



LUND UNIVERSITY

Leaching of concrete : the leaching process and its effects

Ekström, Tomas

2003

[Link to publication](#)

Citation for published version (APA):

Ekström, T. (2003). *Leaching of concrete : the leaching process and its effects*. [Doctoral Thesis (monograph), Division of Building Materials]. Division of Building Materials, LTH, Lund University.

Total number of authors:

1

General rights

Unless other specific re-use rights are stated the following general rights apply:

Copyright and moral rights for the publications made accessible in the public portal are retained by the authors and/or other copyright owners and it is a condition of accessing publications that users recognise and abide by the legal requirements associated with these rights.

- Users may download and print one copy of any publication from the public portal for the purpose of private study or research.
- You may not further distribute the material or use it for any profit-making activity or commercial gain
- You may freely distribute the URL identifying the publication in the public portal

Read more about Creative commons licenses: <https://creativecommons.org/licenses/>

Take down policy

If you believe that this document breaches copyright please contact us providing details, and we will remove access to the work immediately and investigate your claim.

LUND UNIVERSITY

PO Box 117
221 00 Lund
+46 46-222 00 00

LUND INSTITUTE OF TECHNOLOGY
LUND UNIVERSITY

Division of Building Materials

LEACHING OF CONCRETE

The leaching process and its effects

Tomas Ekström

ISRN LUTVDG/TVBM--03/1020--SE(1-296)
ISSN 0348-7911 TVBM
ISBN 91-628-5720-7

Lund Institute of Technology
Division of Building Materials
Box 118
SE-221 00 Lund, Sweden

Telephone: 46-46-2227415
Telefax: 46-46-2224427
www.byggnadsmaterial.lth.se

Errata

- p. 83, equation 3.5: error: $\left(\frac{dV}{dt}\right)_i = k_{w,i} \cdot \nabla P_i - Q_w$
 correction: $\left(\frac{dV}{dt}\right)_i = \nabla(k_{w,i} \cdot \nabla P_i) - Q_w$
- p. 84, in the last section: error: $k_w = \rho_w \cdot B$ correction: $k_w = g \cdot B$
- p. 89, figure 3.9: error: $q = \text{flow (kg/m}^3\text{/s)}$; $dP/dx = \text{pressure gradient (N/m}^2\text{/s)}$
 correction: $q = \text{flow (kg/m}^2\text{/s)}$; $dP/dx = \text{pressure gradient (Pa/m)}$
- p. 113, line 4-5: error: ... in hydraulic head are written ...
 correction: ... in hydraulic head (P_w) are written ...
- p. 113, equation 3.22: error: $u_{mean} = \frac{d^2}{32\mu} \cdot \rho_w \cdot g \cdot \frac{\Delta p}{L}$
 correction: $u_{mean} = \frac{d^2}{32\mu} \cdot \rho_w \cdot g \cdot \frac{\Delta P_w}{L}$
- p. 118, equation 3.45: error: $q_w = -B \cdot \nabla p = -k_w \cdot g \cdot \nabla P_w$
 correction: $v_w = -k_w \cdot \nabla P_w = -g \cdot B \cdot \nabla p / (g \cdot \rho) = -B \cdot \nabla p / \rho$
- p. 161, figure 4.23: The y-scale shall be in mm.
- p. 179, figure 5.23: error: "Relative compressive strength (MPa)"
 correction: "Compressive strength (MPa)"

p. 232:

Rough calculations yield the following results:

- According to table 2.12, $1.83 \cdot 10^{-8}$ mole/l of carbonic acid was assumed to be dissolved in water.
- This amount of H_2CO_3 corresponds to $1.83 \cdot 10^{-8} \cdot (40+12+3 \cdot 16) = 1.83 \cdot 10^{-6}$ g of CaCO_3 /l.
- In total, approximately 150 l of water was led through the 3 holes in a specimen. This gives 50 l/hole.
- If all the CO_2 in the water reacts with Ca^{2+} from the walls of the hole, the amount of CaCO_3 formed becomes $m_{\text{CaCO}_3} = 50 \cdot 1.83 \cdot 10^{-6} = 915 \cdot 10^{-7}$ g.
- If all this CaCO_3 were formed at the walls, it would have a volume of $V = t \cdot \pi \cdot \phi \cdot L / 2 = m_{\text{CaCO}_3} / \rho_{\text{CaCO}_3} \Rightarrow t = m_{\text{CaCO}_3} \cdot 2 / (\pi \cdot \phi \cdot L \cdot \rho_{\text{CaCO}_3}) = 915 \cdot 10^{-7} \cdot 2 / (\pi \cdot 10^{-3} \cdot 40 \cdot 10^{-3} \cdot 2400) = 607 \cdot 10^{-6} \text{ m} = 607 \text{ } \mu\text{m}$.
- If about 3 % of the CO_2 result in CaCO_3 on the wall of the hole it correspond to the measured 20 μm !
- Calculations using the equation (2.12) gives a value of the diffusion coefficient in the solid matrix surrounding the hole of approximately

$$0.002 = \sqrt{\frac{2}{700} k_s \cdot (20 - 0) \cdot 3500 \cdot 3600} \Rightarrow k_s \approx 6 \cdot 10^{-12} \text{ m}^2 / \text{s}$$

which is quite realistic for diffusion in the actual, narrow pores.

p. 239, then last section: error: Figure 7.6 (a) ... Figure 7.6 (b)
correction: figure 7.6 ... figure 7.7

p. 240: The unit of the coloured axis in figure 7.2 and in the y-axis in figure 7.3 is “m/s”.

p. 241-242: The unit of the coloured axis in figures 7.4 (a) and (b) and in the y-axis in figure 7.5 is “mole/m³”.

p.242-243: The unit of the y-axis in figures 7.6 and 7.7 is “mole/m³”.

PREFACE

The work was carried out at the Division of Building Materials at Lund Institute of Technology. The project is part of a National Swedish research programme “Road-Bridge-Tunnel” comprising about 20 projects performed by doctoral students. The research programme was initiated by Professor Kyösti Tuutti, head of the Skanska Research and Development. It was financed by VINNOVA (the Swedish Agency for Innovation Systems), Elforsk AB, Sydkraft AB and Carl Bro Energikonsult AB.

Professor Göran Fagerlund has been my supervisor. I wish to thank him for his support, inspiration and being a source of knowledge.

I would also like to thank my colleagues at the Division of Building Materials for their help and support. Special thanks to Björn Johannesson for the discussions we had about modelling matters, to Mårten Janz for his help with the experimental determination of the water retention curves, to Bertil Person for guidance of determination of non-evaporable water in concrete, to Stefan Backe for his quick and effective help with computers, to Helena Klein for help with literature surveys and finally to Bo Johansson and Ingemar Larsson for their help in the laboratory.

A special thank to Christian Bernstone and Jan Alemo at Vattenfall Utveckling AB and Joakim Jeppsson at Skanska Teknik for good co-operation in matters regarding safety and reliability analysis of dams.

I will also thank Dr. Robert Goldsmith for helping me improving the English text.

I would also express my gratefulness to my employer Carl Bro Energikonsult and their staff for having such patience with my studies.

Finally, I would express my gratitude to my wife Katarina and my children Carolina and Christian for putting up with me these long 6 years of doctoral studies.

ABSTRACT

The present report presents an experimental study of leaching of concrete caused by water percolating through the concrete, or by diffusion from concrete to external water in contact. An apparatus was designed and constructed in which de-ionised water could be forced, by external pressure, through a number of concrete specimens of differing characteristics. It was found that, whereas the initial water flow was normally low and uniform, most specimens showed a rapid increase in water flow after a certain period of time. This was probably due to formation of certain distinct percolation channels. The solid material around these channels was leached, the concrete becoming disintegrated, and almost no continuous cementitious material being left to maintain strength and tightness of the concrete. The chemical composition of the percolated water was analysed, making it possible to calculate the amount of leaching and consequently to theoretically assess the increase in porosity and reduction of strength

Changes in the structure of concrete caused by leaching were also investigated experimentally by measurements of porosity, pore size distribution and strength. ESEM-EDX-studies were made in order to find out the morphology of leached concrete.

Results from all these experimental studies are presented in the report.

A theoretical model of the leaching process and its effects on the material and on the structural stability of real structures was developed. The model is applied to the experimental data.

Key words: concrete dams, leaching, water permeability.

SAMMANFATTNING

Betong är till viss del löslig i vatten. Detta gäller i särskilt hög grad för cementpastafasen i betongen, dvs. reaktionsprodukterna från cementets hydratisering. Även vissa typer av ballast som används i betong har en viss vattenlöslighet. Vattnets förmåga att bryta ner betongen ökas avsevärt om det innehåller vissa lösta ämnen, i synnerhet sådana som sänker dess pH-värde, t.ex. kolsyra.

Det är i första hand kalkhaltiga komponenter i betongen som löses upp, och då framförallt den kalciumhydroxid (Portlandit) som skapades när cementet hydratiserade, men även andra kalkhaltiga hydrationsprodukter kan lösas, t.ex. den kalciumsilikathydrat (C-S-H-gel) som bildades vid cementreaktionen. Upplösningsprocessen kallas därför oftast *kalkurlakning* eller enbart *urlakning*. De båda viktigaste faktorerna som avgör urlakningshastigheten är vattnets *aggressivitet* och betongens *permeabilitet*. Urlakningshastigheten är hög i porös betong med hög permeabilitet eftersom stora vattenmängder kan transporteras genom betongen. Den är låg i tät betong som är sprickfri. I sprucken betong sker stor vattenströmning i sprickor vilket kan medföra stor lokal urlakning i sprickväggarna.

Viktiga faktorer som avgör permeabilitet och därmed urlakning är *porstorleksfördelningen* och porsystemets *grad av kontinuitet*. Det är i första hand cementpastans kapillärporer som bestämmer betongens permeabilitet. Dessa porer kan antingen vara effektivt isolerade från varandra av den extremt finporösa cementgelen eller vara direkt förbundna med varandra. Kapillärporsystemet kan alltså vara mer eller mindre *kontinuerligt*. Vatten kan huvudsakligen strömma genom den kontinuerliga delen av porsystemet vilken därför utgör ett slags *effektiv porositet*. Mycket långsamt diffusionsstyrt vattenflöde kan även ske i de allra minsta kapillärporerna och gelporerna i C-S-H-gelen, men denna vattentransport ger försumbar urlakning. Ökat vattencementtal (vct) medför högre porositet, grövre porsystem och större grad av kontinuitet hos detta. Ökat vct ger därför högre permeabilitet och urlakningshastighet. Även porösa fasgränser mellan ballastpartiklar och cementpasta bidrar till ökad permeabilitet och urlakning.

I föreliggande arbete redovisas ett experimentellt arbete över urlakning. Avsikten med arbetet är att studera urlakningsprocessen och att beskriva urlakningens effekt på betongens egenskaper, främst hållfastheten. I arbetet utvecklas även teoretiska modeller för urlakningsmekanismer och urlakningens tidsförlopp. Dessa modeller verifieras med försöksdata. Avsikten är att dessa modeller skall kunna användas generellt för tillståndsbedömning av olika typer av konstruktioner, främst betongdammar, och för att förutse framtida skadeutveckling förorsakad av urlakning.

Följande typer av experimentella urlakningsförsök genomfördes:

- Homogen genomströmning av avjoniserat vatten (Darcyflöde) genom defektfria vattenmättade betongprover med måttligt hög och mycket hög porositet
- Genomströmning av avjoniserat vatten genom betongprover med förtillverkade defekter i form av hål parallella med vattenflödet.
- Urlakning av betongytor från prover lagrade i stillastående avjoniserat vatten.

Genomströmningsförsöken genomfördes i en nyttillverkad utrustning bestående av följande komponenter; (1) aggregat för avjonisering av vanligt kranvatten, (2) lagringstank för avjoniserat vatten, (3) trycktank ("hydrofor"), (4) ett rörsystem med reduceringsventiler vilket leder fram vatten till en serie av tryckceller, (5) tryckceller med provkroppar så anordnade att endimensionellt vattenflöde genom proverna erhålls, (6) behållare för uppsamling av vatten som transporterats genom proverna. Vattentrycksskillnaden över proverna var normalt 6 bar. För att undvika att ingående vatten på uppströmssidan av proverna förorenades av joner som diffunderar från provernas överyta spolades vattnet på uppströmssidan i provcellerna ut med jämna intervall.

Betongproverna tillverkades med svensktillverkat portlandcement av typ CEM I 42,5 enligt nomenklaturen i europeisk cementstandard. Cementet var dessutom lågalkaliskt och sulfatresistent. Det marknadsförs under namnet "Anläggningscement". Inga tillsatsmedel användes. Ballasten bestod av kvartsit i fraktioner 0-8 mm och 8-12 mm. Vattencementtalet var 0.6, 0.8 och 1.3. Prover lagrades i kalkmättat vatten fram till urlakningsprovning. Vissa prover hettades upp utan torkning (i plastpåsar). Vissa prover både hettades upp och torkades (utan plastpåsar). Före urlakningsprovning vattenmättades dessa prover genom vakuumbehandling följt av vattenlagring. Referensprover som ej användes till urlakningsförsök utsattes i övrigt för samma lagringsförhållanden som urlakningsproverna. Normal storlek hos proverna var 150 mm diameter och 50 mm tjocklek. Även prover med 45 mm diameter provades.

Efter avslutat urlakningsförsök, som pågick under ett antal år, spräcktes alla prover (urlakade och referensprover) i 2 halvor för bestämning av spräckhållfastheten. Små kärnor borrades ur halvorna för bestämning av tryckhållfasthet. Ur den återstående fjärdedelen av ena provhalvan sågades 7 tunna skivor på olika avstånd från den tidigare exponerade överytan. Dessa skivor analyserades med avseende på porositet, porstorleksfördelning och grundämnen (främst Ca och Na).

Den uppmätta permeabiliteten (k_w) hos provkropparna visade sig vara starkt beroende av hur proverna förbehandlats. Prover som aldrig utsatts för någon torkning (jungfruliga prover) hade lågt och tämligen konstant värde på k_w . Detta ökade bara långsamt med ökad urlakningstid.

När prover hettades upp utan torkning (i plastpåsar) genom upp värmning vid tidig ålder och sedan vattenmättades steg värdet på k_w med en faktor ca 100 i förhållande till det jungfruliga provet. Därefter minskade k_w dock gradvis med ökad urlakningstid med en faktor 100 så att ungefär samma värde slutligen erhöles som för det jungfruliga provet. När välhydratiserade prover torkades genom upp värmning och sedan vattenmättades steg värdet på k_w med en faktor ca 100 i förhållande till det jungfruliga provet. För ett flertal prover ökade värdet på k_w drastiskt efter en viss urlakningstid vilket indikerar uppkomsten av genomgående flödeskanaler genom provet.

Uppmätta koncentrationer av Na och K hos det uppsamlade vattnet på nedströmssidan minskade snabbt med urlakningstiden för samtliga prover. Samtidigt sjönk pH till ett värde som motsvarar urlakningen av NaOH och KOH. Värdet sjönk från ca 13.3 till

12.5 som sedan bibehölls under det fortsatta försöket. Detta visar att $\text{Ca}(\text{OH})_2$ fungerar som en stark buffert.

Koncentrationen av Ca hos det genomströmmande vattnet var nästan konstant, ca 0.6 g/liter för alla prover utom de som utsatts för tidig torkning. Ca-koncentrationen för dessa var ca 1.1 g/liter. Ca-koncentrationen i genomströmmat vatten minskade snabbt i de fall där vattenflödet ökade snabbt. Urlakningshastigheten uttryckt i g/s bibehölls emellertid konstant eftersom produkten av flödes hastighet i liter/s och koncentrationen i g/liter var ungefär konstant.

Uppmätt tryckhållfasthet hos urlakade prover uppvisar stor spridning, varierande från samma värde som för icke urlakade referensprover till mycket låga värden. Spridningen beror på stora variationer i urlakning i olika delar av samma prov. Spräckhållfastheten uppvisar mindre spridning vilket kan bero på att brottytan omfattar alla delar av provet.

Porositetsmätningarna hos urlakade prover visar på betydligt större porositetsökning på provets uppströmssida.

Den kemisk analysen visar på en tydlig reduktion av olika grundämnen, särskilt av Ca, på provets uppströmssida.

Huvuddelen av urlakade joner visade sig följa vattenflödet nedströms genom konvektion om betongen har hög permeabilitet. Hos betong med låg permeabilitet skedde huvuddelen av urlakningen genom diffusion mot uppströmsytan. Visuell inspektion visade att den ofta observerade starkt och snabbt ökande genomströmningen efter en viss urlakningstid skedde genom uppkomst av distinkta flödeskanaler. Sådana kanaler innehåller troligen initieellt trånga "flaskhalsar" vilka blir starkt urlakade efter en viss tid. Efter en viss urlakning sker ett genombrott och flödet ökar under kort tid till betydligt högre värden. Hagen-Poiseuilles lag anger att vattenflödet i ett cirkulär cylindriskt rör är proportionellt mot radien upphöjd till 4 vilket medför att även en liten radieökning förorsakad av urlakning ger stor flödesökning. Cementpasta som omger dessa kanaler, och som finns i överytan på urlakade prover, är mycket mjuk, porös och svag och består huvudsakligen av ett urlakat skelett av Si, Al och Fe.

Den teoretiska modellering av urlakningsprocessen som genomfördes var framgångsrik så till vida som modellen kunde förutse den experimentellt uppmätta urlakningsprocessen. Modelleringen baseras på grundläggande fysikaliska jämviktssamband och innehåller såväl information från litteraturen som information framtagen i det här genomförda experimentella arbetet. Modellerna är generella och kan tillämpas såväl på små prover i laboratoriet som på verkliga konstruktioner, t.ex. betongdammar. Det är dock viktigt att de utarbetade modellerna kalibreras ytterligare genom fler laboratorieförsök och observationer på verkliga konstruktioner.

SUMMARY

The hydration products in concrete, and sometimes in the aggregate as well, are to varying degrees soluble in water. The corrosion of concrete by water can be caused by the water itself acting as dissolving agent, or by matter that is dissolved in the water and reacts with the concrete. The most soluble phase in concrete is Portlandite ($\text{Ca}(\text{OH})_2$) formed when Portland cement reacts with water. Also the calcium-silicate-hydrate (C-S-H gel) is soluble in water. Since it is calcium compounds that are attacked, dissolution by water is often called *lime leaching*, or simply *leaching*. The two most important factors influencing leaching are the aggressiveness of the water and the permeability of the concrete. The bulk leaching rate is high in porous concrete in which water can seep through large masses of concrete, whereas it is low in concrete in which the water flows through only a few flow channels, such as in cracks. The degree of local leaching that occurs in a crack on the other hand is often very high.

Pore size distribution and connectivity are two very important factors affecting water permeability and thereby leaching. Pores are void spaces distributed through the material in varying frequency. The pores can be either *interconnected* or *non-interconnected*. Fluids can only percolate through the interconnected parts, which constitute the *effective* pore space. The permeability, or how easily a fluid penetrates a porous medium, is considered to be the single most important property affecting the durability of concrete. The flow of water through concrete represents the sum of all leakage of water, from large-scale flow in large connected, water-filled cracks and cavities to very slight vapour diffusion through capillary pores.

If leaching of the bulk concrete occurs this will negatively affect strength and stiffness, since leaching increases the porosity. It will also negatively affect durability such as frost resistance.

In the present work, leaching was studied by use of models and by performing experiments for verifying the models. The aim of the experiments was to investigate leaching effects in concrete, both in general, and in terms of how the strength of concrete is affected. The aim of the modelling was to develop general calculation methods, applicable to various leaching situations in different types of concrete dams.

In the experimental work concrete was leached in three different ways:

- By the homogenous percolation (Darcian flow) of deionised water through rather porous, defect-free concrete.
- By the percolation of deionised water through artificially-made holes in concrete.
- By leaching from the free surface of concrete lying in stagnant de-ionised water.

The test equipment for leaching consisted of a deionising aggregate for water, a water storage tank, a pump, a pressure water tank and a pipe system leading water out to a number of test cells containing concrete specimens. The water pressure difference across the specimens was mostly 6 bar. The percolating water was collected in vessels at the downstream end and was analysed for relevant ions. In order to maintain the purity of the inlet water, this was replaced at regular intervals.

A sulphate resistant, low-alkali, low-heat Portland cement (“Degerhamn anläggningcement”) of type CEM I 42,5 according to the European Cement Standard

was used. No admixtures or additives were used. The aggregate was quartzite 0-8 mm and 8-12 mm, in a proportion of 85 to 90% of the total concrete mass. W/c ratios of 0.6, 0.8 and 1.3 were used. Some specimens were stored in water until the test started, some were heated without drying (in plastic bags) whereas others were heated and pre-dried (without plastic bags). Before the test started, dried samples were water-saturated by vacuum treatment followed by water absorption.

When the percolation test was ended, both the leached specimens and unleached reference specimens were first split into two halves, which gave the split tensile strength. Three small cylinders were then drilled out and were used for testing the compressive strength. The remaining one-quarter part of each specimen was sliced into seven slices which were analysed with regard to porosity and the content of elements (such as Ca, Na).

The measured permeability (k_w) of the test specimens was found to depend primarily on the way the specimens were cured. Specimens that had never been dried (virgin specimens) had a low and rather uniform k_w , which only increased slowly with time. When the specimens were heated at an early hydration age, the initial k_w was about 100 times as high as in the virgin specimens, but its value decreased again by about 100 times. When well-hydrated specimens were first heated and dried, k_w rose 100 fold compared with the virgin state. Quite often the k_w rose sharply after a certain period of percolation, indicating the formation of individual flow channels, in which leaching was significant.

The measured concentrations of Na and K in the percolating water decreased rather quickly for all the specimens. The pH decreased to a degree, corresponding to the reduction in Na and K, from about 13.3 to 12.5, Ca(OH)_2 acting as a strong buffer.

The concentration of Ca in the percolated water was uniform at approximately 0.6 g/l for all specimens except for the early heated (EH) specimens, in which the concentration was uniform at approximately 1.1 g/l. The concentration of Ca in the percolated water decreased rapidly in cases where the flow of water through the specimens increased rapidly. The leaching rate in terms of g/s however remained constant, since the product of the increased water flow in l/s and the concentration (g/l) remained approximately the same.

The measured compressive strength in the leached specimens showed a large degree of scatter, varying from almost the same values as for the unleached reference specimens down to very low values, depending on whether the cylinders tested were taken from very leached parts of the specimens or from less leached parts. The measured split strength showed a lesser degree of scatter.

Porosity analysis of the leached specimens showed a clear increase in porosity in the upstream part.

Chemical analysis of the leached specimen showed a clear reduction in more soluble elements, calcium in particular, in the upstream part.

In concrete subjected to a water pressure gradient, most of the leached ions appeared to flow downstream with the water if the concrete was permeable, whereas they largely diffused upstream if the concrete was tight. From visual inspection of the specimens tested, it appeared that most of the water, or more correctly, most of the rapid increase in the flow of water, occurred in certain flow channels. These channels probably contain certain narrow bottlenecks that became seriously leached, the leached gel-skeleton

suddenly breaking apart at some time, causing the water flow to increase rapidly. The Hagen-Poiseuille law, stating that the water flow is proportional to the radius raised to 4, makes the rapid increase in the water flow understandable. Around these large channels, and on the upstream surface of the concrete, the cement paste was very soft, porous and weak, consisting mainly of a leached skeleton of Si, Al and Fe which had almost no strength left. In other parts, that were unleached, no signs of a reduction in strength were observed.

The leaching process was theoretically modelled, considering a diffusion of calcium and other ions from the cement paste matrix to water flowing in individual flow channels. The modelling work was rather successful in that the leaching behaviour observed in the experiments could be seen in the models as well. The models are based on basic physical balance laws. The constitutive relations include both traditional relations obtained from the literature, and relations proposed in connection with the present work. The models are sufficiently general to be used both for small experimental samples and for “real” structures (such as concrete dams). It is important, however, that the models developed are calibrated further, not only to experimental data, but also to field data.

SYMBOLS

All symbols are explained where they first appear in the text. Most of the symbols are also presented here. All dimensions are in SI-units.

| Symbol | Definition | SI-unit |
|-------------------|---|-----------------------------------|
| \hat{c}_i | mass source term | (mole/m ³ /s) |
| \bar{c}_i^L | average concentration of species i | (mole/m ³) |
| α | “surface roughness factor”, generally about 0.01-0.2 | (-) |
| μ | dynamic viscosity | (Ns/m ²) |
| ϕ | potential defined as $\mathbf{u} = -\nabla\phi$ | (m) |
| β | empirical dissolution coefficient | |
| φ | contact angle between water and pore wall | |
| α | degree of hydration | (-) |
| ρ | solid bulk density | (kg/m ³) |
| ρ | density of leached material | (kg/m ³) |
| ϕ | diameter of reinforcement bars | (m) |
| δ | diffusion layer in the wall of a solid | (m) |
| μ | dynamic viscosity | (N·s/m ²) |
| ρ | electrical charge density | (J/V/m ³) |
| ν | Poisson’s ratio | (-) |
| τ | reduction tensor for the tortuosity of a pore system | (-) |
| β | safety index | (-) |
| τ | shear stress | (Pa) |
| σ | surface tension between the liquid and the air (0.07275 N/m at +20°C) | (Pa) |
| ε | dielectric field of a medium | (F/m=J/V ² /m) |
| δ | thickness of a diffusion layer | (m) |
| τ | tortuosity factor = s/x | (-) |
| ∇ | Nabla operator $\left(\nabla^T = \left[\frac{\partial}{\partial x} \quad \frac{\partial}{\partial y} \quad \frac{\partial}{\partial z} \right] \right)$ | (1/m) |
| $\phi_{(t)}$ | diameter of leached tubes | (m) |
| δ_0 | thickness of a diffusion layer | (m) |
| η_1 | parameter regarding the depth of concrete under reinforcement bars at casting(-) | |
| η_2 | parameter (1.4 for the profiled bars) | (-) |
| ρ_a | density of aggregate | (kg/m ³) |
| μ_a | loss of mass of aggregate between 105°C and 1050°C | (kg/kg) |
| $\phi_{a(t_0)}$ | initial average diameter of tubes of a size a | (m) |
| $\sum A_{a(t)}$ | cross-sectional area of all leached tubes of a size a | (m ²) |
| $\sum A_{a(t_0)}$ | volume per length of the tubes as a whole | (m ³ /m) |
| μ_c | loss of mass of cement between 105°C and 1050°C | (kg/kg) |
| ε_c | strain in a specimen | (m ³ /m ³) |
| ∇c | concentration gradient | (mole/m ³ /m) |
| ρ_{CH} | density of Ca(OH) ₂ | (kg/m ³) |
| $\sum CO_2$ | total carbonic acid | (mole/l) |

| | | |
|-----------------------|--|-----------------------------------|
| $\delta c_s/\delta t$ | dissolving reaction | (mole/m ³ /s) |
| ρ_{dry} | dry bulk-density of concrete slices | (kg/m ³) |
| γ_i | activity coefficient of species i | (l/mole) |
| μ_i | electrochemical potential of species i | (J/mole) |
| μ_{i0} | standard chemical potential of species i | (J/mole) |
| Δm_{Ca} | loss of calcium due to leaching | (kg) |
| $\Delta m_{ca}(aq)$ | loss of calcium due to leaching the concrete | (kg) |
| σ_N | normal stress | (Pa) |
| Δp | difference in pressure | (Pa) |
| ∇P | pressure gradient | (Pa/m) |
| $\delta p/\delta x$ | pressure gradient | (Pa/m) |
| $\Delta P/L$ | pressure gradient | (Pa/m) |
| σ_s | stress in reinforcement bars | (Pa) |
| σ_{sb} | bond stress between reinforcement and concrete | (Pa) |
| ΔV | change in capillary volume due to normal stresses | (m ³) |
| ρ_w | density of water | (kg/m ³) |
| $(V_{cap})_p$ | capillary volume of cement paste | (m ³) |
| $(V_{cap})_p$ | initial (prior to leaching) capillary pore volume of cement paste | (m ³ /m ³) |
| $(V_p)_a$ | volume of pores in aggregate | (m ³) |
| $(V_p)_p$ | total pore volume of cement paste | (m ³) |
| [A] | real ionic concentration | (mole/l) |
| [Ca(aq)] | measured concentration of ca | (mole/l) |
| [Si(aq)] | measured concentration of Si | (mole/l) |
| A | cross sectional area | (m ²) |
| a | a curve fitting parameter, $a = 1.2$ to fit f_{cc} in Ysberg (1979) | (-) |
| A, B | empirical parameters | (-) |
| a/c | ratio of aggregate to cement | (kg/kg) |
| A_a | cross-sectional area of one capillary of size a | (m ²) |
| $A_{a(t0)}$ | initial cross-sectional area of an individual tube of size a | (m ²) |
| a_i | adjustable parameter corresponding to the size of the ion | (-) |
| A/A_{ges} | ratio of the area of soluble matter to the total area | (m ² /m ²) |
| $A_{pore\ wall}$ | area of the solid in contact with water from which ions are dissolved | (m ²) |
| A_s | area of reinforcement bars | (m ²) |
| A_{tot} | total cross a sectional area | (m ²) |
| A_{wall} | a surface from which ions are dissolved | (m ²) |
| \bar{E}^L | average electric potential in the liquid phase in a representative elementary volume (REV) | (V) |
| b | a curve fitting parameter. $b = 0.5$ to fit f_{cc} in Ysberg (1979) | |
| B | permeability (s) for a gradient in pressure (Pa) | |
| b | slit length perpendicular to the flow direction | (m) |
| c | “Kozeny constant” (0.50, 0.5619) for (circles, squares) | (-) |
| C | cement content | (kg) |
| c | concrete cover | (m) |
| c_{Ca} | calcium concentration | (mole/m ³) |
| $c_{Ca(s)}$ | concentration of Ca in the solid phase | (mole/l) |
| \dot{c}_i | changes in concentration during time period dc/dt | (mole/m ³ /s) |

| | | |
|--------------|---|---------------------------------|
| c_i | concentration of dissolved ions | (mole/m ³) |
| c_i | concentration outside a diffusion layer t | (mole/m ³) |
| c_i | ionic concentration in a free water solution (pore solution) | (mole/m ³) |
| c_{is} | saturation concentration | (mole/m ³) |
| c_l | Ca(HCO ₃) ₂ concentration (kg/m ³) in a solution which is unaffected by the concrete | (mole/m ³) |
| c_s | ionic concentration in a solid phase | (mole/m ³) |
| $c_s(t)$ | concentration of the ions in a solid at time t | (mole/m ³) |
| $c_s(t_0)$ | initial (prior to leaching) concentration of ions in a solid material | (mole/m ³) |
| c_s^* | Ca(HCO ₃) _s concentration (kg/m ³) in the solution surrounding intact concrete | (mole/m ³) |
| $c_{s,Ca}$ | concentration of solid calcium | (mole/m ³) |
| c_{s0} | initial solid-phase concentration | (mole/m ³) |
| c_{sat} | saturation concentration | (mole/m ³) |
| D | damping | |
| d | diameter of a tube | (m) |
| D | diffusion coefficient for Ca(HCO ₃) ₂ (m ² /s) contained in a layer that is destroyed | |
| d | thickness of a concrete layer that is destroyed (leached) | (m) |
| d_c | critical pore diameter | (m) |
| D_{eff} | effective diffusion coefficient, considering the porosity, tortuosity, constrictivity, chemical influences and reactions with the pore walls and with other species | (m ² /s) |
| $D_{eff,Ca}$ | effective diffusion coefficient of Ca ²⁺ in pore solution | (m ² /s) |
| D_f | diffusion coefficient in free water (bulk water) | (m ² /s) |
| D_i | diffusion coefficient for species i | (m ² /s) |
| D_K | Knudsen diffusion in small pores | (m ² /s) |
| D_L | diffusion coefficient of a totally degraded solid at the end of a calcium-leaching process | (m ² /s) |
| dm | mass of leached ions | (kg/m ³) |
| dq_w/dt | amount of water | (m ³ /s) |
| D_s | diffusion coefficient of a solid at any given time | (m ² /s) |
| D_{s0} | initial diffusion coefficient | (m ² /s) |
| E | local electrical potential | (V) |
| f | a property | |
| F | faraday constant | (9.65·10 ⁴ J/V/mole) |
| f_0 | fictitious strength of a solid phase without pores | (Pa) |
| f_0' | fictitious strength of cement gel, with gel pores included | (Pa) |
| f_b | bond strength | (Pa) |
| f_{cc} | a model describing the compressive strength of concrete | (Pa) |
| f_{ct} | a model of the tensile strength of the concrete | (Pa) |
| F_i | total ionic flux | (mole/m ² /s) |
| F_{iu} | diffusion flux of ions | (mole/m ² /s) |
| F_{iv} | ionic flux due to convection | (mole/m ² /s) |
| F_b | bond force capacity | (N) |
| f_{pc} | a model compressive strength of cement paste | (Pa) |

| | | |
|------------------------|--|-------------------------------------|
| F_{s2} | reinforcement force | (N) |
| g | acceleration due to gravity | (m/s ²) |
| $\text{grad}(\mu_i)$ | local gradient of μ | (J/mole/m) |
| h | depth of water | (m) |
| h_1, h_2 | liquid that rises above an arbitrary level | (m) |
| I | ion strength | (mole/l) |
| k | a constant depending on the maximum tolerable error of the number of specimens | (-) |
| k | dissolving rate coefficient | (m ³ /s) |
| k | specific permeability coefficient | (m ²) |
| k | total corrosion of concrete by carbonic acid | (-) |
| K_1 | an empirical parameter depending on the residual content of CH(s) | (-) |
| K_1 | an empirical parameter, given as $2 \leq K_1 \leq 3.5$ in the literature | (-) |
| K_1 | a permeability coefficient | (s) |
| K_2 | an empirical parameter dependent on the leaching ratio | (-) |
| K_2 | an empirical parameter, given as $2 \leq K_1 \leq 3$ in the literature | (-) |
| k_a | specific permeability of all capillaries with a particular size a | (m ²) |
| K_d | a sorption coefficient | (m ³ /kg) |
| k_e | a erosion coefficient | (= dx_e/dt = rate of erosion m/s) |
| k_i | diffusion coefficient of the solution in the tube | (m ² /s) |
| k_i | a diffusion coefficient | (m ² /s) |
| k_{suck} | a capillary constant | (kg/m ² ·√s) |
| k_w | permeability to water | (m/s) |
| k_w | a bulk permeability coefficient | (m/s) |
| $k_w(t)$ | permeability of a leached material | (m/s) |
| $k_w(t_0)$ | permeability of a unleached material | (m/s) |
| L | flow channel length of a slit | (m) |
| L | length of a cantilever | (m) |
| L | length of a concrete specimen | (m) |
| L | length of the crack perpendicular to a flow direction | (m) |
| L | length of a tube | (m) |
| L | length of a filter bed | (m) |
| $M =$ | a constant (5) | |
| M | a bending moment | (Nm/m) |
| M | bending moment of a concrete slab | (N·m) |
| m | a mean value | |
| m | a resistance constant for capillary suction | (s/m ²) |
| $m_{105^\circ C, air}$ | weight of dried (+105°C) slices in air | (kg) |
| m_{1050C} | weight of concrete at +1050°C | (kg) |
| M_{Ca} | molar weight of calcium | (40 g/mole) |
| $m_{Ca(aq)}$ | weight of Ca in a HNO ₃ -solution | (kg) |
| $m_{Ca(t_0)}$ | initial calcium content of unleached concrete at the start of testing | (kg) |
| M_{CaO} | molar weight of calcium oxide | (56 g/mole) |
| m_i | measured weight loss at each pressure step | (kg) |
| m_{rest} | measured insoluble rest of specimens | (kg) |
| m_s | total amount of soluble material in concrete | (kg/m ³) |
| $m_{Si(aq)}$ | measured content of Si in a HNO ₃ solution | (kg) |

| | | |
|-----------------|--|-----------------------------------|
| $m_{Si(aq)}$ | weight of Si in a HNO ₃ -solution | (kg) |
| $m_{Si(t0)}$ | initial content of Si in the each slices of specimens at time $t0$ | (kg) |
| M_w | molar weight of water | (0.018 kg/mole) |
| $m_{wet,air}$ | weight of saturated slices in air | (kg) |
| $m_{wet,water}$ | weight of the saturated slices under water | (kg) |
| N | constant (70 to 100) | (-) |
| n | number of cement particles | (nos.) |
| N | number of classes with diameter of different size | (-) |
| n | number of CO ₂ molecules | (mole) |
| n_a | numbers of tubes of size a that are connected through concrete | (nos./m ²) |
| n_a | number of capillaries of diameter ϕ_a | (nos.) |
| p | hydrostatic pressure | (Pa) |
| P | partial pressure of CO ₂ | (atm) |
| P | total porosity | (m ³ /m ³) |
| P_{air} | air-filled porosity | (m ³ /m ³) |
| $Part$ | the part of the leached volume that lead to an increase in the diameter of the tubes | (-) |
| P_c | porosity of concrete | (m ³ /m ³) |
| $P_{c(t0)}$ | total porosity of concrete at the time when leaching starts | (m ³) |
| P_{cap} | capillary porosity of paste after leaching | (m ³ /m ³) |
| P_i | air pressure applied | (Pa) |
| P_p | total porosity of cement paste | (m ³) |
| P_{p0} | initial porosity of paste | (m ³ /m ³) |
| P_{suck} | porosity available for water suction | (m ³ /m ³) |
| P_{tot} | total porosity | (m ³ /m ³) |
| P_w | water pressure (piezometric) head | (m) |
| P_w | water-filled porosity prior to the start of capillary suction | (m ³ /m ³) |
| q | filter velocity of a fluid | (m/s) |
| Q | mass dissolving | (mole/s) |
| q | water pressure | (kPa) |
| q^* | filtration velocity that would be present if there were no electric effects | (m/s) |
| q_a | water flow in all capillaries with a particular size a | (m ³ /s) |
| Q_{conv} | leaching of calcium by convection to the downstream water | (kg) |
| Q_{diff} | leaching of calcium by diffusion to the upstream water | (kg) |
| q_{iu} | bulk diffusion flow of ions | (mole/s) |
| q_{iv} | bulk convective flow of ions | (mole/s) |
| Q_{leach} | total amount of lime leached by time t | (kg/m ²) |
| q_{osm} | filtration velocity due to electric effects | (m/s) |
| q_{suck} | rate of suction flow | (kg/m ³ /s) |
| Q_w | loss or gain of water inside the concrete | (m ³ /s) |
| q_w | amount of a percolating fluid | (m ³ /s) |
| $q_w(t)$ | water flow in a leached material | (m ³ /s) |
| $q_w(t0)$ | water flow in unleached material | (m ³ /s) |
| $q_{w,crack}$ | leakage of water through a crack | (m ³ /s) |
| $q_{w,tube}$ | flow through a tube | (m ³ /s) |
| R | gas constant | 8.314 (J/(mole·K)) |
| r | radius | (m) |

| | | |
|---|--|-----------------------------------|
| R | strength | |
| r_{∞} | maximum continuous pore radii | (Å) |
| $R \cdot T \cdot \ln(\gamma_i \cdot c_i)$ | difference between any condition for species i and the standard condition | (at 1 atm, 20°C) |
| r_i | circular pore radius | (m) |
| r_w | a reduction parameter considering all deviations from free flow in a straight tube | (-) |
| S | internal surface area | (m ²) |
| S | load effect | |
| s | standard deviation | |
| s | length of a real pore | (m) |
| $share$ | share of the total capillary porosity that are connected through the concrete | (-) |
| $size1, size2$ | length of each side of the small square of fictive volume | (m) |
| \hat{c}_w | source or sink of water | (m ³ /s) |
| S_{por} | molar fraction of portlandite | (mole/l) |
| S_{tot} | molar fraction of total calcium in the hydrated cement paste | (mole/l) |
| T | temperature | (K) |
| t | thickness of the concrete slab at the abutment | (m) |
| t | time | (s) |
| t | time since the start of leaching | (s) |
| u | local velocity of water | (m/s) |
| u_{mean} | mean velocity in a tube | (m/s) |
| W | bending resistance | (m ³) |
| w | crack width (m); $\Delta P/\Delta x =$ pressure gradient | (Pa/m) |
| w | slit width | (m) |
| W | “free” (or unbound) water fraction | (m ³ /m ³) |
| V | volume of trapped air | (m ³) |
| w/c | water cement ratio | (-) |
| W_0 | mixing water | |
| $V_{a(t0)}$ | calculated initial volume of aggregate in concrete slices | (m ³) |
| $V_{a(t0)}$ | initial volume of an individual tube of size a | (m ³) |
| $V_{acetate\ buffer}$ | volume of acetate buffer | (ml) |
| V_{air} | volume of air due to compaction or air additives | (m ³) |
| $V_{air(t0)}$ | measured initial volume of air | (m ³) |
| V_c | volume of concrete | (m ³) |
| V_c | volume of concrete slices | (m ³) |
| V_c | volume of a specimen | (m ³) |
| V_C | volume ratio of cement in paste | (m ³ /m ³) |
| $V_{c(t0)}$ | measured initial volume of concrete slice | (m ³) |
| $V_{collected\ water}$ | test water volume collected | (ml) |
| W_{curing} | water added during curing | |
| V^d | volume fraction of the hydrates other than Portlandite | (m ³ /m ³) |
| V^d_{por} | volume fraction of Portlandite | (m ³ /m ³) |
| W_{forced} | water forced into the concrete during its life cycle | |
| V_{gel} | volume of cement gel | (m ³) |
| W_{hydr} | chemically bounded water present during hydration | |

| | | |
|-------------------|---|---------------------------|
| V^i | volume fraction of the hydrates calculated by subtracting the volume occupied by the Portlandite and the SiO_2 fraction from the total volume of hydrates in a fully hydrated system | (m^3/m^3) |
| V_l/V_{ges} | ratio of the volume of soluble constituents (if insoluble aggregate is employed → volume of hardened cement paste) to the total volume | (m^3/m^3) |
| V_{leach} | leached volume per unit length | (m^3/m) |
| V_{leach} | total volume of leached material | (m^3) |
| W_n | non-evaporable water (chemically bounded) | (kg) |
| V_{NaCl} | volume of NaCl solution employed | (ml) |
| V_p | total volume of cement paste | (m^3) |
| $V_{p(t0)}$ | initial volume of the cement paste prior to leaching | (m^3) |
| V_{rest} | insoluble (in HNO_3) rest found in the container after dissolution of the slices in $\text{HNO}_3(\text{aq})$ (m^3) | |
| $V_{rest,paste}$ | part of the insoluble rest that came from cement paste | (m^3) |
| S_a | assumed solubility of the aggregate in HNO_3 | $(\text{weight } \%)$ |
| $V_{solution}$ | volume of a HNO_3 -solution | (m^3) |
| W_{suck} | total amount of water sucked by capillary action | (kg/m^2) |
| W_{tot} | total water | (m^3) |
| V_{tot} | volume of a concrete specimen | (m^3) |
| v_w | velocity of a pore solution (Darcian velocity) | (m/s) |
| v_w | velocity field in water | (m/s) |
| v_w | velocity of water | (m/s) |
| x | depth of a leached zone | (m) |
| X | gel space ratio | (m^3/m^3) |
| x^* | depth of the leaching front when the rate of erosion is equal to the rate of penetration of a leaching front | (m) |
| x_1 | average position of the dissolution front of Portlandite | (m) |
| x_2 | average position of the dissolution front of C-S-H | (m) |
| z | height above an arbitrary reference level | (m) |
| z | internal lever between reinforcement bars a load resultant | (m) |
| z | penetration depth due to capillary suction | (m) |
| z_i | valence of ionic species i | |

CONTENTS

| | |
|---|-----------|
| PREFACE | 1 |
| ABSTRACT | 2 |
| SAMMANFATTNING | 3 |
| SUMMARY | 6 |
| | |
| 1 INTRODUCTION | 21 |
| 1.1 BACKGROUND TO THE PRESENT WORK | 21 |
| 1.2 CONCRETE DAMS – AN OVERVIEW | 21 |
| 1.3 ENVIRONMENTAL INDUCED DAMAGE IN CONCRETE DAMS | 23 |
| 1.4 LEACHING DAMAGE IN CONCRETE DAMS | 24 |
| 1.5 LACK OF KNOWLEDGE ABOUT LEACHING IN CONCRETE STRUCTURES | 26 |
| 1.6 AIM OF THE WORK | 26 |
| 1.7 LIMITATIONS OF THE WORK | 27 |
| 1.8 ABBREVIATIONS | 27 |
| | |
| 2 LEACHING OF CONCRETE – A LITERATURE SURVEY | 28 |
| 2.1 INTRODUCTION | 28 |
| 2.2 LEACHING DAMAGES | 29 |
| 2.3 WATER QUALITY IN LAKES, RIVERS AND IN THE GROUND | 29 |
| 2.4 LEACHING PROCESSES | 30 |
| 2.4.1 <i>General</i> | 30 |
| 2.4.2 <i>Free surface-leaching</i> | 37 |
| 2.4.3 <i>Leaching due to homogenous percolation of concrete</i> | 41 |
| 2.4.4 <i>Leaching due to percolation through cracks in concrete</i> | 47 |
| 2.4.5 <i>Dissolution reactions</i> | 48 |
| 2.4.5:1 General | 48 |
| 2.4.5:2 Dissolving in stagnant water in which the reaction can reach equilibrium | 49 |
| 2.4.5:3 Dissolving in mobile water in which the reaction cannot go to equilibrium | 51 |
| 2.4.5:4 Dissolving of cement paste | 54 |
| 2.4.6 <i>Diffusion of dissolved ions</i> | 61 |
| 2.4.7 <i>Convection of dissolved ions</i> | 69 |
| 2.5 VARIOUS FACTORS INFLUENCING LEACHING | 69 |
| 2.5.1 <i>Effects of autogenous healing in cracks and self-sealing of concrete</i> | 69 |
| 2.5.2 <i>Effect of type of cement</i> | 71 |
| 2.5.3 <i>Effect of carbon dioxide</i> | 72 |
| 2.5.3:1 General | 72 |
| 2.5.3:2 Carbon dioxide in water | 72 |
| 2.5.3:3 Carbon dioxide in water containing calcium (such as in cement materials) | 74 |
| 2.5.4 <i>Effect of temperature</i> | 75 |
| 2.6 EFFECTS OF LEACHING | 75 |
| 2.6.1 <i>Leaching effects on the permeability</i> | 75 |
| 2.6.2 <i>Leaching effects on the mechanical properties</i> | 75 |
| 2.6.3 <i>Leaching effects on the internal water pressure</i> | 78 |
| | |
| 3 WATER MOBILITY IN CONCRETE OF IMPORTANCE FOR LEACHING | 79 |
| 3.1 WATER FLOW IN POROUS MEDIA | 79 |
| 3.2 CHARACTERISTICS OF WATER | 79 |
| 3.3 WATER IN CONCRETE | 79 |

| | | |
|----------|--|------------|
| 3.4 | DRIVING POTENTIALS FOR THE TRANSPORT OF WATER IN POROUS MATERIALS | 80 |
| 3.5 | PERMEABILITY | 81 |
| 3.5.1 | <i>Introduction</i> | 81 |
| 3.5.2 | <i>Permeability of cement paste</i> | 84 |
| 3.5.3 | <i>Permeability of aggregate</i> | 88 |
| 3.5.4 | <i>The permeability of concrete</i> | 88 |
| 3.5.5 | <i>The permeability of the interfacial zone</i> | 90 |
| 3.6 | FACTORS INFLUENCING THE PERMEABILITY OF CONCRETE TO WATER..... | 90 |
| 3.6.1 | <i>General</i> | 90 |
| 3.6.2 | <i>Cracks or cavities</i> | 91 |
| 3.6.3 | <i>Internal humidity</i> | 91 |
| 3.6.4 | <i>Curing conditions</i> | 95 |
| 3.6.5 | <i>Degree of hydration</i> | 98 |
| 3.6.6 | <i>Water cement ratio</i> | 99 |
| 3.6.7 | <i>Large air- or water-filled pores</i> | 99 |
| 3.6.8 | <i>Porosity and pore size distribution</i> | 100 |
| 3.6.9 | <i>Type, size and amount of aggregate</i> | 103 |
| 3.6.10 | <i>Type of cement</i> | 103 |
| 3.6.11 | <i>Leaching, self sealing or autogenous healing</i> | 104 |
| 3.6.12 | <i>Workability and placing</i> | 105 |
| 3.6.13 | <i>Deposit of material inside a concrete dam</i> | 106 |
| 3.6.14 | <i>The viscosity of the fluid</i> | 106 |
| 3.6.15 | <i>State of stress</i> | 107 |
| 3.6.16 | <i>The shape and dimension of the global structure</i> | 107 |
| 3.7 | WATER FLOW IN SATURATED CONCRETE | 107 |
| 3.8 | TEST METHODS AND MODELLING OF WATER PERMEABILITY..... | 108 |
| 3.8.1 | <i>Permeability test</i> | 109 |
| 3.9 | MODELLING WATER PERMEABILITY IN SATURATED CONCRETE..... | 109 |
| 3.9.1 | <i>Introduction</i> | 109 |
| 3.9.2 | <i>Pore space models</i> | 112 |
| 3.9.3 | <i>A non-pore space model: Darcy's law</i> | 116 |
| 4 | THE EXPERIMENTAL WORK | 121 |
| 4.1 | BACKGROUND | 121 |
| 4.2 | AIM AND GENERAL SETUP | 121 |
| 4.3 | CONCRETE SPECIMENS..... | 123 |
| 4.3.1 | <i>An overview</i> | 123 |
| 4.3.2 | <i>Cement</i> | 128 |
| 4.3.3 | <i>Aggregate</i> | 128 |
| 4.3.4 | <i>Casting</i> | 129 |
| 4.3.5 | <i>Curing</i> | 131 |
| 4.4 | HOMOGENOUS STEADY-STATE PERCOLATION OF WATER THROUGH DEFECT-FREE CONCRETE..... | 132 |
| 4.4.1 | <i>Introduction</i> | 132 |
| 4.4.2 | <i>Apparatus</i> | 133 |
| 4.4.3 | <i>Tested material</i> | 134 |
| 4.4.4 | <i>Test procedure</i> | 135 |
| 4.4.5 | <i>Measurements and presentation of data</i> | 137 |
| 4.4.5:1 | Measuring water flow | 137 |
| 4.4.5:2 | Measuring of ionic flow..... | 137 |
| 4.4.5:3 | Analysis of specimens | 137 |
| 4.4.6 | <i>Validity</i> | 138 |
| 4.4.6:1 | Introduction..... | 138 |
| 4.4.6:2 | Saturated specimens..... | 139 |
| 4.4.6:3 | Curing | 139 |
| 4.4.6:4 | Water-to-cement ratio | 141 |
| 4.4.6:5 | Water aggressiveness..... | 141 |

| | | |
|--------------|--|------------|
| 4.4.6:6 | No atmospheric CO ₂ in contact with the concrete | 142 |
| 4.4.6:7 | The temperature was held constant at 20°C..... | 142 |
| 4.4.6:8 | Size of the aggregate..... | 143 |
| 4.4.6:9 | Hydration effects and type of cement | 143 |
| 4.4.6:10 | The pressure gradient..... | 143 |
| 4.4.6:11 | Loads..... | 144 |
| 4.4.6:12 | Orientation of casting..... | 144 |
| 4.4.6:13 | End effects | 144 |
| 4.4.6:14 | Anisotropic measurements of permeability..... | 144 |
| 4.4.6:15 | Cement..... | 144 |
| 4.4.6:16 | Synergy between degradation mechanisms..... | 145 |
| 4.4.7 | <i>Errors of testing and the reliability of the results.....</i> | 145 |
| 4.4.7:1 | Introduction..... | 145 |
| 4.4.7:2 | Undesired water leakage..... | 145 |
| 4.4.7:3 | End effects | 146 |
| 4.4.7:4 | Decrease in flow area..... | 146 |
| 4.4.7:5 | Carbonation..... | 147 |
| 4.4.7:6 | Effect of air-filled pores in the concrete | 149 |
| 4.4.7:7 | Effect of the presence of air in the inlet water | 149 |
| 4.4.7:8 | Hydration age..... | 149 |
| 4.4.7:9 | Aggregate gradation..... | 149 |
| 4.4.7:10 | Sample size | 149 |
| 4.4.7:11 | Swelling of the concrete..... | 150 |
| 4.4.7:12 | Dissolution and deposition of dissolved substances..... | 150 |
| 4.4.7:13 | Stresses in the specimen..... | 150 |
| 4.5 | PERCOLATION THROUGH HOLES IN THE CONCRETE..... | 151 |
| 4.5.1 | <i>General.....</i> | <i>151</i> |
| 4.5.2 | <i>Test records and presentation of data.....</i> | <i>152</i> |
| 4.5.3 | <i>Validity.....</i> | <i>152</i> |
| 4.5.4 | <i>Errors of test and reliability of results.....</i> | <i>152</i> |
| 4.6 | SURFACE-LEACHING OF CONCRETE | 152 |
| 4.6.1 | <i>General.....</i> | <i>152</i> |
| 4.6.2 | <i>Errors of testing and reliability of the results.....</i> | <i>153</i> |
| 4.7 | CHEMICAL ANALYSIS OF THE WATER SAMPLES..... | 153 |
| 4.8 | SPLITTING TEST | 155 |
| 4.9 | COMPRESSION TEST..... | 156 |
| 4.10 | POROSITY MEASUREMENTS | 156 |
| 4.10.1 | <i>General.....</i> | <i>156</i> |
| 4.10.2 | <i>Pore size distribution</i> | <i>157</i> |
| 4.10.3 | <i>The total porosity.....</i> | <i>158</i> |
| 4.11 | DETERMINATION OF THE NON EVAPORABLE WATER IN THE CONCRETE BY HEATING IT TO +1050°C | 159 |
| 4.12 | CHEMICAL DETERMINATION OF ELEMENTS IN THE SPECIMENS BY ICP AES | 160 |
| 4.13 | ANALYSIS OF CONCRETE AT LEACHED HOLES WITH SEM..... | 160 |

5 RESULTS 162

| | | |
|------------|---|------------|
| 5.1 | HOMOGENOUS STEADY-STATE PERCOLATION OF WATER THROUGH DEFECT-FREE CONCRETE | 162 |
| 5.1.1 | <i>Flow of water through the specimens (convection).....</i> | <i>162</i> |
| 5.1.2 | <i>Flow of ions from the specimens in the downstream direction (convection)</i> | <i>171</i> |
| 5.1.3 | <i>Flow of ions from the specimens in the upstream direction (diffusion)</i> | <i>177</i> |
| 5.1.4 | <i>Determination of changes in compressive and split tensile strength</i> | <i>178</i> |
| 5.1.5 | <i>Determination of changes in pore size distribution</i> | <i>180</i> |
| 5.1.6 | <i>Determination of changes in total porosity</i> | <i>180</i> |
| 5.1.7 | <i>Determination of changes in the remaining compounds and elements contained in the specimens.....</i> | <i>184</i> |
| 5.2 | PERCOLATION THROUGH HOLES IN THE CONCRETE..... | 186 |
| 5.2.1 | <i>Determination of the downstream ion flow (convection)</i> | <i>186</i> |
| 5.2.2 | <i>Determination of the upstream ion flow</i> | <i>187</i> |

| | | |
|----------|--|------------|
| 5.2.3 | <i>Determination of the remaining compounds and elements in the specimens</i> | 187 |
| 5.2.3:1 | Introduction | 187 |
| 5.2.3:2 | Slice 1 (upstream end) | 188 |
| 5.2.3:3 | Slice 7 (near the downstream end) | 195 |
| 5.2.3:4 | Slice 9 (at the downstream end) | 196 |
| 5.3 | SURFACE LEACHING OF CONCRETE | 197 |
| 5.3.1 | <i>Determination of ion flow (diffusion)</i> | 197 |
| 5.3.2 | <i>Determination of the remaining compounds and elements in the specimens</i> | 199 |
| 5.4 | DETERMINATION OF NON-EVAPORABLE WATER IN CONCRETE BY HEATING IT TO +1050°C | 200 |
| 6 | DISCUSSION | 202 |
| 6.1 | HOMOGENOUS, STEADY-STATE PERCOLATION THROUGH DEFECT-FREE CONCRETE | 202 |
| 6.1.1 | <i>Flow of water through the specimens, permeability</i> | 202 |
| 6.1.2 | <i>Flow of ions</i> | 209 |
| 6.1.2:1 | Ion flow in the downstream direction (convection) | 209 |
| 6.1.2:2 | Ion flow in the upstream direction (diffusion) | 212 |
| 6.1.2:3 | Summary of flow of ions | 213 |
| 6.1.3 | <i>Analysis of compressive and split tensile strength</i> | 215 |
| 6.1.4 | <i>Analysis of pore size distribution</i> | 216 |
| 6.1.5 | <i>Analysis of total porosity</i> | 218 |
| 6.1.6 | <i>Analysis of remaining compounds and elements in the specimens</i> | 220 |
| 6.2 | PERCOLATION THROUGH HOLES IN CONCRETE | 231 |
| 6.2.1 | <i>Analysis of downstream ion flow (convection)</i> | 231 |
| 6.2.2 | <i>Analysis of remaining compounds and elements in the specimens</i> | 231 |
| 6.3 | ANALYSES OF NON EVAPORABLE WATER IN CONCRETE BY HEATING THE CONCRETE TO +1050°C | 233 |
| 6.3.1 | <i>Estimation of the degree of hydration on the basis of the literature</i> | 233 |
| 6.3.2 | <i>Estimation of the degree of hydration by tests of the actual concrete</i> | 234 |
| 7 | MODELS VERSUS EXPERIMENTAL WORK – DISCUSSION | 235 |
| 7.1 | INTRODUCTION | 235 |
| 7.2 | GENERAL ABOUT MODELING | 235 |
| 7.3 | MODELING OF THE PORE STRUCTURE OF CEMENT MATERIALS | 236 |
| 7.3.1 | <i>Example: a simple model of pore structures</i> | 236 |
| 7.4 | MODELING OF THE LEACHING PROCESS ON THE MICRO-SCALE | 237 |
| 7.4.1 | <i>Example: flow of water and ions in a small fictive pore</i> | 238 |
| 7.5 | MODELING OF THE LEACHING PROCESS ON A MACRO-SCALE | 243 |
| 7.5.1 | <i>Conceptual model</i> | 243 |
| 7.5.2 | <i>Mathematical models</i> | 245 |
| 7.5.3 | <i>General constitutive relationships</i> | 246 |
| 7.5.4 | <i>The permeability coefficient</i> | 247 |
| 7.5.5 | <i>The dissolving-reaction coefficient</i> | 249 |
| 7.6 | MODEL OF POROSITY CHANGES DUE TO LEACHING | 250 |
| 7.7 | MODEL OF CHANGE OF COMPRESSIVE STRENGTH DUE TO LEACHING | 251 |
| 7.8 | RESULTS FROM CALCULATIONS WITH THE MACROSCOPIC LEACHING MODEL | 254 |
| 7.9 | CONCLUSIONS | 264 |
| 8 | METHODS OF ANALYSIS OF THE EFFECT OF LEACHING ON THE DURABILITY OF EXISTING CONCRETE DAMS | 265 |
| 8.1 | INTRODUCTION | 265 |
| 8.2 | ASSESSMENT PROCEDURE | 265 |
| 8.3 | SERVICE LIFE PREDICTIONS | 267 |
| 8.4 | EXAMPLE OF THE CALCULATION OF THE DURABILITY OF THE FRONT SLAB IN A BUTTRESS DAM | 270 |
| 8.4.1 | <i>Introduction</i> | 270 |
| 8.4.2 | <i>Leaching process</i> | 273 |

| | | |
|-----------|---|------------|
| 8.4.3 | <i>Estimation of the "design service life" by a Lifetime safety factor.....</i> | <i>276</i> |
| 8.4.4 | <i>Estimation of the "design service life" by the Hasofer-Lind method.....</i> | <i>278</i> |
| 8.5 | CONCLUSIONS..... | 280 |
| 9 | CONCLUSIONS..... | 282 |
| 10 | REFERENCES..... | 285 |

Appendix

APPENDIX A STRUCTURE OF CONCRETE

APPENDIX B EXPERIMENTAL RESULTS:

APPENDIX C EXPERIMENTAL RESULTS:

1 Introduction

1.1 Background to the present work

Many concrete dams in Sweden and in other Western countries are old and in a state of degradation. Nevertheless, they are very valuable since they represent a large financial investment and are needed for producing electricity.

Leaching and freeze-thaw are the most common degradation problem in concrete dams in Sweden. In northern Sweden, river water is often relatively free of dissolved ions (*soft water*). Such water is aggressive toward concrete structures due to its dissolving capacity. It is mostly older dams, of very porous concrete with high water permeability that have leaching problems. Yet in the near future more recently built dams, despite better methods having been used in constructing them and their being made of better concrete may also be subjected to leaching damages in a near future. Thus knowledge of how to predict leaching damages is needed now and will be needed even more in the future. The work presented here considers the leaching of hydration products in concrete specimens subjected to soft water.

Studies of leaching in concrete structures and concern for it began during the period of 1910-1920, when many large hydraulic structures were built and many of them began to deteriorate rather rapidly due to lime leaching.

1.2 Concrete dams – an overview

Being a bit witty, one might say there are two types of rocks: natural rocks (sedimentary, magmatic, and metamorphic) and man-made rocks in the form of *concrete structures*.

Concrete is made of approximately the same material as natural rocks. However, since we do not have access to comparable levels of pressure and heat as present when other rocks were formed, concrete rocks need to be made produced chemically. *Cement* is used to create a cement paste that fixes aggregates incorporated into it in a rigid structure. Cement reacts strongly with the water with which it is mixed to form hydration products. During the continuous hydration process that can last for a long period of time, a continuous supply of water is needed. If water is no longer available, hydration ceases.

Concrete structures are usually built in the shape and with the geometry needed to resist loads and meet other requirements.

Concrete dams have been built ever since late in the decade of 1880-1890, when the technique of building by use of stone masonry was on its way to being replaced by building by use of concrete. Concrete dams are commonly denoted by how the water pressure is transferred to the ground, as *gravity*, *buttress* and *arc* dams, respectively (Figure 1.1). A gravity dam possesses stability on the basis of its weight. A buttress dam is also basically a gravity dam, but its stability depends both on its own weight and on the weight of the downward directed water on the sloped front slab. Arc dams, in turn, transmit most of the horizontal pressure of the water behind them to the abutments by means of arc action (Linsley et al 1992). The dominant load on a dam is created by the hydraulic water pressure of the reservoir behind the dam. Some of the most common loads on a dam are shown in Figure 1.2.

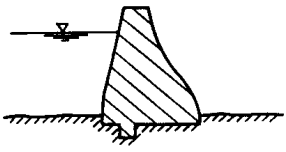
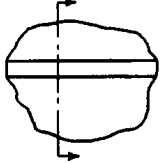
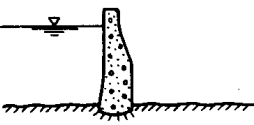
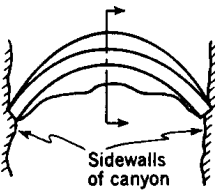
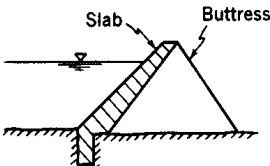
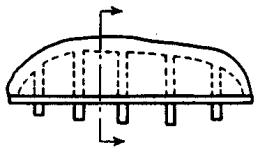
| Type | Material of Construction | Typical cross section | Plan view |
|----------|----------------------------------|---|---|
| Gravity | Concrete, rubble masonry |  |  |
| Arch | Concrete |  |  |
| Buttress | Concrete (also timber and steel) |  |  |

Figure 1.1 Basic types of concrete dams Linsley et al (1992).

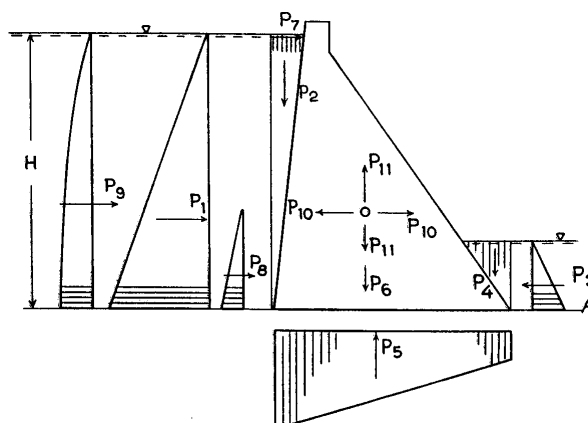


Figure 1.2 Common loads on dams (Reinus 1968). P_1 - P_4 = water pressure, P_5 = uplift, P_6 = weight of the dam, P_7 = ice pressure, P_8 = earth pressure, P_9 - P_{11} = seismic loads. Other loads, not shown here, that may be present are traffic loads and loads stemming from mobile equipment, such as spillway gates.

In Sweden concrete dams have been built ever since the beginning of the 20th Century. During the second decade of the 1900s, the fresh concrete was of very stiff consistency being compacted by stamping. The cement content was 220-240 kg/m³ in the upstream parts and the water-tightening parts, and about 200 kg/m³ in the downstream parts and the supporting parts, in which there were also large stones (Eriksson 2001). During the 1920s, concrete was instead cast of very wet concrete, with about 260 kg/m³ of cement and w/c ratio of around 1.0. This concrete showed very strong water separation. Dams built during the second and third decades of the 1900s usually developed marked leaching damages in their interior (Eriksson 2001), especially in the embedded parts around gates. The surface of the upstream parts was often very tight, with a high content

of cement. Although if this tight surface became cracked or leached with time, leaching damages occurred in the interior. During the 1930s, concrete was vibrated for the first time, making it possible to use stiffer concrete with low w/c ratio. Dams of this decade usually remained in better condition than the earlier dams described above. During the 1940s, part of the cement was exchanged for non-hydrating filler material. This often produced results less satisfactory in terms of durability than achieved during the 1930s. During the 1950s, most dams that were built were made of concrete consisting of slow-hydrating cement (in Sweden called LH-cement) containing aggregate of good quality, air entrainment additives and cast with a carefully controlled raising rate. Dams from this epoch were often of good quality, although the quality was sometimes reduced due to cracking occurring during the cooling phase.

1.3 Environmental induced damage in concrete dams

As said, concrete is often used in water-retaining structures such as dams. It is a porous material that interacts with its immediate environment. Both mechanical and environmental loads affect it. The primary cause of aggressive attack on a dam is often the water contained in the reservoir that the dam impounds (Mason 1990). The water has strong mechanical and environmental effects on the concrete. Environmental degradation processes in the concrete can be of two kinds: physical actions that break the concrete into fragments, and chemical actions that transform the components of the concrete into species of different types.

The most dominant factor in the environmental damage of hydraulic structures is water.

“First, water, which is the primary agent of both creation and destruction of many natural materials, happens to be central to most durability problems in concrete. In porous solids, water is known to be the cause of many types of physical processes of degradation. As a vehicle for transport of aggressive ions, water can also be a source of chemical processes of degradation. Second, the physical-chemical phenomena associated with water movements in porous solids are controlled by the permeability of the solid. For instance, the rate of chemical deterioration would depend on whether the chemical attack is confined to the surface of concrete, or whether it is also at work inside the material. Third, the rate of deterioration is affected by the type and concentration of ions in water and by the chemical composition of the solid. Unlike natural rocks and minerals, concrete is a basic material (because alkaline calcium compounds constitute the hydration products of Portland cement paste); therefore, acidic waters are expected to be particularly harmful to concrete.(...) ..., in practise, deterioration of concrete is seldom due to a single cause; usually, at advanced stages of material degradation more than one deleterious phenomena are found at work. In general, the physical and chemical causes of deterioration are so closely intertwined and mutually reinforcing that even separation of the cause from the effect often becomes impossible. Therefore, a classification of concrete deterioration processes into neat categories should be treated with some care” (Mehta 1986).

A common and severe type of damage of concrete dams is through the concrete being attacked by aggressive water, which either leaches compounds from the concrete or conveys substances into it leading to chemical or physical interactions with compounds contained in the concrete. Examples of such interactions are those of carbonation, sulphate attack, alkali-aggregate reactions, ingress of chloride and

reinforcement corrosion. All these attacks are facilitated by the concrete being permeable.

Another dominant type of damage to hydraulic structures, occurring in cold regions, is freezing and thawing.

In estimating the environmental severity of the deleterious effects to which a dam is subjected, it is important to know where and in what way it is exposed to water and to freezing temperatures. Many water retaining hydraulic structures, such as concrete dams, are mainly exposed to water at the upstream face and are exposed to freezing temperatures at the downstream face. For such structures, it is important to have a tight front slab at the upstream face to prevent water from penetrating the rest of the structure and reaching the cold side. Insulating walls are sometimes installed so as to prevent freezing temperatures from occurring at the downstream face.

1.4 Leaching damage in concrete dams

A hydraulic concrete structure is sooner or later broken down by naturally forces, even if this may take hundreds or even thousands of years. The hydration products contained in the concrete, and sometimes also in the aggregate, vary in their water solubility. Since calcium is present in such large amounts in concrete made of Portland cement and is also present in many readily soluble compounds, such as calcium hydroxide, for example, the degradation of concrete by the dissolution by water is often called *lime leaching* or simply *leaching*. By “lime” is meant different calcium-based compounds, expressed in terms of CaO. The danger of leaching in hydraulic concrete structures was detected at the beginning of the 20th Century (Halvorsen 1966, Moskvin 1980, Mason 1990). *“All concrete structures made with Portland cement have to inevitably undergo lime leaching, and after a certain period of time lose cohesiveness and collapse, as, in fact, they do. Portland cement structures in natural waters are doomed. Destruction from dissolution of lime determined by the nature of Portland cement starts immediately after a cementitious product is put in water. The existence of numerous Portland cement-based water structures is no disproof of this statement, whatsoever. All these structures are decaying, but it takes them extremely long to decompose entirely, for there is a certain something environmentally related that minimising lime leaching.”* (Baikov referred in Moskvin 1980).

The corrosive influence of water on concrete is sometimes classified as follows (Moskvin 1980):

- Deterioration Type 1: The dissolution and removal of hydration products by water which, though it may contain salts that are inert to the cement paste, enhance the solubility of these by increasing the ionic strength.
- Deterioration Type 2: The water containing salts or acids which dissolve hydration products that later are either carried out of the concrete or are precipitated in the pore system without having any binding or load-bearing properties there. Carbonic acid and salts of magnesium, are of this category.
- Deterioration Type 3: The water containing matter that reacts with the concrete to cause its volume to swell (alkali silicon reactions and sulphate attacks).

Water with less than 12.5 in pH is aggressive toward concrete since it destabilises the cementitious hydration products there. In actually however, the rate of chemical attack is a function of both the pH and the permeability of the concrete (Mehta 1986).

In the 1920s, engineers became aware of *soft water* attacks on dams. Soft water has low content of dissolved calcium or magnesium ions.

Pure water in condensation towers, water in nuclear power plants or in low-level nuclear waste and *soft water* from rain or from melting snow or ice may contain little or no calcium ions. When such water comes in contact with Portland cement paste, it tends to dissolve the calcium-containing products in this. If the water penetrates the paste at such a rate that no equilibrium is achieved, the hydrolysis of the paste can continue. If rain or water from melting snow flows over, or through, calcareous ground however, the water becomes *hard* and its aggressiveness decreases. “*Pure soft water has a neutral pH value close to 7. In some cases its erosive capacity has been made worse by the inclusion of dissolved acids, which lower the value of the pH still further. The acids will attack the calcium directly, forming the associated salt of the acid*” (Mason 1990).

“The matrix-forming hydration products of the cement are soluble in water, although their solubility is comparatively low, and therefore most natural waters do not attack the paste. Owing to its low concentration of dissolved ions soft water favours the dissolution of the hydration products, which then may be carried out of the matrix by diffusion, a high concentration gradient acting as driving force, or they are removed from the reaction front by a convective flow, either through the pore system of the paste or at the surface of a concrete member.

The corrosiveness of penetrating soft water is often enhanced by dissolved carbon dioxide. The free carbon dioxide then increases the solubility of calcium hydroxide, calcium hydrates and calcium carbonate by the formation of calcium bicarbonates.

The reaction mechanism demonstrates that a severe attack may occur only provided there is a continuous supply of soft water with or without members or in interior sections if, owing to a very high water permeability of the concrete, the soft water penetrates easily through the concrete.

Although the water permeability of concrete is an important parameter controlling soft water attack, the concentration of soluble compounds as well as the solubility of the paste constituents are additional parameters of equal importance. In the presence of free carbonic acid the type of aggregate must also be considered because calcareous aggregates are vulnerable to dissolution too” (Kropp 1995).

Different types of common leaching damage to a concrete dam are shown in Figure 1.3. The diffusion of dissolved ions to a reservoir occurs at the upstream surface, making the concrete more porous there. This leads to a decrease in strength of concrete and of the reinforcement bond. If water also percolates through the dam, dissolved ions are transported by the water to the downstream surface.

If the downstream surface is in a relative dry condition, the water may evaporate in which case calcite (CaCO_3) curtains are formed at the downstream surface. Since these calcite curtains are tight, they may hinder the further flow of water and ions in that direction. On the other hand, since the moisture content behind the dense curtains might become very high frost damages of the surface might occur.

If the downstream surface is in a humid condition, such as around a spillway or on underwater surfaces on the downstream side of the dam, the atmospheric CO_2 does not have time to react with the calcium ions in the percolated water. Under such conditions,

no tight layer of calcite is formed. Therefore, flow of water is not slowed down why continued leaching takes place.

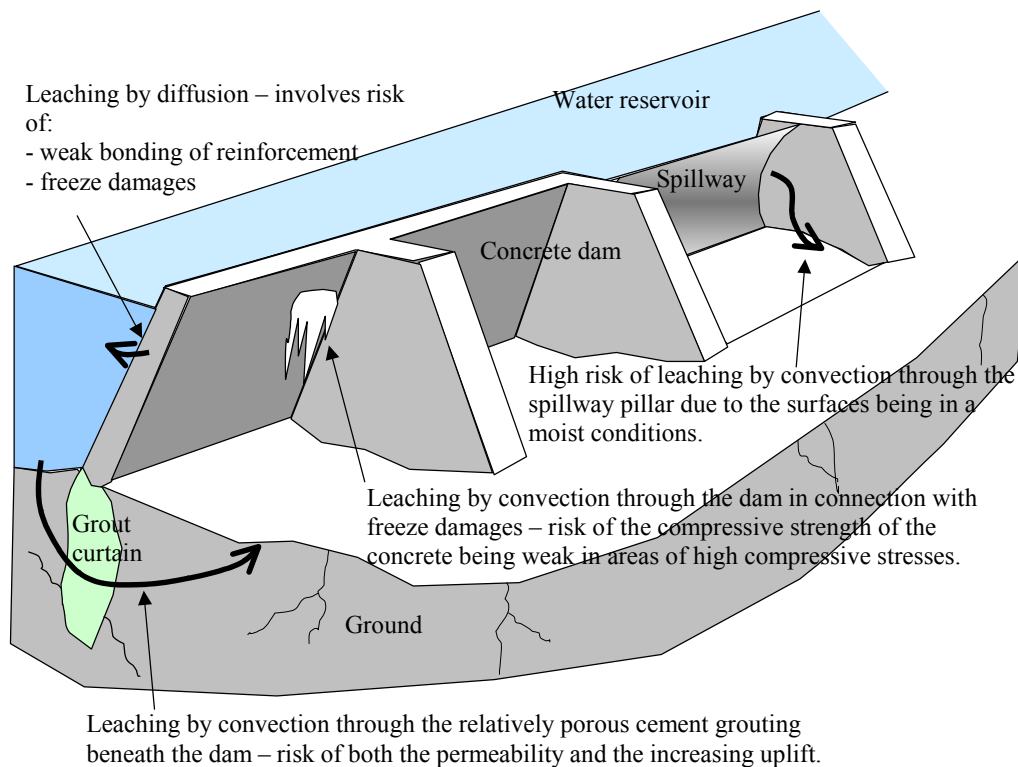


Figure 1.3 Typical leaching damage that occur in concrete dams.

Other locations where leaching damage may occur are in headrace- or outlet tunnels that convey water to and from power stations. The surfaces of such tunnels may be corroded by aggressive water and become rough, leading to reduction of flow. As said above, at locations where leached lime reaches air deposits, calcite curtains may form. In drainage areas such deposits may block water leakage, eventually leading to increased internal uplift pressure within the dam.

1.5 Lack of knowledge about leaching in concrete structures

Models of the entire leaching process in a concrete dam are needed. Such models include dissolving reactions, and diffusion and convection fluxes of ions. The models should also be verified in experiments. Experimental and field test results concerned with the degrading of such mechanical properties as strength and the modulus of elasticity are also needed.

1.6 Aim of the work

The aim of the work presented here was to study the mechanisms of the degradation changes that concrete undergoes in contact with deionised water and also to provide guidelines for estimating the residual life of degraded concrete structures.

The experimental work presented concerns how de-ionised water flows through homogenous concrete and how it affects the leaching process. Changes in *permeability*, *leaching rate* and *strength* are investigated.

The theoretical work seeks a theoretical understanding of the leaching process and aims of developing models, allowing estimates to be made of the permeability, leaching rate and strength of concrete that is subjected to leaching.

1.7 Limitations of the work

The experimental work has the following limitations:

- The w/c ratio of the concrete tested was mainly 0.8, only few specimens with a w/c ratio of 0.6 or 1.3 being used.
- The water pressure difference over the specimens was high, in most cases 6 (bar) (60 meter water head). Thus the pressure gradient was high, normally 120 bar/m.
- The water pressed through the specimens was deionised water containing only normal atmospheric carbonic acid.
- The downstream face was not in contact with air below 100 % RH.
- There were no aggressive substances in the water (except for dissolved atmospheric CO₂, approximately $1.2 \cdot 10^{-5}$ mole CO₂/l).
- The water and specimen temperature was always around +20°C.
- No other degradation mechanisms than leaching were present.
- There was no reinforcement in the specimens.

The modelling has the following limitations:

- The water flow is assumed to occur in a number of *flow tubes* of assumed size distribution. A reduced Hagen-Poiseuilles law assumed to be applicable for calculations of the flow.
- Only the leaching of Ca²⁺- and OH⁻ ions from Portlandite and C-S-H-gel is considered.
- The changes in strength that are assumed to occur are based on a simple strength-porosity relationship, which only takes account of porosity, age, w/c-ratio and amount of aggregate.

1.8 Abbreviations

The following abbreviations are used:

| | |
|--------|---|
| CH(s) | solid Ca(OH) ₂ in the concrete |
| CH(aq) | dissolved Ca(OH) ₂ in the pore solution, i.e. ions of Ca ²⁺ and OH ⁻ . |
| C-S-H | calcium-silicate-hydrate gel |
| ESEM | Environmental Scanning Electron Microscope |
| FEM | Finite Element Method |
| Hcp | hardened cement paste |
| OPC | ordinary Portland cement |
| RH | relative humidity |
| SEM | Scanning Electron Microscope |
| tz | transition zone (the zone between the bulk paste and the aggregate) |

2 Leaching of concrete – a literature survey

2.1 Introduction

Concrete consists of inorganic materials which tend to varying degrees to react with water or, as Moskvin (1980) puts it, “*As the minerals composing hardened cement come in contact with water, equilibrium concentrations of calcium hydroxide common for most soluble compounds are gradually established. Hardened cement is not a homogeneous body either by structure or by properties, one of which is solubility. Besides hydration products, it contains unhydrated grains of clinker. This complex system is in an unstable equilibrium, i.e. is continuously changing. By dissolving one element of the system, the water disturbs equilibrium at a certain point of the system causing it to change into a new equilibrium to satisfy the new conditions. (...) The rate of deterioration is, as a rule, controlled by the rate of internal diffusion. The interaction of an aggressive aqueous solution with the minerals of the hydrated hardened cement results either in the release of the reaction products in the solid phase, or in the degradation of the hardened cement into a conglomerate of insoluble compounds. The kinetics of such degradation also depends on the shape in which new formations separate: whether as loose sediments or dense films which create an increasing obstruction to diffusion in the voids of the solid phase surface layer. In the investigation of such a complex system as a cement matrix, it is incredibly difficult to distinguish among the separate but interconnected processes of capillary, surface, and convection diffusion, or between the interactions of the diffusion ions with various minerals of the hardened cement which are complicated with steric hindrances*” (Moskvin 1980).

A leaching process in concrete might be said to reflect a general ambition of nature to reach lower energy levels. Chemical bonds are broken and solids are dissolved, although the breaking of the chemical bonds require a certain input energy. The energy released when the molecules or ions in question are dissolved by the water results in the total energy level becoming lower and more stable. The pore solution in the concrete is in thermodynamic equilibrium with the solid material. If certain parameters of the thermodynamic relationship, such as the temperature or pressure, are changed, or if any of the dissolved material in the pore solution is carried away, the equilibrium is disturbed.

Lime-leaching refers to CaO (in reality Ca^{2+} and OH^-) being removed from the concrete by being dissolved in water. Leaching enlarges the pore system of the concrete, the permeability of which is thus at least momentarily increased, although dissolved ions may later precipitate in the pore system, reducing the permeability in the parts involved. Water can also cause continued hydration of the as yet unhydrated cement, filling up the pores with increasing amounts of hydration products and thus decreasing the permeability.

Different types of leaching tests have been developed during the last century, for example dissolution tests of crushed cement paste in either non-acidic or acidic water (extraction test) (e.g. Sundius & Assarson 1929, Frost & Virgin 1929), dissolution tests of free surfaces of concrete (e.g. Tremper 1931) and percolation tests (e.g. the Royal Waterpower Board 1927-29, Ruettgers et al. 1935, Markestad 1959, Sällström 1964). The term *percolation* refers to the homogenous passage or trickling of water through concrete. According to Halvorsen (1966), not a single leaching test was carried out for

cracked concrete until 1966. At the same time Halvorsen claims that the literature fails to reveal any case in which leaching occurring in cracks has destroyed a structure of concrete.

2.2 Leaching damages

In the first two decades of the 1900s, the concrete used in Swedish hydraulic structures was often of a very dry character. It was hand-stamped to fill out the mould. The result was often a very in-homogenous and partly very porous concrete. A thin layer of mortar high in cement content and in quality was applied to surfaces in contact with water, ground or air. When this thin layer of mortar was leached, or damaged in some other way, however, the water began to quickly penetrate and leach the thick inner part of concrete that was of poor quality.

The Swedish dam concrete of the 1920s often had a very high ratio of water to cement or low a content of cement, leading to high porosity and permeability. According to Sällström (1968), a mean concrete content of less than 200 kg/m³ and a w/c-ratio of 0.90 or higher was not at all unusual.

As a result of the poor quality of the concrete at the beginning of the 1900s, the leaching of lime from concrete dams posed a serious problem toward the end of the 1920s. Several investigations and seminars in Sweden, Norway and the U.S.A. have dealt with this matter. One investigation carried out during the period of 1920-1929 (see Halvorsen 1966), arrived at the conclusion that leaching attacks on concrete are of three basic types (the Royal Waterpower Board 1929):

- a) Leaching from free surfaces on the concrete
- b) Leaching from the surfaces of cracks in the concrete
- c) Leaching from the interior of concrete that is porous, lean and not at all tight

Of these types, a) was found to often be of little importance, b) was found to be very difficult to deal with and complicated to assess and c) was found to definitely be dangerous and to result in serious damage.

The rate at which leaching occurs depends of course on how rapidly an aggressive substance can reach the interior of the concrete. This depends mainly on how much of the aggressive substance is available and how readily it can penetrate the concrete. Two extreme cases in the leaching of concrete can be conceived, in the one case the leached material forming a protective layer on the surface, thus reducing further attack, and in the other no protective layer being formed or the protective layer formed being removed (by frost, erosion and the like) allowing attacks to continue (Rombèn 1978).

Leaching damages can occur in connection with other degrading mechanisms as well, making the overall damages worse, for example surfaces such as at spillways being exposed to the erosive acting of water flow at high velocity, and surfaces being subjected to leaching, erosion and freezing, all at the same time.

2.3 Water quality in lakes, rivers and in the ground

Table 2.1 presents mean values for the pH and the CO₂ content of waters investigated at Swedish waterpower stations during the years 1925-1928.

Table 2.1 Concentration of H⁺ (pH) and CO₂ in waters at Swedish waterpower stations (mean values) from investigations of the Royal Waterpower Board (1929) 1925-28.

| Location | pH | Free CO ₂ (mg/l) | Bound CO ₂ (mg/l) | Aggressive CO ₂ (mg/l) calculated |
|-------------|-----|--------------------------------|---------------------------------|---|
| Porjus | 6.6 | 3.8 | 3.2 | 5.4 |
| Knutsbro | 6.8 | 7.8 | 12.4 | 7.9 |
| Älvkarleby | 6.5 | 5.5 | 4.5 | 6.2 |
| Norrfors | 6.5 | 6.0 | 4.4 | 6.7 |
| Trollhättan | 6.6 | 3.6 | 4.1 | 4.3 |
| Edsele | 6.6 | 4.1 | 4.1 | 5.0 |
| Motala | 7.2 | 3.0 | 10.6 | 3.0 |

Sundius (1930) indicates that 3-8 and sometimes as much as 15 mg CO₂ per litre of water was not at all unusual in Swedish rivers at the time. The ground water generally has higher concentrations than this, sometimes 80-90 mg /l, due to organic deposits in the ground which the water flows through. In rivers and lakes where the water always moves and is in contact with the atmosphere, excess carbon dioxide in the water can be released to the air. Such water is also frequently warmer than the groundwater, making the carbon dioxide in it more volatile.

Investigations of the surface water in the Swedish provinces of “Skåne”, “Småland” and “Norrland” presented in Granholm et al. (1934) show that

- the water in Skåne is very hard and usually contains no aggressive CO₂, although the northern part of Skåne has soft water containing some aggressive CO₂
- the water in southern Småland is very soft and contains large amounts of aggressive CO₂ (up to 52 mg/l)
- the water in Norrland is almost as aggressive as that in the southern part of Småland, being soft and containing aggressive CO₂ in large amounts (up to 48 mg/l)

According to Myran (1967), the pH-values of the river water at thirty dam locations in Norway vary from between 4.7 to 7.1, the concentrations of CO₂ varying between 1.0 and 19.3 mg/l. Since marshy waters there can contain additional CO₂ and also other acids, such as humic acid, the pH can be as low as 3-4. “...most Norwegian rivers carry a soft, pure water which is often quite acid, and thus does not differ much from distilled water...” (Markestad 1977). Moskvina (1980) cites an example from Siberia of marshy waters that contain as much as 50 mg CO₂/l.

2.4 Leaching processes

2.4.1 General

In cement materials, leaching processes involves mainly the transportation of ions from the interior of the material, through its pore system, outwards into the surroundings. In the leaching process, solid compounds in the concrete are *dissolved* by water that penetrates it and are transported away, either by (i) *diffusion* based on the concentration gradients, or by (ii) *convection* through the flow of water. The narrower the flow paths in the concrete, the less the convection flux (Table 2.2) and the greater the number of ions that flows by diffusion.

Table 2.2 Relation of pore radius to permeability coefficients. Moskvina (1980)

| Pore radius (m) | Permeability coefficient (m/s) | Transfer |
|---------------------|--------------------------------|---------------------|
| $< 10^{-7}$ | $< 10^{-10}$ | Molecular diffusion |
| $10^{-7} - 10^{-5}$ | $10^{-10} - 10^{-9}$ | Molecular flow |
| $> 10^{-5}$ | $> 10^{-9}$ | Viscous flow |

In Figure 2.1, a schematic view of the leaching rate of lime (CaO) in concrete is shown (Moskvina 1980). Between *a* and *b* the water flow is rather slow, the pore water being saturated with lime. In the course of time or if the water flow increases, the pore walls become depleted of solid lime. When this occurs, the concentration of lime in the water decreases, as shown at *b*. In the curve segment *c-d*, the leaching rate is governed totally by the diffusion of Ca(OH)_2 from the interior towards the flow paths.

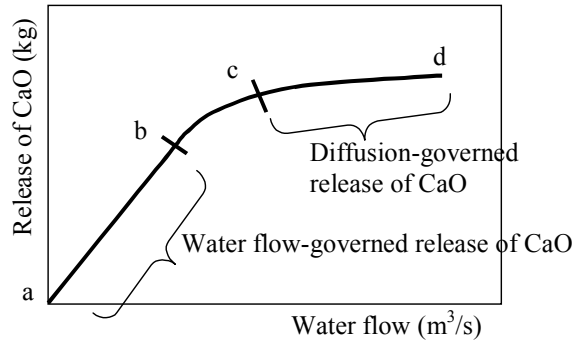


Figure 2.1 Lime leached from concrete vs rate of water percolation (Moskvina 1980). Between *a* and *b*, the water flow is so slight or there is still so much CaO in the walls of the flow paths that the leaching is linearly proportional to the water flow. After *c*, the walls of the flow paths are unable to dissolve CaO at a rate sufficient to maintain a saturated condition, leaching being governed there by how fast new CaO can diffuse from the interior towards the flow paths.

For estimations of the future leaching degradation in concrete, it is important to have adequate knowledge of the kinetics involved and the variables influencing the process as a whole, i.e. from the dissolution of the material inside the concrete to the diffusion and convection of the dissolved ions.

One way of describing the leaching process inside a saturated porous material is to regard it as a balance of mass:

$$\text{Change in mass} = \text{source (or sink)} - \text{convection} - \text{diffusion} \quad (2.1)$$

In an equation in which masses are expressed as concentrations, one obtains

$$\frac{\partial c_i}{\partial t} = \hat{c}_i - \nabla \cdot \mathbf{F}_{iv} - \nabla \cdot \mathbf{F}_{iu} \quad (\text{Balance of ions in the water}) \quad (2.2)$$

where the convective and diffusion flux is often assumed to be

$$\mathbf{F}_{iv} = \mathbf{v}_w c_i; \quad \mathbf{F}_{iu} = -D_{eff} \nabla c_i \quad (2.3)$$

where c_i = concentration of the dissolved ions (mole/m^3); \hat{c}_i = changes in concentration during time period dc/dt ($\text{mole/m}^3/\text{s}$); D_{eff} = effective diffusion coefficient of the pore solution (m^2/s); \mathbf{F}_{iv} = convection flux of ions in the pore solution ($\text{mole/m}^2/\text{s}$); \mathbf{F}_{iu} =

constitutive relation of the diffusion flux of the ions in the pore solution (mole/m²/s); \hat{c}_i = a mass source term, which here is a dissolving-reaction term (mole/m³/s); \mathbf{v}_w = velocity of the water (m/s); and ∇ = the nabla operator.

The first term \hat{c}_i on the right is a source or a sink of the mass provided or lost due to chemical reactions with other substances. The resulting reward in terms of lower and more stable energy levels forces different reactants to react with each other. Heat, pressure and chemical bond energies influence these chemical reactions. A dissolving reaction can be looked upon as involving the diffusion of reactants and products on a molecular scale. The greater the extent to which the water is pure, the dissolving area is large, the diffusivity on the walls of the tube is high and the diffusion layer on the tube walls is thin, the larger the dissolving reaction term \hat{c}_i becomes and the more rapid the leaching process is.

The second term $\nabla \cdot \mathbf{F}_{iv}$ is a convective term indicating how much of the substance is carried away by a velocity field, such as the transport of ions in a water flow. The higher the velocity of the water, the more dissolved material the water flow carries with it.

The third term $\nabla \cdot (\mathbf{F}_{iw})$ is the diffusion due to the concentration gradients (the electrical balance also has an influence here). Intermolecular forces between different ions in the pore solution and between the dissolved ions and the solid molecules influence the diffusion mobility. The larger the ion diffusivity, the more dissolved material is carried away by diffusion. Due to the tortuosity of the flow tubes and due to intermolecular forces between the dissolved ions, or between the ions and the solid material in the tube walls, the diffusion coefficient in a real flow tube, D_{eff} , is smaller than in dilute bulk water.

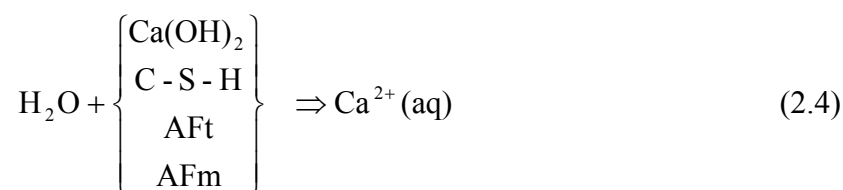
A hypothetical leaching process could be as follows:

- Pure water flowing through concrete causes different hydration compounds to dissolve. If aggregate consisting of readily soluble compounds is also present, these are dissolved as well.
- The order and rate of dissolving of the solid materials depend upon their solubility and where in the pore system they are situated in relation to the pure water and to each other. Substances of lower solubility may be dissolved before other, more soluble substances, if they are surrounded by water which is purer (provided all the other terms in the energy balance, such as temperature, pressure, etc. are equal).
- When dissolved, the ions diffuse towards water in which the content of these same ions is lower. Ions of different types also influence each other due to electrical forces between them.
- If the ions that are dissolved reach certain main flow paths where the water flows through the concrete, the water draws the ions along with it. At the same time as the ions are being carried away by the water flow, they may also diffuse towards purer water, which can be in the direction opposite to that of the water flow.

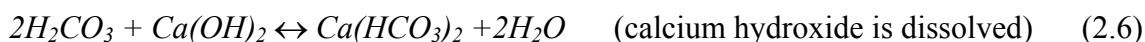
The presence of large internal surfaces, which the water gains ready access to, tends to result in a high leaching rate. If the water is aggressive (soft or containing aggressive substances), the leaching rate would be higher yet. High permeability to water does not

always lead to a high leaching rate (kg/l), however Although the concrete may have several large flow tubes or cracks, sufficient for permeability to be high, the tube walls may quickly become depleted of soluble ions, resulting in the leaching rate as expressed in kg/l being low. The leaching effect is probably maximal when pure water is pressed through a pore system having many large flow-tubes extending through the concrete and many short side pores in the tube walls. The short side-pores contribute to pure water dissolution the solid material. Large flow tubes also provide an ample supply of pure water to which the dissolved ions can diffuse.

Lime that is leached away by the pure water comes mainly from crystals of calcium hydroxide, Ca(OH)_2 , due to its being present in large amounts and to its high solubility. At the same time, as long as there is Ca(OH)_2 left, lime will also be dissolved from the other hydration products - calcium silicate hydrate (C-S-H), calcium aluminium hydrates (C_3A) and calcium aluminium iron hydrate (C_4AF) – although to a much lesser extent.



CO_2 being in contact with the pore solution, also makes a number of additional reactions possible



In the experimental work presented later in the thesis, there was no aggressive carbonic acid in the water, only atmospherically dissolved CO_2 being present.

Assarson & Sundius (1929, see Halvorsen 1966), found a large variation in the degree of leaching of specimens that had already been partly leached. Leaching was not homogenous. Rather, the specimens were found to consist of some parts in which there was no leaching damage and others in which much leaching damage occurred.

Sundius (1930) observed that, when water containing carbonic acid penetrated highly porous and homogeneously permeable concrete, a moving boundary of calcium carbonate (calcite), that extended through the concrete, appeared. The front was moving in the direction of the water flow. Under such conditions, calcite (CaCO_3) is first formed at the downstream surface of the concrete due to the presence of atmospheric CO_2 , either after the wall have been cast, or when it is exposed to water containing carbonic acid. When the water has released the carbonic acid, it becomes very soft and downstream it displays a marked ability to dissolve the calcium hydroxide in the concrete. Further carbonic acid brought in by the water that penetrates the concrete

dissolves the calcite to form calcium bicarbonate ($\text{Ca}(\text{HCO}_3)_2$). Sundius noted that the degradation of highly permeable concrete can be slower when it is exposed to water rich in carbonic acid than when the water contains less amount of carbonic acid. This is due to the pore-filling effect produced by formation of the calcite and to the solubility of this calcite being low. Sundius concluded that tight concrete exposed to water rich in carbonic acid would only degrade the concrete if the flow of water along the surface of the concrete was high.

Sundius referred to leaching experiments in which at the beginning of testing high concentrations of lime were found in the water that penetrated the concrete, the concentration being sharply reduced, however where leaching had progressed for some time.

Sundius (1939) also reported studies at the dam Lilla Edet located in the river Göta älv in the southwest of Sweden. He found a concentration of 0.6 g CaO/litre water in water that had penetrated the concrete walls of the hydropower plant.

Ruettgers et al. (1935) performed large-scale percolation tests of concrete samples prior to construction of Boulder Dam (now Hoover Dam) in the US. The leaching rate and the total amount of lime (CaO) leached in relation to the water that had percolated are shown in Figure 2.2.

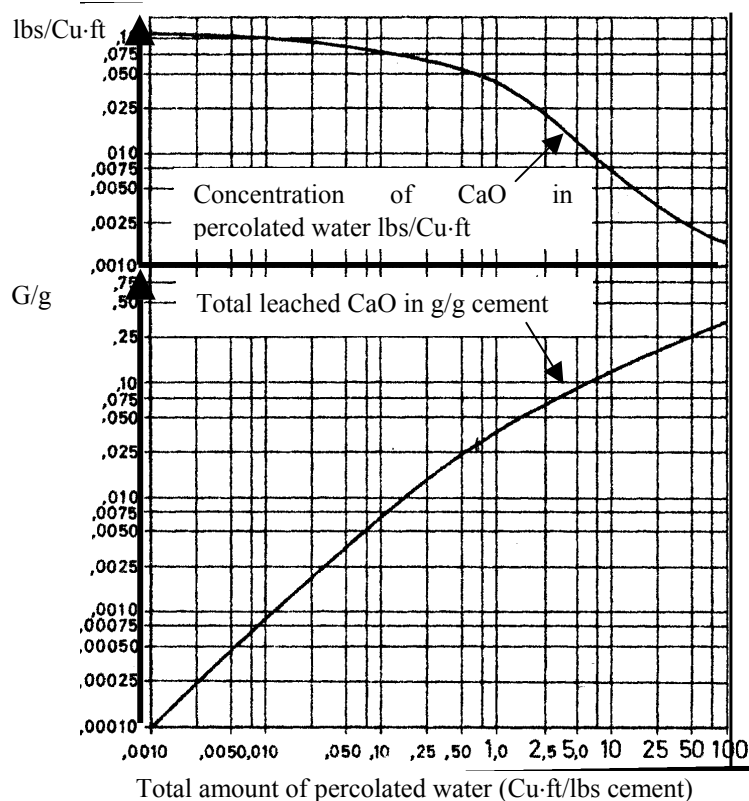


Figure 2.2 Amount of leached lime (CaO) and the concentration of CaO in leached water in relation to amounts of water that percolated (Ruettgers et al. 1935) reported in Halvorsen (1966).

Unsworth, Lota and Hubbard (unknown year of publication) exposed OPC mortar specimens to deionised water at a pressure of 2 MPa, see Figure 2.3. A rapid rise of Na content in the drainage water up to a maximum of about 280 ($\mu\text{g}/\text{l}$) was found when a

volume of water corresponding to two *pore volumes* (PV) had percolated through the specimens. K increased almost as rapidly as Na, rising to about 1200 ($\mu\text{g/l}$) when three PV of water had percolated. The pH value also rose rapidly, to about 13.1, because of the rise in OH-concentration accompanying the rise in Na and K. After the maximum values for Na and K had been reached, the concentration of these components decreased rapidly down to the very low values at the time when a volume of water of about eight PV had percolated through the mortar. As the content of Na and K began to decline, the pH value declined to about 12.5 and the content of Ca in the leached water began to rise (an observation also reported by Markestad 1977). After about ten PV had percolated, the Ca content reached its maximum value of about 530 ($\mu\text{g/l}$) and then decreased only slowly (in a logarithmic time scale) to about 460 ($\mu\text{g/l}$) after about 80 PV had percolated, at which point the test was stopped. The pH value also decreased slowly as the Ca content decreased. The water permeability followed a slowly decreasing curve from about $7 \cdot 10^{-12}$ to $6 \cdot 10^{-12}$ (m/s). The results indicated that Na and K were quickly washed out of the pore system, followed by the dissolving of Ca into the pore solution. Because of the much larger amounts of Ca than Na and K in the mortar, the leaching rate for Ca was rather high during the entire duration of the study. pH 12.5 corresponds to the pH of saturated $\text{Ca}(\text{OH})_2$ -solution.

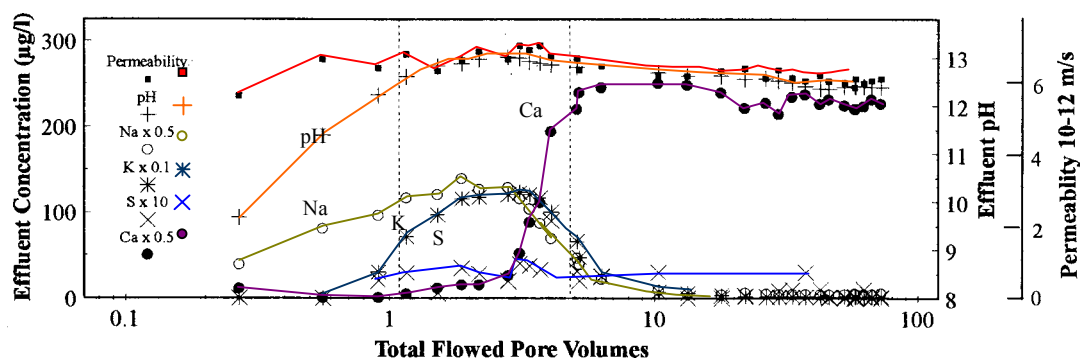


Figure 2.3 The permeability of OPC mortar subjected to 2 MPa water pressure, together with the ion concentrations and pH values in the drainage water. The x-axis is a function of collected drainage water in relation to measured capillary porosity. Unsworth et al. (unknown year)

As both Moskvin (1980) and Sundius (1030) had observed, however, the leaching rate usually decreases when the pore walls in the main flow paths become depleted of lime. The main flow paths can be large-size capillaries, cracks, interfacial areas of contact between the paste and the aggregate, or construction joints. Figure 2.4 presents generalised data from several studies that Moskvin (1980) reported concerning the rate of leaching of lime (CaO) from cement mortar and concrete in relation to the volume of the water percolating through the materials. Moskvin observed that the leaching rate of lime per volume of percolating water decreased after the removal of about 10-20 (g) of lime per kg of the initial cement. Thus, the leaching rate decreased after a certain volume of water had percolated. He concluded that “*fresh supplies of lime to streams of water infiltrating through definite paths of percolation, i.e. continuous large-size capillaries, leaky contacts of the hardened cement to sand and the mortar to large-size*

aggregate, cracks or construction joints, are controlled now by the rate of lime diffusion”.

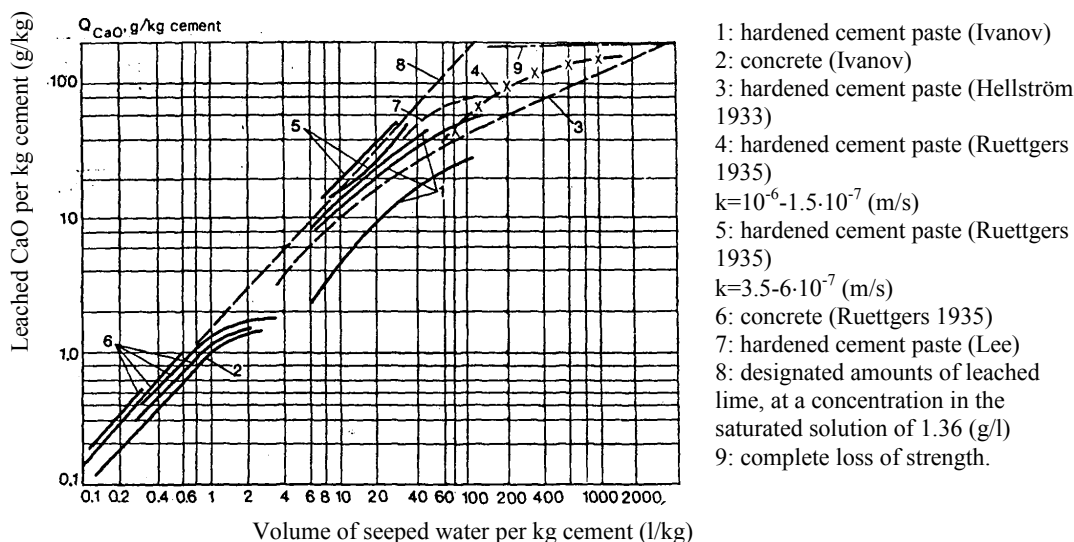


Figure 2.4 Quantity of lime leached from cement mortar or concrete vs volume of seeped (percolated) water, based on data from several authors as presented in Moskvin (1980), where k = permeability (m/s)

“In both the extraction and percolation methods with Portland cements and pure water the concentration tends to keep near to saturation with lime until some 10-15 % of the original weight of cement has dissolved. This probably represents the free calcium hydroxide present as a result of the hydration of the cement” (Lea 1983). The leaching of lime (CaO) probably occurs as an interplay between solid CH, C-S-H of varying composition and unhydrated cement. Ca^+ and OH^- are easily dissolved from the Portlandite, found as separate crystals of $\text{Ca}(\text{OH})_2$ in the concrete. There is also a release of CH from the cement gel, even at early stages of leaching. Unhydrated cement is involved in the leaching process, partly through a hydration process in which new cement gel is formed and then leached, and also when cement is dissolved directly and leached away (Halvorsen 1966). Halvorsen and Larsen (1961) found crystals of solid CH, even in highly leached concrete.

Yokozeki et al. (2000) found a relationship between the mass balance equation for calcium (other components being assumed to be present in only negligible quantities) and experimental results for mortar and concrete.

$$\frac{\partial c_{Ca}}{\partial t} = \frac{\partial}{\partial x} \left(D_{eff,Ca} \frac{\partial c_{Ca}}{\partial x} \right) - \frac{1}{P_p} \frac{\partial c_{s,Ca}}{\partial t} - \frac{v}{P_p} \frac{\partial c_{Ca}}{\partial x} \quad (2.9)$$

where c_{Ca} = calcium concentration (mole/m^3); t = time since the start of leaching (s); $D_{eff,Ca}$ = effective diffusion coefficient of Ca^{2+} in the pore solution (m^2/s); P_p = porosity of the paste (m^3/m^3); $c_{s,Ca}$ = concentration of solid calcium (mole/m^3); and v = velocity of the pore solution (Darcian velocity) (m/s). The porosity was assumed to change due to leaching as follows:

$$P = P_0 + \frac{M_{CH}}{\rho_{CH}}(1 - V_C)(c_{s0} - c_{s,ca}) \quad (2.10)$$

where P_{po} = initial porosity of the paste (m^3/m^3); M_{CH} = molecular weight of $\text{Ca}(\text{OH})_2$ (kg/mole); ρ_{CH} = density of $\text{Ca}(\text{OH})_2$ (kg/m^3); V_C = volume ratio of cement in paste (m^3/m^3); and c_{s0} = initial concentration of solid calcium (mole/m^3). The relationship between the calcium concentration in the pore solution and in the solid phase was assumed to be as shown in Figure 2.5.

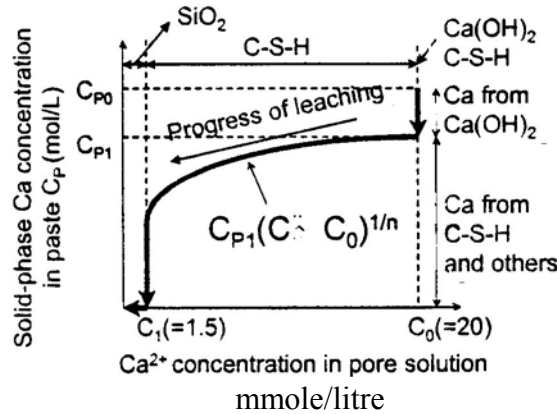


Figure 2.5 Calcium concentration equilibrium relationship in the solid and the liquid state (Yokozeki et al. (2000)). In the leaching process, calcium is first taken from $\text{Ca}(\text{OH})_2$ and then from C-S-H and other compounds.

The reduction in strength due to leaching was estimated by Yokozeki et al. to be as follows:

$$f_c = 0.315 \cdot e^{1.1923 \cdot C_s/C_{s0}} \quad (2.11)$$

where f_c = strength (probably compressive strength) of mortar; c_s = the current solid-phase concentration of Ca in the paste (mole/m^3); and c_{s0} = the initial solid-phase concentration of Ca in the paste (mole/m^3).

With reference to the literature, Halvorsen (1966) proposed there to be three types of leaching: (i) free-surface leaching, (ii) leaching due to homogenous percolation and (iii) leaching due to percolation through cracks in the concrete. Common to these leaching types is the fact that the presence of carbonic acid in the water accelerates leaching if the concrete is carbonated, whereas soft water without CO_2 accelerates leaching in uncarbonated concrete.

2.4.2 Free surface-leaching

A possible conceptual model of free surface-leaching (Sundius 1939, Halvorsen 1966, Markestad 1977, Moskvina 1980, Grube & Rechenberg 1989, Fagerlund 2000) is described in Figure 2.6 and below:

- The surface layer of the concrete is often carbonated by atmospheric CO_2 already before leaching starts.
- The carbonated layer reduces the rate of further leaching due to CaCO_3 having low solubility in water. Deterioration is deterioration of Type 1 (section 1.3).

- If the water contains aggressive CO_2 , this forms a thin layer of calcium carbonate, if such a layer has not already been formed by atmospheric CO_2 . The excess CO_2 gradually dissolves the carbonated layer to form bicarbonate. The deterioration is of Type 2 (section 1.3).
- If the surface of the water is in motion, the dissolved bicarbonate is removed, allowing further bicarbonate to be dissolved from the surface by aggressive water, leaving non-cementitious end-products in the form of silicon, aluminium and iron hydroxide gels with aggregate grain inclusions (Figure 2.7). This **zone I** is termed the zone of destruction. Although the layer may be very weak, it still has a certain diffusion resistance which slows down leaching. If for some reason the leached layer separates from the concrete (e.g. because of freezing and thawing, erosion or spalling), the leaching rate increases.
- The carbonated layer is leached from the outside by aggressive water but grows on the inside when CO_2 penetrates inwards and CH diffuses outwards, allowing the two to react with each other to form new CaCO_3 , this being **zone II**.
- Inside the carbonated layer there is a layer in which CH diffuses towards the surface, this being **zone III**.

The higher the velocity of the water at the surface, and the greater the amount of aggressive CO_2 that the water contains, the faster the leaching process in the concrete progresses. The zone types I to IV are shown in Figure 2.7.

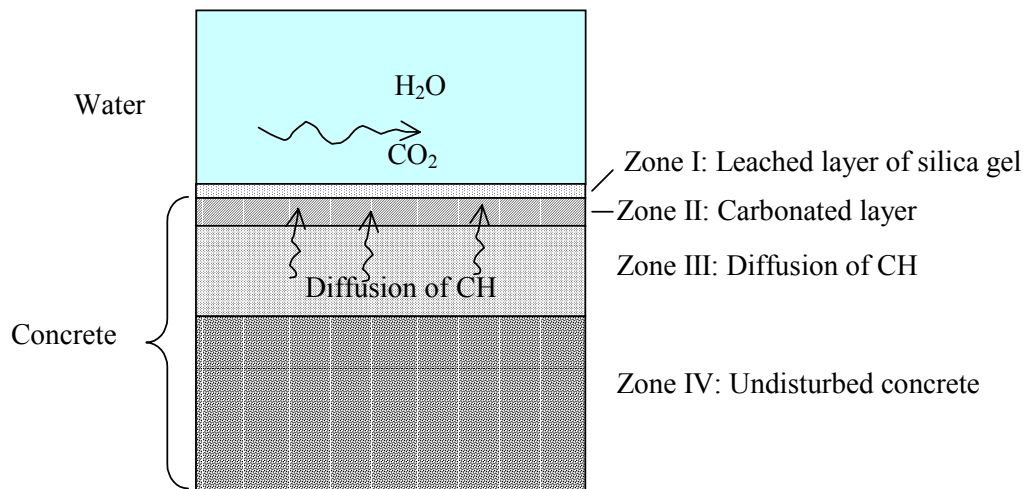


Figure 2.6 Conceptual model of leaching at a free surface of the concrete Halvorsen (1966).

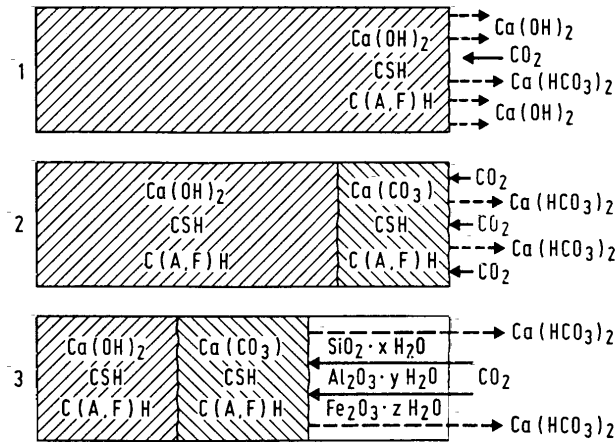


Figure 2.7 The reactions of hardened cement paste in concrete that contains aggressive carbon dioxide (schematic). Calcium carbonate is formed. Hydrate phases of it form a protective layer having stronger diffusion resistance, one that consists of SiO_2 , Al_2O_3 and Fe_2O_3 (Gruber & Rechenberg 1989).

The leaching rate diminishes when the leached layer becomes thicker. Gruber and Rechenberg (1989) refer to experiments involving $4 \times 4 \times 16 \text{ cm}^3$ prisms of Portland cement mortar exposed to carbonic acid (Figure 2.8).

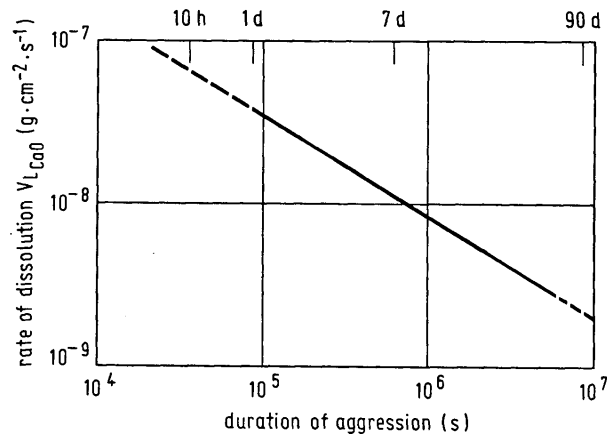


Figure 2.8 Rate of dissolution of calcium oxide from mortar prisms by an aggressive CO_2 solution at $\text{pH} \approx 4.4$, according to Gruber and Rechenberg (1989).

The following equation based on assuming Fick's first law can be applied:

$$d = a \cdot \sqrt{t}; \quad a = \sqrt{\frac{2 \cdot D \cdot A_l}{m_s \cdot A_{ges}} (c_s^* - c_l)} \quad (2.12)$$

where d = thickness (m) of the concrete layer that is destroyed (leached); D = diffusion coefficient for the $\text{Ca}(\text{HCO}_3)_2$ (m^2/s) contained in the layer that was destroyed; m_s = mass of soluble matter, expressed in kg of CaO per m^3 of concrete; $c_s^* = \text{Ca}(\text{HCO}_3)_s$

concentration (kg/m^3) in the solution surrounding the intact concrete; $c_l = \text{Ca}(\text{HCO}_3)_2$ concentration (kg/m^3) in the solution which is unaffected by the concrete; $A_l/A_{ges} =$ ratio of the area of soluble matter to the total area (m^2/m^2); $V_l/V_{ges} =$ ratio of the volume of soluble constituents (if insoluble aggregate is employed \rightarrow volume of hardened cement paste) to the total volume (m^3/m^3); and $A_l/A_{ges} = V_l/V_{ges}$.

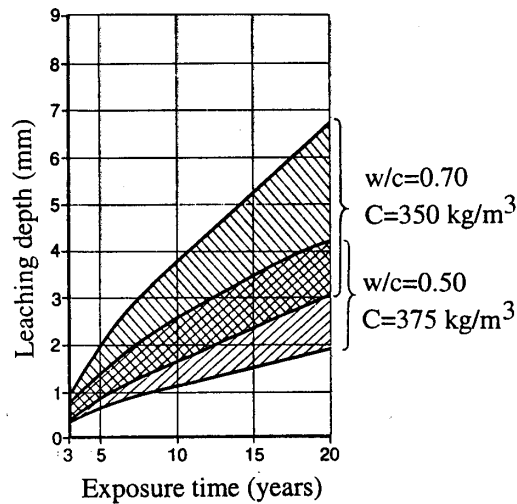


Figure 2.9 Leaching depth in concrete exposed to water at pH 5.6 containing 100 mg aggressive CO_2 (presented in Fagerlund 2000).

If the leached layer is removed mechanically, the leaching process accelerates, as shown schematically by curves I and II in Figure 2.10.

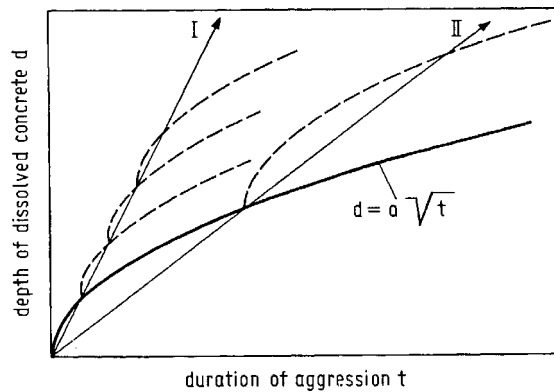


Figure 2.10 Depth of the dissolved material in relation to time – without brushing, with frequent brushing (line I) and with rare brushing (line II) of the gel (Grube & Rechenberg 1989).

Fagerlund (2000) presents a model for the approximate estimation of leaching depth in the case of surface leaching involving erosion:

$$x \approx x^* + k_e \cdot (t - t^*) \quad (2.13)$$

where x = depth of the leached zone (m); x^* = depth of the leaching front when the rate of erosion is equal to the rate of penetration of the leaching front (m); t^* = the time

when this occurs (s); and k_e = erosion coefficient ($=dx_e/dt$ = rate of erosion m/s). The total amount of lime dissolved by time t is

$$Q_{leach} = x \cdot m_s \quad (2.14)$$

where Q_{leach} = total amount of lime leached by time t (kg/m^2); and m_s = total amount of soluble material in the concrete (kg/m^3).

2.4.3 Leaching due to homogenous percolation of concrete

A possible conceptual model of leaching caused by homogenous percolation through very porous concrete is summarised below and in Figure 2.11 and Figure 2.12 (Sundius 1930, Halvorsen 1966, Markestad 1977, Moskvina 1980):

- The surface layer of the concrete has often been carbonated by atmospheric CO_2 already before any leaching starts. This carbonated layer reduces the rate of further leaching because of CaCO_3 having low degree of solubility in water. The deterioration is of Type 1 (section 1.3).
- If the water contains aggressive CO_2 , this forms a thin layer of calcium carbonate if such has not already been formed by atmospheric CO_2 . The excess CO_2 gradually dissolves the carbonated layer to form bicarbonate. The deterioration is of Type 2 (section 1.3).
- The percolated water gradually becomes saturated with bicarbonate, leaving a non-cementitious end product of the destruction of the hardened cement in the form of silicon, aluminium and iron hydroxide gels containing grains of the aggregate. This **zone I** is the zone of destruction.
- The water which continues on its way through the concrete after passing through the carbonated layer is very pure. It deteriorates the concrete through Type 1 deterioration. It is able to dissolve CH very readily up to the point of saturation and then transport it out of the concrete at the downstream surface.
- Further downstream from the point where the calcite just described was dissolved the dissolved calcium bicarbonate may also form new calcite, together with calcium hydroxide that it meets on its way. The carbonated layer increases in thickness at the downstream end and shrinks at the upstream end. The carbonated layer “moves” in a downstream direction, there being a *moving boundary* of carbonated concrete which moves downstream. This **zone II** is the zone of sealing.
- If the downstream surface is in contact with air and the flow of water is so small that the water has a chance to evaporate, atmospheric CO_2 together with the leached CH form curtains of calcite at the surface. If the surface is covered by water or the conditions are humid (e.g. around spillways), or if the flow of water is so large that there is no appreciable chance for it to evaporate, the solutions flow down the surface without there being any formation of calcite-curtains.

The greater the extent of homogenous percolation of water, the more rapidly leaching occurs. If there is a carbonated layer on the upstream face, the leaching is faster when the water contains CO_2 , otherwise it is faster when the water is pure.

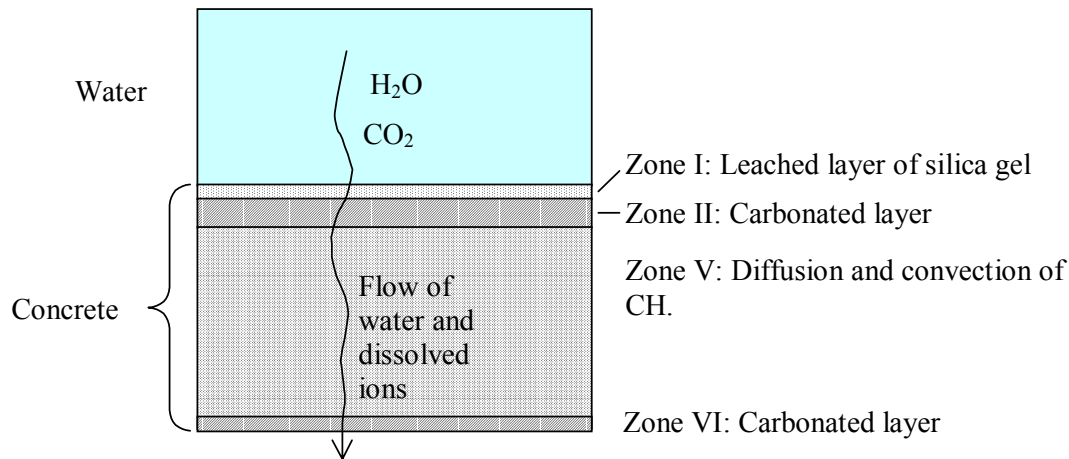


Figure 2.11 Conceptual model of leaching due to homogenous percolation through concrete Halvorsen (1966).

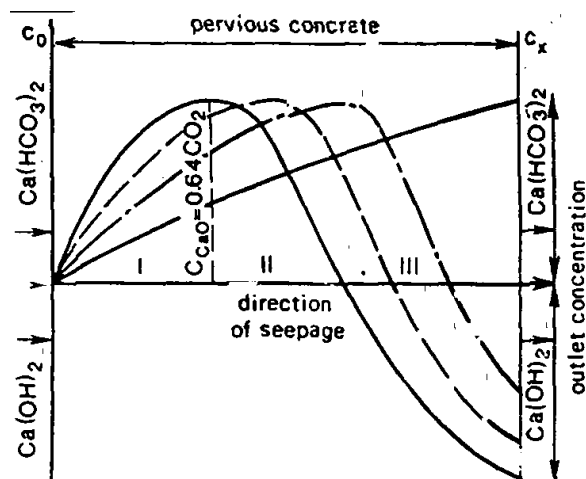


Figure 2.12 Deterioration of concrete from percolation of a CO₂ solution. I – zone of destruction (formation of bicarbonate); II – zone of sealing (precipitation of carbonates); III – zone of leaching. Moskvina (1980).

Moskvina emphasised that when the seepage flow from the downstream surface (the backside of a dam) is greater than the evaporation, the leaching process continues undisturbed. If the evaporation is greater than the flow of water, the concrete surface has the possibility of sealing due to reaction with atmospheric CO₂. Sällström (1968) refers to a possible evaporation level of 10 to 15 mm per month from surfaces at intakes and at spillways in dams where the temperature always is about +5 to +10 and the relative humidity at about 80 %.

On the basis of experimental tests, Tremper (1931) estimated the amount of calcium leached through homogenous percolation to be

$$\text{Log}(Q_{Ca}) = k \cdot \text{log}(T) \quad (2.15)$$

where Q_{Ca} = amount of leached calcium; k = coefficient of proportionality; T = elapsed time. The residual life can be calculated if the amount of leaching that occurred up to a

given time is known. Tremper estimated there to be loss of strength when 50% of the calcium has been leached.

Kjennerud (1974) performed percolation tests of mortar and concrete subjected to differences in water pressure. The water was deionised. Carbonic acid was added for a certain length of time during the test. The results of a test of very porous cement mortar that had been placed in water ever since the demoulding had occurred are shown in Figure 2.13 - Figure 2.18. After 1500 hours of testing, carbonic acid was added to the incoming water fed to the mortar. The large amounts of water that were percolated indicate the mortar to have been very porous. Assuming a pressure gradient of $20\text{m}/0.1\text{m} = 200 \text{ m/m}$ and Darcy's law, the permeability coefficient was found to be $k = 30 \cdot 10^{-6} / (\pi \cdot 0.1^2 / 4) \cdot 200 = 19 \cdot 10^{-6} \text{ m/s}$, which is very high.

To obtain the amount of leached ions in mg/l, the amount of mg/h added needs to be divided by the amount of water percolating, given as g/h, for example $[\text{Ca}^{2+}] = \sim 20(\text{mg Ca}^{2+}/\text{h}) / \sim 30(\text{g/h}) = 667 \text{ mg Ca}^{2+}/\text{l}$.

When only deionised water flowed through the specimens, the flow of water was rather constant. After about 300 hours, the pH value began to drop below the buffering level of the calcium hydroxide (12.5), the amount of leached calcium also beginning to drop. This indicated the walls of the flow channels to have begun to become depleted of calcium. When carbonic acid was added, the amount of calcium in the outflowing water decreased significantly for a short period of time, but then increased very much, to above the level found before the acid had been added. According to Kjennerud, this can be due to an initial carbonatization upstream when the acid was added, the new acid leading after a while, however, to dissolution of this carbonated layer, and also to a more aggressive attack on the flow channel walls. Therefore the amount of leached calcium increased as indicated above. When the addition of carbonic acid had been completed, only the deionised water percolated though, the amount of leached calcium becoming lower again, lower than it had been before the acid had been added. This is due, according to Kjennerud, to the mortar having been carbonated to some degree, and to the calcium carbonate formed being of very low solubility. Unfortunately, the amount of CO_2 was not measured in the outflowing water. Otherwise, it would perhaps have been possible to determine whether the moving boundary of carbonated mortar had penetrated the entire specimen.

When Kjennerud tested dried unsaturated specimens, there was a gradual reduction in the amount of water that percolated. According to Kjennerud, this was due to the blocking effect of the entrapped air. According to Kjennerud, the entrapped air diffuses to larger pores, where the air bubbles are larger. These bubbles flow with the water, and in narrow passages they block the flow of water.

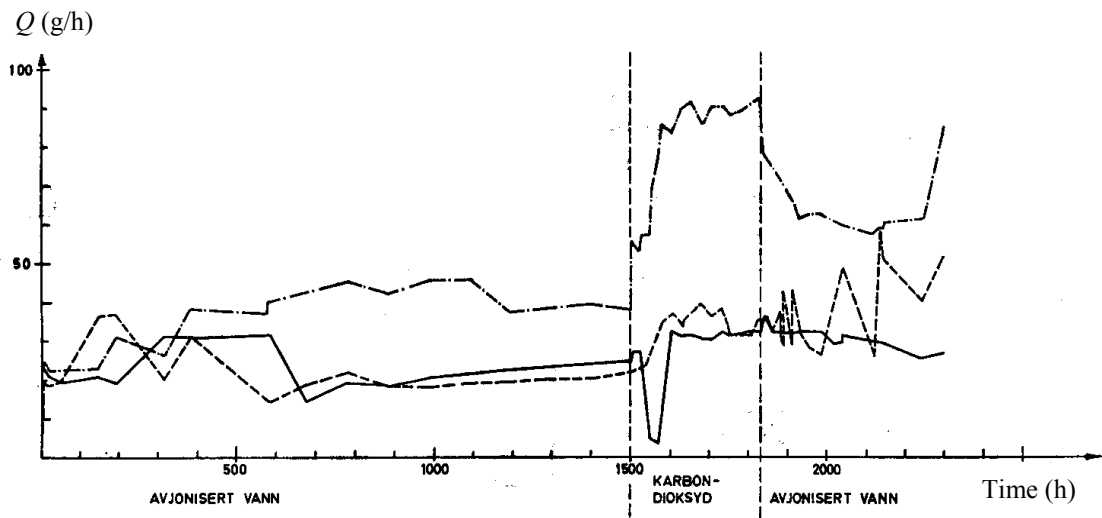


Figure 2.13 Amount of water Q (g/h) percolating through three specimens of highly porous cement mortar that had never been dried or exposed to CO_2 (Kjennerud 1974). “Avjonisert vann” = deionised water; “Karbondioksyd” = addition of CO_2 to the water.

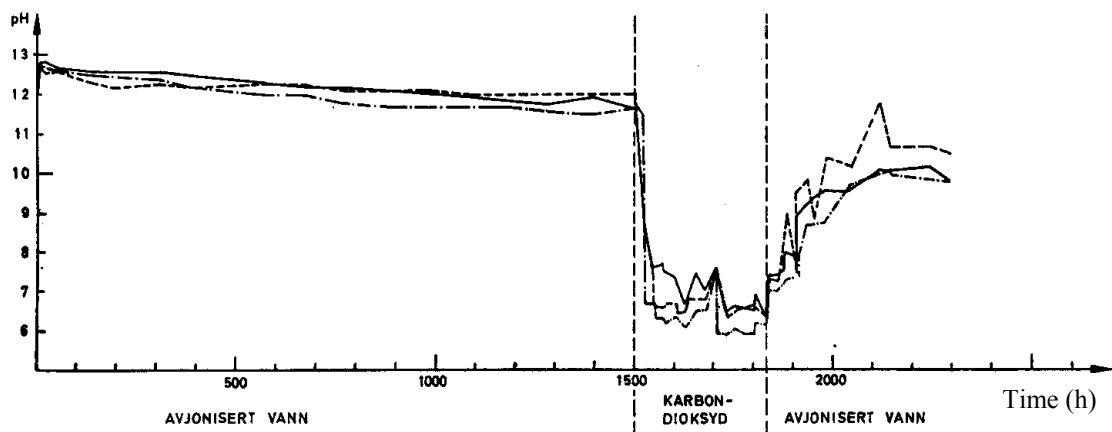


Figure 2.14 Values of pH in the out-flowing water from the mortar as determined by the percolation test described in the text (Kjennerud 1974).

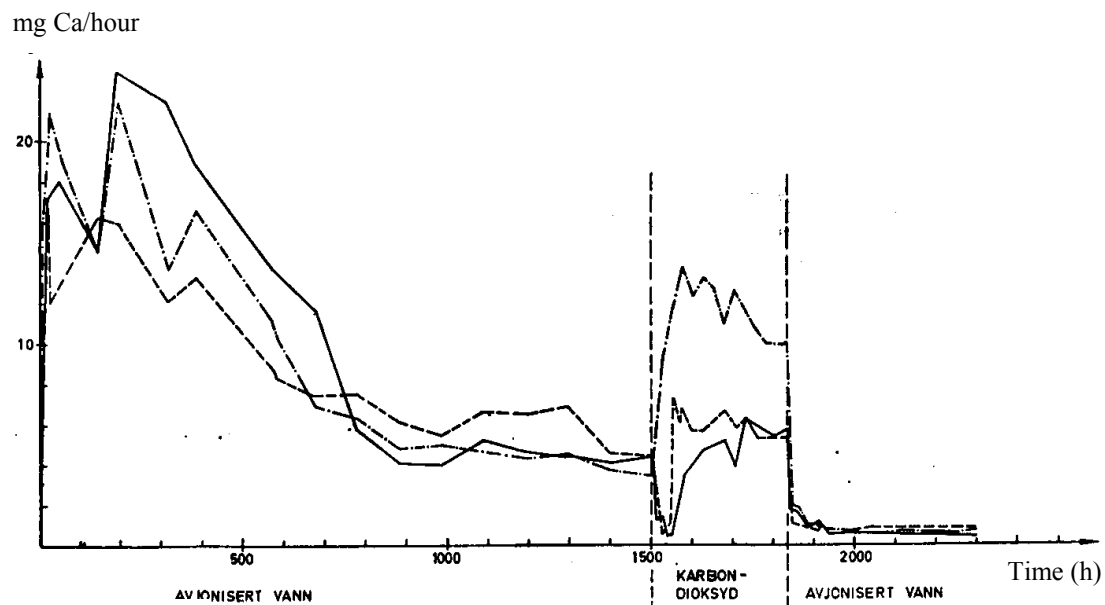


Figure 2.15 Amount of leached calcium (mg/h) in the outflowing water from the mortar as determined by the percolation test described in the text (Kjennerud 1974).

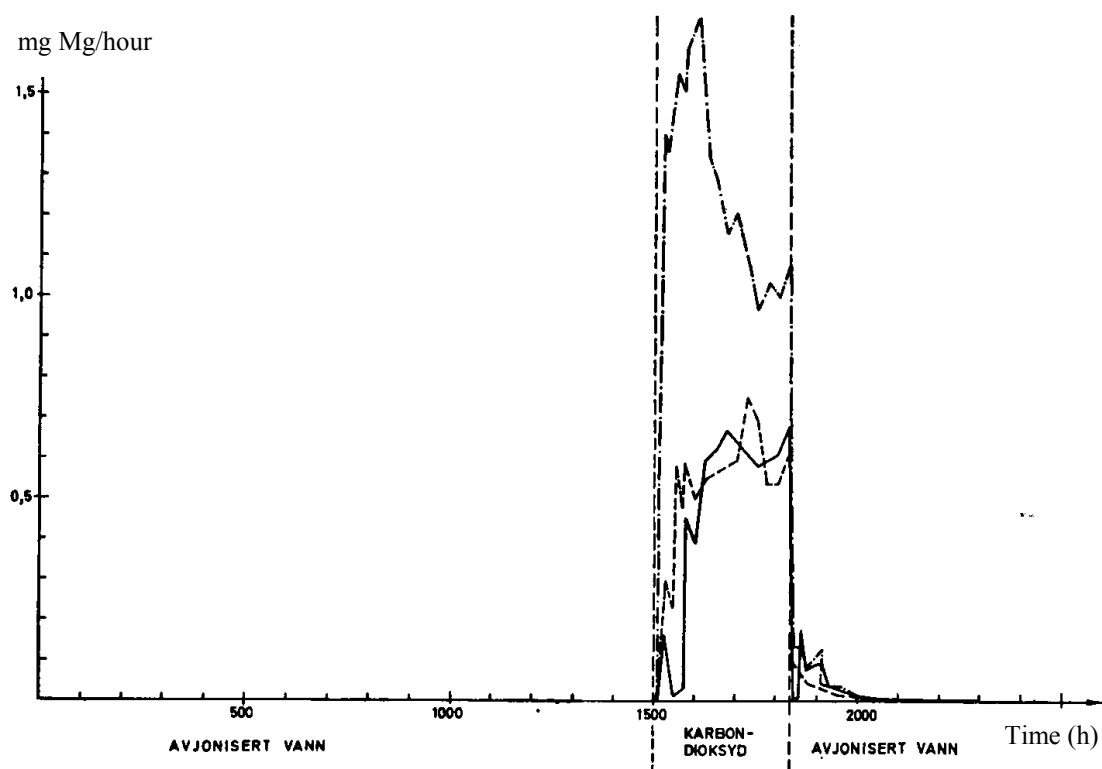


Figure 2.16 Amount of leached magnesium (mg/h) in the outflowing water from the mortar as determined by the percolation test described in the text (Kjennerud 1974).

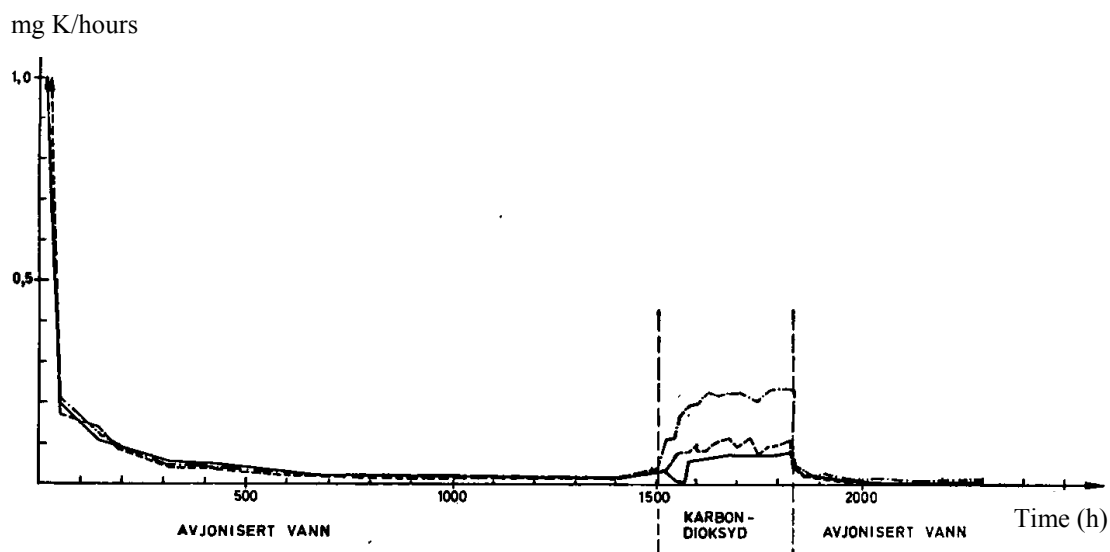


Figure 2.17 Amount of leached potassium (K) (mg/h) in the out-flowing water from the mortar as determined by the percolation test described in the text (Kjennerud 1974).

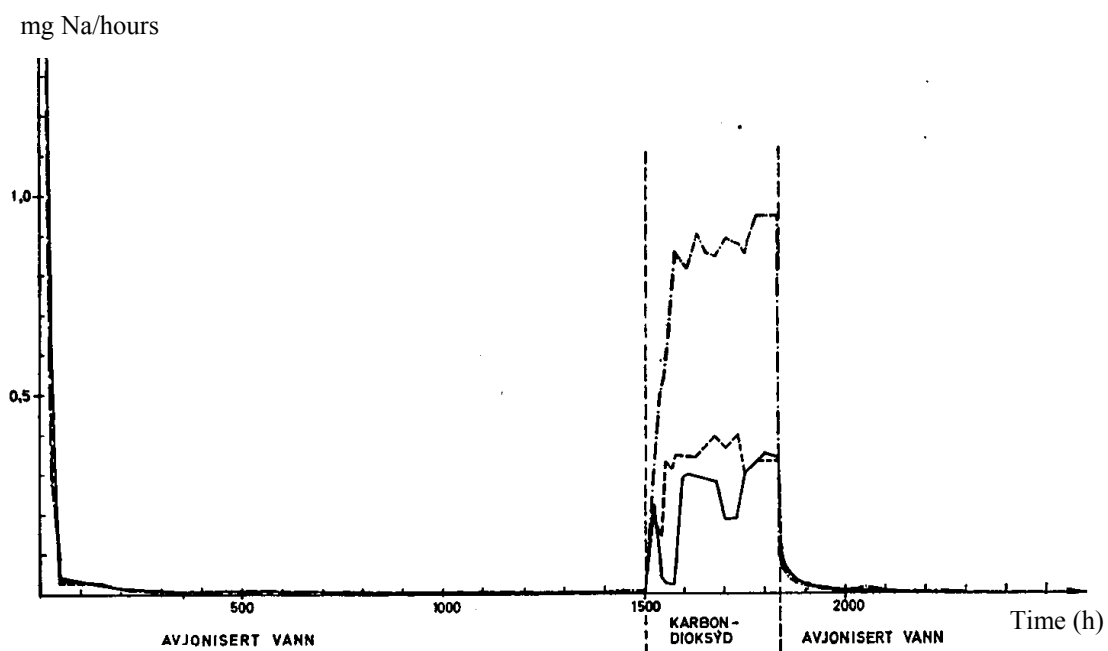


Figure 2.18 Amount of leached sodium (Na) (mg/h) in the out-flowing water from the mortar as determined by the percolation test described in the text (Kjennerud 1974).

Hearn and Morley (1997) found indications of increased leaching of Ca, K and Na compared to the virgin state when 26 years old concrete was dried (Figure 2.19). They assume that the drying caused an exposure of previously unexposed soluble compounds. They found also that the concentration of Ca in the outflow water gradually decreased during the test.

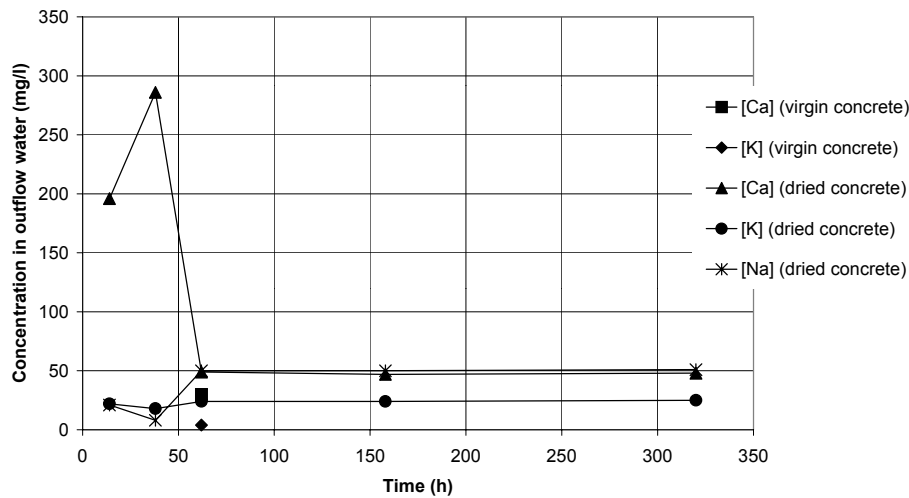


Figure 2.19 Typical changes in the outflow water while the permeability test was being conducted (Hearn & Morley, 1997)

2.4.4 Leaching due to percolation through cracks in concrete

Halvorsen (1966) presents, on the basis of a literature study, a possible conceptual model of leaching due to percolation through cracks in concrete (Figure 2.11). No account is taken in the model of any erosion due to particles present in the flowing water.

The leaching process moves through concrete at both sides of the crack, just as it did in the homogenous percolation of concrete, as described above. In addition, the leaching in a crack progresses as follows:

- If the water percolating through the crack contains no CO_2 , CH moves towards the crack from the interior and then moves away from it and out of the concrete by the convective flow of water through the crack. The crack wall is a **zone V**.
- If the percolating water contain CO_2 , a carbonated layer is formed on the walls of the crack to some extent. Depending on how large the flow of water is through the crack, the dissolved lime either flows out of the crack or forms CaCO_3 in the crack.
- There will be a leached layer of silica gel on the walls of the crack just as on the upstream surface.

When the flow of water is small or stationary cracks can readily seal through the formation of CaCO_3 in the crack. The newly developed calcium carbonate seals the cracks from further penetration by water, the leaching damage therefore ceases. This process is known as *autogenous healing*.

At large mobile cracks or cracks closed to CO_2 , dissolved CH in the concrete diffuses towards the cracks and is then carried away by the water, which causes continuous leaching damage. The concentration of leached material in the percolated

water can be expected to decrease, however, when the walls of the crack become depleted of soluble material.

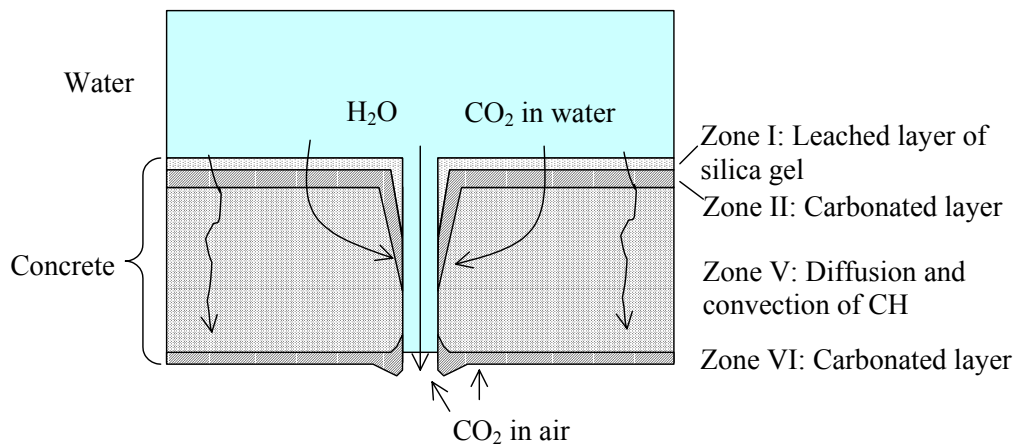


Figure 2.20 Conceptual model of leaching due to homogenous percolation through concrete (Halvorsen, 1966).

The degree of leaching measured near a crack in a concrete dam is shown in Figure 2.21. No leaching of SO_3 is assumed. If in reality such leaching of SO_3 should occur the degree of leaching given in the figure would be too small.

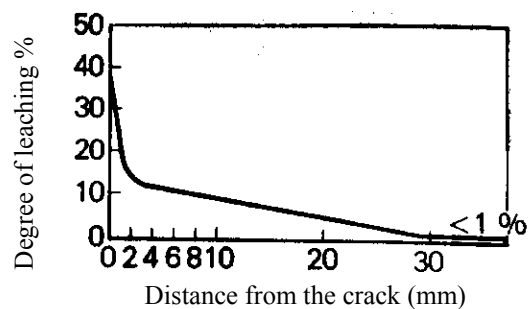


Figure 2.21 Ratio of leached CaO to initial CaO near a crack in the concrete dam at the Storfinnforsen Power Plant, as based on the relationship CaO/SO_3 (Halvorsen, 1966).

The same basic equation as (2.12) can also be used (Fagerlund 2000) for calculating the degree of leaching occurring in cracks.

2.4.5 Dissolution reactions

2.4.5:1 General

The kinetics involved in the dissolution of inorganic material is usually assumed to be very rapid and complete (Gruber & Rechenberg 1989, Atkins & Jones 1997). This is only true, however, if the reactants can reach each other instantaneously. Diffusion resistance always occurs. Data from the literature (e.g. Mainguy et al. 2000) indicates chemical reactions to be much faster than diffusion. For such inorganic substances, such as cementitious materials, water is an excellent solvent. The purer and the more the acid

water, the more aggressive it is. One can distinguish between two types of dissolving reactions:

- Dissolving in stagnant water in which the reaction can reach equilibrium
- Dissolving in mobile or stirred water in which the reaction is not allowed to reach equilibrium, see below.

2.4.5:2 *Dissolving in stagnant water in which the reaction can reach equilibrium*

A solution is said to be saturated when the solvent has dissolved all the solute it can but certain undissolved solute remains (Atkins & Jones 1997). The solubility equilibrium can be determined in various ways. It can be calculated by using equation (2.17) together with data from standard tables, it can be found experimentally, or it can be calculated from thermodynamic properties. The concentration of a pure solid or liquid is a constant, independent of the amount of it that is present, its being defined in equilibrium studies as 1 (Atkins & Jones 1997). Assume the dissolving of a typical *salt* in an aqueous electrolyte:



The reaction quotient Q can be calculated by

$$Q = [A]^a [B]^b / [solid] = [A]^a [B]^b / 1 = [A]^a [B]^b \quad (2.17)$$

For non-ideal solutions the reaction quotient becomes

$$Q = \frac{[\gamma_A(m_A + a \cdot x)]^a [\gamma_B(m_B + b \cdot x)]^b}{1} \quad (2.18)$$

where γ = *activity coefficient* for the ion strength in the electrolyte (l/mole); m = amounts of the ions A and B (molarity) (mole/m³); and x = amount of ions added stepwise (mole/m³).

When the dissolving process is in equilibrium, the solution is saturated and Q becomes the *solubility product*, so that $Q = K_{sp}$. If R is larger than K_{sp} , the solution is over-saturated and the dissolved salt will precipitate until K_{sp} is reached. If R is smaller than K_{sp} , the solution is under-saturated and the salt will dissolve until K_{sp} is reached.

The more dissolved ions there are in a solution, the higher the ion strength becomes, the smaller the activity coefficients are, and the smaller the reaction quotient is, which means that more of the solid can dissolve before K_{sp} is reached. If, in contrast, there already are dissolved ions of the same type as those coming from the solid (m_A and m_B), the reaction quotient R will be larger and less solid can dissolve before K_{sp} is reached. This is known as the “common ion effect”.

If the solubility of a salt AB is S , the relation between the solubility product and the solubility is

$$K_{sp} = (\gamma_a \cdot (m_A + a \cdot S))^a \cdot (\gamma_b \cdot (m_B + b \cdot S))^b \quad (2.19)$$

Note the *common-ion effect*. If the solution already contains salts ions of the same sort as are to be dissolved, the solubility of the added solid compound decreases, sometimes to a very great extent.

The following is an example of how one can determine the solubility product S of $\text{Ca}(\text{OH})_2$ in pure water (ideal solution) at equilibrium for $K_{sp}=5.5 \cdot 10^{-6}$ at $+25^\circ\text{C}$ (Atkins & Jones 1997):

$$K_{sp} = [\text{Ca}^{2+}][2\text{OH}^-]^2 = (S) \cdot (2S)^2 = 4S^3 = 5.5 \cdot 10^{-6} \Rightarrow S=0.011 \text{ mole/l} \quad (2.20)$$

If the solubility S is known and the solubility product is to be determined, K_{sp} is calculated directly from equation (2.20).

Consider too a solution in which 0.1 M NaOH is already dissolved without considering the ion strength. How much $\text{Ca}(\text{OH})_2$ is dissolved? Using equation (2.18) one finds that

| Stage | $\text{Ca}(\text{OH})_2 \leftrightarrow$ | Ca^{2+} | 2OH^- |
|----------------|--|------------------|----------------|
| Start | - | 0 | 0.1 |
| At equilibrium | - | x | 0.1+x |

$$K_{sp} = (x) \cdot (0.1+2x)^2 = x \cdot (0.01+0.4x+4x^2) \Rightarrow x$$

where x is the solubility of $\text{Ca}(\text{OH})_2$ in a solution which already consists of 0.1 M OH^- . For small solubility products, higher orders of x can be neglected. If x^2 and x^3 are neglected in this example, the solubility becomes $x = K_{sp}/0.01 = 5.5 \cdot 10^{-6}/0.01 = 5.5 \cdot 10^{-4}$, i.e. $5.5 \cdot 10^{-4}/0.011=0.05$ of the solubility in pure water, a decrease of 20-fold. If the solution had contained 1 M NaOH, the solubility of $\text{Ca}(\text{OH})_2$ would have decreased $S/K_{sp} = 0.011/5.5 \cdot 10^{-6} = 2000$ times.

To calculate the solubility of different salts in an electrolyte one has to take account of the ion strength. A suitable calculation scheme can be

1. Assume initial amounts of the dissolved salts m_A, m_B, \dots
2. Calculate the ion strength and the activity coefficients for each ion using equation (2.22).
3. Calculate the reaction quotient Q using equation (2.18).
4. Check whether Q is $<$, $=$ or $>$ than K_{sp} .
5. Move toward the saturation point (K_{sp}) by small steps of increasing or decreasing the dissolved amount x .
6. Go to 2. again until the saturation points of all the salts have been reached.

If the reaction quotient $Q > K$, the added salt will precipitate, whereas if $Q < K$, the salt will dissolve.

One of many equations that can be used to calculate the activity coefficient is the Güntelberg equation, which is said to be valid up to about 0.1 (mole/l):

$$\log \gamma_i = - \left(\frac{A \cdot z_i^2 \cdot \sqrt{I}}{1 + \sqrt{I}} \right) \quad (2.21)$$

where the ion strength being calculated as

$$I = 0.5 \cdot \sum z_i^2 \cdot m_i \quad (2.22)$$

where I = ion strength (mole/l); ϵ = dielectric constant (F/m); T = temperature (K); z_i = valence of the ion (-); and $A = 1.82 \cdot 10^6 (\epsilon \cdot T)^{-1.5} \approx 0.5$ for water at 25°C (Stumm (1996)).

2.4.5:3 *Dissolving in mobile water in which the reaction cannot go to equilibrium*

The reaction rates and diffusion velocities of mobile water are important. The kinetics of a dissolving reaction is very difficult to determine and describe. Such a reaction can involve the following steps:

- 1) The time during which the solvent (e.g. water) moves to where the reaction is to take place.
- 2) The dissolution reaction (e.g. $\text{Ca(OH)}_2 \rightarrow \text{Ca}^{2+} + 2\text{OH}^-$)
- 3) The time during which the dissolved products (e.g. Ca^{2+} , OH^-) can leave the location where the reaction occurred.

The rate-determining steps are likely to be 1) and 3), where 1) concerns the diffusion velocity of the solvent and 3) the diffusion velocity of the dissolved products, as well as the influence of the ion strength and the common ion effect.

A dissolving reaction can be considered to be a diffusion process (Hedin 1962), one of the following type:

$$Q = \text{rate}(c_{is} - c_i) = A_{\text{wall}} \frac{k_i}{\delta} (c_{is} - c_i) \quad (2.23)$$

Where Q = the mass dissolving (mole/s); A_{wall} = the surface from which the ions are dissolved (m^2); k_i = the diffusion coefficient (m^2/s); δ = the thickness of the diffusion layer (m); c_{is} = saturation concentration (mole/m^3), which is dependent upon the ion strength and the common ion effect; and c_i = concentration outside the diffusion layer t (mole/m^3).

The assumption on which the equation is based is shown in Figure 2.22. The water molecules diffuse towards a solid particle and force solid atoms or ions to break away from the solid and move away. The dissolved matter may move due to concentration gradients (diffusion) or by means of any flow of water that occur (convection). Electrical balances between different ions may also play a role. If there are small diffusion layers, together with large concentration gradients and ions that easily moving (high diffusion coefficient), the dissolving reaction is rapid. If there is only a small volume of water or if the water is not frequently replaced by new and pure water, the dissolving reaction ceases quickly.

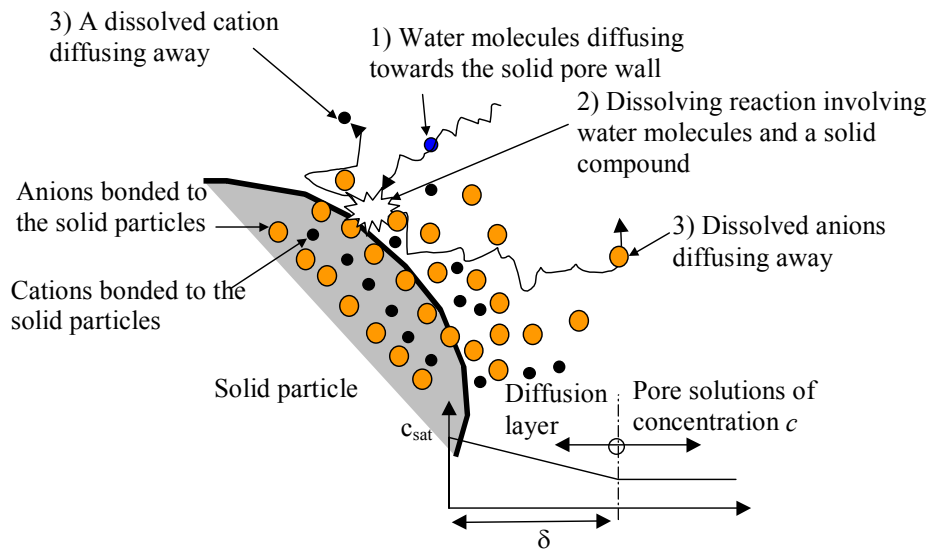


Figure 2.22 Principles involved in the dissolution processes in which water molecules diffuse to a solid pore-wall and dissolve solid compounds there, where c = concentration (mole/l) of the pore solution next to the diffusion layer t , c_{sat} = saturation concentration of a compound (mole/l) in water.

Theoretically, solid compounds are in thermodynamic balance with their dissolved counterparts. When the balance is disturbed however, such as when dissolved ions move away in a leaching process, the order of dissolution for the different substances can be correlated with their solubility, and also with how close to the solvent (the water) each substance is. Substance a , higher in solubility than substance b but not as close to it as pure water, may dissolve more slowly than substance b , despite its greater solubility generally.

Certain information about the reaction rate of crystals of $\text{Ca}(\text{OH})_2$ in water, that is initially pure is available in Hedin (1962) see Figure 2.23.

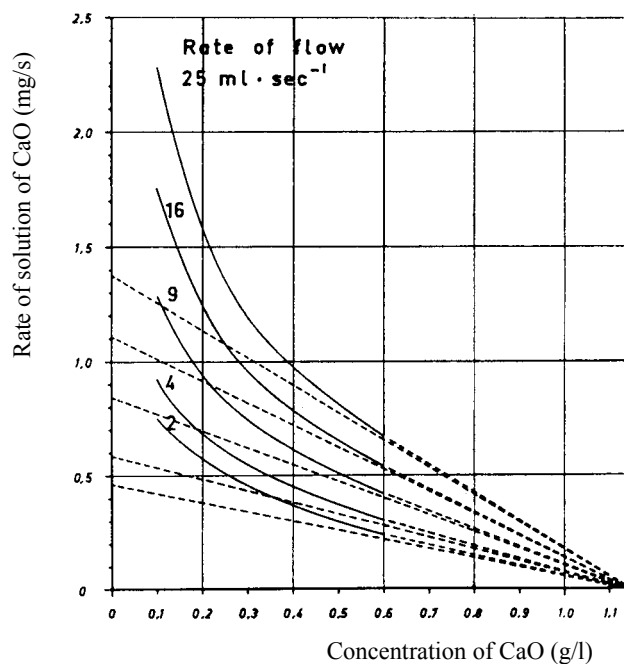


Figure 2.23 Rate of dissolution as a function of concentration at various flow rates (stirring) (Hedin, 1962).

As can be seen, the lower the concentration of dissolved CaO is and the higher the rates of stirring are, the more rapid the reaction involved becomes. The higher rate of dissolving when a solution is stirred is probably caused by a decrease in the diffusion layer nearest the solid particles. When the water is stirred or moves for other reasons, the thin diffusion layer is washed away and the pure water can move closer to the solid. Pure water molecules in direct contact with the solid Ca(OH)_2 dissolve the solid almost instantly. This leads to the conclusion that an ordinary dissolving reaction that occurs in cement paste is probably very much a diffusion-controlled process. The time needed for pure water to diffuse through the solid and for the dissolved ions to diffuse away from it is much greater than the time the pure dissolving reaction takes. Hedin states that only when the solution is stirred at an infinitely rapid rate does the diffusion layer approach zero, then under which conditions of the dissolving reaction being almost instantaneous.

A test of the dissolution of powdered Ca(OH)_2 in deionised water is shown in Figure 2.24. It can be noted (i) that the dissolution reaction is rapid, and (ii) that stirring of the water increases the dissolution rate.

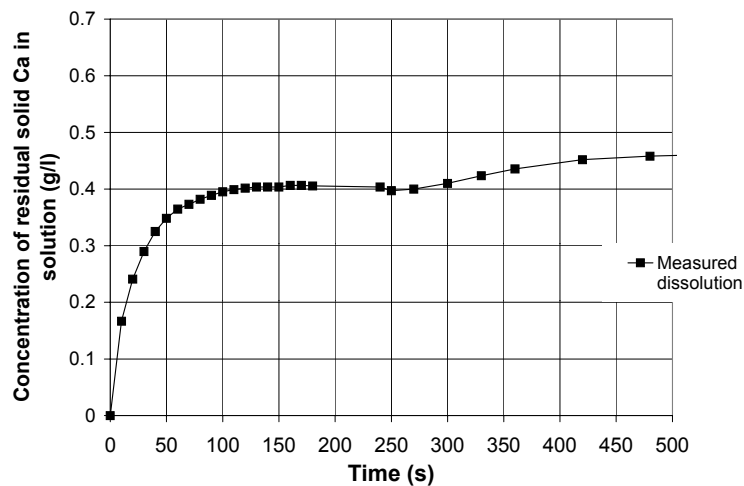


Figure 2.24 Measurements of the dissolution of $\text{Ca}(\text{OH})_2(\text{s})$ in pure water (Ekström 2000).

2.4.5:4 Dissolving of cement paste

There are several types of compounds in concrete, including $\text{Ca}(\text{OH})_2(\text{s})$ and the C-S-H and AF-phases, many of which can differ from each other in composition. These compounds are soluble in water to varying degrees. When the compounds are dissolved in water, the dissolved ions are transported by either diffusion or convection. Dissolution is thus a combination of the transport of the solvent (such as water molecules) to the compounds, a dissolving reaction and a conveying of the dissolved ions then from the place where the reaction occurs.

NaOH and KOH are two compounds easily soluble in concrete. In the pore solution, therefore most of the Na and K are in the dissolved state. Since not much of these compounds are available in the solid phase NaOH and KOH are washed out quickly when concentration gradients are present or when the pore solution is pressed out of the concrete by the flow of water. When NaOH and KOH are washed out, and the new pore solution consists of pure water, the concentration of OH^- in the residual pore solution decreases, making it possible for other, less soluble compounds containing OH^- to be dissolved. CH(s), which has a rather high level of solubility and which is readily available, is likely to be dissolved in the pore solution in particular. The pH drops from about 13.5 in a solution saturated by NaOH and KOH down to about 12.5 when it is buffered by CH. At the same time, although to a much lesser extent, Ca^{2+} and OH^- from the C-S-H and AF-phases are leached away. The more porous the concrete is and the more CH it contains, the more CH is leached. The solubility of CH is further enhanced through its being concentrated in such locations as aggregate-paste interfaces and capillary pores, where the porosity and permeability are also greater (Grattan-Bellow 1990).

“Proton attack will initially result in the consumption of the $\text{Ca}(\text{OH})_2$. Once $\text{Ca}(\text{OH})_2$ is exhausted, the C/S ratio will decrease ... The minimum calcium-to-silica ratio for calcium silicate hydrate is about 0.83... Further acidification will cause the calcium silicate hydrate to decompose to silica gel” (Brown 1987).

However, whether the calcium comes from CH(s) or from cement gel is not easy to determine. Taylor (1990) says, “*The equilibrium suggests that CH will be dissolved before the other phases are attacked, but, in practice, attack is likely to be simultaneous, because of the greater specific surface areas of the hydrated silicate and aluminate phases*”.

Berner (1987) provides a conceptual model of different stages of dissolution, every stage exhibiting its own general range of major component concentrations in the pore-water:

- 1) Dissolution of alkali hydroxides: (Na, K high; Ca, Mg low; Al, Si low; pH high)
- 2) Dissolution of CH(s): (Ca \approx 0.02 M; Mg low; Al, Si low; pH \approx 12.5)
- 3) Incongruent dissolution of calcium silicates, calcium aluminates and calcium aluminosulfates: (Ca, Al, Si low to moderate; Mg low; pH \approx 12.5 to 10.4)
- 4) Dissolution of Mg(OH)₂: (Mg \approx 3·10⁻⁴ M; Al, Si low to moderate; pH \approx 10.4)
- 5) Dissolution of the remaining SiO₂, Al₂O₃ and Fe₂O₃

Berner notes that the time scale for this degradation depends on the physical properties of the concrete (porosity, permeability), on the flux through the concrete (or on its diffusion properties) and on the composition of the leachant. The various stages referred to can overlap, whether they do depending on the relative amounts in the solid phase and on the availability of the solids for being dissolved. Various important chemical reactions in connection with the leaching of concrete were given in section 2.4.1.

According to Halvorsen (1966) and to Hallström (1933) pure water is more aggressive toward crushed cement paste than water containing dissolved CO₂, whereas water containing dissolved CO₂ is more aggressive to carbonated cement paste.

The dissolution of C-S-H is a function of the concentration of CH(aq) in the pore solution. If C-S-H is placed in water or in solutions containing CH(aq), its Ca/Si ratio changes until equilibrium is achieved. Except at low CH concentrations, the SiO₂ concentrations in solutions are very low, so that the transfer between the solid and the solution is almost entirely of CH (Taylor 1990). A curve indicating the equilibrium of solid C-S-H in a solution of CH(aq) is shown in Figure 2.25.

The most calcium-rich C-S-H and Portlandite (CH(s)) is only stable at high concentrations of CH(aq), above 20 mmole CH/l. At this level, CH(s) dissolves in CH(aq) (Ca²⁺ and OH⁻). At concentrations of CH(aq) in the solution of less than 20 mmole/l, CH(aq) is dissolved from C-S-H until a new equilibrium is reached. Below C/s \approx 1.4, the concentration of CH in the pore solution decreases quickly to approximately 2 mmole/l, at which level a large fraction of the total CH in C-S-H is dissolved as shown in Table 2.4.

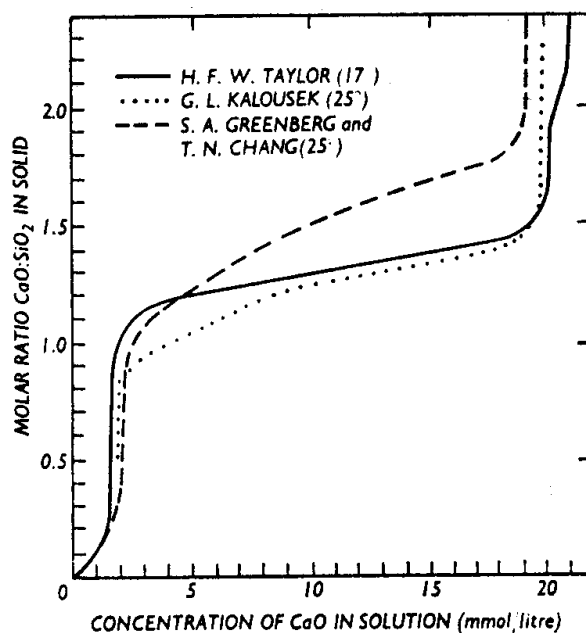


Figure 2.25 Equilibrium between hydrous calcium silicates in solution (Lea, 1983).

The solubility product and solubility in pure water of different compounds that can be found in cement paste are shown in Table 2.3 and Table 2.4.

Table 2.3 Solubility product for different solid compounds in ordinary Portland cement (OPC).

| Hydration product | Solubility S (mole/l) | Solubility product K_{sp} |
|--|--|---|
| Ca(OH)_2 | <ul style="list-style-type: none"> $(70.38-0.17 T) \cdot 10^{-3}$ (large crystals) (Hedin, 1955) e.g. $20.5 \cdot 10^{-3}$ (+20°C) $21.0 \cdot 10^{-3}$ (+19°C) (Basset, 1934) $22.2 \cdot 10^{-3}$ (Duchesne & Reardon, 1995) $25.0 \cdot 10^{-3}$ (cold water) $10.4 \cdot 10^{-3}$ (hot water) $16.2 \cdot 10^{-3}$ (+25°C) (Aylward & Findlay, 1994) | <ul style="list-style-type: none"> $4.68 \cdot 10^{-6}$ (Chem & Phys, 1989) $5.5 \cdot 10^{-6}$ (Atkins & Jones, 1997) $6.4 \cdot 10^{-6}$ (Aylward & Findlay, 1994) $6.3 \cdot 10^{-6}$ (Duchesne & Reardon, 1995) $6.5 \cdot 10^{-6}$ (Harris et al., 2002) |
| C-S-H | See Table 2.4, Figure 2.25, Figure 2.26 and Figure 2.27 | $2 \cdot 10^{-9}$ for Ca/Si ratio of 1-2.5 (Harris et al. 2002) |
| C_3AH_6 | See Table 2.4 | |
| C_3FH_6 | See Table 2.4 | |
| $\text{C}_3(\text{A,F}) \cdot x\text{CaX} \cdot y\text{H}$ | <ul style="list-style-type: none"> CaSO_4: $15.3 \cdot 10^{-3}$ (Chem. & Phys., 1989) $\text{CaSO}_4 \cdot 2\text{H}_2\text{O}$: $14 \cdot 10^{-3}$ (Chem. & Phys., 1989) | <ul style="list-style-type: none"> CaSO_4: $7.10 \cdot 10^{-5}$ (Chem. & Phys., 1989) $\text{CaSO}_4 \cdot 2\text{H}_2\text{O}$: $K=2.6 \cdot 10^{-5}$ (Chem. & Phys., 1989) Ettringite: $\log K_{sp} = -43.13$ (Reardon, 1989) |
| KOH | <ul style="list-style-type: none"> Solubility $S=119\text{g/l}/(39.1+(16+1))\text{g/mol}=2.12\text{M}$ (Aylward & Findlay, 1994) | |

Table 2.3 continued:

| | | |
|------------------------------------|---|---|
| NaOH | <ul style="list-style-type: none"> Solubility $S=114\text{g/l}/(22.99+(16+1))\text{g/mol}=2.85\text{M}$ (Aylward & Findlay, 1994) | |
| CaCO ₃ | <ul style="list-style-type: none"> $13 \cdot 10^{-5}$ (Halvorsen, 1966) | <ul style="list-style-type: none"> $4.96 \cdot 10^{-9}$ $\log K_{sp} = -8.41$ (Reardon, 1989) |
| Ca(HCO ₃) ₂ | <ul style="list-style-type: none"> 1018 (Halvorsen, 1966) | |
| Al(OH) ₃ | <ul style="list-style-type: none"> Begins to dissolve at pH 3-4 (Rombèn, 1978) | |
| Fe(OH) ₃ | <ul style="list-style-type: none"> Begins to dissolve at pH 1-2 (Rombèn, 1978) | |

Table 2.4 Solubility of different concrete hydration products (Moskvin, 1980)

| Compound | Solubility Stable at (g CaO/L) | Releasing |
|--|-----------------------------------|---|
| Ca(OH) ₂ | 1.18 | CH |
| Ca(OH) ₂ supersaturated | 1.6-1.9 | CH |
| Ca(OH) ₂ in 1 % Na ₂ SO ₄ solution | 2.14 | CH |
| Ca(OH) ₂ in 5g/l NaOH solution | 0.18 | CH |
| 2CaO·SiO ₂ ·aq | stable in saturated CH | CH |
| 3CaO·2SiO ₂ ·aq | stable in 1.1 | CH |
| Ca·SiO ₂ ·aq (Wollasonite) | stable in 0.05 | |
| 4CaO·Al ₂ O ₃ ·19H ₂ O (C ₄ AH ₁₉) | stable over 1.15 | CH |
| 3CaO·Al ₂ O ₃ ·6H ₂ O (C ₃ AH ₆) | stable between 0.315-1.15 | CH |
| C ₁₂ A ₇ | | CH and Al ₂ O ₃ (A) |
| C ₂ AH ₈ | | CH and A |
| C ₄ F·aq (4CaO·Fe ₂ O ₃ ·aq) | stable over 1.15 | |
| C ₂ A·aq ----- II ----- | stable between 0.17-0.315 | |
| C ₄ F·aq (4CaO·Fe ₂ O ₃ ·aq) | stable over 1.15 | |
| CF·aq | stable between 0.64-1.15 | |

The dissolving of salts depends on the size of the crystals, since the dissolving reaction is in reality a diffusion process. The solubility of crystals of Ca(OH)₂ of differing size is shown in Table 2.5. Since the dissolution of CH in water is exothermic

$$(\Delta H = -13.8\text{kJ/mole at } +25^{\circ}\text{C}) \quad (2.24)$$

the solubility, thus, decreases with temperature.

Table 2.5 Solubility S (g CaO/l) crystals of $\text{Ca}(\text{OH})_2$ Basset (1934).

| $T^\circ\text{C}$ | 0 | 5 | 10 | 15 | 20 | 25 | 30 | 40 | 50 |
|-------------------|------|------|------|------|------|------|------|------|------|
| Coarse crystals | 1.30 | 1.28 | 1.25 | 1.21 | 1.17 | 1.13 | 1.09 | 1.00 | 0.92 |
| Fine crystals | 1.43 | 1.42 | 1.38 | 1.33 | - | 1.29 | 1.21 | 1.07 | 0.97 |

Table 2.6 and Table 2.8 show the solubility of CH in solutions with differing concentrations of KOH and NaOH.

Table 2.6 Solubility of CaO (g/l) in solutions of KOH or NaOH at $+20^\circ\text{C}$ (Fratini 1949, d'Anselme 1903).

| In KOH solutions | | In NaOH solutions | |
|------------------|-------|-------------------|--------------|
| KOH | CaO | NaOH | CaO |
| | | 0 | 1.177 (1.17) |
| | | 0.4 | 0.94 |
| 1.156 | 0.852 | 1.008 | 0.779 |
| 2.312 | 0.611 | 2.100 | 0.516 |
| 4.186 | 0.381 | 4.140 | 0.281 |
| 5.836 | 0.275 | 5.00 | (0.18) |
| 8.624 | 0.185 | 6.141 | 0.196 |
| 11.9 | 0.151 | 8.361 | 0.146 |
| | | 20.00 | (0.02) |

Table 2.7 Solubility of K^+ and Ca^{2+} (mole/l) in KOH and NaOH solutions at 25°C (Duchesne & Reardon 1995).

| KOH solution | | NaOH solution | |
|------------------|----------------------|-------------------|----------------------|
| K^+ (m) | Ca^{2+} (m) | Na^+ (m) | Ca^{2+} (m) |
| 0 | 0.0222 | 0 | 0.0222 |
| 0.0009 | 0.0220 | 0.0010 | 0.0217 |
| 0.0047 | 0.0210 | 0.0048 | 0.0209 |
| 0.010 | 0.0190 | 0.010 | 0.0197 |
| 0.019 | 0.0172 | 0.019 | 0.0172 |
| 0.047 | 0.0114 | 0.048 | 0.0111 |
| 0.094 | 0.00637 | 0.096 | 0.00573 |
| 0.190 | 0.00328 | 0.193 | 0.00330 |
| 0.482 | 0.00127 | 0.487 | 0.00126 |
| 0.991 | 0.00072 | 0.991 | 0.00065 |
| 1.965 | 0.00036 | 1.965 | 0.00042 |
| 3.860 | 0.00021 | 3.627 | 0.00023 |

In Table 2.8 the solubility product K_{sp} is proposed for C-S-H of differing composition.

Table 2.8 The solubility product K_{CSH} for C-S-H of differing composition as based on experimental data of Jennings (1986) and Berner (1988), taken from Adenot & Richet (1997).

| C/S of C-S-H | 1.65 | 1.45 | 1.30 | 1.15 | 1.05 | 0.95 | 0.90 | 0.85 |
|---|------|------|------|------|------|------|------|------|
| $\text{p}K_{\text{CSH}} = -\log_{10}(K_{\text{CSH}})$ of C-S-H | 11.7 | 10.6 | 9.8 | 8.9 | 8.3 | 7.6 | 7.3 | 6.9 |

Reardon (1989) proposed a chemical equilibrium model for the simulation of reactions between pore-water and the various amorphous and crystalline minerals of cementitious material. The model utilises the Pitzer Ion Interaction model as a basis for the calculation of ion activity coefficients and is said to allow the chemical equilibrium between minerals and water of high solute concentrations to be simulated. A variable compositional model for C-S-H based on the work of Gartner and Jennings is included in it, calculations based on it being shown in Figure 2.26.

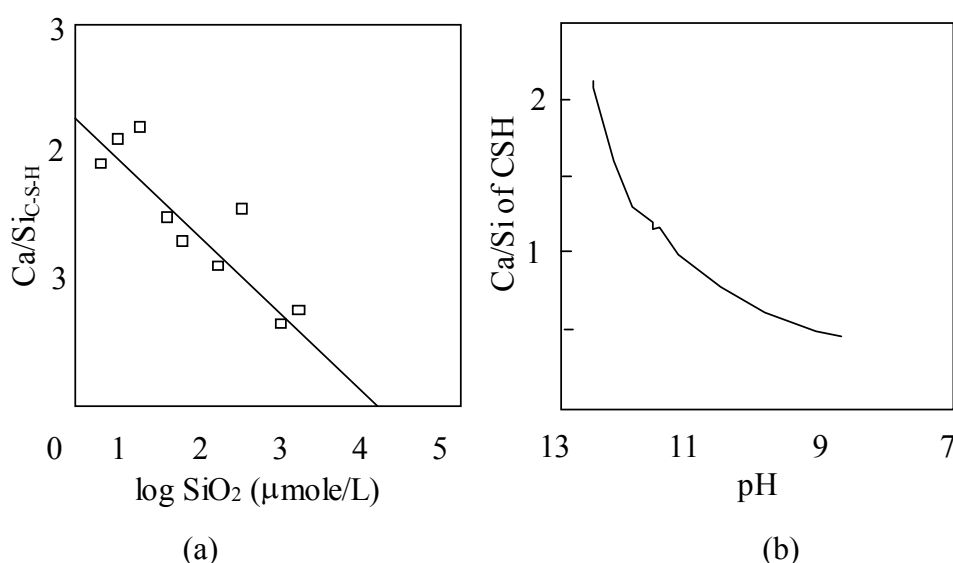


Figure 2.26 (a) Compositional data for the CSH vs. SiO_2 content of the solution, taken from data of Gartner and Jennings (1987) referred in Reardon (1989). (b) Calculated changes in CSH composition with differences in pH (Reardon 1989).

Figure 2.27 compares results of leaching experiments with a leaching model describing the pH value at different values of the C/S-ratio. In the present study, the curves made by Taylor in Figure 2.25 and by Reardon in Figure 2.26 have been transferred into the Figure 2.27 for the sake of comparison. The curve, originally made by Taylor, has here been transformed to be related to pH-values instead of the concentration of CaO (in the solution). It is assumed that pH in the solution is totally governed by the release of OH⁻ ions from $\text{Ca}(\text{OH})_2$ only, i.e. $\text{pH} = 14 + \log(\text{OH}^-) = 14 + \log(2 \cdot \text{CaO})$ (one CaO release two OH⁻ ions). It can be seen that the curves taken from Harris et al., Taylor and Reardon do not correspond so well to each other. The curve calculated from Taylor probably shows the best behaviour for the equilibrium of C-S-H gels in water. The other curves shows probably not equilibrium values in the part of the figure with low values of the calcium-silica ratio.

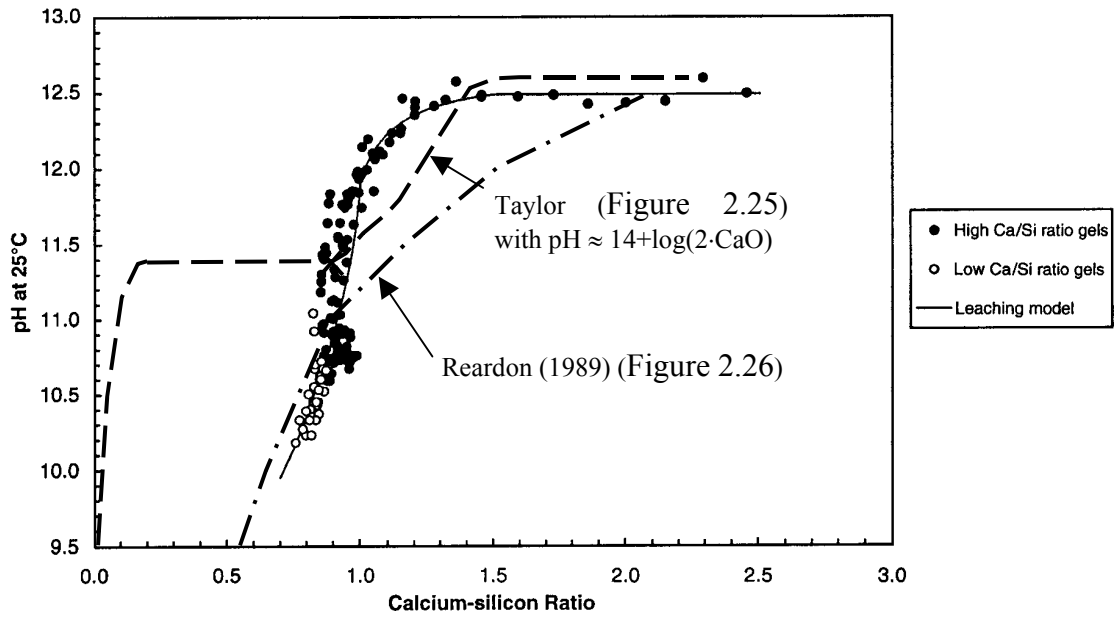


Figure 2.27 Comparison of a leaching model with experimental data (Harris et al. 2002) showing the pH of a solution during the leaching of CSH gels.

Calculated values for the solubility of C-S-H at different values of the molarity of SiO_2 and different pH are shown in Figure 2.28.

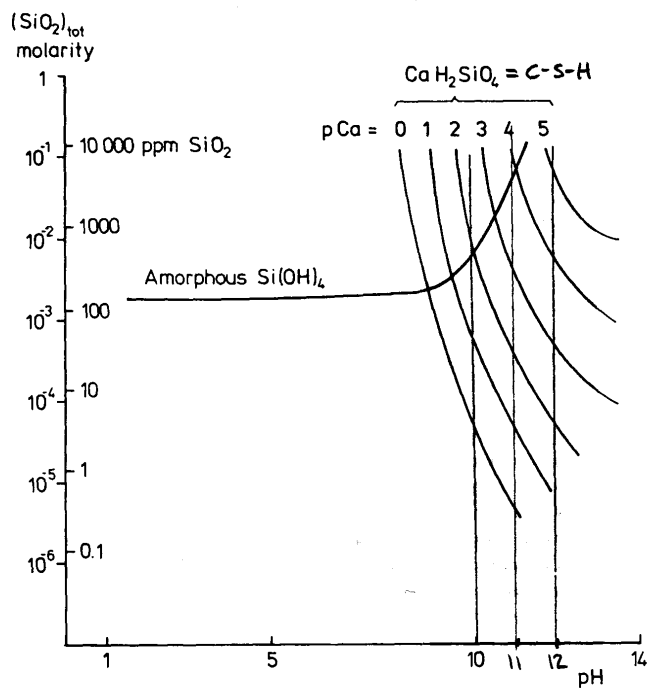


Figure 2.28 Calculated solubility of C-S-H (Rombén, 1979). For example, at $\text{pH} = 11$ and $[\text{SiO}_2] = 10^{-2}$ mole/l, the solubility of Ca in C-S-H being $\text{pCa} = 3.1$, or $10^{-3.1}$ mole/l.

2.4.6 Diffusion of dissolved ions

The diffusive flow of ions in dilute free water is influenced by concentration gradients. Table 2.9 presents values for the diffusivity of different ions in free water as taken from the literature.

Table 2.9 The mass diffusivity D_f of ions in dilute free water.

| Ion | D_f (m^2/s) | Literature reference |
|-------------|----------------------|----------------------|
| Ca^{2+} | $1 \cdot 10^{-9}$ | Moskvina (1980) |
| | $0.79 \cdot 10^{-9}$ | Wallin (1988) |
| K^+ | $1.96 \cdot 10^{-9}$ | Johannesson (1998) |
| Na^+ | $1.33 \cdot 10^{-9}$ | Johannesson (1998) |
| OH^- | $5.27 \cdot 10^{-9}$ | Wallin (1998) |
| | $5.30 \cdot 10^{-9}$ | Johannesson (1998) |
| H^+ | $9.30 \cdot 10^{-9}$ | Wallin (1998) |
| CO_2 | $2.00 \cdot 10^{-9}$ | Wallin (1998) |
| HCO_3^- | $1.20 \cdot 10^{-9}$ | Wallin (1998) |
| CO_3^{2-} | $0.70 \cdot 10^{-9}$ | Wallin (1998) |

In real porous materials, there are no straight flow tubes and the pores are small, leading to the intermolecular forces between the dissolved ions and the walls of the solid having a strong influence. The diffusion flow of ions in a *pore solution* is influenced not only by the concentration gradients, however, but also by the inter-molecular forces between the dissolved ions. Chemical interactions between ions and electrical forces between differently charged ions govern the mobility of ions (Marchand et al., 1999).

Rombén (1979), in his study of acid attack on concrete, speculated there to be a sort of shuttle traffic of the conjugate base A^- of an acid. This carries protons (H^+) from the solution into the reaction layer, releases H^+ , and conveys a dissolved ion (e.g. Ca^{2+}) out of the reaction layer into the solution, where it again encounters H^+ .

The amount (porosity), shape, tortuosity and connections of the pores with each other also influence the mobility (Delagrave et al., 1997). This labyrinth effect as it is called, is often dealt with by use of a *tortuosity factor*. This factor is probably partly a function too of the dwindling size of the flow channels through the material, and of capillary pores and micro-cracks around aggregate. Citing the literature, Rombén (1978) denoted the size of the tortuosity factor to be 1.19 – 1.9 in different ordered balls of the same size. He guessed at the size of the tortuosity factor in the case of concrete, where d_{max}/d_{min} for the particles is in the order of 100, being considerably larger.

A simple way of estimating the steady-state diffusion flow of ions is by use of the linear relationship contained in Fick's law:

$$F_{iu} = D_{eff} \nabla c \quad (2.25)$$

where F_{iu} = diffusion flux of ions ($mole/m^2/s$); D_{eff} = effective diffusion coefficient, considering the porosity, tortuosity, constrictivity, chemical influences and reactions with the pore walls and with other species (m^2/s); and ∇c = the concentration gradient ($mole/m^3/m$).

In Seveque, Cayeux, Elert and Nougier (1992), D_{eff} is suggested to be

$$D_{eff} = \frac{D_f}{P \left(1 + \frac{1-P}{P} \rho K_d \right)} \quad (2.26)$$

where D_f = the diffusion coefficient in free water (m^2/s); P = the bulk porosity (m^3/m^3); ρ = the solid bulk density (kg/m^3); and K_d = the sorption coefficient (m^3/kg).

An experimental determination of the diffusion constant of $Ca(OH)_2$ in calcium hydroxide solutions in the concentration range of 0.05 to 1.1 g CaO/litre at 25°C was conducted by Hedin (1962), using Harned's conductometric method. A diffusion constant D of $1.385 \cdot 10^{-9} m^2/s$ was found for solutions of 1.08 g CaO/l, and up to $1.747 \cdot 10^{-9} m^2/s$ for solutions of 0.064 g CaO/l. The author did not distinguish between Ca^+ and OH^- in reporting his results, D being said to be valid for the diffusion of $Ca(OH)_2$.

Rombén (1979) found in his experiments a relation of the type

$$x = k \cdot \sqrt{t} \quad (2.27)$$

for chemical attack on cement paste, where x = distance of penetration (m); k = a constant ($m \cdot s^{1/2}$); and t = time (s). He stated however, that for ions in solution, the Nernst-Planck's law can predict the ion velocity on the basis of, the electrochemical potential of the solution.

Pereira et al. (1988) provide a simple approach to determining the effective diffusion coefficient, D_{eff} , given as:

$$\frac{1}{D_{eff}} = \frac{1}{D_f \cdot \frac{P}{\tau}} + \frac{1}{D_K} \quad (2.28)$$

where D_{eff} = effective diffusion coefficient regarding porosity, tortuosity and intermolecular forces in small pores (m^2/s); D_f = free water diffusion coefficient (m^2/s); P = porosity (m^3/m^3); τ = tortuosity (-); and D_K = Knudsen diffusion in small pores (m^2/s).

Roy (1988) found the diffusion coefficients for moderately-sized, singly-charged cations in water-saturated porous cementitious materials to generally range between 10^{-11} and $10^{-13} m^2/s$, and the diffusion coefficients for these ions in pure water to be $\sim 10^{-9}$. The reason for the large difference between free water diffusion and diffusion in the pores of cement materials may be the constrictions, the tortuosity and ion-wall interactions along the path of the pores through which the ions migrate in a water-saturated porous matrix.

In cement materials of high hydraulic connectivity (e.g. due to a high w/c ratio), the diffusion coefficient is of course larger. During the leaching of cement materials, the pores are enlarged and the connectivity between the pores becomes greater, which leads to the diffusion coefficient becoming higher. The diffusion coefficient during leaching probably becomes greater for cement materials in which the original diffusion coefficient is low. The ratio of diffusion coefficients in the non-leached to that in the leached state, for example, is higher for materials with low than for materials with high w/c ratio.

Garboczi (1990) expressed the diffusivity of ions as being

$$\mathbf{F}_{iu} = -D_{eff}\nabla c \quad (2.29)$$

$$D_{eff} = D_f P \cdot r_i \quad (2.30)$$

where D_{eff} = effective diffusivity coefficient of the ions (m^2/s); D_f = the diffusivity coefficient for free, dilute water (m^2/s); P = porosity (m^3/m^3); r_i = the reduction parameter considering all deviations from free flow in a straight tube, such as effect of tortuosity, connectivity and the intermolecular forces between the ions and between the ions and the pore-walls (-).

It should be recalled, however, that it is very difficult to determine, or calculate, diffusion coefficients in cement material because of there being so many ions in the pore solution that influence each other. Diffusion is not only influenced by the concentration gradient of each ion but also by the electroneutrality requirements for the solution.

Faucon et al. (1996) and Faucon et al. (1998) describe the leaching process in cement paste subjected to demineralised water without any water pressure gradient as being a leaching process that creates calcium concentration gradients in a layer between the surface and the core of the specimens. These gradients change the chemical equilibrium in the layer, leading to the hydration products calcium hydroxide (CH), calcium aluminium hydrates (C₃A) and calcium aluminium iron hydrate (C₄AF) starting to dissolve. When the calcium content of the pore solution decreases, the calcium silicate hydrate (C-S-H) also loses calcium. At a concentration of Ca²⁺ in the pore solution of about 1.8 (mmole/l) (cf. Figure 2.25), the residual silica matrix in the C-S-H starts to dissolve completely. At that point, however, the residual C-S-H gel has a high ion-exchange capability, the iron and aluminium that are released from the crystallised hydrates, being partially incorporated into the residual C-S-H gel. The incorporation of iron and aluminium into the C-S-H gel enhances its stability and slows down the dissolution to a significant degree.

Many authors, such as Johannesson (1999) and Marchand, Samson and Maltais (1999) have modelled the flow of ions in the pore system of cement materials. The starting point taken is often a mass balance of ions, involving interactions between the solid matrix and the different constituents in the pore solution:

$$\frac{\partial(W c_i)}{\partial t} = (1 - P) \frac{\partial c_{is}}{\partial t} - \text{div}(W \mathbf{F}_i) \quad (2.31)$$

$$\mathbf{F}_i = \mathbf{F}_{iu} + \mathbf{F}_{iv} \quad (2.32)$$

where c_i = ionic concentration in the free water solution (pore solution) ($mole/m^3$); c_s = ionic concentration in the solid phase ($mole/m^3$); \mathbf{F}_i = total ionic flux ($mole/m^2/s$); \mathbf{F}_{iu} = ionic flux due to diffusion ($mole/m^2/s$); \mathbf{F}_{iv} = ionic flux due to convection ($mole/m^2/s$); P = total porosity (m^3/m^3); W = the “free” (or unbound) water fraction (m^3/m^3); and $\delta c_s/\delta t$ = the dissolving reaction ($mole/m^3/s$).

Marchand, Samson and Maltais (1999) used a model termed STADIUM in performing numerical calculations of diffusion. The model which ignores ion flow due to convection and interaction between the dissolved ions in the pore solution, as well as bound ions in the solid phase (that are not part of the dissolving reaction). The equation employed describing diffusion omits the first term (the reaction term) on the right side in equation (2.31):

$$\frac{\partial(W c_i)}{\partial t} = -\text{div}(W \mathbf{F}_{iu}) \quad (2.33)$$

Diffusion is assumed to be caused of local gradients by the electrochemical potential (μ_i).

$$\mathbf{F}_{iu} = -\frac{D_i}{RT} \text{grad}(\mu_i) \quad (2.34)$$

$$\mu_i = \mu_{i0} + R \cdot T \cdot \ln(\gamma_i \cdot c_i) + z_i \cdot F \cdot E \quad (2.35)$$

where D_i = diffusion coefficient for species i (m^2/s); E = the local electrical potential (V); $\text{grad}(\mu_i)$ = the local gradient of μ ; F = the faraday constant ($9.65 \cdot 10^4$ J/V/mole); R = the gas constant (J/K/mole); T = temperature (K); $R \cdot T \cdot \ln(\gamma_i \cdot c_i)$ = difference between any condition for species i and the standard condition (at 1 atm, 20°C); z_i = valence of the ionic species i ; γ_i = activity coefficient of species i ; μ_i = electrochemical potential of species i (J/mole); and μ_{i0} = standard chemical potential of species i (J/mole).

The local electrical field E between different ions is given as

$$\nabla^2 E + \frac{\rho}{\varepsilon} = 0 \quad (2.36)$$

$$\rho = F \sum_{i=1}^n z_i c_i \quad (2.37)$$

where ε = the dielectric field of the medium ($\text{F/m} = \text{J/V}^2/\text{m}$); and ρ = electrical charge density (J/V/m^3). Equation (2.34) was rewritten by the authors to what they called an *extended Nernst-Planck* equation:

$$\mathbf{F}_{iu} = -D_i \left(\text{grad} c_i + c_i \text{grad} \ln \gamma_i + \frac{F z_i}{RT} c_i \text{grad} E \right) \quad (2.38)$$

The authors claimed that through use of this equation both the viscous-drag on the ions and the different electrical forces between the ions are taken into account. The ionic solution produces an electroneutrality that slows down the faster ions and speeds up the slower ones. The authors indicate the equations to be simple to implement in a computer program.

The activity coefficient γ is used in the above equations. Many theories have been developed for calculating the activity coefficient γ , such as expressed in the Debye-Hückel equation, the Pitzer equation (Pitzer, 1991) and the Güntelberg equation (Stumm, 1996). The authors discuss an equation proposed by Samson et al. (1999), said to be suitable for calculating of activity effects in ionic solutions of high concentration:

$$\ln \gamma_i = \frac{A z_i^2 \sqrt{I}}{1 + a_i B \sqrt{I}} + \frac{[4.7 \cdot 10^{-5} \cdot I + 0.2] A z_i^2 I}{\sqrt{1000}} \quad (2.39)$$

$$I = \frac{1}{2} \sum_1^N z_i^2 \cdot c_i; \quad A = \frac{\sqrt{2F^2 e_0}}{8\pi (\varepsilon RT)^{3/2}}; \quad B = \sqrt{\frac{2F^2}{\varepsilon RT}} \quad (2.40)$$

where I = ion strength (mole/l); a_i = an adjustable parameter corresponding to the size of the ion, e.g. 3 (Å) for K^+ , OH^- , 4 (Å) for Na^+ and 6 (Å) for Ca^{2+} , (Stumm 1996).

Ignoring the diffusion caused by gradients in the chemical activity

$$\mathbf{F}_{iu} = -D_i \left(\text{grad } c_i + \frac{F}{RT} z_i c_i \text{ grad } E \right) \quad (2.41)$$

Gjörv et al. (1998) give the values for the diffusion coefficient D_i (or D_{CTH} as they call it in their work) for chloride diffusion in concrete as lying between 2.7 and $9.1 \cdot 10^{-12}$ m^2/s . Other researchers have found even lower values for concrete with very low w/c ratio (0.35-0.40).

In later work, Samson, Marchand and Beaudoin (1999), used the same equation as (2.38) but ignored the diffusion caused by gradients of chemical activity, $-D_i c_i \text{grad} \ln(\gamma_i)$. The variables of interest were also averaged for a representative elementary volume (REV). The averaging method is said to not require any detailed knowledge of the inner structure of the material and the variables included are ones said to be easily measured in practice. The equations (2.33) and (2.38) were rewritten for saturated concrete as

$$\frac{\partial(\bar{c}_i^L)}{\partial t} = \text{div} \left(-D_i \text{grad}(\bar{c}_i^L) - D_i \frac{F z_i}{RT} \bar{c}_i^L \text{grad}(\bar{E}^L) \right) \quad (2.42)$$

the electric field in equation (2.36) being rewritten as

$$\text{div}(W \tau \text{grad}(\bar{E}^L)) + W \frac{F}{\varepsilon} \sum_1^N z_i \bar{c}_i^L = 0 \quad (2.43)$$

where \bar{c}_i^L = average concentration of species i in the liquid phase in a representative elementary volume (REV) (mole/m^3); \bar{E}^L = average electric potential in the liquid phase in a representative elementary volume (REV) (V); and τ = reduction tensor for the tortuosity of the pore system.

Delagrave, Gérard and Marchand (1997) modelled the calcium leaching mechanisms in hydrated cement pastes, assuming (i) the cement to be fully hydrated, (ii) all the solid phases to be in thermodynamic equilibrium, (iii) the dissolving time to be short compared with the transport times, (iv) the system to be saturated, and (v) conditions to be isothermal. The modelling starts with use of the same equation (2.31) as in Marchand et al. (1999). However, they omit the second term $\partial c_{i(s)}/\partial t$ on the right, saying, “*the amount of calcium ion initially in solution is very small in comparison with the amount dissolved by the calcium-bearing hydrates during the leaching process*” and rewrite (2.31) to

$$\frac{\partial c_{Ca(s)}}{\partial c_{Ca^{2+}}} \cdot \frac{\partial c_{Ca^{2+}}}{\partial t} = \text{div}(D_{Ca^{2+}} \text{grad } c_{Ca^{2+}}) \quad (2.44)$$

The first part of the first term on left, $\partial c_{Ca(s)}/\partial c_{Ca}$ is the curve for the equilibrium between Ca^{2+} in the pore solution and the Ca/Si ratio in the solid phase, as shown in Figure 2.25. It is calculated use a complex relationship

$$c_{Ca(s)} = a - b \cdot x^2 + c \cdot x - \left[\frac{e}{1 + \left(\frac{c_{Ca}}{x_2} \right)^N} + \frac{f}{1 + \left(\frac{c_{Ca}}{x_1} \right)^M} \right] \quad (2.45)$$

$$e = S_{por}; \quad f = 0.565(S_{tot} - S_{por}); \quad b = (S_{tot} - S_{por} - f)/400; \quad c = (S_{tot} - S_{por} - f)/20 + 20b; \quad a = S_{por} + b$$

where c_{ca} = concentration of Ca in the pore solution (mmole/l); $c_{Ca(s)}$ = concentration of Ca in the solid phase (mmole/l); S_{por} = molar fraction of Portlandite (mmole/l); S_{tot} = molar fraction of total calcium in the hydrated cement paste (mmole/l); x_1 = average position of the dissolution front of Portlandite (at a calcium concentration of 20 mmole/l); x_2 = average position of the dissolution front of C-S-H (at a calcium concentration of 2 mmole/l); N = constant (70 to 100); and M = constant (5).

As in Samson et al. (1999), and Delagrave et al. (1997), the authors only consider the diffusivity due to concentration gradients and ignore gradients of local chemical activities and local electrical potentials.

The pore system is assumed to become more open when the solid material is leached away. The authors assume diffusivity to increase in the manner described by the equation

$$D_s = D_{s0} \left(\frac{D_L}{D_{s0}} \right)^{\frac{\beta V_{por}^d + \alpha V^d}{V_{por}^e + V^i}} \quad (2.46)$$

$$\alpha = 1 + (1 - \beta) \cdot V_{por}^i / V^i \quad (2.47)$$

where D_s = diffusion coefficient of the solid at any given time (m^2/s); D_{s0} = initial diffusion coefficient (m^2/s); D_L = diffusion coefficient of the totally degraded solid at the end of the calcium-leaching process (m^2/s); V_{por}^d = volume fraction of the Portlandite (m^3/m^3); V^d = volume fraction of the hydrates other than Portlandite (m^3/m^3); V^i = volume fraction of the hydrates calculated by subtracting the volume occupied by the Portlandite and the SiO_2 fraction from the total volume of hydrates in a fully hydrated system (m^3/m^3); β = an empirical coefficient, mainly to account for the effect of the dissolution of calcium hydrates on the diffusion properties of the material.

A higher β value results in a more open pore network, making it easier for ions to move. The authors claim there to be close agreement with the test results, the only parameter needing to be determined in the test being β .

Adenot and Richet (1997) developed a Finite Difference model of the chemical degradation of cement paste, DIFFUZON. The modelling starts with equation (2.33). Like Samson et al. (1999), and Delagrave et al. (1997), however, they consider only diffusivity due to concentration gradients and ignore gradients of local chemical activities, as well as local electrical potentials. Figure 2.29, shows the authors' calculations of the residual Ca and Si content in an OPC paste in which $w/c=0.4$, after degradation for 3 months in essentially deionised water at pH 7. They claim there to be close agreement with experimental results. In the part of the paste nearest to pure water, only silica gel remained. The other compounds leached away by diffusion. Deeper in the specimen, greater amounts of the original hydration compounds were left and larger

amounts of Ca were found in the hydration products. The rate at which the degradation front moved into the material depended not only on the solubility of the hydrates but also on the diffusivity of the ionic species (Gérard, Torrenti, Adenot 1998).

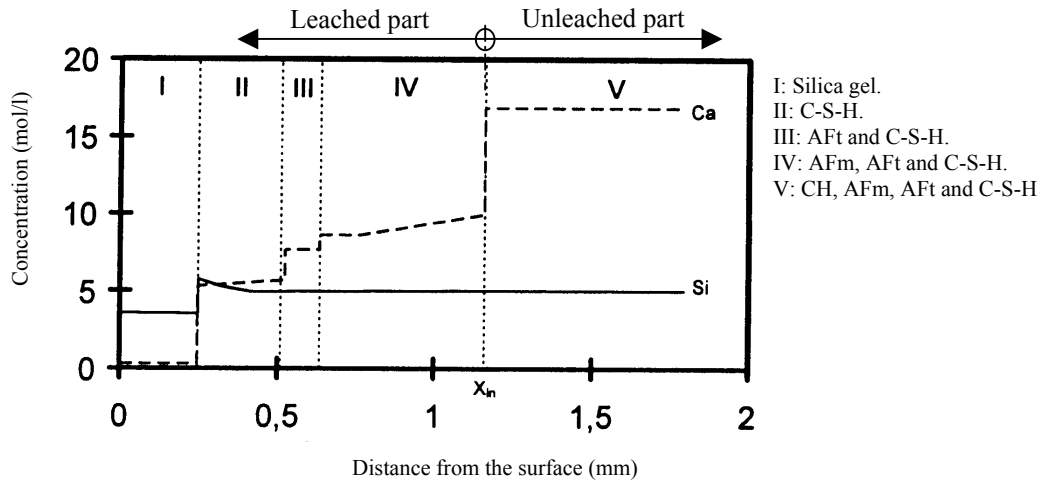


Figure 2.29 Calculated solid phase profiles of calcium, silicon, aluminium and sulphate in a specimen consisting of OPC paste in which w/c 0.4, after 3 months of degradation in essentially deionised water at pH 7 (Adenot and Richet, 1997).

Mainguy et al. (2000) claimed that the leaching of all types of cement-based material in stagnant water can be predicted by the mass balance of calcium alone:

$$\frac{\partial(P \cdot c_i)}{\partial t} = \frac{\partial c_s}{\partial t} - \text{div}[D_e \cdot \text{grad}(c_i)] \quad (2.48)$$

where P = porosity (m^3/m^3); c_i = concentration of calcium in the pore solution (mole/m^3); c_s = calcium concentration in the solid phase; and $\delta c_s/\delta t$ = dissolving reaction of calcium from the solid phase with the pore solution. The diffusion coefficient D_e (m^2/s) is assumed on the basis of the empirical relationship, to be

$$D_e = e^{(9.95 \cdot P - 29.08)} \quad (2.49)$$

The experimental results and the empirical equation (2.49) are shown in Figure 2.30.

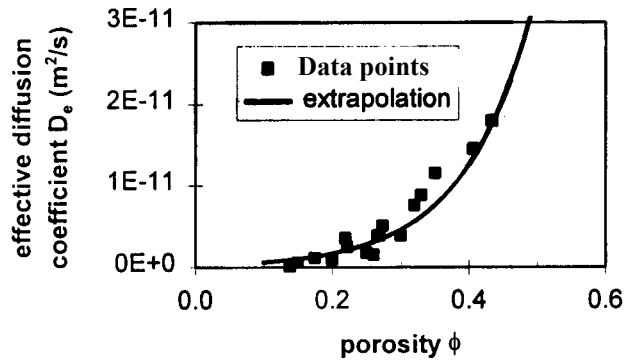


Figure 2.30 Experimental results and extrapolation of the relation between the effective diffusion coefficient and porosity (Mainguy et al. 2000).

Garboczi and Bentz (1996) modelled the diffusivity of ions in a pore system of cement paste for different degree of porosity as based on the degree of hydration, comparing the calculated value with the diffusivity in free water, see Figure 2.31. Although the authors denote the porosity as capillary porosity, using porosity values of 0.34 for a w/c ratio of 0.45 and 0.45 for a w/c ratio of 0.60, one must conclude that they instead mean either the total porosity $(w/c - 0.19\alpha)/(0.32 + w/c)$ or possibly the capillary porosity as a fraction of the total porosity, i.e. $(P_{cap})_p/P_p$. (For w/c ratio of 0.45, the capillary porosity based on the Powers model is: $(P_{cap})_p = (0.45 - 0.39 \cdot 0.9)/(0.32 + 0.45) = 0.13$ and for w/c ratio of 0.6 the capillary porosity is $(P_{cap})_p = 0.27$.) The authors describe their results by the equation

$$D_{eff}/D_f = 0.001 + 0.07 * P_p^2 + H(P_p - 0.18) * 1.8 * (P_p - 0.18)^2 \quad (2.50)$$

where D_{eff} = calculated effective diffusivity (m^2/s); D_f = free water diffusivity (m^2/s); P_p = total porosity of the paste before leaching = $(w/c - 0.39\alpha)/(0.32 + w/c)$ (m^3/m^3); and $H(P_p - 0.18) = 0$ for $P_p < 0.18$ and = 1 for $P_p > 0.18$, where 0.18 is the percolation threshold, based on Bentz and Garboczi (1992), involving an unbroken path from one side of the system to the other appearing for the first time.

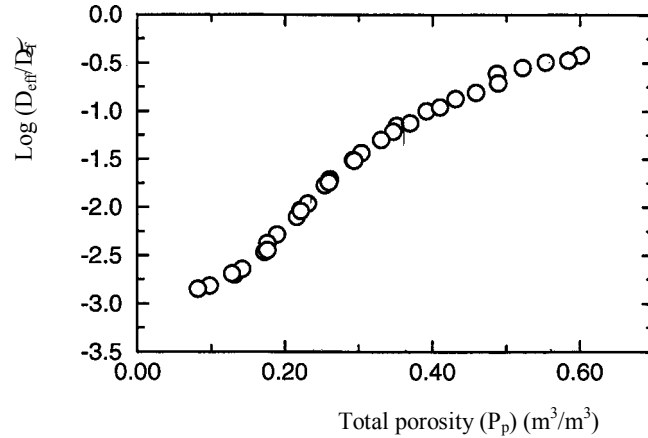


Figure 2.31 Calculated data for the diffusivity of cement pastes, normalized by the free water diffusivity, as a function of the total porosity. Although the from Garboczi and Bentz (1996) data are used the porosity is denoted here as total porosity P_p instead of capillary porosity P_{cap} , as it is in the reference.

Eijk, Brouwers (1998) used the leached capillary porosity instead:

$$D/D_f = 0.0025 - 0.07 * P_p^2 - H(P_p - 0.18) * 1.8 * (P_p - 0.18)^2 + 0.14 P_{cap}^2 + H(P_{cap} - 0.16) * 3.6 * (P_{cap} - 0.16)^2 \quad (2.51)$$

where P_{cap} = capillary porosity of the paste after leaching (m^3/m^3).

2.4.7 Convection of dissolved ions

Convection of ions means that there is a velocity field in which the ions are conveyed. In the case of leaching in concrete subjected to water pressure on one side, the velocity field is the flux of water through the concrete. A mathematical model of the convection of ions in a pore solution is provided by the term $\mathbf{v}_w \cdot \nabla c_i$ in the mass balance

$$\frac{\partial c_i}{\partial t} + \mathbf{v}_w \cdot \nabla c_i + \nabla \cdot (k_i \nabla c_i) - \hat{c}_i = 0 \quad (2.52)$$

where c_i = concentration of ions in the pore solution ($mole/m^3$); \mathbf{v}_w = velocity field in water (m/s); k_i = diffusion coefficient (m^2/s); and \hat{c}_i = supply or sink of ions ($mole/m^3/s$).

2.5 Various factors influencing leaching

2.5.1 Effects of autogenous healing in cracks and self-sealing of concrete

Autogenous healing takes place in cracks, or on the downstream surfaces of the concrete that are exposed to $CO_2(g)$ whereas self-sealing effects take place in “homogenous” concrete not exposed to $CO_2(g)$ (Nycander, 1954, Hearn 1997). Both phenomenons will lead to a gradual reduction in the rate of leaching.

Autogenous healing in cracks:

(Edvardsen 1996, 1999) found there to be a number of different chemical, physical and mechanical causes of autogenous healing and of reduction in water flow in cracks:

- The main cause of self-healing was found to be the formation of CaCO_3 that came from reactions between dissolved $\text{Ca}(\text{OH})_2$ and atmospheric CO_2 . The growth of CaCO_3 decreased when the crack width increased, through the formation of mobile cracks and an increase in water pressure. It was possible to show the occurrence of calcite formation in all the cracks tested, however, also in cracks of large width ($w = 0.30$ mm), in the case of large changes in width of the cracks ($\Delta w = 50\%$), or of high water pressure ($p = 10$ m of water).
- Swelling and hydration of the cement paste was of small importance for leaching;
- Blocking of the flow path by impurities in the water and blocking by concrete particles breaking loose from the surface of the crack were of small importance.

Also Hearn (1992) found the dissolution of $\text{Ca}(\text{OH})_2$, and the formation of CaCO_3 together with CO_2 to be the most important causes of autogenous healing.

In Table 2.10 crack widths with ability to self-heal are shown, Edvardsen (1996).

Table 2.10 Recommendations by Edvardsen (1996) of the maximum crack widths for which autogenous healing in water-retaining structures with stationary or mobile cracks is possible.

| Pressure gradient (m/m) | Crack width (mm) | | |
|-------------------------|-------------------|----------------------|----------------------|
| | Stationary cracks | Mobile cracks | |
| | | $\Delta w \leq 10\%$ | $\Delta w \leq 50\%$ |
| ≤ 10 | 0.20 | 0.20 | 0.10 |
| ≤ 30 | 0.10 | 0.10 | 0.05 |

Figure 2.32 shows the healing rates for different crack widths and water pressures as found by Edvardsen (1996). The water flow recorded in tests decreased rapidly due to self-healing. The author reasoned that the first time that Ca^{2+} is taken directly from the crack surface, crystals of CaCO_3 can grow directly on the surface. Later, due to the increasing thickness of the layer of crystals on the surface, Ca^{2+} needs to diffuse through both the concrete and the crystal layer that has been formed. This slows down the further crystal growth and the rate of self-healing. The following circumstances favour calcite precipitation in a crack:

- Rising water temperatures;
- Rising pH values of the water;
- Falling partial pressures of CO_2 in the water.

The formation of calcite is favoured on walls (where the water velocity is higher) and at a certain distance downstream from the crack-opening where the concentration of Ca^{2+} and OH^- (higher pH) is higher.

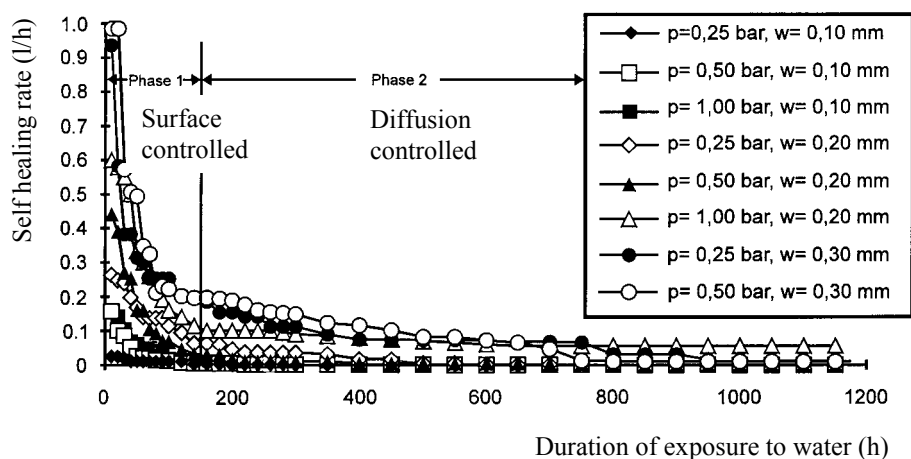


Figure 2.32 Healing rate for different crack widths and water pressures (Edwardsen 1996).

Self-sealing of concrete:

The following are different possible causes of internal self-sealing of concrete (Hearn 1998, Glanville 1931):

2. chemical interaction of water and hydrated or unhydrated cement paste
 - a) continued hydration of residual clinker
 - b) dissolution and deposition of soluble hydrates such as $\text{Ca}(\text{OH})_2$ along the flow path
 - c) carbonation of dissolved $\text{Ca}(\text{OH})_2$
4. swelling of hydrated cement paste due to water absorption
5. Presence of additives that can gradually bind lime, such as silica fume, fly ash, trass or slag.

Many researchers have attributed self-sealing to the hydration of previously not unreacted cement upon exposure to water (Hearn 1994). Hearn refers to data from a permeability test by Hearn (1992) concerning virgin concrete hydrated continuously for 26 years with or without having been oven-dried ($+105^\circ$) (Figure 3.26). “*Backscattered electron images show that virtually no un-hydrated cement remains in these specimens, yet they exhibit self-sealing behaviour*”. Instead of considering self-sealing to be due to continued hydration (there was no unhydrated cement left), Hearn speculates that, in the specific older specimens she examined, the self-sealing effect was probably due to the dissolution and redeposition of CH.

2.5.2 Effect of type of cement

The presence of a large amount of calcium in the concrete, especially in the form of $\text{Ca}(\text{OH})_2(\text{s})$, increases the amount of leaching. Any additives that can bind $\text{Ca}(\text{OH})_2$ therefore decrease the leaching rate (Sällström 1962 and 1964). On the other hand, when less $\text{Ca}(\text{OH})_2$ is left to form calcite and facilitate autogenous healing, and self-sealing become less effective in protecting the concrete against further leaching.

2.5.3 Effect of carbon dioxide

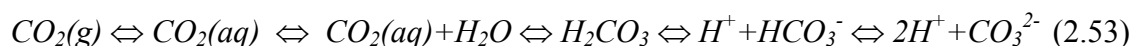
2.5.3:1 General

As mentioned above in sections 2.4.1 to 2.4.4, CO₂ in connections with the concrete has a great influence on the leaching of concrete. The two major effects of carbon dioxide on the leaching of concrete are the following:

- Carbonation of Ca(OH)₂. This is what happens in autogenous healing, when the pores of cracks in the concrete are more or less filled with CaCO₃. This slows down the leaching process due to both the flow of water and the solubility being decreased, see also section 2.5.1, Edvardsen (1996) and below.
- The amount of carbonic acid which is free to attack the concrete, see below.

2.5.3:2 Carbon dioxide in water

Carbon dioxide exists in different forms in water: as dissolved carbon dioxide CO₂(aq); as carbonic acid H₂CO₃, as bicarbonate HCO₃⁻ and as carbonate CO₃²⁻



The equilibrium constants are shown in Table 2.11. Further equilibrium constants are presented in Edvardsen (1996).

Table 2.11 Equilibrium constants in the system CaO-CO₂-H₂O (Taylor 1990 tab. 12.1).

| Reaction | Definition of K | Log K |
|--|--|--------|
| CO ₂ (g) ⇌ CO ₂ (aq) | [CO ₂]/p _{CO₂} | -1.42 |
| CO ₂ (aq)+H ₂ O ⇌ H ₂ CO ₃ | [H ₂ CO ₃]/[CO ₂ (aq)] | -2.8 |
| H ₂ CO ₃ ⇌ H ⁺ +HCO ₃ ⁻ | {H ⁺ }[HCO ₃ ⁻]/[H ₂ CO ₃] (K ₁) | -3.5 |
| HCO ₃ ⁻ ⇌ H ⁺ +CO ₃ ²⁻ | {H ⁺ }[CO ₃ ²⁻]/[HCO ₃ ⁻] (K ₂) | -10.25 |
| CaCO ₃ (calcite) ⇌ Ca ²⁺ +CO ₃ ²⁻ | [Ca ²⁺][CO ₃ ²⁻]/1 | -8.35 |

According to Halvorsen (1966), CO₂ is mainly found in water in the form of dissolved gas and only in small amount as carbonic acid, H₂CO₃. Only about 1 % of the CO₂ is in the form of carbonic acid, the rest being in gaseous form (Poulsen et al. 1985). For Table 2.11, the figure is 10^{-2.8}/10^{-1.42} = 0.04, 4% of the aquatic CO₂ being in the form of H₂CO₃.

Although the carbonic acid, bicarbonate and carbonate content make up the total content of carbon dioxide ΣCO₂ their proportions depend on the hydrogen ion concentration (Moskvina 1980):

$$[H_2CO_3] = [H^+] \cdot A \quad (2.54)$$

$$[HCO_3^-] = K_1 \cdot [H^+] \cdot A \quad (2.55)$$

$$[CO_3^{2-}] = K_1 \cdot K_2 \cdot A \quad (2.56)$$

$$A = \frac{\sum CO_2}{[H^+]^2 + K_1 \cdot [H^+] + K_1 \cdot K_2} \quad (2.57)$$

where ΣCO_2 = total carbonic acid (mole/l); K_1 , K_2 = see Table 2.11. The equations are also plotted in Figure 2.33. Atmospheric CO_2 contributes with about 0.6 mg/l of the carbon dioxide (or $CO_2(aq)$), leading to a reduction in the pH-value of the water. Biochemical processes in contact with the water or interaction with sedimentary calcareous rocks, however, can result in much higher concentrations.

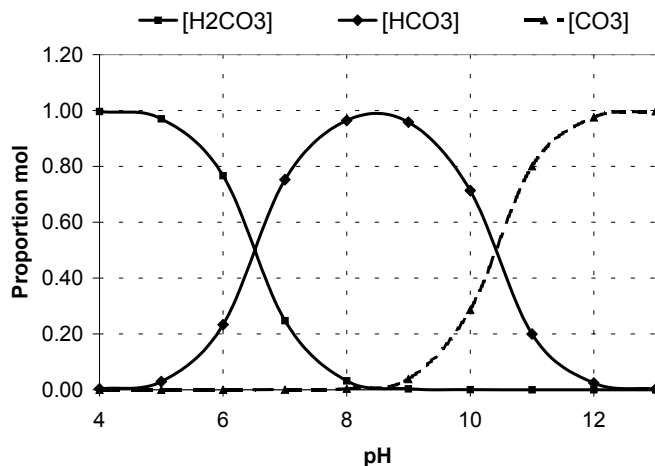


Figure 2.33 Equilibrium of CO_2 in water as calculated from equations (2.54) - (2.57).

Example 2.1

An example will be given of the estimation of the pH of pure water in contact with air. The partial pressure p of CO_2 at $+25^\circ C$ and 1.00 atm is $p = 3.04 \cdot 10^{-4}$ atm (Atkins & Jones 1997). Since the concentrations of H^+ are so small, the autoprotolysis of water must also be taken into account. According to Table 2.11, the concentration of H^+ (pH) is

$$\begin{aligned}
 [H^+]_1 + [H^+]_2 + [H^+]_{\text{autoprotolysis}} &= \\
 &= 1.83 \cdot 10^{-8} + 9.87 \cdot 10^{-10} + 10^{-7} = 1.19 \cdot 10^{-7} = 10^{-6.92} \text{ mole/l} \quad (2.58)
 \end{aligned}$$

or pH=6.92.

Table 2.12 Calculation of pH in pure water containing atmospheric CO_2 .

| | | |
|-------------|--|--|
| First step | $CO_2(g) \leftrightarrow CO_2(aq)$ | $[CO_2(aq)] = K \cdot p = 10^{-1.42} \cdot 3.04 \cdot 10^{-4} = 1.16 \cdot 10^{-5} \text{ mole/l}$ |
| Second step | $CO_2(aq) \leftrightarrow H_2CO_3$ | $a = [H_2CO_3] = K \cdot [CO_2(aq)] = 10^{-2.8} \cdot 1.16 \cdot 10^{-5} = 1.83 \cdot 10^{-8} \text{ mole/l}$ |
| Third step | $H_2CO_3 \leftrightarrow H^+ + HCO_3^-$ a-x x x | $ [H^+]_1 = x = -\frac{10^{-3.5}}{2} \pm \sqrt{\left(\left(\frac{10^{-3.5}}{2}\right)^2 - 1.83 \times 10^{-8} \cdot 10^{-3.5}\right)} $ $ = 1.83 \cdot 10^{-8} \text{ mole/l} $ |
| Fourth step | $HCO_3^- \leftrightarrow H^+ + CO_3^{2-}$ x-y y y | $ [H^+]_2 = y = -\frac{10^{-10.25}}{2} \pm \sqrt{\left(\left(\frac{10^{-10.25}}{2}\right)^2 - 1.83 \times 10^{-8} \cdot 10^{-10.25}\right)} $ $ = 9.87 \cdot 10^{-10} \text{ mole/l} $ |

2.5.3.3 Carbon dioxide in water containing calcium (such as in cement materials)

Carbon dioxide is found in water together with calcium in different forms, as both bound and free carbon dioxide. The bound carbon dioxide is divided into combined and semi-combined CO₂ (calcium carbonate CaCO₃ and calcium bicarbonate Ca(HCO₃)₂). The free carbon dioxide is divided into associated and aggressive CO₂ (CO₂ in H₂CO₃ or dissolved in water as a gas). The equilibrium of CO₂, Ca and water is



combined + associated (+aggressive) \Leftrightarrow semi-combined

The same balance applies to magnesium. Additional CO₂ disturbs the equation and drives it to the right, creating conditions for the dissolution of carbonates to form bicarbonates, the water then acquiring aggressive properties. An excess of CO₂ is thus referred to known as aggressive carbonic acid (Moskvin 1980). Water that is rich in bicarbonates can contain a large amount of dissolved CO₂, without its being aggressive.

Granhölm et al. (1934) presents a table indicating the aggressiveness of different types of water, as based on work concerning the leaching of concrete pipes.

Table 2.13 Different types of water and its aggressiveness toward concrete (Granhölm et al. 1934) .

| Type of water | Composition of the water | | Aggressiveness of the water |
|---------------|--------------------------|---|-----------------------------|
| | Hardness (mg CaO/l) | Aggressive carbonic acid (mg H ₂ CO ₃ /l) | |
| I | >20 | <15 | None |
| II | >20 | 15-40 | Insignificant |
| | 2-20 | <15 | |
| III | >20 | 40-90 | Substantial |
| | 2-20 | 15-40 | |
| | <2 | <15 | |
| IV | >20 | >90 | Large |
| | 2-20 | >40 | |
| | <2 | >15 | |

Carbon dioxide in water dissolves calcium carbonate or calcium hydroxide to form calcium bicarbonate:

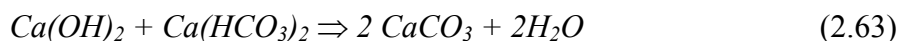


The total corrosion of concrete due to carbonic acid, expressible as the sum of the two equations (2.60) and (2.61), can be written

$$k = k_1 + k_2 \quad (2.62)$$

where k = total corrosion of concrete by carbonic acid (-); k_1 = corrosion of concrete according to equation (2.60); and k_2 = corrosion of concrete according to equation (2.61).

Calcium bicarbonate can react with calcium hydroxide to form calcium carbonate:



It is difficult to calculate the exact equilibrium conditions for these processes in water, since the various equilibrium constants, dissociation constants and solubility products depend on the temperature and on the ion concentration.

One should recall that other ions in the pore solution influence the equilibrium of carbon and lime in water both by common ion effects and by their changing the ion strengths. *”The presence of ions which do not directly participate in the reaction but, through increasing the ionic strength of the solution, accelerate it, changes the equilibrium in the system and promotes the dissolution of yet a larger quantity of carbonate. (...) Sometimes, with the same content of bicarbonate, carbonate and H₂CO₃ in the solution, even the direction of the reaction changes as the ionic strength of the solution increases. In a solution with certain proportions of [HCO₃⁻], [CO₃²⁻], [Ca²⁺] and [H₂CO₃], bicarbonates spontaneously decomposed (owing to lack of equilibrium carbonic acid) and calcium carbonate precipitated. The solution in this case was not aggressive to concrete. In a similar solution but with 3 % NaCl a reverse reaction proceeded: solid calcium carbonate dissolved. The solution then exhibited distinct aggressive properties towards concrete. Therefore, the presence of NaCl alters not only quantitatively but also qualitatively the interaction of the aqueous medium with concrete”* (Moskvin 1980).

A mass transfer model is presented in Wallin (1988).

The effects of aqueous CO₂ on concrete can be summarised as follows (Nycander 1954):

- If there is an excess of CO₂ in the water (aggressive CO₂), the water will be aggressive towards the concrete and dissolve lime from it.
- If the water is hard and contains much bicarbonate, it is not aggressive. Bicarbonate can react in an opposite way with the lime in the concrete to form calcium carbonate, which has the ability to seal the concrete against further attacks.

2.5.4 Effect of temperature

Increasing the temperature increases the permeability of the water and the diffusion of ions. On the other hand, increasing the temperature also decreases the dissolution of CH (see section 2.4.5) although it increases the dissolution of other compounds (C-S-H, etc.) (Gérard et al. 1998).

2.6 Effects of leaching

2.6.1 Leaching effects on the permeability

According to Halvorsen (1966), Ruetters (1935) reported no increase in permeability for a degree of leaching as high as 30% of the initial lime. No other results on the effect of leaching on permeability have been found.

2.6.2 Leaching effects on the mechanical properties

Some authors have observed a total loss in strength when 50 % of the initial content of calcium has been leached from the concrete (Tremper 1931). There are other authors who, according to Granholm et al. (1934), consider concrete to be “destroyed” when 20

% (Sundius 1930) or 30 % (Westerberg 1933) of the total content of lime has been leached.

Ruettgers (1935) performed comprehensive percolation studies of homogenous, highly porous concrete. The connections he found between the content of lime (CaO) that had been leached and the compressive strength of the concrete are shown in Figure 2.34. Moskvin (1980) points out that since the results on which the figures in question are based had a wide scatter, they are not altogether reliable. Note that the relations given are for wet leached specimens as compared with dry unleached specimens. Since wet specimens can be assumed to be lower in strength than dry specimens, this can be one cause of the strength-reduction the data indicate. The strength of a wet specimen may increase by 10-15 % when it is allowed to dry (Möller et al. 1994), just as shown in the figure.

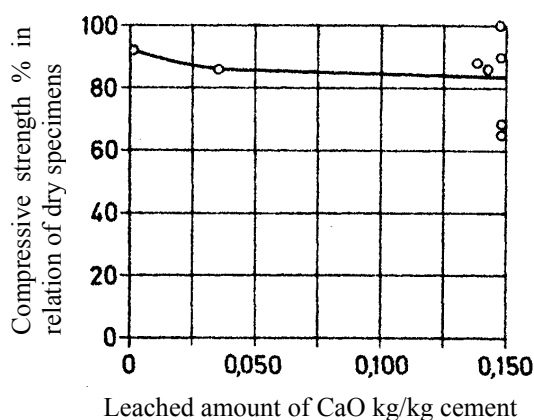


Figure 2.34 The effects of leaching on the compressive strength of concrete specimens through which water had been percolated (Ruettgers et al., 1935) as reported in Halvorsen (1966).

Mary (1937), as Halvorsen (1966) indicated, pointed out that the relation between the amount of water percolated and the reduction in compressive strength reported is only valid for concrete with a continuous pore system, and not when the water percolation is concentrated to cracks or surfaces.

Figure 2.35 shows results obtained by Ruettgers (1936), Tremper (1931), Terzaghi (1948), Takemoto (1959) and Sällström (1964). Those of Tremper and Terzaghi show a substantially higher reduction in strength than the results do that Ruettgers (1935) reported. One explanation of this which Terzaghi suggested is that both he and Tremper used water with a high content of aggressive CO_2 , whereas Ruettgers used water containing no carbonic acid. Terzaghi considered that lime may very well have been leached out through the pore spaces in the upstream part, but have re-crystallised as CaCO_3 further downstream. Tremper and Ruettgers only measured the lime that came from the specimens. One can note that since the total strength of the specimens was probably governed by their weakest link, in this case the leached upper part of the specimens, the measured leached ratio of CaO was too low in comparison with the measured strength. On the other hand, Meyers (1935), considers the “Denver City water” used in the Ruettgers et al. experiment to be a possible cause of salts depositing at the downstream side of the concrete. The two sets of values from Terzaghi (1948) plotted in Figure 2.35 are from two specimens only, and it is also not certain how much

of the reduction in strength that was found depended upon a combination of leaching and sulphate reactions, since both mechanisms were current. The reduction in strength that Sällström (1964) found in his experiment was also large. He used ordinary municipal tap water containing almost no aggressive carbon dioxide but fairly large amounts of bicarbonate as percolating test water. The explanation above of Terzaghi's result concerning the deposit of CaCO_3 in the downstream end may also hold in this case because of the possibility of reactions between bicarbonate and $\text{Ca}(\text{OH})_2$ occurring in the mortar.

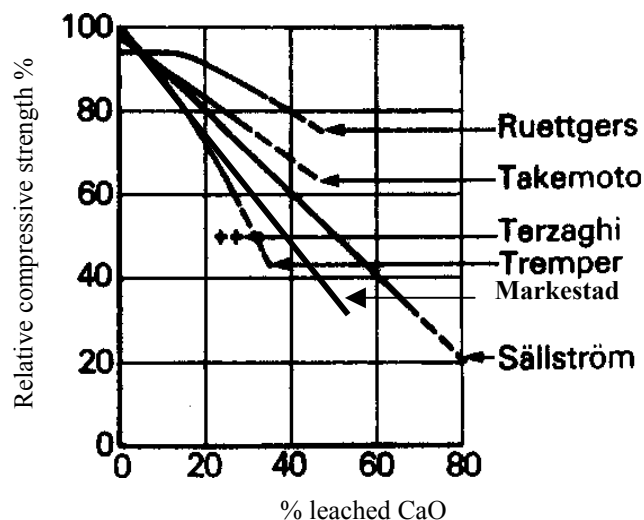


Figure 2.35 Relation between lime leaching and compressive strength. Results of different authors cited in Halvorsen (1966). The dashed lines indicate the extrapolations of results to have been carried out by the authors. The results that Markestad (1977) reported are also plotted.

According to Halvorsen (1966), Hallström (1933) considered $\text{Ca}(\text{OH})_2$ in the form of crystals to contribute to a large extent to the strength of the concrete. Both Mather (1950) and Terzaghi (1950) agree on the reduction in strength being due to the leaching of both free $\text{Ca}(\text{OH})_2$ -crystals and Ca in the cement gel. Terzaghi believes, on the other hand, that the main reduction in strength is caused by dissolution of the cement gel. In studying Figure 2.35, one can note that in some authors estimates the compressive strength is found to go down from the start, whereas in others the strength shows a flat part when the leaching of CaO begins (Figure 2.34). If the strength goes down at the start of leaching, one can conclude that free CH also contributes to the strength here. On the other hand, if the reduction in strength first starts after some of the CaO has been leached, one can conclude that free CH contributes to no appreciable extent to the load-bearing capacity. The tests conducted by Ruettgers et al. indicate there to first be a loss of strength after 10-15 % of the lime has been leached away, which corresponds to the total amount of CH in the specimens. According to Sällström (1964), his specimens of mortar containing LH-cement showed an almost linear decrease in compressive strength all the way, from the very start of testing.

Sällström (1964) showed that at a given leaching ratio mortar shows a larger reduction in strength when the cement includes trass or slag. On the other hand, this is

more than adequately compensated for by the lowering of the amount of leaching for cement with use of such additives.

Figure 2.36 shows measured values for the compressive strength of leached concrete which Markestad had presented. Water percolating through the concrete being found to leach the concrete.

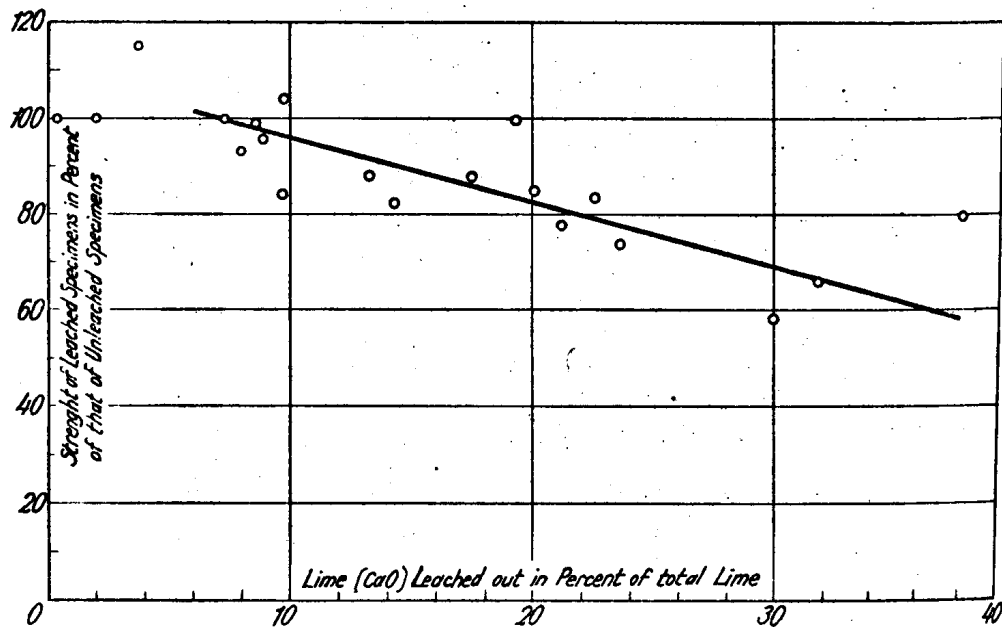


Figure 2.36 Relation between lime leaching and compressive strength (Markestad, 1977).

Carde et al. (1996) considered, on the basis of both modelling and experimental results, that removal of Ca from Portlandite ($\text{Ca}(\text{OH})_2$) increases the macro-porosity of the material, resulting in a decrease in strength, whereas removal of Ca from the C-S-H-gel leads primarily to an increase in microporosity, which has no very appreciable effect on the strength of the material. *“The dissolution of this calcium hydroxide is the essential parameter governing both decrease in strength and increase in porosity”*.

Mindess (2000) concludes: *“Calcium hydroxide appears to be about as strong as the C-S-H. However, because of its morphology at the cement-aggregate interface, it provides a plane of weakness along which cracks can propagate more easily, this providing the weak link in ordinary concrete”*.

2.6.3 Leaching effects on the internal water pressure

The dissolution of hydration products and their possible later precipitation further downstream can change the internal pore pressure. The pressure increases in the upstream part but decreases in the downstream part, leading to the risk of delamination or uplift of the concrete structure (Ruetters et al. 1935, Gruner 1967).

Ruetters et al. noted that water can flow through a dam along reinforcement bars, increasing the total water leakage. When the downstream face of a dam is exposed to air, the leached ions in the water can precipitate in the pores close to the face. This can transfer the water pressure as a whole to the concrete covering of this face, possibly resulting in delamination.

3 Water mobility in concrete of importance for leaching

3.1 Water flow in porous media

Pores are void spaces distributed through the material. They can be either *interconnected* or *non-interconnected* (Scheidegger 1960). Fluids can only percolate through the interconnected parts, or the *effective* pore space. The smaller the pores, the greater the effect of the pore walls on the hydrodynamic phenomena. The ratio of the volume of the pores as a whole to the total volume is called the *porosity*. If only the interconnected pores are taken in account, the resulting value is termed the *effective porosity*. Another well-defined geometrical measure applied to a porous medium is that of its *specific internal area*. Although it would be desirable to be able to find a geometric quantity for characterising the size of pores generally, they unfortunately dwindle back and forth, diverge and converge as well as differing markedly in scale, making them very difficult both to measure and to model.

3.2 Characteristics of water

The shape of a water molecule and bonding of two water molecules are shown in Figure 3.1.

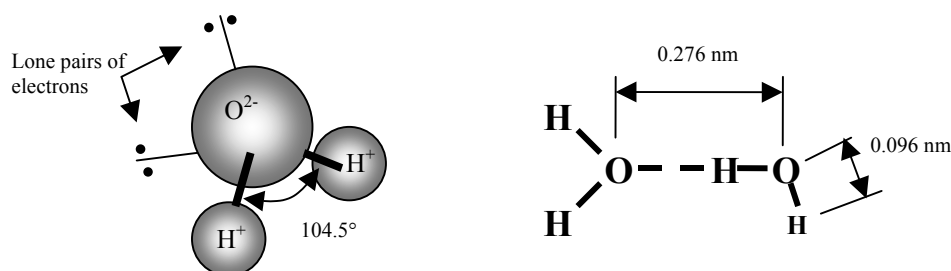


Figure 3.1 Structure of the water molecule and the hydrogen bond (Horn 1969)

Because of the fairly strong hydrogen bond between water molecules, water has a high boiling temperature, a low vapour pressure and a high viscosity. The strong dipole character of water molecules favours interactions between them and other polar molecules or ions. Examples of interactions between water molecules and other polar-bonded atoms are the wetting ability of material containing oxygen atoms or OH-groups (e.g. the capillary action within narrow pores) and the dissolution of hydration products in concrete.

3.3 Water in concrete

Concrete is an extremely fine porous material with a strong ability to bind water hygroscopically (Powers and Brownard, 1948). The gel pores in concrete have a size of $\approx 10^{-9}$ m, about 4 to 5 times that of a water molecule. Capillary pores have a size of less than 10^{-6} m. They can be filled with water by capillary condensation.

The water in concrete is usually assumed to be of three types: chemically bound water, adsorbed water and free water (Powers (1960)). At a relative humidity of less than 45%, the water molecules tend to be absorbed on the internal surfaces of the pores, the amount of water absorbed being proportional to the internal surface area. At a humidity of more than 40-45%, the amount of water a dry specimen takes up depends on it

porosity. Below a humidity of 40% the water tends to be held by adsorption, whereas over 45% it is mostly held by capillary condensation. At an RH of 100% all pores are basically filled with water. Hysteresis phenomena in porous materials involving both adsorption and desorption have been observed. This is attributed mostly to an *ink bottle effect*, in which the small capillaries remain filled during desorption, preventing the larger connecting ones from being properly emptied (Scheidegger 1960).

The water contained in concrete stems from different phases of construction and curing. For example,

$$W_{tot} = W_0 + W_{curing} - W_{hydr} + W_{forced} \quad (3.1)$$

where W_{tot} = total water; W_0 = mixing water; W_{curing} = water added during curing; W_{hydr} = chemically bounded water present during hydration; and W_{forced} = water forced into the concrete during its life cycle, e.g. by capillary suction or as a result of external water pressure being imposed.

3.4 Driving potentials for the transport of water in porous materials

Driving potentials causing water to flow have their ultimate origin in thermodynamic balances of energy and entropy. It can be illuminating to examine the energy balance equation so as to identify the basic driving forces involved.

$$dE = dq_h + dw_{mech} + dw_{gravitational} + dw_{kinetic} + dw_{chemical} + dw_{electrical} + dw_{surface} + others \quad (3.2)$$

where on the left side dE = change in energy (J), and where on the right side change in dq_h = changes in heat energy, such as caused by differences in temperature; dw_{mech} = changes in mechanical energy, such as caused by differences of the pressure or friction; $dw_{gravitational}$ = changes in gravitational energy level; $dw_{kinetic}$ = changes in kinetic energy (e.g. turbulence); $dw_{chemical}$ = changes in chemical energy levels, such as caused by concentration gradients in diffusion and in dissolving reactions as well as osmotic pressures gradients; $dw_{electrical}$ = changes in electrical potentials; and $dw_{surfaces}$ = changes in energy level attributed to surface phenomena (such as absorption and capillary suction).

Each of the different terms in equation (3.2) concerned with energy differences can be individual. In combination they can also be driving forces in the transport of water. A dam subjected to one-side hydraulic water pressure is rather dry a long time after the reservoir is filled with water. The water tends to first penetrate the dam by vapour diffusion. When the pore system becomes more filled with water, meniscus are formed in the pores. Water is now forced in by capillary suction. When the pores become even more filled with water, the water penetrates the dam through a combination of capillary suction and flux due to the external water overpressure applied to the upstream surface of the dam. On the downstream side of the dam, the concrete is in dynamic equilibrium with the atmosphere. Changes in the humidity of the air, as well as rain or sunshine, can change the diffusion and fixation of water on the outer surface of the dam. If there is a water table on the downstream surface, the water transport below a certain level may involve Darcian flow (flow in completely filled pores by over-pressure) all the way from the upstream to the downstream surface.

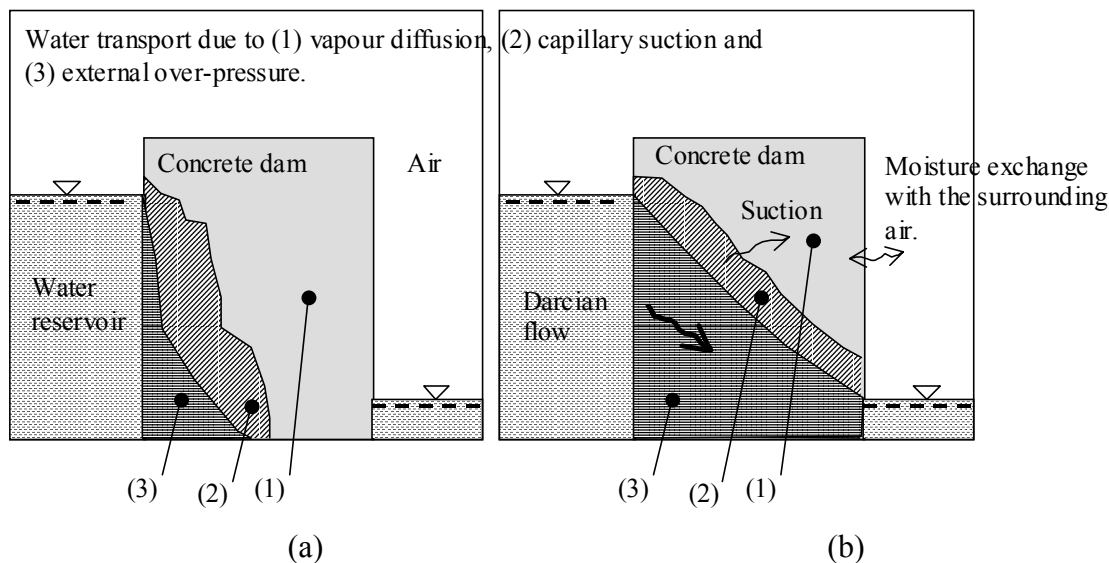


Figure 3.2 Driving potentials for the flow of water in a concrete dam exposed to water at the one side and either air or water at the other, where (a) shows the conditions found a relative short time after the reservoir has been filled and (b) the conditions long after the reservoir has been filled.

Most of the driving potentials are at least partly influenced by the degree of saturation.

Some of the driving potentials (such as the capillary potential) are partly related to the geometry of the interfaces between the different phases in the porous media involved.

3.5 Permeability

3.5.1 Introduction

The permeability of a porous medium, or how readily a fluid penetrates it, is regarded as the single most important property determining the durability of concrete.

The flow of water through concrete is the sum of all leakage of water through it, ranging from large-scale flow in large connected, and water-filled cracks and cavities to very low levels of vapour diffusion through the capillary pores. The flow channels involved can differ very much in shape and origin. During the lifetime of concrete, flow channels can be formed, changed and closed again. The greater the number of flow channels there are in concrete and the broader, less tortuous, smoother and more connected the flow channels are, the less the resistance is against water mobility and the greater the extent is to which water can be distributed.

“Percolation through concrete structures is of two kinds: that which passes through large openings (honeycombs, various imperfections of placement, cracks), which are by far the most important, and that which follows the capillary channels inherent in concrete generally conceived as homogenous and dense and which characterises and defines the technical term permeability of concrete. Considered in this limited sense, the permeability of concrete plays but a secondary role in the general problem of making structures water tight if one considers merely the total amount of water given passage. The study of this property is of importance only if one considers

with it the progressive destruction of concrete by percolating water and outside agents. As slow as it might be, percolating water dissolves considerable quantities of lime” (Mary 1935).

The transport of fluids in concrete occurs in pores or defects in the concrete. The amount of pores present in the cement paste phase is in on the order of 35-50% of the volume. In ordinary Swedish aggregate it represents approximately 0.5-1% of the volume. Within the concrete the porosity is on the order of 10-20 %. The flux of a fluid tends to occur where it can flow most easily, i.e. in large connected pores. In defect-free concrete, such pores consist of capillary pores and the porous transition layer around the aggregate. Defects in concrete, such as cracks, can have permeability many orders as high as that of the concrete itself, its level depending on the size of the cracks and on how connected they are within the concrete.

Water permeability is often used to denote a number of different mass transfer mechanisms. The diffusion of water moisture, the absorption or desorption of water on the pore walls, liquid flow due to capillary suction, and unsaturated or saturated liquid flow due to external pressure have all been referred to rather loosely in the literature as permeability.

Many investigations of permeability have been carried out during the last century. Comprehensive summaries of many such investigations have been presented by Halvorsen (1966), (1986) and Hearn (1992), for example. Most of the permeability tests performed concern the percolation of water in relation to different w/c ratios, degree of hydrations, curing conditions and aggregate distributions. Although many of these studies have used obviously *saturated* specimens for which moisture protection at the downstream end (Darcian flow) has been provided, for many others this have not been the case. Concrete can be unsaturated at the beginning of tests or it can become unsaturated due to self-dessication or to the downstream end not being located underwater. In some cases, the hydraulic head has been so slight that the flow of water has not been a true Darcian flow but has been due mostly to capillary suction or diffusion.

Transport phenomena in porous media are sometimes regarded (Van Brakel 1975) as involving two types of transport: capillary and non-capillary liquid transport. In the case of capillary transport, both the driving force and the transport coefficient are a function of the geometry of the pore space, whereas in other cases the transport coefficient alone is a function of the geometry.

The mobility of water through concrete is governed mainly by the size and shape of the flow channels within the concrete and the connections between them, on the humidity inside the concrete, and on the type of driving forces acting on the water.

The flow of water in a porous material can be characterised by the pushing potential present that forces water through the pores, and by the resistant forces that slow down the flow.

Hall (1994) divides the flow of liquids in cement materials into:

- Saturated single-phase flow: A considerable volume of scientific work has been done on permeability of this type (saturated conductivity) in cement materials. No systematic comparisons of the permeability of well-defined materials, or of the boundary conditions of different fluids at well-defined temperatures appear to have been made, however.

- Unsaturated single-phase flow: The author knows of little experimental work that has been done involving the analysis of mixed cases of absorption, diffusion, capillary suction and saturated flow due to overpressure.
- Flow of two miscible liquids: Most of the work here has been done on the diffusion of ions in cement materials, little work having been concerned with the convective flow of ions, apart from diffusion.
- Two-phase flow involving immiscible liquids: No experimental data on this is available.

The experimental and modelling work in the dissertation deals only with the mass transfer of water in a saturated pore system that is due to an external pressure, sometimes referred to as true Darcian permeability (Hearn 1992), see also the term *saturated single-phase flow* referred to above. Other types of water transfer are reviewed in this chapter as well.

Garboczi (1990) expresses the diffusivity of water in saturated cement material as

$$v_w = -k/\mu \cdot \nabla P \quad (3.3)$$

$$k = d_c^2 \cdot P \cdot r_w \quad (3.4)$$

where v_w = water velocity (m/s); k = specific permeability coefficient (m^2); μ = dynamic viscosity ($\text{N}\cdot\text{s}/\text{m}^2$); ∇P = pressure gradient (Pa/m); d_c = *critical pore diameter* representing the smallest pore diameter measured determining the connectivity of a fluid across a specimen; P = porosity (m^3/m^3); and r_w = a reduction parameter pertaining deviations of all types from free flow in straight tubes such as tortuosity, connectivity and intermolecular forces both between ions and molecules and between ions or molecules and the pore-walls. Compare equation (2.30) for ion flow.

The mobility of water through saturated concrete can be described by equation (3.5) below. The rate of accumulation (dV/dt) of water inside the concrete depends on the rate of water transport through the concrete ($k\nabla P$) and the mass supply of water inside the concrete (\hat{c}). A driving potential (∇P) arising from thermodynamic differences pushes or sucks water through the concrete, the flow resistance k hindering the flow of water. The driving potential can be vapour gradients, capillary suction, osmotic effects or hydraulic overpressure. The flow resistance k , for example, depends on the geometric shape of the pore system, on the humidity and on the temperature. The volume supply can be absorption or desorption on the internal walls of the pores, loss of water due to hydration, or the accumulation of water from dissolution processes in solid material.

$$\left(\frac{dV}{dt}\right)_i = k_{w,i} \cdot \nabla P_i - Q_w \quad (3.5)$$

where $(dV/dt)_i$ = accumulation of water due to a driving potential i (m^3/s); $k_{w,i}$ = flow resistance to the driving potential i (e.g. m^3/s); ∇P_i = driving potential i (e.g. m/m); and Q_w = loss or gain of water inside the concrete (m^3/s).

In most cases, the total flow would be a composite of various flow types, its being the sum of the individual types of flow (Wisnicki et al. 1969):

$$\frac{dV}{dt} = \sum_1^n \left(\frac{dV}{dt} \right)_i \quad (3.6)$$

In a porous material water moves from regions of higher to regions of lower energy level, in concrete dams the energy being essentially that due to gravitational influences and to pressure.

Permeability is strongly influenced by the polar nature of water molecules. Intermolecular forces between the water molecules and between these and the pore walls, for example, slow down the flow. Sometimes, the intermolecular forces increase the permeability, as in capillary suction, and sometimes the flux of water is stopped through its reacting chemically with various compounds, as when cement is hydrated.

The permeability of concrete depends on the permeability of each phase of the concrete (Wisnicki 1969, Fagerlund 1980, Lawrence 1982), (Hearn 1992), and thus on

- the permeability of the paste
- the permeability of the aggregate
- the permeability of the interfacial zone

The permeability of the concrete is generally higher the higher the permeability of the cement paste in the concrete. This is usually blamed on the interfacial zones between the aggregate and the cement paste, which are weak and relatively porous and are vulnerable to differential strains between the cement paste and the aggregate induced by drying shrinkage, thermal shrinkage and externally applied loads, such strains resulting in microcracks.

3.5.2 Permeability of cement paste

In cement paste which is free of defects (such as cracks), the degree of permeability depends on the number, size, shape and connectivity, as well as the RH of the pores. The greater the amount of mixing water available, the greater the extent is to which pores are formed during hydration. During the hydration process, the pores are filled to varying degrees with hydration products which lead to a decrease in porosity and connectivity thus to a drop in permeability (see Table 3.1).

Table 3.1 Reduction in the permeability of cement paste (w/c 0.7) as hydration progresses (Powers et al. 1954).

| Age (days) | Fresh | 5 | 6 | 8 | 13 | 24 | Ultimate |
|--------------------------------|------------|-------|-------|------|----|----|----------|
| Permeability (10^{-13} m/s) | 20 000 000 | 4 000 | 1 000 | 4000 | 50 | 10 | 6 |

Figure 3.3 presents results of a study by Powers et al. (1954) concerning Darcian permeability in cement paste that was very well hydrated ($\approx 93\%$). (The relation between the permeability coefficient k_w (m/s), which depends in the gradients of hydraulic head (m/m), and the permeability coefficient B (s), which depends on pressure gradients in Pa, can be expressed as $k_w = \rho_w \cdot B$.) As one can note, the permeability increases very rapidly when certain levels of the w/c ratio or of capillary porosity are reached. The fact that the relation appears to be about the same in both figures is not surprising, since in Powers structural model capillary porosity is proportional to the w/c ratio. The very rapid increase in permeability at a capillary porosity of about 30% is probably due in part to the interconnection between capillaries increasing and to the

tortuosity being less at this point. Another cause may be that the flow of water in a fictive flow channel is proportional to the fourth power of the radius, which results in a very rapid increase if a part of the increase in capillary porosity is due to an increase in radius. It seems clear that the permeability of cement paste is controlled by its capillary porosity.

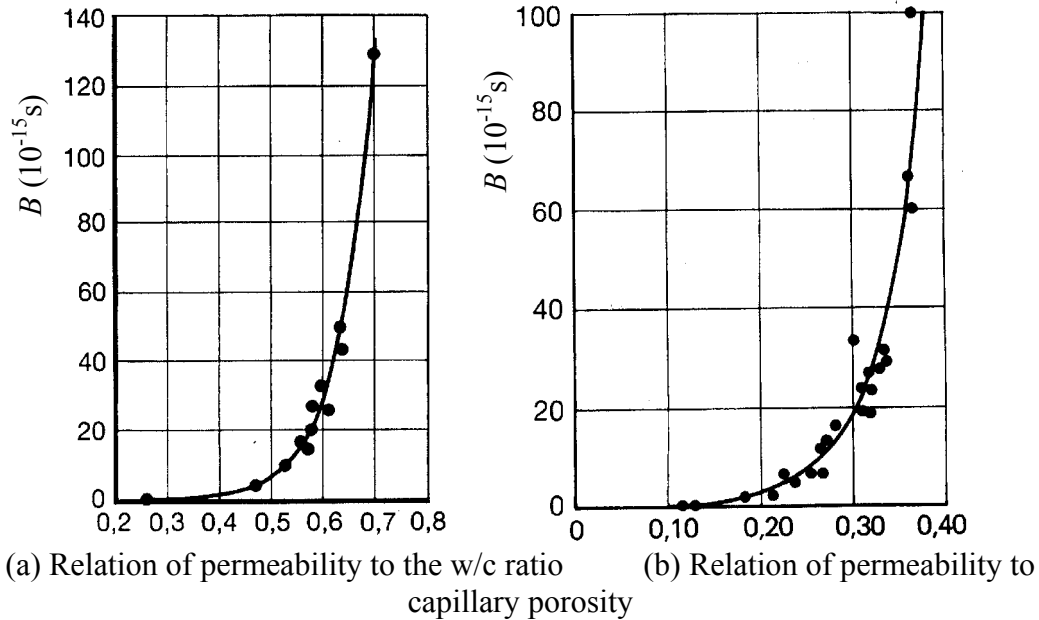


Figure 3.3 Water permeability of cement paste in relation to (a) the w/c ratio (Powers et al. 1954), and (b) capillary porosity (Powers et al. 1954). The figures are taken from Fagerlund (1980).

Figure 3.4 shows the permeability of hardened cement on the basis of data reported by various authors.

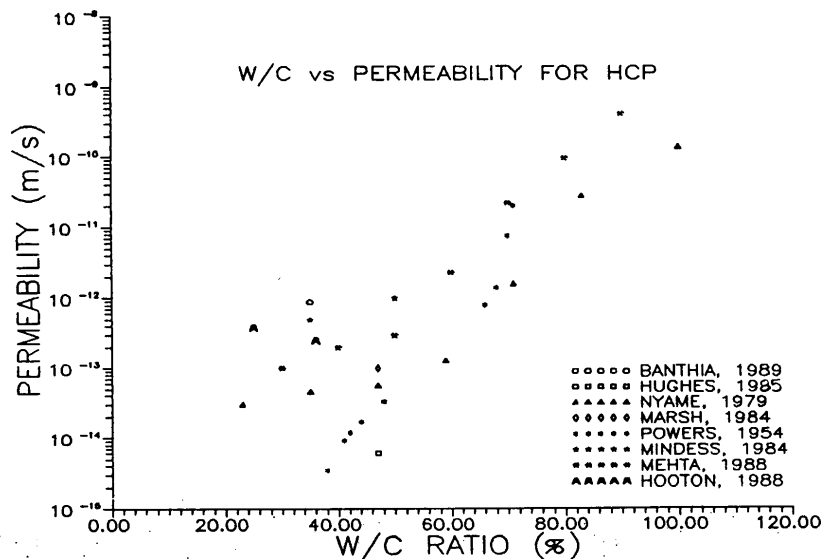


Figure 3.4 Correlation between the w/c-ratio and the water permeability of hardened cement paste as based on data reported in various studies (Hearn 1992 fig. 3.7).

Nyame and Illston (1980) conducted a study of paste containing OPC with a composition of 64% C_3S , 13% C_2S , 6.8% C_3A , 7.3% C_4AF and 3.6% $CaSO_4$, mixed with distilled water at w/c ratios of 0.23, 0.47, 0.71 and 1.0, and hydrated continuously in water for periods of up to 20 months. Conical specimens sealed with a silicone rubber jacket were used for tests of steady-state permeability. The majority of the specimens were exposed to water pressures of 7 to 14 MPa, after which the total porosity and the pore size distribution were measured by drying the specimens to $+105^\circ C$ and then performing a mercury intrusion porosimetry (MIP) assessment. The effects of hydration on permeability, of the w/c ratio on the cumulative and frequency pore-size distributions, and the relationship between total porosity and saturated permeability are shown in Figure 3.5 to Figure 3.7. The permeability values represent mean values based on 3 to 8 samples, for each w/c ratio the coefficients of variation in permeability typically being in excess of 50%. There was a small but significant decrease in permeability over the time elapsed since pressure was first applied. The authors adjudged this to be the result of continuous hydration and the clogging of pores, as well as constrictions that arose from the application of pressure.

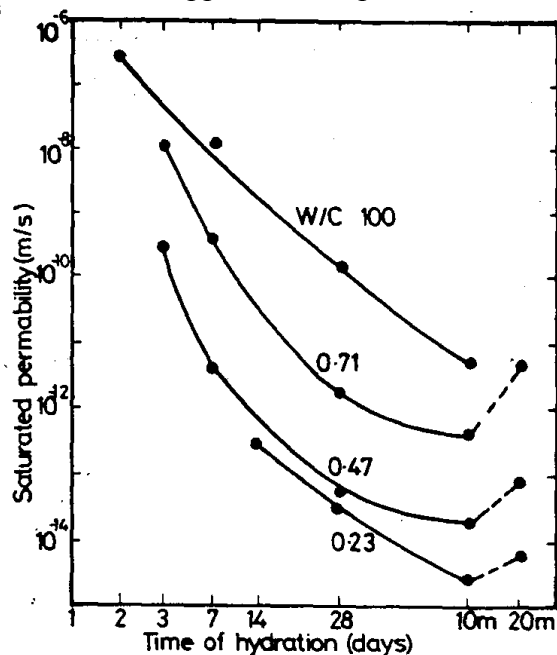


Figure 3.5 Effect of hydration on the water permeability of hardened cement pastes of differing w/c ratio (Nyame & Illston, 1980).

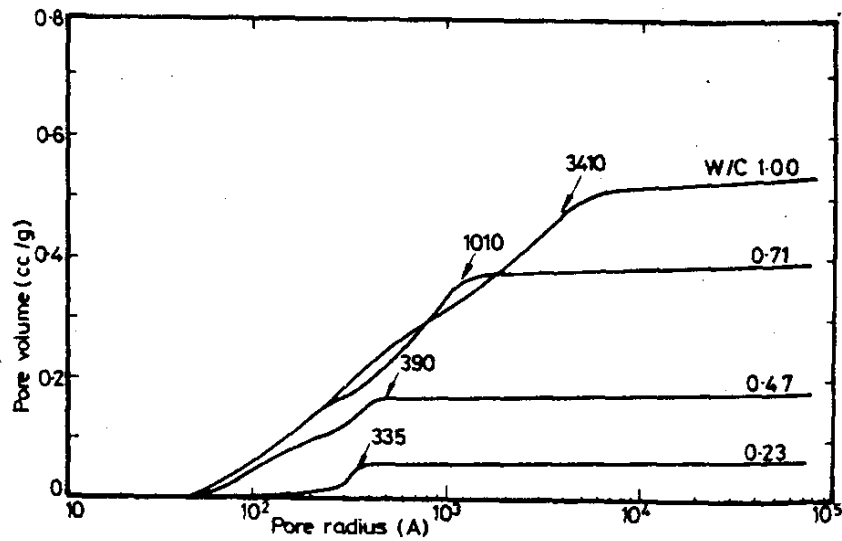


Figure 3.6 Effect of the w/c ratio on the cumulative pore size distribution of hep kept in water for 20 days (Nyame & Illston, 1980), as measured by mercury intrusion porosimetry.

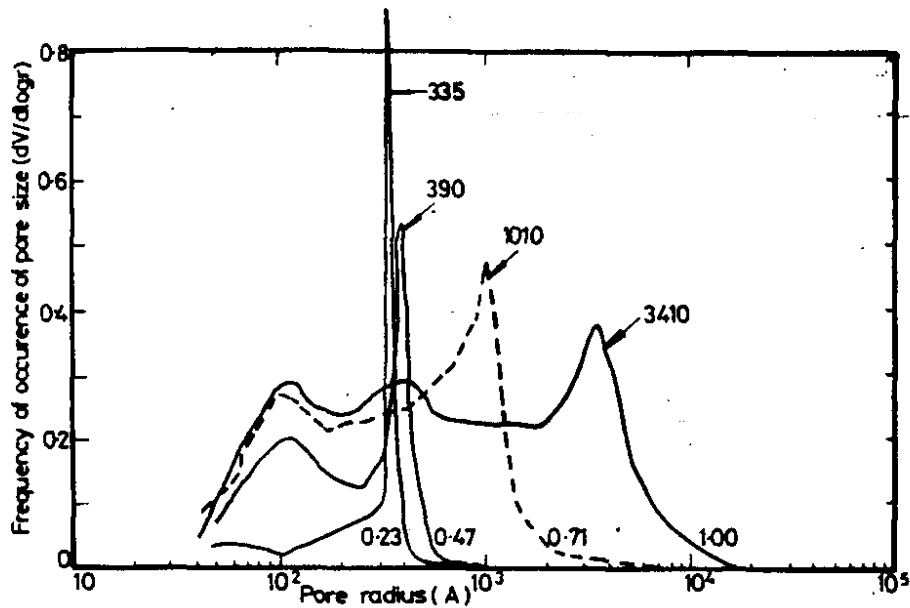


Figure 3.7 Effects of the w/c ratio on differential pore size distributions of hardened cement paste kept in water for 20 days (Nyamer & Illston, 1980).

Hooton (1986) investigated the permeability of various cement pastes. The pastes were mixed under vacuum and were cast in a cylindrical steel mould. The cylinders of paste obtained were then sliced into 40-mm disks. The disks were saturated with water under vacuum for 24 hours. It is uncertain whether the disks were also dried prior to the vacuum saturation. De-aired and deionised water was applied under a pressure of 172 kPa to specimens 7 days old and under a pressure of 690 kPa to older specimens. The permeability coefficients of the pastes are shown in Figure 3.8. The average coefficient

of variation for the permeability results was calculated based on the basis of 79 sets of 3-replicate tests to be 51.9%.

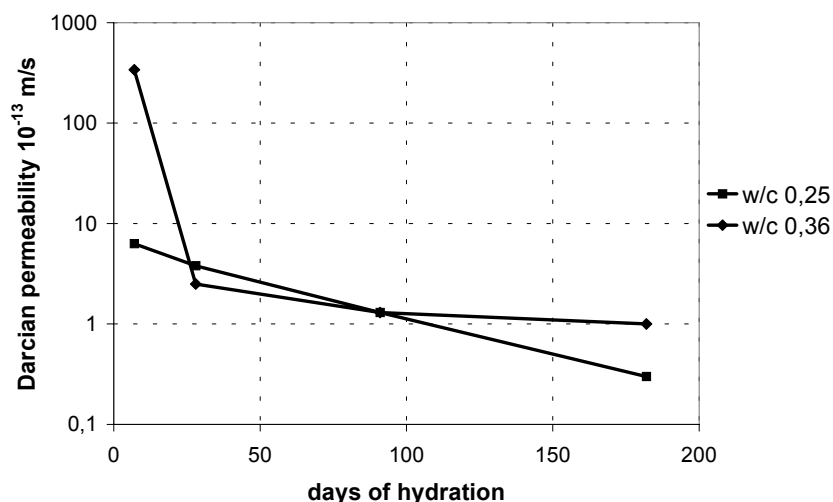


Figure 3.8 Permeability (10^{-13} s) of cement paste in relation to the w/c ratio and to degree of hydration prior to the permeability test (Hooton 1986). “Darcian” permeability = permeability calculated on the basis of Darcy’s law.

3.5.3 Permeability of aggregate

Despite its generally low porosity (below 3%), aggregate tends to have about the same level of permeability as cement paste (Powers 1958, Mehta 1986), see Table 3.2. This can be explained by the difference in typical size between the capillary pores in the paste (10 to 100 nm) and in aggregate (larger than 10 μm in average) (Mehta 1986).

Table 3.2 Comparison of the permeability of rocks and of cement paste (Powers 1958).

| Type of rock | Permeability (m/s) | W/c ratio of mature cement paste of the same permeability |
|----------------|----------------------------|---|
| Quartz diorite | $8.24 \cdot 10^{-14}$ | 0.42 |
| Marble | $2.39-57.7 \cdot 10^{-13}$ | 0.48-0.66 |
| Granite | $5.35-15.6 \cdot 10^{-11}$ | 0.70-0.71 |
| Sandstone | $1.23 \cdot 10^{-10}$ | 0.71 |

3.5.4 The permeability of concrete

Although the reduction in flow area (when the porosity is lower for the aggregate than for the cement paste), segmenting of the flow channels and lengthening of the effective flow channels suggest that the permeability of concrete should be less that of cement paste (Hearn 1992), the permeability of concrete is in fact about 100 times as high as that of the corresponding cement paste (Young 1988). The major explanation for this is that the addition of aggregate produces a porous *interfacial zone* between the aggregate and the paste and that microcracks are formed there during hydration. (Mehta, 1986). The permeability of concrete (and cement paste) on the basis of different studies is shown in Figure 3.9, Figure 3.10 and Figure 3.11.

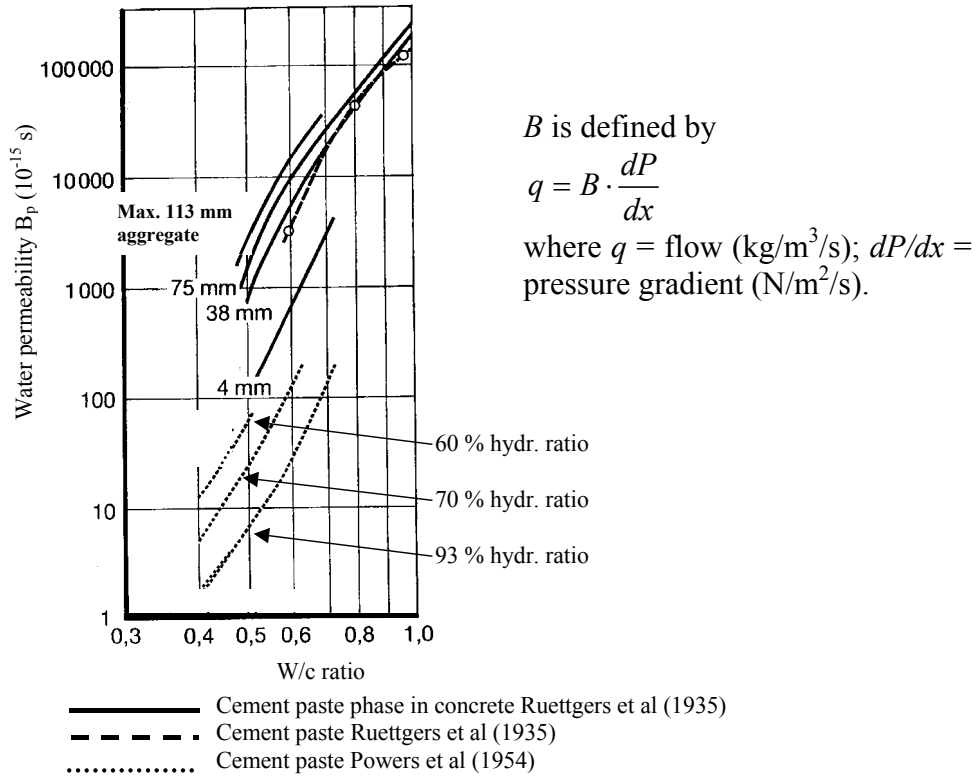


Figure 3.9 Permeability to water of cement paste for the various cement pastes phase in concrete (presented in Fagerlund 1980).

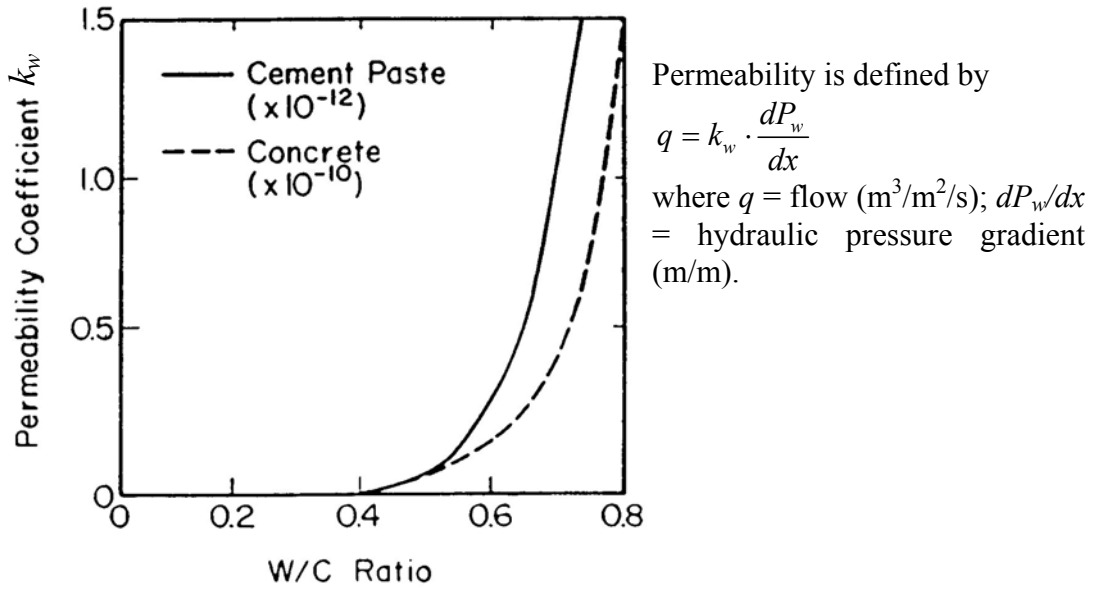


Figure 3.10 Water permeability for cement paste and for concrete (Young 1988).

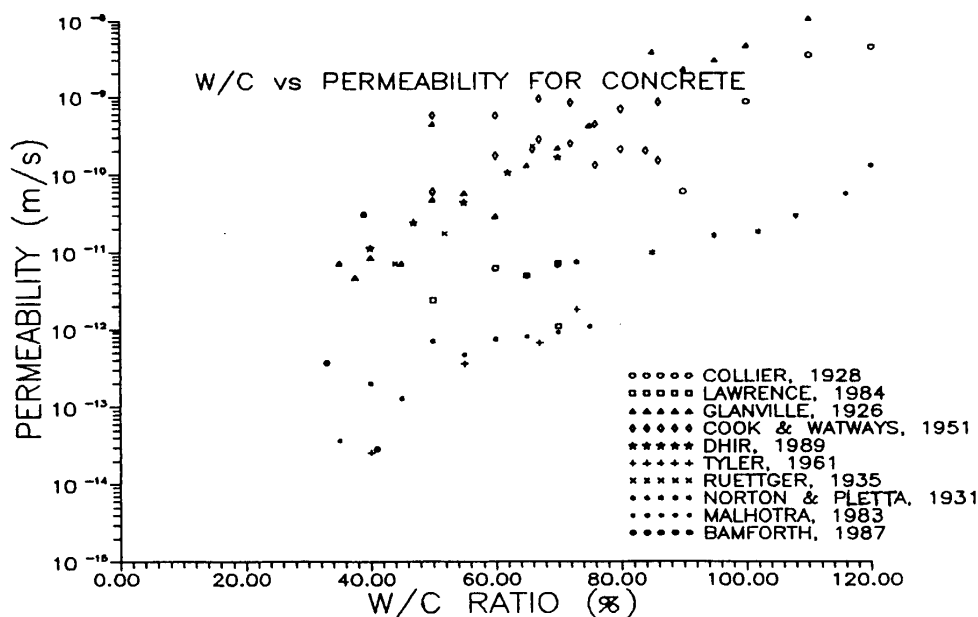


Figure 3.11 Correlation between the w/c-ratio and the permeability of concrete on the basis of data from different studies (Hearn, 1992).

3.5.5 The permeability of the interfacial zone

The permeability of the interfacial zone is governed mainly by

- The pore size distribution within the zone.
- The crystals within the zone (mainly $\text{Ca}(\text{OH})_2$).
- Microcracks within the zone.

There are no direct measurement of the permeability of the interfacial zone.

3.6 Factors influencing the permeability of concrete to water

3.6.1 General

It can be said generally that all factors that enlarge, connect or straighten existing flow channels or create new flow channels increase the permeability of the concrete. Since the flow of water can be said to be approximately proportional to the pore diameter raised approximately to the power of 4 and to crack thickness raised raised approximately to the power of 3, the flow obviously increases rapidly as pores and cracks become wider and more connected. The following factors influence the permeability of concrete (cf. McMillan & Lyse 1930, Ruettgers 1935, Mary 1935, Mather & Callan 1950, Nycander 1954, Nilsson 1994):

- 1) Cracks or cavities
- 2) The internal humidity
- 3) Curing conditions
- 4) The w/c ratio
- 5) The degree of hydration
- 6) The presence of air-filled pores
- 7) The pore-size distribution.

- 8) The type, size and amount of the aggregate
- 9) The pressure gradient applied (although not for Darcian flow)
- 10) The type of cement
- 11) Interactions between the water and the solid material in the concrete (e.g. leaching, self-sealing and autogenous healing)
- 12) The mixing-and-placing properties of the fresh concrete, such as its coherency properties, consistency, stability and bleeding
- 13) Flow channels along the reinforcement bars due to water separation and to settlement of the concrete mass
- 14) The presence of substances clogging the pore system
- 15) The viscosity of the fluid
- 16) The ionic strength in the pore solution
- 17) The stresses to which the structure is subjected
- 18) The shape and dimensions of the global structure

A further factor influencing the permeability, in the case of thick, concrete dams is:

- 19) The depositing of material inside the dam

3.6.2 Cracks or cavities

Microcracks can be formed due to various factors: shrinkage during the cooling period after casting, shrinkage due to drying, deflection due to changes in temperature and elastic strain and creep due to loads. The cracks are found mainly in the interfacial zone, but are found in the paste as well. Microcracks are always larger than capillary pores. They propagate from one discontinuity to another, creating more or less continuous flow channels throughout the cement matrix (Hearn 1992). The curing period is particularly important, since drying and cooling produce large variations in stress in the concrete when it has not yet obtained any large degree of strength. The sooner the water curing of concrete starts, the more quickly the concrete gains in strength and the smaller the stresses due to differences in temperature and moisture are. In dams that are thick, cracks are easily formed due to large temperature differences during production, unless actions (such as cooling) are undertaken to prevent cracks from being formed.

Leakage through a crack is usually quantified as (Edvardsen 1996)

$$q_{w,crack} = \alpha \frac{w^3 \cdot \Delta P}{\mu \cdot \Delta x} \cdot L \quad (3.7)$$

where $q_{w,crack}$ = leakage of water through the crack (m^3/s); α = “surface roughness factor”, generally about 0.01-0.2; w = crack width (m); $\Delta P/\Delta x$ = pressure gradient (Pa/m); μ = dynamic viscosity (kg/ms); and L = length of the crack perpendicular to the flow direction (m).

3.6.3 Internal humidity

The humidity of the concrete has big influence on the permeability. The solid phase changes due to shrinkage or swelling or to chemical reactions, leading to changes in the geometry of the pore system. The moisture content itself influences the extent to which water can flow through the pore system.

The degree of humidity of the concrete is influenced by the amount of mixing water present in relation to the amount of cement, by the curing conditions and by the

later boundary conditions. Concrete with a low w/c ratio may have parts located in the interior which have a humidity of less than 100 %, even if the concrete is always covered with water. The reason is self-desiccation caused by “Chemical shrinkage” of water bound to cement.

The water contained in concrete is often classified into non-evaporable water (W_n) (also denoted as chemically bound water), and evaporable water (W_e). The evaporable water is often classified into water adsorbed on the pore walls (W_{gel}) and mobile water (W_m). As can be understood by its name, mobile water is mainly involved in the mass transfer of water. How the water is fixed within the concrete depends on the geometry of the pore system, the type of solid material in the matrix, the humidity, and the thermodynamic balance between the pore system and the surroundings.

Under dry conditions, below 45 %RH, if no overpressures occur, the water vapour *diffuses* due to differences in vapour concentration within the more or less empty pore system (Figure 3.12). The broader, straighter, smoother and more connected the pores are, the more readily the transport of water can occur. Some of the water molecules become adsorbed to the pore walls, are stuck in very narrow pores or react chemically with substances in the pore walls.

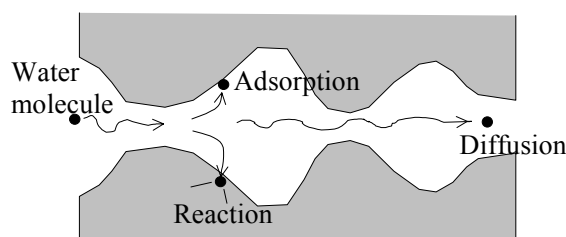


Figure 3.12 Movements or fixation of water molecules in dry pores of the cement material: Adsorption to the walls of the pore, hydration of compounds in the solid walls or diffusion. The broader the pores, the less collision with the pore walls and attraction to them occurs and the more readily diffusion through the pores can take place.

If the relative humidity in the pores increases, more water is adsorbed to the pore walls and a film of liquid water is formed. In this film, the water molecules nearest the pore walls are strongly adsorbed to the walls and are hardly mobile, whereas the subsequent layers are attracted less and may slide over the layer underneath as in bulk water, although probably with a higher level of viscosity. As indicated above, changes in the thermodynamic energy level may alter the mobility of the water. Higher pressure or higher temperature, for example, makes the water molecules vibrate more intensively and lead to decreased viscosity and to reduced interaction with the pore walls, therefore the water moving more readily. According to Hearn (1992), Peer (1990) has shown that pores smaller than 10^{-7} m in diameter and with a length/diameter ratio of 2 or less do not contribute significantly to the water permeability of cement paste for water. Gases with a polar arrangement of their molecules, such as are water vapour, are probably more strongly attracted to the water film and are absorbed and mainly transported there, whereas non-polar gases are transferred by diffusion.

Under conditions of continuously increasing humidity, curved water menisci are formed in narrow passages, leading to capillary condensation. This occurs at an RH above about 45 %. The flow of water then changes to *capillary suction*, which is a much

more rapid, transport being a combination of film transfer, diffusion and capillary suction (Figure 3.13). Water is transported from one water meniscus, to another by film-transfer or by diffusion to the adjacent meniscus. Water is being sucked through the meniscus to the next air-filled pore. The higher the humidity, the greater the extent to which the transport is based on capillary suction and the more rapid the mass transfer of water becomes.

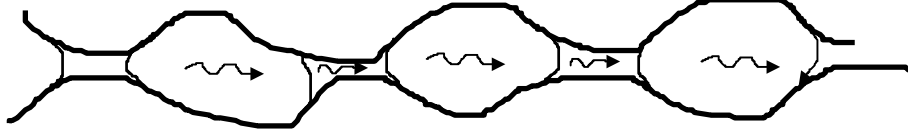


Figure 3.13 Diffusion and capillary suction of water in fictive pores in cement material. The higher the humidity, the larger the amount of water transported by capillary suction is.

At an RH of close to 100%, the cement paste is almost completely filled with water. Then, water transport is being governed mainly by capillary suction. Some pores are so isolated and difficult to reach that they are first filled with water after a long period of water suction.

By the period of time t , water has been sucked into the material to a depth of z . A simple relationship between the penetration depths of the water front and time elapsed is

$$z = \sqrt{\frac{t}{m}} \quad (3.8)$$

where z = penetration depth due to capillary suction (m); t = time (s); and m = the resistance constant for capillary suction (s/m^2). The magnitude of m is independent of the total porosity but depends on the pore size distribution. The smaller the pores, the larger the resistance m (Fagerlund 1980b). The total amount of water that is sucked in during the period time t can be calculated as

$$W_{suck} = \frac{\rho_w \cdot P_{suck}}{\sqrt{m}} \cdot \sqrt{t} = k_{suck} \cdot \sqrt{t} \quad (3.9)$$

where W_{suck} = total amount of water sucked by capillary action (kg/m^2); ρ_w = density of water (kg/m^3); P_{suck} = porosity available for water suction (m^3/m^3); and k_{suck} = capillary constant ($\text{kg/m}^2 \cdot \sqrt{\text{s}}$). The capillary constant k_{suck} depends on the pore structure (influencing m), the pore volume and the humidity (influencing P_{suck}). The rate of capillary suction at each moment can be calculated as

$$q_{suck} = \frac{k_{suck}}{2} \cdot \frac{1}{\sqrt{t}} \quad (3.10)$$

where q_{suck} = rate of suction flow ($\text{kg/m}^3/\text{s}$). The rate decreases over time, as the equation indicates. Not all the pore volume is available for capillary suction, which can be stated generally as

$$P_{suck} = P_{tot} - P_{air} - P_w \quad (3.11)$$

where P_{tot} = total porosity (m^3/m^3); P_{air} = air-filled porosity (m^3/m^3); and P_w = water-filled porosity prior to the start of capillary suction (m^3/m^3), Fagerlund (1980).

When a pore system is completely filled with water, any transport of dissolved ions or gases proceeds by slow diffusion in water.

The transport of water in the range of 0-100 % RH when subjected to *overpressure* applied to water follows the same principles as described above for 0-100 % RH under lack of overpressure, although transportation is faster, especially when the water content of the concrete is high. (Figure 3.14). In small pores between 10^{-9} and 10^{-6} m in size (Hearn 1992), however, the water flow due to external pressure is of negligible size compared to that caused by capillary suction. It is a time-consuming process to replace one of two immiscible fluids by another, such as air by water. Air can easily act as a plug in the pore system when water presses upon it and must either get around it or “wait” for the dissolution or collapse of the air voids that prevent its advance. The collapse of air voids can be due to the pressure becoming so high that the air is finally pressed out of bottlenecks that have developed or is dissolved by the water and transported downstream. When the pressure finally decreases near the downstream face, however, air voids that have been dissolved may be formed again and stop the water flow there.

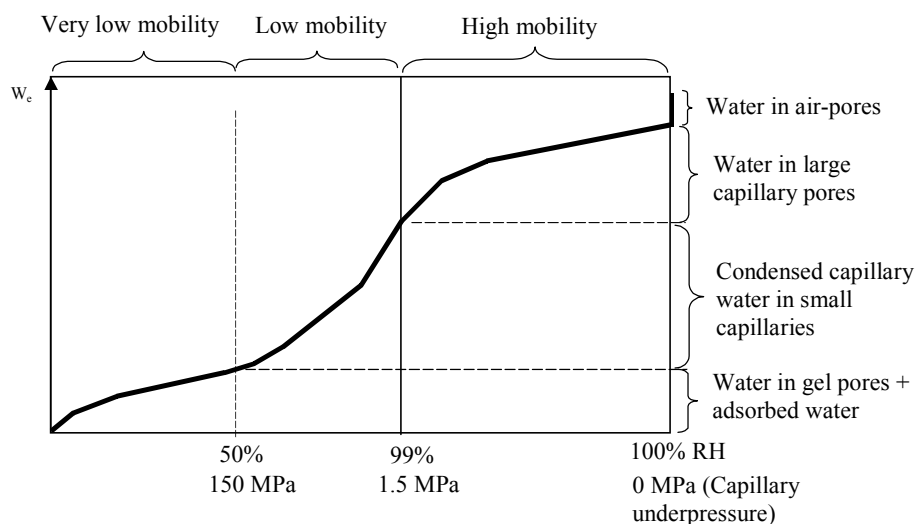


Figure 3.14 Basic picture of the sorption isotherm and of the mobility of water due to over-pressure effects in concrete at different relative humidities (Fagerlund, 2000).

To summarise,

- for RH values below 45 %, water transport is controlled by vapour diffusion, adsorption and possibly surface film transfer (at a RH of close to 45 %).
- For RH values between 45 and 100 %, water transport is controlled by vapour diffusion and by capillary suction. The higher RH is, the greater the amount of capillary suction is which occurs.
- In saturated concrete under steady-state conditions, water transport is due to external overpressure and can be described in terms of laminar flow in which there is a certain degree of viscosity and be calculated according to Darcy’s law.

Gjörv and Löland (1978) who took account of evaporation from the downstream side of concrete specimens in a permeability test, found the increase in the effect of capillary

action to be of the same order as that of a hydraulic gradient of approximately 20 MPa/m.

In a real structure, such as a dam, there may be the same combination of moisture conditions throughout the structure, the flow of water being a function of many different types of transport mechanisms, see Figure 3.2.

3.6.4 Curing conditions

Both the curing of concrete at an early degree of hydration, and the treatment conditions, present at later stages influence the permeability of the concrete very much in terms of the formation of micro-cracks. These can be the result of drying shrinkage, carbonation shrinkage, thermal shrinkage and externally applied loads (see also section 3.6.2). The access to water, and use of an appropriate curing temperature, are of great importance for the tightness of concrete. Figure 3.15 shows the dependence of the tightness of the concrete on the duration of water curing prior to water penetration in the case of curing that starts one day after casting. Figure 3.16 indicates the great importance it has that curing with water begins soon after casting. Figure 3.17 shows the water penetration in concrete as affected by different methods of curing.

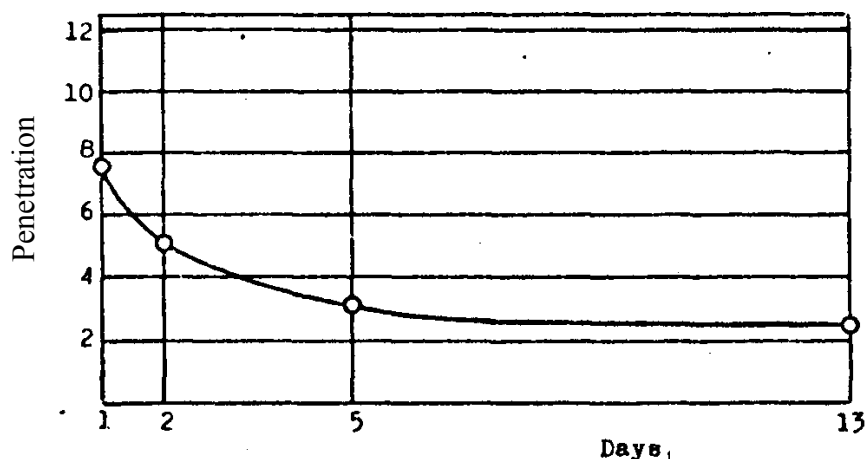


Figure 3.15 The dependence of the duration of water curing prior to the penetration of water into the concrete for a w/c ratio of 0.7 and testing at a degree of hydration of 28 days when curing starts one day after casting (Nycander, 1954).

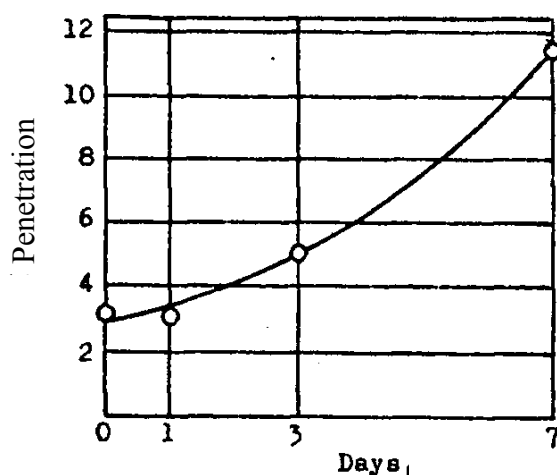


Figure 3.16 Dependence of the starting time for water curing of five day duration on the penetration of water in concrete for a w/c ratio of 0.7 and testing at a degree of hydration of 28 days (Nycander, 1954).

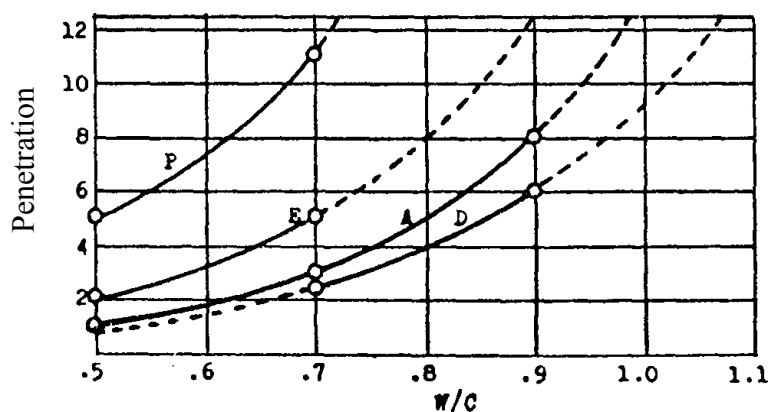


Figure 3.17 The dependence of different curing conditions and w/c ratios on the penetration of water in concrete tested at a degree of hydration of 28 days. P = conditions of the concrete's being 14 days in watertight moulds and afterwards in laboratory air; E, A and D = the concrete's spending 2, 5 and 13 days respectively in water prior to its being in laboratory air (Nycander, 1954).

Powers and Copeland (1954) showed that even in the case of a very slow drying to 79 % RH and re-saturation the coefficient of permeability increased seventy-fold.

Vuorinen (1985) found the permeability to increase 100 times in initially fog-cured specimens if they were first dried at +105°C and then resaturated.

As can be seen in Figure 3.18, a high curing temperature enlarges the pore size found in the cement paste, this in turn increasing the permeability (Figure 3.19).

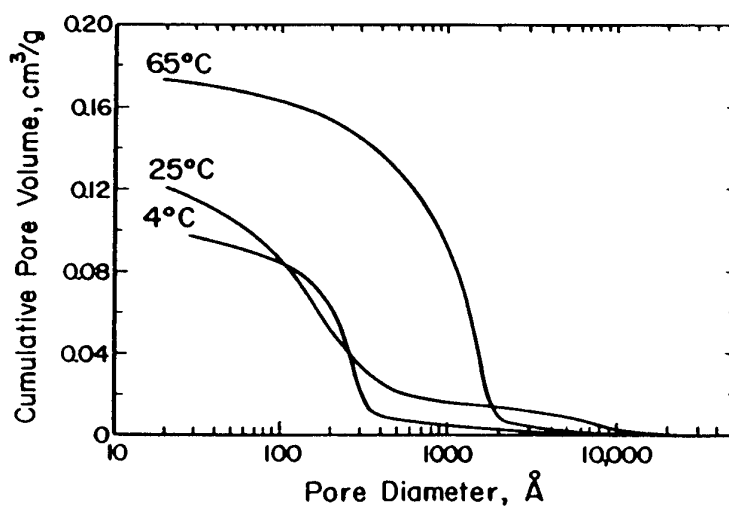


Figure 3.18 Effects of curing the temperature on the pore size distribution (data for the C_3S pastes from Young (1970), as given in Young (1988)).

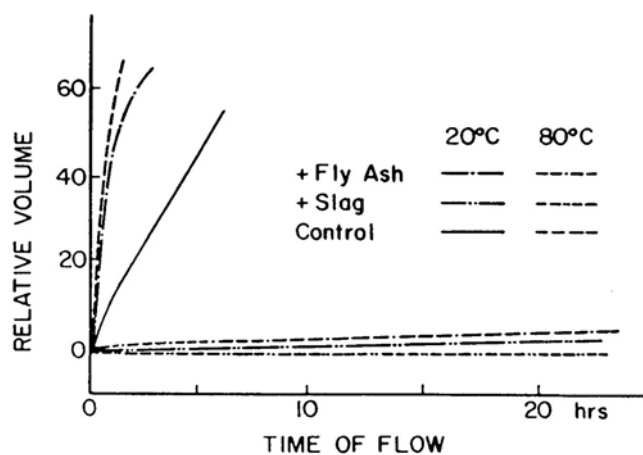


Figure 3.19 Effect of the curing temperature on water flow through pastes made with and without mineral admixtures (data from Bakker (1983), as given in Young (1988)).

The importance of water curing for achieving a low degree of permeability can be seen in Figure 3.20. Even a short period of drying after demoulding can “destroy” the tightness of concrete, due to the formation of microcracks.

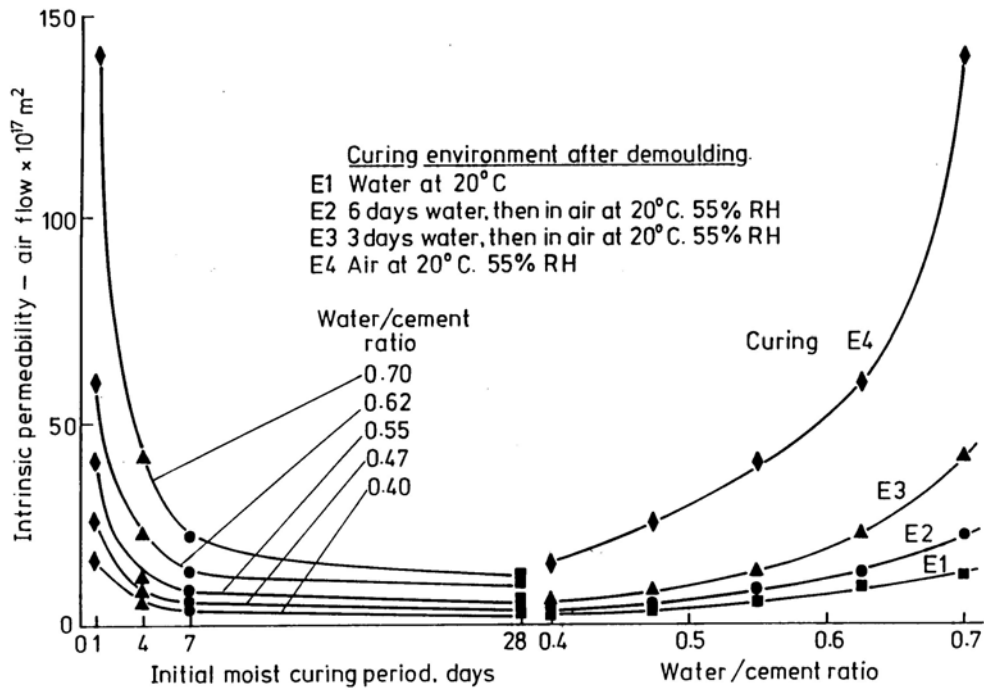


Figure 3.20 Effects of curing and conditioning on the permeability of concrete (Dhir et al. 1989, as presented in Hearn 1992).

3.6.5 Degree of hydration

The permeability of concrete, mortar and cement paste is sensitive to the degree of hydration or age at which a permeability test is started. The permeability is much greater when testing is started at a young age than at an old age (McMillan & Lyse 1930, Ruetters et al. 1935, Powers et al. 1954), cf. Figure 3.21. Concrete exposed to penetrating water at an early age may seal due to continuous hydration.

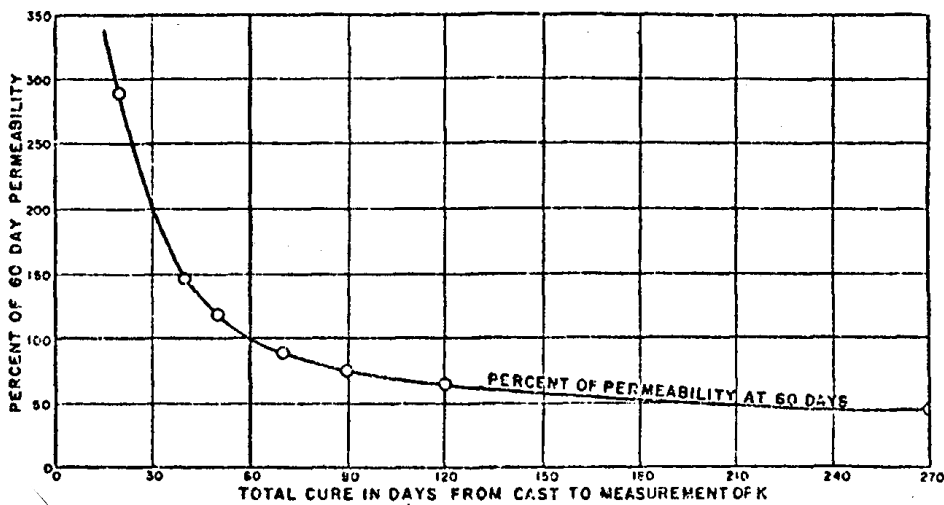


Figure 3.21 Effects of length of cure on permeability (Ruetters et al. 1935).

3.6.6 Water cement ratio

Figure 3.9 shows results of studies of the permeability of cement paste and homogenous concrete. Powers and Copeland (1954) did not treat viscosity separately in defining the coefficient of permeability. This is defined by the equation

$$\frac{dq_w}{dt} = K_1 \frac{\Delta P}{L} A \quad (3.12)$$

where dq_w/dt = amount of water (m^3/s); K_1 = the permeability coefficient (s) including the viscosity ($K_1 = K_2/\mu$ where μ = dynamic viscosity $\text{N}\cdot\text{s}/\text{m}^2$); $\Delta P/L$ = pressure gradient (Pa/m); and A = cross sectional area (m^2). As the “true” viscosity appears to be a function of the size of the pore size, it is difficult to measure the coefficient K_2 .

As can be seen, the higher the w/c ratio, the higher the permeability of both the cement paste and the concrete. Figure 3.4 and Figure 3.11 present results of several investigations concerning the dependency of w/c on the permeability. The data in the figures include only specimens that were cured for at least 28 days and were tested without any pre-conditioning. The data show large scatter, especially in the case of concrete. Only for cement paste with a high w/c ratio the scatter is somewhat smaller. According to Hearn (1992), the results of individual studies have shown a direct proportionality between permeability and the w/c ratio, although the data for different studies show a high degree of scatter in relation to each other. This is probably due to differences in specimen treatment and in test procedures.

3.6.7 Large air- or water-filled pores

The greater the extent to which the bigger air voids in hardened concrete are filled with air, the more difficult it is for water to penetrate the concrete. As the pressure increases, the air is compressed, possibly allowing the water to pass by blocking air the bubble. Besides, the air bubble will gradually be filled by water. A long time is required before the air voids are completely filled with water, permitting the permeability to increase. Many authors (e.g. Ruetters et al. 1935, Carlson 1950, Bažant 1975) emphasise the long period of time, possibly hundreds of years, that may be required before the water pressure becomes steady across a wide section of a dam, such as a large gravity dam. An example is shown in Figure 3.22. In reality, of course, water may penetrate more quickly in large, interconnected flow channels than in smaller, unconnected pores. Water may possibly also be sucked into the dam by capillary suction, increasing the saturation rate. A long time is required, nevertheless, before saturation is completed.

The higher the pressure, the easier it is for the air in voids to be dissolved in water. If air is introduced into the headwater at higher than atmospheric pressure, it may be released again when the water penetrates the concrete, the pressure sinking from the headwater to the tailwater

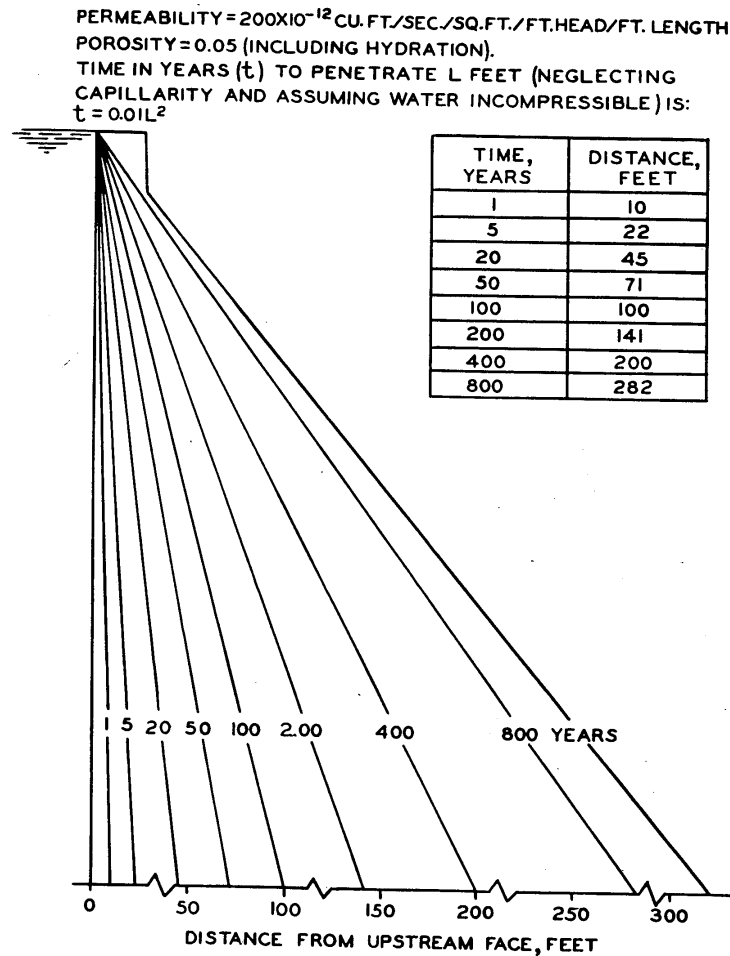


Figure 3.22 Calculated penetration of water into a 400-ft wide concrete dam for various durations of hydraulic head (Carlson 1950).

Cook (1951) observed that permeability test samples which were vacuum-saturated possessed a consistently higher level of permeability than samples that were pressure-saturated, i.e. in which the water was pressed in rather than being sucked in as in vacuum saturation. The reason is probably that vacuum saturation produces higher degree of saturation.

By applying a hydraulic gradient of 80 MPa/m and reducing the air content of the water to approximately 33 % compared to that of saturated air at atmospheric pressure, Gjörv and Löland (1978) achieved an increase in hydraulic conductivity of 550 and 88 % for a concrete with a w/c ratio of 0.5 and 0.6, respectively. By successively reducing the hydraulic gradient from 80 to 20 MPa/m, a reduction in hydraulic conductivity of about 50 % was obtained, the exact result depending on the air content of the system. The authors considered that the observed effect was due to air having a blocking effect on the pore system.

3.6.8 Porosity and pore size distribution

The hydration of cement paste results in two forms of pores: gel pores and capillary pores. Gel pores are very small (15 to 20Å). The intermolecular forces between the

water molecules (viscosity effects) and between the water molecules and the pore walls (absorption effects) in such very small pores (only about 5 times as large as a water molecule) result in low mobility of gel-pore water. Therefore, the main flow of water is in the capillary pores (or cracks if these are present), which are much larger, ranging from 10 nm up to 1 μm in size.

With increasing degree of hydration, the capillary pore system becomes less connected, becoming filled with hydration products. Below a w/c ratio of approximately 0.7, the connections within the capillary pore system become largely blocked, whereas above w/c 0.7 no total blocking occurs (Fagerlund 1980b).

Due to the highly complex pattern of the pore system in a porous material, no simple relation between porosity and permeability can be found (Scheidegger 1960).

Nyame and Illston (1980 and 1981) conducted a study of the relationship between the permeability of hardened cement paste and its porosity and pore size distributions with the aim of gaining a better understanding of the significance of the *threshold diameter* (see below) in connection with permeability.

The authors concluded that porosity, specific area and the hydraulic radius were not uniquely related to permeability, but that the hydraulic radius of the pore system describes the measured permeability rather well, except for pore sizes of close to molecular dimensions, see Figure 3.23. They found permeability not to be a unique function of porosity, but to be dependent upon the w/c ratio as well, as can be seen in Figure 3.24. The authors assumed continued hydration to subdivide the pore system into many unconnected pores. They suggested water flow to occur in distinct *flow channels*.

They also found what they termed a “maximum continuous pore radius”, r_∞ , which apparently was the pore radius for which the frequency curve has a maximum, see for example the pore radius of $r=1010 \text{ \AA} \approx 10^{-7} \text{ m}$ for cement paste with a w/c ratio of 0.71 in Figure 3.7. A pore radius of this size or larger apparently has a strong influence on permeability.

(Note: the pore size *maximum continuous pore radius* is termed in different ways in the literature, for example, *continuous pore radius*, *threshold diameter* and *critical pore radius*).

The critical pore diameter, is said to “represent the minimum diameter of pores which are geometrically continuous throughout all regions of the hydrated cement paste” (Winslow and Diamond 1970) and it is the diameter of the last pore filled before a connected pathway is formed from the one side of the specimen to the other. Expressed in other words, “a continuous capillary pore system through which Darcian flow can occur” (Young 1988). The moment when the first unbroken path from one side to another appears (Bentz & Garbotczi 1991) or when a connected system is no longer connected (as in the hydration of cement paste) is called the percolation threshold. The diameter involved can be calculated, by mercury intrusion pressure porosimetry, as the diameter at the inflection point on the cumulative intrusion curve.

Mehta and Manmohan (1980) found the same thing for a threshold diameter of approximately 1320 \AA . Nyame and Illstone found the relationship between these maximum continuous pore radii r_∞ and permeability to be

$$k_w = 1.684 \cdot r_\infty^{3.284} \cdot 10^{-22} \quad (3.13)$$

where k_w = permeability (m/s); r_∞ = maximum continuous pore radii (\AA). The relationship between total porosity and permeability was found to be

$$k_w(t) = k_0(t) \cdot P_p^{b(t)} \tag{3.14}$$

where $k_w(t)$ = permeability at time t (m/s); and P_p = total porosity of the cement paste; and $k_{w0}(t)$ and $b(t)$ are the constants shown in Table 3.3.

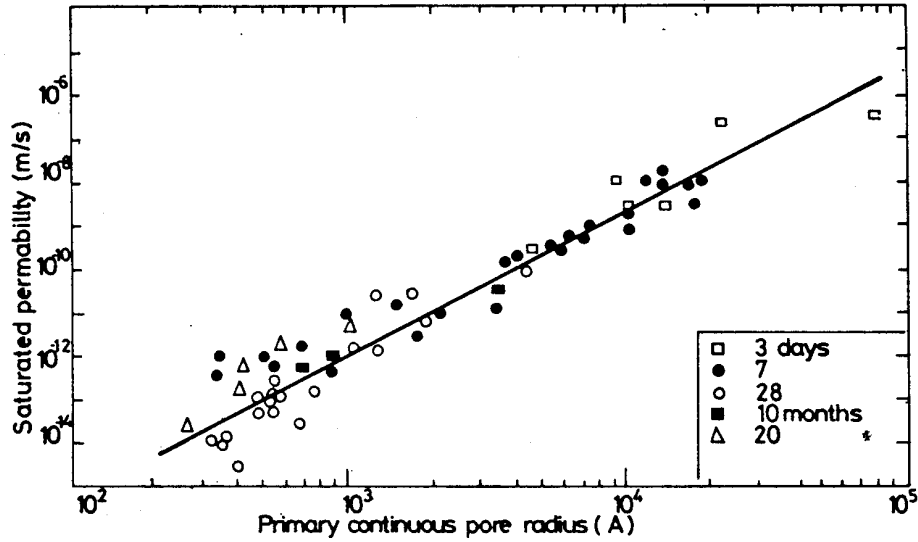


Figure 3.23 The relationship between the “continuous pore radius” and the saturated permeability of hcp (Nyame & Illston, 1980).

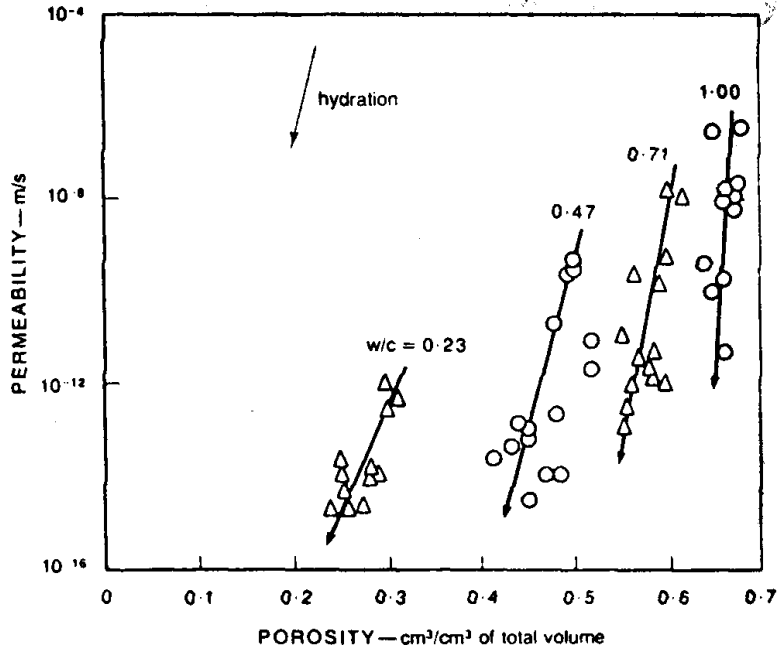


Figure 3.24 Permeability of cement paste as a function of the total porosity (Nyame and Illston, 1981).

Table 3.3 Regression constants for the relationship between the total porosity and the permeability of hardened cement paste (Nyame & Illston 1980 tab. 1).

| Time of hydration (days) | $Kw_0(t)$ | B(t) | Correlation coefficient |
|--------------------------|----------------------|-------|-------------------------|
| 3 | $4.19 \cdot 10^{-5}$ | 16.18 | 0.8811 |
| 7 | $4.19 \cdot 10^{-5}$ | 12.98 | 0.8323 |
| 28 | $4.19 \cdot 10^{-5}$ | 9.02 | 0.7031 |
| 10 months | $4.19 \cdot 10^{-5}$ | 6.44 | 0.9378 |
| 20 months | $4.19 \cdot 10^{-5}$ | 7.95 | 0.9661 |

Hooton (1986) found a large scatter in the relationship of permeability and r_{∞} , in the results reported by Nyame and Illston. Hooton also noted that many studies had reported approximately the same size of the so-called critical pore radius: 790 Å (Mehta & Manmohan 1980), 750 Å (Goto & Roy 1981), and 590 Å (Feldman 1981). The critical pore radius is similar to the maximum continuous pore radius described by Nyame and Illson (1980) and the threshold diameter described by Winslow and Diamond (1970). However, Hooton found there to be no unique relationship between any of the pore radii and permeability.

According to Young (1988), Hughes (1985) employed pore size distributions based on the *second* mercury intrusion curve, which is considered to cover all pores that are emptied after the first mercury intrusion, a curve considered to be a measure of the continuous pore system, which is permeable to water.

3.6.9 Type, size and amount of aggregate

Use of larger and more porous aggregate makes the concrete more permeable. For a given water-to-cement ratio, the tightest concrete can be achieved by use of such an aggregate, which has a shape and a size distribution that require a minimum of mixing water. The aggregate should have a grading curve with as much of the space between the larger particles as possible being filled with smaller particles. Thus reducing the amount of cement paste.

Unstable mixes leading to bleeding might produce channels in the concrete and cavities under big aggregate particles. This will increase the permeability. The grading curve of aggregate shall be such that stable mixes are produced.

The larger the aggregate is, the greater the risk is of microcracks, the permeability thus increasing (Nycander 1954). The work of Ruettgers et al. in 1934 indicated the use of a larger aggregate concrete more permeable (Figure 3.9 b). Other researchers, however, have not found there to be any strong relationship between the gradation of the aggregate and permeability (Mary 1935, Markestad 1977).

3.6.10 Type of cement

Ingredients in the cement that consume CH such as pozzolanic material, often decrease the permeability of the concrete. On the other hand, the amount of autogenous healing (see section 3.6.11) may be reduced.

The more finely the cement is ground, the tighter the concrete becomes (Nycander 1954). On the other hand, Powers and Copeland (1954) maintain that after some time pastes made from coarsely ground cement are just as impermeable as pastes made of finer cement.

3.6.11 Leaching, self sealing or autogenous healing

See also section 2.5.1.

The permeability of concrete may change due to the removal or the formation of material inside the concrete or on the surfaces.

The dissolution and precipitation of calcium hydroxide may lead to a change in the permeability. If solid material is leached away, the permeability in the area in question increases. Ruetggers (1936) claimed, however, that in the experiment he conducted, there was no increase of permeability, even when 1/3 of the lime had been leached away. Meyers (1936) argued that for the type of specimens that Ruetggers employed no account was taken of the effect of carbonation. CO_2 that reacts with lime in the pore solution can both open and fill the pores, the permeability changing as a result of this. If leached material come in contact with carbon dioxide, or bicarbonate comes in contact with calcium hydroxide, the resulting precipitation of CaCO_3 may decrease the permeability in the area. The cement paste in concrete may also seal due to continued hydration, which is discussed in section 3.6.5. Another example of this is shown in Figure 3.25 for the pure paste that Powers studied.

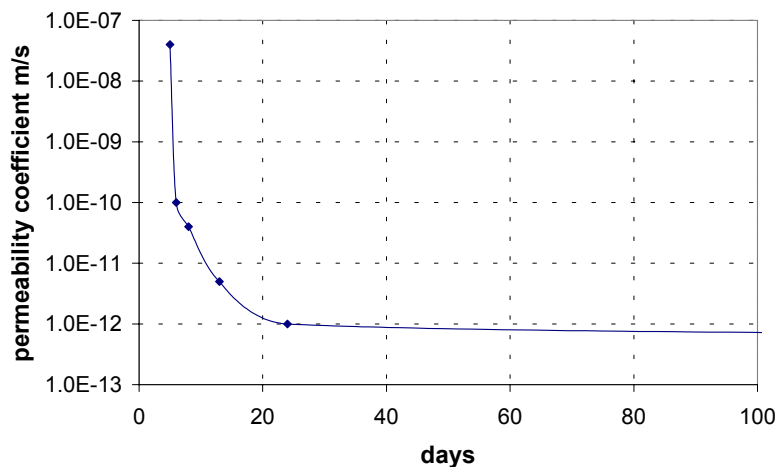


Figure 3.25 Reduction in permeability through continued hydration during a test of permeability (Powers, 1954).

Hearn and Morley (1997) conducted a percolation study of 26-year old homogenous concrete both in its virgin state and after drying in order to determine its self-healing properties. The permeability of virgin concrete was found to be constant (Figure 3.26). When the concrete was dried, the permeability increased by a factor of about 100, although it gradually decreased later on in the test. The authors claimed that the decrease in permeability was due to self-healing caused by the dissolution of soluble species such as $\text{Ca}(\text{OH})_2$ on the upstream face and the deposition and crystallisation of the same species on the downstream face. No self-healing due to the continued hydration of cement was assumed to occur in the specimens, no unhydrated, cement being assumed to be left in the concrete either. The deposition and crystallisation of species was assumed to take place when the pressure along the flow channel dropped. This presumes that there is a pressure effect on the solubility of the species. However,

Constantiner and Diamond (1995) found no significant pressure effect on the solubility of alkali or of calcium hydroxide.

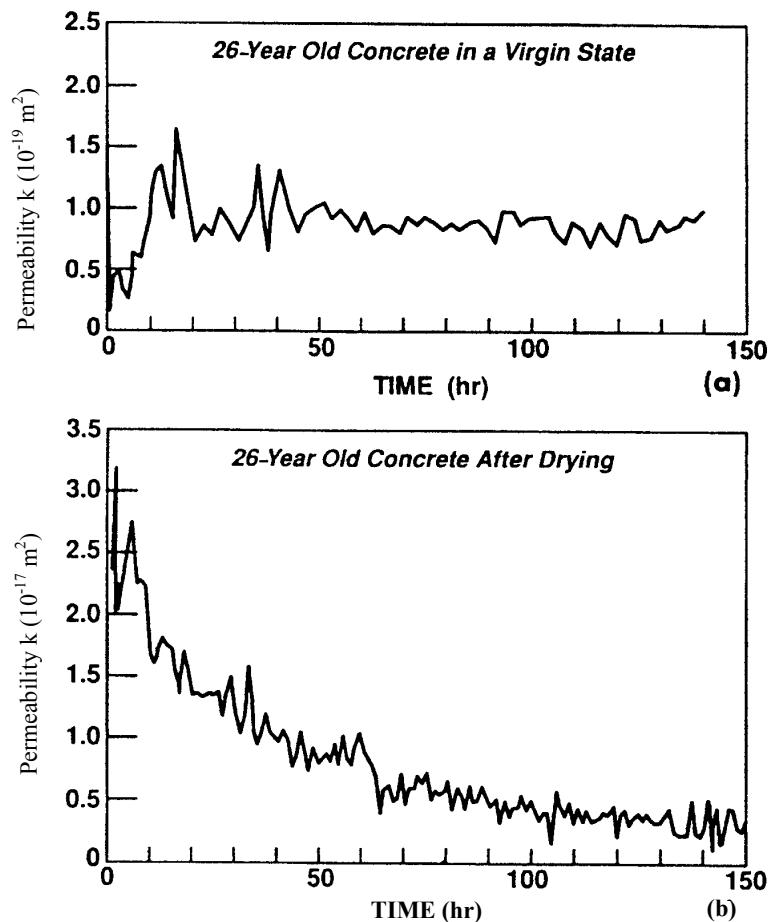


Figure 3.26 Typical variations in permeability during the testing of (a) a 26-year old concrete that never dried; and (b) the same concrete oven-dried at $+105^{\circ}\text{C}$ and resaturated (Hearn and Morley 1996).

3.6.12 Workability and placing

The workability of concrete is important for tightness. The concrete needs to fill out the mould and enclose the reinforcement. The grading of aggregate is decisive for the workability, consistency and stability of the concrete. Experience shows that a stiff consistency results in concrete that is less tight than if the concrete has a more plastic consistency (Nycander 1954). In old concrete dams made of stamped concrete, there is a considerable risk of the concrete not being tight, especially at joints between different batches of concrete.

“Potentially, entrained air, entrapped air or honeycombing (large irregular voids due to poor compaction) are less damaging than bleeding, as they are isolated and do not form continuous flow paths in the cement matrix. Bleeding has more serious effects. The formation of bleeding channels creates continuous flow paths and the deposition of water pockets underneath coarse aggregate particles” (Hearn 1992).

3.6.13 Deposit of material inside a concrete dam

According to Mayers (1935), material can readily deposit inside a thick concrete dam:

- ✓ Both $\text{Ca}(\text{OH})_2$ and CaCO_3 are more soluble at lower than at higher temperatures and some of this material will be precipitated in the central portion of the concrete mass.
- ✓ Cement forms supersaturated solutions from which more stable forms slowly precipitate; thus, as the supersaturated water flows from the upper face zones to the central zones deposition of Portlandite might occur.

3.6.14 The viscosity of the fluid

The flow resistance of a liquid is highly dependent on its viscosity. In large flowing channels, the viscosity of the water depends on the temperature. In very small channels, such as in many of the pores in cement paste, large intermolecular forces develop between different ions in the water and between ions in the water and ions bounded in compounds in the pore walls. When strong intermolecular forces need to be exceeded, the viscosity becomes greater. Although all the evaporable water in cement materials is mobile when subjected to hydrostatic pressure, some of it has a high degree of viscosity.

Powers, Mann and Copeland (1958) remarked that, within the range of porosity found in the paste, part of the evaporable water, and perhaps all of it, is adsorbed to the pore walls. Boundary layers near the surface of particles possess a viscosity that differs from that of the bulk. This is of importance in filtrating liquids in fine-porous media (Derjaguin & Zachavaeva 1965). The viscosity is higher than that of free water. Van Brakel (1974) restricts pores not to being smaller than 0.1 – 2000 μm for the viscosity of free water to apply. The viscosity is increased by the presence of solutes and also depends on the kind and amount of the dissolved material.

Therefore, the viscosity of the water contained in pores in concrete cannot be treated as being a constant at a given temperature; rather it is a function of the dimensions of interparticle space, and of the kind and amount of dissolved material (Powers et al. 1958). They found that all evaporable water also water in gel pores appeared to be mobile. He also found the rate of flow to be temperature-dependent, being higher at higher temperatures, indicating water viscosity in cement paste to have a relatively high activation energy.

Powers (1960) calculated the effect of w/c-ratio on the viscosity. His data are given in Table 3.4.

Table 3.4 Computed relative viscosity of the fluid in saturated cement pastes, as based on eq. 62 in Powers (1960).

| W/c | Porosity ϵ | Hydraulic radius (\AA) | Factor for the increase in viscosity |
|------|---------------------|-----------------------------------|--------------------------------------|
| 0.38 | 0.280 | 7.8 | 47 600 |
| 0.45 | 0.346 | 10 | 2 700 |
| 0.50 | 0.395 | 12 | 600 |
| 0.60 | 0.461 | 16 | 134 |
| 0.70 | 0.489 | 18 | 78 |

Powers noted that the permeability is 5-6 times as great when pure water permeates a given cement paste than when salts, particularly NaOH and KOH, are dissolved in the

water. Powers and Copeland (1954) also observed that the permeability increased when alkali was removed from the pore solution.

Some reports means that the roughness of the walls of the channels may extend through the laminar layer, causing turbulent flow. The true viscosity also includes the turbulent viscosity (Kou 1996).

3.6.15 State of stress

Experiments conducted by Wisnicki et al. (1969) indicated there to be no significant reduction in permeability due to 2-dimensional stress being applied. A stress of maximally 75% of their compressive strength was applied in the experiment. It appeared that the main effect of stress upon the permeability of concrete was that of closing major cracks.

3.6.16 The shape and dimension of the global structure

The permeability is influenced by the tortuosity of the channels in which most of the water flows. The proportion of the channels that are connected within the structure is probably smaller when the structure is thicker (Figure 3.27).

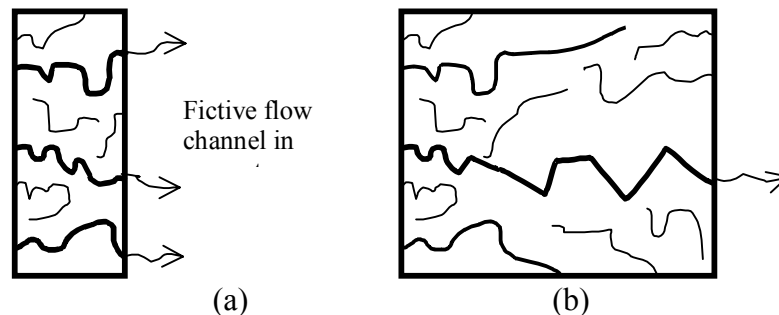


Figure 3.27 There are probably a greater number of connected flow channels in thinner (a) than in thicker concrete (b).

3.7 Water flow in saturated concrete

There are various advantages in studying permeability, or water flow, in saturated concrete:

- There is only viscous laminar flow of water under such conditions, no absorption, moisture diffusion or capillary suction taking place.
- The flow can be calculated with the simple use of Darcy's law, assuming there to be a homogenous, viscous flow.
- The flow is steady over time.
- There is no shrinkage or swelling.

The disadvantage in only studying Darcian flow in saturated concrete is that such concrete is not very frequent in real structures. The boundaries of the concrete in real structures are often exposed to air, at least during certain periods of time.

A permeability test of concrete and mortar discs ($\phi 150 \times 50$ mm) performed by McMillan and Lyse (1930) showed the following:

- tests of permeability are very sensitive. “Minor defects in concrete that would make no appreciable change in compressive strength affect the flow of water through the specimen under pressure to a marked degree”.
- an increase in watertightness occurs when the curing time is increased and when the w/c ratio is decreased.

Ruettgers et al. (1935) showed on the basis of data from two specimens that the downstream discharge of water was linearly proportional to the pressure. The test water was, however, not treated to eliminate dissolved air.

Sällström (1968) studied relations between a standard method of testing non-steady state water penetration due to combined capillary suction and over-pressure and one for testing water permeability, Figure 3.28. There was an increase in penetration as the permeability became greater, although the relationship was not a linear one, which could be expected since the mechanisms behind the flow are about the same.

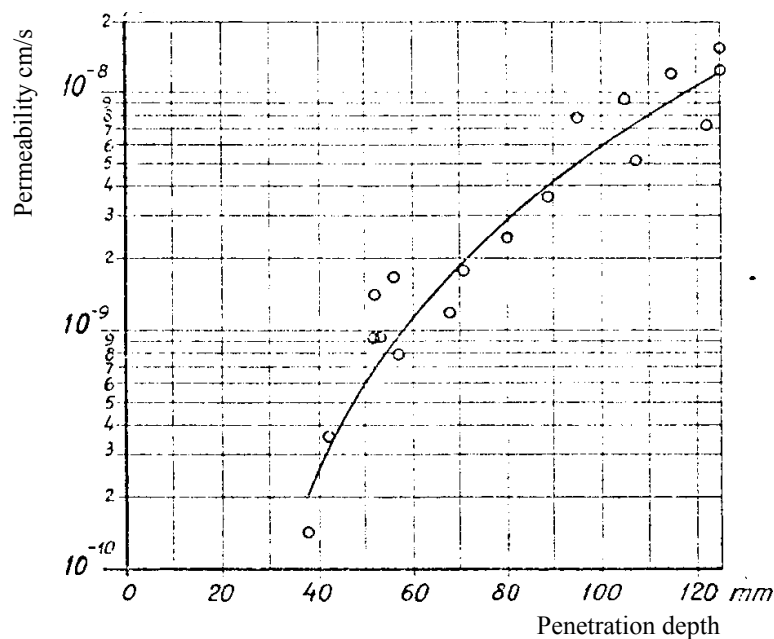


Figure 3.28 Relations between permeability and penetration depth for concrete composed of low-heat cement and 4 to 6 percent air (Sällström, 1968)

3.8 Test methods and modelling of water permeability

Measuring water mobility in concrete is a very difficult task. Unsaturated concrete can be penetrated by water by means of a number of different mechanisms such as adsorption, diffusion, chemical reactions, capillary suction and viscous flow caused by over-pressure. The pore system may change its geometry due to the formation or leaching of compounds or to swelling or shrinking. This means that permeability tests need to be selected very carefully.

Permeability measurements suffer from a lack of standardisation. It is usually very difficult to compare the results of different permeability tests due to differences in test setups and procedures.

3.8.1 Permeability test

If Darcian flow is to be tested, both in-flow and out-flow assumed by need to be measured in order to ensure the presence of the equilibrium conditions Darcy's equation. If the flows in and out are not equal, this may be due to the consumption of water through hydration, to the specimen not having been completely saturated or to change in the pressure head not yet being communicated across the thickness of the specimen (Hooton 1989).

Hooton notes that the variability of permeability test results is large. In the very few publication providing statistical data, that he found, the coefficient of variation was about 40 to 50%. The variation with respect to the permeability of concrete is much more variable than properties such as strength. Alterations in preparation of the specimen, or in testing procedures, can lead to large differences in the calculated permeability.

The degree of saturation of probably the concrete is the major cause of discrepancies when results obtained in different laboratories are compared (Cabrera & Hassan 1997).

3.9 Modelling water permeability in saturated concrete

3.9.1 Introduction

Many models describing the mobility of water in a porous material such as concrete have been developed through the years.

It should be emphasised that the complexity of the microstructure of cement paste, mortar and concrete is so great that it is not possible to derive their macroscopic properties from simple flow rules on a micro-scale without efforts being made to model the structure itself (Breysse & Gérard 1997). It is above all the enormous scale differences in the material, ranging from a 2 nm to approximately 100 nm pore diameter size and to the atomic size of the elements that are difficult to include in a model.

Methods for measuring fluid motion are usually classified into two groups, the one being *microscopic* methods and the other *macroscopic* methods. Microscopic methods describe the motion involved in terms of each of the small tubular conduits in the porous medium, using a statistical approach. Macroscopic methods describe the fluid as a unit moving at a macroscopic-average velocity which can be given, for example, by Darcy's law (Deju 1970).

A commonly used procedure for calculating the permeability of concrete is to

- a) estimate the pore-size distribution on the basis of experiments;
- b) assume a geometric or mathematical micromodel, such as for percolation or flux in slits or in tubes; and finally
- c) transform of the micromodels employed to pertain to flow on a continuous macro-scale.

Van Brakel (1974) divided the modelling of porous media into two main types: *pore space* and *non-pore space* models. Pore space models can involve the conception of

connected tubes or discrete particles in one, two or three dimensions (Figure 3.29 - Figure 3.31). These are often suitable for examining microscopic behaviour. Non-pore space models can be empirical correlations (such as Darcy's equation), discrete particle models, continuum models or statistical models, often suitable for analysing macroscopic behaviour. Van Brakel is of the opinion that even non-pore space models need always to some extent to be attached to a pore space model. With respect to capillary liquid transport in particular, he regards the sensibility of using the continuum approach as being disputable. van Brakel (1974) has provided a substantial survey of the literature.

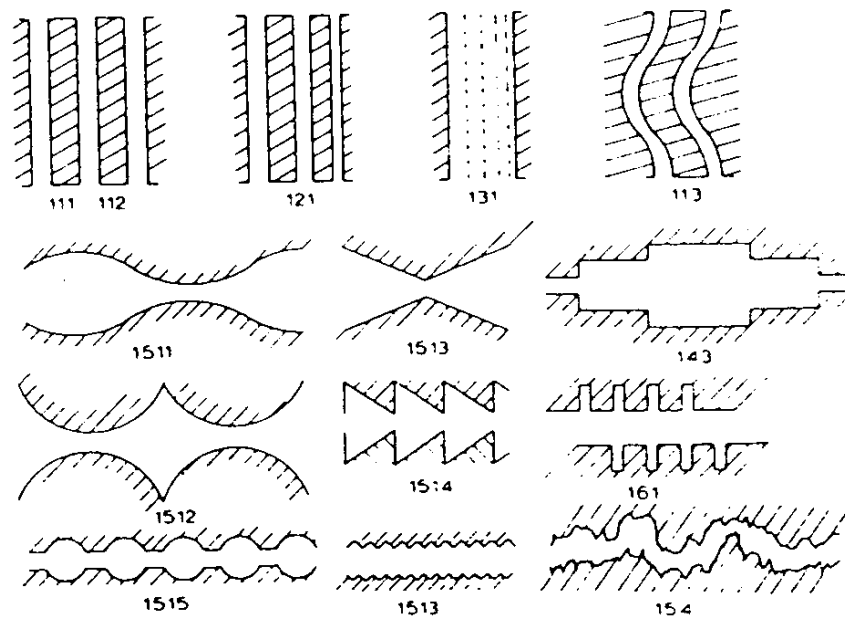


Figure 3.29 Elements of pore space models involving one-dimensional connectivity (Van Brakel, 1974)

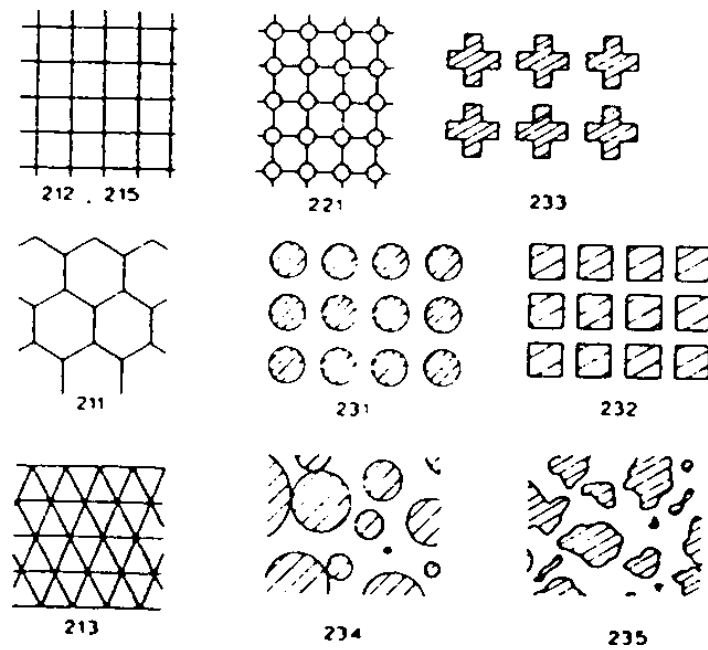


Figure 3.30 Figure 3.1 Elements of pore space models involving two-dimensional connectivity (Van Brakel, 1974)

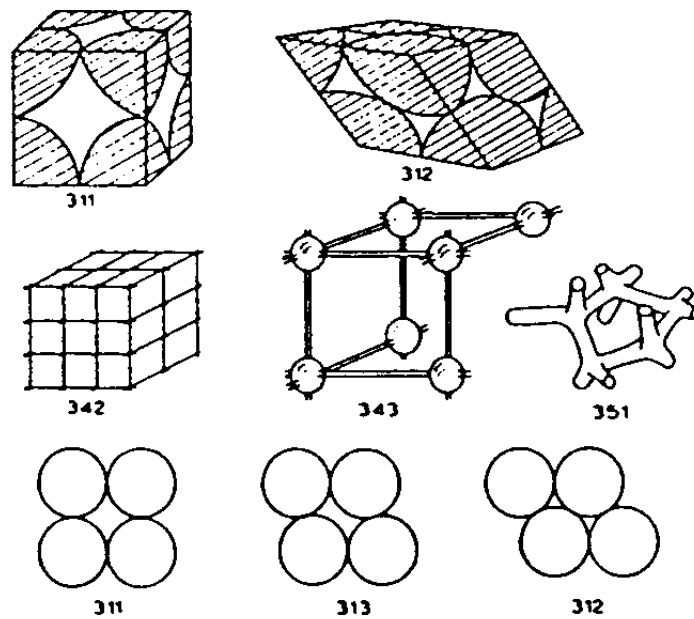


Figure 3.31 Elements of pore space models involving three-dimensional connectivity (Van Brakel, 1974)

Balance equations of varying suitability can be applied to the pore space or non-pore space model one selects.

3.9.2 Pore space models

According to Scheidegger (1960), flow through porous media appears to take place along flow channels at the local (pore) velocity, v . The macroscale filter velocity q of the fluid is smaller than the local velocity v , as often described by the Dupuit-Forchheimer equation:

$$q = P \cdot v \quad (3.15)$$

where q = filter velocity of the fluid (m/s); P = porosity (m^3/m^3); and \mathbf{u} = local velocity of the fluid in the flow channels (m/s). The local velocity v is assumed to fluctuate both between channels and along channels. In the Fochheimer equation, v is an average velocity.

A pore space model of the flow of a fluid through a porous medium is often based in some way on the *Navier-Stokes* equations for *incompressible fluids*. Note that the designation of the velocity of the fluid is changed here to \mathbf{u} (instead of $\dot{\mathbf{x}}$).

$$\nabla \cdot \mathbf{u} = 0 \quad (3.16)$$

$$\rho_w \frac{\partial \mathbf{u}}{\partial t} + \rho_w \mathbf{u} \cdot \nabla \mathbf{u} + \nabla p - \mu \nabla \cdot (\nabla \mathbf{u} + \nabla \mathbf{u}^T) + \rho_w \mathbf{g} = \mathbf{0} \quad (3.17)$$

where ρ_w = density of water (kg/m^3); \mathbf{u} = local velocity of water (m/s); p = hydrostatic pressure (Pa); μ = dynamic viscosity (Pa·s); and \mathbf{g} = acceleration due to gravity (m/s^2).

Note also that the velocity \mathbf{u} is the velocity within each small flow channel and not the bulk velocity of the material.

If one assumes slow (creeping), steady-state, viscous and incompressible flow without the effects of inertia, the balance of momentum becomes (Zienkiewicz & Taylor 1989)

$$\nabla \cdot \mathbf{u} \quad (3.16)$$

$$\nabla p - \nabla \cdot (\boldsymbol{\tau}) + \rho_w \mathbf{g} = \mathbf{0}; \quad \boldsymbol{\tau} = \mu (\nabla \mathbf{u} + \nabla \mathbf{u}^T) \quad (3.18)$$

where $\boldsymbol{\tau}$ = shear stress (MPa). Assuming steady-state flow, a straight, smooth and horizontal circular tube, laminar flow and the velocity of the fluid being zero on the walls of the tube allows Navier-Stoke flow to be integrated with the *Hagen-Poiseuille equation*:

$$u_{mean} = \frac{d^2}{32\mu} \cdot \frac{\Delta p}{L} \quad (3.19)$$

where u_{mean} = mean velocity in the tube (m/s); Δp = pressure gradient (Pa); L = length of the tube (m); d = diameter of the tube (m). The variation in the velocity u in a cross-section of a flow tube is

$$u = \frac{\left(\left(\frac{d}{2} \right)^2 - r^2 \right)}{4 \cdot \mu} \cdot \frac{\Delta p}{L} \quad (3.20)$$

where \mathbf{u} = local velocity of the fluid (m/s); r = distance from the middle of the tube in a radial direction. The total flow of water through the tube is

$$q_{w,tube} = u_{mean} \cdot \frac{\Delta p}{L} \cdot A_{tube} = \frac{d^2}{32\mu} \cdot \frac{\Delta p}{L} \cdot \frac{\pi \cdot d^2}{4} = \frac{\pi \cdot d^4}{128 \cdot \mu} \cdot \frac{\Delta p}{L} \quad (3.21)$$

where $q_{w,tube}$ = flow through the tube (m³/s). Fluxes caused by gradients in hydraulic head are written in terms of the same equations as above but are multiplied by the fluid density ρ_w and the gravity coefficient g :

$$u_{mean} = \frac{d^2}{32\mu} \cdot \rho_w \cdot g \cdot \frac{\Delta p}{L} \quad (3.22)$$

For real flow tubes in cement materials, reductions due to deviation from a large smooth cylinder (that the Hagen-Poiseuille equation assumes) should probably be assessed with use of a reduction factor.

Under these same conditions the integration of Navier-Stoke for the flow of fluids through smooth parallel slits gives

$$q_w = \frac{b \cdot w^3}{12 \cdot \mu} \cdot \frac{\Delta p}{L} \quad (3.23)$$

where L = flow channel length of the slit (m); w = slit width (m); and b = slit length perpendicular to the flow direction (m). When the surface of the slit is not smooth, use is commonly made of a “surface roughness factor”, α , (generally about 0.01-0.2) by which equation (3.23) is multiplied.

Assuming ideal fluids (without viscosity or compressibility) and isothermal conditions, and introducing a potential $\phi = -\nabla \dot{\mathbf{x}}$, Navier-Stokes can be written (Zienkiewicz & Taylor 1989) as

$$\frac{\partial \phi}{\partial t} + \frac{\mathbf{u}^2}{2g} + \frac{p}{\rho_w g} + z = \text{constant} \quad (3.24)$$

where z = height above an arbitrary reference level (m); and ϕ = a potential defined as $\mathbf{u} = -\nabla \phi$ (m). In steady-state flow, equation (3.24) provides the *Bernoulli* equation:

$$\frac{\mathbf{u}^2}{2g} + \frac{p}{\rho_w g} + z = \text{constant} \quad (3.25)$$

A very simple *capillarie* model of flow in one direction only is that of a bundle of straight parallel capillaries of uniform diameter together with the Hagen-Poiseuille equation (Figure 3.32).

$$q_a = -\frac{n_a \phi_a^2}{32\mu} \cdot A_a \cdot \frac{\partial p}{\partial x} = -\frac{k_a}{\mu} \cdot A_a \cdot \frac{\partial p}{\partial x} \quad (3.26)$$

$$k_a = \frac{n_a \phi_a^2}{32} \quad (3.27)$$

where q_a = water flow in all capillaries with a particular size a (m^3/s); k_a = specific permeability of all capillaries with a particular size a (m^2); $\delta p/\delta x$ = the pressure gradient (Pa/m); n_a = the number of capillaries of diameter ϕ_a (nos.); and μ = the dynamic viscosity (Ns/m^2); and A_a = the cross-sectional area of one capillary of size a (m^2).

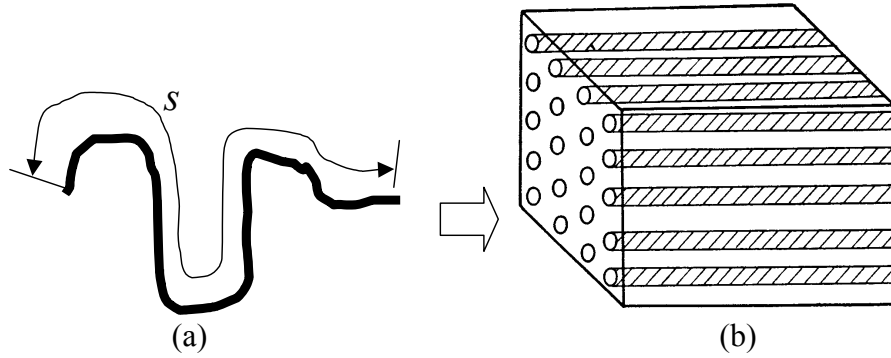


Figure 3.32 “Real” and dwindling flow channels (a) modelled by (b) a parallel straight type model (Scheidegger 1960).

A plausible objection to this model is that the pores probably are not as perfect straight cylinders as the equation assumes. A *tortuosity factor* $\tau = ds/dx$ is commonly used to describe the difference between the length of a real pore (ds) and that of a strait cylinder (dx):

$$q_a = -\frac{n_a \phi_a^2}{32\mu} \cdot A_a \cdot \frac{\partial p}{\partial s} = -\frac{n_a \phi_a^2}{32 \cdot \mu} \cdot A_a \cdot \frac{1}{\frac{\partial s}{\partial x}} \cdot \frac{\partial p}{\partial x} = -\frac{n_a \phi_a^2}{32 \cdot \mu} \cdot A_a \cdot \frac{1}{\tau} \cdot \frac{\partial p}{\partial x} = -\frac{k'_a}{\mu} \cdot A_a \cdot \frac{\partial p}{\partial x} \quad (3.28)$$

where s = the length of a real pore (m).

$$k'_a = \frac{n_a \phi_a^2}{32 \cdot \tau} \quad (3.29)$$

This tortuosity factor is probably governed by the effects of the dwindling route of a flow channel through the material, and by dwindling micro-cracks or capillary pores around the aggregate.

The porosity P (m^3/m^3) of n cylinders is:

$$P = n \cdot \frac{\pi \phi^2}{4} \cdot \frac{s}{x} = n \cdot \frac{\pi \phi^2}{4} \cdot \tau \quad (3.30)$$

Eliminating n from the equation (3.29) yields:

$$k_a = \frac{P}{8 \cdot \pi \cdot \tau^2} \quad (3.31)$$

Use is sometimes made of an internal specific area, S (m^2). Let $S_a = n\pi\phi_a$:

$$k_a = \frac{S_a \cdot \phi_a}{32 \cdot \pi \cdot \tau} \quad (3.32)$$

Modifying the model to make it valid for three orthogonal directions involves dividing the equations by 3, e.g.

$$k_a = \frac{n_a \phi_a^2}{3 \cdot 32 \cdot \tau} \quad (3.33)$$

This is not very much better than the first equation of (3.27), however, concerning the large uncertainties connected with the other variables. The number 3 can easily be included in the tortuosity factor τ . The dividing of k_a by 3 in analysing three dimensions is not a good model of real pores, since these dwindle back and forth in many directions.

The parallel type model described above has the drawback of only going from one side to the other. A variant to the parallel type model is a model of the serial type with varying radius along its axis (Figure 3.33).

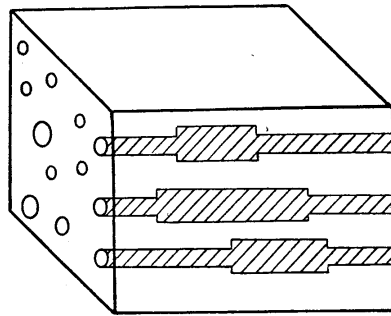


Figure 3.33 A serial type model (Scheidegger 1960).

Another pore space model is a *branching type model* in which a fluid flow channel can branch into several others, which later on, can join together again; see 343 and 351 in Figure 3.31.

The models of hydraulic radius theory are linked with the hypothetical channels in which flow is assumed to take place. A possible measure of a hydraulic radius, for example, would be the ratio of the volume to the surface of the pore space (Scheidegger 1960). The so-called Kozeny equation is

$$k = \frac{c P^3}{\tau S^2} \quad (3.34)$$

where k = specific permeability (m^2); c = “Kozeny constant” (0.50, 0.5619) for (circles, squares); P = porosity (m^3/m^3); τ = tortuosity factor = s/x ; and S = internal surface area (m^2).

The equation is similar to equation (3.32), except for the Kozeny constant c and how the tortuosity τ enters the equations. A variant of the Kozeny equation is the Kozeny-Carman equation. Two disadvantages of the Kozeny-Carman equation are that the porosity overestimates permeability and that the internal surface of all the small pores has a too large influence on the permeability.

Garboczi (1990) reviewed the Katz-Thompson permeability theory:

$$k = \phi_c^2 \cdot c/F \quad (3.35)$$

Where k = specific permeability (m^2); c/F = corresponds to $P \cdot r_w$ in section 2.4.6; c is calculated to 1/226 in Garboczi (1990); $F = D_{\text{bulk}}/D_{\text{eff}}$ = the quotient of the bulk diffusivity in diluted free water and of the effective diffusivity in small pores (measured in terms of electrical conductivity or diffusion); ϕ_c = critical pore diameter (m), see also section 3.6.8.

3.9.3 A non-pore space model: Darcy's law

Darcy (1856), in filtrating water through sand in a circular tube, found the following empirical relationship (*Darcy's law*) concerning homogenous flow in saturated, porous media:

$$q_w = -k_w \cdot A_{\text{tot}} \cdot \frac{(h_2 - h_1)}{L} \quad (3.36)$$

where q_w = the amount of the percolating fluid (m^3/s); k_w = the bulk permeability coefficient, which depended on both the porous media and the fluid (m/s); A_{tot} = the cross sectional area of the filter bed (m^2); h_1, h_2 = liquid that rises above an arbitrary level at the inlet or outlet end of the filter bed (m); and L = the length of the filter bed (m). See Figure 3.34.

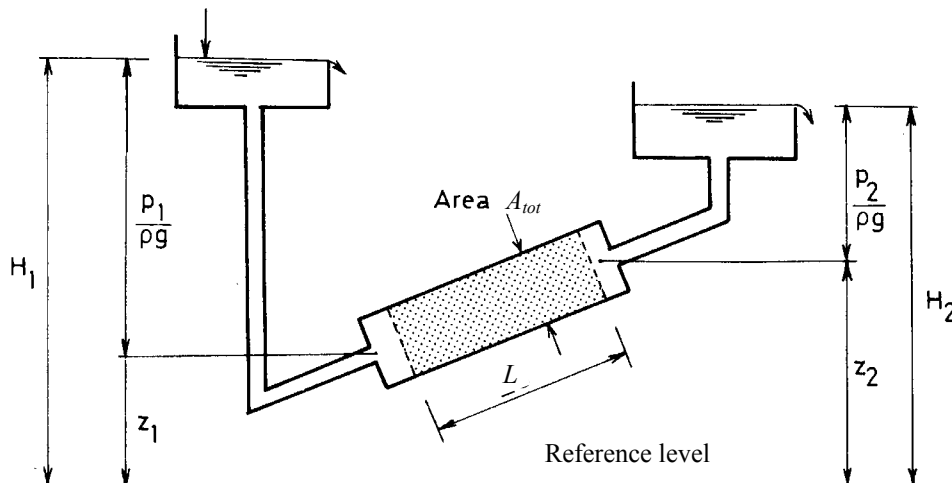


Figure 3.34 A principal figure in Darcy's experiment (Cederwall and Larsen 1976)

In its original form, Darcy's law overlooked hydrodynamic microscopic flow in a complicated system of pores. The law is an *averaging macroscopic* one (De Wiest 1969). The macroscopic approach is commonly used in modelling work and is the perhaps the only approach that can be verified experimentally. In practice, it is the value k_w that is usually measured and reported. According to Collins et al. (1986), there is evidence, however, (Ruetters et al. 1935, Powers et al. 1958) that the flow of water through saturated concrete, mortar and hardened cement paste very closely approximates Darcy's law.

Darcy's law is limited in some aspects. It is essentially valid for the following (Lage 1998):

- Homogenous, steady-state flux in saturated, porous media

- The permeability coefficient k_w , which is fluid-dependent (it depends on the viscosity)
- Incompressible fluids
- Isothermal conditions
- Creeping, laminar flow (very low velocity)
- Newtonian fluid
- Flow through a relatively long, uniform and isotropic porous medium
- A low level of hydraulic conductivity in the medium

Deviations from Darcy's law can occur (Hearn 1992) when:

- voids are incompletely saturated
- the pore structure and the volume change over time (e.g. due to continued hydration or to leaching)
- surface effects of the internal pore surfaces cannot be simply neglected
- there are osmotic effects
- under non-steady state conditions (e.g. involving changes in pressure)
- turbulent flows occur (although, probably not in concrete)

It would appear that there can scarcely be a "real" osmotic flow of water, caused by a hydraulic head. To build up osmotic pressure, there must be a semi-permeable membrane that lets only certain types of molecules or ions pass through. For example, water can pass through the membrane into an electrolyte, but the ions cannot pass out of the electrolyte through the membrane. Yet since concrete ions can pass through the matrix into the pure water on the upstream face, no osmotic pressure exists here.

Darcy's equation can be restated in terms of the pressure p and the density ρ of the liquid. The pressure at the two ends (see Figure 3.34) can be written as (Scheidegger 1960)

$$h_1 = p_1/(\rho \cdot g) + z_1; \quad h_2 = p_2/(\rho \cdot g) + z_2 \quad (3.37)$$

where $p/(\rho g)$ = pressure head (m); and z = height above an arbitrary reference level.

Darcy's equation can be reformulated to

$$q_w = -k_w \cdot A \cdot \frac{(p_2 - p_1) / (\rho \cdot g) + z_2 - z_1}{L} = -k_w \cdot A \cdot \frac{(\Delta p / \rho g) + \Delta z}{L} \quad (3.38)$$

Trying to write the equation for infinite filter lengths Δl and at the same time simplify by introducing a *hydraulic potential* (sometimes called a *piezometric head*), $P_w = p/\rho g + z$, and assuming no variation of K_w or ρ , Darcy's equation becomes:

$$v_w = -k_w \cdot \nabla P_w \quad (3.39)$$

where v_w = seepage velocity (m/s). Note that the velocity v_w is to be understood as the bulk velocity and not as the velocity u in an individual flow channel. For an an-isotropic porous medium, permeability becomes a tensor:

$$v_w = -\mathbf{k}_w \cdot \nabla P_w \quad (3.40)$$

A balance of the water volume can be written as

$$D \frac{\partial P_w}{\partial t} = \hat{c}_w - \nabla \cdot (v_w) \quad (3.41)$$

where D = damping; and \hat{c}_w = source or sink of water (m^3/s). Under steady-state conditions, the partial time derivatives and source term \hat{c}_w vanish. Combined with Darcy's law, the continuity equation becomes

$$\nabla \cdot (v_w) = \nabla \cdot (-k_w \cdot \nabla P_w) = 0 \quad (3.42)$$

To separate the influence of the porous medium from that of the liquid, the constant can be reformulated to the Hazen-Darcy equation:

$$k_w = k/\mu \cdot \rho_w \cdot g \quad (3.43)$$

where k = the specific (sometimes termed intrinsic) permeability coefficient, independent of the fluid (m^2).

In Scheidegger (1960), a number of investigations that were reviewed indicate Darcy's law to not be valid for seepage velocities above a "certain" value. This appears to be due to the non-linearity of the laminar fluid flows in real, curved tubes, and to end effects.

Also, molecular effects, boundary effects, surface effects and ion strength effects make Darcy's law fail, according to Scheidegger. In an electrolyte, the movement of the fluid past the boundary of the solid causes a downstream transport of the ionic charges in the upper part of the layer nearest the boundary. Powers et al. (1954) estimated the osmotic flow of water to be about 10% for hcp. This displacement creates a streaming potential, that results in the transport of ions ("electro-osmosis") in a direction opposite to the fluid flow. The total flow of an electrolyte through a porous medium is

$$q = q^* - q_{osm} \quad (3.44)$$

where q = total filter velocity (m/s); q^* = filtration velocity that would be present if there were no electric effects (m/s); and q_{osm} = filtration velocity due to electric effects (m/s).

Darcy's law is sometimes expressed as

$$q_w = -B \cdot \nabla p = -k_w \cdot g \cdot \nabla P_w; \quad k_w = g \cdot B \approx 10 \cdot B \quad (3.45)$$

where B = permeability (s) for a gradient in pressure (Pa).

Hagen-Poiseuille's law for liquid flow in cylindrical tubes is used below (Ruetters 1935) in an attempt to identify the permeability involved. Assume that water permeates through a number n_a of flow tubes of differing diameters ϕ_a that are connected through the concrete. Let there be N different size of diameters.

$$q_w = \sum_1^N (-n_a \cdot k_a \cdot A_a) \cdot \frac{\Delta P_w}{L_a} = \sum_1^N \left(-n_a \cdot \left(\frac{\phi_a^2}{32\mu} \rho_w \cdot g \right) \cdot A_a \cdot \frac{L}{L_a} \right) \cdot \left(\frac{\Delta P_w}{L} \right) \quad (3.46)$$

Darcy's law gives

$$q_w = -k_w \cdot A_{tot} \cdot \frac{\Delta P_w}{L} = \sum_1^N \left(-n_a \cdot \left(\frac{\phi_a^2}{32\mu} \rho_w \cdot g \right) \cdot \frac{A_a}{A_{tot}} \cdot \frac{L}{L_a} \right) \cdot \left(\frac{\Delta P_w}{L} \right) \cdot A_{tot} \quad (3.47)$$

Identifying k_w gives

$$k_w = \sum_1^N \left(n_a \cdot \left(\frac{\phi_i^2}{32\mu} \rho_w \cdot g \right) \cdot \frac{A_a}{A_{tot}} \cdot \frac{L}{L_a} \right) \quad (3.48)$$

or

$$k_w = \sum_1^N \left(\left(\frac{\phi_a^2}{128\mu} \rho_w \cdot g \right) \cdot \frac{n_a \cdot \pi \cdot \phi_a^2}{A_{tot}} \cdot \frac{L}{L_a} \right) \quad (3.49)$$

The permeability k_w depends on the viscosity μ , the effective diameter of the tube ϕ_i , the density of the fluid ρ , the ratio of the apparent to the true length of the tube, L/L_a and the term $n_a \phi_a^2 / A_{tot}$, which describes the amount (porosity) and distribution of tubes in relation to the area as a whole. The viscosity depends on the temperature and the type of fluid involved. The viscosity of the water flowing in such small channels as found in cement paste depends on the size of the channel, as was discussed in section 3.6.14.

Nycander (1954) presents the following relations concerned with the flow of water through concrete:

$$q_w = k \left(\nabla P_w + \frac{1}{8} (\nabla P_w)^2 \right) \quad (3.50)$$

For low-pressure gradients, the second term in the equation is neglected. The water flows as in the sand that Darcy's law describes. For high-pressure gradients, the first term is neglected. Nycander explains the second term with the assumption of the flow channels widening due to elastic strains in the material or to the compression of entrapped air.

Powers (1979) proposed a permeability coefficient for water movement in very fine gel pores. It assumes the particles to be spherical and to depend on the internal specific surface area and the free energy of activation for flow:

$$q = K_1 \frac{\Delta h}{L} A \quad (3.51)$$

where

$$K_1 = \frac{2\rho_w g}{\eta_i A_{int}^2} \frac{P}{1-P} e^{-\frac{\Delta G}{RT}} \quad (3.52)$$

where K_1 = the coefficient of permeability for the hydraulic head, seen as a pressure gradient (m/s); Δh = the hydraulic head (m); L = the thickness of a specimen (m); A = the cross-sectional area of a specimen (m²); ρ_w = the density of water (kg/m³); η_i = the coefficient of viscous resistance under ideal conditions; A_i = the internal area (m²); P = porosity (m³/m³); ΔG_{ex} = Gibbs free energy of activation for flow in excess of that present under ideal flow conditions (J/mole); R = the ideal gas constant (8.314 J/K/mole); and T = temperature (K).

Powers using experimental data from tests of the permeability of cement paste specimens, suggested that the free energy of activation for flow varies with porosity is

$$\frac{\alpha}{T} \cdot \frac{(1-P)}{P} = \frac{\Delta G_{ex}}{R \cdot T} \quad (3.53)$$

where α = a constant. Powers investigated the permeability of different cement pastes at differing temperatures. He obtained estimates of the internal surface A_{int} that he

compared with data obtained using the BET method. He concluded that all evaporable water, also the gel pore water, moves under an externally produced pressure gradient. However, since in practice permeation in concrete mostly involves capillary flow, the equation is not particularly applicable (Young 1988).

4 The experimental work

4.1 Background

A hydraulic structure of concrete, such as a dam, will sooner or later be broken down by nature, even if it may take hundreds or thousands of years. Hydration products in concrete, and sometimes in the aggregate as well, are soluble in water to varying degrees, especially in soft water. On the upstream surface of a dam, leaching takes place as a diffusion of dissolved ions into the water reservoir. Some of the dissolved ions follow the water flow through the structure and out the backside of the dam (Figure 4.1). If the backside of the dam is exposed to water or to air of high humidity, such as around spillways, the flow of water, and ions may not stop. If the water at the backside is vaporised, calcium ions can readily precipitate to form calcite “curtains”, and the flow of water and ions decrease.

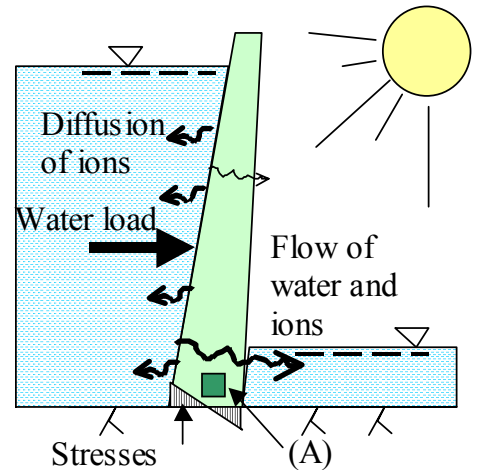


Figure 4.1 A concrete dam subjected to lime leaching. (A) = fictive place for tested concrete.

The concrete tested in this work is assumed to have almost the same properties and exposed to almost the same boundary condition as concrete in the location (A) in a fictive dam as shown in Figure 4.1.

4.2 Aim and general setup

The aim of the experimental work carried out was to study the leaching process and its effect on the mechanical properties of concrete.

The concrete examined was subjected to leaching in three different ways:

1. By the homogenous, steady-state percolation of deionised water through concrete that was rather porous, though “defect-free”
2. By the percolation of deionised water through artificially-made holes in the concrete
3. By diffusion-controlled leaching at the free surfaces of the concrete laying in stagnant, de-ionised water

By the “homogenous, steady-state percolation of water through defect-free” concrete is meant the macroscopic, homogenous, steady-state percolation (Darcian flow) of water in concrete in which no holes, cracks or other types of flow paths have been made artificially. On a microscopic scale, of course, no flow of water through concrete is homogenous, but on a larger scale, in concrete that has been produced in a normal way, the flow of water can usually be assumed to follow Darcy’s law. More concerning Darcy’s law is taken up in section 3.9.3.

All the concrete specimens studied were saturated with water prior to the leaching tests being carried out. This condition corresponds to location (A) in Figure 4.1. Three different water-to-cement ratios (w/c), 0.6, 0.8 and 1.3, were involved. The concrete was cured and was treated in five different ways, being *virgin (V)*, *early-heated (EH)*,

late-dried (LD), late-dried after being leached while in a virgin state (V-LD) and late-dried after being leached while in an early-heated state (EH-LD). A more precise account of the various test methods, the concrete and the states which the concrete was tested is presented in the sections that follows.

The basic principles behind the three different types of leaching tests are shown in Figure 4.2. Figure 4.3 is a photograph of the laboratory where the testing took place. Figure 4.4, finally, presents the complete test program in brief.

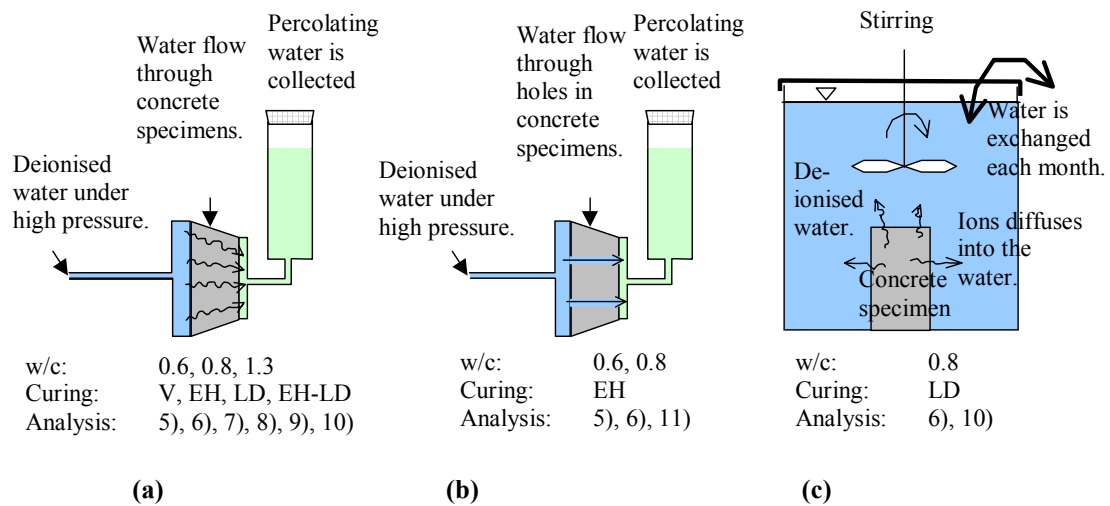


Figure 4.2 Experiments performed in the present work, (a) “homogenous percolation of water through defect-free” concrete, (b) percolation through artificially-made holes in the concrete and (c) leaching from free surfaces of concrete placed in stagnant, deionised water. Figure 4.4 serves to clarify the curing that takes place and the various types of analyses performed.

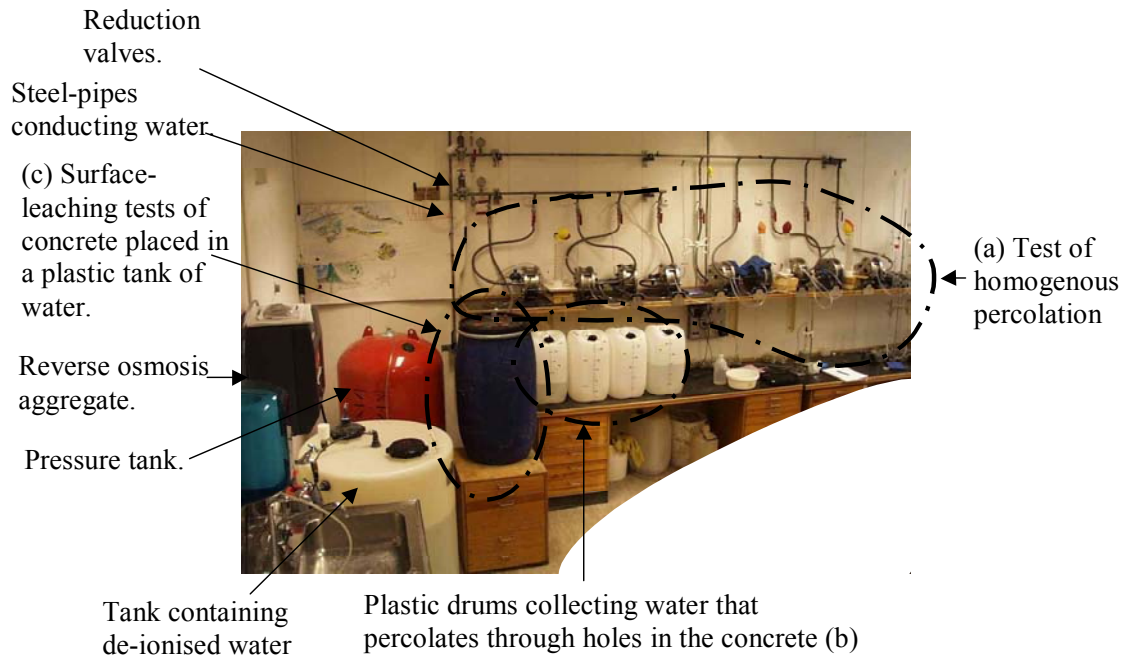


Figure 4.3 Photo of the laboratory showing the test equipment. See Figure 4.2 for explanations of the tests (a), (b) and (c).

4.3 Concrete specimens

4.3.1 An overview

Concrete specimens with w/c ratio of 0.6, 0.8 and 1.3 were tested. No admixtures or additives were used. The amount and type of the aggregate in the concrete differed somewhat for the different w/c ratios. The recipes used for producing the different types of concrete are shown in Table 4.1. The specimens are classified in two major ways. First, they are classified in terms of the different w/c ratio 0.60, 0.80 and 1.29 (Table 4.1). Secondly, they are classified in terms of how the specimens were cured or treated, as *V*, *EH*, and *LD*. It turned out that a very important factor for the water permeability was how the specimens were treated before the test, (see section 4.3.5). The specimens used in any of the three types of leaching tests (see section 4.2) are termed *test specimens*. Reference specimens, basically the same as the leached specimens except for their not being subjected to any aggressive form of water are termed *reference specimens (R)*. The reference specimens were always exposed to lime-saturated type.

Before the test started, all dried samples (*LD*, *V-LD*, *EH-LD*) were water-saturated by vacuum treatment followed by water absorption.

Table 4.1 Recipes for the different types of concrete employed.

| ID, W/c ratio | Curing ¹⁾ | C ²⁾ (kg/m ³) | A ₀₋₈ ³⁾ (kg/m ³) | A ₄₋₈ ³⁾ (kg/m ³) | A ₈₋₁₂ ³⁾ (kg/m ³) | A ₁₂₋₁₆ ³⁾ (kg/m ³) | V _p ⁴⁾ (m ³ /m ³) | V _a ⁵⁾ (m ³ /m ³) | V _{air} ⁴⁾ (m ³ /m ³) | ρ _c ⁶⁾ (kg/m ³) |
|------------------|-------------------------|---|--|--|---|--|---|---|---|--|
| 0.60 | EH, EH-LD | 335 | 1232 | 555 | - | - | 0.31 | 0.68 | 0.013 | - |
| 0.80a | V, LD | 241 | 936 | - | 469 | 467 | 0.27 | 0.72 | 0.008 | 2370 |
| 0.80b | V, V- LD | 241 | 938 | - | 469 | 469 | 0.27 | 0.72 | 0.006 | 2375 |
| 0.80c | EH-LD | 289 | 1179 | 571 | - | - | 0.32 | 0.67 | 0.013 | 2325 |
| 1.29 | V, LD | 177 | 916 | - | 459 | 459 | 0.28 | 0.71 | 0.008 | 2317 |

¹⁾ See section 4.3.5 for description of the curing methods.

²⁾ Portland cement with a moderate heat of hydration of the type CEM I 42,5 (“Degerhamn anläggningcement”).

³⁾ Aggregate: Kvidinge sand (2640 kg/m³) 0-8 mm, Hardeberga quartzite (2550 kg/m³) 4-8, 8-12 and 12-16 mm. The fraction of the aggregate between 8 and 16 mm represented only 1.8 % of the total aggregate in terms of weight.

⁴⁾ V_p = volume of paste calculated as = C(0.32+w/c)/1000.

⁵⁾ Total volume fraction of the aggregate.

⁴⁾ Air content, measured by the pressure method in *Bluhm and Feurherdt* a apparatus of 8.0 litre content.

⁶⁾ Measured density of test cement.

Table 4.2 gives the number of specimens of the different types of concrete.

Table 4.2 Numbers of specimens¹⁾ of different w/c ratio, diameter and curing type.

| Curing ²⁾ | ID (see Table 4.1) | | | | | |
|----------------------|--------------------|--------|------------|--------|-------|--------|
| | 0.6 | | 0.8a, 0.8b | 0.8b | | 1.29 |
| | Specimen diameter | | | | | |
| | 155 mm | 45 mm | 155 mm | 155 mm | 45 mm | 155 mm |
| V | - | - | 6 (2) | - | - | 1 (1) |
| EH | 4 (4) | 1 | - | - | - | - |
| LD | - | - | 2 (1) | - | - | 3 (1) |
| V-LD | - | - | 3 (5) | - | - | - |
| EH-LD | - | 11 (9) | - | 2 (1) | 6 (5) | - |

¹⁾ The numbers with and without brackets denote reference specimens leached specimens, respectively.

²⁾ V = virgin, EH = early heated, LD = late dried. V-LD and EH-LD means specimens first being leached in a V or of EH state and then being further leached in a LD state.

Figure 4.4, presents the complete test program, all the specimens tested being shown.

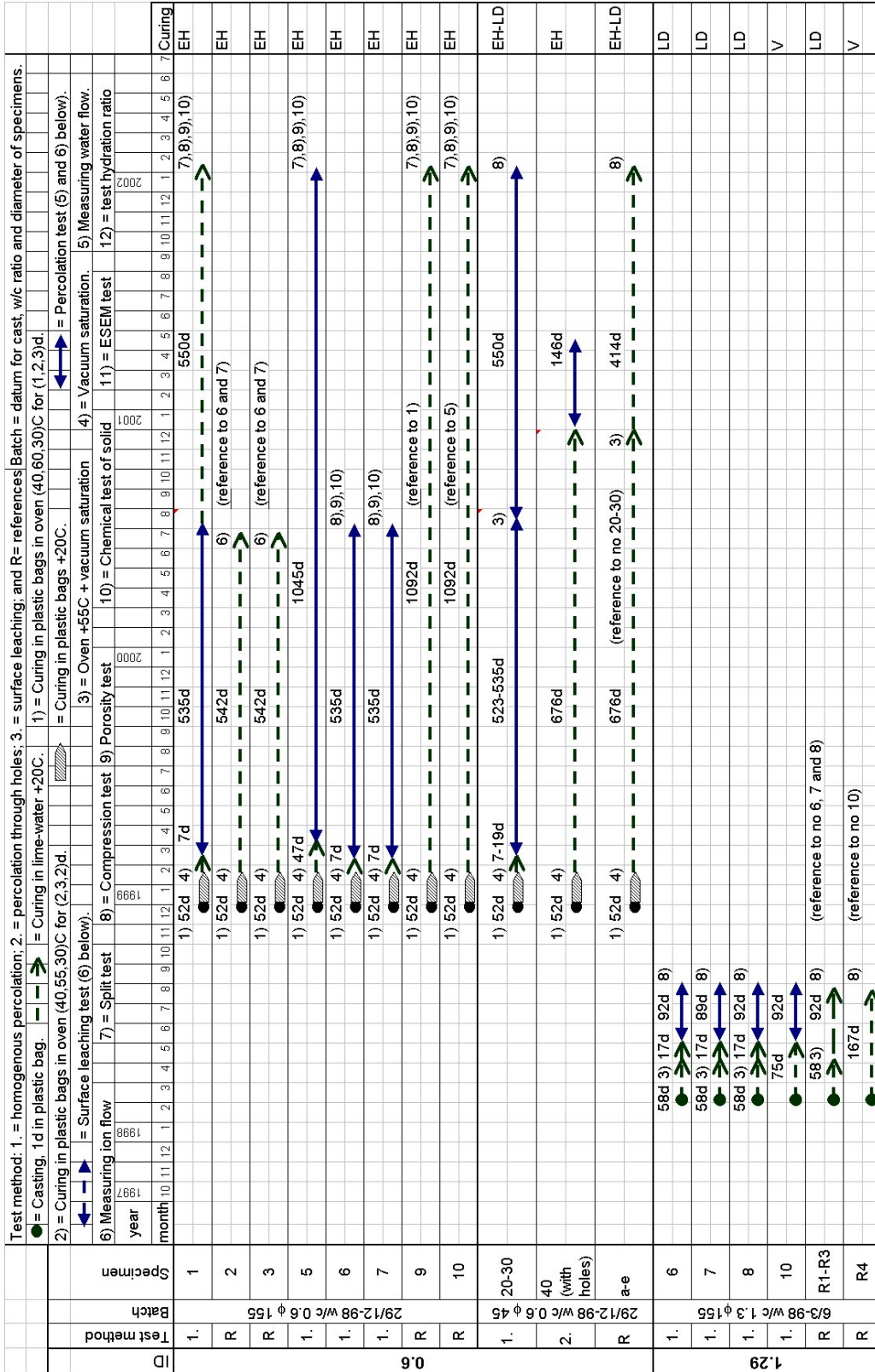


Figure 4.4 Complete test program for all specimens with a w/c-ratio of 0.60 or 1.29 that were tested.

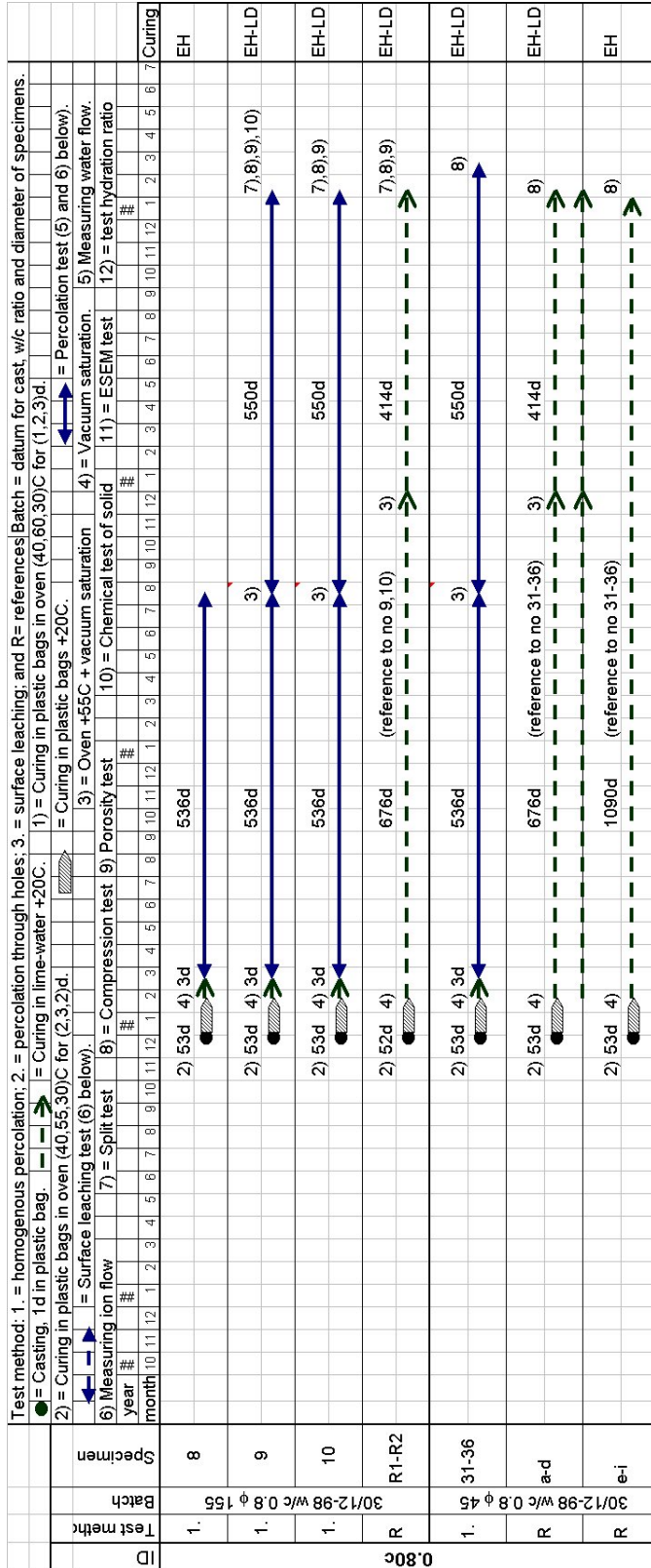


Figure 4.6 Complete test program for all specimens of the 0.80c that were tested (all with a w/c-ratio of 0.80).

4.3.2 Cement

A low alkali sulphate resistant Portland cement with moderate heat of hydration (“Degerhamn anläggningcement”) of the type CEM I 42,5 according to the European Standard was used for all concrete studied. Table 4.3 shows the average chemical composition of the cement during 1997 and 1998. Cement from 1997 was used for the concrete denoted as 0.80a, 0.80b or 1.29, see Table 4.1. Cement from 1998 was used for the concrete denoted as 0.60 or 0.80c.

Table 4.3 Average chemical composition of the cement that was used during 1997 and 1998. The analyses were performed by CEMENTA, Sweden.

| Cement | Oxides % | | | | | | | | | | Clinker minerals | | | |
|-------------|----------|------|------------------|--------------------------------|--------------------------------|------------------|-------------------|------|-----------------|-----|------------------|------------------|------------------|------------------|
| | Type | CaO | SiO ₂ | Al ₂ O ₃ | Fe ₂ O ₃ | K ₂ O | Na ₂ O | MgO | SO ₃ | Cl | Ignition | C ₃ S | C ₂ S | C ₃ A |
| Period 1997 | 65.5 | 22.7 | 3.56 | 4.32 | 0.57 | 0.05 | 0.45 | 2.07 | 0.02 | - | 55.7 | 22.8 | 2.1 | 13.1 |
| Period 1998 | 65.4 | 22.7 | 3.5 | 4.2 | 0.6 | 0.1 | 0.7 | 2.1 | 0.0 | 0.4 | 57.3 | 21.8 | 2.1 | 13 |

4.3.3 Aggregate

Aggregate of the type *Hardeberga quartzite* 2630-2640 (kg/m³) and *Kvidinge sand* 2599 (kg/m³) was used. All aggregate is assumed to be non-porous with the same bulk density as the compact density. The modulus of elasticity, compressive strength, tensile strength and ignition loss for the two types of aggregate have been studied by Hassanzadeh (1994) (Table 4.4).

Table 4.4 Modulus of elasticity (E), compressive strength (f_{cc}), tensile strength (f_{ct}) and ignition loss for the two used types of aggregate used (Hassanzadeh, 1994).

| Aggregate type | E (Gpa) | f_{cc} (MPa) | f_{ct} (MPa) | Ignition loss (%) |
|----------------------|---------|----------------|----------------|-------------------|
| Hardeberga quartzite | 60 | 330 | 15 | 0.3 |
| Kvidinge sand | 61 | 150 | 10 | 0.8 |

Figure 4.7 shows the sieve curves for the individual fractions of aggregate as well as the size distribution of the two types of aggregate mixture used in the concrete.

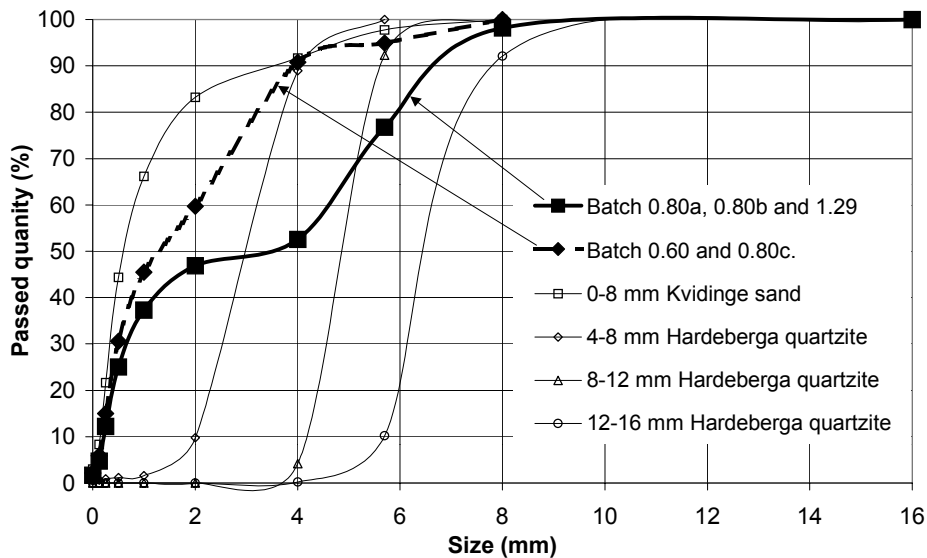


Figure 4.7 Sieve curves for the different individual fractions of aggregate employed and the size distributions of the two different aggregate mixtures used in the concrete batches.

The gradation curves of the two aggregate mixtures for the concrete used are quite normal for Swedish concrete. No optimal curve with regard to impermeability was sought. Note that for batches 0.80a, 0.80b and 1.29 the fraction of aggregate between 8 and 16 mm was only 1.8 % of total the aggregate weight.

4.3.4 Casting

The concrete was mixed in an ordinary laboratory concrete mixer. The cement and aggregate were mixed for about 3 minutes, whereupon ordinary municipal tap water was added and the mixing continued for about another 3 minutes. Two sizes of conical specimens were cast, the one having a top-diameter of 158 mm and a bottom diameter of 150 mm and the other having a top-diameter of 51 mm and a bottom diameter of 45 mm. All the specimens had a height of approximately 50 mm.

All the test specimens were cast in steel cylinders (Figure 4.8). The cylinders were smeared with grease on the inside circumference prior to casting so as to be easier to remove when demoulding them. The steel cylinders were the same ones that the concrete specimens were placed in during the percolation test that was later performed. The thickness of the specimens (~50 mm) was adjusted to the correct value by use of a piece of wood. The steel cylinders with the fresh concrete inside were placed on a piece of hard fibreboard and were vibrated on a vibrating table for approximately 15-20 seconds.

Certain water separation occurred on top of those specimens that had a w/c ratio of 1.29.

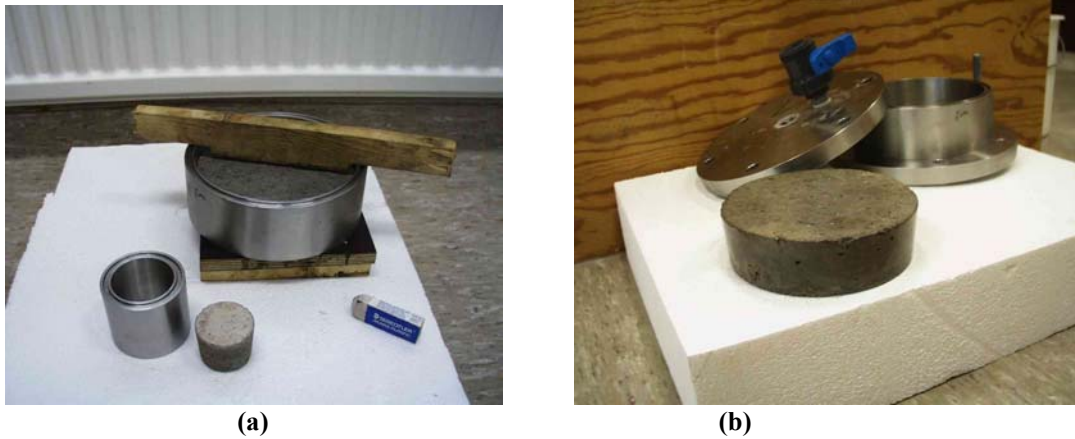


Figure 4.8 The test specimens were cast in steel cylinders placed on fibreboard. The proper size was achieved by use of a piece of wood (a). A test specimen 150 mm in diameter placed next to the test cell in which it was later subjected to water percolation (b).

Some of the ϕ 45 mm diameter specimens were made with holes that penetrated them. The holes were produced by letting 3 pieces of 0.7 mm steel wire be fixed in each mould during casting, see Figure 4.9. The wires were smeared with grease to make them easier to remove at demoulding.



Figure 4.9 Some specimens of those ϕ 45 mm in diameter were cast with steel fibres of only 0.7 mm in diameter sticking through them. After demoulding, the steel fibres were removed, leaving thin holes through the specimens. The wire in the figure is not stretched as it would be during casting.

Reference specimens were produced in 300-mm long steel cylinders with diameter 150 mm and were cut a few days after casting into disks 150 mm in diameter and 50 mm thick. Some of the conical specimens described above were also used as reference specimens.

After being kept in their moulds placed in plastic bags for about 24 hours, all the specimens and cylinders were unmoulded.

The ends of the specimens were neither brushed nor treated in any other way prior to the leaching tests being performed.

4.3.5 Curing

The experimental specimens were divided into five groups with respect to how they were cured or treated (see also Figure 4.4):

1. *V* = *virgin* specimens. These had never been dried or leached before the leaching test was carried out. They were placed in lime-saturated water and were kept there until the leaching test was begun.
2. *EH* = *early heated* specimens. After demoulding, the concrete was put in plastic bags and was placed in ovens. Concrete with a w/c ratio of 0.6 was put in an oven at 40, 60 and 30°C for 1, 2 and 3 days, respectively, the concrete with a w/c ratio of 0.8 being put in an oven at 40, 55 and 30°C for 2, 3 and 2 days, respectively. After being taken out of the oven, the specimens remained in the plastic bags in air at +20 °C for some time. This type of curing is assumed to be comparable to adiabatic curing in a real dam (“mass curing”, as Ruettggers 1935 denoted it). The concrete was heated but was not dried. The specimens were water-saturated by vacuum just before the leaching tests began
3. *LD* = *late-dried* specimens. These were hardened virgin specimens (*V*) that were placed in an oven +55°C when they were 58 days old (specimens 1.29, see Figure 4.4) or 201 days old (specimens 0.80a, see Figure 4.5). They were kept there for seven days without any protection against evaporation of moisture.
4. *V-LD* = specimens being first leached in a virgin state (*V*) for a number of days (see specimens 0.80b in Figure 4.5) and then dried at +55°C for 5-7 days without drying protection.
5. *EH-LD* = specimens being first leached in an early-heated state (*EH*) for a number of days (see Figure 4.4 and Figure 4.6) and then dried at +55°C 5-7 days without drying protection.

The specimens that were heated or dried were water-saturated by vacuum treatment, followed by water absorption, just before the leaching test started. Since the virgin (never dried) specimens were assumed to already be water saturated, no vacuum treatment was carried out.

Figure 4.4 provides a more precise account of how the individual specimens were treated.

Figure 4.10 provides an overview of the curing methods employed.

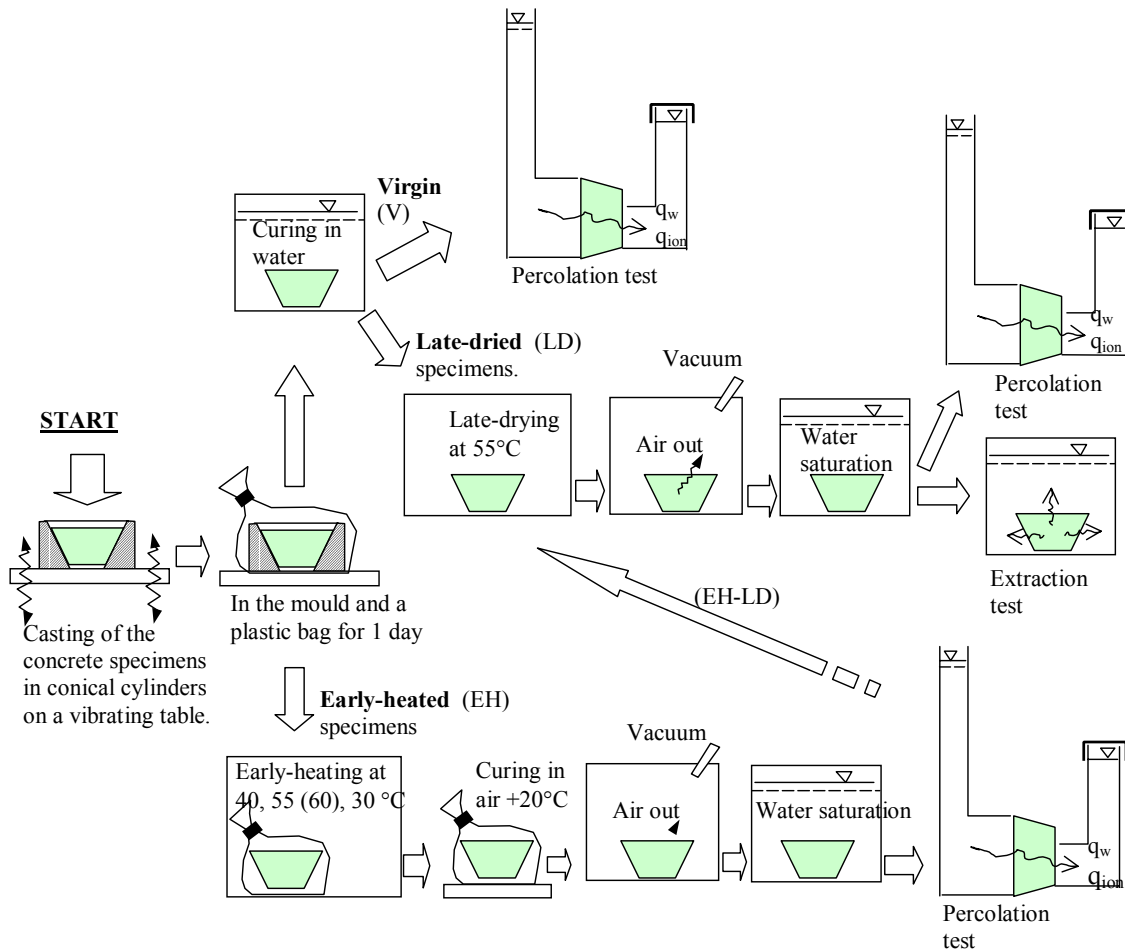


Figure 4.10 Curing history of the different concrete specimens employed in the present work.

4.4 Homogenous steady-state percolation of water through defect-free concrete

4.4.1 Introduction

To observe the leaching process in concrete in as similar conditions as possible to the position (A) in Figure 4.1, a test equipment was constructed in which water was allowed to percolated homogeneously through the concrete specimens. *Homogenous steady-state percolation* can be equated with Darcian saturated flow, the porous medium (the concrete) being assumed to be homogenous and isotropic and to contain randomly oriented pores. The leaching is a sort of “homogeneous internal leaching with water pressure gradient” (Fagerlund 2000). The equipment consisted of a deionising aggregate, a water tank storing deionised water, a pump, a pressure tank, a pipe system conveying water to a number of test cells containing concrete specimens and finally to measuring vessels for collecting the water that percolated (Figure 4.11). The water pressure difference applied to the specimens was in most cases 6 bar corresponding to an average pressure gradient of 12 MPa/m.

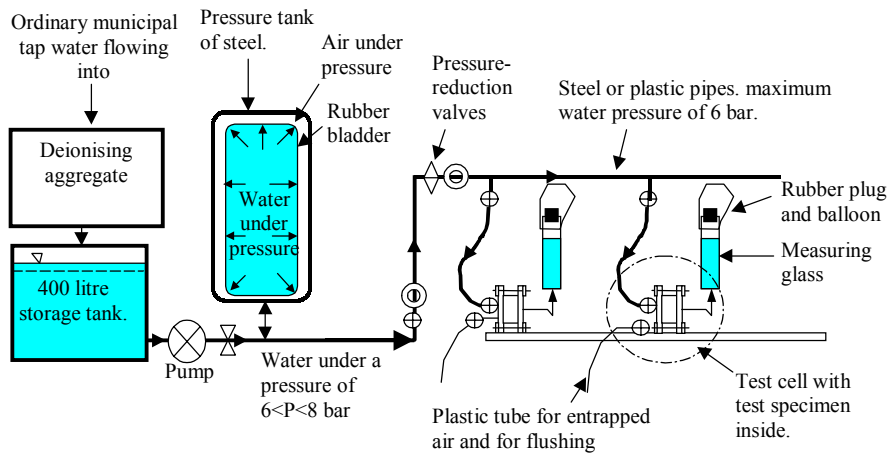


Figure 4.11 Permeability equipment, consisting of a deionising aggregate, a storage tank, a pump, a pressure tank, pressure reduction valves and a number of test cells containing concrete specimens.

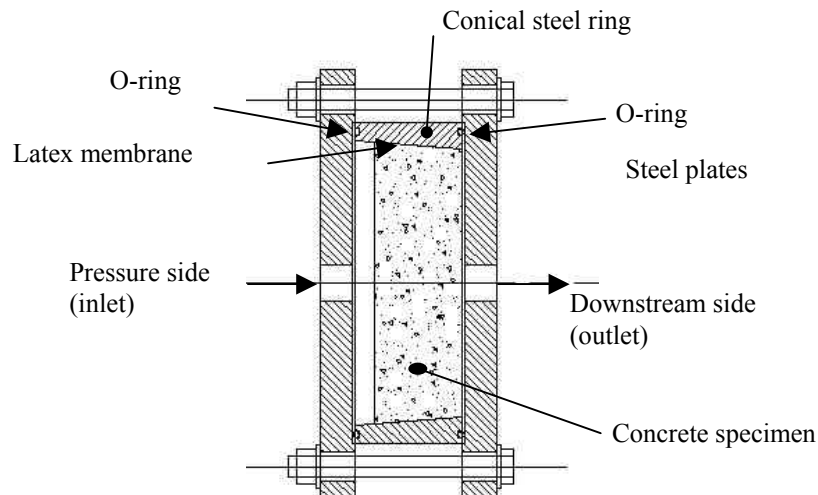


Figure 4.12 A test cell containing a concrete specimen.

4.4.2 Apparatus

The deionising aggregate was an ordinary reverse-osmosis aggregate, filtrating out most of the ions contained in the tap water. The conductivity of the water was reduced from about 300 to about 2-4 $\mu\text{S}/\text{cm}$, shown by the conductivity meter mounted on the aggregate. Table 4.5 shows the result of an analysis of the water after it had passed the through deionising aggregate.

Table 4.5 The properties of the deionised test water.

| <i>Property</i> | <i>Value</i> |
|-----------------------------------|--|
| $pH^{1)}$ | 6.25 |
| <i>Alkalinity</i> ¹⁾ | 3.25–4.5 mg CaCO ₃ /l |
| <i>Hardness</i> ¹⁾ | 0.20 mg CaCO ₃ /l |
| <i>Conductivity</i> ¹⁾ | 8.7 $\mu S/cm$ (2-5 according to the ELGA's meter) |
| $Ca^{2)}$ | 1.034 mg/l |
| $Mg^{2)}$ | 0.045 mg/l |
| $Na^{2)}$ | 1.337 mg/l |
| $K^{2)}$ | 0.316 mg/l |

1) Measured by titration and by ion selective electrodes.

2) Measured by ICP-AES (see section 5.2.3)

After passing through the de-ionising aggregate, the water was stored in a 400 litre plastic tank. It was then pumped into an ordinary pressure tank designed for apartment buildings, containing a rubber container inside a steel tank. As the rubber container was filled, the air pressure between it and the steel tank increased. This led to an increase in the water pressure in the rubber container. The pump was set to automatically shut off when the water pressure had reached 8 bar. By “water pressure” is meant *overpressure* above atmospheric pressure.

From the pressure tank, the water flowed in a stainless steel pipe to three pressure-reduction valves. The valves were set to maintain a certain pressure at the outflow side, despite changing inflow pressure when water was drained from or flowed into the pressure tank. These valves made it possible for the three outlet pipes to have different pressure.

From the pressure-reduction valves, the water flowed to a series of test cells through stainless steel pipes. A shut-off valve was located before each of the test cells so that individual cells could be taken out of the system at any time. Another shutoff valve was mounted to the upstream steel plate of each the test cells, used for flushing out water from the inlet, just upstream the specimens. Because of the water being very pure, all parts in the system were made of acid-proof material.

The test cells were made of acid-proof stainless steel. Two sizes of cells were employed, one for specimens about $\phi 155$ mm in diameter and the other for specimens about $\phi 45$ mm in diameter.

Each test cell was composed of a cylindrical part and two endplates, see Figure 4.12. Rubber O-rings were placed between the plates and the cylinder. The concrete specimens were cast directly in the cylinders. The cylinders were conical inside so that the water pressure applied during the leaching test would press down the concrete specimen and tighten it against the steel through a thin latex membrane..

Entrapped air under the upstream lid was led out by way of the shutoff valves.

The percolating water was collected in burettes, beakers or plastic drums, depending upon the flow rate and amount of water involved. In order to maintain the purity of the inlet water, this was flushed out and renewed once a week.

4.4.3 Tested material

All of the specimens shown in Figure 4.4 except for specimens 0.80a:R2 and 0.60:40 were tested under conditions of homogenous steady-state percolation. Specimens

0.80a:R2 and 0.60:40 were tested by the surface leaching test and the test of percolation through specimens with artificially-made holes are described in the sections that follows.

4.4.4 Test procedure

The test specimens were taken from the curing water one by one. After being in open air for about 2-3 minutes, silicon grease was smeared on the outer, cylindrical and conical surface of each specimen. A latex tube was forced around the cylindrical surface. Further silicon grease was applied to the latex tube and to the inside surface of the steel cylinder in which the specimen was later mounted. The grease and the latex tube were used to achieve a perfect sealing. A 100-150 mm long soft plastic tube for conveying percolated water from the specimens to the measuring vessels during the leaching test was mounted onto the outlet nipple on the bottom lid of each test cell. An O-ring was mounted on the bottom end of the steel cylinder and the cylinder was placed on the bottom lid. The cylinder was filled with deionised water. The concrete specimen was then placed inside the cylinder, entrapped air and some water from the bottom of the cylinder being pressed out during the mounting of the specimen. The water had the function of preventing carbon dioxide from coming into contact with the downstream end of the concrete specimen and preventing the bottom end from drying before the test started. The top lid with its O-ring was mounted and the cell was assembled by a number of steel bolts. The inlet tube from the steel-pipe system to the cells was fixed to the top of the lid and the desired water pressure was applied through use of the shutoff valve. The entrapped air was released through the air valve located atop the lid of the test cell.

The test cells were placed on a shelf, the cylindrical surface of each laid on its side, the measuring vessels being connected to the soft plastic outlet tubes.

To prevent moisture leakage from the measuring vessels and CO₂ from coming in contact with the percolating water during the test, rubber plugs and balloons were mounted atop the vessels. When larger drums were used to collect the percolating water, plastic tubes were placed around the soft plastic tube that led from the test cell into the hole in each drum.

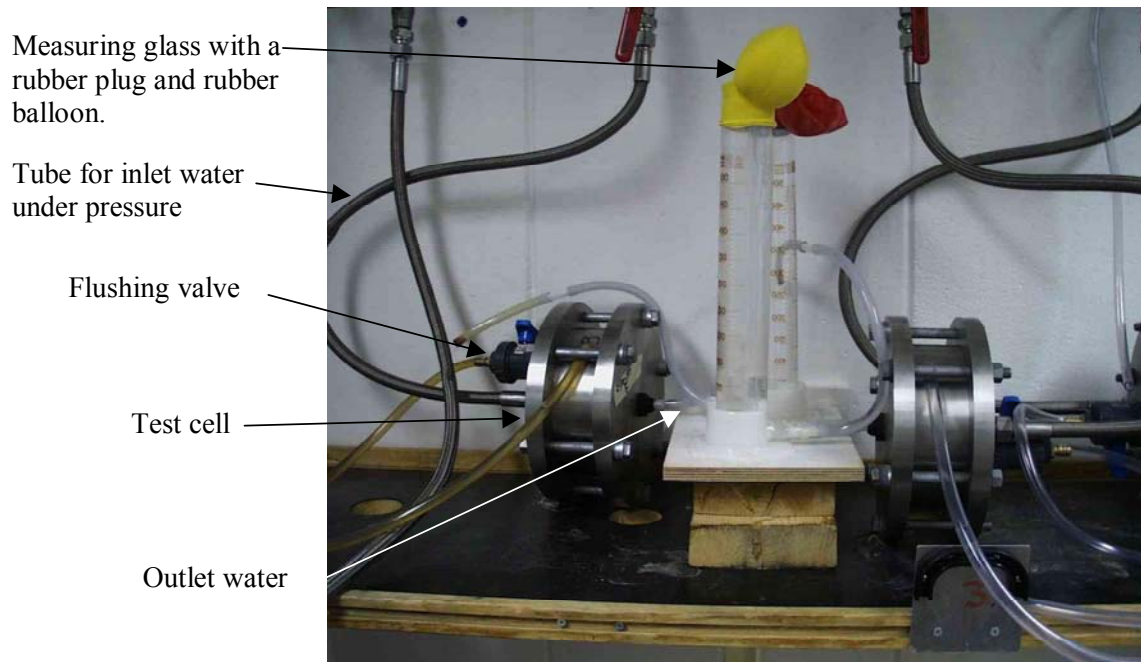


Figure 4.13 Test cells with incoming and outgoing water tubes and collecting vessels for (a) test specimens 150 mm in diameter and (b) test specimens 45 mm in diameter.

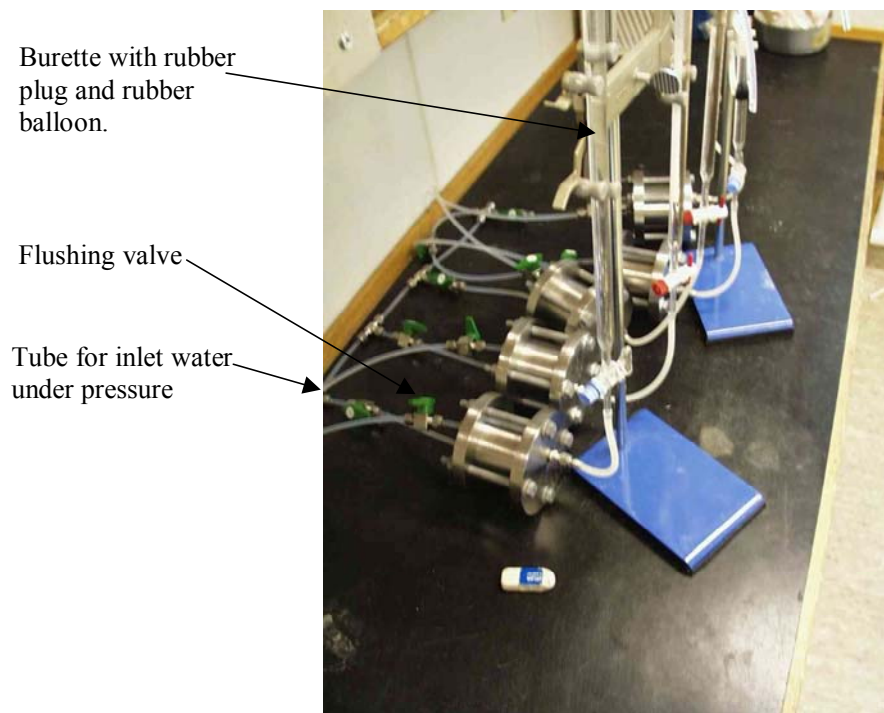


Figure 4.14 Test cells with incoming and outgoing water tubes and collecting vessels for (a) test specimens 150 mm in diameter and (b) test specimens 45 mm in diameter.

4.4.5 Measurements and presentation of data

4.4.5:1 Measuring water flow

The amount of water that percolated (sometimes called *drainage water*) was measured regularly by reading the water level in the measuring vessels. When a water-collecting vessel was full, and the amount of water had been measured, the vessel was emptied into the sink or was collected in small plastic bottles, holding *drainage water samples* for further chemical analysis.

4.4.5:2 Measuring of ionic flow

The pH and ion concentrations in the drainage water that was collected were checked and recorded regularly, pH being measured by pH electrodes and the concentrations of calcium by Ca^{2+} selective electrodes or by ICP AES (section 4.7).

In a real dam, with a large water reservoir at its upstream face, the dissolved ions from the concrete do not influence the ion concentration in the inlet (upstream) water very much. In the experiments conducted, however, the small volume of the upstream water was contaminated rather quickly with dissolved ions coming (diffusing) from the test specimens. To avoid this, the inlet water was flushed through the air valves on the upper lid once or twice a week. Doing this enabled rather pure water condition to be maintained on the upstream face of each specimen, at least during the first one or two days after each flushing. The volume flushed on each occasion was about 2 litres per specimen for the $\phi 150$ mm specimens and 0.2-0.3 litres for the $\phi 45$ mm specimens. The water flushed out was occasionally collected and analysed chemically in the same way as the drainage water.

4.4.5:3 Analysis of specimens

When the percolation test was completed, each of the leached specimens and unleached reference specimens was first split into two halves (Figure 4.15) so as to obtain the split tensile strength. Three small cylinders were then drilled out from each of the 150 mm diameter specimens and were tested for compressive strength. The quarter of each specimen that remained was then cut into a number of slices (usually 7), each being analyzed with regard to porosity and the elements it contained (Ca, Na, etc). The analyses are described later in the chapter.

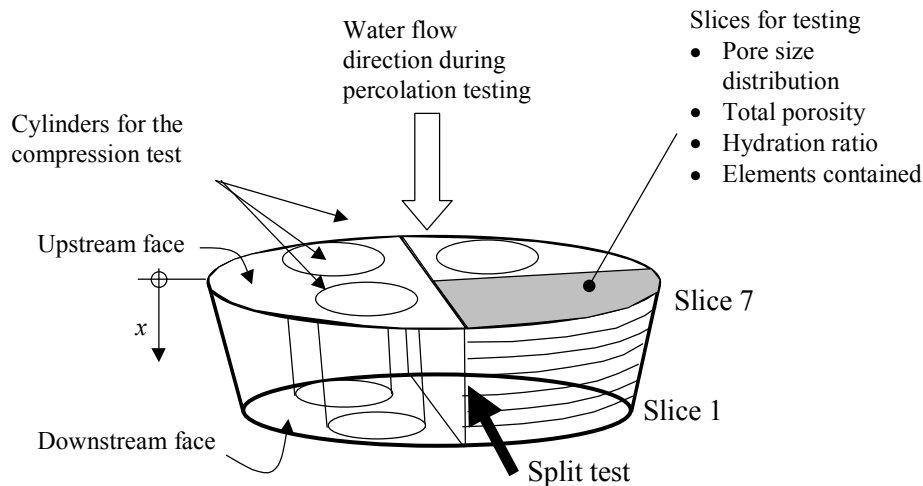


Figure 4.15 Analyses performed on the specimens.

4.4.6 Validity

4.4.6:1 Introduction

The aim of the experimental testing carried out was to imitate percolation through concrete at location (A) in a dam shown in Figure 4.1. One can question how valid the results are for concrete situated in real dams surrounded by a real environment.

The test specimens can, of course, not be of the same geometric size as a real structure. Also, a real environment is very difficult to predict and imitate. The chemical, physical, mechanical and biological impacts the environment can have on a dam can vary considerably during the lifetime of a dam. In real dams there are often several, degradation mechanisms all in effect at the same time, possibly also working together in synergy and thus leading to more rapid degradation.

There would have been no point in attempting to investigate the entire spectrum of factors that could influence the leaching process in a concrete dam. This would have involved too many parameters to all be considered at the same time.

The methods of investigation employed must thus be considered to be lacking in validity in some respects. The effects of the following factors are probably greater in the test than they would be in the case of a real dam:

1. The curing and treatment methods; e.g. drying
2. The water pressure gradient; 12 MPa/m compared to < 0.03 MPa/m in reality
3. The water to cement ratios; as high as 1.29
4. The aggressiveness of the water; deionised
5. The lack of any contact between atmospheric CO₂ and concrete.

The effects of the following factors may cause an underestimation of the effects they could be expected to have on a real dam:

1. The lack of aggressive ions (such as CO₂, H⁺ and SO₄²⁻) in the water. Some CO₂ from the air was dissolved by the water storage tank, however, producing to a pH of about 6-7.
2. The temperature; 20°C instead of a normal value of +5 - +8°C
3. Loads; constant load, confined concrete

4. Synergy between different degradation mechanisms; only leaching is investigated
5. Size of the aggregate; smaller than in a real structure

To increase the validity of the conclusions of this investigation field studies of real dams ought to be conducted in the future.

Various factors that could influence the validity of the results are discussed below.

4.4.6:2 *Saturated specimens*

In reality, dams and other hydraulic structures are probably not always completely saturated with water. The degree of saturation depends on the initial and boundary conditions and the geometry of the structure. In a saturated specimen, a steady-state flow of water occurs. In unsaturated concrete the flows is smaller. In the present investigation, all the specimens were saturated, this representing an accelerating factor.

4.4.6:3 *Curing*

In real dams, the curing conditions may differ considerably. The skill of the builder, the type of curing system employed, the type of concrete involved, the size and geometry of the structure, and the moisture and temperature conditions in the surroundings may all influence the results of curing. When sufficient water is supplied during hydration and small temperature gradients are involved, concrete can be a tight and strong material. Inside a real dam which is thick and lacks any cooling, large amounts of heat can be released during hydration, resulting in fairly high temperatures, up to 80°C (Fagerlund 1997c). This heat can influence the composition of the hardened concrete. Both swelling due to a gain in heat during hydration and shrinkage during the heat loss that occurs during the cooling period may cause the concrete to crack. If cooling is employed during the hydration period, problems of cracks can be largely avoided. The thinner the structure, the easier it is for heat and moisture to flow out (or in) through the surface of the structure. The temperature rises in thin structures becomes smaller during hydration than it does in the interior of a thick structure. During the filling of the reservoir behind a dam, the water gradually penetrates the pore system of the dam until the concrete is saturated to a certain level above the ground. Above this level, the concrete has a relative humidity of less than 100%. In massive dams, the filling of the pore system of the entire dam with water may take many decades or even centuries. In a thin specimen stored in water the filling might be complete after a few days.

Below the “hydrostatic pressure line”, or in parts of the dam where capillary forces are active the concrete is largely saturated. If the water level upstream or downstream rises, previously dried concrete becomes saturated again, if the new water level is maintained for some time. If the water level upstream or downstream is lowered, and the water level remains low for some time, drying of the concrete occurs. If the ambient temperature is high or the sunshine is intense, the concrete is also heated. It is important to note that the changes in moisture content referred to take time, especially in the case of thick dams.

In the present work, five different types of curing (or treatment) were used, V, LD, EH, V-LD and EH-LD, cf. section 4.3.5. A major aim in employing different types of curing was to achieve rapid and reliable leaching rates comparable to those in real dams. Different locations in which these five types of curing are likely to occur in real

dams, provided the concrete is similar in all other respects (w/c, type of cement, aggregate, etc.), are indicated in Figure 4.16.

V (*virgin specimens*): Concrete of this type has never been dried, except a certain self-desiccation the first day, when it was hardening in plastic bags. The high water-to-cement ratio, the small specimen size and the fact that the specimens were put in a water tank after demoulding, probably resulted in almost no drying and in the temperature gradients being small, resulting in few micro-cracks.

The quality of the concrete tested may be quite similar to that of the concrete found in real dams, situated below the water surface (e.g. at location V in figure Figure 4.16).

LD (*late-dried specimens*): Concrete of this type was dried for one week at +55°C after being immersed 2 to 6.5 months in lime-saturated water. After drying, it was resaturated. The specimens were therefore well-cured with a degree of hydration of about 0.7-0.9 when the drying started. +55°C is a rather moderate drying temperature, which might occur in a real structure. The curing and treatment are quite similar to that concrete in real dams which for some reason dries fast (e.g. because of curing being momentarily stopped or the water table being lowered during a very warm summer period of intense sunlight) and is then re-saturated through the water table rising. Such concrete could be located at LD in Figure 4.16.

EH-S (*early-heated specimens*): Concrete of this type was heated in plastic bags placed in an oven immediately after unmoulding and then saturated with water after being cured for some time.

Such concrete could represent location EH in Figure 4.16. There, the concrete is at high temperature and has no loss of moisture during hydration, except for water losses due to chemical reactions. After the filling of the reservoir, the pore system of the dam is gradually saturated with water. The filling of the pore system with water in the present test specimens through use of vacuum treatment is of course much more rapid than the filling of the pores in a real concrete dam. Leaching starts also quicker than in real dams.

V-LD (*late-dried specimens first leached in a virgin state*): Concrete of this type was first leached in a virgin state, then dried in an oven at +55°C, re-saturated and leached again. Such concrete could represent location V-LD in Figure 4.16, where leached and saturated concrete has been dried and heated again (such as because of a lowering of the water table during a warm and sunny period) and then resaturated (because of a subsequent rise in the water table).

EH-LD (*late-dried specimens first leached in an early-heated state*): Concrete of this type was first leached in an early-heated state, then dried in an oven at +55°C, resaturated and leached again. Such concrete could represent location EH-LD in Figure 4.16, where early-heated saturated concrete has been dried and heated again (e.g. because of a lowering of the upstream water table during a warm and sunny period) and then resaturated (because of the upstream water table rising again).

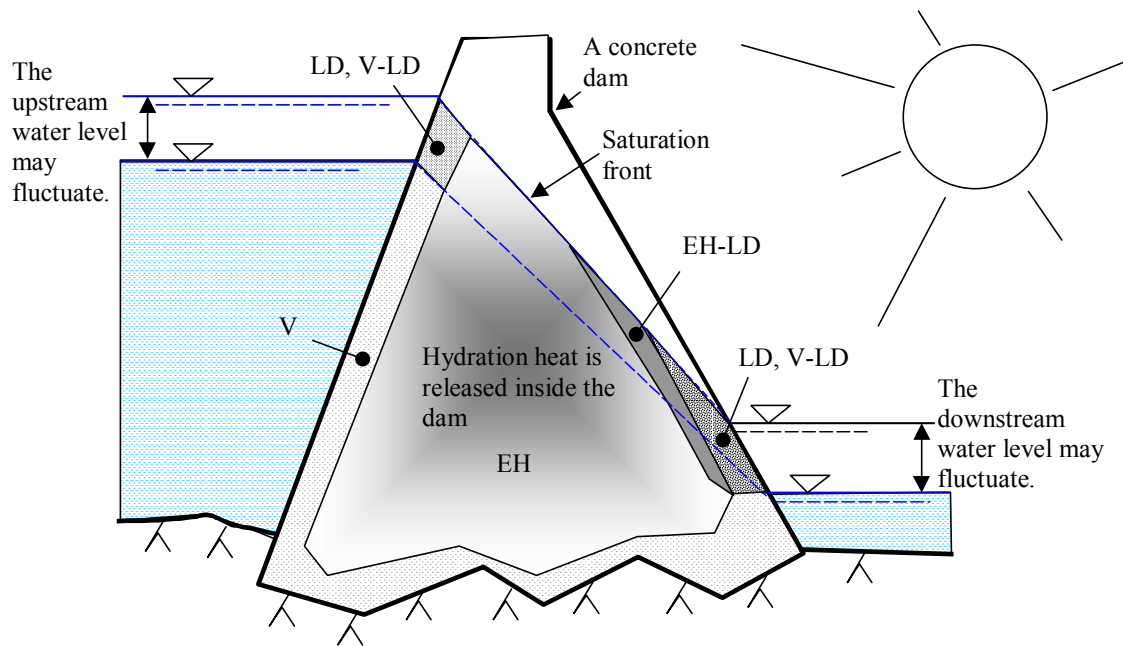


Figure 4.16 Curing conditions in real dams.

Common to all the concrete and curing types tested is that the moisture changes and the re-saturation were much more rapid than they would be in real concrete.

4.4.6:4 Water-to-cement ratio

In modern watertight structures the w/c ratio usually does not exceed 0.55-0.60. In some structures, however, badly cast or older, higher w/c ratios are possible. Supporting parts in dams, such as the main section of an RCC-dam, an old dam of a massive type or the pillars in a buttress-dam, may often have high w/c ratio. In such cases, any cracks in the tight front slab may lead to high water leakage through the supporting parts, with corresponding leaching.

In the present experiments, the water cement ratios tested were 0.6, 0.8 and 1.29. These rather high values were selected with of the aim of attaining a high level of permeability, of imitating the behavior of old concrete dams and of studying the *leaching process*. It is doubtful whether a w/c ratio of 1.29 is found in any real structures, although it may possibly be found in parts of dams where the casting has failed, in the supporting parts of older dams, or in the grout curtains located beneath certain dams. It was difficult to cast concrete having as high a w/c ratio as 1.29 and the specimens probably received certain initial flow paths due to water separation. A small amount of the water separated from the upper surface of the concrete during casting probably evaporated, making the w/c ratio somewhat less than 1.29. At the same time, the water separation probably led to certain flow paths around the aggregate remaining when the water disappeared, making the permeability higher.

4.4.6:5 Water aggressiveness

Much of the water in nature is *soft*, such as water from melting snow or rainwater flowing over or through insoluble ground materials. Water of this type is rather common in mountainous terrain of the type found in northern Sweden in which the soil

contains granite or gneiss often covered by peat. Such water has a very strong ability to dissolve hydration products from concrete. If acids are also dissolved in the water, the aggressive effect may be still greater. Natural waters that interact with the atmosphere or come from areas of decomposing organic matter contain such ions as CO_2 , H^+ and SO_4^{2-} that are aggressive towards concrete. According to Myran (1967), the pH-values in river water at thirty dam locations in Norway vary between 4.7 and 7.1 and the concentration of CO_2 between 1.0 to 19.3 mg/l. Since marshy waters can contain large amounts of CO_2 , as well as other acids such as humic acid, the pH there can be low, perhaps as low as pH 3-4. Moskvin (1980) provides an example of marshy waters in Siberia that contain up to 50 mg CO_2 /l. The aggressiveness of different types of water was discussed in chapter 2.

In the present study, the test specimens were exposed to deionised water in which only atmospheric carbon dioxide was dissolved. The pH was measured to be 6.25. See Example 2.1, where carbonic acid of $1.83 \cdot 10^{-8}$ mole/l gave a pH of 6.92, which is higher than the measured value obtained. Perhaps the concentration of dissolved H_2CO_3 was somewhat higher in the experiment than assumed. If the concentration of H_2CO_3 in the example presented were increased to $[\text{H}_2\text{CO}_3] = 4.6 \cdot 10^{-7}$ mole/l ($K_{\text{CO}_2(\text{aq}) \leftrightarrow \text{H}_2\text{CO}_3} = -1.4$), the pH value would decrease to the measured value 6.25.

Since the downstream surface of the test specimens was exposed to percolated water only, the ion types there were the same as in the pore water inside the specimens.

It can be said that in the experiments used the water conditions on the upstream surface of the concrete were more aggressive, but on the downstream surface more non-aggressive in comparison with the conditions in a real dam.

4.4.6:6 *No atmospheric CO_2 in contact with the concrete*

The surfaces of real dams that are in contact with air are also in contact with atmospheric CO_2 either before or during the test. If water percolates through a dam, calcium contained in this water, together with atmospheric CO_2 , often form calcite curtains on the downstream surfaces of the dam. This leads to a reduction in the permeability of the dam and to further leaching.

The concrete specimens used the present work had no contact with atmospheric CO_2 . The test methods employed thus represent an aggravation of the processes normally occurring in dams that have surfaces which are in contact with atmospheric air.

4.4.6:7 *The temperature was held constant at 20°C*

In real concrete dams, the temperature differs with the season, with the location and size of the dam, with the orientation of the dam towards the sun and with where in the dam the section of concrete of interest is located. Below the water table, the temperature may vary between perhaps 4 and 10°C. Above the water table, the temperature follows the air temperature, which can of course differ considerably during the course of the year. Inside the dam, the temperature varies between that on the upstream face, the ground and the downstream face of the dam. The thicker a dam, the stronger the influence of the ground temperature on the temperature of the dam. Temperature changes on the surface are too slow to influence the interior of the dam. The interior temperature of a thick dam can be expected to be about 5 to 10°C most of the year. When the temperature in a thinner dam changes, the concrete may either expand or shrink. The

resulting tensions can cause the concrete to crack. The solubility of the solid materials in the concrete also differs with the temperature. For calcium hydroxide, $\text{Ca}(\text{OH})_2$, the constituent most decisive for leaching, the solubility at decreasing with increasing temperatures.

The present test equipment was placed in a room held at a constant temperature of $+20^\circ\text{C}$. The fact that the temperature in the experiment was rather high compared with the temperatures in real dams and that it was held constant throughout testing, was probably a clear limitation of the test method employed.

4.4.6:8 *Size of the aggregate*

The aggregate used was smaller than that used in real dams. This probably resulted in the permeability being lower than in real dams.

4.4.6:9 *Hydration effects and type of cement*

The shortest curing time before the leaching test began was 83 days (1992 hours) for the water-cured specimens with a w/c-ratio of 0.8, and 58 days (1392 hours) for the water-cured specimens with a w/c-ratio of 1.3. This means that for most of the specimens the degree of hydration at the beginning of the leaching tests was probably high, between about 0.7 and 0.9. Two batches (0.60 and 0.80c) were cured in plastic bags (membrane cured) and were not water-cured as the others. They were cured for 52 days (1248 h), which probably means that the degree of hydration was somewhat lower. The cement used in many older dams in Sweden was of a slower type in terms of rate of hydration development.

The degree of hydration reached in the tests is, however, probably in parity with the that reached in real dams.

4.4.6:10 *The pressure gradient*

A *massive gravity dam* often has a pressure gradient of about a 1.1 to 1.4 meter water head per meter of width of the structure (mwh/m), a 100 m high dam being about 70 to 90 m wide at the base. The major parts of such dams may have water-to-cement ratios as high as those used in the present study, only the upstream parts usually tending to have lower w/c ratio. The pressure gradient in such a dam is generally steeper over the tighter parts and flatter over the more permeable supporting parts of the dam. For massive gravity dams with a separate *front slab*, the water pressure gradient over the latter can be as high as about 40 (mwh/m). *Arc dams* can have pressure gradients of up to 20 (mwh/m). *Buttress dams* can have gradients of about 30 to 40 (mwh/m) over their front slabs. The pillar itself may have a more complex pattern of gradients, the complexity depending on the geometry, the possible cracks that leak water and the moisture conditions close to the pillar.

The tight front layer in massive dams and arc dams and the front slabs in buttress dams are usually of very good quality concrete, however, with a low w/c, so that the high pressure gradients are not particularly dangerous, although around embedded parts such as joint bands, gate abutments or gate folders, where the concrete can be difficult to cast, the pressure gradient can be high (perhaps 100-200 mwh/m) and the concrete can be of bad quality.

In the 50 mm thick specimens in the homogenous percolation tests of concrete presented here, the pressure difference was 60 meter, i.e. 1200 mwh/m. This is much

higher than in real dams, even if it might occur in certain exceptional cases. A high gradient leads to a strong water flow and a high leaching rate. The pressure gradients were sometimes changed during the tests to study the influence of pressure on permeability.

4.4.6:11 Loads

Real dams can crack from stresses caused by external or internal loads. Cracks increase the permeability, making hydration products accessible to water, which in turn results in higher leaching rates. If the stresses vary in intensity, the cracks also vary, which can hinder any autogenous sealing or self-sealing that might occur.

The specimens examined in the percolation test were supported along their circumference. The conical shape of the specimen and of the steel cylinder in which the specimen was mounted meant that water pressure therefore could be used to force the specimen downwards and outwards. The water pressure only produced normal stresses in the specimens. The stresses in the experiments were always constant.

4.4.6:12 Orientation of casting

In the leaching test performed the direction of water flow was the same as the direction of the cast. The upstream surface in the leaching test was also the same as the upper surface during casting. If the water content is high, however, the concrete tends to develop vertical channels during the bleeding period (Powers 1954). Thus, in the present test, the permeability might have been lower if the water had been pressed through the specimens in the other direction (perpendicular to the cast direction).

In real dams the cast is often oriented perpendicular to the direction of water flow. This often leads to the permeability being higher due to incomplete compaction, the presence of horizontal lift-joints, etc. It is difficult to say whether the direction of the cast for the present specimens led to the permeability being higher than in real dams.

4.4.6:13 End effects

There may have been an end effect in the specimens, decreasing the permeability as compared with longer specimens (cf. Ruettgers et al. 1935). A possibly better way of producing the test specimens would have been to cast them in longer cylindrical steel cylinders and to then cut off a bit of the upper and lower part and only use the middle section.

4.4.6:14 Anisotropic measurements of permeability

Later in this study, calculations of the permeability coefficient based on different quantities of water measured in the experiments are presented. This permeability coefficient is calculated as if the flow of water was laminar and occurring in an isotropic porous medium in one direction only. In reality, the concrete specimens probably did not possess isotropic permeability.

4.4.6:15 Cement

Cement in old dams is not exactly of the same type as that used in the studies reported here, but the old types, often coarsely ground with high content of C_2S , are not manufactured any longer. The cement used, however, is the most similar type available on the market in Sweden today.

4.4.6:16 *Synergy between degradation mechanisms*

In reality, there are many other degradation mechanisms than those studied here that act on the concrete simultaneously (such as leaching, freeze-thawing, alkali-silica reactions and erosion). Frost damage can cause substantial cracking of concrete, its of course increasing the permeability.

No other degradation mechanisms than leaching were studied in this study.

4.4.7 Errors of testing and the reliability of the results

4.4.7:1 *Introduction*

The reliability of test results depends on the accuracy of the test methods employed. The reliability can be quantified by use of variation coefficients based on large numbers of test results. If a variation coefficient is low this implies that the test method in question possesses good reliability. Any source of error known should be taken account of in estimating reliability. Two types of reliability can be distinguished:

- ✓ *Repeatability*: This involves there being a low degree of variation in the test results when a test is repeated using the same batch of material, the same test equipment and the same test personnel.
- ✓ *Reproducibility*: This involves there being a low degree of variation in the test results when a test is repeated using for the same batch of material, but conducting testing in another laboratory by other test personnel using other test equipment.

In this report, only repeatability is taken into account. The reproducibility of the results the test methods employed not having been checked in any other laboratory. The reliability of the test results as whole depends on the reliabilities of the different test methods used for determining leaching and permeability.

4.4.7:2 *Undesired water leakage*

Any possible leakage of water between the concrete specimen and the steel cylinder rather than through the concrete specimen provides wrong and misleading results. If there is evaporation from the measuring vessels, this also gives wrong and misleading results.

(i) Water leakage between the specimen and the steel cylinder:

The very uniform flow of water obtained in the experiments indicates all or almost all of the water volume to have permeated the concrete and not to have passed through the boundary between the specimen and the cell wall. If water had passed through this boundary, its flow would probably not have been as uniform as it was. In case of leakage, the silicon grease used at the boundary would probably have been eroded and the water flow has increased with time. Although there in many cases was a gradual increase in water flow, in such cases distinct *channels* through the concrete specimens involved were always observed. No signs of water flow through the slot between the specimen and steel cylinder were observed. When dismantled, none of the concrete specimens showed any sign of corrosion on the surface that had been placed against the steel cylinder. The surfaces in question were smooth, showing no signs of leaching at the surface, even for those specimens through which large amounts of water had flowed.

In order to test the tightness of the boundary between the specimen and the cell wall, the top surface and the side of one of the concrete specimens were covered by a tight latex foil. No flow of water was observed, suggesting the boundary to be completely tight.

(ii) Evaporation from measuring the vessels:

If the water collected were to evaporate, the flow of water measured would be too small and the content of dissolved ions as measured too high. If CO₂ enters the water that is collected, it reacts with the dissolved calcium in the water, so that calcite is produced and the pH is reduced. Under such conditions, later examination of the Ca²⁺ content and the pH gives wrong and misleading results. Thus, it is important that there be a tight layer between the air and the vessel used to collect the water. This is especially important for tight specimens in which the flow of water is low.

The soft plastic tube leading the water that is collected from the test cells to the burettes was made to be as short as possible. When a burette was used as measuring vessels, a rubber plug and a rubber balloon were placed on top of it to prevent moisture diffusion to the air and CO₂ diffusion from the air.

The specimens using a measuring glass as a measuring vessel had the same short soft-plastic tube and rubber balloon placed on top.

The very permeable specimens that used a plastic drum for collecting the drainage water had a longer soft-plastic tube from the test cells to the drums, about 0.5m in length. Because of the high level of water flow the evaporation of moisture and the dissolving of CO₂ in the water were not as important as for the other specimens.

The tightness of the rubber plugs and the balloons that were used in the percolation tests were studied in a special test. One measuring glass and one burette, each with a rubber plug and a balloon on top were filled with water. The decrease of the water level was measured over a period of time. The results indicate only an insignificant evaporation through the plug and balloon. The largest degree of evaporation measured in this test compared with the smallest measured flow of water in the percolation test was in a ratio of 1 to 30.

4.4.7:3 *End effects*

Because of the manner of preparing specimens for testing, or for reasons other than this, there can be an end effect that makes short specimens less permeable, for a given unit of length, than long specimens are (Ruetters 1935). It can be suspected that certain end effects were present in the work reported here as well. When concrete is cast in such small forms as the steel forms $\phi 155$ and $\phi 45$ in diameter and 50 mm in depth that were used here, the cement paste and the aggregate may not be very uniformly distributed within the specimen.

Regarding permeability, however, any effects of this sort were of no critical importance, since it was not the aim of this work to determine the permeability of concrete in general. The major aim of testing was to study the *leaching process*.

4.4.7:4 *Decrease in flow area.*

When the specimens were taken out of the test cell after testing was finished, it could be seen in some cases that *the latex tube* around the concrete had been pressed out about 1 cm on the top and the bottom end of the specimen. The out-pressed part of the tube was

so loose that water had no problem in going beneath it. The flow area involved had not decreased.

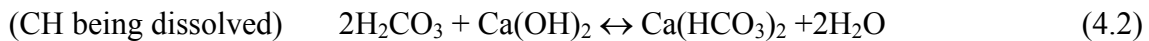
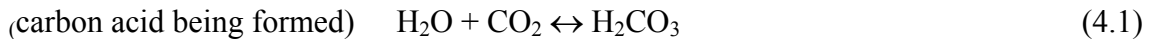
4.4.7:5 Carbonation

There is always a risk of atmospheric *carbon dioxide* CO_2 , coming in contact with the calcium hydroxide in the concrete, either by way of the water on the inlet side or on the outlet side, resulting in carbonation. If the concrete is carbonated, its permeability is likely to decrease. Also, the drainage water on the outlet side may become carbonated if CO_2 leaks into the measuring vessel. If the drainage water becomes carbonated, there is a risk that the measured ion content and the pH will be too low.

(i) Water at the inlet side:

Some CO_2 from the atmosphere can be assumed to have been dissolved in the water of the storage tank. It was earlier estimated that about 0.31 mg/l of atmospheric CO_2 dissolves in water under ordinary partial pressure. This 0.31 mg CO_2 means that $0.31 \cdot 10^{-3} \text{ g} / 44 \text{ g/mole} = 7.0 \cdot 10^{-6} \text{ mole H}_2\text{CO}_3$ is formed in each litre of water.

When CO_2 is in contact with the pore solution, the following reactions can occur:



As can be seen in equation (4.2), two moles of H_2CO_3 can dissolve one mole of Ca(OH)_2 to produce one mole of $\text{Ca(HCO}_3)_2$. The one mole of calcium bicarbonate produced may either flow out of the concrete by convection or diffusion, or react with one mole Ca(OH)_2 to form one mole of CaCO_3 (equation (4.3)).

Later, more H_2CO_3 , may reach this CaCO_3 , dissolve it and then flow through the concrete and out of it, equation (4.4). If only Ca(OH)_2 is leached, the capillary porosity and the permeability may increase, but if CaCO_3 is formed as well, the permeability may decrease again.

Example:

The following example indicates how the permeability can be influenced if reaction equations (4.2) and (4.3) applied to specimen 0.80a:3.

At the end of the leaching test, 12 litre of water had penetrated the specimen. The dimension of the specimen were $V_{\text{specimen}} = \pi \cdot 0.155^2 / 4 \cdot 0.050 = 9.4 \cdot 10^{-4} \text{ m}^3$. The capillary pore volume of the specimen was assumed to be $V_{\text{cap}} = (w/c - 0.39\alpha) \cdot C / 1000 \cdot V_{\text{specimen}} = (0.8 - 0.39 \cdot \alpha) \cdot 245 / 1000 \cdot 9.4 \cdot 10^{-4} = 0.110 \text{ m}^3 / \text{m}^3 \cdot 9.4 \cdot 10^{-4} \text{ m}^3 = 1.0 \cdot 10^{-4} \text{ m}^3$.

The molar weights of Ca(OH)_2 and CaCO_3 is $74.08 \cdot 10^{-3}$ and 100.08 kg/mole , respectively. The densities of Ca(OH)_2 and CaCO_3 is approximately 2300 and 2700 kg/m^3 respectively.

If only equation (4.2) applies, the volume of dissolved calcium hydroxide is approximately

$$V_{\text{Ca(OH)}_2, \text{leach}} = n_{\text{Ca(OH)}_2} \cdot M_{\text{Ca(OH)}_2} / \rho_{\text{Ca(OH)}_2} \cdot V_w = \frac{1}{2} \cdot 7 \cdot 10^{-6} \cdot 74.08 \cdot 10^{-3} / 2300 \cdot 12 = 13.6 \cdot 10^{-10} \text{ m}^3$$

The calcium bicarbonate formed may flow out of the concrete by convection or diffusion, or react with more Ca(OH)_2 to form CaCO_3 . If this happens, as described in equation (4.3), and no backward reaction occur, the volume of calcium carbonate formed will be approximately:

$$V_{\text{CaCO}_3, \text{leach}} = n_{\text{CaCO}_3} \cdot M_{\text{CaCO}_3} / \rho_{\text{CaCO}_3} \cdot V_w = 7 \cdot 10^{-6} \cdot 100.08 \cdot 10^{-3} / 2700 \cdot 12 = 31.1 \cdot 10^{-10} \text{ m}^3$$

Both the increase in capillary volume due to the leaching of Ca(OH)_2 and decrease in capillary volume due to the crystallisation of CaCO_3 , as the theoretical example above shows, are insignificantly small compared with the capillary volume of $9.4 \cdot 10^{-4} \text{ (m}^3\text{)}$, their thus not being able to influence the permeability.

If the water has percolated through only a few main channels, however, there may be a significant increase in permeability. Assume hypothetically there to be one hundred channels in form of flow tubes with an initial diameter of 0.1 mm, which makes the volume of these channels (or tubes) to $V_{100 \text{ tubes}} = 100 \cdot \pi \cdot (10^{-4})^2 / 4 \cdot 0.05 = 393 \cdot 10^{-10} \text{ m}^3$. If the water had only leached Ca(OH)_2 as described in equation (4.2), the diameters of the hundred channels could have increased to $(4 \cdot (13.6 + 393) \cdot 10^{-10} / (100 \cdot \pi \cdot 0.05) - (10^{-4})^2)^{0.5} = 0.14 \cdot 10^{-3} \text{ m}$ and, in accordance with the Hagen-Poiseuille law, the permeability could have increased $(0.14/0.1)^4 = 4$ times. Thus, if there were very few channels, this could influence the permeability. Similarly, the CaCO_3 which is formed may lead to a significant decrease in permeability, if there are only a few channels to take account of.

(ii) At the outlet side:

At the outlet side, the drainage water is in contact with concrete all the time. The vessels in which the drainage water is stored are sealed from atmospheric CO_2 by rubber plugs and balloons. When the plugs and balloons were removed to empty the vessel, some CO_2 came in contact with the drainage water, but the emptying was so rapid that no significant amount of CO_2 could be dissolved. Some CO_2 was trapped inside the vessels however, when they were emptied.

Assuming 1 litre of air to have been trapped, a total pressure of 1 atm, a temperature of 25 °C and a partial pressure of CO_2 to $3 \cdot 10^{-4} \text{ atm}$ (Atkins & Jones 1997 p. 535) gives

$$n = PV/(RT) = 3 \cdot 10^{-4} \cdot 1 / (8.206 \cdot 10^{-2} \cdot 293) = 12 \cdot 10^{-6} \text{ mole} \quad (4.5)$$

where n = number of CO_2 molecules (mole); P = partial pressure of CO_2 (atm); V = volume of trapped air (litre); R = gas constant (litre·atm/K/mole); and T = temperature (K).

This amount of $\text{CO}_2(\text{aq})$ can carbonate about $0.5 \cdot 12 \cdot 10^{-6} = 6 \cdot 10^{-6} \text{ mole Ca(OH)}_2(\text{aq})$ to CaCO_3 . Since in one litre of drainage water, however, there is about $15 \cdot 10^{-3} \text{ mole Ca(OH)}_2$, the drainage water acts as a large buffer that traps any CO_2 there before it reached the concrete. Whatever leakage of CO_2 to the outlet side occurs is thus assumed to not influence the permeability.

4.4.7:6 *Effect of air-filled pores in the concrete*

When the test started, some of the concrete specimens had not been saturated, by means of the vacuum saturation method described earlier, but since they had been stored in a water tank all the time they were probably almost completely saturated, possibly except for some remaining air-filled compaction pores. Measurements of the air content of the concrete when it was cast, showed the volume of the air to typically be about 0.6- 1.3 % of the volume of the concrete. For the specimens with the dimensions of $\phi 155\text{mm} \cdot 50\text{mm}$, this meant that there was about $1.0\% \cdot 0.155^2 \cdot \pi / 4 \cdot 0.055 = 9.4\text{ ml}$ air in each specimen. During the experiment, air bubbles were sometimes observed escaping to the water surface in the outlet water, which could mean that not all air had been removed prior to testing. However, the fact that the water flow during testing was very uniform appears to indicate that the air bubbles had already been absorbed during in the water storage stage before the test began. The cause of the observed bubbles in the outlet water was probably due to that air had been trapped in the outlet at the start of the test.

4.4.7:7 *Effect of the presence of air in the inlet water*

The air the water was in contact with was at atmospheric pressure, conditions that are likely to be found in the headwater of a dam. Air bubbles released in the concrete due to the gradually lowering of the water pressure in the specimen could be thought of to decrease the permeability. The water used in testing was, however, only in contact with air under ordinary atmospheric pressure. Since the water pressure was raised above atmospheric pressure by a pump and was returned again to atmospheric pressure when the water flowed through the specimen, there should be no release of air bubbles inside the specimen, this because of the pressure never dropping below the pressure of 1.0 atm at which the air was first dissolved. The fact that a steady flow of water without abrupt fluctuations was always found also implied that the flow channels were not blocked by air.

4.4.7:8 *Hydration age*

Despite the curing period having been relatively long one should not overlook the fact that when the tests started hydration had not yet been completed. The percolation test in particular is very sensitive since water that seeps out can come in contact with non-hydrated cement. This is a problem in most of the investigations of leaching that have been reported in literature.

4.4.7:9 *Aggregate gradation*

There is no guarantee that all individual specimens contain aggregate with exactly the same amount and gradation. There are always a certain variation in a mix. This can be one reason for the scatter in results.

4.4.7:10 *Sample size*

According to Collins et al. (1986), no investigations of the minimum sample size for the biggest coarse aggregate have been carried out. For lack of a better guideline, one saying that the ratio of the smallest dimension of a specimen to the largest dimension of the stones being at least 3 to 1 has been followed in the present work.

4.4.7:11 Swelling of the concrete

Swelling of concrete specimens occurs when they are resaturated after drying. Since when testing was started the specimens were probably almost completely saturated, swelling can be neglected.

4.4.7:12 Dissolution and deposition of dissolved substances

The dissolution and deposition of soluble species can occur along the flow path. If solid material is dissolved by water and is carried away from its original location by water flow, this results in an increase in local permeability. If the dissolved material is deposited in any other place, the permeability decreases there. It is difficult to say what the resulting change in the global permeability of the specimen will be. There was probably no deposition of material that was already dissolved, however, and thus no reduction of the permeability because of this. There are several reasons for assuming this:

- the solubility of the species in the specimen is not pressure dependent
- the temperature did not change either within the specimen or over time
- the entire specimen was saturated with water
- the concrete was not carbonated
- no other property that influences solubility was changed

4.4.7:13 Stresses in the specimen.

The bending moment and supporting tension at the circumference of the steel cylinder, could possibly change the permeability.

The bending moment of the $\phi 155$ (mm) circular specimen exposed to a water pressure of 6 bar is

$$M = \frac{qr^2(3+\nu)}{16} = 600 \text{ kN/m}^2 \cdot 0.0775^2 \text{ m}^2 \cdot (3+0.2)/16 = 0.72 \text{ kNm/m} \quad (4.6)$$

The stress due to this moment is

$$\sigma_M = \pm M \cdot 6/W = \pm 0.72 \text{ kNm/m} \cdot 6 / (1 \text{ m} \cdot 0.05^2 \text{ m}^2) = \pm 1730 \text{ (kPa)} \quad (4.7)$$

The normal stress in the specimen due to the supporting force at the circumference is (see Figure 4.17)

$$\sigma_N = q \cdot \text{upstream face area} / (\tan \theta \cdot \text{circumference area}) = 600 \text{ kN/m}^2 \cdot \pi \cdot 0.155^2 / 4 \text{ m}^2 / (8.3/50 \cdot \pi \cdot 0.155 \cdot 0.05) = 2790 \text{ kPa} \quad (4.8)$$

where M = bending moment (kNm/m); q = water pressure (kPa); r = radius (m); ν = Poisson's ratio; W = bending resistance (m^3); and σ_N = normal stress (kPa).



Figure 4.17 The conical shape of the specimens

The total normal stress σ at the upstream face is

$$\sigma = \sigma_M + \sigma_N = +1730 + 2790 = +4520 \text{ kPa (compressive stress)} \quad (4.9)$$

The total normal stress in downstream face is

$$\sigma = \sigma_M + \sigma_N = -1730 + 2790 = +1060 \text{ kPa (compressive stress)} \quad (4.10)$$

If an elasticity modulus of about 30 GPa is assumed, the strain ε_c of the entire concrete specimen is

$$\varepsilon_c = \Delta V/V_c = \sigma/E = 4520 \cdot 10^3 \text{ Pa}/30 \cdot 10^9 \text{ Pa} = 0.15 \cdot 10^{-3} \quad (4.11)$$

If only the capillary pores in the cement paste, $(V_{\text{cap}})_p$ are assumed to be compressed, the initial capillary pore volume will decrease by

$$\Delta V = \varepsilon_c \cdot V_c / (V_{\text{cap}})_p = \varepsilon_c \cdot 1000 / (C \cdot (w/c - 0.39 \cdot \alpha)) \quad (4.12)$$

where ε_c = strain in the specimen (m^3/m^3); ΔV = change in capillary volume due to normal stresses (m^3); V_c = volume of the entire specimen (m^3); $(V_{\text{cap}})_p$ = capillary volume of the paste (m^3); w/c = water-to-cement ratio; C = cement content (kg); and α = degree of hydration.

Example:

For the specimen 0.80a:3 it is assumed that $\Delta V = 0.15 \cdot 10^{-3} \cdot 1000 / (245 \cdot (0.8 - 0.39 \cdot 0.9)) = 1.36 \cdot 10^{-3} = 0.14 \%$ of the initial capillary pores.

For the test cells with a diameter of ϕ 45 mm, the corresponding value is about 0.03%.

Also, since both the upstream and the downstream side of the specimen were found to be compressed, virtually no cracks should appear and the permeability should thus not increase due to cracking.

4.5 Percolation through holes in the concrete

4.5.1 General

To imitate the flow of soft water through cracks, or through other large flow paths in the concrete when subjected to water under pressure, deionised water was pressed through artificial holes (see section 4.3.4) in four concrete specimens (0.60:40, 0.60:41, 0.80c:42 and 0.80c:43). 0.7 mm steel wires were inserted in the mould before casting to produce holes parallel to the water flow. After casting the wire was removed (see section 4.3.4). To get rid of any plugs of hydration products in the holes, a 1.4 mm steel wire was put through and taken out again, just before the test started. This produced holes 1.4 mm in diameter. The amount of water that flowed through the specimens (drainage water) and the concentrations of ions in it were measured. After testing of this type of specimen was finished, one specimen (0.60:40) was analysed by means of SEM (Scanning Electron Microscope) in order to see how leaching in the hole-wall had occurred.

The testing equipment and the mounting of specimens were the same as for the homogenous percolation test of concrete (section 4.4). The water pressure was set to a very low level by adjustment of the reducing valve and of the shutoff valve just before each test cell was closed. Otherwise, the flow of water would have been too large. This produced a slow and easily managed flow of water through the specimens.

The water that passed through the holes in the specimens was ordinary municipal tap water that had been deionised by a reverse-osmosis aggregate as described in 4.4.2.

The water from the specimens was led to 25 litre plastic drums.

4.5.2 Test records and presentation of data

The water flow was measured using the same method as for the homogenous percolation test described in section 4.4.5:1.

The drainage water collected was analysed in the same way as described in section 4.4.5:2. Since the flow of water was so large that one could assume there to be no risk of the deionised water in the inlet being contaminated by dissolved ions diffusing upstream, no flushing of the shutoff valve of the test cell was carried out.

4.5.3 Validity

The validity of the tests performed for the conditions found in real dams was judged to be about the same as described in section 4.4.6:1 to 4.4.6:9.

4.5.4 Errors of test and reliability of results

Since the flow of water fluctuated considerably during testing it was difficult to obtain a precise flow, with the equipment available.

4.6 Surface-leaching of concrete

4.6.1 General

Two specimens of virgin concrete with a w/c ratio of 0.8, namely specimens 0.80a:R2 and 0.80a:R3, hydrated in water for 35 months (almost 3 years), were cut into four sections and laid in a plastic tank containing 100 litres of deionised water, stirred by a propeller. The test setup is shown in Figure 4.18.

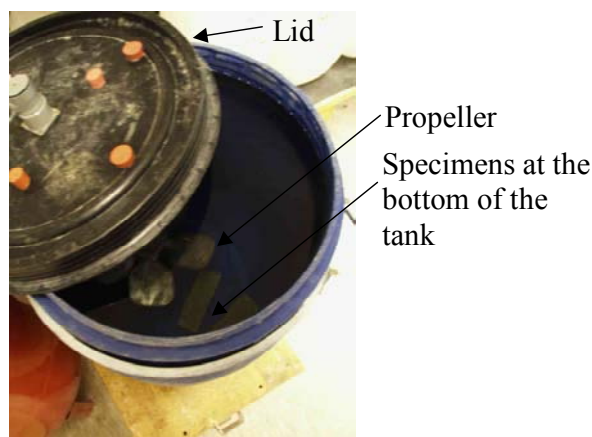


Figure 4.18 Four sections of concrete were laid at the bottom of a 100-litre plastic tank filled with deionised water that was stirred constantly.

The water was replaced once a month. Because the volume of water being large and the water being replaced at regular intervals, the ion strength of the water remained relatively low and the aggressiveness of the water remained strong. The pH was

measured at each refilling of new water, never exceeding 10.5. After 613 days (~1.7 years), the specimens were taken out of the container. Slices were cut from different distance from the initial cut surface, see Figure 4.19. The slices were 50x50 mm in size and 3 mm thick. The total porosity of the slices was measured in the manner described in sections 4.10.1 and 4.10.3. The slices were then powdered. The powder from each slice was collected in a plastic container. The powder was then dissolved in HNO₃ and examined by ICP AES. The aim of this experiment was to study the loss of calcium from the specimen to the bulk of deionised water and to determine the diffusion coefficient. The chemical analysis is described in section 4.12

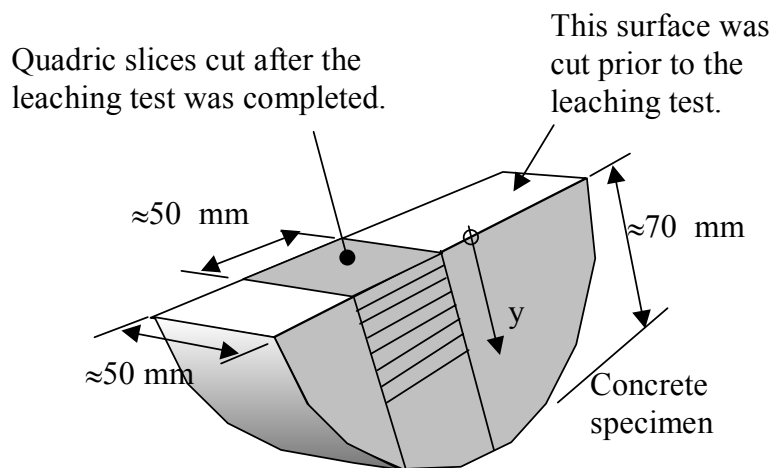


Figure 4.19 Slices was cut from the specimens. The slices were then grounded to powder.

4.6.2 Errors of testing and reliability of the results

The cut slices were undesirably thick, making it difficult to obtain exact measurements of the leaching gradient. It was not possible, however, to cut thinner slices.

4.7 Chemical analysis of the water samples

The concentration of H⁺ (pH) and of certain other important ions (Ca, Na and K in particular) was measured both in water that had been in contact with concrete on the upstream surface and in water that had percolated through the concrete. The pH was measured by pH-electrodes and the concentration of calcium by Ca²⁺-selective electrodes or by ICP AES (Inductive coupled plasma atom emission spectroscopy).

pH measurements:

The pH values were measured by an *Orion 720A ISE/pH meter* together with a *Beta Sensor pH Electrode model G-200-PC*. Magnetic stirrers were used to obtain as stable values as possible as quick as possible. The temperature in both the buffers and the water samples that were collected was the same, +20°C.

- ❖ *Calibration.* The pH electrode was calibrated on every measuring occasion against three buffer solutions with pH values on both “sides” of the pH of the water sample that was tested, so that the values measured could be obtained by interpolation. In

most cases, buffer solutions with pH values of 9, 11 and 13 were employed since most of the water samples had pH values of about 11 to 13.

- ❖ *Measuring.* The pH in the small bottles of drainage water samples that were collected was measured directly (Figure 4.20).
- ❖ The *reliability* of the pH-tests appeared to be good. The variation in pH-value was about 0.05.

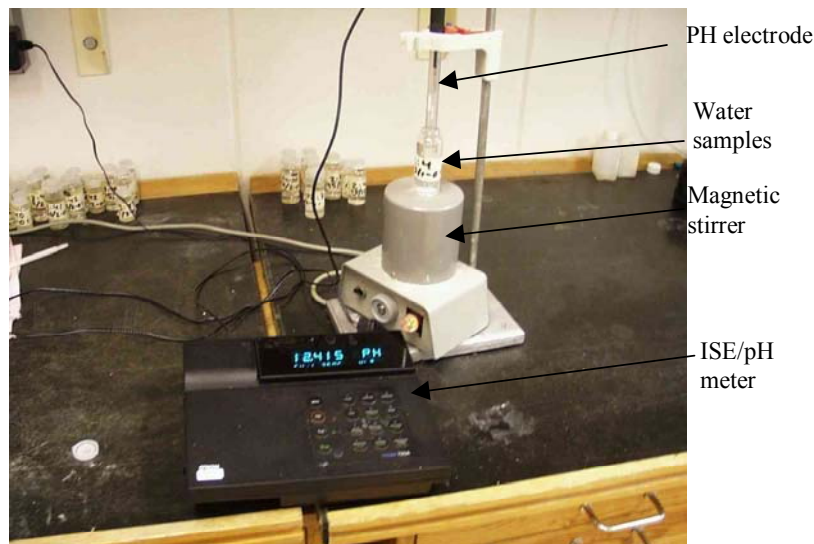


Figure 4.20 Measuring the pH of the water samples collected.

Measurement of calcium by an ion selective electrode:

The electrodes used for measuring calcium concentration were an Orion 720A ISE/pH meter together with a Beta Sensor calcium selective electrode of model ISE-400-P, and a Beta Sensor reference electrode of model R-860-S. Magnetic stirrers were used to obtain more stable values, and to obtain them more quickly. The temperature in both the standards and the collected water samples was the same, +20°C.

- ❖ *Calibration:* The electrodes were calibrated on every measuring occasion in three different standards of 40 ml 0.1M NaCl + 0.4 ml acetate buffer + x CaCl₂, where x was 0.4 ml of 0.001, 0.01 and 0.1 M CaCl₂, respectively, which gave solutions of 0.39, 3.9 and 39.3 mg Ca²⁺/l, respectively.

Acetate buffer and sodium chloride were added to ensure that the test water samples and the standards were at the correct pH and were similar in ionic strength, as well as to reduce the effects of interfering ions. The acetate buffer consisted of acetic acid (CH₃COOH) and sodium acetate (NaCH₃COO). The acetate buffer was at $\text{pH} = \text{pK}_a + \log\left(\frac{[\text{A}^-]}{[\text{HA}]}\right) = 4.75 + \log 1 = 4.75$.

Because an ion selective electrode only detects free ions, the pH needs to be rather low to avoid ion bonding between the ion studied and other ions. The measured pH was in the range of 4.5 to 4.8 for both the calibration standards and the test specimens.

The ionic strength for both the standards and the test water samples was about 0.1.

❖ *Measuring*: So as to be alike in pH, ionic strength and sensitivity to interfering ions, the test water samples were composed of solutions of 20 ml 0.1 M CaCl + x of collected water + y acetate buffer (or multiples of it). Although it was found that x and y were dependent to some extent on the ionic strength of the drainage water sample, they were usually set at to x=0.4 and y=0.4 ml so as to have the same ionic strength as the calibration solutions. The pH was about 4.5 to 4.8.

The ionic concentrations in the water samples were

$$[A] = \text{read value} * \frac{(V_{\text{NaCl}} + V_{\text{collected water}} + V_{\text{acetate buffer}})}{V_{\text{collected water}}} \quad (4.13)$$

where [A] = real ionic concentration in the test water (mole/l); read value = value read off the ion meter (mole/l); V_{NaCl} = volume of NaCl solution employed (ml); $V_{\text{collected water}}$ = test water volume collected (ml); and $V_{\text{acetate buffer}}$ = volume of acetate buffer (ml) employed.

❖ The *reliability* was not very high. The variation was about $\pm 10\%$ when the values were compared with values received from ICP-AES, as described below. The last two years of testing, only ICP-AES values have been employed.

Calcium measured by ICP-AES:

To check the reliability of the ion-selective electrode measurements, to measure other ions than calcium, and in the two last year of testing, to obtain more reliable results, analyses were also performed by means of a *Purcin-Elmer Optima 3000 DV* making use of a ICP AES technique (Inductive coupled plasma atom emission spectroscopy). Since during the last two years of testing, the measurements by the selective electrodes described above were not fully reliable all measurements of ions were performed by use of the ICP AES method. According to the test centre at the Department of Plant Ecology at Lund University, where the equipment was placed, the accuracy of this technique is $\pm 5\%$. Other elements checked, besides Ca were Na, K, Al, Fe, S and Mg.

4.8 Splitting test

When the percolation test was finished, both the leached specimens and the unleached reference specimens were first split into two halves (Figure 4.15), to obtain the split tensile strength. As can be seen in the figure the split load was applied by means of 10 mm wide and 2 mm thick fiberboard. The lower point of load was slightly inclined to compensate for the conical form of the specimen, so that the load could be applied vertically. The two small pieces of wood that can be seen at the bottom at both sides of the vertical line was withdrawn when the load was applied. The specimens were taken directly from the leaching experiment or water-storage bath and were still water-saturated. The load-application rate was 0.5 kN/s, which correspond to 0.045 MPa/s.



Figure 4.21 Splitting test of a concrete specimen.

4.9 Compression test

Tests of compressive strength were performed on small cylinders obtained from the test specimens and from reference specimens. The sample cylinders tested were of two types: (i) small cylinders with a diameter of 40 mm that were drilled out of the concrete specimens 155 mm in diameter, see Figure 4.15, and (ii) the specimens 45 mm in diameter that were tested as they were. The specimens were taken directly from the leaching experiment and were still water saturated. Cylinders with poor end surfaces were ground so that good surface contact with the pressure plates could be obtained.

After the geometry of the cylinders had been measured, the cylinders were tested in an ordinary strength-testing machine. A 0.5 kN/s load was applied. A value of the E-modulus was determined by measuring the load-displacement curve.

The compressive strength and the modulus of elasticity obtained here cannot be compared directly with those obtained with use of standard tests because of the differences in specimen sizes and in procedure. The test, however, indicates changes in compressive strength and in E-modulus for the leached as compared with the unleached specimens.

The reliability was decreased because of the fact that some of the drilled-out cylinders came from parts of the specimens that were obviously very strongly leached whereas others came from parts that were to a much lesser extent leached.

4.10 Porosity measurements

4.10.1 General

A number of both leached and unleached specimens were analysed with regard to pore size distribution and total porosity. One quarter of each of the specimens was cut into a number of slices, often seven (Figure 4.15). Because of this slicing, it was possible to measure differences in the distribution and total volume of the pores in the direction in which the water had flowed earlier in the percolation test. Each slice was a 40x40 mm square with a thickness of 3 to 7 mm. When the porosity measurements began all the slices were still saturated.

The porosity was determined in three steps. First the weight of the wet slices in air and when submerged in water was determined, $m_{wet,air}$ and $m_{wet,water}$.

Secondly, the size distribution of coarser pores was determined by use of pressure plates, or suction tests. Third, the total porosity was determined by heating the slices in an oven to +105°C and determining the dry weight, $m_{105°C}$.

A source of possible error in the slices that were analysed by the suction test described below is that continued hydration may have occurred during the rather time-consuming suction test (which took 4 to 6 months). However, the specimens were very old when the test started (3-4 years) and had access to water all the time, so the hydration must have been nearly complete when the suction tests began. Also, during the suction test, water is removed, which should reduce the risk of further hydration.

4.10.2 Pore size distribution

This test was carried out with help of a suction test, using a pressure plate apparatus as described in Janz (1997), see Figure 4.22. The procedure involved the following:

- 1) The specimen is placed on a water-saturated fine-porous ceramic plate. A layer of kaolin, topped by a fine-porous cloth, placed between the plate and the specimen in order to achieve perfect hydraulic contact between water in pores in the specimen and water in pores in the plate.
- 2) The porous plate is mounted as a lid to a water-filled container. Water in the container is under normal atmospheric pressure.
- 3) The assembly is placed in a pressure-vessel.
- 4) Air pressure in the vessel is increased in steps. The pores in the plate are so small that they stay water-filled also at the highest air-pressure. Thus the plate takes the pressure difference between air in the vessel and the atmospheric pressure in the water-filled container.
- 5) The amount of water that was pressed out of the chamber being measured by a burette.
- 6) When no more water could be pressed out of the specimen, it was taken out and measured by weight.
- 7) Procedure 4) to 7) were repeated for a sequence of higher air pressures, using steps of 1, 2, 4, 10, 20, 40, 70 and 100 bar.

Water in the specimen is forced out of the specimen, by means of overpressure, through the cloth, kaolin clay, ceramic plate, and then out of the vessel. An internal screen prevents the neoprene diaphragm from clogging the underside of the ceramic plate when pressure is applied. The connection between the internal screen and the outside surface of the vessel (the outflow tube) produces atmospheric pressure beneath the ceramic plate. A high-quality manifold pressure regulator regulates the overpressure that is applied.

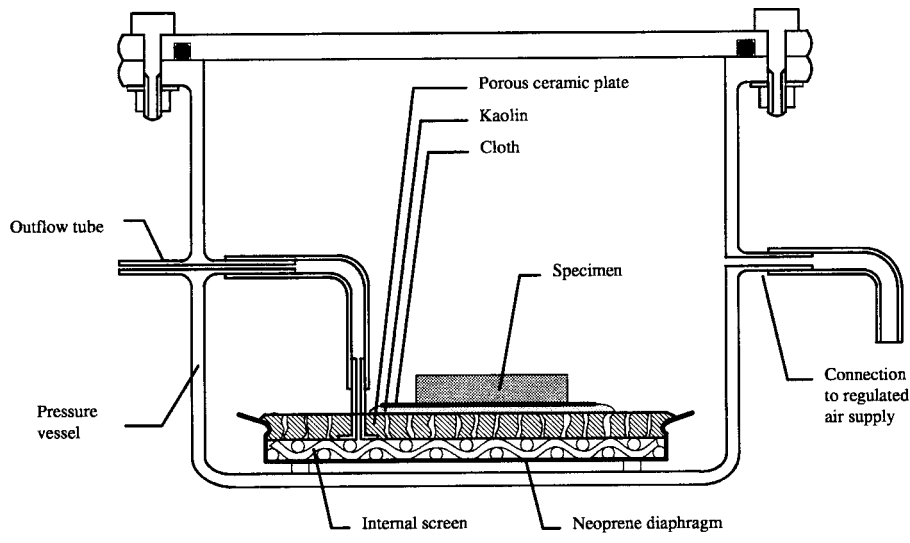


Figure 4.22 Drawing of a pressure plate extractor mounted in a pressure vessel (Janz 1977).

If one assumes the pores to be circular tubes or channels, the relation of the air pressure to the pore size according to the Laplace equation becomes.

$$r_i = \frac{2 \cdot \sigma \cdot \cos \varphi}{P_i} \quad (4.14)$$

where r_i = circular pore radius (m); σ = surface tension between the liquid and the air (0.07275 N/m at +20°C); φ = contact angle between water and pore wall; and P_i = air pressure (Pa) applied.

The contact angle φ is assumed to be zero, i.e. water wets the surface of the solid completely. Radii between approximately 10 000 Å and 200 Å can be detected, which corresponds to a pressure of 0.15 to 7.25 MPa and a relative humidity, RH, of approximately 0.999 and 0.96, respectively, according to the Kelvin equation:

$$\ln RH = -\frac{\sigma \cdot M_w}{R \cdot T \cdot \rho_w} \cdot P_i = -\frac{\sigma \cdot M_w}{R \cdot T \cdot \rho_w} \cdot \frac{2}{r_i} \quad (4.15)$$

where M_w = molar weight of water (0.018 kg/mole); R = gas constant 8.314 (J/(mole·K)); ρ_w = density of water (kg/m³); and T = temperature (K).

The weight loss during each pressure step corresponds to the volume of the pores V_i (m³), using the assumed radius contained in the following expression:

$$V_i = m_i / \rho_w \quad (4.16)$$

where m_i = measured weight loss at each pressure step (kg).

4.10.3 The total porosity

The porosity was determined from measurements of the saturated weights in air and water and the dry weight, see section 4.10.1.

The volume V_c of the concrete slices was calculated as

$$V_c = \frac{m_{wet,air} - m_{wet,water}}{\rho_w} \quad (4.17)$$

where V_c = volume of the concrete slices (m^3); $m_{wet,air}$ = weight of the saturated slices in air (kg); $m_{wet,water}$ = weight of the saturated slices under water (kg); and ρ_w = density of water (kg/m^3).

The dry bulk-density ρ_{dry} was calculated as:

$$\rho_{dry} = \frac{m_{105^\circ C,air}}{V_c} \quad (4.18)$$

where ρ_{dry} = dry bulk-density of the concrete slices (kg/m^3); and $m_{105^\circ C,air}$ = weight of the dried ($+105^\circ C$) slices in air (kg).

The total porosity P_c of the concrete based on drying at $+105^\circ C$ is

$$P_c = \frac{m_{wet,air} - m_{105^\circ C,air}}{\rho_w \cdot V_c} = \frac{m_{wet,air} - m_{105^\circ C,air}}{m_{wet,air} - m_{wet,water}} \quad (4.19)$$

where P_c = porosity of the concrete (m^3/m^3).

4.11 Determination of the non evaporable water in the concrete by heating it to $+1050^\circ C$

The degree of hydration α was measured for cut slices (Figure 4.15) of some specimens as a continuation of the measuring of the total porosity in section 4.10.3:

- 1) The slices were dried at $+1050^\circ C$.
- 2) The slices were cooled to approximately $+700^\circ C$ in the oven
- 3) The slices were cooled to $+20^\circ C$ in an exsiccator
- 4) The slices were measured by weight in air, $m_{1050^\circ C, air}$

The degree of hydration was calculated as described in Byfors (1980) as

$$\alpha = 4 \cdot \frac{W_n}{C} = 4 \cdot \frac{m_{105^\circ C} \cdot (1 - A) - m_{1050^\circ C}}{m_{1050^\circ C} - B \cdot m_{105^\circ C}} \quad (4.20)$$

$$A = \frac{\mu_c + a/c \cdot \mu_a}{1 + a/c}$$

$$B = \varepsilon \frac{a/c}{1 + a/c}$$

$$\varepsilon = 1 - \mu_a$$

where α = degree of hydration (-); C = cement content (kg); W_n = non-evaporable water (chemically bounded) (kg); $m_{105^\circ C}$ = weight of concrete at $+105^\circ C$ (kg); $m_{1050^\circ C}$ = weight of concrete at $+1050^\circ C$ (kg); a/c = ratio of aggregate to cement (kg/kg); μ_a = loss of mass of the aggregate between $105^\circ C$ and $1050^\circ C$ in fraction of mass at $+105^\circ C$ (kg/kg); and μ_c = loss of mass of the cement between $105^\circ C$ and $1050^\circ C$ in fraction of the mass at $+1050^\circ C$ (kg/kg).

4.12 Chemical determination of elements in the specimens by ICP AES

The slices for which the porosity was analysed, as described in section 4.10 was analysed by ICP AES to determine the content of the elements contained in the samples. The procedure was

- 1) The slices were ground to form powdered samples (if these had not already been powdered).
- 2) The samples were measured by weight in air, $m_{\text{dry,air}}^{\text{powder}}$
- 3) The powder was boiled in a solution of water and HNO₃ for 2.5 weeks at 130°C. When the boiling was stopped, all except 80 ml of the solution was removed by boiling. The residual solution was diluted to 1000 ml by de-ionised water.
- 4) The solution was analysed by ICP AES (see section 4.7) with regard to the amounts of the elements Al, Ca, Fe, K, Mg, Mn, Na, S and Si.
- 5) Dissolving of the powder also yields a residual insoluble solid part, as sediment at the bottom of the measuring glass. This was dried and measured by weight.
- 6) Because of the uncertainty regarding how much of the residual, non-dissolved, part came from the aggregate and how much came from the cement paste, an additional chemical analysis was performed. In this analysis, only aggregate was dissolved according to point 2) to 4) above, the solubility of the aggregate in HNO₃ being determined.

4.13 Analysis of concrete at leached holes with SEM

The specimens used in the percolation test of concrete specimens with holes, were cut into 9 slices (Figure 4.23). Small parts of these around one of the holes were removed and were studied by means of a Scanning Electrode Microscope (SEM). Changes in the crystalline and element composition and in the topography were studied from the surface of the hole inwards into the concrete. The water that had flowed through the holes was expected to have dissolved material from the surface of the holes and carried it away. SEM-analysis was performed by Dr. Möser at FIB in Weimar. Examining the *secondary electrons* (SE) and the *back-scattered electrons* (BSE) allowed the topography and morphology of the surface of the samples of concrete to be observed. A qualitative estimation of the compounds present could also be made. An EDX (Energy Dispersive X-ray)-analysis of the surface of the samples allowed a quantified assessment of the elements present to be made.

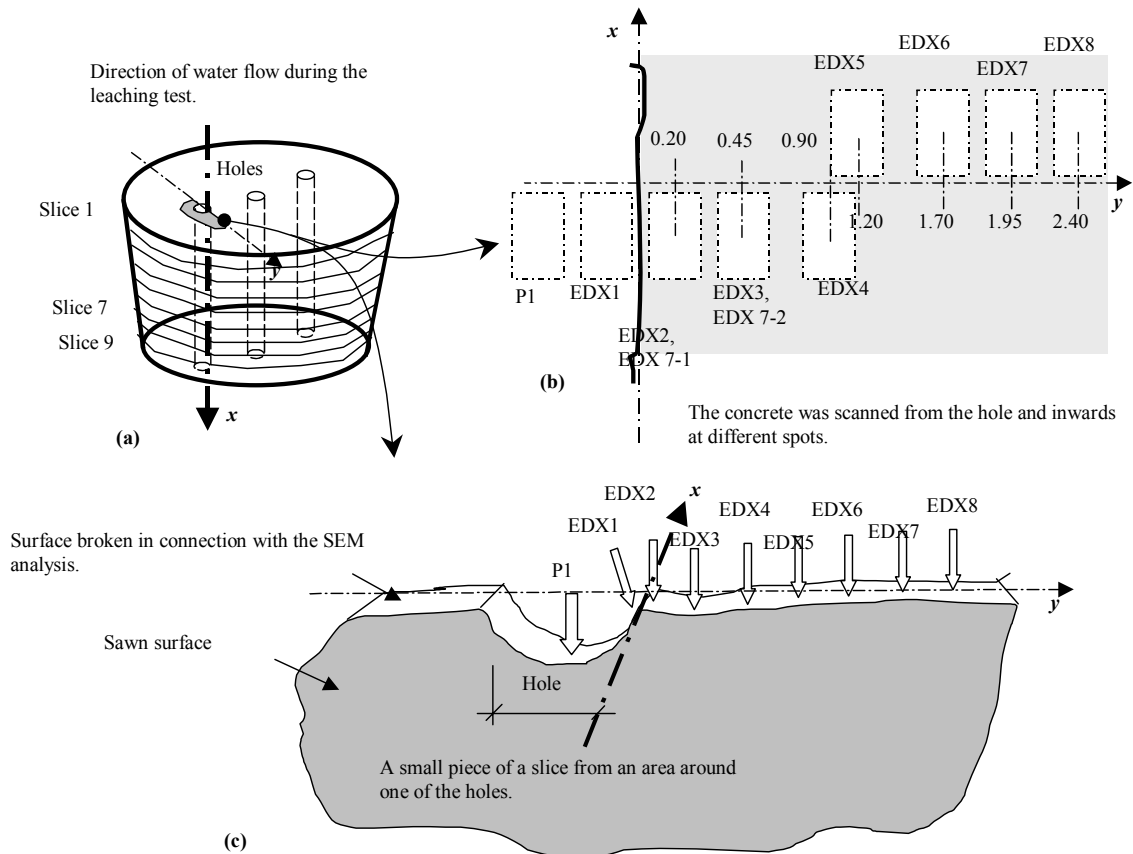


Figure 4.23 The specimens employed in the percolation test of concrete containing holes were cut into nine slices. One small part from the wall of one of the holes was broken from each of the slices 1, 7 and 9. These three small parts were studied using SEM. The locations of the different “spot-areas” in which EDX-analyses were carried out are shown as small dotted frames in the figure. The diameter of the holes was approximately 1.4 mm.

5 Results

5.1 Homogenous steady-state percolation of water through defect-free concrete

5.1.1 Flow of water through the specimens (convection)

Figure 5.1 - Figure 5.13 summarize the results for permeability in connection with the homogenous percolation of deionised water through defect-free concrete. Figure 5.1 to Figure 5.10 show permeability versus time. Figure 5.11 to Figure 5.13 show permeability versus the total volume of the water that percolated. In the APPENDIX B, the measured flow of water and ions, together with the permeability (calculated using equation (4.21)) is given for each of the specimens with a diameter of $\phi 155\text{mm}$, but not, due to lack of space, for those with a diameter of 45 mm. For an account of the type of concrete involved and the testing history, see Table 4.1 and Figure 4.4. The results obtained are discussed in section 6.1.1.

What is meant by the “homogenous steady-state percolation of water through defect-free concrete” is the macroscopic, homogenous and steady-state percolation (Darcian flow) of water through in concrete in which no holes, cracks or other types of flow paths were made artificially. Although on a microscopic scale, no flow of water through concrete is homogenous, on a larger scale water flow can be assumed to follow Darcy’s law. See more about Darcy’s law in section 3.9.3.

The flow of water can be described in either of two ways, (i) as water flow q_w (m^3/s) or as (ii) water permeability k_w . What is meant here by water permeability is the Darcy permeability, k_w , defined by the equation

$$k_w = q_w \cdot \frac{L}{\Delta P_w} \cdot \frac{1}{A_{tot}} \quad (4.21)$$

where k_w = permeability (m/s); q_w = measured flow of water (m^3/s); L = measured length of the specimen in the flow direction (m); ΔP_w = measured difference in water pressure between the upstream and the downstream end of the specimen (m); and A_{tot} = measured cross-sectional area (m^2). Because the specimens were conical, the area was based on the measured diameter at half of the height the specimens.

A brief summary:

- The permeability of (EH)-specimens with a w/c of 0.6 and
 - a diameter of 155 mm was initially about 10^{-10} m/s (Figure 5.1), but it decreased by a factor of approximately 100 down to about 10^{-12} m/s during a period of about 400 days after of the leaching test began.
 - The specimens with a diameter of 45 mm (specimens 20-30 in Figure 5.2) showed the same basic development, but the permeability was approximately 10 times as low as for the specimens with a diameter of 155 mm. When the $\phi 45$ mm-specimens were late-dried (EH-LD) after about 14 000 hours, the permeability rose by a factor of about 10 and then continued at this level.

- The permeability of (**V**)-specimens with a **w/c** of **0.8** and a diameter of 155 mm was initially about $0.5 \cdot 10^{-12}$ m/s ($\pm 0.5 \cdot 10^{-12}$ m/s) (Figure 5.3 to Figure 5.5), thereafter remaining constant over time. One specimen (0.80b:2) was tested over a very long period of time (about four years), the permeability being found to remain basically constant, increasing only slowly. At four years of age, k_w was approximately 1.5 times the initial value. One of the specimens, 0.80a:5, was found to have increase very much in permeability (by a factor of 100) after about 290 days of testing.
- When the virgin (**V**) specimens with a **w/c** of **0.8** and a diameter of 155 mm were late-dried (**V-LD**), the permeability increased by a factor of about 100 just after the drying, as compared with the permeability they had in the Virgin state (Figure 5.6). After a further period of time, the permeability increased often very rapidly, by a factor of about 100.
- The permeability of the specimens with a **w/c** of **0.8** and a diameter of 155 mm that were late-dried (**LD**) after a curing time of 5000 hour, was initially about 10^{-10} m/s (Figure 5.7), which was about 10 times as high as for the V-specimens with a w/c of 0.80. Rather quickly, there was a decrease of k_w by a factor of approximately 10 to about 10^{-11} m/s during a period of about 120 days after the leaching tests had begun. After the initial decrease of permeability, one of the specimens (0.80a:3) was found to have increased in permeability by a factor of about 5, whereas the other (0.80a:4) showed a further slow decreasing permeability by a factor of about 2.
- The permeability of the (**EH**)-specimens with a **w/c** of **0.8** and
 - a diameter of 155 mm was initially about 10^{-10} m/s (Figure 5.8), which was about 100 times as high as for the V-specimens with a w/c of 0.80. The permeability then decreased by a factor of approximately 100 to about 10^{-12} m/s during a period of about 600 days after the leaching tests started. When the specimens were late-dried (**EH-LD**) after about 14 000 hours, the permeability rose by a factor of about 10 and then slowly decreased.
 - a diameter of 45 mm was initially about 10^{-11} m/s (Figure 5.9), which was about 10 times lower than for the EH-specimens with diameter of 155 mm, referred to above. The permeability then decreased by a factor of approximately 10 to about 10^{-12} m/s during a period of about 500 days after the leaching tests begun. At this time the specimens were late-dried (**EH-LD**), the permeability rising by a factor of about 10. The permeability was then uniform or decreased, though only slowly.
- The permeability of the (**V**)-specimens with a **w/c** of **1.29** and a diameter of 155 mm was initially about $3 \cdot 10^{-11}$ m/s, but rather quickly (during a period of 2000 hours) increased to 10^{-8} m/s (Figure 5.10 a).
- The permeability of the specimens with a **w/c** of **1.29** and a diameter of 155 mm that were late-dried (**LD**) after a curing time of 2000 hours was initially about

$2 \cdot 10^{-10}$ m/s, but increased rather quickly (during a period of 1000-1800 hours) to between $7 \cdot 10^{-9}$ and $4 \cdot 10^{-8}$ m/s (Figure 5.10 b).

Some of the concrete specimens in which the water flow increased were dismantled to determine whether any visual changes had occurred. At the upstream face of the concrete specimens, small brown areas could be observed in all cases. These brown areas contained compounds of Al, Fe, Si and some Ca, which were probably residual parts of leached C-S-H and AF phases. In the centre of the brown areas, small holes leading into the concrete could be observed. These holes had obviously served as main flow paths for the water during the leaching tests, or in the final parts of the leaching tests at least. At the beginning of testing, no such holes were observed. After being formed, they increased in width as the testing progressed.

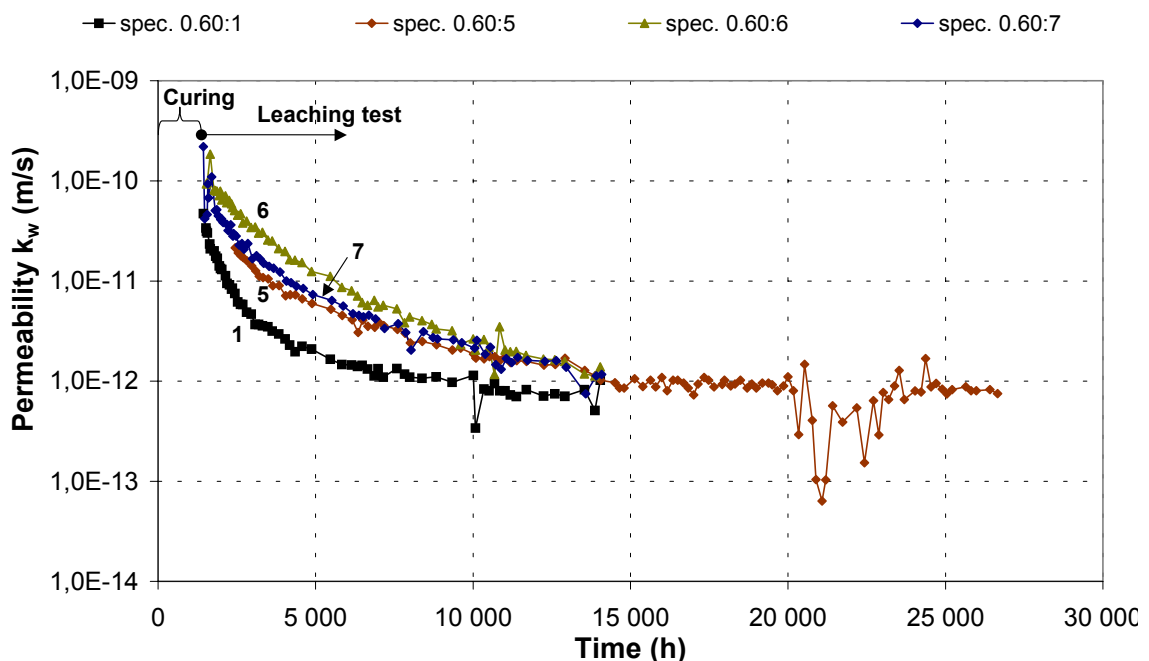


Figure 5.1 Flow of water and permeability in the leached EH-specimens with a w/c of 0.60 and a diameter 155 mm. The leaching tests started at a hydration age of approximately 1570 hours.

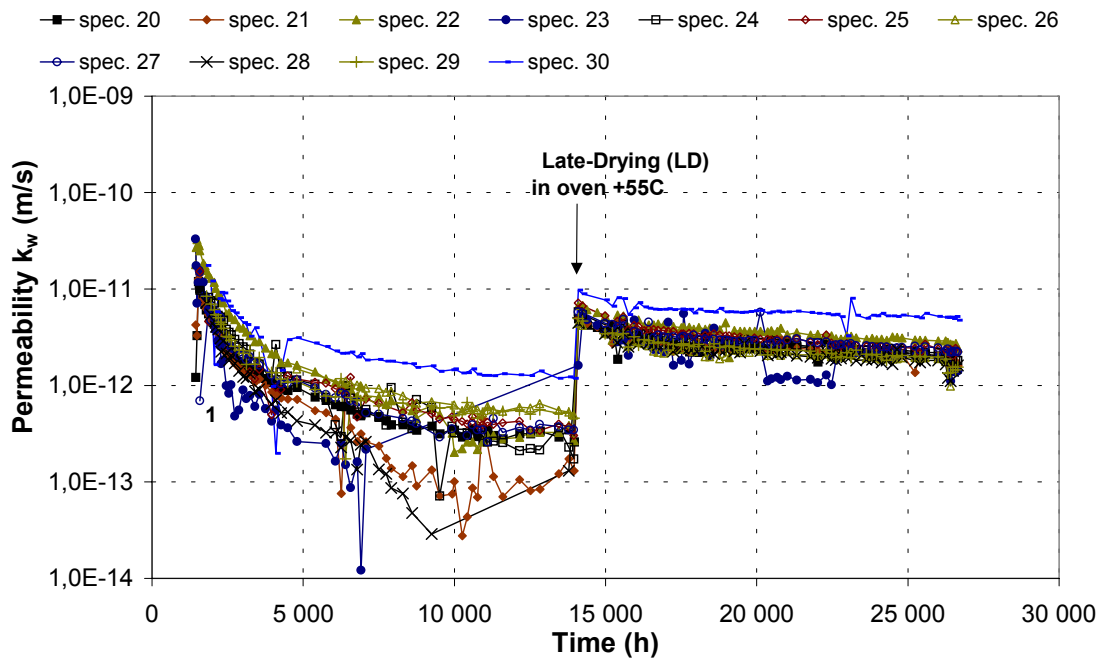


Figure 5.2 Flow of water and permeability in the leached EH-specimens with a w/c of 0.60 and a diameter 45 mm. LD = means that the specimens have been “late-dried”, see section 4.3.5.

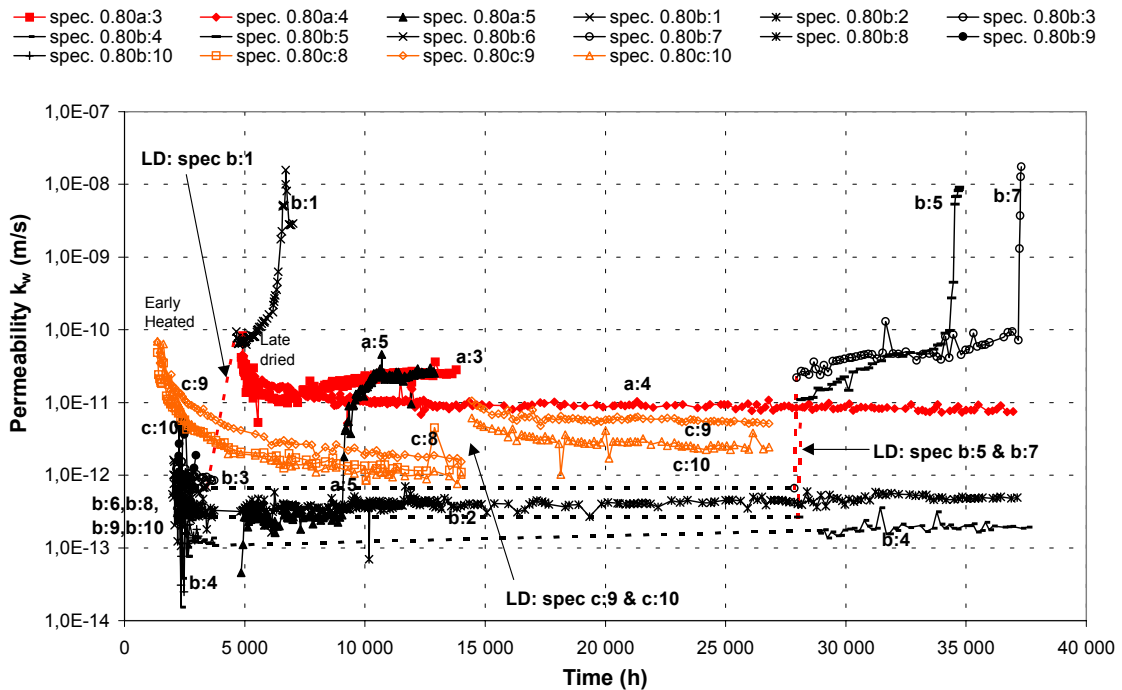


Figure 5.3 Flow of water and permeability in all the leached specimens (V, V-LD, LD, EH) with a w/c of 0.80 and a diameter 155 mm.

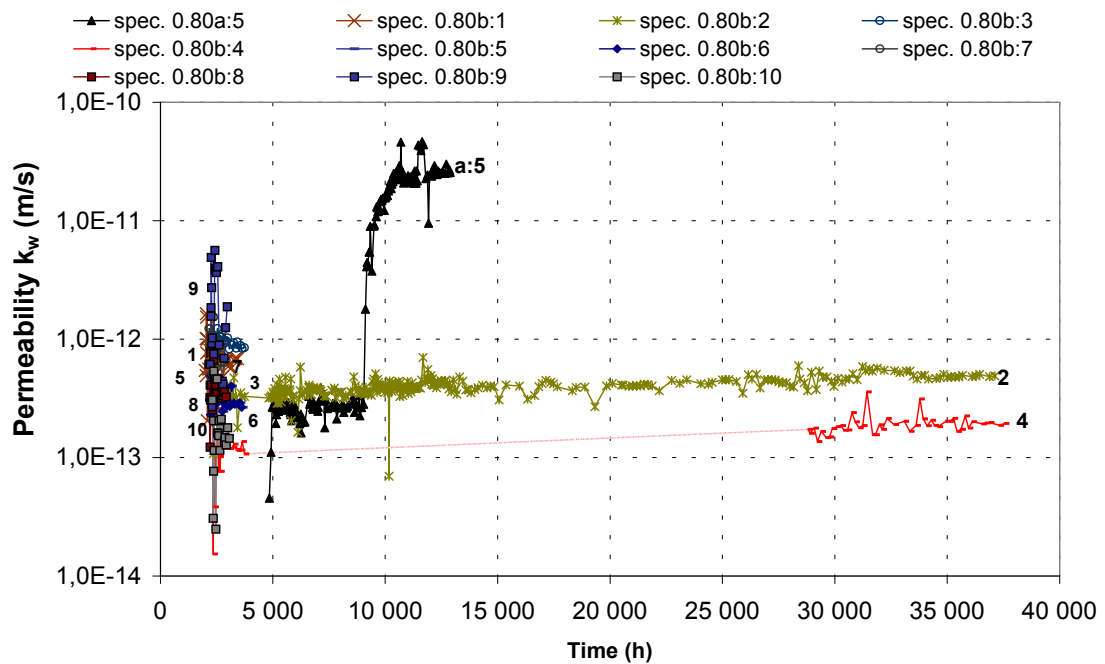


Figure 5.4 Flow of water and permeability in the leached virgin (V) 0 – 40000 hour specimens with a w/c of 0.80 and a diameter of 155mm. All the specimens were subjected to the leaching tests after approximately 2000 hours of curing, except for specimen 0.80:a5, for which testing was started after 4850 hours of curing.

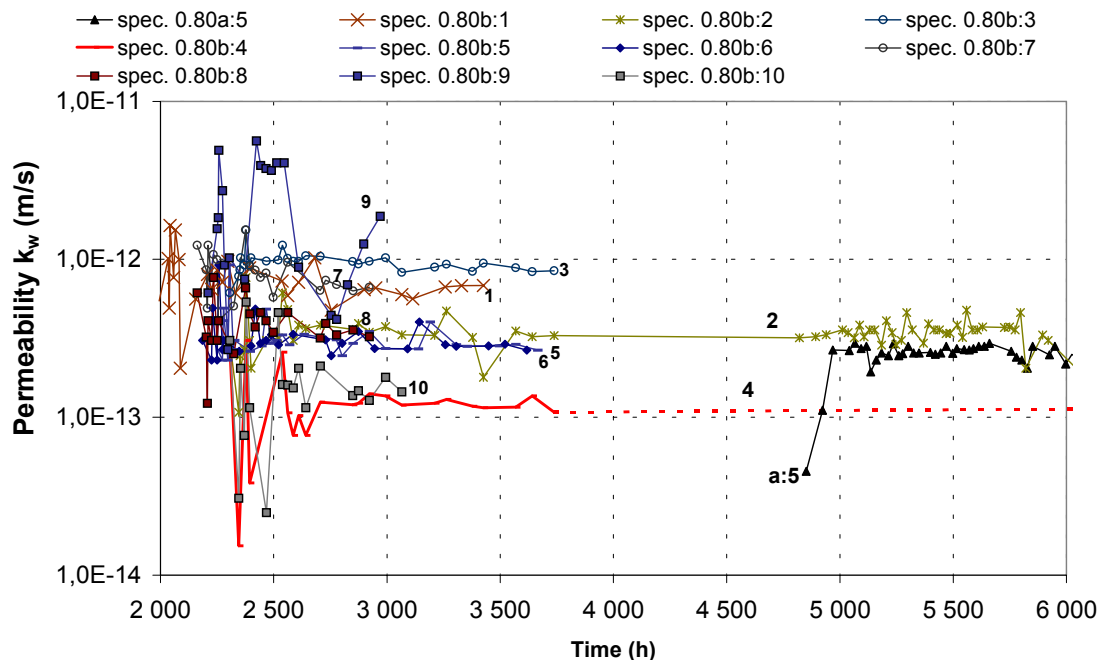


Figure 5.5 Flow of water and permeability in the leached virgin (V) 2000 – 6000 hour specimens with a w/c of 0.80 and a diameter of 155mm. The data presented pertain to the same specimens as in Figure 5.4 but involve a shorter testing time.

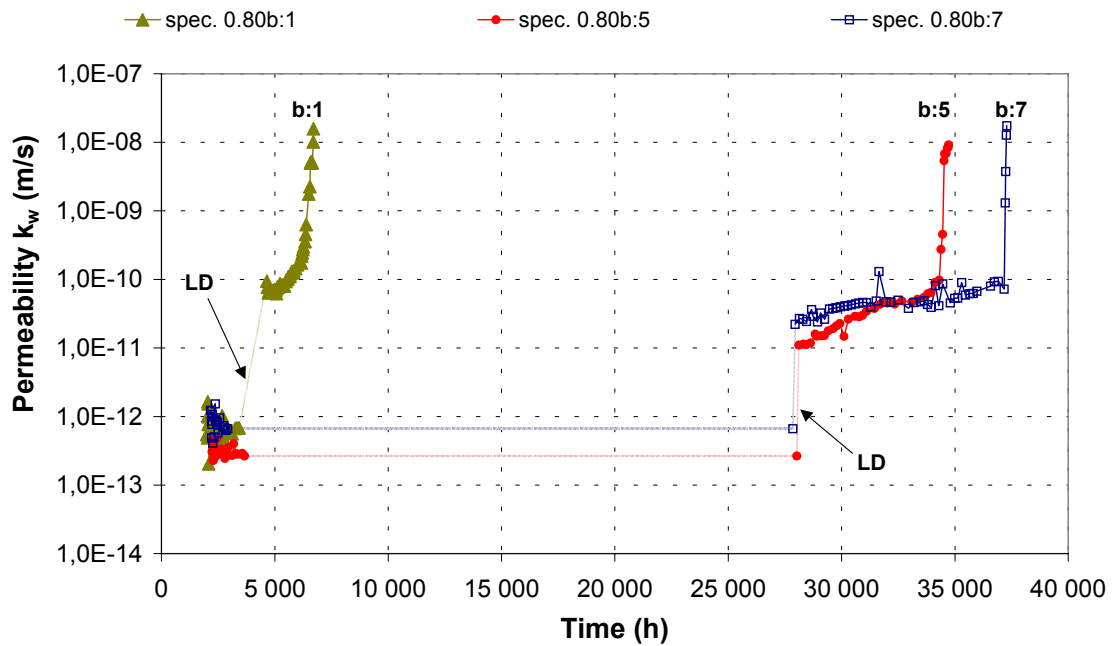


Figure 5.6 Flow of water and permeability in the leached late-dried (V-LD) specimens with a w/c of 0.80 and a diameter of 155mm that were late-dried (V-LD) at 5 000 and 28 000 hours. The specimens were also leached in a virgin state during the period between 2000 and 3500 hours.

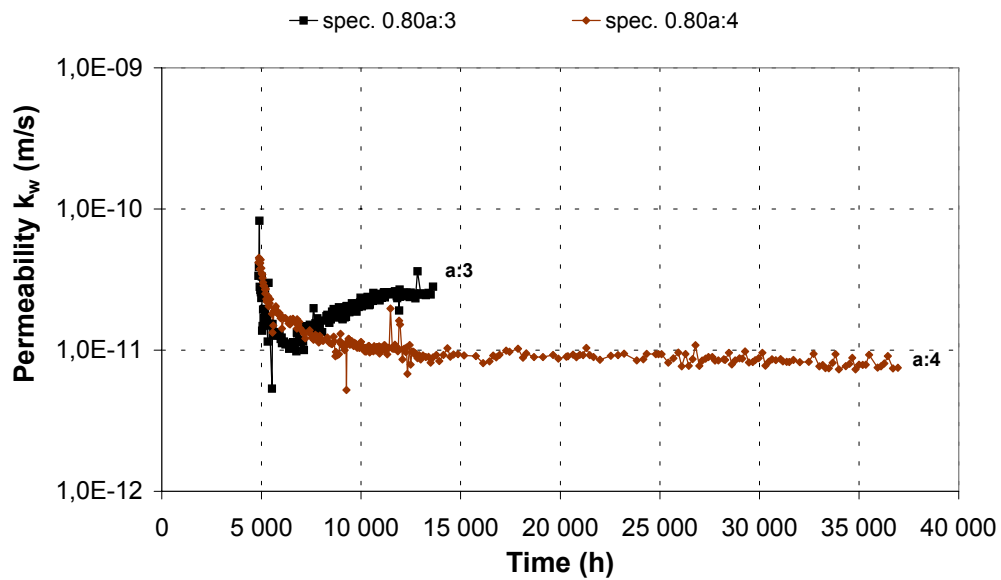


Figure 5.7 Flow of water and permeability in the leached late-dried (LD) specimens with a w/c of 0.80 and a diameter of 155mm.

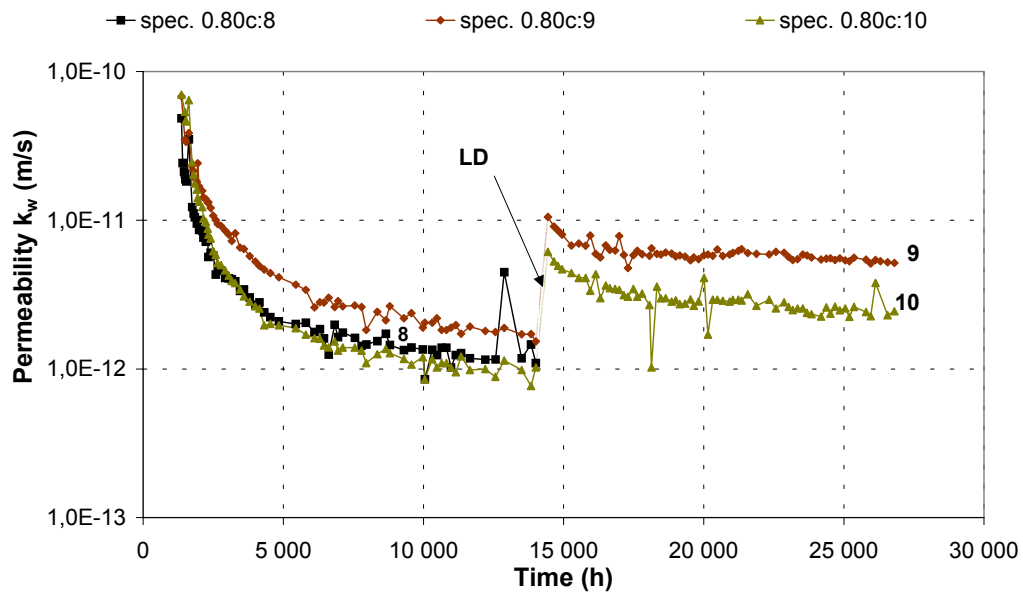


Figure 5.8 Flow of water and permeability in the leached EH-specimens with a w/c of 0.80 and a diameter of 155mm that were late-dried (E-LD) at 14 000 hours.

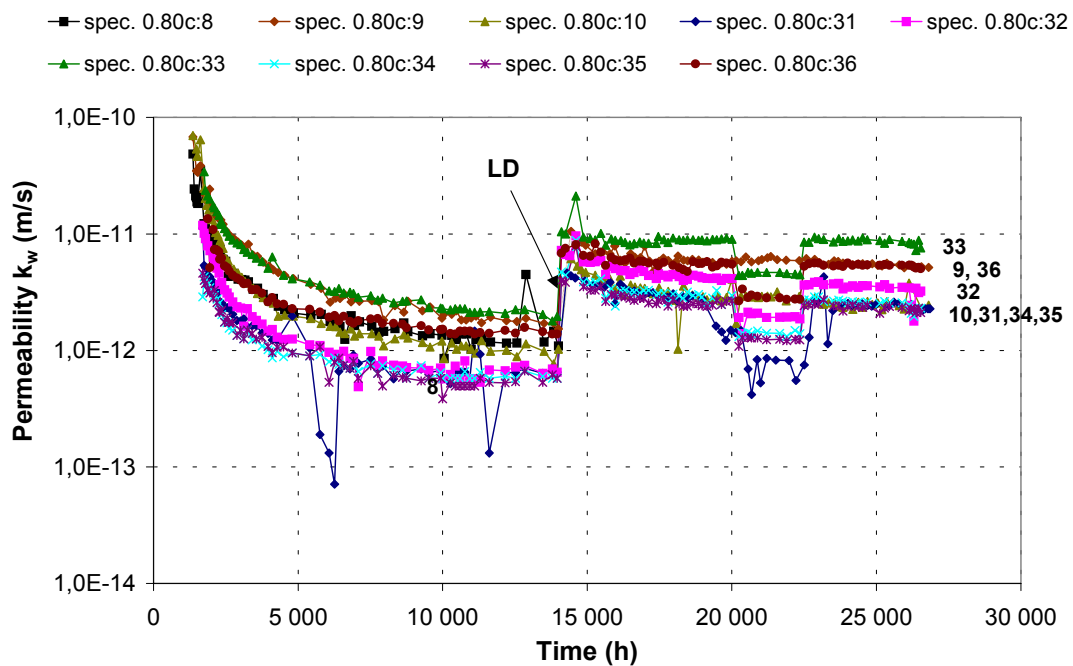


Figure 5.9 Flow of water and permeability in the leached EH-specimens with a w/c of 0.80 and a diameter of 45mm that were late-dried (E-LD) at 14 000 hours.

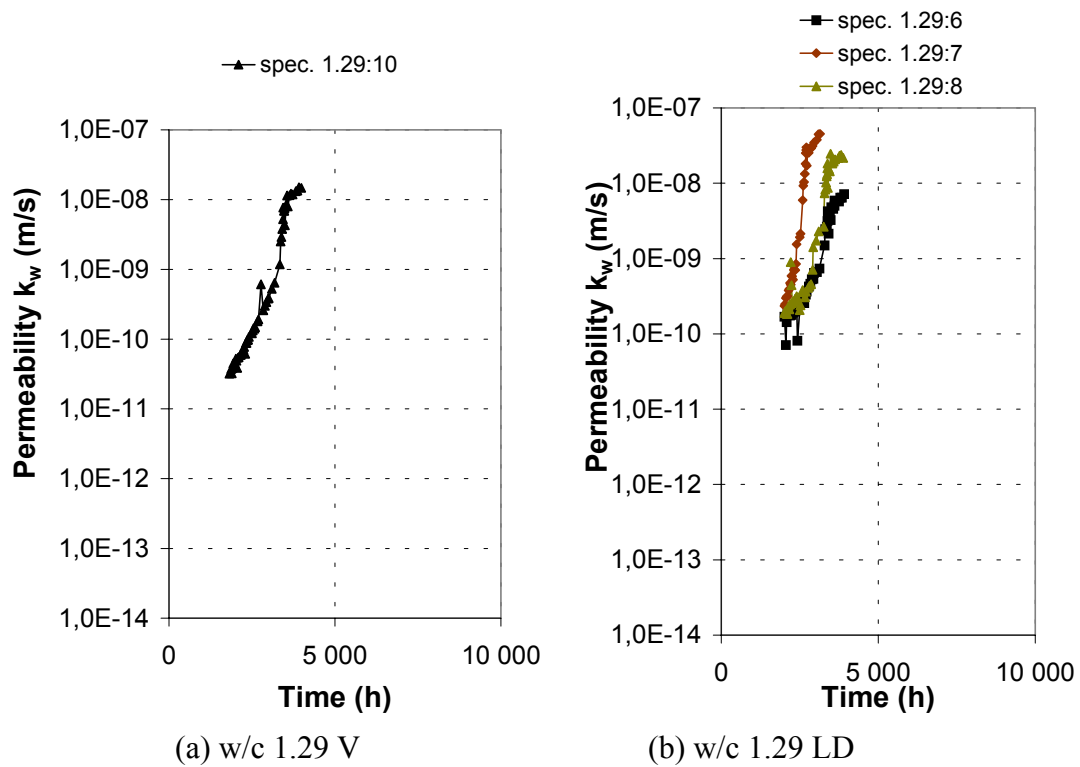


Figure 5.10 Flow of water and permeability in the leached specimens with a w/c of 1.29.

In Figure 5.11 to Figure 5.13 the same data as presented in the preceding figures is shown, but is presented as permeability versus the total volume of water that percolated. These figures are also discussed in section 6.1.1.

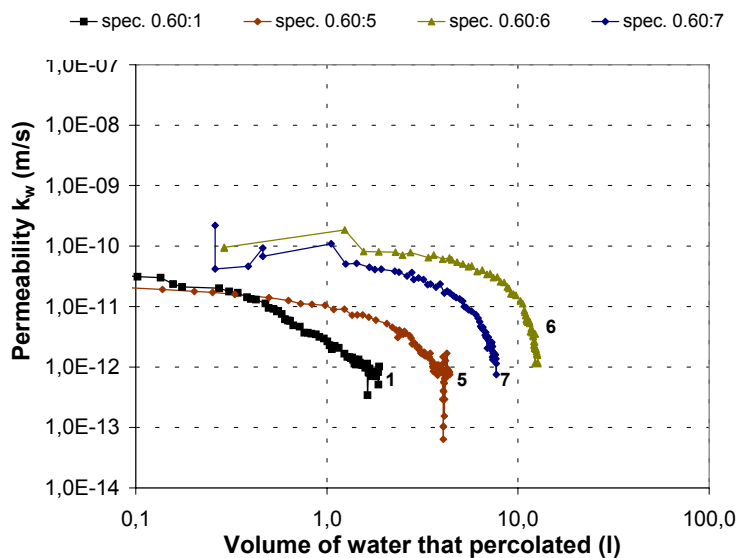


Figure 5.11 Permeability versus total flow of water in the leached EH-specimens with a w/c of 0.60 and a diameter of 155 mm.

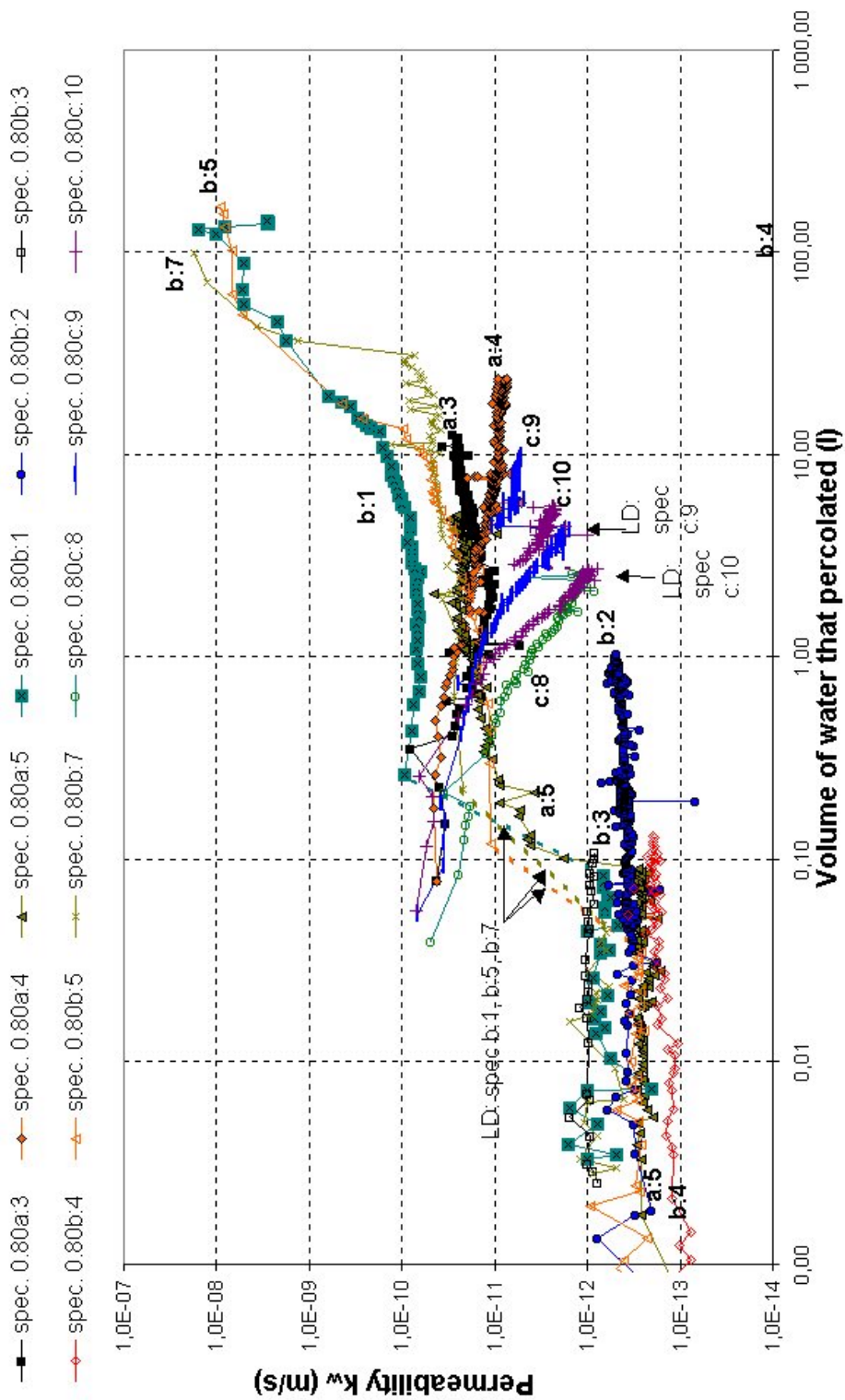


Figure 5.12 Permeability versus the total flow of water in all the leached specimens (V, V-LD, LD, EH) with a w/c of 0.80 and a diameter of 155 mm.

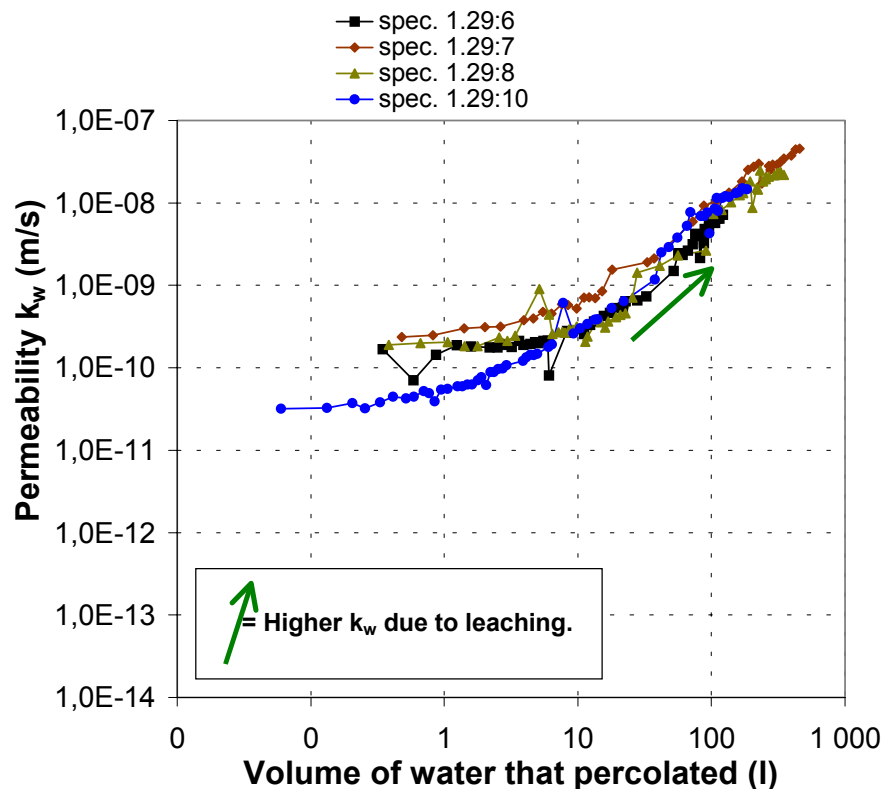


Figure 5.13 Permeability versus total flow of water in the leached specimens with a w/c of 1.29 and a diameter of 155 mm. Specimen 1.29:10 is a V-specimen, the others are LD-specimens.

5.1.2 Flow of ions from the specimens in the downstream direction (convection)

A summary of the results for the leaching of ions by the percolating water, as described in section 5.1.1, is presented in Figure 5.14 to Figure 5.22. The measured flow of ions for each specimen with a diameter of $\phi 155\text{mm}$ is given in the APPENDIX B. The results for specimens with a diameter of only 45 mm is not there for reasons of space. See Table 4.1 and Figure 4.4 for an account of the type of concrete involved and of the testing history. A discussion of the results is given in section 6.1.2.

The water that percolated through the specimens was collected on the downstream side, the concentrations of the elements it contained being measured. The elements involved were Ca, K, Na, S, Al, Fe, Mg and Mn. The measured concentrations of calcium in the percolated water is presented in the following ways in Figure 5.14 to Figure 5.20. The results are for all the specimens with a diameter of 150 mm and w/c ratios of 0.6, 0.8 and 1.29, all the curing and treatment types involved being represented.

1. In Figure 5.14 to Figure 5.16 are shown the concentration of Ca^{2+} in the water that percolated in relation to
 - a. the volume of the water that percolated;
 - b. how much of the initial calcium was carried away by the water that percolated;

- c. the volume of the water that percolated per kg of cement used in mixing the concrete.
2. In Figure 5.17 to Figure 5.20 are shown the accumulated weight of the calcium that was leached in relation to
 - a. the volume of the water that percolated;
 - b. the volume of the water that percolated per kg of cement used in mixing the concrete, and the time relationships involved.
3. Figure 5.21 shows the calculated residual content of calcium in the concrete specimens in relation to the initial calcium content. The calculations are based on the measured amounts of Ca that were leached by the water that percolated. The amounts of Ca that leached in the upstream direction are not taken account of here.
4. Figure 5.22 shows the measured pH in the collected percolated water.

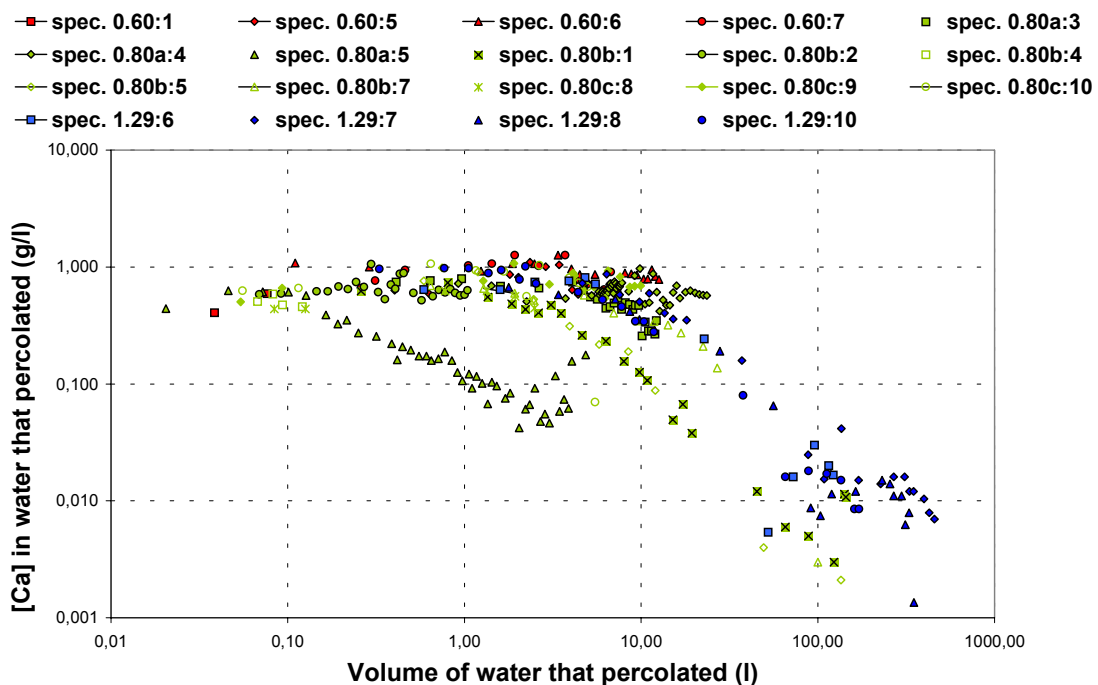


Figure 5.14 Measured concentrations of calcium in the percolated water in relation to the volume of water that percolated.

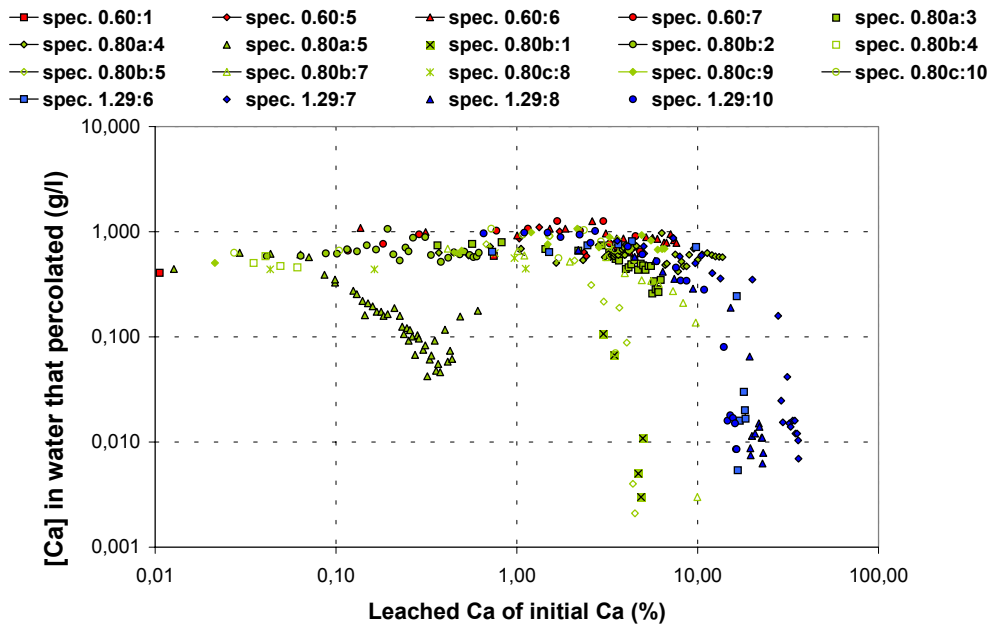


Figure 5.15 Measured concentrations of calcium in the percolated water in relation to the leaching ratio. The leaching ratio is the ratio of the total flow of calcium in the water that percolated as measured, to the estimated initial calcium content in the specimens based on the recipe for the concrete.

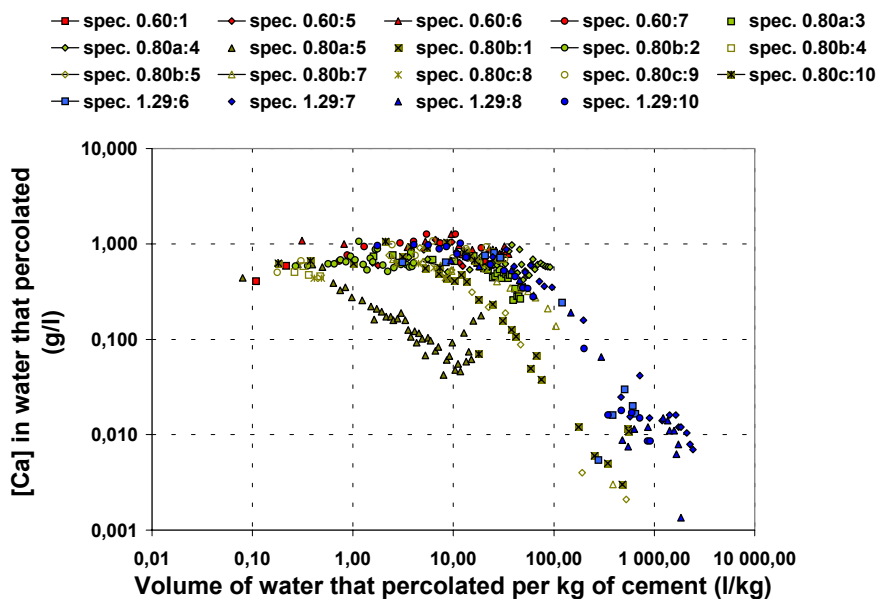


Figure 5.16 Measured concentrations of calcium in the percolated water in relation to the water that percolated. The volume of water that percolated per kg of cement represents the volume of percolating water as measured in relation to estimated cement content based on the recipe for the concrete.

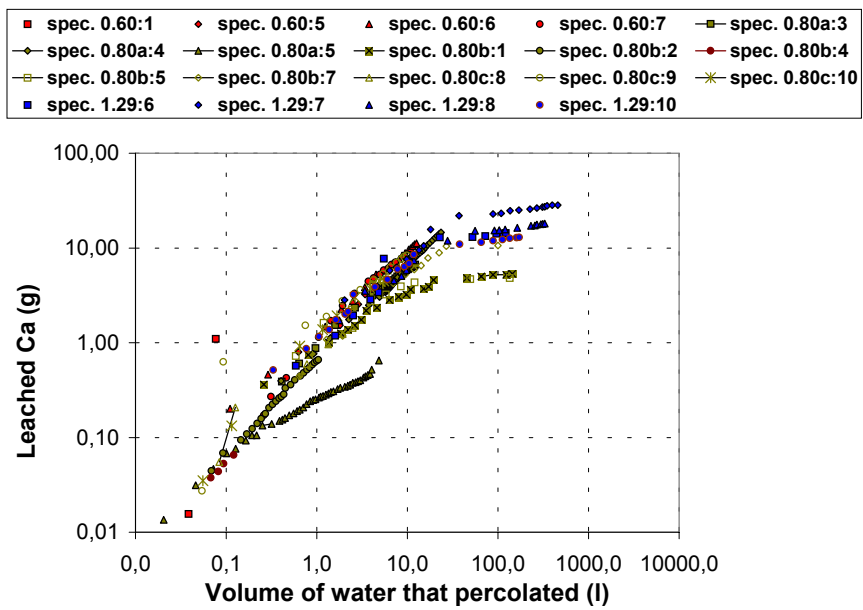


Figure 5.17 Leached calcium (g) in the percolated water as measured in relation to the measured volume of water that percolated.

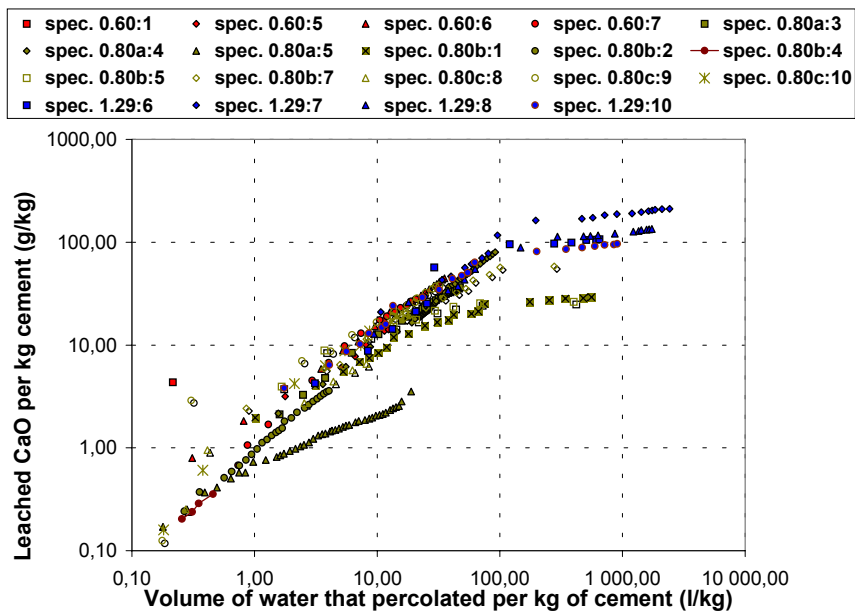


Figure 5.18 Leached g of CaO in the water that percolated per kg of cement, as measured in relation to the measured volume of water that percolated per kg of cement.

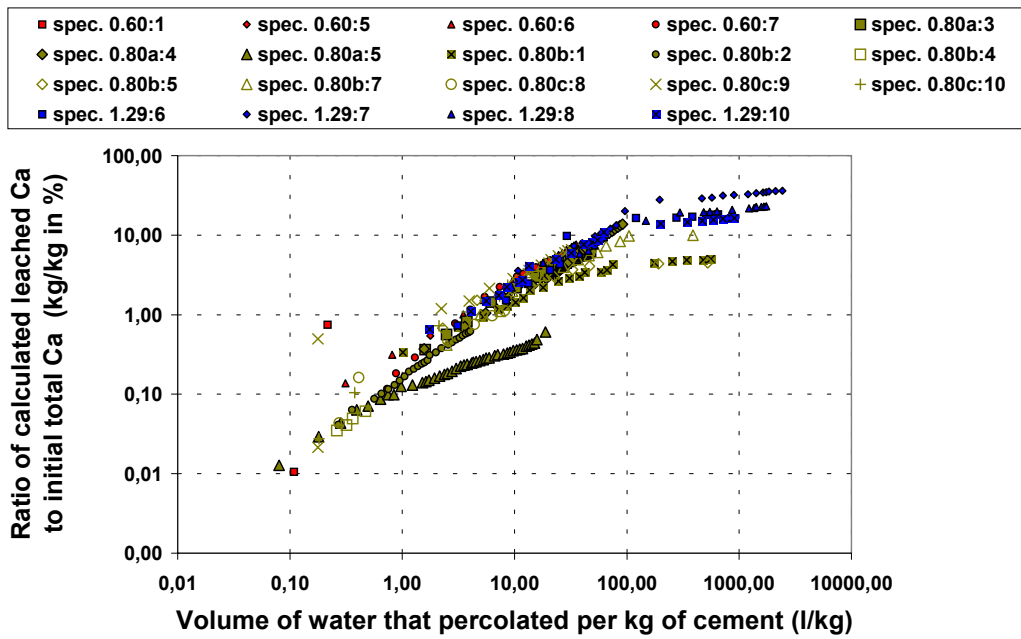


Figure 5.19 Ratio between the calculated total amount of Ca that was leached the initial total amount of Ca (kg/kg in %) in relation to the volume of the water that percolated per kg cement (l/kg).

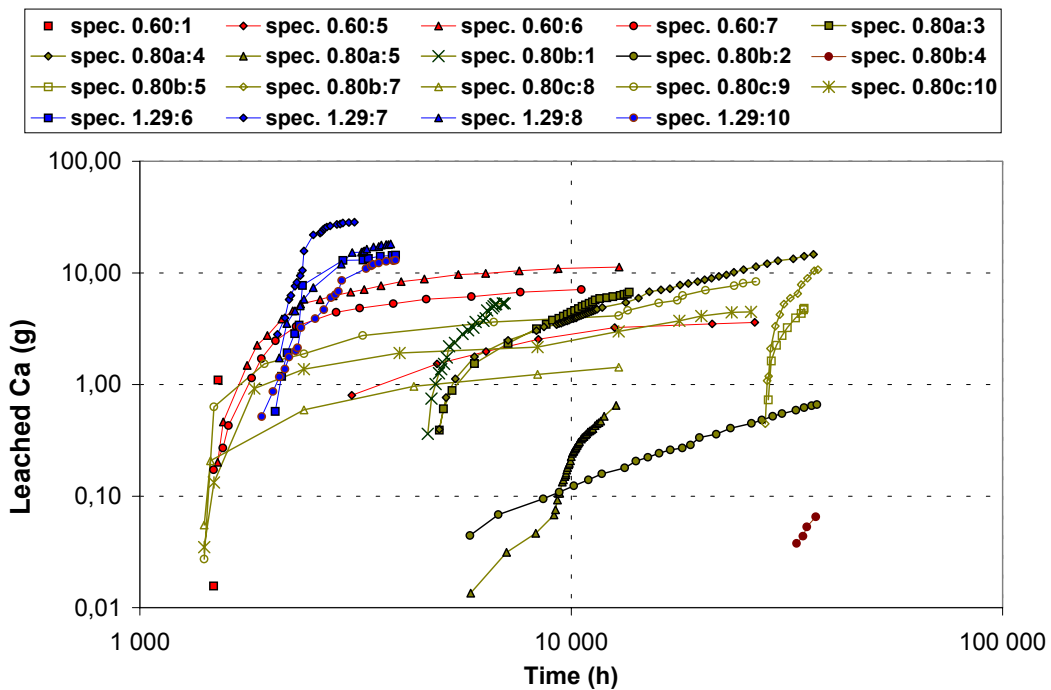


Figure 5.20 Calculated total amount of leached Ca in relation to time.

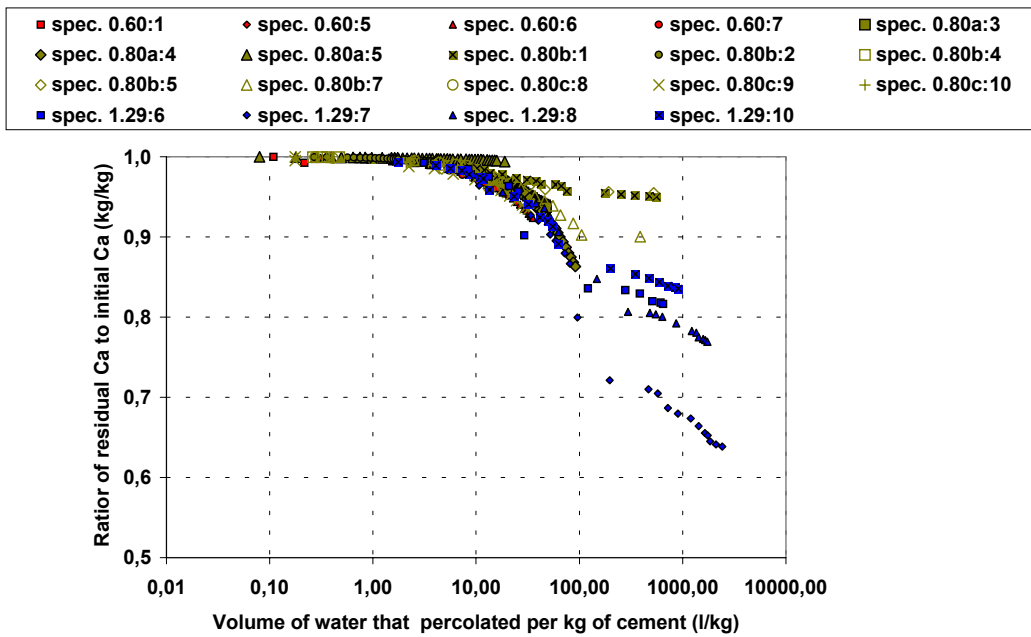


Figure 5.21 Residual total content of calcium in relation to initial total calcium content (%).

pH:

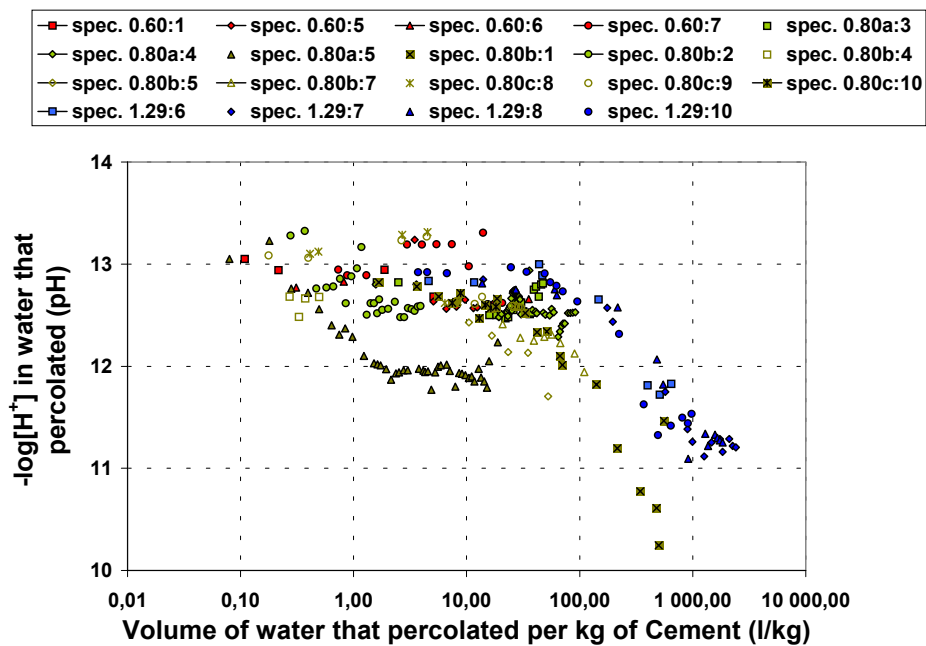


Figure 5.22 Measured pH in percolated water in relation to the measured volume of water that percolated.

Table 5.2 Measured concentrations of ions in the water on the upstream surface of the specimens. Sample volume = the volume of water the ions and the pH were measured in.

| Specimen | Cum. time (h) | Cum. Flushing (l) | Time since last flushing (h) | pH (g/l) | Ca (g/l) | K (g/l) | Na (g/l) | S (g/l) |
|---------------------|---------------|-------------------|------------------------------|----------|----------|---------|----------|---------|
| 0.80a:4 and 0.80b:2 | 26676 | 526 | 120 | 9,67 | 0,0073 | 0,0005 | 0,0011 | 0,0021 |
| | 27012 | 530 | 72 | 9 | | | | |
| | 27516 | 536 | 96 | 9,8 | | | | |
| | 28164 | 544 | 72 | 9,64 | 0,0064 | 0,0098 | 0,0014 | 0,0014 |
| | 29844 | 564 | 192 | 10,56 | 0,019 | 0,0005 | 0,0024 | 0,0007 |
| 0.80b:2 | 31668 | 586 | 119 | 10,12 | 0,01 | 0,0004 | 0,0005 | 0,0004 |
| | 33349 | 598 | 169 | 9,212 | 0,0084 | 0,0003 | 0,0005 | 0,0002 |
| | 34837 | 614 | 146 | 9,176 | 0,0061 | 0,0001 | 0,0004 | 0,0001 |
| | 36445 | 630 | 168 | 10,272 | 0,0091 | 0,0002 | 0,0004 | 0,0003 |
| 0.80a:4 | 23452 | 548 | 72 | 10,78 | | | | |
| | 31492 | 586 | 119 | 9,37 | 0,005 | 0,0002 | 0,0004 | 0,0002 |
| | 33173 | 598 | 169 | 7,972 | 0,0056 | 0,0002 | 0,0005 | 0,0002 |
| | 34661 | 614 | 146 | 7,559 | 0,0041 | 0,0001 | 0,0004 | 0,0001 |
| | 36269 | 630 | 168 | 7,241 | 0,0017 | 0,0001 | 0,0004 | 0,0001 |
| 0.80b:4 | 28890 | 68 | 72 | | 0,0128 | 0,001 | 0,001 | 0,003 |
| | 30282 | 84 | 192 | 11,05 | 0,017 | 0,001 | 0,003 | 0,001 |
| | 32106 | 106 | 119 | 10,43 | 0,013 | 0,0005 | 0,0005 | 0,0005 |
| | 33787 | 118 | 169 | 9,338 | 0,013 | 0,0006 | 0,0005 | 0,0003 |
| | 35275 | 134 | 146 | 9,655 | 0,008 | 0,0002 | 0,0004 | 0,0002 |
| | 36883 | 150 | 168 | 10,373 | 0,0098 | 0,0003 | 0,0004 | 0,0002 |
| 0.80b:5, 7 | 28914 | 70 | 72 | 9,76 | 0,0138 | 0,0005 | 0,0011 | 0,0023 |
| | 30306 | 86 | 192 | 10,4 | 0,014 | 0,0004 | 0,0013 | 0,0007 |
| | 32130 | 108 | 119 | 10,3 | 0,011 | 0,0041 | 0,0031 | 0,0004 |
| | 33811 | 120 | 169 | 9,047 | 0,01 | 0,0002 | 0,0004 | 0,0003 |
| | 35131 | 148 | 146 | 0 | 0,006 | 0,0001 | 0,0004 | 0,0002 |
| | 36739 | 164 | 168 | 0 | 0,005 | 0,0001 | 0,0004 | 0,0002 |
| 0.80c:9,10 | 14440 | 144 | 240 | 7,45 | 0,0062 | 0,0005 | 0,0012 | 0,0022 |
| | 15952 | 158 | 168 | 9,56 | 0,0054 | 0,0004 | 0,0022 | 0,0013 |
| | 16312 | 162 | 168 | 9,84 | | | | |
| | 16648 | 166 | 144 | 9,57 | 0,0061 | 0,0003 | 0,0013 | 0,0012 |
| | 17152 | 172 | 168 | 9,33 | | | | |
| | 17800 | 180 | 168 | 9,5 | 0,0058 | 0,0002 | 0,0011 | 0,0008 |
| | 19528 | 200 | 192 | 10,53 | 0,008 | 0,0006 | 0,0016 | 0,0004 |
| | 21352 | 222 | 119 | 9,77 | 0,007 | 0,0002 | 0,0004 | 0,0003 |
| | 21352 | 222 | 119 | 9,77 | 0,007 | 0,0002 | 0,0004 | 0,0003 |
| | 24521 | 250 | 146 | 7,504 | 0,0048 | 0,0001 | 0,0004 | |
| 26129 | 266 | 168 | 7,542 | 0,0029 | 0,0003 | 0,0005 | | |

5.1.4 Determination of changes in compressive and split tensile strength

The measured values for the relative compressive strength and relative split tensile strength of the leached specimens are shown Figure 5.23 in relation to the mean strength of the non-leached specimens. A discussion of the results is provided in section 6.1.3.

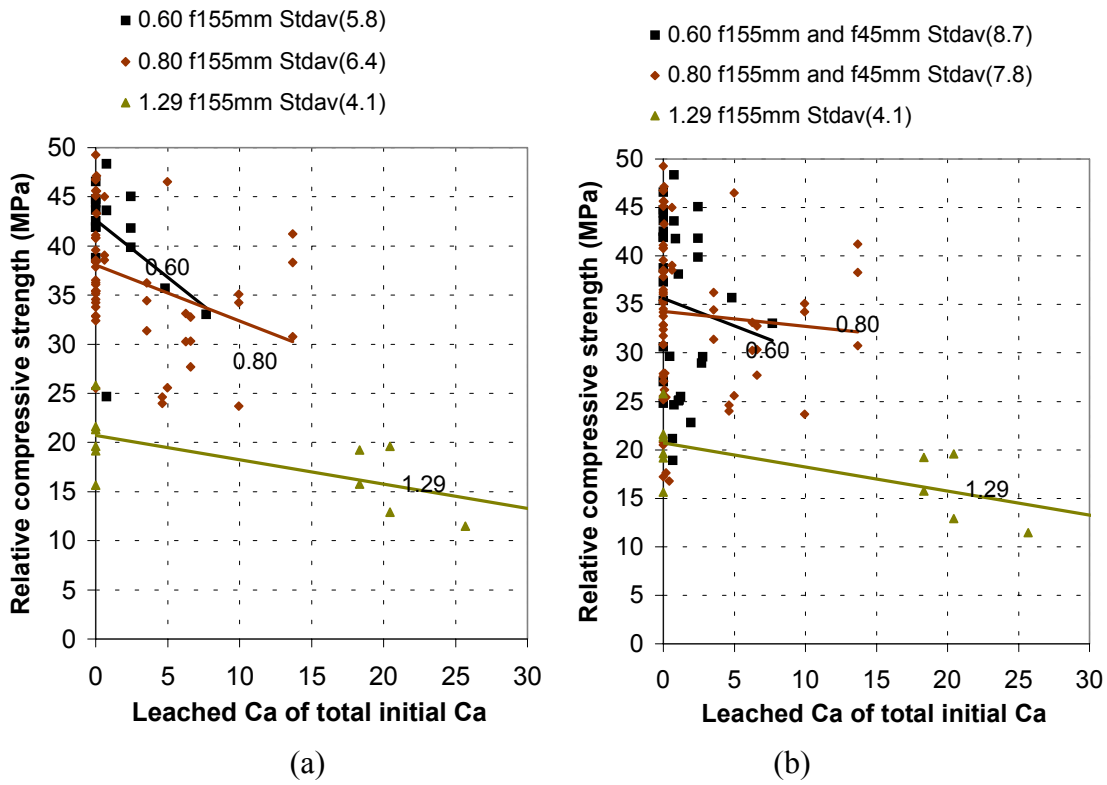


Figure 5.23 Relative compressive strength (a) of all specimens $\phi 155$ mm in diameter; and (b) of all specimens of both $\phi 155$ and $\phi 45$ mm diameter, in relation to the leaching ratio.

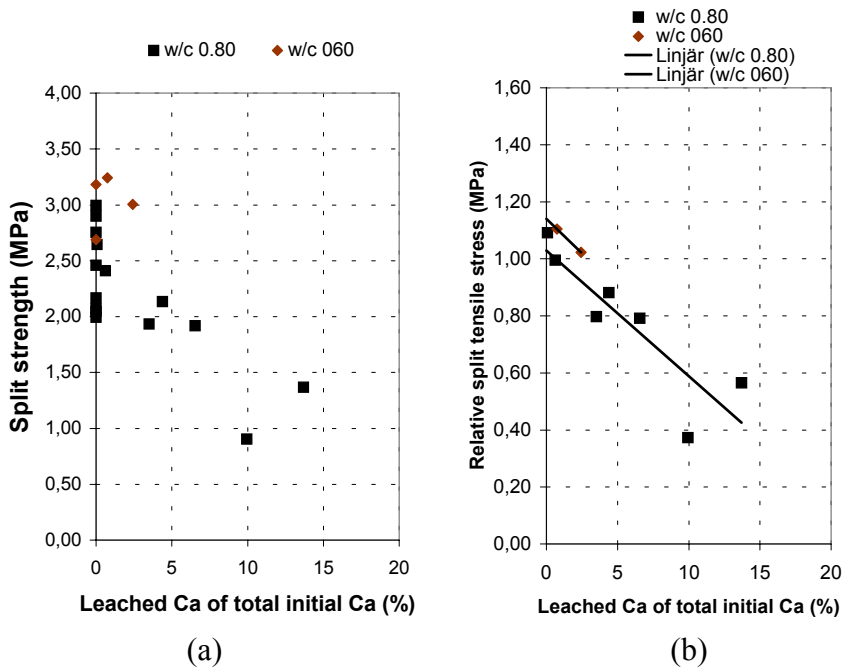


Figure 5.24 (a) Split strength of all the specimens $\phi 155$ mm in diameter; and (b) the relative split strength of the leached specimens $\phi 155$ in diameter in relation to non-leached specimens.

5.1.5 Determination of changes in pore size distribution

Slices of some the specimens were gradually drained of water by use of suction equipment, as described in section 4.10.2. The volume of the drained water allowed the pore size distribution in the upper pore size range $200 \text{ \AA} - 10\,000 \text{ \AA}$ to be estimated. The accumulated volume of water that was pressed out from pores of differing size (the assumptions made being taken up in section 4.10.2) are shown in the APPENDIX C. One can note that above a certain pore size, or critical pore diameter ϕ_{crit} , the water volume drained was almost insignificant, but that below this critical pore diameter the volume of water pressed out increased very much. It can be seen in the figures in the APPENDIX C, that ϕ_{crit} was measured to about 10^{-7} m , except for specimens 0.60:9R, 0.80b:2 and 0.80b:5, for which ϕ_{crit} was about $0.4 \cdot 10^{-7} \text{ m}$. A discussion of the results is provided in section 6.1.4.

5.1.6 Determination of changes in total porosity

The total porosity was measured after drying of the specimens in the oven $+105^\circ\text{C}$ (see section 4.10.3).

- The results for all the specimens with a w/c ratio of 0.60 and 0.80 and a diameter of 155 mm are presented in Figure 5.25 and in Figure 5.25.
- The results for the same specimens as in Figure 5.26 are also presented in Figure 5.27 - Figure 5.29. In these figures a differentiation have been made for different batches: 0.80a, 0.80b and 0.80c.
- The results for the same specimens as in Figure 5.26 are also presented in Figure 5.30 - Figure 5.32. There, the differentiation has been made in terms of the different curing methods involved: V, LD and EH.

A discussion of these results is provided in section 6.1.5.

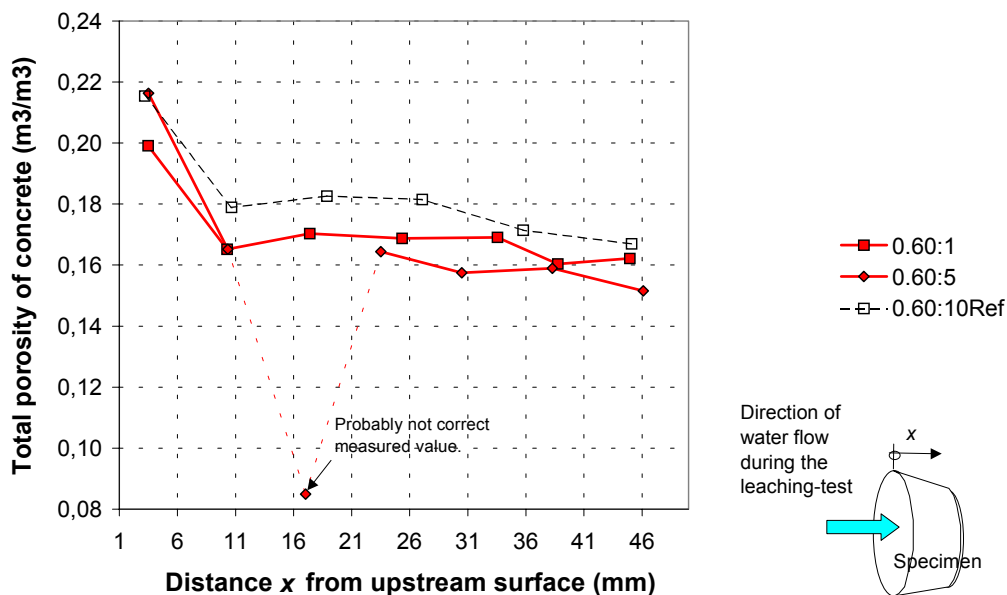


Figure 5.25 Total porosity of the leached EH specimens 0.60:1 and 0.60:5 and the reference EH specimen 0.60:10Ref at different distance from the surface.

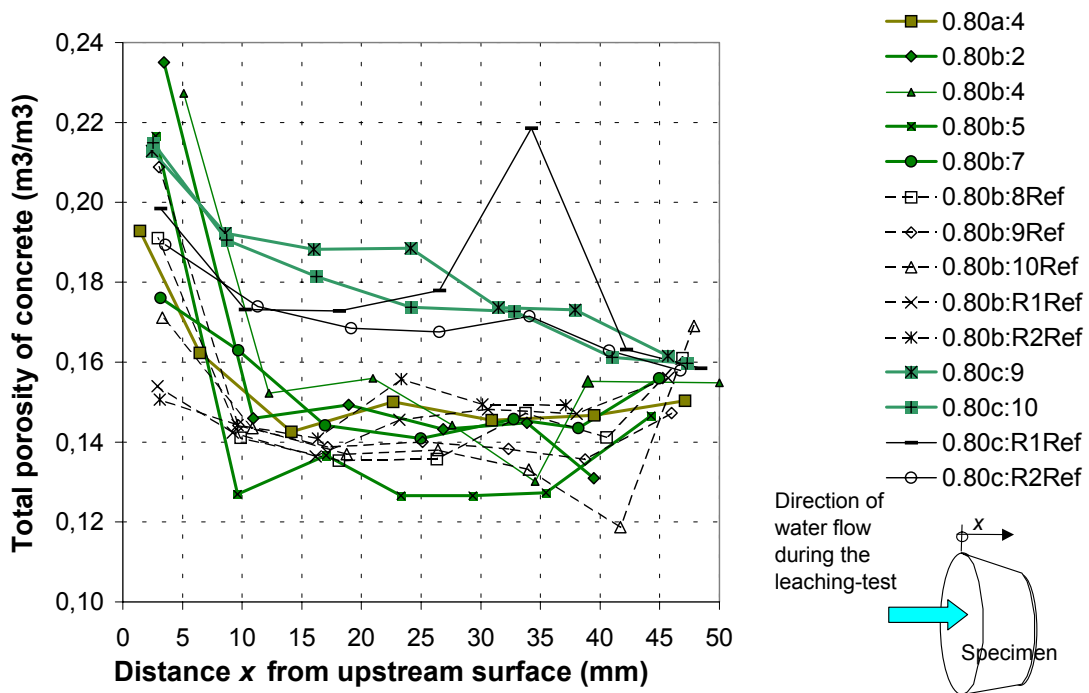


Figure 5.26 Total porosity of all the leached specimen with a w/c ratio of 0.80, at different distance from the surface.

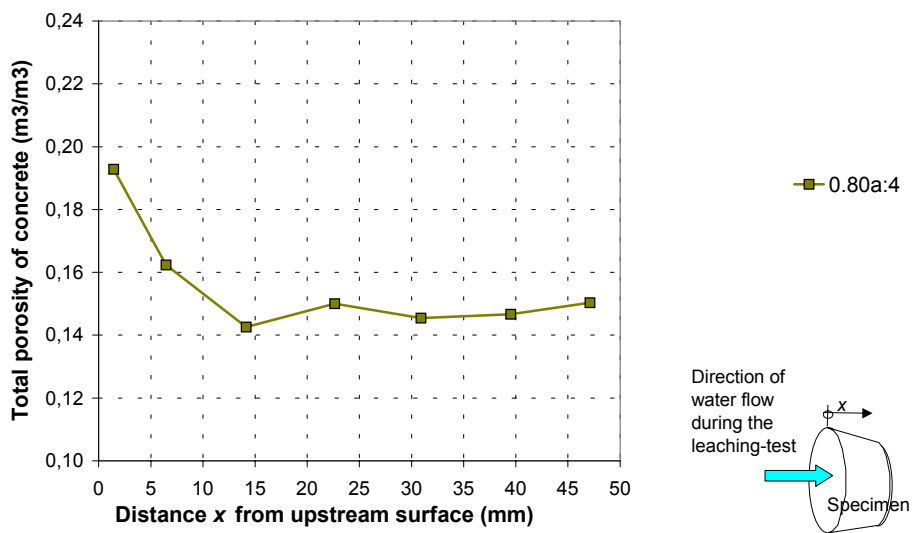


Figure 5.27 Total porosity of the leached LD specimen 0.80a:4 at different distance from the surface.

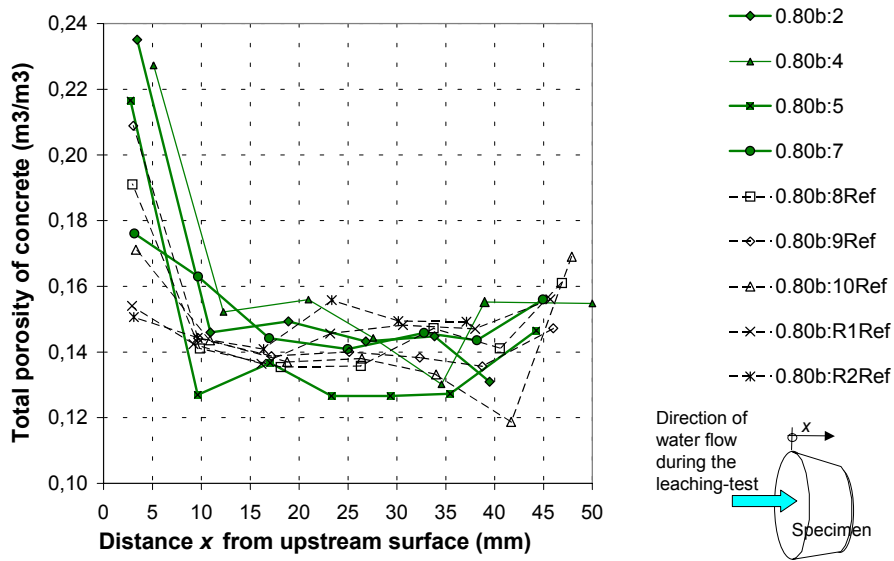


Figure 5.28 Total porosity of leached specimens 0.80b:2, 0.80b:5 and 0.80b:7 and reference specimens 0.80b:8Ref, 0.80b:9Ref and 0.80b:10Ref at different distance from the surface.

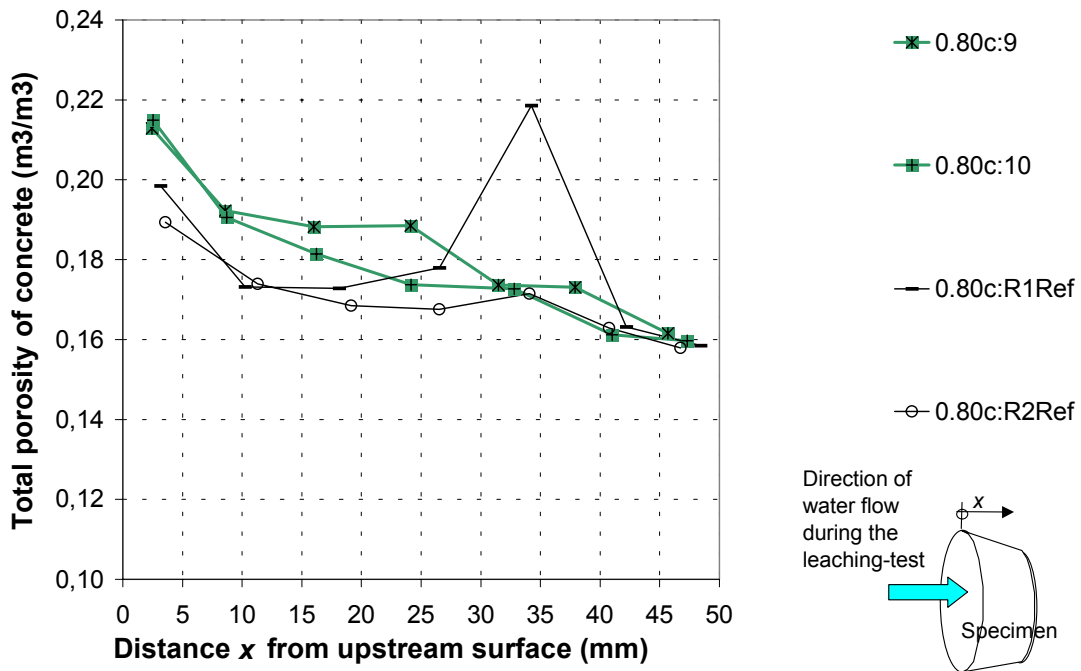


Figure 5.29 Total porosity of leached specimens 0.80c:9 and 0.80c:10 and reference specimens 0.80c:R1 and R2 at different distance from the surface.

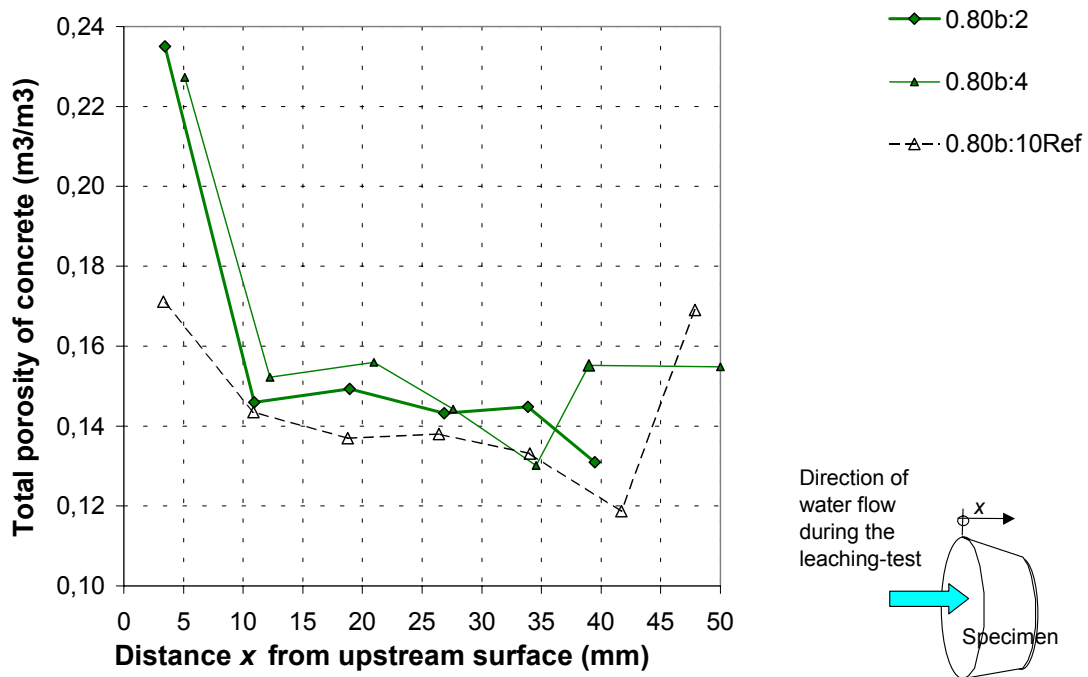


Figure 5.30 Total porosity of the (V)-specimens 0.80 at different distance from the surface.

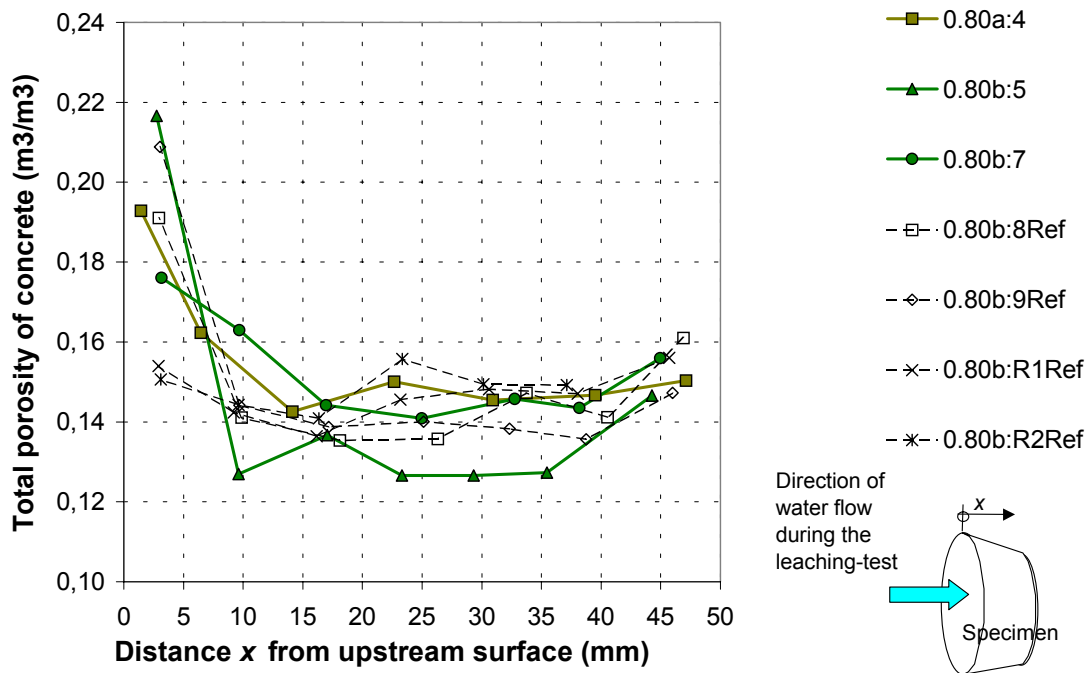


Figure 5.31 Total porosity of the (LD)-specimens 0.80 at different distance from the surface.

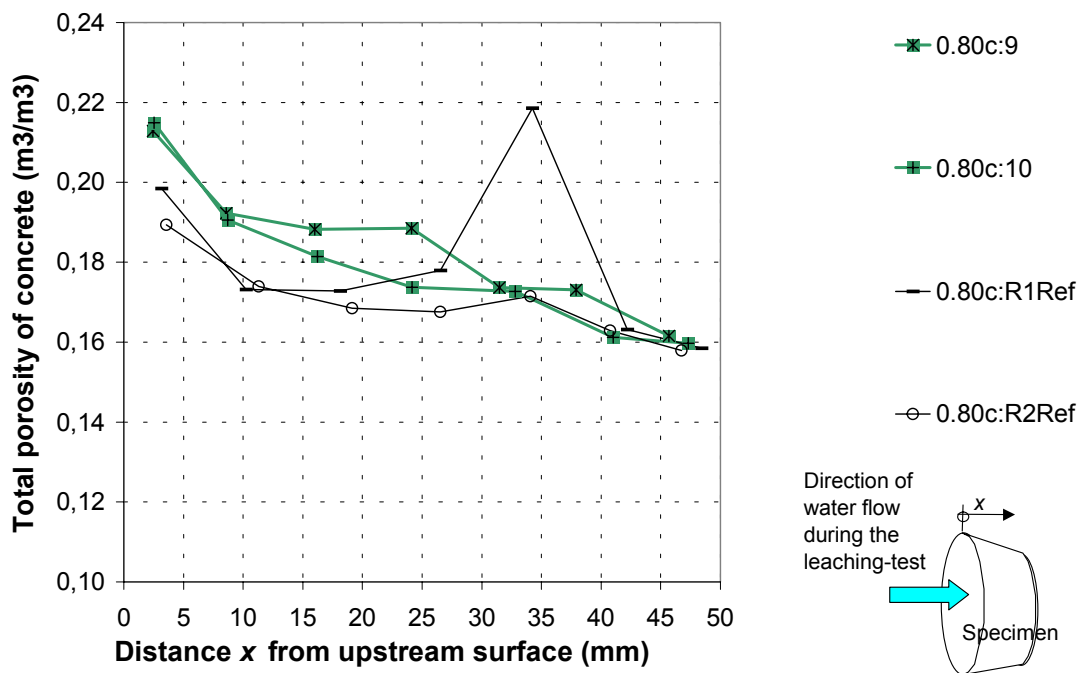


Figure 5.32 Total porosity of the (EH)-specimens 0.80 at different distance from the surface.

5.1.7 Determination of changes in the remaining compounds and elements contained in the specimens

After the leaching tests had been completed, the concrete specimens were cut into seven slices. Each slice was pulverised and was dissolved in HNO_3 (see Figure 4.15 and section 4.12). The data in Table 5.3 are results of this chemical analysis. In order to estimate how much of the dissolved elements came from the paste and how much from the aggregate, a second study was conducted involving only the aggregate. This second study was performed in the same way and with the same type and amount of aggregate as used for concrete specimen 3, see Table 5.4.

A discussion of the results is provided in section 6.1.6.

Table 5.3 Measured values for the remaining elements contained in slices taken from leached and non-leached concrete specimens. x = distance from the upstream face (see Figure 4.15).

| Specimen | x mm | Al mg/l | Ca mg/l | Fe mg/l | K mg/l | Mg mg/l | Mn mg/l | Na mg/l | S mg/l | Si mg/l | slices g | Pow- der g | Cy- lin- der ml | Rest g |
|----------|-----------|------------|------------|------------|-----------|------------|------------|------------|-----------|------------|-------------|------------------|--------------------------|-----------|
| 0.60:6 | 45 | 757 | 5 240 | 1 342 | 147 | 132 | 37 | 27 | 177 | 13 | | 117.1 | 1000 | 96.4 |
| | 35 | 595 | 4 120 | 1 181 | 132 | 112 | 28 | 21 | 137 | 10 | | 109.7 | 1000 | 91.6 |
| | 25 | 644 | 4 830 | 1 127 | 133 | 108 | 31 | 21 | 190 | 10 | | 111.1 | 1000 | 92.8 |
| | 15 | 369 | 2 720 | 633 | 134 | 73 | 18 | 11 | 107 | 10 | | 60.1 | 1000 | 49.6 |
| | 5 | 715 | 4 740 | 1 323 | 148 | 146 | 41 | 28 | 182 | 15 | | 114.6 | 1000 | 92.4 |
| 0.60:9 | 46 | 1 396 | 10 377 | 1 800 | 151 | 310 | 46 | 200 | 333 | 19 | 35.6 | 35.6 | 200 | 31.3 |
| | 39 | 1 397 | 10 669 | 1 740 | 141 | 273 | 44 | 157 | 323 | 28 | 34.9 | 34.4 | 200 | 30.0 |
| | 33 | 1 259 | 8 056 | 1 703 | 153 | 305 | 38 | 139 | 184 | 9 | 24.6 | 24.6 | 200 | 21.4 |
| | 26 | 1 574 | 13 164 | 2 003 | 162 | 303 | 50 | 183 | 288 | 15 | 38.3 | 38.4 | 200 | 32.7 |
| | 19 | 1 456 | 11 433 | 1 824 | 146 | 321 | 47 | 175 | 281 | 15 | 36.8 | 36.8 | 200 | 32.4 |
| | 11 | 1 468 | 10 914 | 1 855 | 158 | 287 | 51 | 176 | 296 | 29 | 38.9 | 38.8 | 200 | 34.2 |
| | 3 | 1 514 | 12 174 | 2 077 | 149 | 308 | 49 | 181 | 333 | 13 | 32.8 | 32.8 | 200 | 27.9 |
| 0.80a:3 | 45 | 757 | 5 240 | 1 342 | 147 | 132 | 37 | 27 | 177 | 13 | | 117.1 | 1000 | 96.4 |
| | 35 | 595 | 4 120 | 1 181 | 132 | 112 | 28 | 21 | 137 | 10 | | 109.7 | 1000 | 91.6 |
| | 25 | 644 | 4 830 | 1 127 | 133 | 108 | 31 | 21 | 190 | 10 | | 111.1 | 1000 | 92.8 |
| | 15 | 369 | 2 720 | 633 | 134 | 73 | 18 | 11 | 107 | 10 | | 60.1 | 1000 | 49.6 |
| | 5 | 715 | 4 740 | 1 323 | 148 | 146 | 41 | 28 | 182 | 15 | | 114.6 | 1000 | 92.4 |
| 0.80a:4 | 47 | 898 | 4 672 | 1 579 | 173 | 275 | 54 | 23 | 204 | 11 | 24.6 | 24.6 | 200 | 20.2 |
| | 40 | 1 079 | 6 013 | 1 970 | 223 | 296 | 57 | 18 | 270 | 14 | 40.4 | 40.5 | 200 | 35.8 |
| | 31 | 946 | 5 559 | 1 556 | 183 | 218 | 54 | 13 | 231 | 6 | 33.2 | 33.3 | 200 | 29.3 |
| | 23 | 994 | 7 092 | 1 987 | 116 | 253 | 58 | 12 | 241 | 13 | 37.5 | 37.6 | 200 | 32.6 |
| | 14 | 737 | 5 577 | 1 483 | 104 | 227 | 55 | 10 | 266 | 13 | 35.2 | 35.3 | 200 | 31.1 |
| | 6 | 1 005 | 5 055 | 1 584 | 193 | 244 | 56 | 14 | 286 | 16 | 30.2 | 30.2 | 200 | 26.0 |
| | 1 | 529 | 2 399 | 779 | 132 | 130 | 28 | 8 | 88 | 10 | 12.1 | 12.1 | 200 | 9.7 |
| 0.80b:2 | 46 | | | | | | | | | | | | | |
| | 39 | 770 | 5 075 | 1 063 | 83 | 148 | 28 | 92 | 142 | 8 | 25.7 | 25.7 | 200 | 23.3 |
| | 34 | 989 | 7 536 | 1 226 | 88 | 194 | 35 | 113 | 211 | 25 | 29.9 | 29.9 | 200 | 26.5 |
| | 27 | 1 489 | 11 097 | 1 910 | 130 | 236 | 43 | 140 | 262 | 17 | 39.5 | 36.5 | 200 | 35.5 |
| | 19 | 1 251 | 9 276 | 1 578 | 127 | 243 | 41 | 150 | 280 | 13 | 38.7 | 38.6 | 200 | 34.8 |
| | 11 | 1 290 | 8 874 | 1 594 | 141 | 289 | 43 | 180 | 276 | 13 | 40.1 | 40.0 | 200 | 36.2 |
| | 3 | 1 253 | 7 344 | 1 847 | 94 | 268 | 49 | 125 | 181 | 16 | 32.3 | 32.1 | 200 | 29.1 |
| 0.80b:5 | 44 | 994 | 7 332 | 1 336 | 66 | 131 | 34 | 65 | 111 | 10 | 27.7 | 27.7 | 200 | 24.8 |
| | 35 | 1 202 | 9 218 | 1 612 | 78 | 134 | 32 | 78 | 152 | 15 | 43.7 | 43.6 | 200 | 40.2 |
| | 29 | 1 140 | 8 393 | 1 635 | 100 | 144 | 34 | 90 | 140 | 13 | 35.1 | 35.0 | 200 | 31.9 |
| | 23 | 958 | 7 649 | 1 158 | 79 | 122 | 29 | 77 | 124 | 11 | 31.3 | 31.3 | 200 | 28.5 |
| | 17 | 936 | 7 014 | 1 102 | 76 | 125 | 28 | 69 | 119 | 11 | 32.5 | 32.5 | 200 | 29.8 |
| | 10 | 967 | 7 165 | 1 174 | 86 | 126 | 27 | 84 | 105 | 10 | 32.6 | 32.6 | 200 | 29.9 |
| | 3 | 2 054 | 16 175 | 3 075 | 164 | 218 | 47 | 160 | 221 | 12 | 60.0 | 60.0 | 200 | 54.4 |
| 0.80b:8 | 47 | 1 419 | 8 088 | 1 984 | 302 | 314 | 62 | 25 | 281 | 27 | 30.4 | 30.7 | 200 | 24.1 |
| | 41 | 1 207 | 6 845 | 1 755 | 254 | 248 | 56 | 19 | 219 | 9 | 32.1 | 32.3 | 200 | 27.0 |
| | 34 | 1 486 | 9 688 | 2 194 | 243 | 260 | 63 | 18 | 300 | 10 | 34.8 | 35.0 | 200 | 29.3 |
| | 26 | 1 074 | 7 182 | 1 543 | 250 | 214 | 48 | 13 | 234 | 7 | 38.7 | 38.9 | 200 | 33.3 |
| | 18 | 1 422 | 8 456 | 1 938 | 334 | 290 | 63 | 17 | 365 | 14 | 42.4 | 42.7 | 200 | 36.1 |
| | 10 | 1 410 | 9 141 | 2 229 | 274 | 281 | 64 | 26 | 406 | 22 | 39.3 | 39.6 | 200 | 32.7 |
| | 3 | 1 436 | 9 883 | 2 444 | 253 | 301 | 62 | 22 | 250 | 33 | 28.3 | 28.7 | 200 | 21.1 |
| 0.80b:10 | 48 | 886 | 5 763 | 1 360 | 180 | 199 | 47 | 11 | 169 | 9 | 20.8 | 20.8 | 200 | 16.6 |
| | 42 | 954 | 7 472 | 1 883 | 167 | 249 | 59 | 15 | 269 | 10 | 41.1 | 41.1 | 200 | 35.9 |
| | 34 | 990 | 8 211 | 1 935 | 157 | 225 | 51 | 15 | 298 | 16 | 35.8 | 35.9 | 200 | 30.5 |
| | 26 | 1 282 | 9 696 | 2 751 | 179 | 314 | 78 | 18 | 327 | 21 | 39.9 | 40.0 | 200 | 33.6 |
| | 19 | 1 339 | 8 691 | 2 086 | 259 | 280 | 58 | 25 | 224 | 11 | 36.2 | 36.3 | 200 | 30.4 |
| | 11 | 1 364 | 9 675 | 2 146 | 267 | 319 | 71 | 25 | 339 | 14 | 42.3 | 42.3 | 200 | 35.8 |
| | 3 | 1 003 | 8 168 | 1 770 | 153 | 238 | 56 | 11 | 282 | 22 | 32.5 | 32.5 | 200 | 26.1 |

Table 5.4 Measured values for the remaining elements for the aggregate.

| Aggregate | Al mg/g | Ca mg/g | Fe mg/g | K mg/g | Mg mg/g | Mn mg/g | Na mg/g | S mg/g | Si mg/g | rest g |
|-------------------------|------------|------------|------------|-----------|------------|------------|------------|-----------|------------|-----------|
| Hardeberga quartzite | 1.65 | 0.62 | 2.09 | 0.64 | 0.19 | 0.03 | 0.25 | 0.16 | 0.00 | 98.7 |
| Kvidinge sand | 4.27 | 3.71 | 13.9 3 | 0.08 | 1.44 | 0.29 | 0.00 | 0.03 | 0.02 | 94.9 |

5.2 Percolation through holes in the concrete

5.2.1 Determination of the downstream ion flow (convection)

With the equipment available it was quite difficult to maintain a constant water flow through the holes of the specimens. The varying water flow lead to varying pH (Figure 5.33) and varying concentrations of ions (Figure 5.34 in the outlet water. When the water flow was high, the concentration of ions and the pH decreased in the outlet water and when the water flow was low the outlet water became richer in ions.

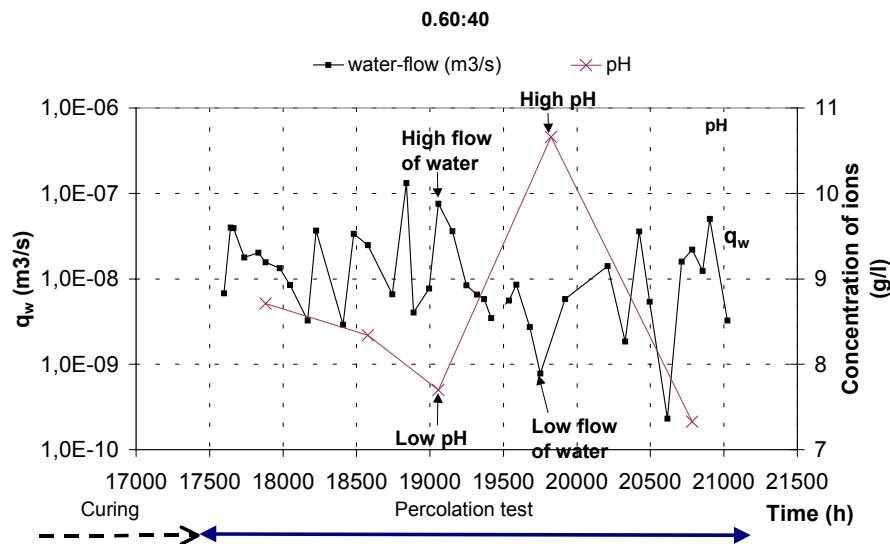


Figure 5.33 pH in water flowing through the holes in specimen 0.60:40. The “saw-tooth”-shape of the water flow q_w is due to difficulties in maintaining constant flow rate. The valve that led the water in through the holes was not designed for such a task. “Curing” means here the test specimens being stored in lime-water for 1750 hours prior to the test.

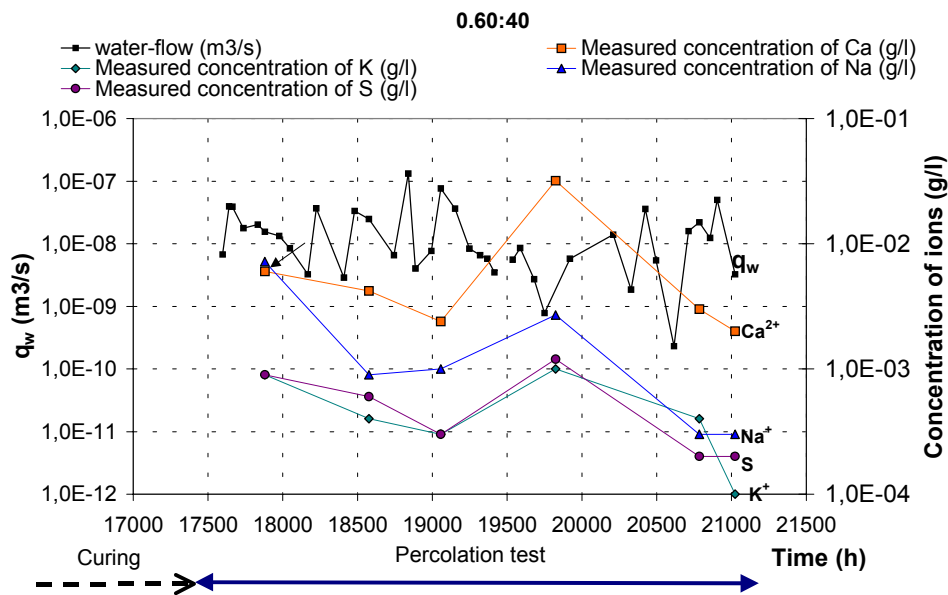


Figure 5.34 Concentration of ions in water flowing through the holes in specimen 0.60:40.

5.2.2 Determination of the upstream ion flow

Of course there was diffusion upstream of ions but the flow of water was sufficiently fast to be any net flow of ions in the upstream direction.

5.2.3 Determination of the remaining compounds and elements in the specimens

5.2.3:1 Introduction

An examination of one leached concrete specimen 0.60:40 (see sections 4.3, 4.5 and 4.13) was performed at FIB in Weimar by means of SEM (Scanning Electron Microscope). The results are presented below, together with an initial discussion of them. Further discussion of the result is to be found in section 6.2.2. The concrete specimen had been cast with three holes extending from the one side to the other, see Figure 4.23. De-ionised water flowed through these holes for some time, see Figure 5.33. After the leaching tests had been completed, the specimen was sawed into nine slices. A small piece was broken off from each of the three slices 1, 7 and 9 and examined by use of a SEM. Slice no. 1 was from the most upstream part of the specimen and slice no 9 from the most downstream part. The pieces were taken from a small area around one of the holes. The SEM-examination was performed on the surface of these small pieces, from the surface of the hole and along a line y perpendicular to the hole (Figure 4.23).

Pictures, see below, of the topography and morphology were obtained by use of Secondary Electrons (SE) and Back-Scattering Electrons (BSE). The darker areas in the pictures indicate the presence of denser compounds. By means of an EDX (Energy Dispersive X-ray) analysis conducted on the observed surface, chemical elemental analysis was also performed.

The EDX-examination provides mean values for the concentration of elements in the *spot-areas* that were studied. Although no precise distribution of the different elements within these spot-areas was obtained the distribution can be observed to some extent on the basis of the texture and the colour in the pictures (based on SE and BSE). Although it is not possible either to quantify exactly from which compounds the different elements came, the Ca for example, may have come from $\text{Ca}(\text{OH})_2$, C-S-H gel, the AF-phases or the aggregate. It is often obvious from the shape and texture one can observe in the pictures that certain compounds are fairly common, although no precise figures can be given. The smaller the spot-area studied is, the more exactly the distribution of the elements in it can be determined. The time required would of course increase if larger parts were to be examined in detail since a great number of spot-areas would need then to be studied.

The x-rays in the EDX analysis penetrate about 2-5 μm into the material. Therefore, material that is visually hidden beneath the surface influences the element analysis. For example, an EDX analysis of an observed crystal of $\text{Ca}(\text{OH})_2$ may give peculiar results indicating a high content of silicon when there is a particle of aggregate just beneath the crystal analysed.

Accordingly, the text below presents largely qualitative conclusions regarding the distribution of elements and compounds.

The aggregates employed were Hardeberga quartz and Kvidinge sand. Kvidinge sand consists of about 75 % gneissic granite, which is a morphologically transformed granite. Granite consists mainly of quartz and feldspar. Feldspar has a chemical composition of XZ_4O_8 where $\text{X} = (\text{Na}, \text{K}, \text{Ca})$ and $\text{Z} = (\text{Al}, \text{Si})$.

5.2.3:2 *Slice 1 (upstream end)*

Figure 5.35 - Figure 5.41 show the shape and texture of the surface of a piece of concrete, showing both the hole and the matrix. A summary of the EDX analysis of the elements in the entire area the picture (a) covers is presented in Table 5.6.

It can be said generally that:

- There is a very thin layer of about 1-3 μm of calcite (CaCO_3) on the inner surface of the hole. The calcite was probably formed during the leaching test built up by calcium from the wall of the hole and dissolved $\text{CO}_2(\text{aq})$ in water.
- There was no Portlandite ($\text{Ca}(\text{OH})_2$) closer to the hole than approximately 1.5 mm from it, Portlandite occurring more frequently at a distance of 2 mm or more from the hole-wall.

Table 5.6 Numbers of atoms of the total in % from the spot-areas selected as contained in slice 1.

| Element | y (mm) | Ca | Si | Na | K | Al | S | Fe | O | Cr | Ni | Sum | Ca/Si |
|---------------------------|-----------|------|------|------|------|------|------|------|------|-----|------|------|-------|
| Molar weighth (g/mole) | | 40.1 | 28.1 | 23.0 | 39.1 | 27.0 | 32.1 | 55.8 | 16 | 52 | 58.7 | | |
| Spot-area | | | | | | | | | | | | | |
| Figure 5.37 (a) | Hole | 18,4 | 10,0 | 0,5 | 0,8 | 3,6 | 4,1 | 1,3 | 60,2 | - | - | 98,9 | 1.8 |
| EDX-Bild3 | Hole | 0,8 | 5,6 | 1,1 | 0,05 | 1,9 | 0,1 | 22,3 | 60,0 | 5,4 | 2,5 | 99,9 | - |
| EDX2 | Hole | 15.4 | 15.1 | 1.4 | 1.0 | 3.1 | 0.3 | 2.9 | 59.0 | - | - | 98.2 | 1.0 |
| EDX1 | 0.20 | 19.5 | 11.3 | 0.4 | 0.6 | 3.2 | 0.1 | 5.3 | 58.1 | - | - | 98.4 | 1.7 |
| EDX3 | 0.50 | 12.0 | 22.5 | 0.4 | 0.1 | 1.3 | 0.1 | 1.0 | 62.0 | - | - | 99.4 | 0.5 |
| EDX4 | 0.95 | 16.1 | 17.7 | 1.3 | 0.6 | 2.4 | 0.2 | 1.5 | 59.7 | - | - | 99.4 | 0.9 |
| EDX5 | 1.20 | 19.4 | 14.5 | 0.3 | 0.9 | 2.6 | 1.2 | 1.5 | 59.2 | - | - | 99.4 | 1.3 |
| EDX6 | 1.70 | 16.6 | 16.6 | 0.2 | 0.6 | 2.8 | 0.7 | 1.4 | 60.0 | - | - | 99.0 | 1.0 |
| EDX7 | 2.00 | 18.2 | 15.8 | 1.1 | 0.12 | 2.6 | 1.1 | 1.0 | 60.0 | - | - | 99.6 | 1.2 |
| EDX8 | 2.40 | 23.8 | 11.9 | 0.8 | 0.2 | 2.2 | 1.7 | 0.9 | 58.2 | - | - | 99.8 | 2.0 |

Figure 5.35 and Figure 5.36 displays the surface of the hole (location P1 in Figure 4.23) at two different levels of magnification, (b) showing a thin layer of calcite-crystal clustered on the underlying aggregate or on the C-S-H gel.

No K and Na from the pore solution should be left on the surface, since the pore solution had already been leached for a considerable period of time by storage in de-ionised water. Since K and Na had been washed out long before the leaching tests had been completed, most of the Na, K (and Al) found are presumably from the feldspar in the aggregate. The Si probably stems mainly from the quartz in the aggregate, and to some extent from the residual gel of C-S-H.

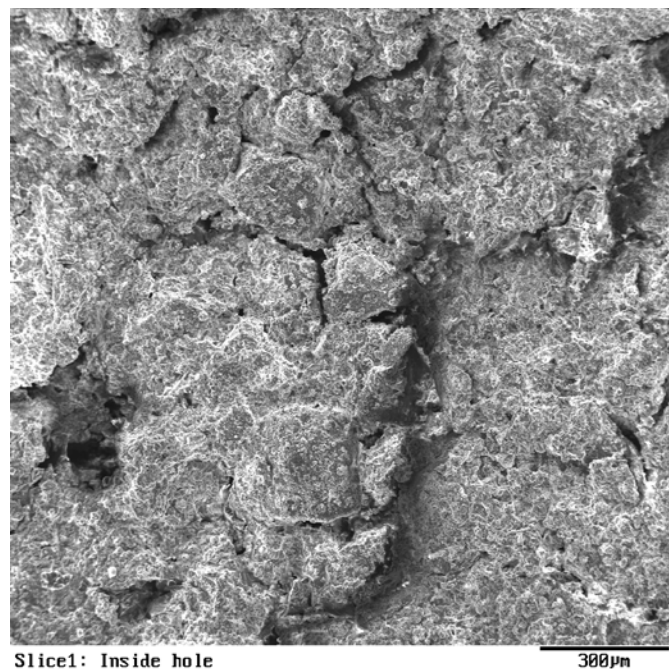


Figure 5.35 SEM-picture taken from the position p1 inside the hole (see Figure 4.23) at (a) a magnification of 50:1. The spot-area was as big as the whole picture.

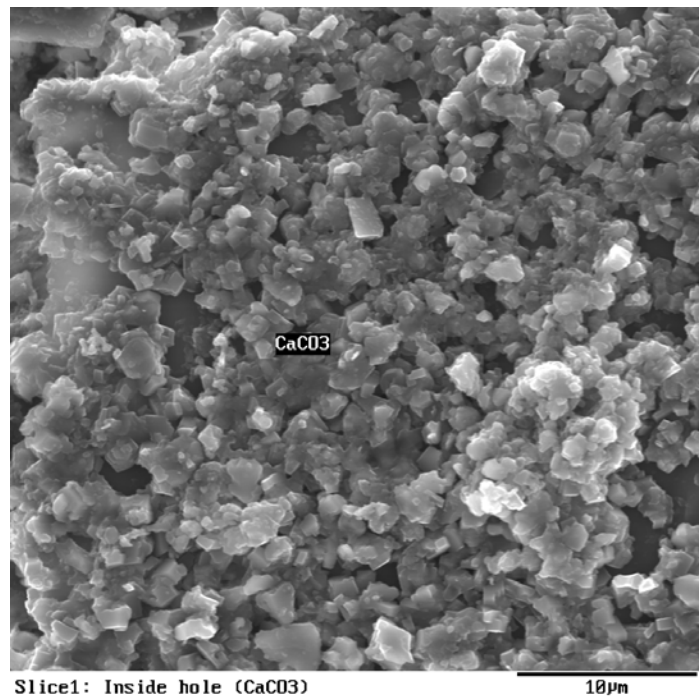


Figure 5.36 SEM-picture taken from the position p1 inside the hole at a magnification of 2000:1.

Figure 5.37 likewise presents a view of the surface of the hole, but at a magnification of 3000. This picture is taken at another location than that shown in Figure 5.35 (b). The element analyses, indicating considerable Na, Al and Si to be present, indicates that the area selected is probably located on a section of aggregate. The relatively large amounts of Cr and Ni and most of the Fe probably come from water that flowed through the hole during the leaching test.

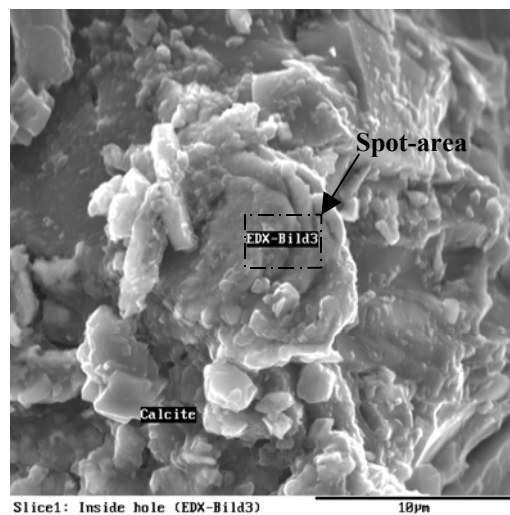


Figure 5.37 SEM-picture from position p1 inside the hole (see Figure 4.23) at a magnification of 3000:1. The spot-area EDX-Bild3 selected for x-ray examination is shown as a dotted frame

Figure 5.38 shows the boundary between the hole and the matrix of the concrete at a magnification of 70:1. The edge of the hole can be seen extending in a horizontal direction at the middle of the picture. The spot-areas selected for EDX1, EDX2 and EDX3 (see Figure 4.23) are shown in the figure. Their size was 600x250 μm .

The element analysis EDX2 of the inner surface of the hole reveals rather much Fe, probably stemming mostly from the period of flow of water during the leaching test referred to earlier. Most of the Ca is probably bound up in the calcite (CaCO_3). The Na, Al and Si probably come from aggregate located between the CaCO_3 -crystals or just beneath them.

The element analyses EDX1 of the surface in the matrix just outside the hole reveals rather much Fe. Fe probably comes to a major part from the water that percolated the hole.

The amount of Ca observed in the area between the wall of the hole and at a point approximately 1.5 mm into the matrix (EDX3, EDX4, EDX5, shown in Figure 5.39 - Figure 5.41), is probably mostly from the C-S-H gel. No Ca(OH)_2 or CaCO_3 was detected in that section. Most of the Fe is probably present in the AF-phases. The Na and Al probably stem from feldspar in the aggregate. The Si probably comes from aggregate (feldspar or quartzite) and from C-S-H gel, to what extent from each of these sources being difficult to say. No Cr or Ni was detected.

The low Ca/Si-ratio in EDX6 is probably due to the presence of a large aggregate particle in the spot-area.

At a distance of about 1.5 mm from the hole, crystals of Ca(OH)_2 begin to appear, and at a distance of 2 mm from the hole rather large quantities of Ca(OH)_2 can be observed, see Figure 5.42 and Figure 5.43. No CaCO_3 was detected there. The concrete matrix was scanned extensively at rather high magnification, from left to right and from the hole and outwards. There appeared to be a rather distinct boundary 1.5 mm from the hole, where solid Ca(OH)_2 was found. Closer to the hole the Ca(OH)_2 had obviously diffused away to the pure water that flowed through the hole during the leaching test.

The amounts of Na and K observed were greater at a distance of approximately 3 mm from the hole, indicating there to be some Na and K left in the pore solution at the end of the leaching test.

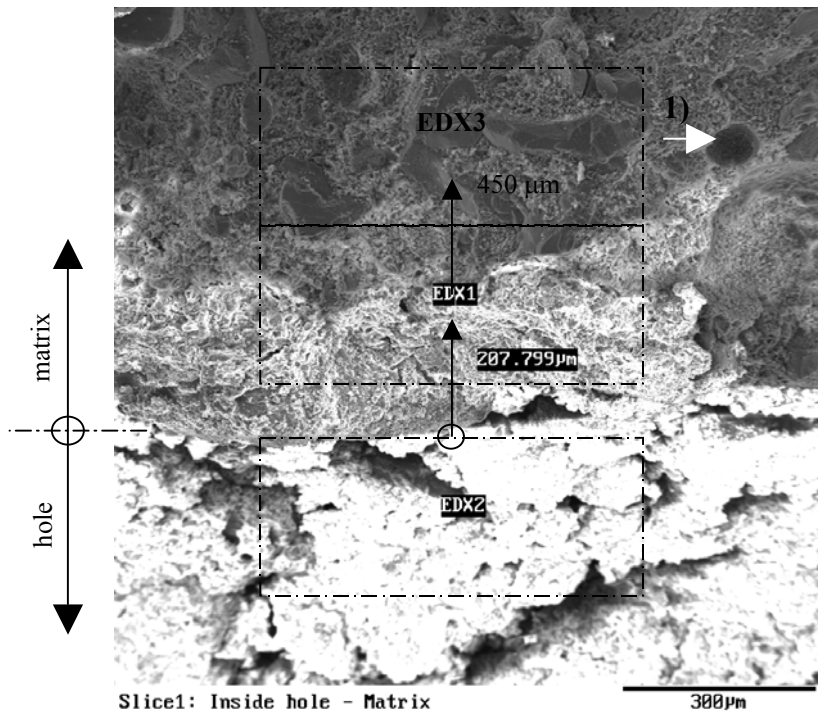


Figure 5.38 SEM-picture from a position at the boundary of the hole at a scale magnification of 70:1. The spot-areas EDX 1, EDX2 and EDX3 selected for x-ray examination are shown as dotted frames. For orientation, arrow at 1) is also found in Figure 5.39.

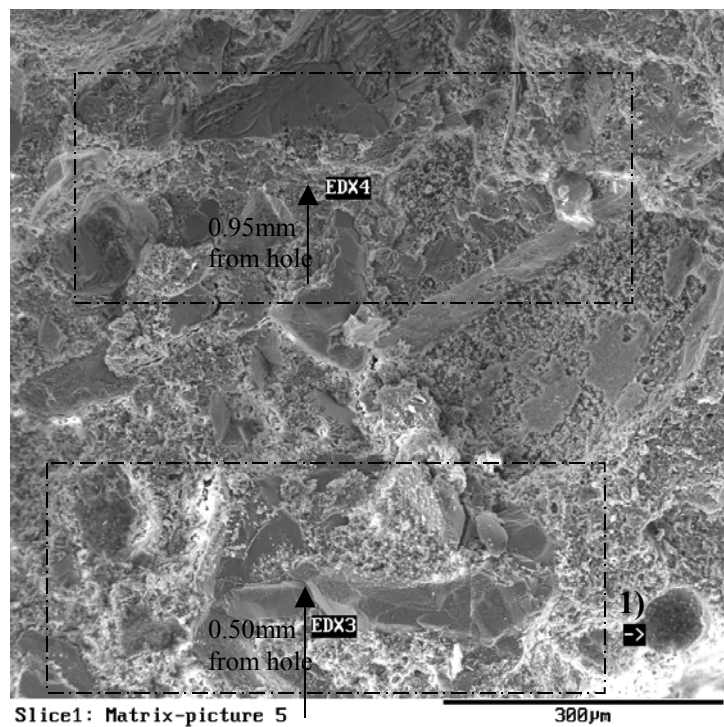


Figure 5.39 SEM-picture at a magnification of 1:100. The spot-areas EDX3 and EDX4 selected for x-ray examination are shown as dotted frames. For orientation, the arrow at 1) is also found in Figure 5.38.

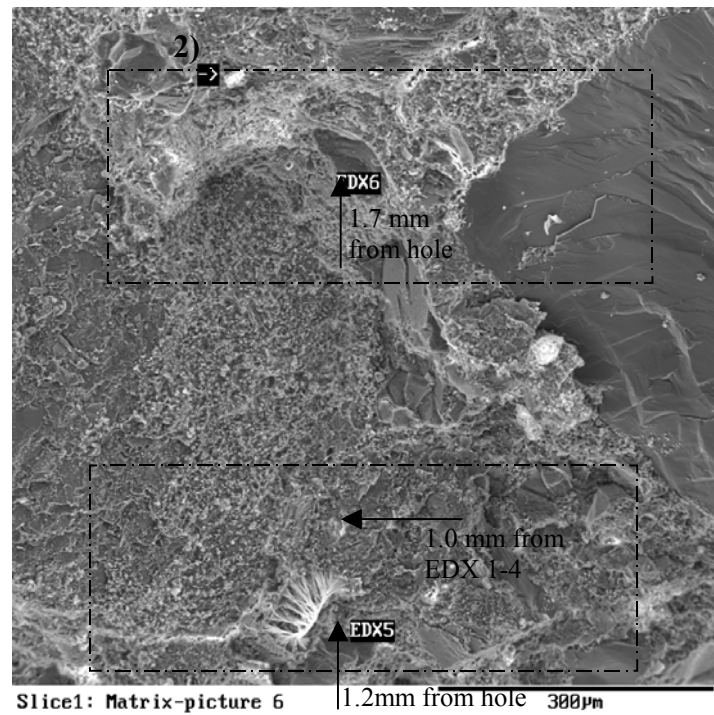


Figure 5.40 SEM-picture at a scale magnification of 1:100. The spot-areas EDX5 and EDX6 selected for x-ray examination are shown as dotted frames.

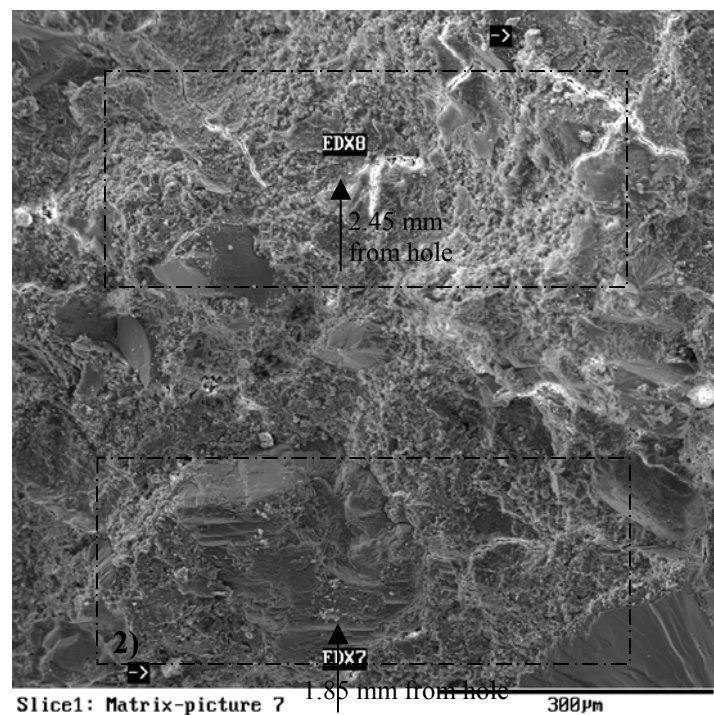


Figure 5.41 SEM-picture at a scale magnification of 1:100. The spot-areas selected for x-ray examination are shown as dotted frames. For orientation, arrow at 2) is also found in Figure 5.40.

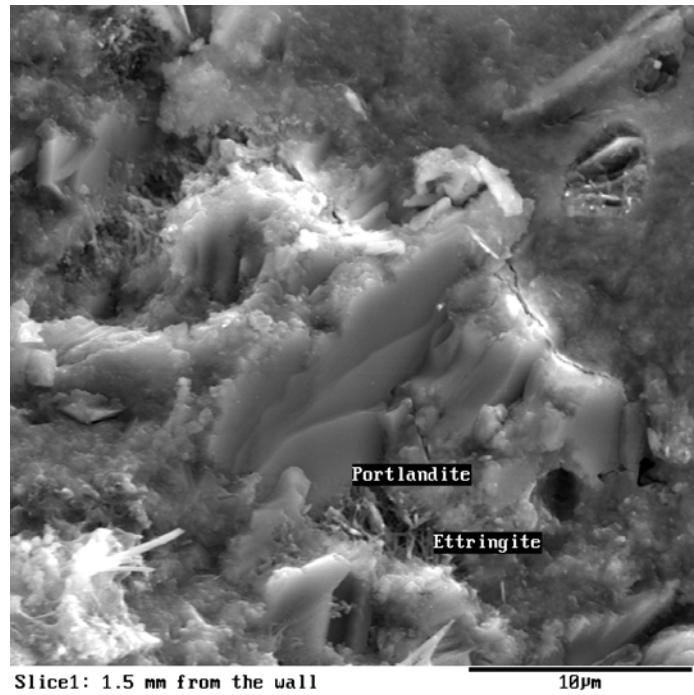


Figure 5.42 $\text{Ca}(\text{OH})_2(\text{s})$ as observed in the concrete 1.5 mm from the hole.

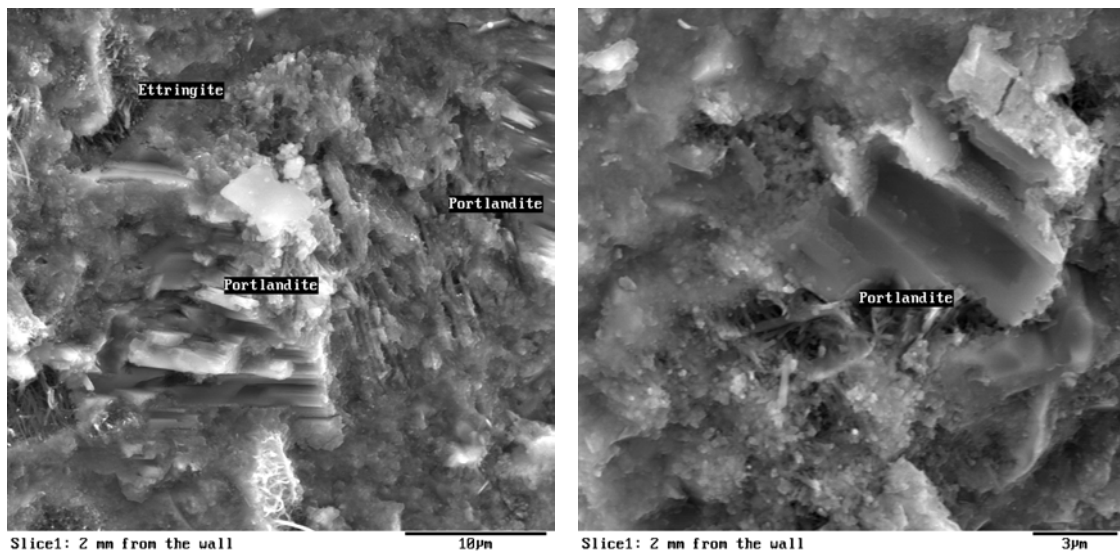


Figure 5.43 $\text{Ca}(\text{OH})_2(\text{s})$ as observed in the concrete 2.0 mm from the hole.

Slice 1, particularly the air voids contained large amounts of secondary ettringite (Figure 5.44).

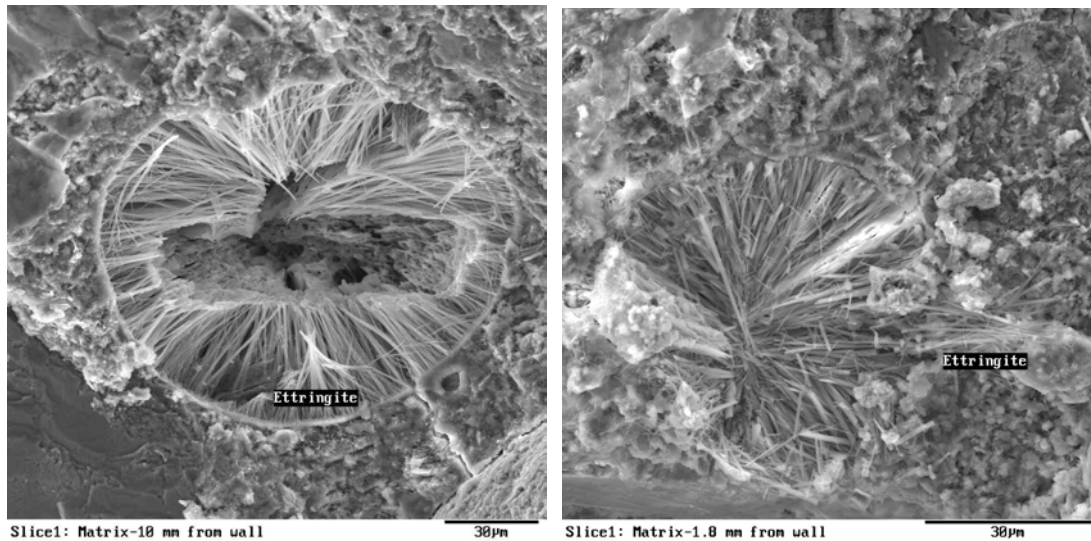


Figure 5.44 Ettringite as observed in air voids located in slice 1 at a distance of 1.0 and 1.8 mm, respectively from the walls of the hole.

5.2.3:3 Slice 7 (near the downstream end)

Figure 5.45 shows the shape and texture of the surface of the piece of concrete at an area extending, from the hole and into the matrix. A summary of the EDX analyses of the elements in this segment of the picture (a) is presented in Table 5.7.

Generally, it can be said that

- At the walls of the hole the layer of calcite (CaCO_3) found was thicker ($17\ \mu\text{m}$) than at the walls of the hole in slice 1, the thickness of the layer in slice 1 being almost negligible.
- There was no Portlandite (Ca(OH)_2) closer to the hole than approximately 0.7 mm from it, which was closer than in slice 1 (1.5 mm).

Table 5.7 Number of atoms in terms of % of the total in the spot-areas in slice 7 that were selected.

| Element | y (mm) | Ca | Si | Na | K | Al | S | Fe | O | Cr | Ni | Sum | Ca/Si |
|------------------------|--------|------|------|------|------|------|------|------|------|----|------|------|-------|
| Molar weighth (g/mole) | | 40.1 | 28.1 | 23.0 | 39.1 | 27.0 | 32.1 | 55.8 | 16 | 52 | 58.7 | | |
| Spot-area | | | | | | | | | | | | | |
| EDX7-1 | 0.20 | 18.0 | 18 | 0.3 | 0.2 | 1.3 | 1.0 | 0.6 | 60.3 | - | - | 99.8 | 1.0 |
| EDX7-2 | 0.45 | 21.4 | 14.7 | 0.2 | 0.3 | 1.6 | 1.4 | 0.9 | 59.3 | - | - | 99.6 | 1.45 |
| EDX7-3 | 0.80 | 20.9 | 13.2 | 0.8 | 1.2 | 3.3 | 0.8 | 1.3 | 58.1 | - | - | 99.6 | 1.44 |
| EDX7-4 | 1.25 | 20.0 | 14.6 | 0.8 | 0.7 | 2.6 | 1.1 | 1.0 | 59.0 | - | - | 99.6 | 1.37 |
| EDX7-5 | 1.5 | 22.4 | 13.9 | 0.1 | 0.4 | 1.8 | 1.0 | 1.4 | 59.7 | - | - | 99.6 | 1.61 |

The element analyses at EDX7-1 showed small amounts of Fe, probably stemming from the AF-phases. Yet there was far less Fe than in slice 1, and no Cr or Ni, indicating no deposits from the water that flowed earlier. The amount of Ca, constituting 17.98 % of total number of atoms, was probably mostly bound in C-S-H gel, as well as in CaCO_3 located close to the hole. The Na and Al present probably stemmed from feldspar in the

aggregate. The Si found probably came from aggregate (feldspar or quartzite) and from C-S-H gel, difficult to say in what proportions, however.

The element analyses at EDX7-2 revealed a small amount of Fe, probably stemming from the AF-phases. The amount of Ca found, constituting 21.35 % of total numbers of atoms, is probably mostly bound in C-S-H gel. The amounts of Na and Al probably come from feldspar in aggregate. The Si probably comes from aggregate (feldspar or quartzite) and from C-S-H gel, the proportions of each being uncertain.

The concrete matrix was scanned extensively at rather high magnification, both from left to right and from the hole outwards. There appeared it be a rather distinct boundary located 0.7 mm from the hole where solid $\text{Ca}(\text{OH})_2$ was found. This distance was shorter than the 1.5 mm in the case of slice 1. The water in the hole in slice 7 was saturated with Ca^{2+} and OH^- to a greater extent, reducing the driving potential for diffusion. The carbonated layer in slice 7 probably also decreased the diffusion there because of its being tighter material with a lower diffusion coefficient.

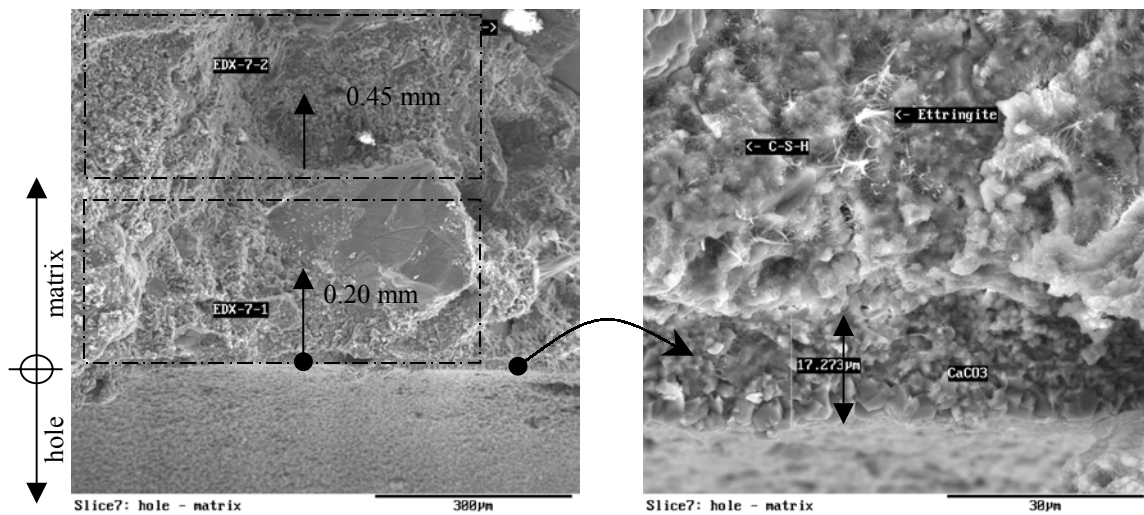


Figure 5.45 Two SEM-pictures taken from a position near the hole, at a (a) magnification of 100:1 and (b) at a magnification of 1000:1. The spot-areas EDX7-1 and EDX7-2 selected for x-ray examination are shown as dotted frames.

5.2.3:4 Slice 9 (at the downstream end)

On slice 9 Portlandite ($\text{Ca}(\text{OH})_2$) was found approximately 0.7 mm from the wall of the hole (Figure 5.46).

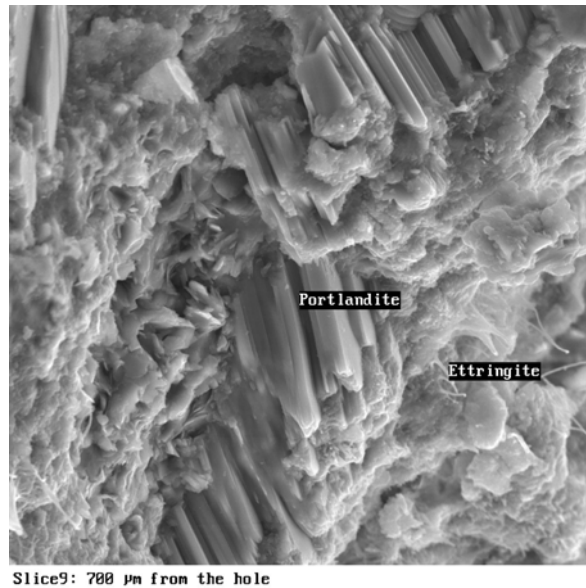


Figure 5.46 Crystals of $\text{Ca}(\text{OH})_2$ (Portlandite) found at a distance of 0.7 mm from the wall of the hole found in slice 9.

5.3 Surface leaching of concrete

5.3.1 Determination of ion flow (diffusion)

For measuring the diffusion coefficient, four concrete samples were placed in a tank containing about 100 litres of de-ionised water that was stirred (see section 4.6). The water was exchanged once a month when the concentrations of Ca, K, Na and S were measured by means of ICP-AES and when the pH was measured by use of a pH electrode. The results are shown in Table 5.8. The same data are also shown in Figure 5.47 and Figure 5.48. The “saw-tooth” shape is due to the fact that after each exchange of water only pure water was present in the tank.

Table 5.8 Measured concentration of Ca^{2+} , K^+ , Na^+ , S and H^+ in the water tank in which the concrete specimens were placed. No. = number of exchanges of water in the tank (for new, deionised water). If no values are entered (empty squares), this means that only water was exchanged, no measures being taken.

| No | Accu- mulated time (h) | Ca (g/l) | K (g/l) | Na (g/l) | S (g/l) | pH |
|----|------------------------------|----------|---------|----------|---------|-------|
| 1 | 0 | | | | | |
| 2 | 432 | | | | | |
| 3 | 840 | | | | | |
| 4 | 1 272 | | | | | 9,3 |
| 5 | 1 992 | | | | | |
| 6 | 2 472 | | | | | 9,9 |
| 7 | 3 552 | | | | | 10,2 |
| 8 | 4 344 | | | | | 10,6 |
| 9 | 5 016 | 0,043 | 0,0006 | 0,0018 | 0,0009 | 10,52 |
| | 5 016 | 0,065 | 0,0007 | 0,0024 | 0,0014 | 10,5 |
| 10 | 5 664 | 0,011 | 0,0035 | 0,0023 | 0,0003 | 7,95 |
| 11 | 6 432 | 0,012 | 0,0012 | 0,0012 | 0,0003 | 9,47 |
| 12 | 7 104 | | | | | |
| 13 | 7 872 | | | | | |

Table 5.8 continued

| | | | | | | |
|----|--------|--------|--------|--------|--------|-------|
| 14 | 8 400 | 0,007 | 0,0004 | 0,0007 | 0,0002 | 9,48 |
| 15 | 9 072 | 0,008 | 0,0005 | 0,0007 | 0,0008 | 7,521 |
| 16 | 9 816 | 0,0085 | 0,0012 | 0,0014 | 0,0006 | 8,119 |
| 17 | 10 488 | 0,0078 | 0,0009 | 0,001 | 0,0005 | 7,679 |
| 18 | 11 328 | 0,0093 | 0,0004 | 0,0004 | 0,0005 | 7,766 |
| 19 | 12 096 | 0,0095 | 0,0002 | 0,0003 | 0,0005 | 8,141 |
| 20 | 12 744 | 0,009 | 0,0004 | 0,0005 | 0,0002 | 7,7 |
| 21 | 13 488 | 0,0088 | 0,0004 | 0,0006 | 0,0002 | 7,65 |
| 22 | 14 256 | 0,0088 | 0,0002 | 0,0004 | 0,0002 | 8,02 |
| 23 | 14 760 | 0,0077 | 0,0008 | 0,001 | 0,0002 | 8,06 |

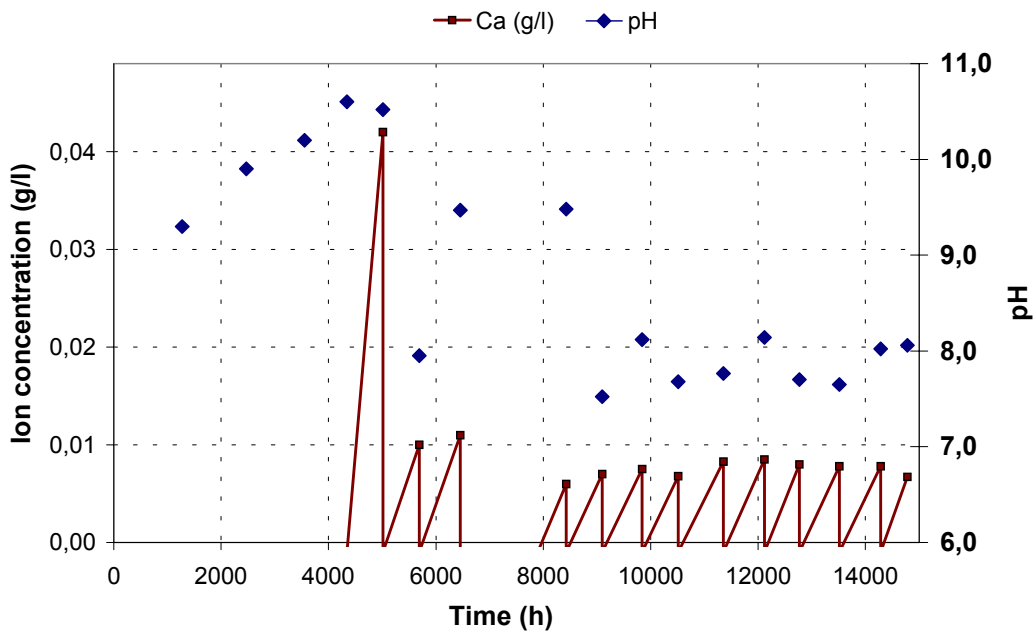


Figure 5.47 Concentrations of Ca and pH in the water of the tank in which concrete specimens subjected to surface leaching were placed. The “saw-tooth”-shape is a simplified presentation of how the concentration of ions rises from zero in the newly, exchanged deionised water, to the concentration measured when the next exchange of water occurs.

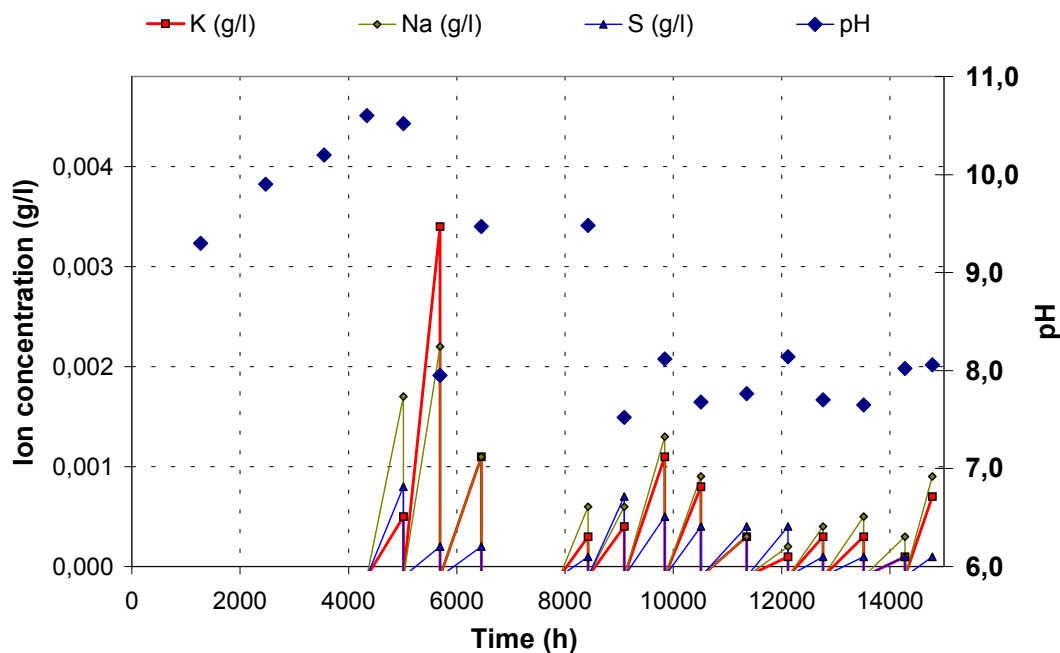


Figure 5.48 Concentrations of K, Na, S and pH in the water of the tank in which concrete specimens subjected to surface leaching were placed.

5.3.2 Determination of the remaining compounds and elements in the specimens

After the leaching tests had been carried out, one concrete sample was cut into seven slices (see section 4.6 and Figure 4.19). Each slice was pulverised and was dissolved in HNO_3 (see section 4.12) into a solution with volume 200 ml. The data in Table 5.3 is from this chemical analysis.

The “Rest” category in the table represents the remainder of the solid particles located at the bottom of the vessel, particles not soluble in $\text{HNO}_3(\text{aq})$ and consisting mainly of insoluble aggregate. Before the chemical analysis was carried out, the weight of the powder was determined.

It is clearly seen that the concentration of ions, like Ca^{2+} , is smaller close to the surface than deeper in the concrete. At a distance of 34 mm from the surface the values are smaller again, but this can probably be explained by the fact this slice was located nearer to the cylindrical surface at the other side of the specimen, see Figure 4.19, compared with the slice at the distance of 29 mm from the “first” surface. The concentration gradient of Ca could principally be used for a calculation of the diffusivity of Ca-ions in concrete. Also the diffusivity of other ions might be calculated. These analysis are, however, not made in this report.

Table 5.9 Measured (ICP-AES) ions in solutions of concrete dissolved in HNO₃(aq).

| Distance y from surface (mm) | Al mg/l | Ca mg/l | Fe mg/l | K mg/l | Mg mg/l | Mn mg/l | Na mg/l | S mg/l | Si mg/l | Powder g | Amount of solution ml | Rest g |
|------------------------------|---------|---------|---------|--------|---------|---------|---------|--------|---------|----------|-----------------------|-------------|
| 4 | 423 | 3 469 | 858 | 84 | 114 | 22 | 6 | 138 | 2 | 16,5 | 200 | 14,3 |
| 9 | 359 | 2 967 | 774 | 70 | 104 | 19 | 18 | 95 | 2 | 12,8 | 200 | 10,9 |
| 13 | 436 | 3 886 | 1 036 | 82 | 123 | 24 | 5 | 124 | 4 | 16,8 | 200 | 14,3 |
| 18 | 552 | 3 667 | 1 124 | 140 | 123 | 23 | 11 | 134 | 5 | 20,2 | 200 | 17,6 |
| 23 | 634 | 4 254 | 1 132 | 160 | 146 | 25 | 8 | 163 | 5 | 23,5 | 200 | 20,3 |
| 29 | 669 | 5 394 | 1 151 | 132 | 172 | 34 | 10 | 185 | 5 | 22,6 | 200 | 19,4 |
| 34 | 506 | 3 766 | 1 050 | 117 | 139 | 37 | 21 | 127 | 5 | 17,6 | 200 | 14,9 |

5.4 Determination of non-evaporable water in concrete by heating it to +1050°C

The non-evaporable water contained in the aggregate, the unhydrated cement and the concrete specimens were determined by heating the samples to +1050°C in an oven. The results were used for determining the degree of hydration of the concrete at the start of the leaching tests. The results are shown in Table 5.10 and Table 5.12. The data are raw-data. They are transported to the degree of hydration in section 6.3.

Table 5.10 Measurement of the non-evaporable water contained in the cement, the aggregate and the non-leached concrete used in the present experiments. m_{105C} = weight after oven heating at +105°C; and m_{1050C} = weight after oven heating at +1050°C.

| Material | m_{105C} , air (g) | m_{1050C} , air (g) |
|----------------------|----------------------|-----------------------|
| Cement | 45,112 | 44,656 |
| Hardeberga quartzite | 81,765 | 80,181 |
| Kvidinge sand 0-3 mm | 42,046 | 41,753 |
| Kvidinge sand 0-8 mm | 63,019 | 62,551 |
| 0.80b:-a, 92d | 69,024 | 67,471 |
| 0.80b:-b, 92d | 69,606 | 68,003 |
| 0.80b:, 121d | 227,581 | 221,88 |
| 0.80b:-a, 201d | 107,29 | 104,764 |
| 0.80b:-b, 201d | 105,39 | 102,403 |
| 0.80b:-c, 201d | 108,91 | 106,425 |
| 1.29:-a, 63d | 65,118 | 63,62 |
| 1.29:-b, 63d | 65,601 | 64,025 |
| 0.60:-a, 99d | 68,73 | 66,525 |
| 0.60:-b, 99d | 69,127 | 66,95 |
| 0.60:-98, 105d | 274,379 | 265,185 |
| 0.80c:-M, 56d | 15,893 | 15,461 |
| 0.80c:-98-K, 56d | 17,102 | 16,565 |

Table 5.12 Measurement of the non-evaporable water contained in the leached concrete used in the present experiments. m_{105C} = weight after oven +105°C; and m_{1050C} = weight after oven +1050°C.

| Material | Slice | $m_{105C, \text{air}}$ | $m_{1050C, \text{air}}$ |
|----------|---------|------------------------|-------------------------|
| 0.60:9 | 1 | 36,813 | 35,564 |
| | 2 | 35,976 | 34,874 |
| | 3 | 25,488 | 24,615 |
| | 4 | 39,918 | 38,335 |
| | 5 | 38,113 | 36,814 |
| | 6 | 40,159 | 38,859 |
| | 7 | 34,136 | 32,815 |
| 0.80b:2 | 2 | 26,305 | 25,689 |
| | 3 | 30,749 | 29,916 |
| | 4 | 40,521 | 39,495 |
| | 5 | 39,708 | 38,685 |
| | 6 | 41,133 | 40,088 |
| | 7 | 33,207 | 32,285 |
| | 0.80b:5 | 1 | 61,674 |
| 2 | | 33,388 | 32,594 |
| 3 | | 33,323 | 32,524 |
| 4 | | 32,095 | 31,314 |
| 5 | | 35,946 | 35,056 |
| 6 | | 44,525 | 43,666 |
| 7 | | 28,662 | 27,73 |

6 Discussion

6.1 Homogenous, steady-state percolation through defect-free concrete

6.1.1 Flow of water through the specimens, permeability

Introduction:

Permeability is an important parameter in connection with both leaching and flow of water through cementitious material. In the experiments carried out, the permeability was determined approximately every second day by measuring the volume of percolating water collected on the downstream side of each specimen. In section 5.1.1, the resulting flow of water measured in m^3/s is shown for various of the specimens. What is meant by permeability is Darcian permeability, see equation (4.21). Various aspects of the result are discussed below.

A brief summary:

Concrete of differing w/c-ratios (0.60, 0.8 and 1.29) cured in different ways (V, EH, LD, V-LD and EH-LD, see section 4.3.5) was tested. Three different patterns are evident in the water flows obtained:

- constant water flow
- accelerating water flow
- successively retarded water flow

Note in the figures that are shown that the last water flow level shown for each specimen is not the final water flow but rather the water flow at the time when the specimen was removed from the pressure cell. If further leaching had occurred, this could have changed the value of the permeability coefficient k_w . Figure 6.1 is a basic presentation of the results. The permeability k_w of the specimens was found to depend to a considerable extent on the way in which the specimens were cured (see section 4.3). The permeability of well-hydrated virgin (V) specimens was found to be low and rather uniform, increasing only slowly over time, although sometimes it increased more rapidly. When well-hydrated specimens were heated and dried (LD), the permeability rose 100 fold compared with the virgin state. The permeability of the LD-specimens often rose sharply after their being percolated for some time. If the specimens were heated at an early hydration age but not dried, (EH), the initial permeability was about 100 times as high as for virgin specimens, although it later decreased by a factor of about 100.

Note that all the specimens in the work conducted were saturated with water and had a high degree of hydration when the leaching test began. It was found that for such specimens it was easy to obtain steady-state flow of water. Both leaching effects and hydration can effect the flow of water.

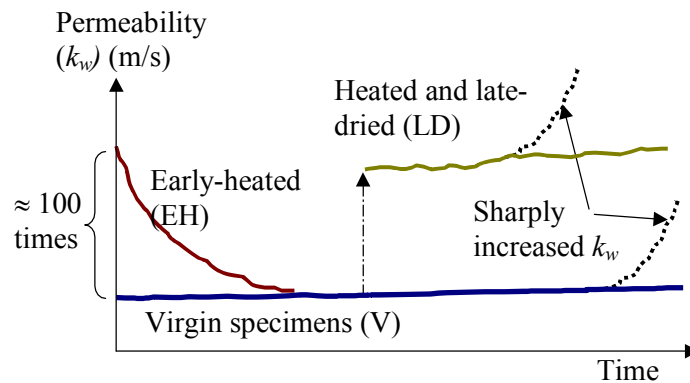


Figure 6.1 Basic pattern of measured k_w values in different specimens of cured concrete .

Although a strong influence of the w/c-ratio on permeability could be noted, there were no appreciable differences in permeability between w/c-ratios of 0.60 and of 0.80, but there was a clear difference in permeability between w/c-ratios of 0.80 and of 1.29.

When the flow of water rose rapidly, it appeared that the increase in flow took place in only a rather few individual flow channels that had been broadened through material being leached away from the channel walls. In such cases the flux could not be described in terms of a steady-state Darcian flow, since the permeability coefficient increased in relation to the amount of water that had flowed through the concrete. In Figure 5.12 and Figure 5.13 it was observed that the permeability often increases considerably after some 10 litres of water has percolated through the concrete. This can be seen in Figure 5.19 to correspond to about 1 – 4 % of the initial content of calcium having been leached by the water.

Comparison with literature:

Figure 6.2 and Figure 6.3 indicate the permeability of the concrete specimens that were tested for different w/c-ratios and curing types, together with relevant results from the literature. The permeability of the EH-specimens with a w/c-ratio 0.6 found in the present study was approximately 10 times as high as was found for concrete of the same type in Ruettgers' study. Early-heating made the concrete more permeable, probably due to micro-cracking. On the other hand, the permeability became lower toward the end, when self-sealing of the specimens had occurred. The V-specimens in the present study with a w/c-ratio of 0.8 showed lower permeability than the corresponding specimens in the Ruettgers study, whereas for late-dried specimens the permeability was about the same in both studies. After an extended period of percolation of water, the specimens in the present study became leached and the permeability rose. Also, the specimens with a w/c-ratio of 1.29 became much more permeable after leaching.

The large scatter in the result reported in the literature appears to, at least partly, be due to lack of standardisation of the experiments. For example, the studies differ in curing and hydration age. The lack of standards in measuring permeability is a major obstacle to comparing results of different studies.

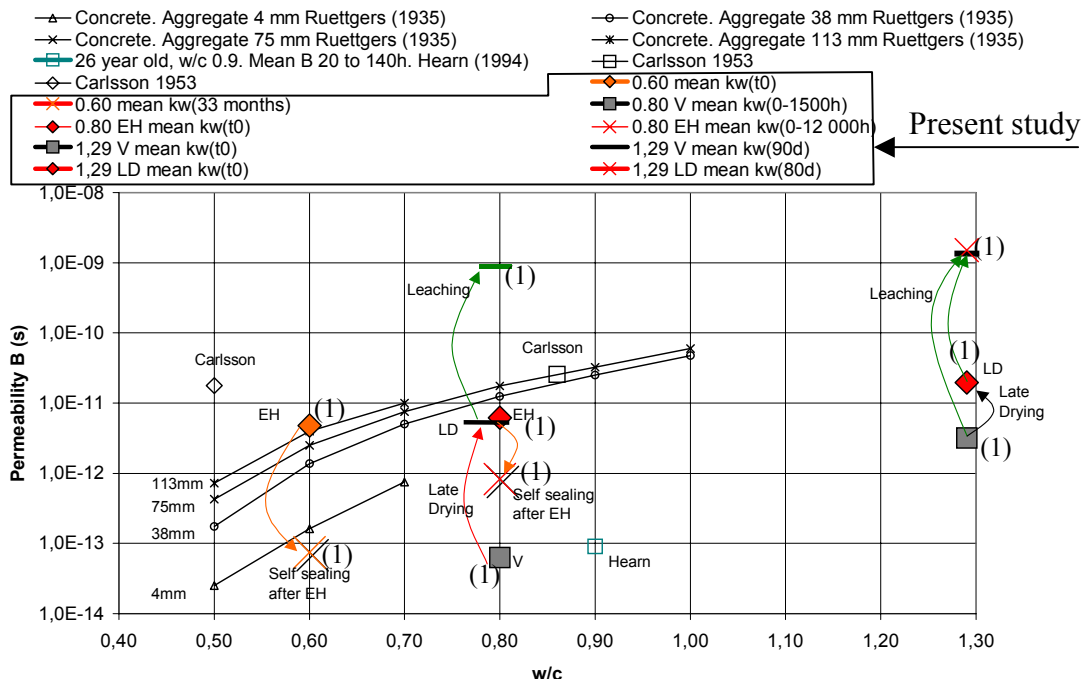


Figure 6.2 Permeability versus w/c-ratio for leached concrete specimens as found in the present work (1) and as reported in the literature. The arrows in the figure represents changes in permeability through leaching, self-sealing (hydration) or drying.

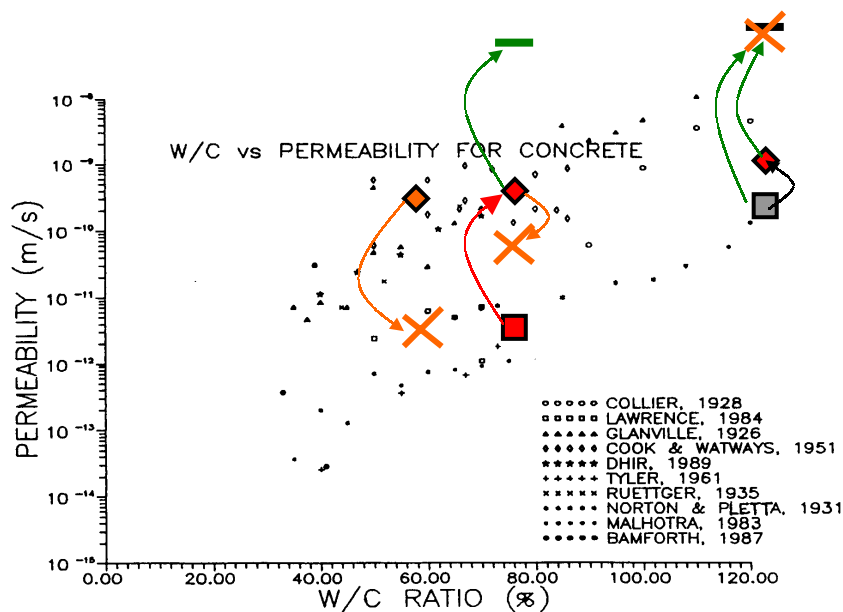


Figure 6.3 Permeability versus w/c-ratio for leached concrete specimens in the present work and as reported in the literature. See Figure 6.2 for a explanation of the symbols.

Influences of curing:

The effects on permeability found for curing (EH versus V) and for treatment (LD) were much larger than the effects of any of the other factors considered. The effects of the

heating and the drying of the specimens led, as was just indicated, to a 100-fold increase in permeability, which is in basic agreement with results other authors have obtained (section 3.6.4).

Virgin (V) specimens:

The (V) specimens were well-hydrated, periods of some 93 days (0.80b) and 201 days (0.80a:5) being involved, and were well-cured in lime-water, as well as being held at constant temperature. According to sections 3.6.4 and 3.6.5, the permeability of the concrete at the ages involved here should be fully developed, so that a curing time of a few days more or a few days less before the leaching test begins should not change the permeability appreciably. Because of their being well cured, the specimens received no micro-cracks or only few cracks. One of the w/c 0.80 specimens (of the eleven virgin w/c 0.80 specimens altogether), namely 0.80a:5, showed a rapid increase in water flux after about 4 000 hours of testing. Also the only virgin specimen with a w/c ratio of 1.29, namely 1.29:10, showed quite a sharp increase in permeability almost immediately (approximately a 30-fold increase after 1500 hours), and thereafter an even more rapid increase in permeability (a further 10-fold increase after 100 hours).

Late-dried (LD) specimens:

As already indicated, the heating and drying in LD-treatment resulted in a 100-fold increase in permeability, whereupon constant permeability followed. The cause of this was very likely an extensive micro-cracking in parts of the cement paste. The concrete was well-cured at the time of late-drying, and there was probably not much continued hydration that could have sealed the cracks.

Early-heated (EH) specimens:

The characteristic behaviour of the EH specimens was the approximately 100-fold increase in permeability as compared with the permeability of virgin specimens. Another characteristic is the fact that the permeability decreased later in a $\sqrt{\text{time}}$ -shaped pattern. When the permeability had decreased to about the same values as in the virgin state, the permeability became constant with time. The reason for the increase in permeability at the beginning of testing was probably that the concrete was heated before its having attained a high degree of strength. The swelling due to the increase in temperature in the oven, and the shrinkage due to the decrease in temperature when taken out of the oven, probably led to micro-cracking of the concrete. These cracks increased the permeability. Another contributing explanation to the higher permeability compared with the virgin specimens was probably that the EH-specimens were somewhat younger (~56 days) than the others (90-96 days). On the other hand, the aggregate of the EH-specimens was somewhat smaller (8 mm maximum as compared with 12-16 mm maximum). Therefore, one might have expected lower permeability.

Influences of saturation:

All specimens are assumed to have been completely water saturated when the leaching test began. The virgin (V) specimens had been stored in water, whereas the other specimens (EH and LD) had been saturated by vacuum treatment. One observation, providing support for this, is that the measured flux of the water was always showed steady state characteristics when the leaching test began.

Influences of pressure:

The influence of different hydraulic pressure-gradients was studied by changing the external water pressure. The results show close agreement with Darcy's law. There was a linear proportionality between the pressure applied and the resulting flow of water. The permeability coefficient k_w was constant for the different pressures examined, when the other variables were hold constant.

Influences of self-sealing and leaching:

Self-sealing was observed in EH-specimens. It is discussed below. An influence of leaching on permeability was observed in most of the specimens, permeability becoming higher as leaching progressed. In many of the specimens, permeability rose sharply as was indicated above.

Influences of viscosity:

The viscosity of the inflow and outflow water was not analysed. The temperature was constant, being at +20°C throughout.

Influences of mechanical stresses:

There was probably no significant reduction in permeability due to specimens being compressed when they were forced down into their conical steel cylinders, see section 4.4.7:13.

Constant, decreasing or increasing flow:

The results can be divided into:

- constant water flow
- accelerating water flow
- increasingly retarded water flow

A **constant** water flow could be noted for most of the specimens, except for the EH-specimens. The main reasons for the water flow being constant were probably the following:

- (i) The filtration of water occurred through a very large number of flow channels. Since the flow of water in each was so slight, the leaching of solid material from the walls of the channels was so limited that the permeability remained virtually unchanged.
- (ii) The testing time was not sufficient for any marked changes to occur. Although all the concrete specimens would probably sooner or later have become so leached that the permeability would have increased, this would have taken some time.

A certain **increase** in the flow of water did appear: (i) when the concrete was late-dried or early-heated, the permeability was immediately found to be higher as compared with the virgin state, (ii) some specimens showed an increase in flow over time. The reasons for this were probably the following:

- (i) The initial increase in water flow was presumably caused by microcracks that formed when the concrete was dried and/or heated.

- (ii) The increase in flow over time was probably due to most of the flow occurring in flow channels that became leached. If the w/c ratio was higher and the concrete was late-dried, the probability of an increase in water flow became greater. Through leaching, the flow channels became wider and, since the water flow is approximately proportional to the hydraulic radii of the channels raised to the power of four, the flow could sometimes increase very rapidly. The smaller the number of flow channels available, the more rapid the leaching effects in these channels were, and the more rapid the increase in permeability was. On the upstream surface of the concrete, small round spots, that were brown in colour could be seen. There the solid material were was soft and small, and distinct channels, leading into the concrete could be noted. The leaching observed on the upstream surface due to the diffusion of ions to the bulk water in the inlet probably did not produce any appreciable increase in permeability, since only short segments of the flow channels were widened. For a higher permeability to be attained, longer sections of the flow channel would need to be widened. Since the late-dried concrete probably had only a small amount of unhydrated cement available for continuous hydration able to tighten the concrete, no appreciable self-sealing effects occurred in this type of concrete.

The **decrease** in water flow that appeared rather quickly after the start of the leaching test in the early-heated specimens was probably due to self-sealing. Continued hydration is probably the most likely reason for the decrease in permeability that occurred. The concrete was heated immediately after de-moulding, when it had not yet attained a high level of strength and therefore many microcracks were likely to have already developed. These microcracks increased the permeability and also increased the possibilities for unhydrated cement to react. Since during the entire curing process, the concrete specimens were placed in plastic bags, no further water was available to allow continuous hydration to take place. When water penetrating the concrete during the leaching test reached unhydrated cement, much of it was probably hydrated, the new hydration products filling up the pore system and resulting in a decrease in the permeability.

There was probably no self-sealing caused by air contained in the pore system. The specimens were all saturated with water when the test started and no air in the penetrating water was probably dissolved as air-bubbles in the concrete.

If the early-heating had led to creating of fragments, physical clogging resulting in self-sealing might have occurred. This is not likely to be a significant cause of self-sealing, however. For one thing, the flow of water should then have decreased more abruptly than it did. For another, if there were fragments that blocked the water flow in the specimens the permeability should not have increased as much as it did later when the same specimens were late-dried

The dissolution or deposition of crystals of $\text{Ca}(\text{OH})_2$ could be no more than a minor cause of the self-sealing that occurred.

There was too little carbonic acid in the water for carbonation to be any reasonable cause of the relatively fast self-sealing that was noted. It was only the EH-specimens in which self-sealing was observed. If carbonation was a cause of the self-sealing there, self-sealing should also have been noted in specimens of the other types.

General viewpoints of permeability studies:

Estimation of the permeability of concrete specimens of differing characteristics could be obtained in at least two ways:

1. By conducting a large number of experiments involving concrete of differing characteristics under highly standardised conditions so as to obtain statistically reliable results.
2. By developing mathematical models of the permeability of concrete based on principles that are physically and chemically sound and are verified by experiments.

Employing a statistical model requires that a sufficient number of samples are tested under specific conditions. If the conditions (involving such factors as curing, temperature level and boundary conditions), or the material (such as w/c ratio, and amount and type of aggregate) are not absolutely constant, the statistical model cannot be used to estimate the change in water flow. In the present study, the statistical approach is not particularly useful because of the rather few test samples available. The statistical data are not large enough to draw very adequate conclusions regarding the influence of the parameters, although certain tendencies can be noted, see above, such as that permeability was influenced in particular by curing.

A physical model based on a realistic conception of the pore structure, and taking account of the physical and chemical processes involved, can be highly robust and can also be employed if the conditions or the materials used should change. In the next chapter, approach number 2 above is used in conjunction with mathematical and numerical models of permeability that are compared with experimental results; see chapter 7.

The mathematical models available often distinguish between microscopic and macroscopic models. *Microscopic* models of water flow in porous materials are often based on the Navier-Stokes equations for incompressible fluids and on the Hagen-Poiseuille equation for tubes, see section 3.9.2.

The measured flow of water observed in the present experiments, however, can be said to be macroscopic in character. No knowledge of the pore size distribution or the shape and connections of any flow channels was available. After the leaching test was completed, the porosity was measured. This did not enable any secure estimation of the pore size distribution to be made, however.

A continuity equation used in conjunction with Darcy's equation can provide a *macroscopic*, physically-based model of porous materials

$$D \frac{\partial P_w}{\partial t} = Q_w - \nabla \cdot (v_w) \quad (5.1)$$

$$v_w = -k_w \nabla P_w \quad (5.2)$$

where D = a damping parameter; Q_w = source or sink of water ($\text{m}^3/\text{s}/\text{m}^3$); v_w = macroscopic water velocity or filtration velocity, which is the mean velocity of the water in a continuous porous body and not the water velocity in each separate flow channel in the material (m/s); k_w = permeability coefficient (m/s); and ∇P_w = pressure gradient (m/m). The total flow of water can be written as

$$q_w = v_w \cdot A_{tot} \quad (5.3)$$

where q_w = flow of water (m^3/s); and A_{tot} = cross-sectional area (m^2). Since the pressure gradient ∇P_w was sometimes changed back and forth, it was possible to determine whether the permeability coefficient k_w was dependent upon these changes in pressure. However, since the temperature was constant, being at $+20^\circ\text{C}$ during all of the tests, the intrinsic permeability k could not be determined.

6.1.2 Flow of ions

6.1.2:1 Ion flow in the downstream direction (convection)

The water that percolated through the specimens was collected at the downstream side, the concentrations of elements being measured. The elements measured were Ca, K, Na, S, Al, Fe, Mg and Mn. The elements exist in ionic form in the pore solution. It was assumed that, when the leaching tests began, the ions contained in the pore solution were in equilibrium with the solid matrix. The equilibrium was disturbed when deionised water began penetrating the pore system. The ions in the pore solution were transported away either by diffusion or by the flux of water, leading to further ions, stemming from the solid matrix to be dissolved in the pore solution.

B Potassium and Sodium:

The drainage water from the specimens contained high concentrations of both potassium (K) and sodium (Na). However, the concentrations decreased quite rapidly, especially for the specimens that showed an increase in water flow. The rapid reduction in the concentrations of these two ions is caused by the fact that large amounts of K and Na were already dissolved in the pore solution at the start of testing not much being bound to the pore walls. Thus, when the pore solution was washed out in the leaching test, large amounts of the K and Na were washed out too. Figure 6.4 and Figure 6.5 summarise findings for all of the specimens. One can note that during the percolation of 0.10 litre of water the concentration of K^+ and Na^+ in the water decreased in a basically linear way on log – log scale.

It took some time after the leaching test began, however, before the first measurements of chemical contents could be performed. Some of the K and Na had probably already been leached before the first chemical analysis were performed. The volume of capillary pores in a 0.80a –specimen, for example, was approximately $V_{cap} = C \cdot (w/c - 0.39 \cdot \alpha) \cdot V = 241 \cdot (0.80 - 0.39 \cdot 0.9) \cdot \pi \cdot (0.155^2/4) \cdot 0.05 = 0.10$ litre. For many of the specimens, the first measurement was performed when about 0.10 litre of water, an amount corresponding to one pore volume, had passed through, the specimens. According to Unsworth et al. (unknown year of publication), the decrease in alkali and the increase in Ca in the pore solution occurs when approximately 2 pore volumes have flowed through the concrete.

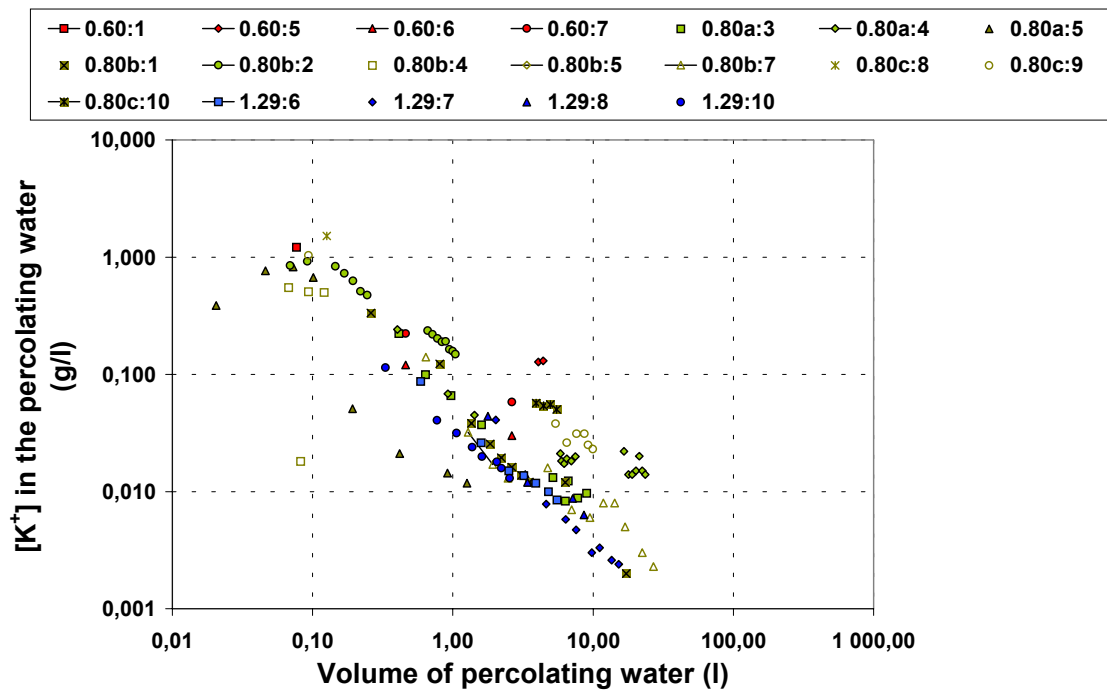


Figure 6.4 Measured concentrations of K^+ in the percolating water in relation to the initial level of K.

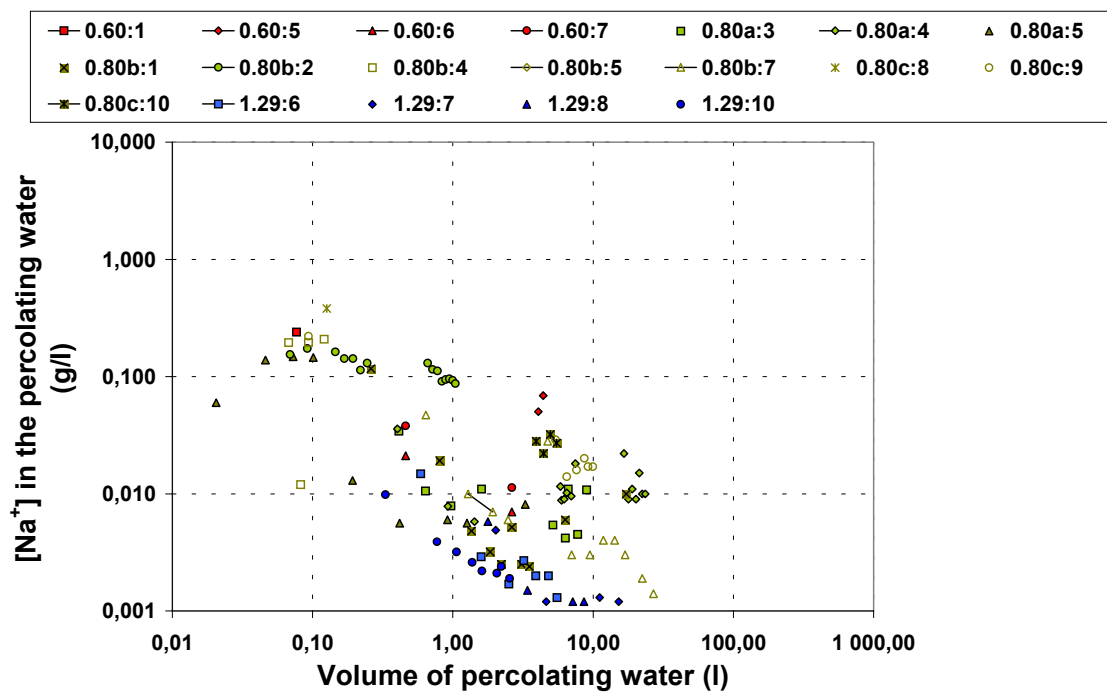


Figure 6.5 Measured concentrations of Na^+ in the percolating water in relation to the amount of initial Na.

Calcium:

The concentration of calcium (Ca^{2+}) in the drainage water was constant during the first part of testing. For the virgin (V) and late-dried (LD) specimens, the mean concentration at the start of testing was about 0.6 g/l whereas for the early-heated (EH) specimens it was higher, about 1.0-1.1 g/l. These results are in agreement with the literature. For specimens in which the water-flow increased during testing, the concentration of Ca decreased, as indicated above.

The finding of large amounts of Ca at the start of testing is somewhat confusing, since it could be thought to have been much lower, in view of the common ion effect of OH^- stemming from the large amounts of K and Na that were rapidly dissolved at the start of the leaching test (see Unswort et al. in Figure 2.3). As indicated above, however, it took some time after the leaching test, had begun before the first measurements of the chemical content were performed. The fact that a certain amount of K and Na had probably already been leached before the first chemical analyses were conducted probably resulted in a concentration of Ca already at the first measurement.

The reason why the concentration of calcium was higher in the EH-specimens than in the other specimens at beginning of testing may, as discussed above, might be that more, unhydrated cement in the EH-specimens was available already at the start of the leaching test.

Figure 5.14 shows the concentration of Ca^{2+} in the water that percolated in relation to the total volume of water that percolated. As can be seen, the leaching rate began to slow down after approximately 5-10 litres of water had percolated through the specimens. When the concentration of Ca in the water that seeped through decreases this indicates the walls of the flow channels to have been depleted of easy soluble ions. The ions also had to diffuse from the interior through an increasingly thick diffusion layer before reaching the walls of the channel, where they were transported away by the flow of water. For specimen 0.80a:5, this occurred already when 0.10 litre, had flowed indicating that the water seeped out of the specimen through a rather small amounts of *flow channels*. This led to the walls of the pores becoming depleted of calcium rather quickly.

Lea (1983) reported having found the drainage water coming from concrete exposed to water pressure to be saturated with calcium until a calcium content corresponding to 10-15 % of the weight of the cement had been leached. In the present study, the drainage water obtained was found to have been saturated with calcium until an amount of calcium corresponding to about 5 % (except for specimen 0.80a:5) of the initial calcium content of the cement had been leached (see Figure 5.15). This correspond to 11% of the weight of the cement, assuming that Ca made up 47% of the weight of the cement ($5/(0.47) \approx 11\%$). When this values had been reached, the concentration of Ca in the drainage water decreased rapidly. Possible explanations of this could be (i) that the Ca from the Portlandite has to diffuse through a thick leached layer before it reach the flow channels; and (ii) that when the pore-walls begin to be depleted of Portlandite, Ca is taken from other compounds, such as C-S-H, which are less easily dissolved than Portlandite.

The leaching that occurs can be estimated not only in terms of how many ions the percolating water contains (their concentration), but also (and better yet) by the leaching rate, i.e. how many ions are leached per time unit, computed as the flux of water times

the ion concentration, see Figure 5.17. At a total volume that had percolated of about 10-30 litres, the leaching rate, as expressed in gram Ca/l began to decrease.

Sulphate:

The concentration of sulphate (S) in the drainage water was low and nearly constant in all the tests, decreasing only slowly. The S probably comes from AFt and AFm compounds. There is less S than Ca in concrete, sulphate compounds having a lower solubility than most other compounds. Accordingly, the concentration of S in the drainage water was lower than that of K, Na and Ca. On the other hand, the concentration of S remained almost constant, in contrast to the concentrations of K and Na. About 1 to 5% of the initial amount of S was leached out of the specimens.

Aluminium, ferrite and magnesium:

The concentrations of magnesium (Mg), iron (Fe) and silicon (Si) in the drainage water were very low in all the tests. Hardly any concentrations of Mg, Fe and Si could be detected in the drainage water. The hydration products that were primarily lost were Ca, Na, K and S. The residual products probably consisted of a leached, porous and weak skeleton of the, insoluble compounds that contained Mg, Fe and Si.

pH:

The pH in the pore solution of unleached OPC concrete at equilibrium was approximately 13.2-13.4. The leaching of hydroxide ions (OH^-) strongly follows the leaching of K, Na and Ca. When hydroxide ions are leached, the pH decreases. The pH of the drainage water from all the specimens $\phi 155$ mm in diameter is shown in the APPENDIX B. At pH values above 12.5, dissolved K^+ and Na^+ ions were still found, and at pH 12.5 dissolved CH. Thanks to the large amount of CH in cementitious materials, the pH normally remains at 12.5 for a long period of time during leaching, CH acting as a strong buffer. When the walls of the flow channels became depleted of CH in CH compounds that are easily soluble (such as Portlandite), the pH falls below 12.5. When this occurs, OH^- -ions are also dissolved from other compounds, such as C-S-H-gel.

6.1.2:2 Ion flow in the upstream direction (diffusion)

Measurements of ions moving in the upstream direction to the deionised water during the percolation test were incomplete and could not be performed very adequately. The major reason for this was that the equipment was not constructed in such a way that the diffusion of ions in the upstream direction could be measured in a regular and reliable way. Usually 2 litres of water were flushed each second day from the inlet side of a specimen in order to maintain a constant boundary condition of pure water. The steel pipes leading to the specimens were of such small diameter that water from about 2 meter of pipe from each specimens was flushed upstream at each flushing. This means that the water flushed may to some extent have come from the inlet side of neighbouring specimens. A more adequate testing equipment should have provided a larger container of water on the upstream surface of each specimen so that no ions would be able to diffuse to neighbouring specimens. Measurements of the ions in the flushed water should also have been conducted for one specimen at a time. Instead,

water from more than one specimen at a time was investigated, which resulted in uncertainty regarding what ions had come from each specimen.

In Table 5.1 and Table 5.2 many results of measurements of ions and pH in flushed water from concrete are shown. The flushed volume for the data in Table 5.2 was 2 litres per specimen and occasion for specimens of the $\phi 155$ mm type. It was noted that at the start of the leaching test the concentration of Ca^{2+} in the flushed water was about 0.02-0.03 g/l and that it was about 0.002 g/l after about 40 000 hours of leaching. These data can be used for a rough estimating of the total amount of Ca that was diffused upstream, see Figure 6.7. The measured values can later be used for calibration purposes (provided exactly the same boundary and time conditions are employed).

6.1.2:3 *Summary of flow of ions*

A brief summary of the observed concentrations of different ions in the water that percolated is as follows:

- the measured concentrations of Na and K in the water that percolated decreased rather quickly for all of the specimens (Figure 6.6). Concrete contains Na and K, in only a small amounts nearly all of that present being initially dissolved in the pore solution due to its high solubility. When pure water was pressed through the concrete, the small amounts of Na and K present were washed out rather quickly.
- The pH of the percolating water decreased to an extent correspondingly to the reduction in the content of Na and K, from about 13.3 to 12.5, $\text{Ca}(\text{OH})_2$ acting as a strong buffer.
- the concentration of Ca in the water that percolated remained at about 0.65 g/l. The concentration of Ca was probably lower at the start when the alkali concentration (K and Na) was high. The concentration of Ca remained steady because of there being so much Ca in the concrete, its being bound in different compounds.
- in cases in which the walls of the flow channels become leached of calcium and the flow of water increases rapidly, the concentrations of all the ions and the pH-value decrease very much, although the leaching rate of Ca in g/s remains rather constant.

The flow of water and of ions for all the specimens (of diameter ($\phi 155$ mm)) is shown in APPENDIX B.

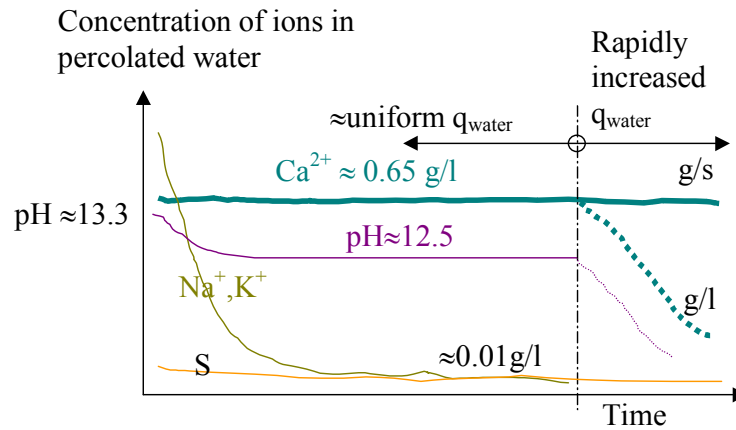


Figure 6.6 Graph of the measured concentrations of ions in the water that percolated.

The amount of ions that diffused upstream and were flushed out through the flushing valve were probably quite large as evident in Figure 6.7 and Figure 6.8. The measured values shown in Figure 6.7 are taken from specimen 0.80a:4, which consisted of rather permeable concrete, which led to the leaching of ions by convection (by the percolating water) being higher than by diffusion upstream. The measured values in Figure 6.8 are taken from specimen 0.80b:2 consisting of a less permeable form of concrete, which led to the leaching of ions by convection (by the percolating of water) being lower than leaching by diffusion upstream. The accumulated diffusion of Ca given in the figures was estimated by interpolation from Table 5.2.

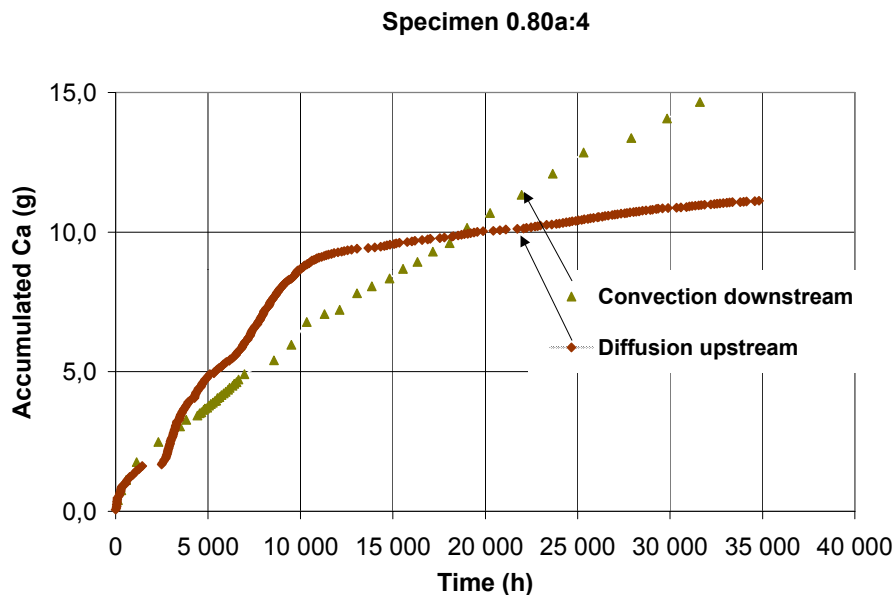


Figure 6.7 Estimated diffusion of Ca^{2+} in an upstream direction in comparison with the convection of Ca^{2+} in a downstream direction for specimen 0.80a:4. The diffusion curve is assumed to be more less valid for all the specimens.

Specimen 0.80b:2

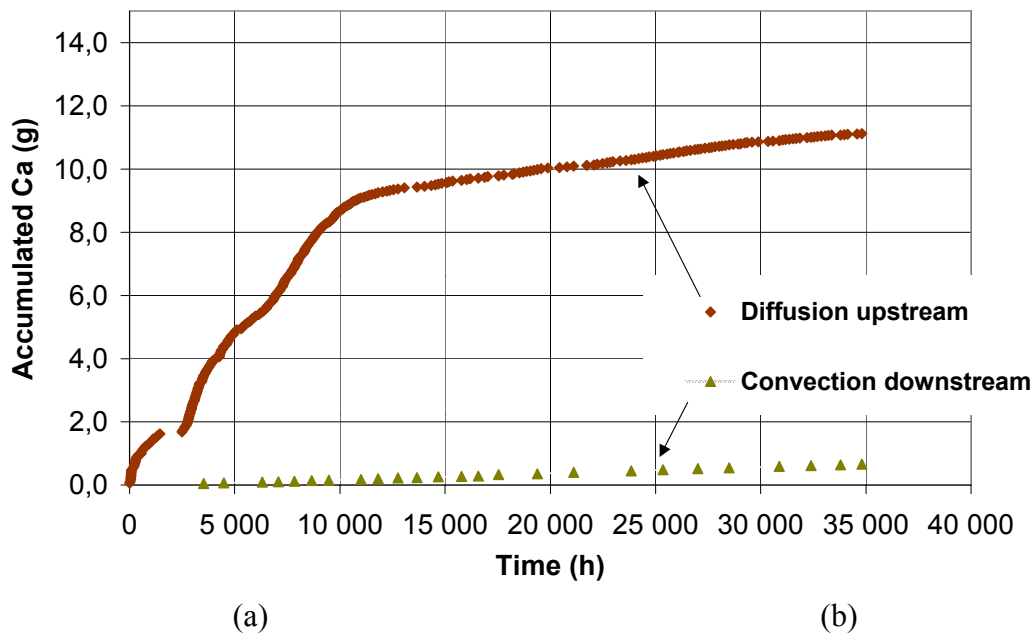


Figure 6.8 Estimated diffusion of Ca^{2+} in an upstream direction in comparison with the convection of Ca^{2+} in a downstream direction for specimen 0.80b:2.

6.1.3 Analysis of compressive and split tensile strength

The measured strength of the leached specimens shows a large scatter, from almost the same values as for the unleached reference specimens down to very low values. In chapter 5.1.1, the presence of small brown areas on the upstream surface of some specimens was described. In these areas, small holes leading into the specimen were observed, where the major flow of water had evidently taken place, probably along with leached solid material. During the compression test, it was noted that cylinders drilled from parts of the specimens containing many such brown areas and flow channels had lost much of their strength.

Around some of the larger flow channels going through the entire specimens, such large amounts of hydration products had been lost that the concrete had no cohesive strength left. The strength as tested depended on whether the cylinders were drilled from these highly leached parts of the specimens or from other parts (Figure 6.9). This is evident in Figure 5.23 (a), which shows a large degree of scatter in measures of compressive strength. Cylinders from unleached parts were of almost the same strength as the reference specimens. It therefore seems as if the influence of leaching on the compressive strength of the specimens was very much a local effect.

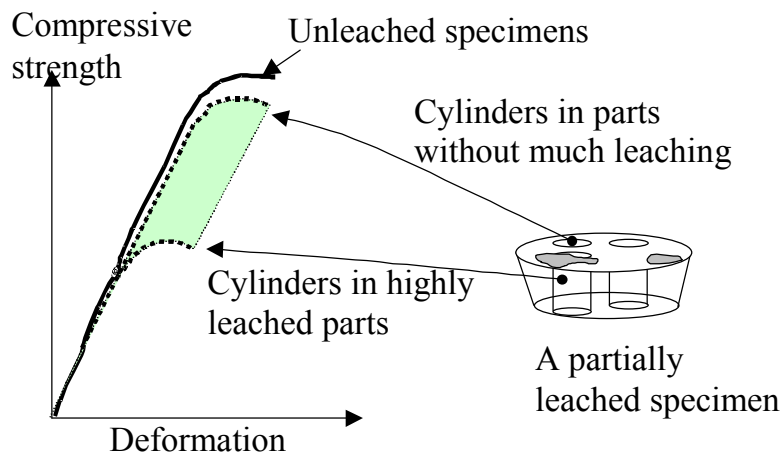


Figure 6.9 Principle figure of the measured strength.

In contrast to the compressive strength, the splitting strength, Figure 5.23 (b), found to be reduced considerably when the specimens were leached, the result showing relatively small scatter. The reduction in splitting strength associated with a given leaching ratio was similar in all of the specimens tested. The most important cause of this behavior is probably that the specimens were split into two halves the strength being affected by leaching in all parts of the specimen, all local effects were included. A possible further cause could be that the load bearing area resisting the split load had decreased when the upstream end of the specimens was leached.

6.1.4 Analysis of pore size distribution

Note that the slices used for measuring the pore size distribution represented only a quarter of each specimen (Figure 4.15). In view of the inhomogenous leaching that was observed (see section 5.1.1 and APPENDIX C), the distribution of pore sizes in other parts of the specimens may have differed considerably from what was found in the remainder of each specimen. The aim of this study was to determine what connections there were between the measured pore size distribution and the measured flow of water and ions. It was hoped that the measured pore size distributions could serve as an input in pore space models for modelling of the leaching process.

As was indicated in section 5.1.5, the volume of water pressed out increased rapidly at certain *critical pore diameter* ϕ_{crit} .

One explanation of this sharp increase may be that the pore size distribution varied very much along the flow channels in the concrete. Certain narrow pores, or “bottlenecks”, along the flow channels could be thought to resist the movement of water. As long as the gas pressure applied in the pressure plate or suction test is less than what is needed to press the pore solution through these narrow bottlenecks, the pore water pressed out is less than the total water volume in each flow channel. When the applied pressure is larger than that corresponding to the bottle-neck radius, all water along that flow channel is pressed out, see for example the flow channel (c) in Figure 6.10.

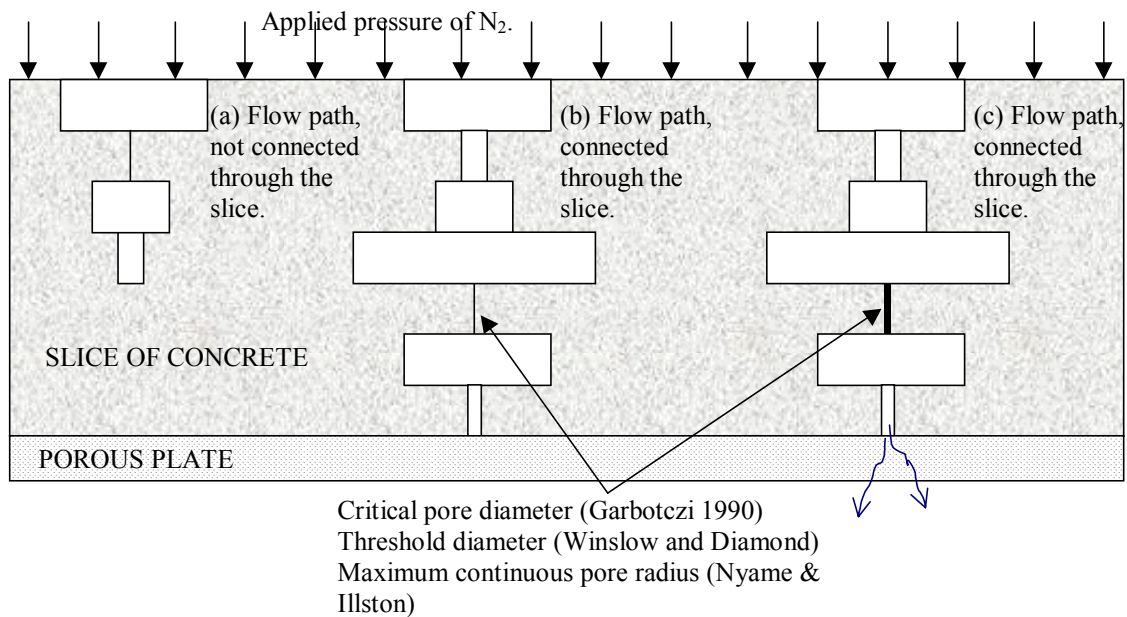


Figure 6.10 Schematic diagram of channels in which drainage water can be conducted through or into slices of concrete in the suction test: (a) a flow channel, not connected through the slice and thus not drained; (b) a flow channel, connected through the slice but with a pore diameter too narrow for the water to be drained at the prevailing pressure level; and (c) a flow channel, connected through the slice, with a pore diameter sufficiently large that the water can be drained at the pressure level.

In the figures presented in the APPENDIX C, it can be seen that ϕ_{crit} was often measured to 10^{-7} m, except for specimens 0.60:9R, 0.80b:2 and 0.80b:5, where ϕ_{crit} was about $0.4 \cdot 10^{-7}$ m.

For specimen 0.80b:2, ϕ_{crit} was approximately $4 \cdot 10^{-8}$ m for each of the slices, except for the slice from a depth of 3 mm below the surface. For this slice, the critical pore diameter was approximately 10^{-7} m, probably due to this slice, that was taken from the upstream end of the specimen, being leached to a greater extent than the other slices. Large amounts of material had been dissolved from this slice and diffused into the pure water at the inlet. There had been a coarsening of the pore system where material had been leached away.

Attempting to connect the observed ϕ_{crit} with the observed flow of water in the specimens in question, is not an easy task. Specimen 0.80b:5 showed a high degree of permeability at the end of the leaching test but, as can be seen in Figure 6.11, the critical pore diameter is nevertheless *smaller* than for each of the slices in the comparable specimen 0.80b:4, and is also smaller than for slice 3 in specimen 0.80b:2. Although the permeability of specimen 0.80b:2 was greater than that for specimen 0.80b:4, ϕ_{crit} was *smaller* than for the slices of specimen 0.80b:4 (except slice 3 of specimen 0.80b:2). One explanation of the discrepancy between a high level of permeability and a not particularly large critical pore diameter can be that the large flow channels, responsible for the high level of permeability in specimen 0.80b:5 could have been located in another part in the specimen than that which was investigated. At the same time, the

late-drying (LD) of specimen 5 should have coarsened the pores in a rather inhomogeneous way.

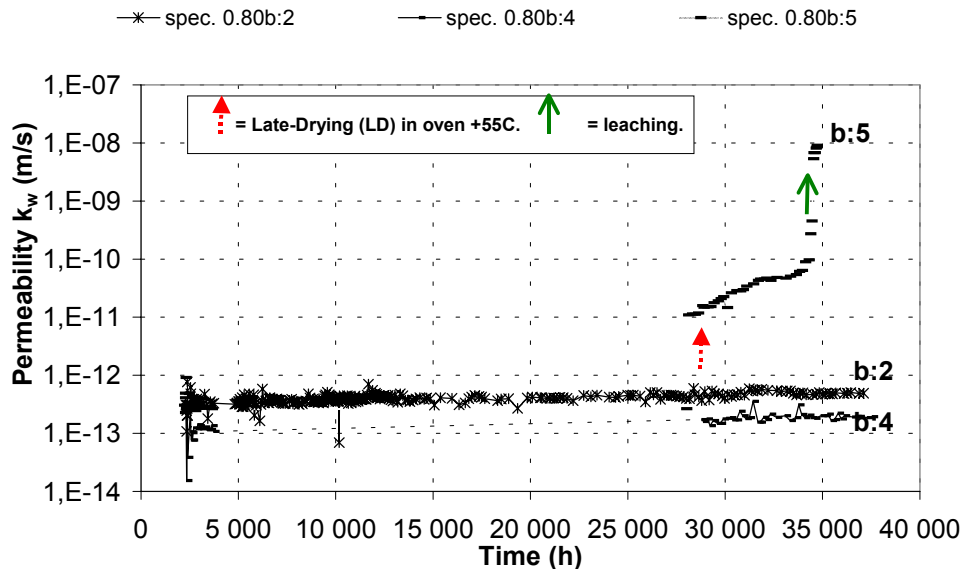


Figure 6.11 The measured permeability of the specimens 0.80b:2, 4 and 5.

The critical pore diameter as measured in the present investigation was about 1 magnitude smaller than values found in literature. Winslow and Liu (1990) and Winslow et al. (1994) using mercury porosimetry obtained $\phi_{crit} \approx 10^{-7}$ m for cement paste and $\phi_{crit} \approx 10^{-6}$ m for concrete and mortar (figures A.15 and A.16 in APPENDIX A). Note, however, that in the present investigation a method for estimating pore sizes was employed in which the *pore solution* in a saturated slice was pressed out by a pressure of N_2 that was applied, whereas the authors referred a method in which *mercury* was pressed in (MIP), two different pressure potentials and two different fluids being used.

6.1.5 Analysis of total porosity

Measurements of the total porosity of the leached specimens and of comparable enleached specimens are presented in section 5.1.6. All the specimens except for the reference specimens marked by “R” showed a greater porosity in the upstream part than in the rest of the specimen. There are two possible explanations for the greater porosity found in the upstream part:

- the upstream end of each of the conical specimens was upwards during casting, which probably led to a somewhat higher content of cement at that end being higher, which in turn led to the porosity being greater
- since the upstream end of the specimens that were leached was exposed to de-ionised water, there was probably a larger amount of material in that part that was leached.

A brief discussion of each of the specimens is provided below. Porosity is discussed further in section 6.1.6.

The greater porosity at the upstream end of specimen 0.60:5 than of specimen 0.60:1 (Figure 5.25), can perhaps be explained by the fact that specimen 0.60:5 was exposed to the deionised water at the upstream face for a longer period of time (1011 days as compared with 526 days). More material had diffused from the upstream end to the inlet water, leading to higher degree of porosity there. In the other parts, further downstream, of the specimens, the porosity was approximately the same for the different specimens, which can be explained by the fact that calcium leached by the drainage water was about the same (Figure 5.20).

In Figure 5.26 one notes that the porosity of the w/c 0.80 EH-specimens is greater than that found throughout the specimens in all the slices cut with use of the other curing methods, V and LD, for w/c 0.80. This is probably due to the early heating having caused such expansion and shrinking when the mechanical properties of the concrete had not yet been fully developed, that a greater number of microcracks developed than in the case of the other curing types.

In Figure 5.30 one can note that the porosity of the upstream part of V-specimens 0.80b:2 and 0.80:4 is high. This indicates the specimens to have lost considerable material in the upstream direction to the deionised water through leaching. This is not strange when one recalls that these specimen were exposed to deionised water for long periods of time, 1436 days (almost 4 years) in the case of specimen 0.80b:2 and 465 days in the case of specimen 0.80b:4. In the downstream direction, as seen in Figure 5.20, approximately 0.66 and 0.07 g of calcium were leached out of specimens :2 and :4, respectively, by the water that had percolated through the specimens. As can be seen in Table 6.1, this correspond to about 0.0006 and 0.0001 m³/m³, respectively, if one assumes that all calcium that was leached came from Ca(OH)₂(s). This is so small amount compared with the total porosity of about 0.15 m³/m³ that no definite conclusions can be drawn regarding differences in porosity between the middle and downstream parts of the three specimens.

Table 6.1 Increase in total porosity ΔP_c (m³/m³) due to the leaching of Ca(OH)₂, calculated as $\Delta P_c = m_{CH}/\rho_{CH}/V_c$, where m_{CH} = measured weight of leached calcium in the drainage water; ρ_{CH} = density of CH (2240 kg/m³); and V_{CH} = volume of the entire specimen ($\pi \cdot \phi^2/4 \cdot h = \pi \cdot 0.155^2/4 \cdot 0.05 = 0.000943$ m³).

| Specimen | 0.60:1 | 0.60:5 | 0.80a:4 | 0.80b:2 | 0.80b:4 | 0.80b:5 | 0.80b:7 | 0.80c:9 | 0.80c:10 |
|---|--------|--------|---------|---------|---------|---------|---------|---------|----------|
| ΔP_c (m ³ /m ³) | 0,0010 | 0,0031 | 0,0128 | 0,0006 | 0,0001 | 0,0042 | 0,0093 | 0,0073 | 0,0039 |

In figure Figure 5.31 one can note that the conical LD-specimens, both those that were leached and the reference ones, were higher in porosity in the upstream part. The difference is too small, however, that no definite conclusions can be drawn. Perhaps the 43 days of leaching that the “reference” specimens 0.80b:8 and 0.80b:9 were exposed to, led to the porosity of the upstream part being higher. The fact that the upstream slices were 6 mm in thickness meant that they may have been leached to such an extent that this could explain the high level of porosity. The low porosity of the upstream part of the reference specimens 0.80b:R1 and 0.80b:R2 can depend on that they were cast in a long cylinder and were then cut into individual specimens therefore they were more homogenous in their porosity.

In figure Figure 5.32 one can note that in the upstream part there is a more marked difference between leached specimens and reference specimens. The reference specimens were of the type that were made in long steel cylinders and were then cut into individual specimens. The higher porosity in the “upstream” end of them is therefore somewhat strange, since one would have expected there to be a uniform porosity.

6.1.6 Analysis of remaining compounds and elements in the specimens

The aim of this study was to estimate the amount of residual elements found in the leached concrete.

The specimens studied were cut into slices perpendicular to the direction that the water had flowed during the leaching test (see Figure 4.15). The slices were dissolved in $\text{HNO}_3(\text{aq})$ and were then examined by ICP AES technique (see section 4.12) with regard to the amount of the elements Al, Ca, Fe, K, Mg, Mn, Na, S, Si.

When the slices had been dissolved, a solid rest appeared at the bottom of the container. This solid probably came mainly from the aggregate and also to some extent from the cement paste. To estimate the amount of aggregate that was dissolved in the HNO_3 , a second test was performed in the same way as before, but only with respect to the aggregate. A leaching model for estimating content of calcium and of the aggregate and the porosity in the tested specimens is proposed below.

Leaching-model: (content of solid compounds and porosity after leaching):

The measured (section 5.1.7) amounts of residual elements found in each slice after leaching (time $t1$) are in this section compared with the estimated *initial* amounts of these elements in each slice prior to leaching (time $t0$). The residual content of calcium (Ca) in the specimens is compared with the measured concentrations of the Ca in the drainage water obtained from the same specimen. In addition, the estimated porosity of this specimens prior to leaching was compared with the measured porosity (see section 5.1.6).

The following assumptions were made:

- The structural model of Powers is appropriate (see Appendix A.3.5 for abbreviations);
- The aggregate contains no pores
- The volume of air is the same throughout the cement paste.

The procedure employed in the calculations can be described briefly as follows:

- The initial content of cement C content prior to leaching is calculated, on the basis of the chemical investigation (section 4.12 and 5.1.7).
- The initial calcium content prior to leaching is calculated from the content of C and is compared with the measured content of cement in the leached slices. The differences should be equal to the measured flow of calcium to the upstream and downstream water.
- The initial content of the aggregate is calculated and is compared with the measured content of the slices.

- The initial porosity is calculated and is compared with the measured porosity of the slices.

The volume of the leached concrete slices ($V_{c(tl)}$) is calculated from the measures of porosity (section 5.1.6).

The total volume of each concrete slice is the sum of the initial volume of cement paste ($V_{p(t0)}$), the initial volume of air-voids due to insufficient compaction ($V_{air(t0)}$) they contain, and the volume of the aggregate ($V_{a(t0)}$):

$$V_{c(t0)} = V_{p(t0)} + V_{air(t0)} + V_{a(t0)} \quad (5.4)$$

Where $V_{c(t0)}$ = measured initial volume of each concrete slice calculated from the weight of the slices both above water and below (equation (4.17)) (m^3); $V_{p(t0)}$ = calculated volume of cement paste (m^3); $V_{air(t0)}$ = measured initial volume of air (see Table 4.1) (m^3); and $V_{a(t0)}$ = calculated initial volume of aggregate in the concrete slices (m^3).

It is assumed that the volume of concrete $V_{c(tl)}$ did not change during the leaching test, i.e. that $V_{c(t0)} = V_{c(tl)}$. It is also assumed that the volume of the cement paste remained unchanged during leaching, only the porosity of the paste having increased. Although this is not completely true for the slice from furthest upstream, from which there possibly was very little of the surface volume that leached away, no account is taken to this.

The initial volume of the paste is calculated as

$$V_{p(t0)} = \frac{C}{1000} (0.32 + w/c) \quad (5.5)$$

where $V_{p(t0)}$ = initial volume of the cement paste prior to leaching (m^3); C = initial content of cement prior to leaching (kg); and w/c = w/c-ratio. For the calculation of this paste-volume, the w/c ratio is assumed to be the same throughout the cement paste.

$V_{a(t0)}$ is assumed to be the observed solid rest found after the dissolution test had been conducted, minus the estimated part of the silicon which came from the cement paste, increased then by the factor with which the aggregate had been reduced through being dissolved during the test (Figure 6.12):

$$V_{a(t0)} = \frac{V_{rest} - V_{rest,paste}}{(1 - S_a)} = \frac{m_{rest} - (m_{Si(t0)} - m_{Si(aq)})}{\rho_a \cdot (1 - S_a)} \quad (5.6)$$

where V_{rest} = the insoluble (in HNO_3) rest found in the container after dissolution of the slices in $HNO_3(aq)$ (m^3); $V_{rest,paste}$ = the part of the insoluble rest that came from the cement paste (m^3); S_a = assumed solubility of the aggregate in HNO_3 (weight %); m_{rest} = measured insoluble rest of the specimens (kg); $m_{Si(t0)}$ = assumed initial content of Si in the each slices of the specimens at time $t0$ (kg); $m_{Si(aq)}$ = measured content of Si in the HNO_3 solution of (kg); and ρ_a = assumed density of aggregate (kg/m^3).

A separate test of the solubility of the aggregate in HNO_3 indicated (1- S_a) it to be 94.0 % by weight for *Kvidinge sand* and 98.72 % by weight for *Hardeberga quartzite*. The density ρ_a is assumed to 2550 (kg/m^3) for *Kvidinge sand* and 2630-2640 (kg/m^3) for *Hardeberga quartzite* (see 4.3.3). S_a and ρ_a are related to the mass-fraction given in Table 4.1 as

$$S_a = \text{Agg}_{Kvidinge} \cdot (1-0.940) + \text{Agg}_{Hardeberga} \cdot (1-0.987) \quad (5.7)$$

$$\rho_a = \text{Agg}_{K\text{vidinge}} \cdot 2599 + \text{Agg}_{\text{Hardeberga}} \cdot 2640 \quad (5.8)$$

where $\text{Agg}_{K\text{vidinge}}$ = fraction of the aggregate *Kvidinge sand*, or $1232/(1232+555) = 0.69$ (kg/kg) for the concrete specimens of type 0.60; and $\text{Agg}_{\text{Hardeberga}}$ = fraction of the aggregate which is *Hardeberga quartzite*, or $555/(1232+555) = 0.31$ (kg/kg) for the same type of concrete.

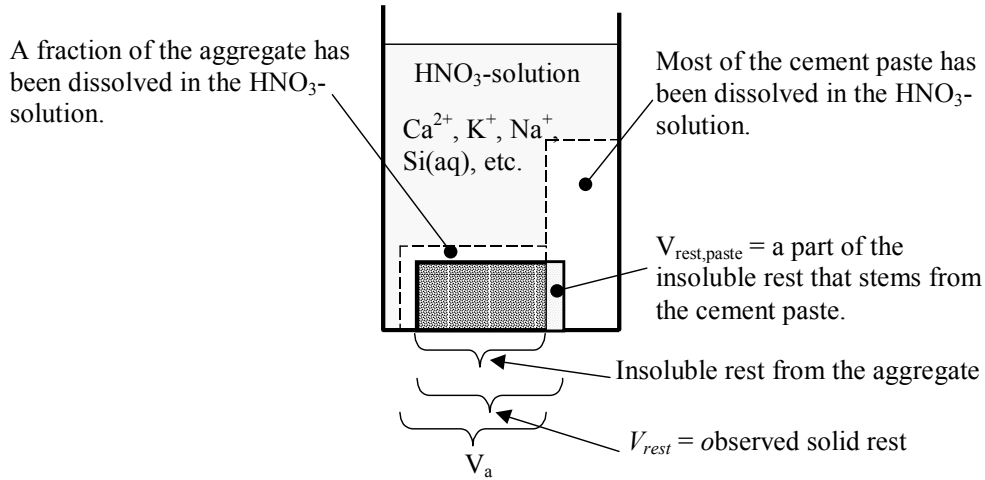


Figure 6.12 A slice of concrete dissolved in HNO₃.

The initial content $m_{\text{Si}(t_0)}$ of Si in the cement paste was assumed to be

$$m_{\text{Si}(t_0)} = 0.227 \cdot 28 / 60 \cdot C = 0.106 \cdot C \quad (5.9)$$

where C = cement content (kg) of the concrete, and where 0.227, 28 and 60 are the weight-% of SiO₂ (**Table 4.3**), the mole-weight of Si and the mole-weight of SiO₂ respectively. The Si content of the aqueous HNO₃ is

$$m_{\text{Si}(aq)} = [\text{Si}(aq)] \cdot V_{\text{solution}} \quad (5.10)$$

where $m_{\text{Si}(aq)}$ = weight of Si in the HNO₃-solution (kg); $[\text{Si}(aq)]$ = measured concentration of Si in the HNO₃-solution; and V_{solution} = volume of the HNO₃-solution (m³).

The volume of the cement paste can be estimated if the total volume of concrete, the air content of it, the amount of undissolved rest V_{rest} , and the concentration of silicon in the HNO₃(aq) are known. If equations (5.5), (5.6) and (5.9) are used, equation (5.4) can be written as

$$V_{c(t_0)} = \frac{(m_{\text{rest}} - (0.1061 \cdot C - m_{\text{Si}(aq)}))}{\rho_a \cdot (1 - S_a)} + \left[\frac{C}{1000} (0.32 + w/c) \right] + V_{\text{air}(t_0)} \quad (5.11)$$

Reformulating the equation gives

$$C = \frac{\left(V_{c(t_0)} - \frac{m_{\text{residual}} + m_{\text{Si}(aq)} - V_{\text{air}(t_0)}}{\rho_a \cdot (1 - S_a)} \right)}{\left(\frac{0.32 + w/c}{1000} \right) - \frac{0.1061}{\rho_a \cdot (1 - S_a)}} \quad (5.12)$$

The amount of initial calcium in the concrete can then be calculated:

$$m_{Ca(t0)} = 0.655 \cdot C \cdot M_{Ca} / M_{CaO} = 0.47 \cdot C \cdot 40 / 56 = 0.47 \cdot C \quad (5.13)$$

where $m_{Ca(t0)}$ = initial calcium content of the unleached concrete at the start of testing (kg); 0.655 = CaO content according to Table 4.3; M_{Ca} = molar weight of calcium (40 g/mole); and M_{CaO} = molar weight of calcium oxide (56 g/mole).

The amount of residual calcium in a leached slice is assumed to be the amount of calcium as measured in the HNO₃-solution:

$$m_{Ca(t1)} = m_{Ca(aq)} = [Ca(aq)] \cdot V_{\text{solution}} \quad (5.14)$$

where $m_{Ca(aq)}$ = weight of Ca in the HNO₃-solution (kg); $[Ca(aq)]$ = measured concentration of ca in the HNO₃-solution.

The loss of Ca is defined as the difference between the assumed initial content and the measured residual content found in the leached specimen.

$$\Delta m_{Ca(s)} = m_{Ca(t0)} - m_{Ca(t1)} \quad (5.15)$$

where Δm_{Ca} = loss of calcium due to leaching, as measured for the leached solid concrete (kg). This loss of calcium due to leaching can be compared with the observed leaching of calcium in both the upstream and downstream waters, as measured in the leaching test.

$$\Delta m_{ca(aq)} = Q_{\text{diff}} + Q_{\text{conv}} \quad (5.16)$$

where $\Delta m_{ca(aq)}$ = loss of calcium due to leaching, as observed in the water both upstream and downstream from the concrete (kg); Q_{diff} = leaching of calcium by diffusion to the upstream water (kg); Q_{conv} = leaching of calcium by convection to the downstream water (kg).

Q_{diff} is estimated from Figure 6.7 with the real leaching time for each specimen (see Figure 4.4).

The two losses of calcium, the observed loss in the solid specimen and the observed loss to the water, should be the same, since it is the same calcium that is involved. All calcium that leached from the specimens entered the water upstream through diffusion and the downstream water by convection.

When the content of cement had been estimated, the initial porosity was calculated as

$$P_{c(t0)} = \frac{V_a \cdot (V_p)_a + \frac{C}{1000} \cdot (w/c - 0.19 \cdot \alpha) + V_{\text{air}(t0)}}{V_c} \quad (5.17)$$

where $P_{c(t0)}$ = porosity (m³/m³) of the concrete based on the calculated content of C , the measured $V_{\text{air}(t0)}$ and the measured volume of each slice, V_c ; and $(V_p)_a$ = volume of pores in the aggregate, assumed in this model to be zero. This porosity $P_{c(t0)}$ is compared with the measured porosity of the leached slices and also compared with the initial porosity, assuming an even content of cement throughout the specimen, and the cement content as based on the recipe (Table 4.1).

Results of Leaching model 1 and of measurements:

The calcium content (kg/m^3) of the concrete and the volume fraction (m^3/m^3) of the aggregate and of the pores at times t_0 and t_1 are given in the tables and figures below. By t_0 is meant the time at which the leaching test was started and by t_1 the time at which the leaching test was finished. The degree of hydration, assumed to 0.90, has a significant influence on the porosity only.

The results for a reference specimen 0.60:9Ref that had never been leached, only lying submerged in lime-water, are shown in Table 6.2 and Figure 6.13. One can note that the upstream end of the specimen had a higher initial Ca content of than the rest of the specimen. Since this was probably due to separation of the aggregate during casting, the upstream part of the specimen became richer in cement paste. The calculations give a total initial cement content of 336 kg/m^3 , as compared with 335 kg/m^3 in the bulk batch of the concrete on the basis of the recipe, results which are in excellent agreement. The calculations indicate 14.8 g of the calcium to have been leached, which is impossible, however, because it is an unleached reference specimen. Examining the figure, one can note that the curves of “Ca (initial calculated)” and “Ca leached, measured” have the same shape but lie at some distance from each other. They should lie at the same level. There is no good explanation for this discrepancy.

Table 6.2 Comparison of residual Ca with leached Ca for specimen 0.60:9Ref. See also Figure 6.13. For explanations of symbols, see the text.

| Specimen | x | ρ_a | S_a | $m_{\text{Si(aq)}}$ | m_{rest} | C | C | $m_{\text{Ca}(t_0)}$ | $m_{\text{Ca}(t_1)}$ | $\Delta m_{\text{Ca}}(\text{s})$ | Q_{diff} | Q_{conv} | $\Delta m_{\text{Ca}}(\text{aq})$ |
|-----------|----|-----------------|-------|----------------------|----------------------|-----------------|-----------------|----------------------|----------------------|----------------------------------|-------------------|-------------------|-----------------------------------|
| | mm | kg/m^3 | - | 10^{-6} kg | 10^{-2} kg | kg/m^3 | kg/m^3 | kg/m^3 | kg/m^3 | g | g | g | g |
| 0.60:9Ref | 46 | 2732 | 0.032 | 3,73 | 3,13 | 318 | 336 | 142 | 126 | 13.9 | 0 | 0 | 0 |
| | 39 | | | 5,66 | 3,00 | 342 | | 153 | 130 | | | | |
| | 33 | | | 1,88 | 2,14 | 331 | | 148 | 140 | | | | |
| | 26 | | | 3,02 | 3,27 | 344 | | 154 | 147 | | | | |
| | 19 | | | 3,04 | 3,24 | 320 | | 143 | 133 | | | | |
| | 11 | | | 5,83 | 3,42 | 322 | | 144 | 120 | | | | |
| | 3 | | | 2,50 | 2,79 | 376 | | 168 | 153 | | | | |

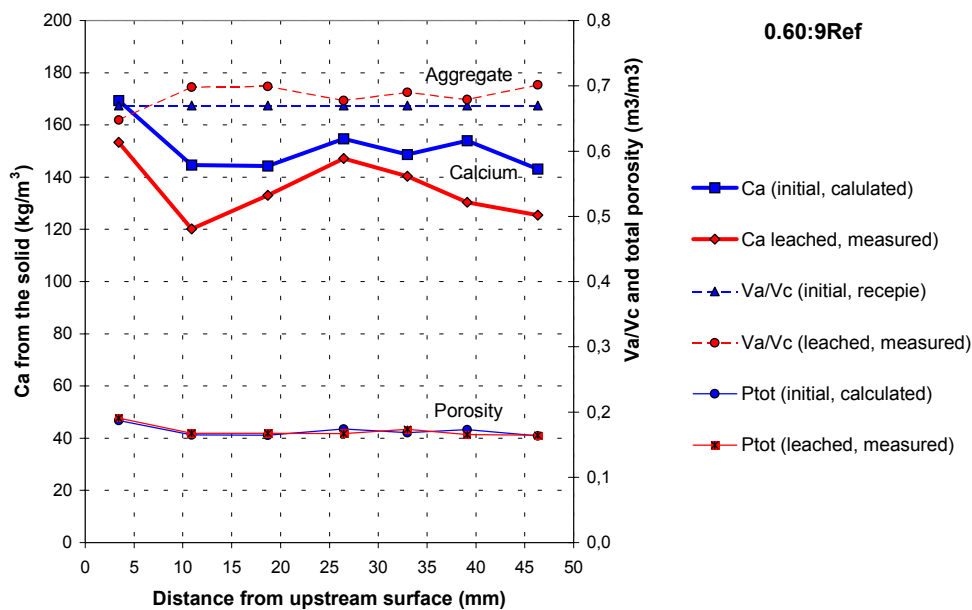


Figure 6.13 Calcium content (kg/m^3) and volume fraction (m^3/m^3) of aggregate and pores at times t_0 and t_1 in the unleached concrete specimen 0.60:9Ref. See also Table 6.2.

Table 6.3 and Figure 6.14 shows the result for specimen 0.80a:3. As can be seen, the upstream end of the specimen has a higher initial Ca content than the rest of the specimen. This was probably due to separation of the aggregate during casting making the upstream part richer in cement paste. In the leached specimen, the Ca content of is much lower in the upstream part, probably due to the extensive diffusion of ions to the de-ionised water on the upstream surface. In a region 35 mm from the upstream face, a decrease in Ca was also found, perhaps due to a greater amount of aggregate there, resulting in larger number of interfacial zones between the paste and the aggregate. Such zones are porous and rich in Portlandite. The Ca may then have more easily leached from this region. It can also be noted that the porosity is higher, and the content of aggregate lower, in the upstream part, which is what one would expect. The calculations give a total initial cement content of 240 kg/m^3 , as compared with 242 kg/m^3 based on the recipe, figures which agree closely. The calcium leached was calculated to be 12.1 g, which is also in close agreement with the leaching of calcium as measured in the upstream and downstream waters.

Table 6.3 Comparison of residual Ca and leached Ca for specimen 0.80a:3.

| Specimen | x | ρ_a | S_a | $m_{Si(aq)}$ | m_{rest} | C | C | $m_{Ca(t0)}$ | $m_{Ca(t1)}$ | $\Delta m_{Ca}(s)$ | Q_{diff} | Q_{conv} | $\Delta m_{Ca}(aq)$ |
|----------|----|-----------------|-------|----------------------|----------------------|-----------------|-----------------|-----------------|-----------------|--------------------|------------|------------|---------------------|
| | mm | kg/m^3 | - | 10^{-6} kg | 10^{-2} kg | kg/m^3 | kg/m^3 | kg/m^3 | kg/m^3 | g | g | g | g |
| 0.80a:3 | 45 | 2620 | 0.036 | 12.6 | 9,64 | 222 | 240 | 100 | 103 | 12.1 | 5.7 | 6.7 | 12.4 |
| | 35 | | | 9.94 | 9,16 | 216 | | 97 | 86 | | | | |
| | 25 | | | 10.4 | 9,28 | 213 | | 96 | 100 | | | | |
| | 15 | | | 9.65 | 4,96 | 229 | | 103 | 103 | | | | |
| | 5 | | | 14.8 | 9,24 | 305 | | 137 | 86 | | | | |

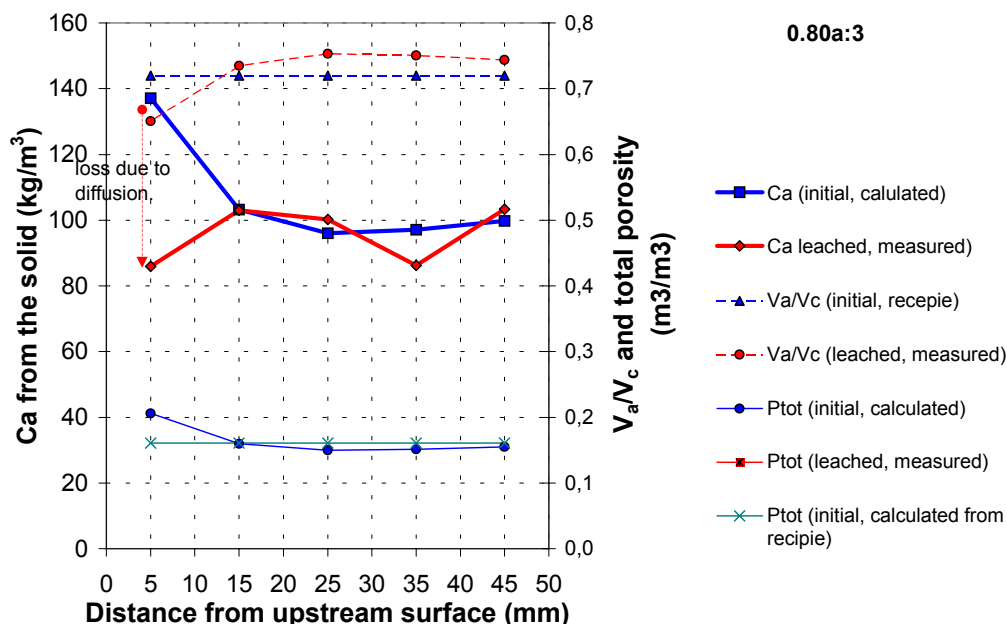


Figure 6.14 Calcium content (kg/m^3) and volume fraction (m^3/m^3) of aggregate and pores at time t_0 and t_1 in the unleached concrete specimen 0.80a:3.

The results for specimen 0.80a:4 are shown in Table 6.4 and Figure 6.15. One can note that the upstream end of the specimen has a higher initial Ca content than the rest of the specimen. Since this was probably due to separation of the aggregate during casting, the upstream part became richer in cement paste. In the leached specimen, the Ca content in the upstream part is much lower probably due to the extensive diffusion of ions to the de-ionised water. More calcium was leached from the rest of the specimen than in the case of specimen 0.80a:3, probably due to the transport of dissolved Ca by the flow of water (convection). The calculations give a total initial cement content of 205 kg/m^3 , as compared with 242 kg/m^3 according to the recipe. The deviation is quite large and is difficult to explain. The calculated amount of leached calcium is 14.3 g , which is less than the estimated leaching based on measurements in the upstream and downstream waters, namely 25.7 g . It can also be seen that the measured porosity of the leached specimen is somewhat too high in comparison with the initial state.

If the density of the aggregate is assumed to be 5% higher, than the nominal values as stated by the manufacturer, the calculated values becomes more realistic: $C = 239 \text{ kg/m}^3$, $\Delta m_{\text{Ca}}(\text{s}) = 28.2 \text{ g} \approx \Delta m_{\text{Ca}}(\text{aq}) = 25.7 \text{ g}$. The porosity and the amount of aggregate become more realistic, see Figure 6.16. This shows that the leaching calculations are sensitive to variations in the aggregate density.

Table 6.4 Comparison of residual Ca with leached Ca for specimen 0.80a:4.

| Specimen | x | ρ_a | S_a | $m_{\text{Si(aq)}}$ | m_{rest} | C | C | $m_{\text{Ca}(t0)}$ | $m_{\text{Ca}(t1)}$ | $\Delta m_{\text{Ca}}(\text{s})$ | Q_{diff} | Q_{conv} | $\Delta m_{\text{Ca}}(\text{aq})$ |
|----------|----|-----------------|-------|----------------------|----------------------|-----------------|-----------------|---------------------|---------------------|----------------------------------|-------------------|-------------------|-----------------------------------|
| | mm | kg/m^3 | - | 10^{-6} kg | 10^{-2} kg | kg/m^3 | kg/m^3 | kg/m^3 | kg/m^3 | g | g | g | g |
| 0.80a:4 | 47 | 2620 | 0.036 | 2,25 | 2,02 | 240 | 205 | 108 | 86 | 14.3 | 11.0 | 14.7 | 25.7 |
| | 40 | | | 2,81 | 3,58 | 179 | | 81 | 68 | | | | |
| | 31 | | | 1,19 | 2,93 | 186 | | 84 | 76 | | | | |
| | 23 | | | 2,55 | 3,26 | 201 | | 90 | 85 | | | | |
| | 14 | | | 2,53 | 3,11 | 184 | | 83 | 72 | | | | |
| | 6 | | | 3,19 | 2,60 | 223 | | 100 | 74 | | | | |
| | 1 | | | 1,99 | 9,65 | 300 | | 135 | 84 | | | | |

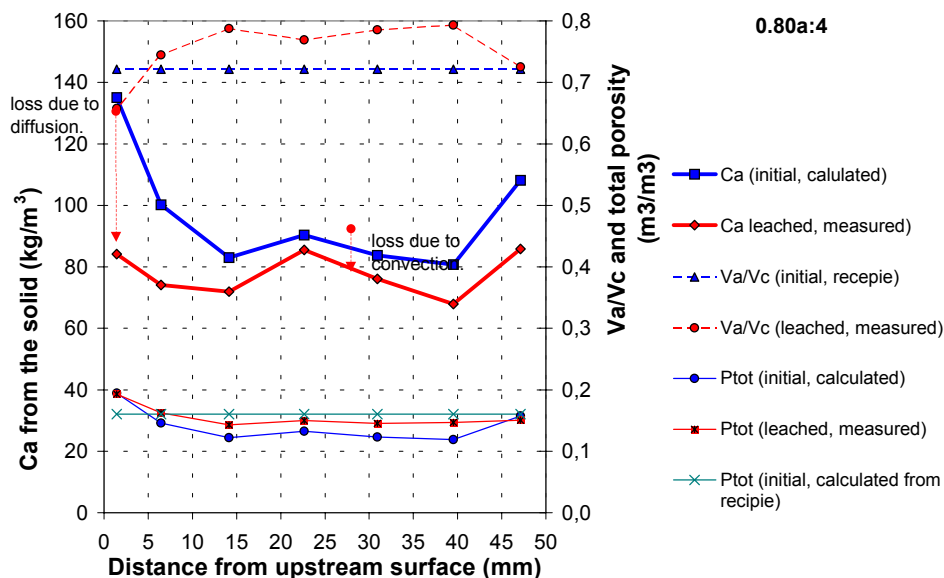


Figure 6.15 Calcium content (kg/m^3) and volume fraction (m^3/m^3) of aggregate and pores at times t_0 and t_1 in the unleached concrete specimen 0.80a:4, with density $\rho_a = 2620 \text{ kg/m}^3$

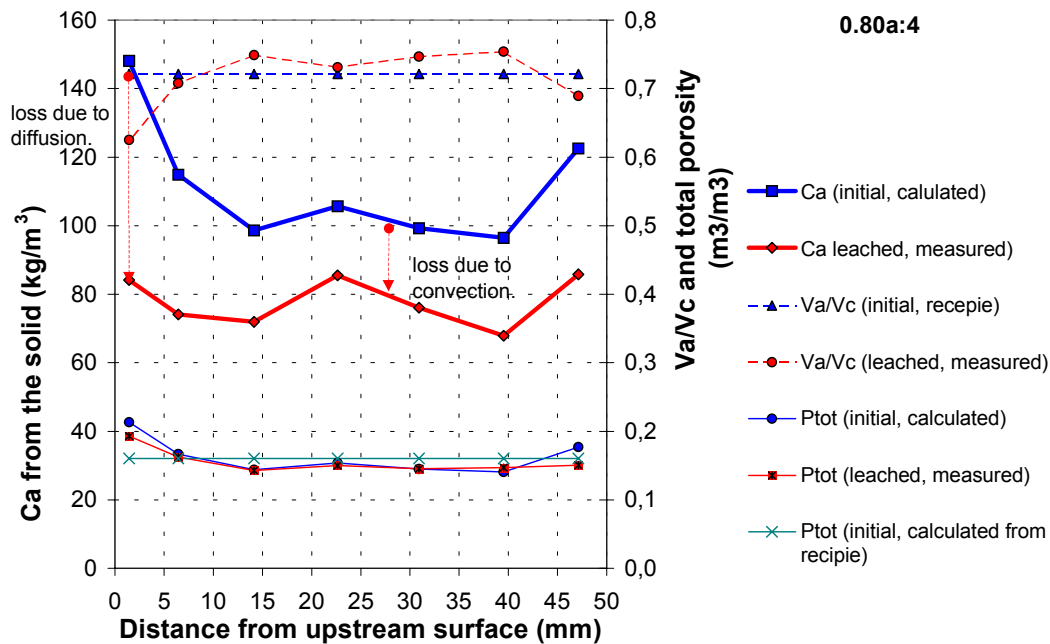


Figure 6.16 Calcium content (kg/m^3) and volume fraction (m^3/m^3) of aggregate and pores at times t_0 and t_1 in the unleached concrete specimen 0.80a:4, with density $\rho_a = 2751 \text{ kg/m}^3$.

Table 6.4 and Figure 6.15 give the results for specimen 0.80b:2. The results as calculated seem quite reasonable, the calculated content of cement $C = 246 \text{ kg/m}^3$ being almost the same as in the recipe, 242 kg/m^3 . The shape of the curves, the Ca content, the amount of aggregate and the porosity agreeing closely with each other as well. The only noteworthy discrepancy is that the calculated amount of leached calcium is somewhat lower than that estimated on measurements made in the upstream and the downstream water. However, the estimated 11.0 g of diffused calcium to the inlet in the table is a rough estimation based on measurements and might very well be lower.

Table 6.5 Comparison of residual Ca with leached Ca for specimen 0.80b:2.

| Specimen | x | ρ_a | S_a | $m_{\text{Si(aq)}}$ | m_{rest} | C | C | $m_{\text{Ca}(t_0)}$ | $m_{\text{Ca}(t_1)}$ | $\Delta m_{\text{Ca}}(s)$ | Q_{dif} | Q_{conv} | $\Delta m_{\text{Ca}}(\text{aq})$ |
|----------|----|-----------------|-------|----------------------|----------------------|-----------------|-----------------|----------------------|----------------------|---------------------------|------------------|-------------------|-----------------------------------|
| | mm | kg/m^3 | - | 10^{-6} kg | 10^{-2} kg | kg/m^3 | kg/m^3 | kg/m^3 | kg/m^3 | g | g | g | g |
| 0.80b:2 | 39 | 2751 | 0.036 | 1,63 | 2,33 | 205 | 246 | 92 | 89 | 7.8 | 11.0 | 0.7 | 11.7 |
| | 34 | | | 4,96 | 2,65 | 237 | | 106 | 111 | | | | |
| | 27 | | | 3,32 | 3,55 | 275 | | 124 | 115 | | | | |
| | 19 | | | 2,68 | 3,48 | 226 | | 102 | 106 | | | | |
| | 11 | | | 2,63 | 3,62 | 222 | | 100 | 98 | | | | |
| | 3 | | | 3,16 | 2,91 | 299 | | 134 | 90 | | | | |

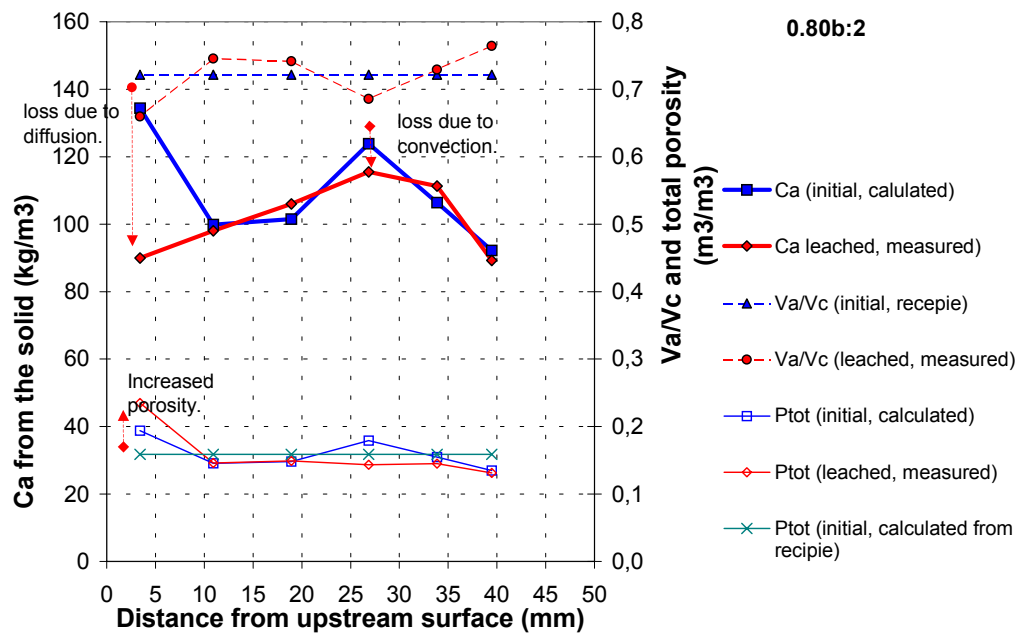


Figure 6.17 Calcium content (kg/m^3) and volume fraction (m^3/m^3) of aggregate and pores at time t_0 and t_1 in the unleached concrete specimen 0.80b:2.

Table 6.6 and Figure 6.18 present the results for specimen 0.80b:5. The calculated results for the leaching model are quite good, the calculated cement content $C = 243 \text{ kg/m}^3$ being the same as in the recipe, 242 kg/m^3 , although the assumed density of the aggregate is somewhat higher, 2804 kg/m^3 , than for the specimens described above. The shape of the curves for the Ca content, the amount of aggregate and the porosity agree well. However, the porosity in the upstream end should have been lower in the leached specimen than in the unleached one. The calculated amount of leached calcium is somewhat lower than the estimate based on the measurements made in the upstream and downstream water.

Table 6.6 Comparison of residual Ca with leached Ca for specimen 0.80b:5.

| Specimen | x | ρ_a | S_a | $m_{\text{Si(aq)}}$ | m_{rest} | C | C | $m_{\text{Ca}(t_0)}$ | $m_{\text{Ca}(t_1)}$ | $\Delta m_{\text{Ca}(s)}$ | Q_{diff} | Q_{conv} | $\Delta m_{\text{Ca}(aq)}$ |
|----------|----|-----------------|-------|----------------------|----------------------|-----------------|-----------------|----------------------|----------------------|---------------------------|-------------------|-------------------|----------------------------|
| | mm | kg/m^3 | - | 10^{-6} kg | 10^{-2} kg | kg/m^3 | kg/m^3 | kg/m^3 | kg/m^3 | g | g | g | g |
| 0.80b:5 | 44 | 2804 | 0.022 | 2,37 | 5,44 | 249 | 243 | 112 | 118 | 3.8 | 7.4 | 4.8 | 12.2 |
| | 35 | | | 2,08 | 2,99 | 224 | | 101 | 99 | | | | |
| | 29 | | | 2,24 | 2,98 | 222 | | 100 | 97 | | | | |
| | 23 | | | 2,11 | 2,85 | 226 | | 102 | 110 | | | | |
| | 17 | | | 2,54 | 3,19 | 240 | | 108 | 106 | | | | |
| | 10 | | | 2,95 | 4,02 | 220 | | 99 | 95 | | | | |
| | 3 | | | 2,08 | 2,48 | 325 | | 146 | 104 | | | | |

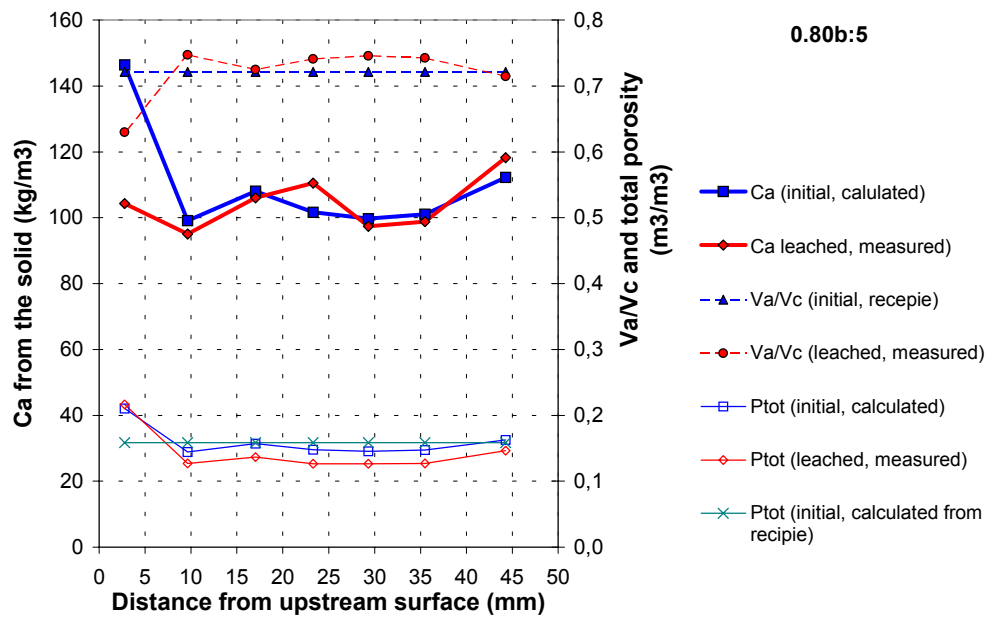


Figure 6.18 Calcium content (kg/m^3) and volume fraction (m^3/m^3) of aggregate and pores at times t_0 and t_1 in the unleached concrete specimen 0.80b:5.

Table 6.7, Table 6.8, Figure 6.19 and Figure 6.20 shows the results obtained for specimens 0.80b:8Ref and 0.80b:10Ref, i.e. reference specimens, which had been leached for 42 days in early age. The calculated results agree well with the measured values. The cement content was about 242 kg/m^3 . The shape of the curves for Ca, the amount of aggregate and the porosity as shown in the figures are about as what one would expect on basis on the recipe.

Table 6.7 Comparison of residual Ca with leached Ca for specimen 0.80b:8Ref.

| Specimen | x | ρ_a | S_a | $m_{\text{Si(aq)}}$ | m_{rest} | C | C | $m_{\text{Ca}(t_0)}$ | $m_{\text{Ca}(t_1)}$ | $\Delta m_{\text{Ca}(s)}$ | Q_{diff} | Q_{conv} | $\Delta m_{\text{ca(aq)}}$ |
|------------|----|-----------------|-------|----------------------|----------------------|-----------------|-----------------|----------------------|----------------------|---------------------------|-------------------|-------------------|----------------------------|
| | mm | kg/m^3 | - | 10^{-6} kg | 10^{-2} kg | kg/m^3 | kg/m^3 | kg/m^3 | kg/m^3 | g | g | g | g |
| 0.80b:8Ref | 47 | 2660 | 0.036 | 5,32 | 2,41 | 280 | 244 | 126 | 119 | 0.6 | 1.3 | 0 | 1.3 |
| | 41 | | | 1,74 | 2,70 | 228 | | 103 | 97 | | | | |
| | 34 | | | 1,91 | 2,93 | 231 | | 104 | 126 | | | | |
| | 26 | | | 1,45 | 3,33 | 208 | | 93 | 85 | | | | |
| | 18 | | | 2,76 | 3,61 | 215 | | 97 | 91 | | | | |
| | 10 | | | 4,43 | 3,27 | 234 | | 105 | 106 | | | | |
| | 3 | | | 6,56 | 2,11 | 339 | | 152 | 151 | | | | |

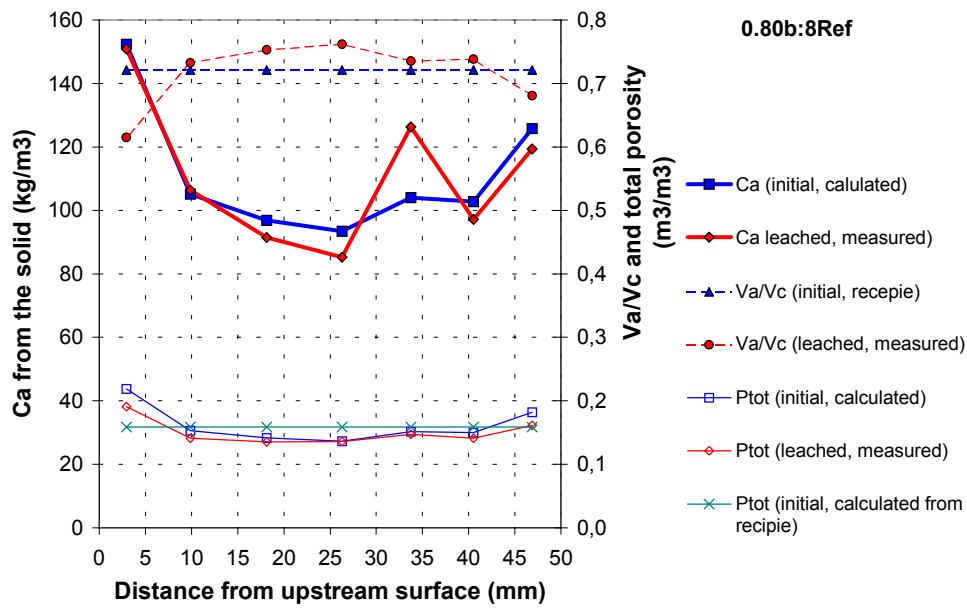


Figure 6.19 Calcium content (kg/m^3) and volume fraction (m^3/m^3) of aggregate and pores at times t_0 and t_1 in the unleached concrete specimen 0.80b:8Ref.

Table 6.8 Comparison of residual Ca with leached Ca for specimen 0.80b:10Ref.

| Specimen | x | ρ_a | S_a | $m_{\text{Si(aq)}}$ | m_{rest} | C | C | $m_{\text{Ca}(t_0)}$ | $m_{\text{Ca}(t_1)}$ | $\Delta m_{\text{Ca}}(\text{s})$ | Q_{diff} | Q_{conv} | $\Delta m_{\text{Ca}}(\text{aq})$ |
|-------------|----|-----------------|-------|----------------------|----------------------|-----------------|-----------------|----------------------|----------------------|----------------------------------|-------------------|-------------------|-----------------------------------|
| | mm | kg/m^3 | - | 10^{-6} kg | 10^{-2} kg | kg/m^3 | kg/m^3 | kg/m^3 | kg/m^3 | g | g | g | g |
| 0.80b:10Ref | 48 | 2646 | 0.018 | 1,87 | 1,66 | 291 | 238 | 131 | 122 | 1.2 | 1.3 | 0 | 1.3 |
| | 42 | | | 1,97 | 3,59 | 190 | | 85 | 85 | | | | |
| | 34 | | | 3,28 | 3,05 | 219 | | 99 | 106 | | | | |
| | 26 | | | 4,23 | 3,36 | 232 | | 105 | 111 | | | | |
| | 19 | | | 2,11 | 3,04 | 236 | | 106 | 110 | | | | |
| | 11 | | | 2,78 | 3,58 | 235 | | 106 | 104 | | | | |
| | 3 | | | 4,43 | 2,61 | 291 | | 131 | 110 | | | | |

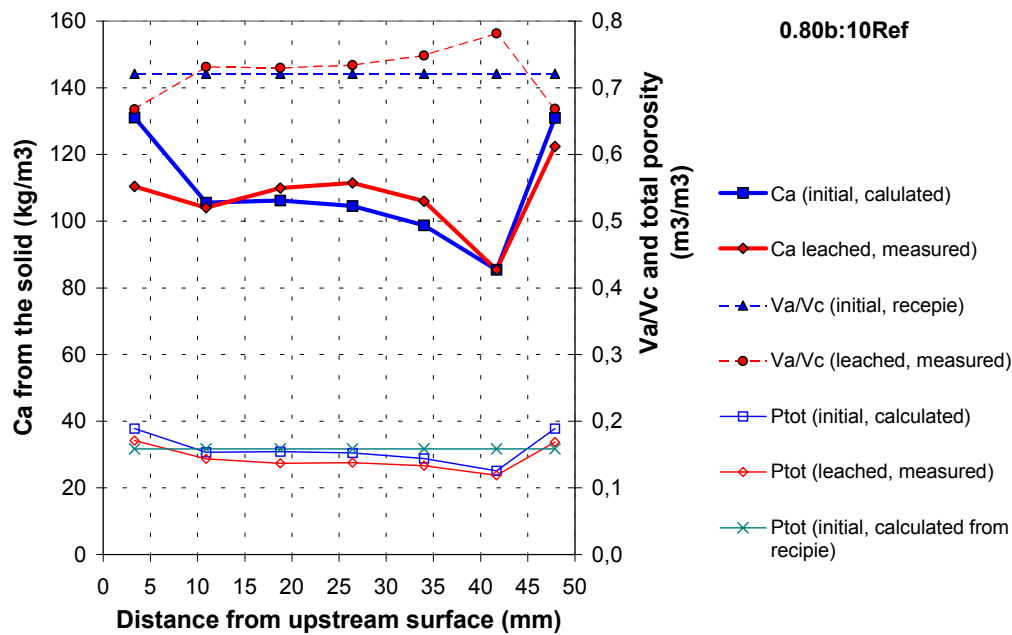


Figure 6.20 Calcium content (kg/m^3) and volume fraction (m^3/m^3) of aggregate and pores at times t_0 and t_1 in the unleached concrete specimen 0.80b:10Ref.

6.2 Percolation through holes in concrete

6.2.1 Analysis of downstream ion flow (convection)

The leaching in the hole occurred by diffusion of ions from the interior of the concrete to the wall of the hole, the ions then being transported by the water flux through the hole and out of the concrete. Since the diffusion velocity of the ions was low compared with the water velocity, no ions diffused in an upstream direction.

6.2.2 Analysis of remaining compounds and elements in the specimens

The most important results of this analysis were the following:

- the matrix around the hole was leached of Portlandite at a distance of about 1.5 mm at the inlet to the hole (see Figure 6.21) and about 0.5 mm at the outlet of the hole.
- There was a very thin layer of calcite (approximately 1-3 μm) on the surface of the hole-wall at the inlet to the hole, whereas the layer was somewhat thicker (20 μm) on the hole-wall at the outlet of the hole.

The reason why of the calcite layer being thicker at the outlet end than at the inlet end was probably the following:

- That atmospheric CO_2 was dissolved in the inlet water;
- That the pH of the flowing water rose, from just below 7 at the inlet to higher levels along the flow channel as more and more CH became dissolved from the walls of the hole;

- That the concentration of CO_3^{2-} was higher in the outlet end due to higher pH (see Figure 2.33);
- That the concentrations of Ca^{2+} and CO_3^{2-} were higher in the outlet end. Thus, more CaCO_3 was formed there. Edvardsen (1999) also observed this in studies of cracks.

Rough calculations yield the following results:

- According to Table 2.12, $1.83 \cdot 10^{-8}$ mole/l of carbonic acid was assumed to be dissolved in water.
- This amount of H_2CO_3 corresponds to $1.3 \cdot 10^{-8}$ g CO_2 /l.
- In total, approximately 150 l of water was led through the 3 holes in a specimen. This gives 50 l/hole.
- If all the CO_2 in the water reacts with Ca^{2+} from the walls of the hole, the amount of CaCO_3 formed becomes $m_{\text{CaCO}_3} = 150 \cdot 1.3 \cdot 10^{-8} \cdot 100/44 = 435 \cdot 10^{-7}$ g.
- If all this CaCO_3 were formed at the walls, it would have a volume of $V = t \cdot \pi \cdot \phi \cdot L/2 = m_{\text{CaCO}_3} / \rho_{\text{CaCO}_3} \Rightarrow t = m_{\text{CaCO}_3} \cdot 2 / (\pi \cdot \phi \cdot L \cdot \rho_{\text{CaCO}_3}) = 435 \cdot 10^{-8} \cdot 2 / (\pi \cdot 10^{-3} \cdot 40 \cdot 10^{-3} \cdot 2400) = 1 \cdot 10^{-6}$ m = 10 μm , which is in parity with the measured results of 18 μm . Since in reality, the measured pH of the inlet water was 6.25, which is lower than the 6.92 assumed in Table 2.12, there might have been more than $1.83 \cdot 10^{-8}$ mole/l of carbonic acid (H_2CO_3) giving even better agreement between calculated and measured thickness of the calcite layer.
- Calculations using the equation (2.12) gives a value of the diffusion coefficient in the solid matrix surrounding the hole of approximately

$$0.002 = \sqrt{\frac{2}{\sim 700} k_s \cdot (20 - 0) \cdot 3500 \cdot 3600} \Rightarrow k_s \approx 6 \cdot 10^{-12} \text{ m}^2 / \text{s}$$

which is quite realistic for diffusion in the actual, narrow pores.

The SEM-EDX-analysis, performed in the present investigation without use of other supplementary examination techniques, can be said to be only qualitative. However, it is an excellent technique for visualising the topography, shape and texture of the concrete. By sweeping back and forth over a large area, general tendencies can be detected. For example, between the wall of the hole and up to a definite distance from the hole, few $\text{Ca}(\text{OH})_2$ -crystals were found by the SEM-EDX-analysis. A carbonated layer on the wall of the hole could be seen. Yet to analyse a larger area takes time and the operator needs to be skilled. It is possible that with a more detailed analysis of each spot-area by EDX and of the relative amount of aggregate, more precise estimates could have been made of the Ca/Si- relation in the paste, allowing an estimation of the leaching ratio to be made. Possibly, if the SEM-analysis had been supplemented by an Electron Backscatter Diffraction (EBSD), a better understanding of the different compounds in relation to the distribution of elements could have been obtained.

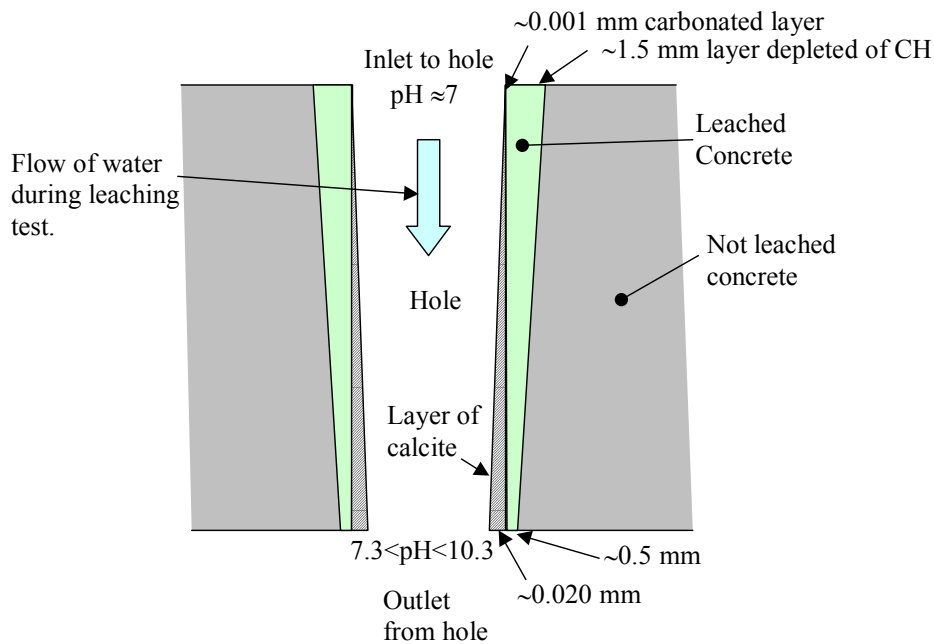


Figure 6.21 A schematic view of changes in wall of the hole and in the matrix surrounding the hole, after the leaching test. The diameter of the hole is enlarged in relation to the length of in this view.

6.3 Analyses of non evaporable water in concrete by heating the concrete to +1050°C

The degree of hydration is important when estimating the porosity at the beginning of a leaching test. The degree of hydration can be estimated in two ways: (i) by using other authors' data or models or (ii) on the basis of one's own experiments on concrete.

6.3.1 Estimation of the degree of hydration on the basis of the literature

Byfors (1980) has proposed that the degree of hydration could be described by

$$\alpha = e^{a \cdot (\ln t)^b} \quad (5.18)$$

where α = degree of hydration; t = time (hours); and a , b = parameters that depend on the type of cement and the hydration temperature. The degree of hydration is plotted for $a = -10$ and $b = -2$ in Figure 6.22. These coefficients are valid for Swedish Standard cement cured at +20°C. The hydration age for the concrete specimens at the start of the leaching test in the present work is also plotted in the figure.

Table 6.9 shows the degree of hydration obtained by Persson (1992) for concrete similar to those used in the leaching tests.

If 1 kg of cement is assumed to react with 0.25 kg of water at complete hydration, Table 6.9 gives the following degree of hydration in water-cured concrete after 90 days.

$$\alpha = 4 \cdot W_n / C = 4 \cdot 0.207 = 0.83 \quad (5.19)$$

which agrees very well with the curve in Figure 6.22.

Table 6.9 The ratio of the chemically bound water to the cement content, W_n/C , from Persson (1992). The cement employed is of the CEM I 42,5 type (Degerhamn anläggning).

| Batch | Cement (kg/m ³) | Aggregate | | W/c | Curing | Age | | |
|-------|--------------------------------|-----------|------|------|----------|-------|-------|-------|
| | | 0-8 | 8-12 | | | 28 d | 90 d | 450 d |
| 2 | 302 | 808 | 1144 | 0.58 | Water | 0.188 | 0.207 | 0.204 |
| | | | | | Air | 0.173 | 0.197 | 0.195 |
| | | | | | Membrane | 0.186 | 0.198 | 0.216 |

6.3.2 Estimation of the degree of hydration by tests of the actual concrete

The experimentally determined ignition loss between 105°C and 1050°C was 1.0, 1.9 and 0.7 % for unhydrated cement, Hardeberga quartzite and Kividinge sand, respectively. Unfortunately these data are not reliable. More plausible values would have been 0.4, 0.3 and 0.8 % respectively. The degree of hydration shown in Figure 6.22 is calculated in accordance with section 4.11 and data from Table 5.10, for a measured mass loss of between 105°C and 1050°C for the concrete studied here, but with ignition loss of unhydrated cement and aggregate in accordance with the “plausible” values.

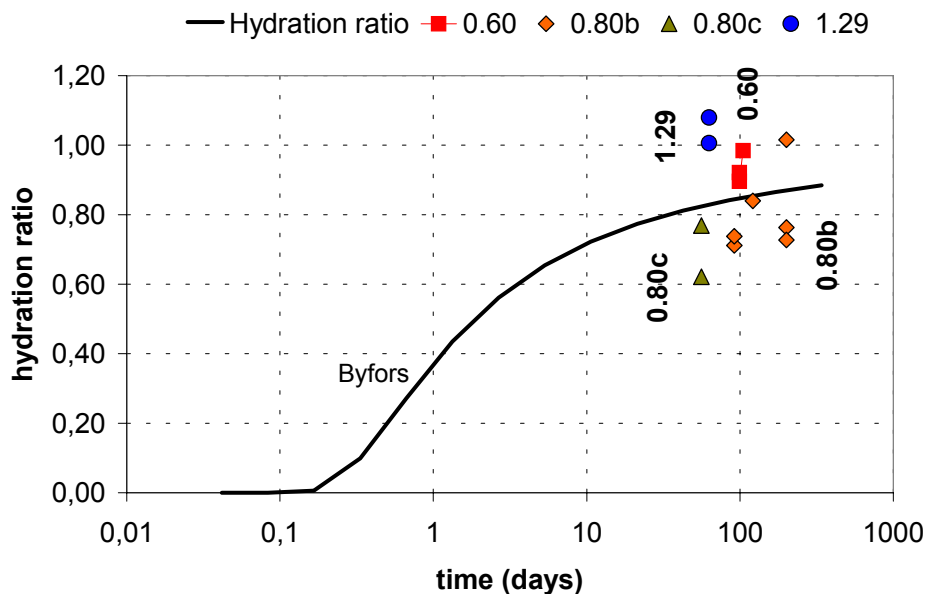


Figure 6.22 Hydration curve based on Byfors (1980), involving equation (5.18) where $a = -10$ and $b = -2$.

7 Models versus experimental work – discussion

7.1 Introduction

A porous medium consists of a *solid matrix* in which *void space* is always included. The void space is occupied by one or more fluid phases, such as air or water. A *phase* is defined as a chemically homogenous portion of space separated from other phases by well-defined physical boundaries. There may be only a single gaseous phase in the void space, since all gases are completely *miscible* and no distinct interfaces between them are maintained. Also, there may be a number of (*immiscible*) liquid phases, each occupying a well-defined portion of the void space (Bear 1987).

In porous media there always are difficulties in choosing the size of the smallest volume to be studied. If the volume selected is too small, there are difficulties in verifying the results of calculations, whereas if too large a volume is studied, one consisting of a very large number small separated volumes, calculations require a very large amount of computer effort. If the smallest volume studied is too large, important properties and processes on a small-scale level cannot be investigated. Most numerical modelling tools assume there to be a *continuum* which is studied within the material.

7.2 General about modeling

The objective in investigating *processes*, or phenomena involving the transport of extensive quantities of material in the domain (system) of a porous medium is to predict responses of the system of interest as a whole, or a phase or a component of the latter to excitation(s). The response takes the form of spatial and temporal variations in the values of state variables (such as pressure, density or temperature) that describe the behaviour of the system. In practice no model of a given domain can be used without the model coefficients relevant to the domain being known, coefficients that can be obtained by experiments. A typical experiment consists of exciting the system and observing its responses, while applying the same excitation (under the same initial and boundary conditions) to the model of the system. The values of the coefficients are obtained by comparing the response predicted by the model with that actually observed in the real system (in the field or in the laboratory). There is never an identical sets of values of this sort, only a “best fit” between them (Bear 1987).

A model is always a simplified version of the real system, one that approximates the excitation and its effects of relevance to the problem on hand. There is no unique model for a given porous-medium domain, or for a given problem. Usually the modelling processes involve the use of *conceptual*, *mathematical*, *numerical* and *statistical* models.

A *conceptual* model describes the composition of the system, the processes taking place within it, the mechanics governing it, the relevant properties of the medium, its boundary and initial conditions and finally, the assumptions that are made.

Because of the difficulties in describing a porous media at a *microscopic* level due to variations within the phases, its complex geometry, changes on phase boundaries and the impossibility of validating the model by measurements at that level, modelling is commonly performed at a *macroscopic* level. At that level it is easier to formulate problems and solve them. Any lack of information is compensated for by *coefficients* that are determined experimentally in the laboratory or in the field.

A *mathematical* model transforms the conceptual verbal model into mathematical relations consisting, for example, of physical balance equations that are relevant to the problem, constitutive relations between the phases and components involved, initial conditions, and boundary conditions. This conception of a mathematical model can be used at both a microscopic and a macroscopic level, but at the microscopic level, as just indicated, the model becomes exceedingly complex, and validation becomes impossible. The mathematical models may, for example, involve Darcy's law, the Navier-Stoke equation for incompressible fluids or the Hagen-Poiseuilles law, dependent on the assumptions and simplifications that are made.

Because of the complexity of most problems (irregular shape, heterogeneity domains, and the irregular temporal and spatial distribution of the various excitations), it is impossible to achieve analytical solutions. Instead, *numerical methods* (such as the Finite Element Method) are commonly used. A number of assumptions and simplifications are made, in addition to those made in the mathematical model.

There may be *uncertainty* as to whether or not the conceptual model represents the real structure or process. There may be uncertainty regarding the distribution of the basic underlying variables and coefficients obtained from experiments or measurements. There may be uncertainty concerning experimental or test errors in the observed data used for the calibration of coefficients. Modelling processes of all types (conceptual, mathematical, numerical or statistical) introduces uncertainties.

The types of uncertainties involved (ISO 2394 E.2) can be

- Inherent uncertainties
- Lack of knowledge
- Statistical uncertainties

Stochastic models are used in connection with statistical uncertainties. It is often difficult to draw sharp boundaries between the different types of uncertainty. Many statistical uncertainties can perhaps be explained if the processes involved are investigated thoroughly, and knowledge increases.

7.3 Modeling of the pore structure of cement materials

If one could model the intricate pore structure of a cement-based material, many phenomena could be studied theoretically, such as the flow of water and the leaching of ions. To model a microscopic pore structure, not only must the composition and geometry of the real structure be digitalised and transferred to a numerical computer program, but the results of the calculations must also be verified by experiments. The greatest difficulty lies in the fact that very large computer resources are required to perform calculations on such a mass of elements as is needed (millions) and that the results obtained on the micro-scale are difficult to verify by experiments.

Below, an example with a very simple stochastic model of a cement paste illustrates, however, certain tendencies that have been found regarding the pore structure of a cement-based material.

7.3.1 Example: a simple model of pore structures

In the present model a certain number of cement-particles were “thrown” into a digitised “cement paste volume” by use of a random function. The model is of a same type as used Bentz and Garboczi (1991a). The particles were all of the same size.

Growth simulating what happens to cement particles during hydration occurred randomly at the surfaces of each particle, the particles growing to somewhat more than double their origin size. The number of particles was

$$n = 0.32/(0.32+w/c) \cdot \text{size1} \cdot \text{size2} \cdot a^2 \quad (7.1)$$

where n = number of cement particles; $0.32/(0.32+w/c)$ = volume of unhydrated cement in the paste (m^3/m^3); size1 , size2 = length of each side of the small square of fictive volume that was studied, see Figure 7.1 (a); and a^2 = area of each particle before growth (m^2).

With a little extra effort, cement particles of different size can be employed and particles of aggregate can also be “thrown” into the paste. Portlandite can be modelled as growing within the cement gel. This should result in a more realistic pore structure.

Three different calculations are shown in Figure 7.1, (a) and (b) both involving cement with a w/c ratio of 0.80, and (c) with a w/c ratio of 0.60. Not only does the paste with a w/c of 0.60 appear to have a smaller number of pores, but the pores are also less connected as they are for the paste with a w/c of 0.80. A slight tendency was found, after many series of calculations involving the same w/c-ratios, that the porosity was higher near the boundary of the volume studied.

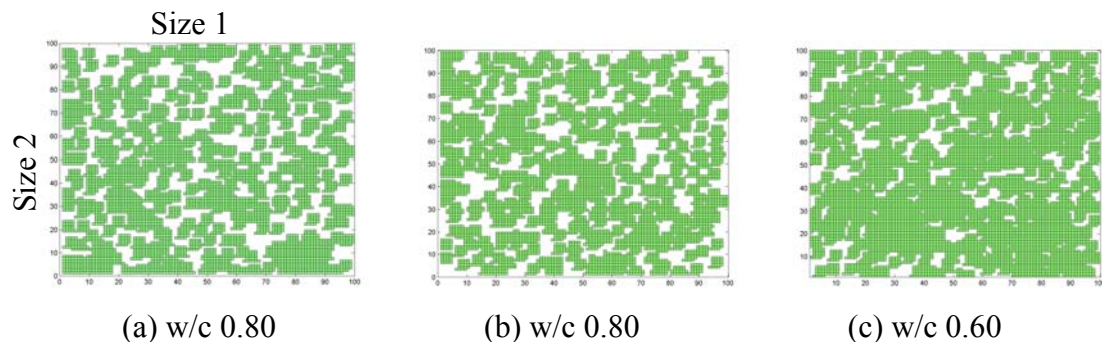


Figure 7.1 Calculated pore structure in an OPC paste. In (a) and (b) two sets of calculations were performed on material with a w/c ratio of 0.80 and in (c) a calculations on material with a w/c ratio of 0.60.

Theoretically, the digital pore models obtained are easy to transfer to a FEM-program for performing further calculations for example microstructure, permeability, strength, E-modulus, etc. The difficulties, however, in transferring the digital data to a FEM-program, and the tremendous calculation time required, meant that no further efforts were made to model “real” microscopic pore structures. In the next section, an account is provided of how the pore structure at the micro-scale was modelled in a much simpler way.

7.4 Modeling of the leaching process on the micro-scale

As indicated above, an ultimate modelling strategy of porous materials would involve the use of as small a geometry as possible in the calculations, since more processes and effects can then be simulated. However, for a porous material such as cement-based material, with its differences in length and the complexity of its pore system, the computer resources needed to perform calculations are too great. There are also

difficulties in verifying a model by means of experiments if the scale is too small. Nevertheless, a highly simplified example is shown below as an illustration of the following:

- That in a cement material, soluble compounds are first leached from the walls of larger flow tubes
- The greater the solubility of a solid compound is and the closer it is into pure water, the more quickly the dissolution of the compound occurs.

7.4.1 Example: flow of water and ions in a small fictive pore

Deionised water flows from left to right in a small fictive pore with 3 side pores in cement material (see Figure 7.2). When the initial content of calcium is washed out by the water, more calcium is dissolved from solid C-S-H in domain 1 and from solid CH in domain 3. The calculations are performed by use of a commercially available FEM-program (FEMLAB, see references). The equations calculated are

$$\begin{aligned} \text{Flow of water:} \quad & \nabla \cdot \mathbf{u} = 0 \\ & \nabla \cdot \mu (\nabla \mathbf{u} + (\nabla \mathbf{u})^T) + \nabla p = 0 \quad (\text{Navier-Stoke}) \end{aligned} \quad (7.2)$$

$$\text{Ions in the flow channel:} \quad \frac{\partial c_i}{\partial t} + \mathbf{u} \nabla c_i - \nabla \cdot (k_i \nabla c_i) = 0 \quad (\text{Balance of mass}) \quad (7.3)$$

$$\text{Ions in pores in solids:} \quad \frac{\partial c_i}{\partial t} - \nabla \cdot (k_i \nabla c_i) - \hat{c}_{is} = 0 \quad (\text{Balance of mass}) \quad (7.4)$$

$$\text{Ions in solids:} \quad \frac{\partial c_s}{\partial t} + \hat{c}_{is} = 0 \quad (\text{Balance of mass}) \quad (7.5)$$

where \mathbf{u} = local velocity vector (m/s) of the water in the x- and y-directions (u,v) in the flow channel, the initial conditions being $\mathbf{u}(0) = \mathbf{0}$ and the boundary conditions $\mathbf{u}(\text{inlet}) = (3 \cdot 10^{-3})$ m/s, with no slipping at the boundary to the solids; μ = dynamic viscosity of water = $1 \cdot 10^{-3}$ N·s/m²; p = pressure (Pa) in the pore solution with the boundary condition of $p = 0$ at the outlet; $c_i = c_{Ca}$ = concentration (mole/m³) of calcium in the pore solution in both the flow channel and the small pores assumed to be located in the solid phases of C-S-H and CH, at an initial concentration of $c_{Ca(t0)} = 20$ mole/m³ in all three domains; k_i = diffusion coefficient for calcium in the pore solution, assumed to be 10^{-9} m²/s in the flow channel and 10^{-11} m²/s in the small pores assumed to be located in the solid phases; \hat{c}_{is} = dissolving reaction of calcium from the solid phases of C-S-H and CH (mole/s), see below; and c_s = concentration of calcium (mole/m³) in the solid phases of C-S-H and CH, with initial conditions of 1000 (a simplified value) mole/m³ for both C-S-H and CH.

The dissolving reactions are assumed to be

$$\hat{c}_{is} = k \cdot (c_{sat} - c_i) \quad (\text{if } c_i > c_{sat}) \quad (7.6)$$

$$k = \frac{k_i \cdot A_{wall}}{\delta} \quad (7.7)$$

where k = dissolving rate coefficient (m^3/s); c_{sat} = saturation concentration (mole/m^3) of calcium from the respective solid phase, using assumed values of $2 \text{ mole}/\text{m}^3$ for C-S-H and $20 \text{ mole}/\text{m}^3$ for CH; $A_{pore\ wall}$ = area of the solid in contact with water from which the ions are dissolved (m^2); and δ = diffusion layer in the wall of the solid (m).

Using an assumed diffusion coefficient $k_i=10^{-9}$ and an diffusion layer of $\delta=10^{-7}$ m, the rate coefficient becomes $k = 10^{-2} \text{ m}^3/\text{m}^2/\text{s}$, which is used in the calculations.

Figure 7.2 shows the flow of water calculated by use of equation (7.2). The velocity profile across the flow channel has a parabolic shape, extending from zero velocity at the wall of the channel to a maximum value in the middle of the channel (Figure 7.3). Where the velocity is highest, the water is also purest because the dissolved ions are more quickly washed away. In Figure 7.4 (a) it can be seen how, during the first 10 seconds of the penetration of pure water, calcium in the pore solution is washed out from left to right. Inside the side-pores the water velocity is zero and the ions are only transported by diffusion. The diffusion is driven by the concentration gradients between the high concentration of calcium near the walls and inside the side-pores, and the purer water in the main channel of water flow. This can be seen more clearly, after 360 seconds, in Figure 7.4 (b). Then the main channel of flow contains pure water but the side pore still having high concentrations of Ca^{2+} . In Figure 7.5 the concentrations of Ca^{2+} in different cross sections, A-A, B-B and C-C, can be seen. Electric balance between the differently charged ions in the pore solution, and between the ions in the pore solution and the solid components in the pore walls, are not taken into account in the calculations. It can be supposed, however, that in a channel of flow in which the alkali ions (K^+ and Na^+) have already been leached and no other ions are present to any significant extent, except for ions of Ca^{2+} and OH^- , no significant electric imbalances are found. In dissolving $\text{Ca}(\text{OH})_2$ from Portlandite or C-S-H gel, opposite charges of the same strength (two + and two - from each $\text{Ca}(\text{OH})_2$) are introduced into the pore solution. If the diffusion velocity of the Ca^{2+} and OH^- are the same, there are no electric gradients that can slow down or speed up the diffusion of ions of the respective types. In the literature, however, the speed of OH^- is reported as being about five times as high as that for Ca^{2+} (table 8.8). The OH^- -ions diffuse more quickly than the Ca^{2+} -ions. This produces an imbalance in the electrical charges in the solution, which should mean that the diffusion of Ca^{2+} as calculated in this example is a bit too slow.

One can see in Figure 7.6 that the difference in the assumed solubility concentrations of C-S-H ($2 \text{ mole}/\text{m}^3$) and of CH ($20 \text{ mole}/\text{m}^3$) leads to CH dissolving faster than C-S-H. As can be seen in Figure 7.6 (a) the concentration of solid calcium decreases fastest of the cross sections in the channel of flow where the water is purest. At 3600 s (Figure 7.6 (b)), the calculated leaching front in crosssection B-B extends about 0.1 mm into the CH phase and has lost about 70% of its content of Ca at the surface, whereas across the channel of flow the C-S-H phase has scarcely lost any of its Ca.

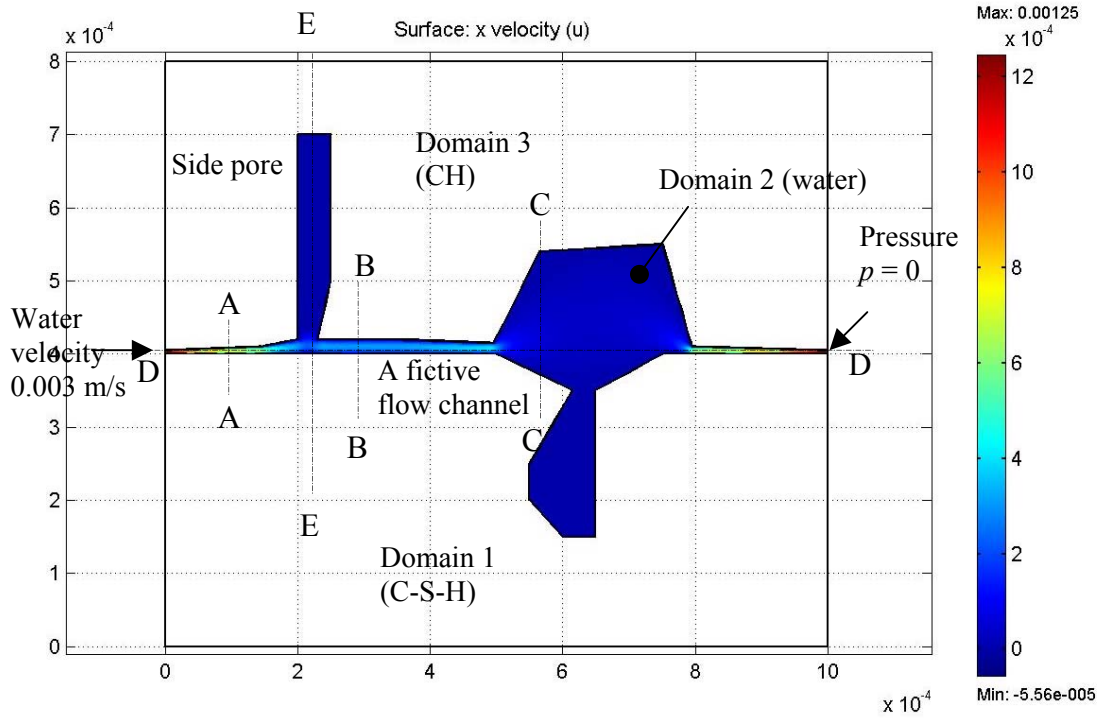


Figure 7.2 Flow of water as calculated by use of Navier-Stoke in a fictive flow channel (domain 2) surrounded by C-S-H (domain 1) and CH (domain 3).

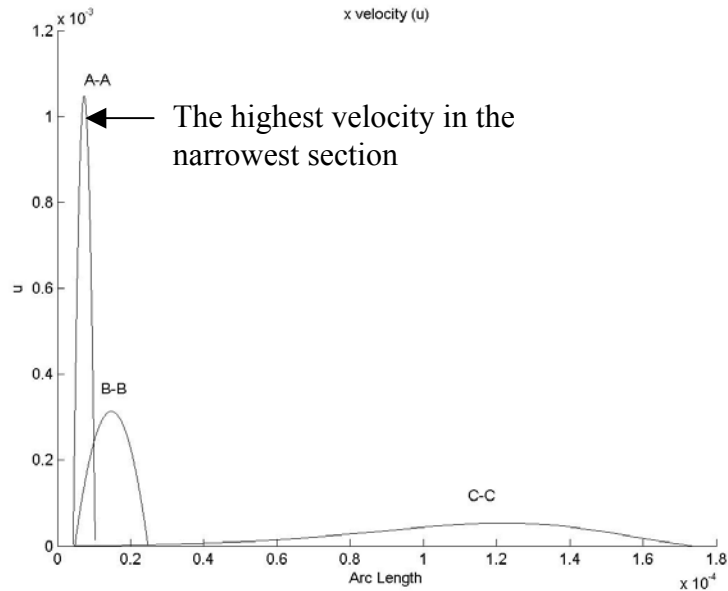
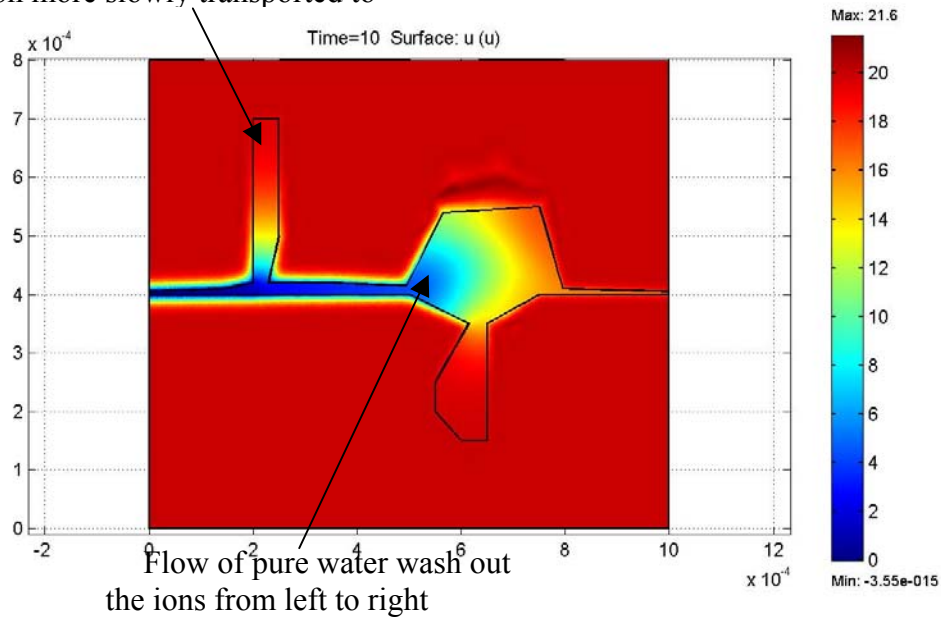
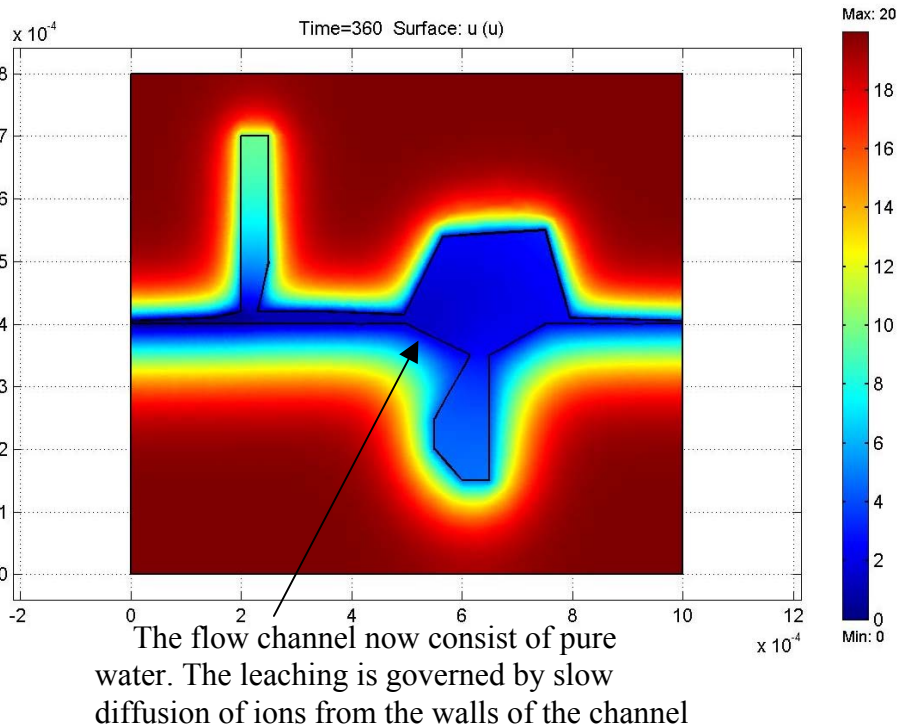


Figure 7.3 Calculated velocities of water flow at three different cross sections, A-A, B-B and C-C.

Ions in the side pore are by diffusion more slowly transported to



(a)



(b)

Figure 7.4 The calculated concentration of calcium in the pore solutions at (a) 10 s and at (b) 360 s.

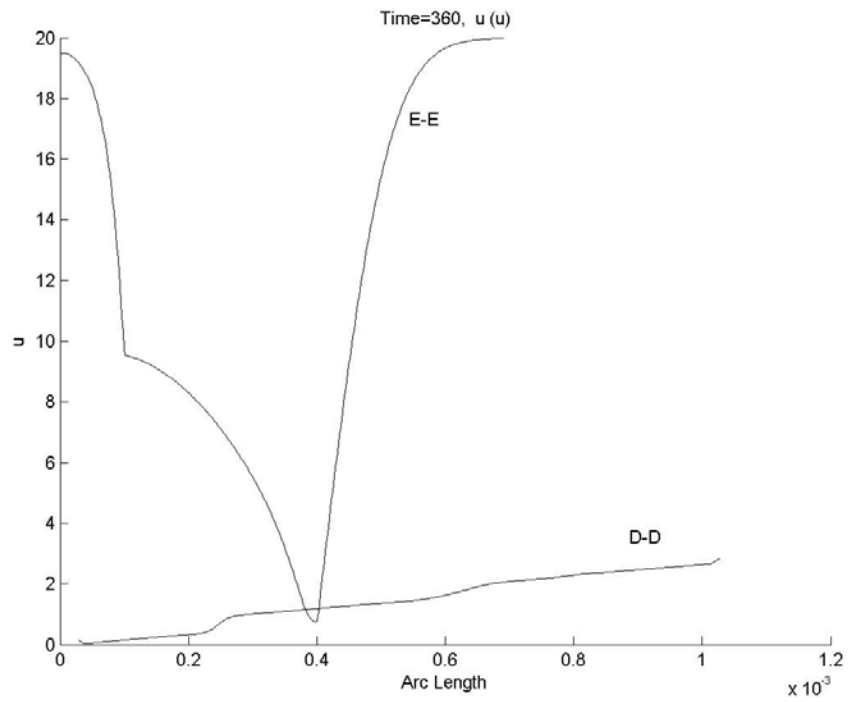


Figure 7.5 The calculated concentrations of Ca^{2+} in the pore solution at two different cross sections, D-D and E-E, see Figure 7.2.

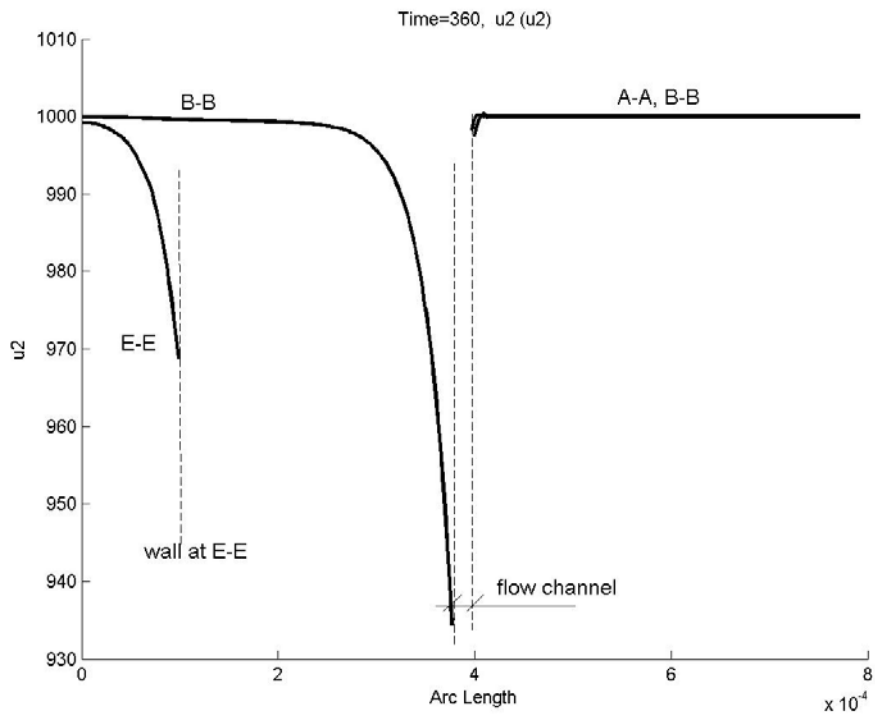


Figure 7.6 The calculated concentration of calcium in the solids at the cross sections A-A and B-B at 360 s.

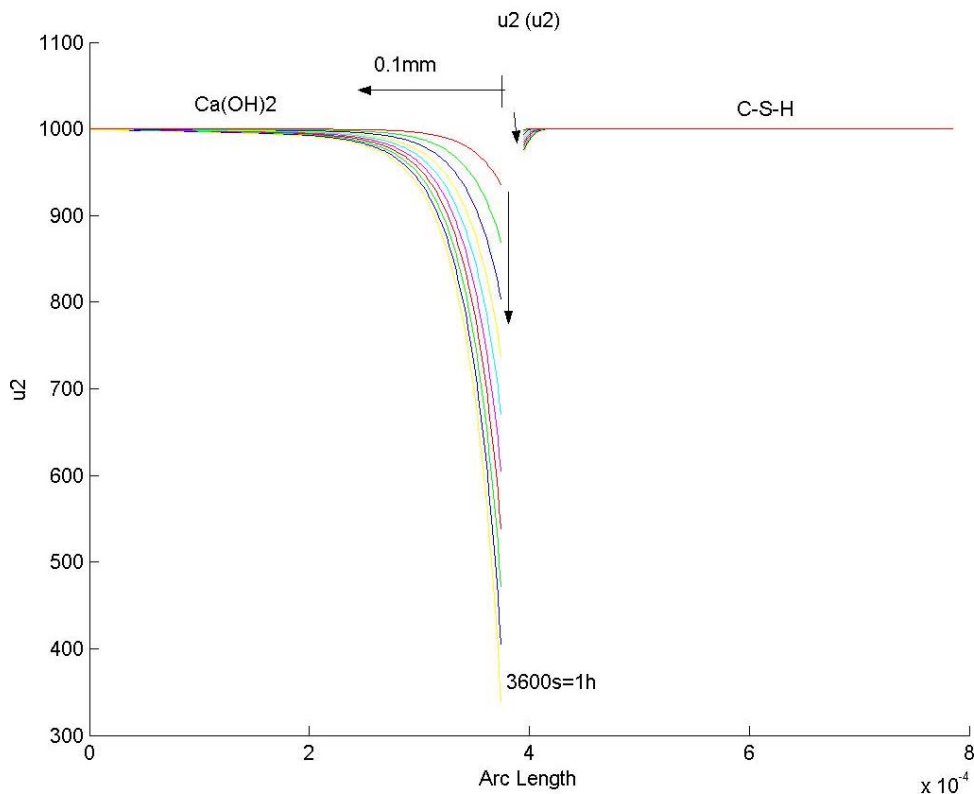


Figure 7.7 Calculated concentration of calcium in the solids at cross-section B-B for different leaching times of (0-3600s).

7.5 Modeling of the leaching process on a macro-scale

7.5.1 Conceptual model

For calculations concerned with leaching processes to be useful, use must be made of macro-scopic models.

Various demands must be met by a macro-scale model of a porous material (such as a cement-based material) for it to be considered satisfactory:

1. It should be able to take account of the microscopic behaviour of the material.
2. It should be as simple as possible and be easy to understand.
3. It should be based on natural mechanisms and laws of balances and not simply on the “curve-fitting” of experimental results.
4. The model should be possible to verify on the basis of experiments.
5. It is highly advantageous if the model can also be used to real structures, which means not experimental specimens produced only for use in investigations, but rather structures such as dams, tunnels, bridges, and the like. A major difficulty in calculating the flux of fluids in a concrete structure is that of the very great differences there are in the scales involved, extending from nanometric to metric dimensions. The goal of the models presented below is to perform calculations on a

metric scale on real structures (such as dams), at the same time as account is taken of the flux of water and ions on a micrometric scale.

The present model concerns the homogenous percolation of water through cement-based materials. Although the calculations are performed on the **bulk cross section area**, they are based on the assumed presence of microscopic flow tubes in the material. The flow of water and ions is to take place in a number of tubes of a particular diameter and degree of connectivity. Tortuosity effects and intermolecular effects on the flow of water and ions are dealt with by use of simple models. The calculations on a metric scale are done by assuming there to be a particular number of these tubes per cubic or square meter of the specimen or structure. The water flowing into the material is assumed to be deionised. When the water washes out the initial content of calcium, more calcium is dissolved from solid C-S-H and solid CH in the walls of the tubes.

The dissolving reactions are assumed to arise when Ca^{2+} and OH^- are dissolved from CH, C-S-H and CAF compounds. Hydroxide ions stemming from potassium hydroxide (KOH) and sodium hydroxide (NaOH) are assumed to have already been washed out by the water. Thus the concentration of OH^- when the calculations begin, corresponds to a pH-value of about 12.5-12.6, or 40 mole/m³.

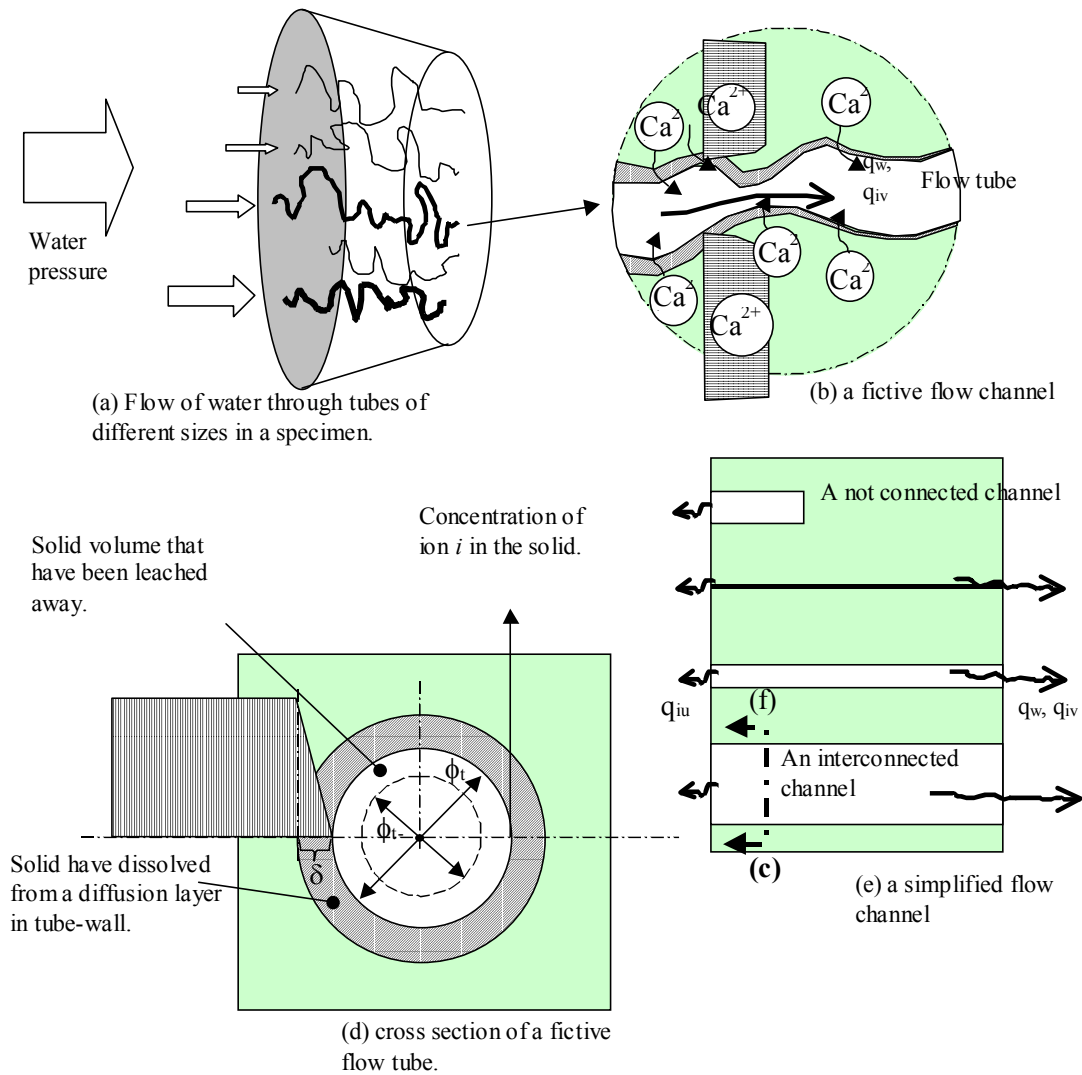


Figure 7.8 The flow of water and ions in a real concrete specimen (a) is assumed to occur in tortuous and more or less distinct flow tubes, which in reality are geometrically highly complex (b). The flow of water and ions depends on chemical interactions and reactions in these often very small flow tubes. In the model employed the flow of water and of ions is assumed to occur in simplified flow tubes (c) of a particular diameter that is the same throughout. The water dissolves solid materials from the tube walls (d).

7.5.2 Mathematical models

The flow of water and ions is calculated per *bulk* area or volume of the material.

Flux of water: $\nabla \cdot (v_w) = 0$ (continuity) (7.8)

Flux of ions in the tube: $\frac{\partial c_i}{\partial t} = \sum \hat{c}_{is} - \nabla \cdot (F_{iv} + F_{iu})$ (Balance of mass) (7.9)

Ions in the solids:
$$\frac{\partial c_i}{\partial t} = -\sum c_{is} \quad (\text{Balance of mass}) \quad (7.10)$$

where v_w = bulk-water velocity (m/s); c_i = ion concentration in the pore solution (mole/m³); F_{iv} = convective flux of ions by means of the flow of bulk water (mole/m²/s); F_{iu} = bulk diffusion of ions due to concentration gradients (mole/m²/s); and \hat{c}_{is} = bulk dissolving reaction (mole/m³/s).

7.5.3 General constitutive relationships

Water:

The homogenous flow of water is assumed by Darcy's law to be

$$v_w = -k_w \nabla P_w \quad (7.11)$$

$$q_w = v_w \cdot A_{tot} \quad (7.12)$$

where k_w = bulk water permeability (m/s); P_w = water pressure (piezometric) head (m); ∇P_w = gradient of water pressure (m/m); q_w = bulk water flow (m³/s); and A_{tot} = cross sectional area in the flow direction (m²). In the macroscopic approach taken here, the permeability, k_w , of the material as a whole (bulk) is assumed to be the sum of the permeability for each of the number n of flow tubes per unit of cross-sectional area.

It is assumed that the main flux of water and ions occurs in a particular numbers n of *flow tubes*. Assume that only a certain *share* of the total capillary porosity are connected through the concrete - that the flow tubes that let water through correspond to this share of the capillary porosity.

$$n_a = share \cdot \frac{(V_{cap})_p}{N \cdot V_{a(t0)}} \cdot \frac{V_{tot}}{A_{tot}} = share \cdot \frac{(V_{cap})_p}{N \cdot A_{a(t0)} \cdot L} \cdot \frac{A_{tot} \cdot L}{A_{tot}} = share \cdot \frac{(V_{cap})_p}{N \cdot A_{a(t0)}} \quad (7.13)$$

where n_a = numbers of tubes of size a that are connected through the concrete (nos./m²); *share* = share of the total capillary porosity that are connected through the concrete (-); $(V_{cap})_p$ = initial (prior to leaching) capillary pore volume of the cement paste (m³/m³); V_{tot} = volume of the concrete specimen (in the present experiment $\pi \cdot 0.154^2 / 4 \cdot L$ (m³); $V_{a(t0)}$ = initial volume of an individual tube of size a (m³); $A_{a(t0)}$ = initial cross-sectional area of an individual tube of size a (m²); L = length of the concrete specimen (m); and N = number of classes with diameter of different size.

$$A_{a(t0)} = \pi \cdot \phi_{a(t0)}^2 / 4 \quad (7.14)$$

where $\phi_{a(t0)}$ = initial average diameter of the tubes of size a (m). The initial (unleached) volume per length of all the tubes of size a is

$$\sum A_{a(t0)} = n_a \cdot \pi \phi_{a(t0)}^2 \quad (7.15)$$

where $\sum A_{a(t0)}$ = volume per length of the tubes as a whole (m³/m). With n_a from above $\sum A_{a(t0)}$ can also be written as

$$\sum A_{a(t0)} = n_a \cdot A_{a(t0)} = share \cdot \frac{(V_{cap})_p}{N \cdot A_{a(t0)}} \cdot A_{a(t0)} = share \cdot \frac{(V_{cap})_p}{N} \quad (7.16)$$

$$\text{i.e. } \sum A_{1(t0)} = \sum A_{2(t0)} = \sum A_{3(t0)} = \sum A_{N(t0)} \quad (7.17)$$

$$(V_{cap})_p = C \cdot (w/c - 0.39 \cdot \alpha) / 1000 \quad (7.18)$$

where C = cement content (kg/m^3); w/c = water cement ratio (kg/kg); α = degree of hydration (-).

The flow of water in each flow tube is assumed to follow the Hagen-Poiseuille's law, but with a reduction factor of r_w , due to the discrepancy between the flow in a relatively large perfect cylinder and the flow in a small tortuous flow path in concrete.

$$q_a = -k_a \cdot A_a \cdot \nabla P_w = - \left(\frac{\phi_a^2}{32 \cdot \mu} \cdot \rho_w \cdot g \cdot r_w \right) \cdot A_a \cdot \nabla P_w \quad (7.19)$$

where q_a = water flow in a single flow tube of size a (m^3/s); k_a = permeability for water in a single flow tube of size a (m/s); A_a = cross-sectional area of a flow tube of size a (m^2); r_w = reduction coefficient due to the discrepancy between the flow in a real tortuous flow tube and that in a perfect cylinder (-); ϕ_a = diameter of a flow tube of size a (m); and μ = dynamic viscosity (Ns/m^2).

Ions:

The ions in the pore solution are transported either by the flux of water (convection) or by diffusion:

$$F_{iv} = v_w c_i \quad (\text{convection}) \quad (7.20)$$

$$F_{iu} = -k_i \nabla c_i \quad (\text{diffusion}) \quad (7.21)$$

$$q_{iv} = A_{tot} \cdot F_{iv} \quad (7.22)$$

$$q_{iu} = A_{tot} \cdot F_{iu} \quad (7.23)$$

where k_i = diffusion coefficient of the solution in the tube (m^2/s); q_{iv} = bulk convective flow of ions (mole/s); and q_{iu} = bulk diffusion flow of ions (mole/s).

The **diameter** of the tubes and the thickness of the **diffusion layer** in the tube walls are assumed to increase as the tube-walls become leached. Assume that only a certain *Part* of the total leached volume results in an increase in the diameter of the tube, the rest (*1-Part*) leading instead to an increase in the thickness of the diffusion layer in the tube walls.

7.5.4 The permeability coefficient

Leached volume:

Although the permeability is assumed to increase when solid material is leached from the walls of the individual flow tubes, the estimates of the leached volume are based on the bulk residual content of solid material. The leached volume in relation to the bulk material is calculated by

$$V_{leach} = dm/\rho = (c_{s(t0)} - c_{s(t)}) \cdot M/\rho \quad (7.24)$$

where V_{leach} = leached volume per unit length, corresponding to all leached ions from the solid bulk material (m^3/m); dm = mass of the leached ions (kg/m^3); ρ = density of the leached material (kg/m^3); $c_{s(t0)}$ = initial (prior to leaching) concentration of the ions in the solid material (mole/m^3); $c_{s(t)}$ = concentration of the ions in the solids at time t

(mole/m³); A_{tot} = cross-sectional area of the material (m²); and M = molarity weight (kg/mole).

The tubes are assumed to grow wider when material is leached.

$$\sum A_{a(t)} = n_a \cdot \pi \phi_{a(t)}^2 / 4 = \sum A_{a(t_0)} + Part \cdot V_{leach} / N \quad (7.25)$$

where $\sum A_{a(t)}$ = cross-sectional area of all the leached tubes of size a (m²); $\phi_{(t)}$ = diameter of the leached tubes (m); and $Part$ = the part of the leached volume that lead to an increase in the diameter of the tubes (-). The division by N means that a same part of the total leached volume V_{leach} is divided on the different classes of tube sizes.

Equations (7.15) and (7.25) can be reformulated as

$$\phi_{a(t_0)} = \sqrt{\frac{4}{n_a \cdot \pi} \cdot \sum A_{a(t_0)}} \quad (7.26)$$

$$\phi_{a(t)} = \sqrt{\frac{4}{n_a \cdot \pi} \cdot (\sum A_{a(t_0)} + Part \cdot V_{leach} / N)} \quad (7.27)$$

The sum of flow of water in all the small tubes corresponds to the bulk water flow:

$$q_w = \sum_{a=1}^N (-n_a \cdot k_a \cdot A_a) \cdot \nabla P_w = -k_w \cdot \nabla P_w \cdot A_{tot} \quad (7.28)$$

Where k_w = permeability for water of the bulk body of the material (m/s). Reformulating equation (7.28) leads to an expression for the bulk permeability in terms of the permeability of the tubes:

$$k_w = \sum_{a=1}^N (n_a \cdot k_a \cdot A_a) / A_{tot} = \sum_{a=1}^N \left(n_a \cdot \left(\frac{\phi_{a(t)}^2}{32 \cdot \mu} \cdot \rho_w \cdot g \cdot r_w \right) \cdot \frac{A_a}{A_{tot}} \right) \quad (7.29)$$

The quotient of the initial (unleached) water flow and the water flow in the leached material is

$$\frac{q_{w(t)}}{q_{w(t_0)}} = \frac{k_{w(t)} \cdot \nabla P \cdot A_{tot}}{k_{w(t_0)} \cdot \nabla P \cdot A_{tot}} = \frac{\sum_1^N \left(n_a \cdot \frac{\phi_{a(t)}^2}{32 \cdot \mu} \cdot \rho_w \cdot g \cdot r_w \cdot \frac{A_{a(t)}}{A_{tot}} \right) \cdot \nabla P \cdot A_{tot}}{\sum_1^N \left(n_a \cdot \frac{\phi_{a(t_0)}^2}{32 \cdot \mu} \cdot \rho_w \cdot g \cdot r_w \cdot \frac{A_{a(t_0)}}{A_{tot}} \right) \cdot \nabla P \cdot A_{tot}} = \frac{\sum_{a=1}^N (n_a \cdot \phi_{a(t)}^4)}{\sum_{a=1}^N (n_a \cdot \phi_{a(t_0)}^4)} \quad (7.30)$$

where $k_{w(t_0)}$ = permeability of the unleached material (m/s); $q_{w(t_0)}$ = water flow in unleached material (m³/s); $k_{w(t)}$ = permeability of the leached material (m/s); and $q_{w(t)}$ = water flow in the leached material (m³/s).

Using equations (7.26), (7.27) and (7.30) gives

$$\frac{\sum_{a=1}^N (n_a \cdot \phi_{a(t)}^4)}{\sum_{a=1}^N (n_a \cdot \phi_{a(t_0)}^4)} = \frac{\sum_{a=1}^N \left(n_a \cdot \left(\frac{4}{n_a \cdot \pi} \cdot (\sum A_{a(t_0)} + Part \cdot V_{leach} / N) \right)^2 \right)}{\sum_{a=1}^N \left(n_a \cdot \left(\frac{4}{n_a \cdot \pi} \cdot \sum A_{a(t_0)} \right)^2 \right)} \quad (7.31)$$

Using equations (7.16), (7.17) and (7.24) in equation (7.31) gives

$$\begin{aligned} \frac{\sum_{a=1}^N (n_a \cdot \phi_{a(t)}^4)}{\sum_{a=1}^N (n_a \cdot \phi_{a(t_0)}^4)} &= \left(\frac{\sum A_{a(t_0)} + Part \cdot V_{leach} / N}{\sum A_{a(t_0)}} \right)^2 = \left(1 + \frac{Part \cdot V_{leach} / N}{\sum A_{a(t_0)}} \right)^2 = \\ &= \left(1 + \frac{Part \cdot M}{share \cdot \rho \cdot (V_{cap})_p} \cdot (c_{s(t_0)} - c_{s(t)}) \right)^2 = \left(1 + a \cdot (c_{s(t_0)} - c_{s(t)}) \right)^2 \end{aligned} \quad (7.32)$$

where $a = Part \cdot M / (\rho \cdot share \cdot (V_{cap})_p)$.

Using equations (7.30) and (7.32), the flow of water at time t in a material contains n number of leached tubes can be written then as

$$\begin{aligned} q_{w(t)} &= q_{w(t_0)} \cdot \frac{\sum_{a=1}^N (n_a \cdot \phi_{a(t)}^4)}{\sum_{a=1}^N (n_a \cdot \phi_{a(t_0)}^4)} = \\ &= \sum_{a=1}^N \left(n_a \cdot \frac{\phi_{a(t_0)}^2}{32 \cdot \mu} \cdot \rho_w \cdot g \cdot r_w \cdot \frac{A_{a(t_0)}}{A_{tot}} \right) \cdot \nabla P \cdot A_{tot} \cdot \left(1 + a \cdot (c_{s(t_0)} - c_{s(t)}) \right)^2 = \\ &= \sum_{a=1}^N \left(n_a \cdot \frac{\phi_{a(t_0)}^4}{128 \cdot \mu} \cdot \pi \cdot \rho_w \cdot g \cdot r_w / A_{tot} \right) \cdot \left(1 + a \cdot (c_{s(t_0)} - c_{s(t)}) \right)^2 \cdot \nabla P \cdot A_{tot} \\ &= (k_{w(t_0)}) \cdot \left(1 + a \cdot (c_{s(t_0)} - c_{s(t)}) \right)^2 \cdot \nabla P_w \cdot (A_c) \end{aligned} \quad (7.33)$$

The relationship between the bulk permeability of the leached and of the unleached material can then be written as

$$k_{w(t)} = k_{w(t_0)} \cdot \left(1 + a \cdot (c_{s(t_0)} - c_{s(t)}) \right)^2 \quad (7.34)$$

where the initial permeability coefficient is

$$k_{w(t_0)} = \sum_{a=1}^N \left(n_a \cdot \frac{\phi_{a(t_0)}^4}{128 \cdot \mu} \cdot \pi \cdot \rho_w \cdot g \cdot r_w / A_{tot} \right) \quad (7.35)$$

7.5.5 The dissolving-reaction coefficient

The assumed mathematical model of the dissolving-reaction coefficient \hat{c}_i is

$$\begin{aligned}\hat{c}_i &= k \cdot (c_{is} - c_i) = n \cdot \frac{k_{is} \cdot \pi \cdot \phi_t}{\delta} \cdot (c_{is} - c_i) / K1 = \\ &= \sum_{a=1}^N (n_a \cdot \phi_{a(t_0)}) \cdot \frac{k_{is} \cdot \pi}{\delta} \cdot (c_{is} - c_i) / K1\end{aligned}\quad (7.36)$$

where k = reaction rate for dissolution; k_{is} = diffusion coefficient for calcium ions in the solid diffusion layer of the pore walls (m^2/s); δ = thickness of the diffusion layer in the pore walls (m); and $K1$ = an empirical parameter, assumed to be 1 when there is still CH(s) left and to have a different value (e.g. 100) when so much Ca has been leached that no more CH(s) is found (-).

The immediately decrease of the solubility when all CH has been leached is here assumed to be regarded by the factor $K1$. The value of this factor can of course be discussed. In Figure 2.25 it can be seen that the ratio ($K1$) between the point at CH is dissolved (20 mmole CaO/litre) and the point when C-S-H starts to be dissolved at larger amounts (2 mmole/litre) is about 10 (20/2). In (Harris et al. 2002) the solubility for C-S-H was about 0.2 mmole/litre, here corresponding to $K1 = 20/0.20 = 100$.

The thickness of the diffusion layer is assumed to increase as the wall of the flow tubes loses material due to leaching.

$$\delta = \delta_0 \cdot \left(\frac{c_{s(t_0)}}{c_{(t)}} \right)^{K2}\quad (7.37)$$

where δ_0 = thickness of the diffusion layer in the pore walls before leaching takes place (m); and $K2$ = an empirical parameter reflecting the fact that the diffusion layer increases when the walls of the flow tubes becomes depleted of soluble substances (-).

7.6 Model of porosity changes due to leaching

The total porosity of concrete subjected to leaching is assumed to change as

$$P_c = [(V_p)_a + (V_p)_p + V_{air} + V_{leach}] / V_c = P_{c(t_0)} + \frac{V_{leach}}{V_c}\quad (7.38)$$

where V_c = volume of the concrete (m^3); $(V_p)_a$ = volume of the pores in the aggregate (m^3); $(V_p)_p$ = total pore volume of the cement paste (m^3); V_{air} = volume of air due to compaction or air additives (m^3); V_{leach} = total volume of the leached material (m^3); and $P_{c(t_0)}$ = total porosity of the concrete at the time when leaching starts (m^3). See section A.6.

The total porosity of the cement paste subjected to leaching is assumed to change as

$$P_p = \frac{(V_p)_p}{V_p} + \frac{V_{leach}}{V_p}\quad (7.39)$$

where P_p = total porosity of the cement paste (m^3); $(V_p)_p$ = total pore volume (m^3); V_p = total volume of the cement paste (m^3); and V_{leach} = total volume of the leached material (m^3). See section A.3.5.

7.7 Model of change of compressive strength due to leaching

The strength of concrete depends on the amount and strength of its solid constituents. Due to scatter in the distribution of hydration products, micro-cracks, stress concentrations, stress redistribution, different modulus of elasticity of hydration products and aggregate, etc, it is difficult to give any precise value of the strength by any theoretical model. Stress concentrations and micro-cracks around pores and in the not perfect homogenous solid phase lower the strength. Aggregates will probably to some extent “trap” micro-cracks and by that increase the strength. The smaller the size and higher the amount of the aggregate, the better crack-trapping ability and the higher strength is probably achieved. On the other hand, aggregate can result in stress concentrations and stress re-distribution due to differences in elasticity and strength between the aggregate and the cement paste, and because of that aggregate can also lead to decreased strength.

Because the main effect of leaching is an increased porosity, it is tempting to use a strength model, which involves only the porosity of the cement paste. An increase in the porosity due to leaching will cause a reduction of the strength of the cement paste. Therefore it will also cause a reduction in the strength of concrete.

In the principles showed by figure 3-4, the strength of the concrete is assumed to approximately follow the strength of the cement-paste. In high w/c ratios, the aggregate probably increase the concrete’s strength a bit compared to the paste’s strength and vice versa for low w/c ratios Fagerlund (1987).

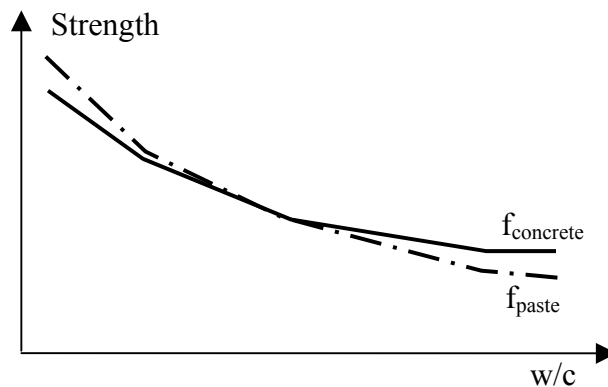


Figure 7.9 Principle relations between compression strength of concrete and paste. $f_{\text{concrete}} \approx f_{\text{paste}}$.

Two simple relationships for estimates of the strength of cement paste based on porosity are shown below.

Alternative 1: The compressive strength of cement paste is estimated by use of a model taken from Bal’shin (1949) and Fagerlund (1995). The solid phase $(V_0)_p$ of the paste, with solid gel and unhydrated cement, takes the entire load. Pores do not carry any load, see Figure 7.10.

$$f_{pc} = f_0 (1 - P_p)^{K_1} \quad (7.40)$$

The porosity of the cement paste is defined as:

$$P_p = \frac{w/c - 0.19 \cdot \alpha}{w/c + 0.32} \quad (7.41)$$

Where f_{pc} = the compressive strength of cement paste (Pa); f_0 = the fictitious strength of the solid phase without pores (Pa); K_1 = an empirical parameter, given as $2 \leq K_1 \leq 3.5$ in the literature (-); P_p = the porosity of the cement paste (no air pores are included) (m^3/m^3); w/c = water to cement ratio (kg/kg); and α = degree of hydration (-).

Alternative 2: Another model of the compressive strength for cement paste is taken from Powers (1958). The cement gel V_{gel} , with gel pores, takes the entire load. Unhydrated cement and capillary pores takes no load, see Figure 7.10.

$$f_{pc} = f_0' \cdot X^{K_2} \quad (7.42)$$

The gel space ratio is defined as:

$$X = \frac{V_{\text{gel}}}{V_{\text{gel}} + (V_{\text{cap}})_p} = \frac{0.71 \cdot \alpha}{0.32 \cdot \alpha + w/c} \quad (7.43)$$

Where f_0' = the fictitious strength of the cement gel, with gel pores included (Pa); K_2 = an empirical parameter, given as $2 \leq K_2 \leq 3$ in the literature (-); X = the gel space ratio (m^3/m^3); V_{gel} = the volume of the cement gel (m^3); and $(V_{\text{cap}})_p$ = the volume of the capillary pores in the cement paste (m^3).

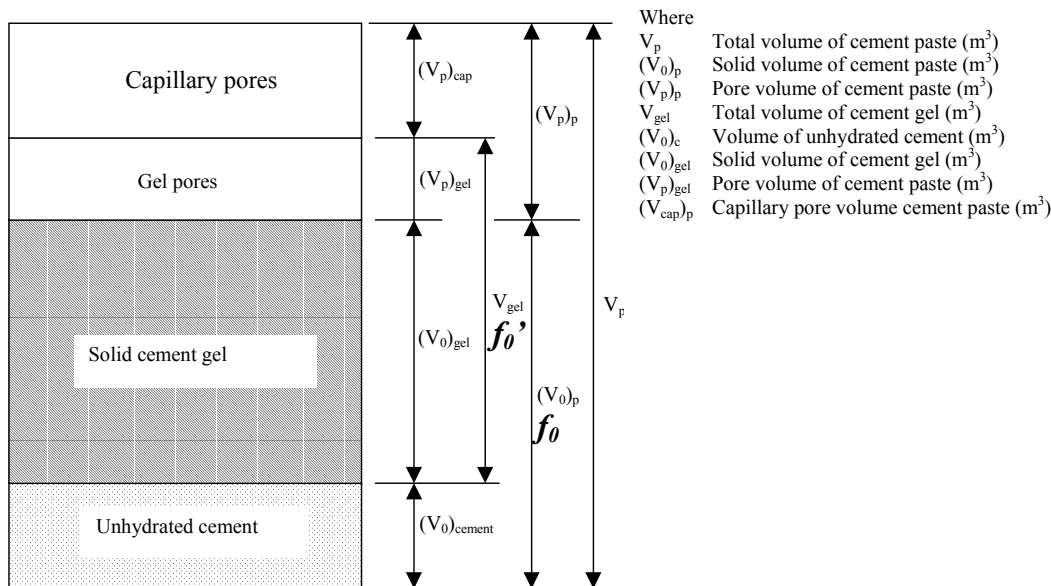


Figure 7.10 Schematic volume fractions in cement paste

The “fictitious” strength is in alternative 1 the strength of the solid phase without pores and in alternative 2 the cement gel with gel pores included. Because the fictitious strength in the second alternative includes gel pores it should be lower than in the first alternative.

In Figure 7.11, calculations of the compressive strength as a function of w/c ratio are shown for the strength-structure relations described by alternative 1 and 2 above. The parameters K_1 and K_2 are both chosen to 2.5. In the figure are also shown results from a laboratory test on the compressive strength of concrete made of Swedish standard cement and aggregate (Ysberg, 1979). No values of the fictitious strength are available in this work. The fictitious strength in the strength-structure relations is proposed to $f_0 = 210$ MPa and $f_0' = 100$ Mpa, so the curves fit well to the compressive strength given by Ysberg for w/c 0.7. It is interesting to note that the two alternative curves of the relations alternative 1 and 2, have very much the same shape. However, as it was assumed in Figure 7.9, the curves for the strength-structure relations in Figure 7.11, which describe the strength of the cement paste, are a bit steeper than the curve for concrete presented by Ysberg.

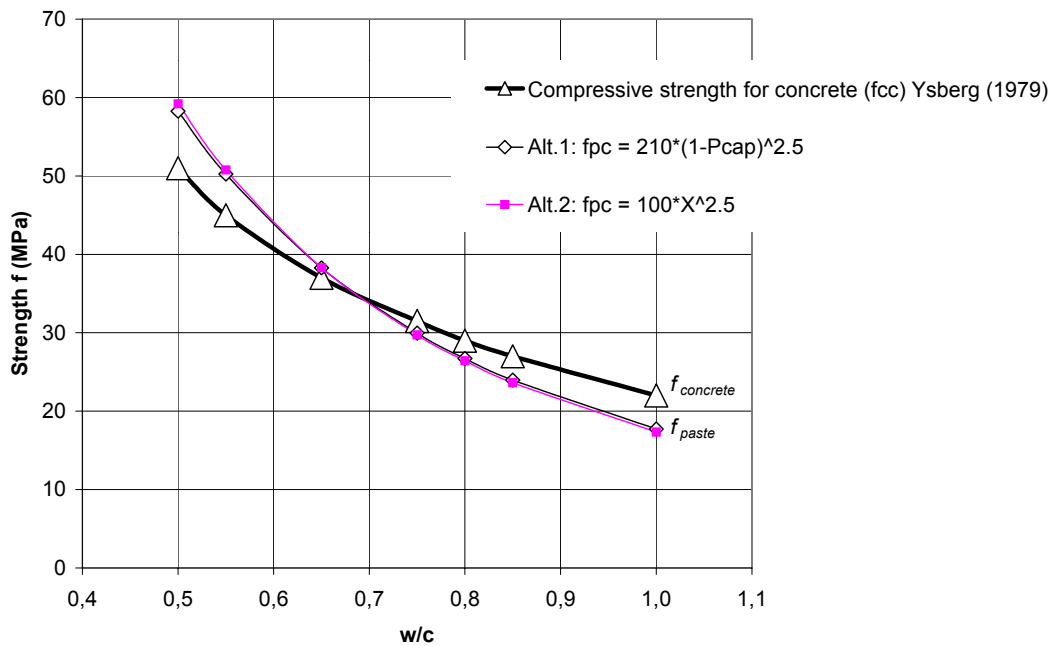


Figure 7.11 Calculated compressive strength relations (Alternative 1 and 2 from the text) compared with laboratory test results of compressive strength of Swedish concrete Ysberg (1979).

In Figure 7.12, the strength-structure relations for the cement paste are modified to fit the whole curve of the compressive strength presented by Ysberg. The modifications are only made by pure curve fitting in order to transform the calculated strength of cement paste to an assumed strength of concrete. With $a=1.2$ and $b=0.5$ in the model f_{cc} below, the relations turns out to be close to the compressive strength presented by Ysberg.

$$f_{cc} = f_{pc} \cdot a \cdot (w/c)^b \quad (7.44)$$

where f_{cc} = a model describing the compressive strength of concrete (Pa); f_{pc} = the compressive strength of cement paste by any of the strength relations alternative 1 and 2 described above (Pa); a = a curve fitting parameter, $a = 1.2$ to fit f_{cc} in Ysberg (1979); b = a curve fitting parameter. $b = 0.5$ to fit f_{cc} in Ysberg (1979).

The strength model may be used for comparison with experimental results in this work and for static checks of real structures in the future. For such use, more verification must, however, be done.

An important reflection is that the strength of the concrete is rather closely related to the strength of the cement paste. Is there, for example, a reduction by 10 % of the strength of the cement paste in the concrete (e.g. due to leaching), there will also be a reduction by 10 % of the strength of the concrete.

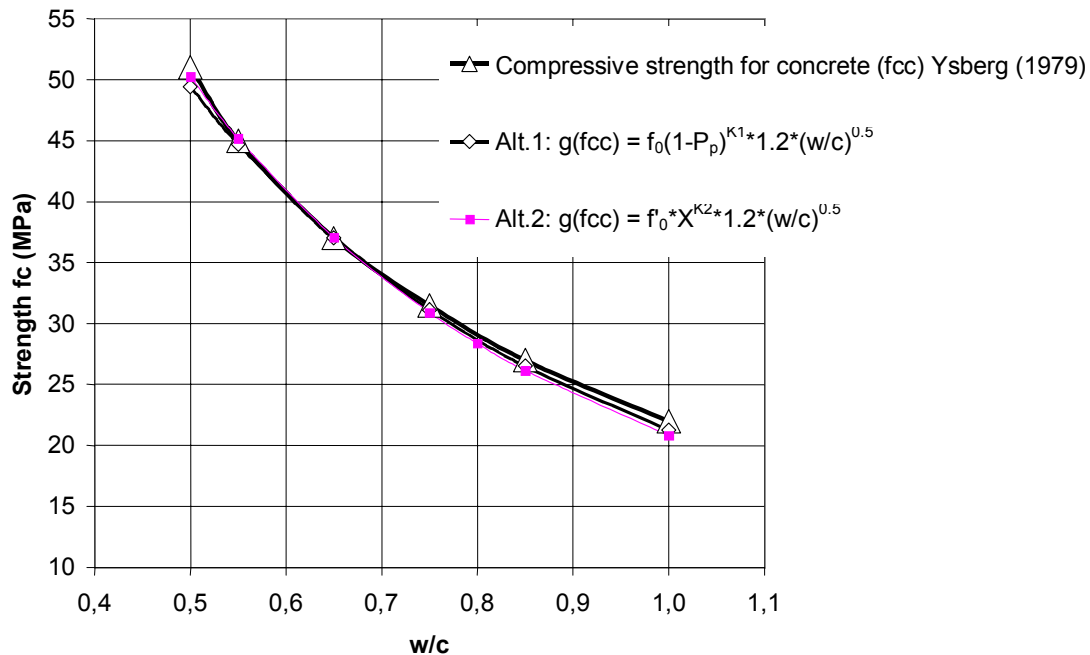


Figure 7.12 Modified compressive strength relations from figure 3-6 compared with laboratory test results of compressive strength of Swedish concrete Ysberg (1979).

7.8 Results from calculations with the macroscopic leaching model

Results using the presented model were calculated by a commercially available FEM-program (FEMLAB, see the reference manual available from Comsol AB in Sweden). The solver used in FEMLAB is the “time-dependent solver” in “General form” without any solver options such as “iterative solver” or “streamline diffusion”. The elements used in the FEM-calculations are “Lagrange – Quadratic” elements, i.e. three-node elements. A three-node element gives a more exact numerical solution than a two-node element does.

In the calculations, the parameters are chosen so that the leaching behaviour and leaching effects obtained are similar to those obtained for the leached specimens in the experiment “*Homogenous, steady-state percolation of water through concrete*” described in section 5.1 and 6.1. The balance equations used in the calculations are summarised in

Table 7.1. The parameters that are not varied across the different calculations are shown in Table 7.2 and those that are varied in Table 7.3. The results of the calculations are shown in Figure 7.14 to Figure 7.21. In the model, the leaching behaviour is governed by various physical variables, such as

1. the number of flow tubes that are connected through the specimens (*share*) and how coarse they are (ϕ_0)
2. the reduction coefficient r_w based the discrepancy between the water flow in real, narrow pores in concrete and large straight cylinders
3. the diffusion coefficients of the flow tubes and in the small pores in the solid (k_i and k_s)
4. how much of the leached material leads to an increase in the diameter of the flow tubes (*Part*)
5. how rapidly the dissolving reaction occurs which depends on how much of the solid has been leached away (*K1* and *K2*).

By varying these variables in a realistic way, different leaching behaviour is obtained. Calculated leaching is compared with the results from the experimental study in chapter 6. An objection to the calculations might be that the calculations is a form of “circle proof”, but it is only partly true. One can not choose the parameters no matter how. For example, by choosing *share*, ϕ_0 and r_w to certain values leads to a certain permeability at the start of the leaching. This value of permeability together with assumptions of the parameters k_i , k_s , *Part*, *K1* and *K2* gives a certain permeability over the time and a certain leaching behaviour that is compared with the experimental results.

The model is shown in Figure 7.13. In this example only Ca^{2+} - and OH^- -ions coming from CH and C-S-H are regarded. It is, however, possible to involve other ions and compounds too in the model.

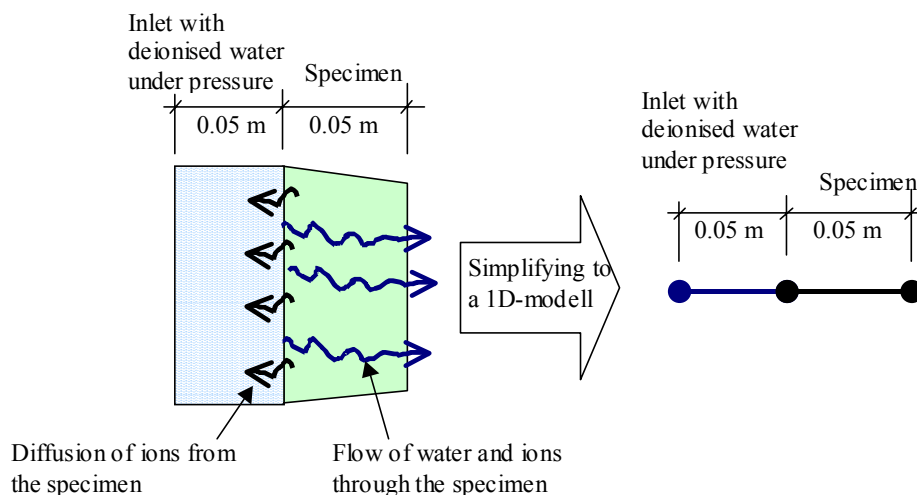


Figure 7.13 A fictive concrete specimen subjected at the one side to deionised water under pressure is modelled by use of a 1-dimensional FEM-modell.

Table 7.1 Balance equations for the domain studied in the FEM-calculation.

| Constituent | Equation | Boundary condition | Initial condition |
|--|--|---|---------------------|
| Water | $\nabla \cdot (v_w) = 0$ | $P_w = 60 \text{ m}$ | $P_w \cdot (1-x/L)$ |
| Ca^{2+} in pore solution | $\frac{\partial c_i}{\partial t} = \sum \hat{c}_{is} - \nabla \cdot (F_{iv} + F_{iw})$ | Diriclet $c=0$ at node 1 Neumann $q=g=0$ at node 2 | c_s |
| Ca^{2+} in solid | $\frac{\partial c_i}{\partial t} = -\sum c_{is}$ | Neumann $q=g=0$ at both node 1 and 2 | c_0 |
| $v_w = -k_w \nabla P_w; k_{w(t)} = (k_{w(t0)}) \cdot \left(1 + \frac{Part \cdot M \cdot (c_{s(t0)} - c_{s(t)})^2}{\rho \cdot share \cdot (V_{cap})_p} \right)$ $\hat{c}_i = n \cdot \frac{k_{is} \cdot \pi \cdot \phi_t}{\delta} \cdot (c_{is} - c_i); \quad \delta = \delta_0 \cdot \left(\frac{c_{s(t0)}}{c_{s(t)}} \right)^{K1} / K2$ | | | |

Table 7.2 Parameters that do not change during the calculations.

| M_{Ca} | M_{CH} | M_{CSH} | C | W/c | α | CSH | $Ca(OH)_2$ |
|--------------------------------|---------------------|---------------------|---------------------|-------------------|--------------------------------|--------------------------------|--------------------------------|
| Kg/mole | Kg/mole | Kg/mole | Kg/m ³ | - | - | Kg Ca/m ³ | Kg Ca/m ³ |
| 0.040 | 0.074 | 0.342 | 240 | 0.80 | 0.90 | 49.9 | 28.8 |
| CAF | c_0 | $CH-stop$ | C_s | ρ_s | $(V_p)_p$ | $(V_{cap})_p$ | V_p |
| Kg Ca/m ³ | Mole/m ³ | Mole/m ³ | Mole/m ³ | Kg/m ³ | m ³ /m ³ | m ³ /m ³ | m ³ /m ³ |
| 19.2 | 2668 | 1968 | 20 | 2300 | 0.151 | 0.108 | 0.269 |
| V_{air} | L | V_c | A_c | P_w | δ_0 | | |
| m ³ /m ³ | M | m ³ | M ³ | m | m | | |
| 0.008 | 0.05 | $9.3 \cdot 10^{-4}$ | $1.9 \cdot 10^{-2}$ | 60 | 10^{-7} | | |

Table 7.3 Parameters that are changed from one calculations to another. The symbol “-“ means that the same value is used as in the case (above) preceding it.

| Cal. No. | Diameter ϕ_0 | share | Nos. of tubes n | k_i | k_s | Part | r_w | $K1$ ₁₎ | K2 | a | k | k_w |
|----------|-----------------------------------|-----------|--|-------------------|-------------------|------|-----------|--------------------|----|-------------------|-------------------|--------------------|
| | m | - | | m ² /s | m ² /s | - | - | - | - | - | - | m/s |
| 1 | $10^{-6}/5 \cdot 10^{-6}/10^{-5}$ | 10^{-3} | $4 \cdot 10^7/2 \cdot 10^6/4 \cdot 10^5$ | 10^{-10} | 10^{-12} | 0.1 | 10^{-2} | 100 | 3 | $3 \cdot 10^{-2}$ | $2 \cdot 10^{-3}$ | $6 \cdot 10^{-12}$ |
| 2 | - | - | - | - | 10^{-13} | - | - | - | - | - | $2 \cdot 10^{-4}$ | - |
| 3 | $5 \cdot 10^{-5}$ | 10^{-4} | $5 \cdot 10^4$ | - | 10^{-12} | - | - | - | - | $3 \cdot 10^{-1}$ | $9 \cdot 10^{-7}$ | $8 \cdot 10^{-11}$ |
| 4 | $10^{-6}/5 \cdot 10^{-6}/10^{-5}$ | 10^{-3} | $4 \cdot 10^7/2 \cdot 10^6/4 \cdot 10^5$ | - | 10^{-13} | - | - | 1 | 5 | $3 \cdot 10^{-2}$ | $2 \cdot 10^{-4}$ | $6 \cdot 10^{-12}$ |

¹⁾As long as there are CH left in the solid ($c_s > CH-stop$) is K2 set to 1. K1 is set to the value in the table when no CH is left.

Figure 7.14 shows, for the calculation number 1, the calculated concentration of calcium in the inlet water and in the pore solution of a fictive specimen. By inlet water is meant the water volume that is found just ahead of the specimen. This water is deionised when it is let into the test equipment and is subjected to an overpressure corresponding to a 60 m hydraulic head. Due to the sharp gradients in the ion concentration between the pore solution in the specimen and the inlet water, the

diffusion of ions into this inlet water is high. The figure shows how the concentration of calcium in the pore solution is reduced at the upstream end of the specimen when calcium is transported to the inlet water by diffusion.

Six months after the fictive leaching began, the pore solution at a depth of approximately 6 mm has begun to lose ions, the “leaching front” in the pore solution having extended 6 mm into the specimen. At 36 months, the “leaching front” in the pore solution has extended approximately 20 mm into the specimen. During this time, the concentration of Ca in the inlet water has changed. Initially, the concentration is zero (deionised water). The concentration increases then as ions diffuse into the water. In the model, the ions in the inlet water diffuse away from right to left because there is a boundary condition of zero-concentration at the left side.

(Note: This zero condition corresponds approximately to the inlet water being “flushed” once or twice a week in the real experiment. After each flushing, the inlet water was again very free of ions. Approximately the same amount of calcium disappears through the left side of the inlet water as did in flushing in the experiments. Whereas the calcium was removed instantly flushing, however, it is removed only slowly by diffusion in the model).

After some time however, the calculated concentration in the inlet water in the model is reduced because of the diffusion of ions from the specimens not being large enough to compensate for the loss by diffusion through the left side of the inlet water. The upstream end of the specimen becomes leached and the thickness of the diffusion layer increases. When the diffusion layer increases, diffusion from the specimen to the inlet water decreases.

Accordingly, at 6 months the concentration of Ca in the inlet water was approximately 0.4 g/l, whereas at 36 months the concentration is approximately 0.1 g/l. The figure also shows (as indicated above) that in only the first 20 mm are the pores not saturated with calcium, the pores in the rest of the specimen in the downstream direction being saturated. Thus, the water that percolates through the specimen and out through the right side is saturated with calcium. Since, for many of the specimens in the experiment described earlier in this report, the percolated water that was collected was saturated with calcium. Therefore, the calculated results do not appear unrealistic. The fictive specimen shown in Figure 7.14 was so tight (permeability $k_w = 6 \cdot 10^{-12}$ m/s) and the concentration gradient of ions so large on the upstream surface that the major transport of calcium by the initial leaching was by diffusion, only a smaller amount being by convection, as indicated in the figure.

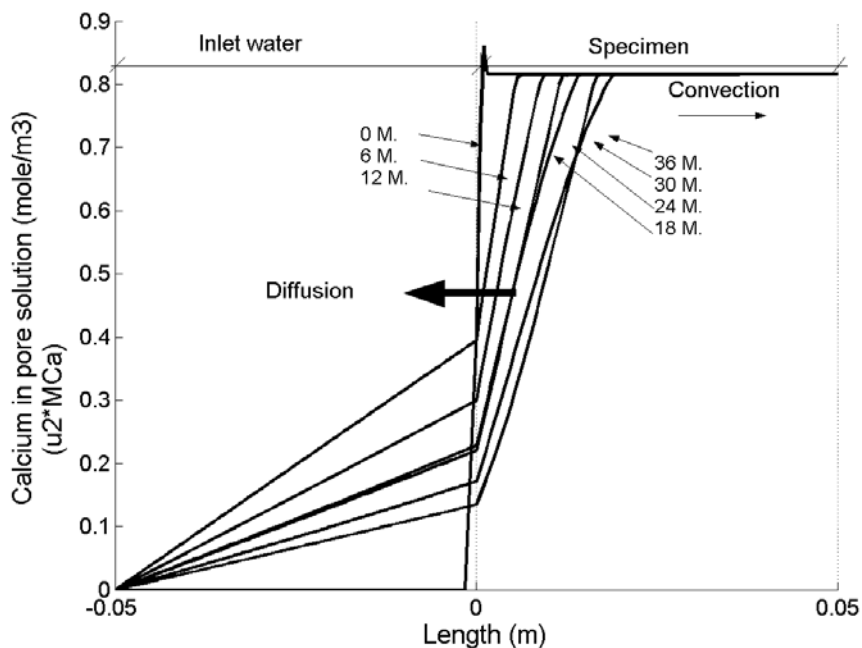


Figure 7.14 Calculated concentration of calcium in the inlet water (to the left) and in the pore solution within the specimen (to the right). 0 M., 6 M., etc. indicate the result at time zero, 6 months, etc. after the calculations of leaching were begun. “Diffusion” = most of the calcium that was leached diffused upstream to the inlet water. “Convection” = a certain amount of the calcium that was leached was transported away by the water flow. “Length 0” = the upstream end of the specimen and “Length 0.05” = the downstream end.

Figure 7.15 shows the calculated concentration of calcium in the solid material in the fictive specimen. Due to the high level of diffusion, as described in connection with Figure 7.14, the solid is heavily leached at the upstream end. Later on in the leaching the convective flow of ions also transports a large part of the calcium through the specimens and out through the downstream end. In the latter case, the deionised water dissolves calcium at the upstream end and transports it through the specimen under saturated conditions. No further calcium is dissolved by the water along the specimen since the concentration of the flowing water is at the saturation level. On the upstream surface the concentration of Ca decreases from 107 kg/m^3 down to approximately 25 kg/m^3 . After 36 months of leaching, the leaching front in which calcium has been leached from the solid, extends into the specimen to a depth of 20 mm. This loss of calcium m_{loss} corresponded approximately to the following amount:

- $m_{loss} = V \cdot \Delta c = \pi \cdot \phi^2 / 4 \cdot L / 2 \cdot (c_0 - c_i) = \pi \cdot 0.155^2 / 4 \cdot 0.020 / 2 \cdot (107 - 25) = 0.015 \text{ kg} = 15 \text{ g}$

The division of L by 2 is because of the shape of the leached front, as shown in Figure 7.15, the calcium decreasing in an almost linear manner from 107 to 25 kg/m^3 . The loss of calcium $m_{loss} = 15 \text{ g}$ is due both to diffusion upstream and to convection downstream, where

- Diffusion upstream: $m_{loss,diff} \approx$ (see Figure 7.16) $\approx (1 - 0.15) \cdot 10^{-6} \text{ g/s} \cdot 2.6 / 2 \cdot 10^6 \text{ s} + 0.15 \cdot 10^{-6} \text{ g/s} \cdot (93.3 - 2.6) / 2 \cdot 10^6 \text{ s} = 7.9 \text{ g}$

- Convection downstream: $m_{loss,conv} \approx$ (see Figure 7.17) $\approx 1.02 \cdot 10^{-7} \text{g/s} \cdot 2 \cdot 10^7 \text{s} + (1.02 + 1.42) / 2 \cdot 10^{-7} \text{g/s} \cdot (9.3 - 2) \cdot 10^7 \text{s} = 10.9 \text{ g}$
- Total leaching: $7.9 + 10.9 = 18.8 \text{ g} \approx 15 \text{ g} = m_{loss}$ (the curve in Figure 7.15 for 36 M. is not exactly linear)

It can be concluded that when the major part of calcium loss begins, the loss is by diffusion in the upstream direction, but that in time, when the diffusion layer has increased at the upstream end and the permeability has increased, the major part of the loss is by convection. The total loss of calcium during the 3-year period for which it was calculated is due more to convection (10.9 g) than to diffusion (7.9 g).

It can also be concluded that the amount of loss due to diffusion and convection corresponds closely to the experimental results. Note for example, for specimen 0.80a:4 that in Table 6.4 the loss by diffusion was estimated to have been $m_{loss,diff} = 11.0 \text{ g}$ and by convection $m_{loss,conv} = 14.7 \text{ g}$. Although the values are slightly higher than in the calculation example provided above, in view of the fact that the specimen was leached for 3.7 years, which is longer than the 3 years in the calculation example presented, the agreement can be seen as close.

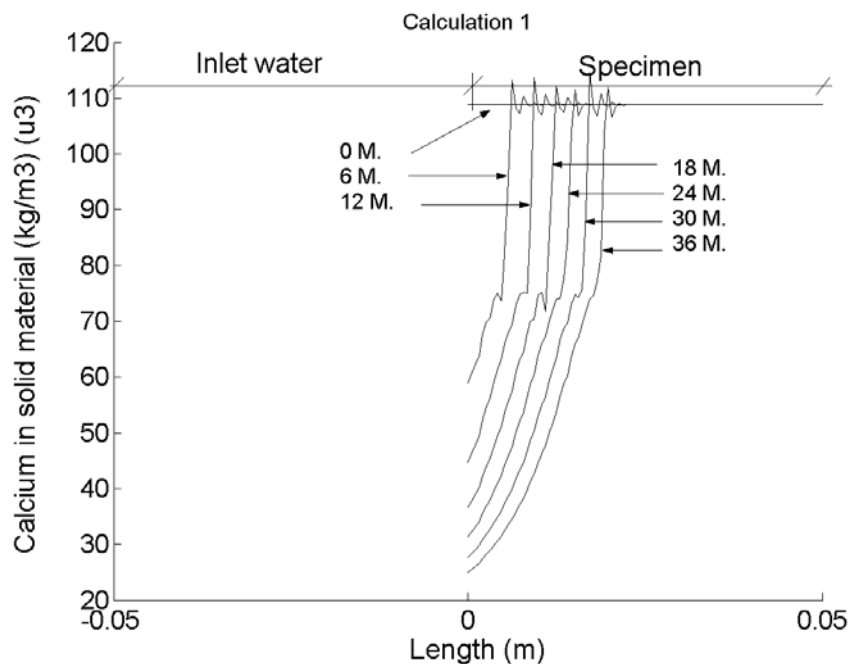


Figure 7.15 Calculated concentrations of calcium in the solid material in the specimen (to the right).

Figure 7.16 shows the leaching rate of calcium that diffuses to the inlet water from the fictive specimen. As can be seen, the diffusion rate at the start of the leaching is high, but it decreases rapidly at an early stage of leaching. This is caused by the fact that the concentration gradient is very large initially when the inlet water is still deionised and the diffusion layer on the upstream end is still thin, which results in a high diffusion rate. When the diffusion layer increases and the inlet water becomes “polluted” by dissolved calcium ions, diffusion rate decreases.

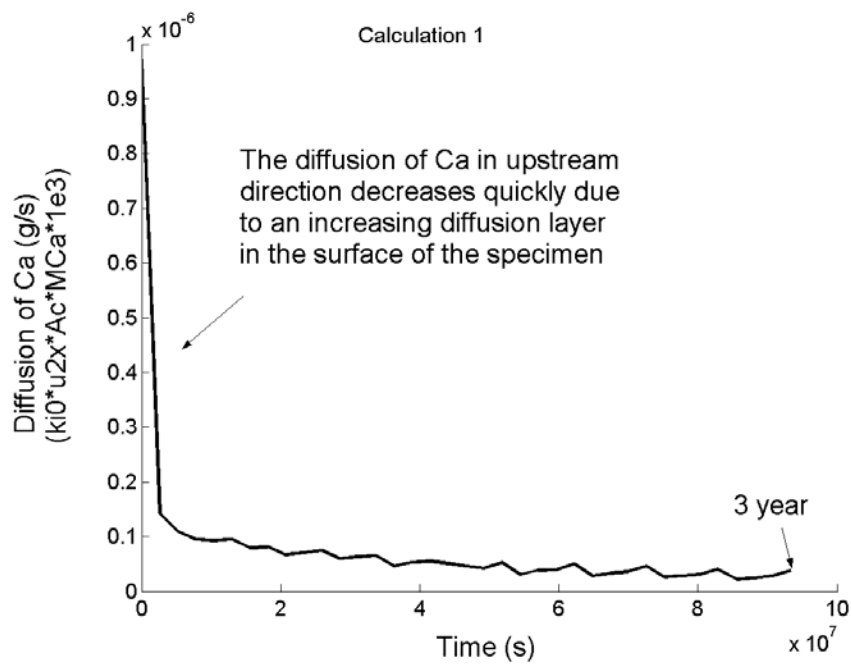


Figure 7.16 Calculated diffusion of calcium from the specimen into the inlet water over time.

Figure 7.17 shows the convective flow of calcium out of the specimen at the downstream end. This convection of calcium is governed by the flow of water. The flow of water increases with time, since the permeability increases as solid material is leached away. Comparing Figure 7.16 and Figure 7.17 shows that at the start of leaching the diffusion in the upstream direction is approximately $1 \cdot 10^{-6}$ g/s, whereas the convection is approximately $1 \cdot 10^{-7}$ g/s, so that $1/10^{\text{th}}$ of the total leached calcium flows with the water in a downstream direction, whereas the rest diffuses upstream. After 3 years of leaching, however, the diffusion has decreased to approximately $0.5 \cdot 10^{-7}$ g/s, whereas the convective flow has increased to approximately $1.4 \cdot 10^{-7}$ g/s.

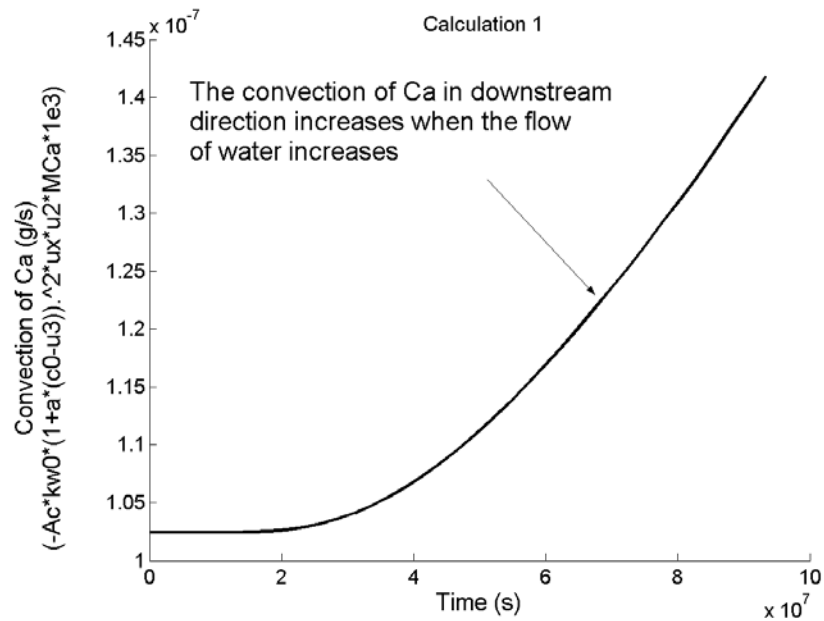


Figure 7.17 Calculated convection of calcium from the specimen by the flow of water downstream.

Figure 7.18 shows the increase in the calculated permeability as the specimens lose solid material from the walls of their flow tubes, the permeability increasing most at the upstream end, from which most of the solid material was leached.

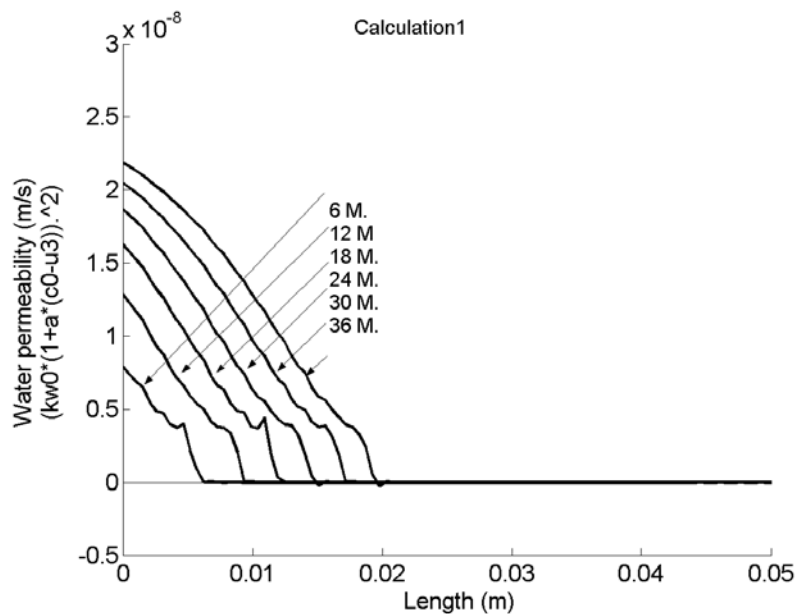


Figure 7.18 Calculated water permeability along the 0.05 m thick specimen at different times after leaching had started.

Figure 7.19 and Figure 7.20 show the calculated concentrations of calcium in the pore solution and in the solid material of the fictive specimen for different choices of the

variables shown in Table 7.3. The difference between Calc. 1 and Calc. 2 is that the diffusion coefficient k_s for the small pores of the solid is set to 10^{-12} m²/s in Calc. 1 and to 10^{-13} m²/s in Calc. 2. This leads to the calcium not being able to diffuse as rapidly to the walls of the flow tubes from the interior of the solid. This leads to the concentration of calcium in the flow tubes decreasing to below the saturation point when the water transports Ca in a downstream direction. When the concentration decreases below the saturation point, calcium is dissolved from the walls of the tubes in accordance with equation (7.36). Because of the dissolving being slower reaction in Calc. 2 than in Calc. 1, the concentration of calcium decreases to below the saturation point at a distance farther into the specimen in Calc. 2 than in Calc. 1. This leads to calcium being leached from the solid material a greater distance into the specimen in Calc. 2 than in Calc. 1, as can be seen in Figure 7.20.

In Calculation 3, there are fewer and larger flow tubes than in the other calculations. This leads to the dissolving reaction being less and the flow of water greater (higher permeability). This, in turn, as can be seen in Figure 7.19 and Figure 7.20, leads to the flow tubes becoming totally depleted of calcium ions ($c_{Ca} \approx 0$) and the solid material being leached homogeneously throughout the specimen, the remaining concentration of Ca being approximately 82 kg/m³. A similar behaviour was observed in the experiments for example for specimens 0.80b:1, 0.80b:5, 0.80b:7 and the specimens with a w/c-ratio of 1.29.

As indicated above, the solubility of C-S-H varies with how much calcium it contains. The solubility of C-S-H differs also somewhat in literature sources. To see the influence of the solubility of the C-S-H a calculation 4 was performed. Calculation 4 is identical to Calculation 2, except that the coefficient K1 in equation (7.36) is set to 1 instead of 100. The lower value of K1 means that there is no distinct level at which the dissolving of calcium from CH and C-S-H decreases, as there is when K was set to 100. The dissolving rate decrease, however, a bit more rapid, K2 is set to 5 instead of 3.

The only sign of the dissolving of Ca from the calcium-pores of C-S-H being slower than when CH still left is the coefficient K2, which is set to 5 in Calculation 4. Figure 7.19 shows that the leaching behaviour obtained for Calculation 1 and for Calculation 4 are about the same. More calcium is taken from the upstream end of the specimen in Calculation 4 than in Calculation 1.

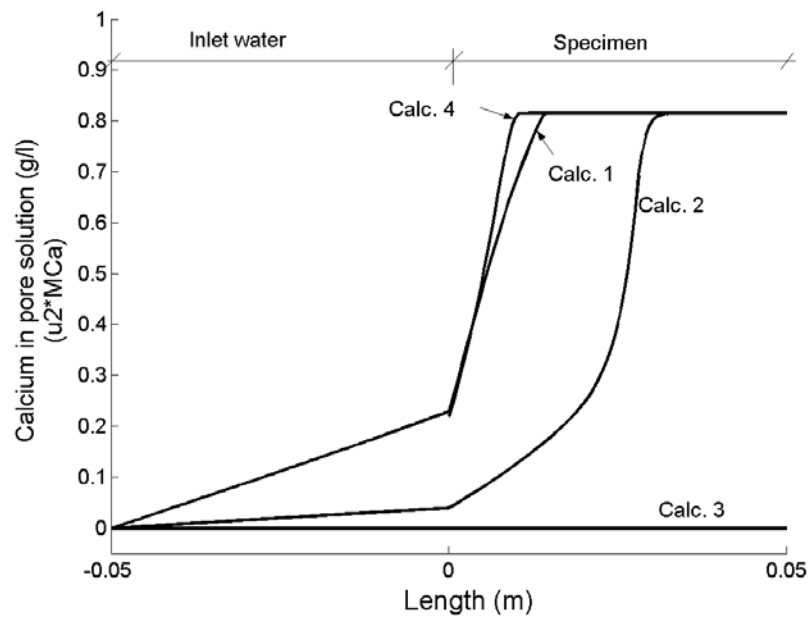


Figure 7.19 Calculated concentrations of calcium in the pore solution of the specimen for the four different calculations 1, 2, 3 and 4 at a time 2 years after leaching began.

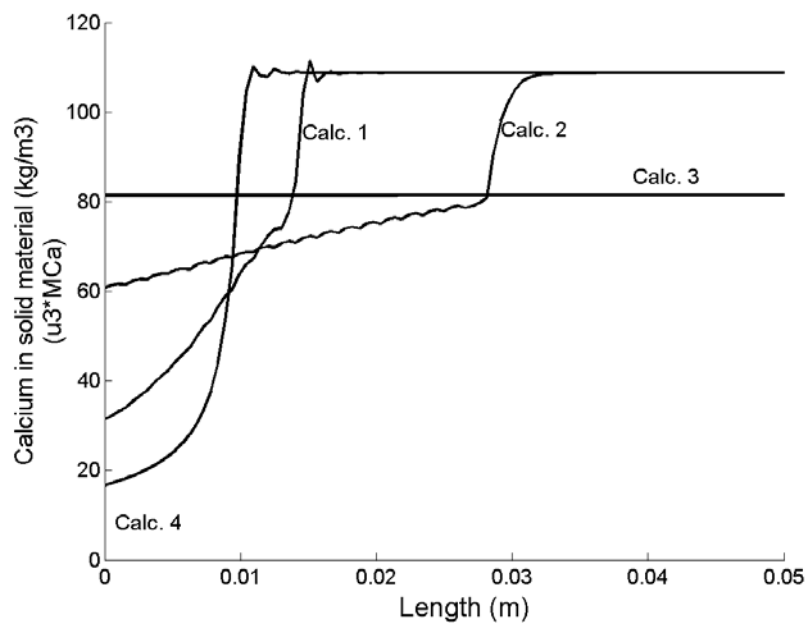


Figure 7.20 Calculated concentration of calcium in the solid material of the specimen for the four different calculations 1, 2, 3 and 4 at a time 2 year after leaching began.

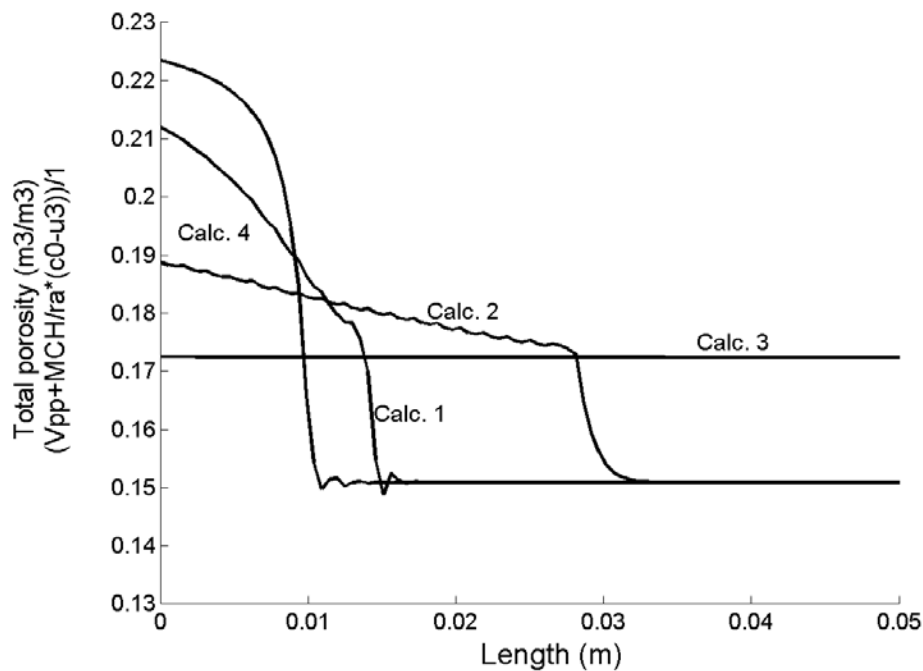


Figure 7.21 Calculated total porosity of the specimen for the four different calculations 1, 2, 3 and 4 at a time 2 year after leaching began.

7.9 Conclusions

The results of the calculations reported in sections 7.4 and 7.5 are encouraging. It seems as a FEM-formulation of the balance equations for water and for ions as described in equations (7.2) to (7.5) and equations (7.8) to (7.10) represents a suitable way of modelling leaching processes. The constitutive relationship that was assumed in this chapter and was that used in the balance equations, however, can be investigated further. An advantage of using such basic balance equations in general FEM-programs is that it enables the geometry of specimens or structures and changes over time to be calculated under almost all leaching conditions. Thus, the same balance equations and constitutive relationships can be used for different specimens and structures.

8 Methods of analysis of the effect of leaching on the durability of existing concrete dams

8.1 INTRODUCTION

Many concrete structures such as bridges and dams are located in harsh climates, making them prone to environmental attacks. For predictions of their remaining lifetime to be made with any certainty, the bearing capacity (R) needs to be sufficiently larger than the load effects (S) expected to occur during the lifetime of the structure. Estimates of R confronts the engineer with difficulties, however, since the degradation model (D) assumed need to be appropriate, and statistical variations in the parameters involved need to be taken into account.

8.2 Assessment procedure

A procedure for the assessment of the structure stability of degraded concrete structures, based on the Contecvet-manual (2001), is proposed in Figure 8.1. The following procedures, performed stepwise are involved:

- starting with a preliminary qualitative assessment, based on visual inspections, and simple engineering judgments of structural safety;
- thereafter making preliminary quantitative assessments using calculations based on basic empirical data obtained from investigations of the structure.

If the safety level is found to be only borderline or less, further action can be taken, such as

- a detailed assessment of the situation with use of data obtained by more detailed investigations of the structure, such as measurements of the residual strength in critical sections, measurements of ongoing corrosion, measurements of degree of leaching, etc.
- carrying out of repair.
- replacing the structure

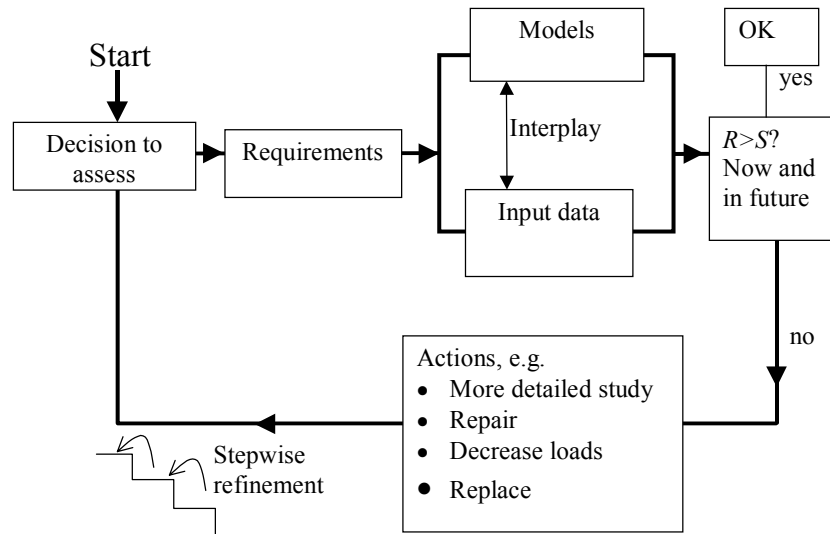


Figure 8.1 A proposed procedure for the assessment of degraded concrete structures.

Each step of refinement of assessing the structure follows a new cycle in the figure. The reason for carrying out an assessments could be, for example, that earlier assessments had shown the safety level to be low, that an accident had occurred, that environmental damage is considered to have gone too far, creating of new guidelines for structural design, new owners having taken over, etc. The requirements placed on the structure may be set either by the owner or by society. Performing safety calculations requires that certain *basic data* (ISO 1998) be estimated, such as geometric values, material properties, load characteristics, and the like. These estimates can be ones based on literature, on site-specific documents (such as “as-built drawings”, test results, previous assessments, repair or damage) or on investigations of material properties, load characteristics, and the like that have been carried out recently.

It is essential that the gathering and evaluation of such basic data involve an interplay between the material engineer and the structural engineer and that certain simple calculations of static relationships be performed before extensive investigations are carried out. It is important to study the special characteristics of each structure. A buttress dam in Figure 8.2 is shown as an example. It has certain sensitive points that need to be taken account of in further investigation:

- (A) If the reinforcement bars are corroded on the upstream surface of the front slab supported by the pillar, they may be unable to withstand the large tensile force F_s there or, if the concrete on the downstream side of the slab is leached, the concrete may be unable to withstand the compression stress.
- (B) If the upstream surface of the front slab is leached, the reinforcement bars may not be bonded sufficiently to the concrete.
- (C) If the pillar has been damaged by frost or leaching the compression forces may not be transferred to the ground.
- (D) If there has been leaching or frost damages in the pillar at its foot, the tensile strength of the concrete is lowered.

Properties of major concern for (A) are the tightness of the concrete, the degree to which corrosion has been propagated and the compressive strength of the concrete. The

property of major concern for point (B) is the bond strength between the concrete and the reinforcement bars. For point (C) it is the compressive strength of the concrete and for point (D) the tensile strength of the concrete. The modulus of elasticity (E_c), which is basic to the possible re-distribution of internal stress, is of central importance to all statically non-determined structures. All tests made on the structure should aim at determining properties of concrete and reinforcement required for an analysis of the structure capacity and safety of the entire structure in all its parts. All samples tested should be as representative as possible with regard to location, direction of loads and possible damage. Priority needs to be given to investigating damaged parts with small structural margin.

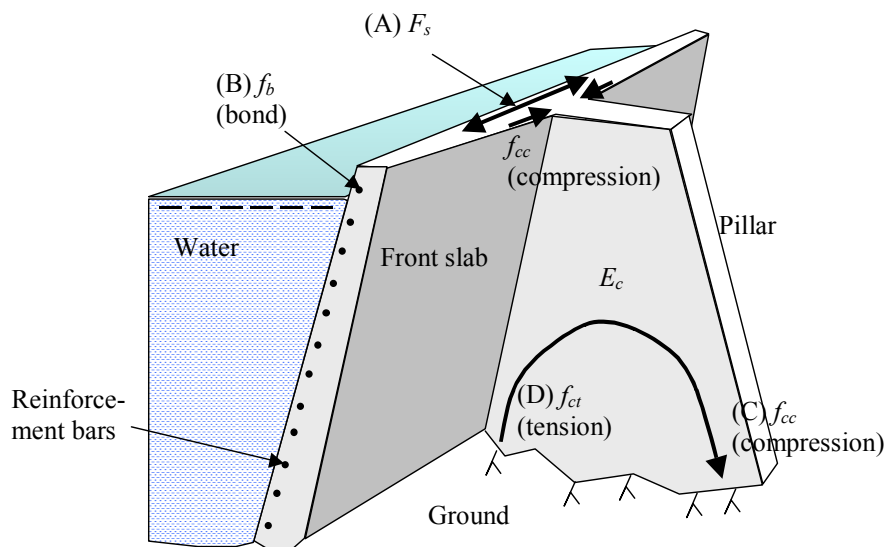


Figure 8.2 Static and environmentally sensitive parts of a buttress dam.

8.3 Service life predictions

In assessing the safety of real structures, one needs to estimate both the load resistance R and the load effects S . Figure 8.3 shows a fictive assessment performed at time t_1 with the goal of estimating the structural safety both at time t_1 and in the future. The estimate of R and S at time t_1 can be obtained in various ways, the following being examples:

- If a material property that is sought cannot be investigated in the current structure, the value of that property at time t_1 can be assumed in a very rough way on the basis of an empirical model based on some other test or tests, on other structures, exposed to similar environmental conditions (see examples in the manual Contecvet 2001);
- If the material property sought is known from tests conducted on the current structure at time t_0 , the value of that property at the future time t_1 can be assumed by use of a degradation model (D), using input data from the test at time t_0 ;
- If the material property sought is known from tests conducted on the current structure at time t_1 , the estimate of R and S and thus the estimate of whether $R > S$ can be calculated directly.

The estimate of the values R and S and thus the estimate of structural safety of the future is difficult, since there must be a realistic degradation model (D). The greater the number of test values that are available from different times in the history of the object in question, the easier it is to predict the future.

Fictive test values from samples taken from a fictive structure at times t_0 and t_1 are shown in Figure 8.3 (a). Such values usually have a distribution that is transformed to characteristic values to be used in assessments by use of some statistical model, such as $f = m \pm k \cdot s$, where f = property; m = mean value; k = a constant depending on the maximum tolerable error %. K is also a function of the number of specimens; and s = standard deviation.

The great difficulty lies in predicting a probable degradation curve (D), see the curve in Figure 8.3 (b). Questions to be answered are, what degradation mechanisms are present; what variables influence degradation; when does degradation start; at what rate does degradation occur? Is there any synergy between different degradation mechanisms? What variation in degradation is there over time.

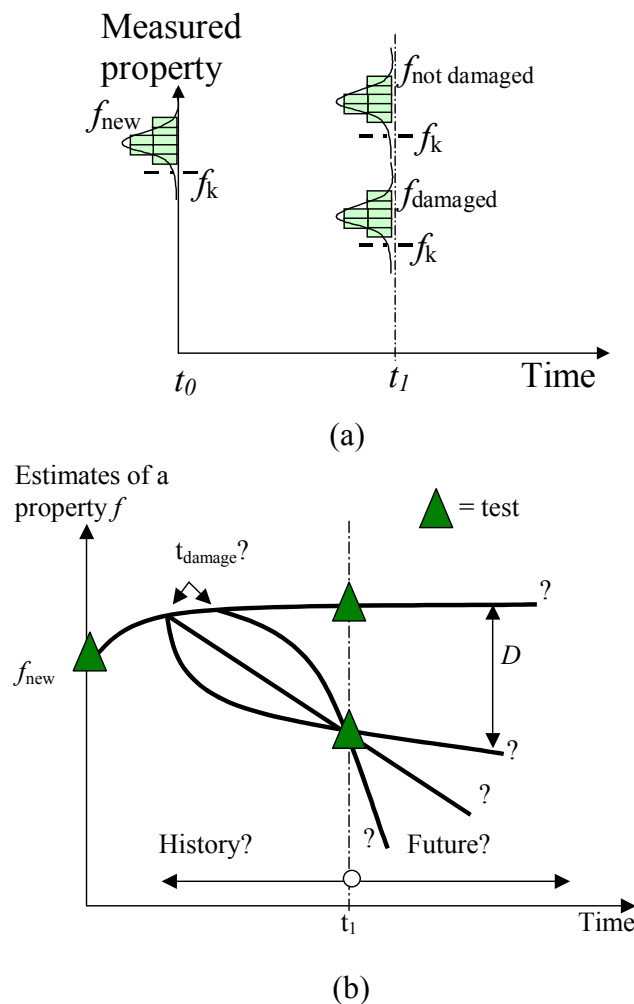


Figure 8.3 Principles involved in estimating degradation by use of test values and degradation models.

Statistical variations in R and S are commonly considered by use of either probabilistic methods or semi-probabilistic methods (e.g. the *partial coefficient method*). Figure 8.4 shows the principles involved in computing a life-curve for a fictive structure. The structure is calculated by use of the partial coefficient method to fail at time t_γ and by use of a probabilistic method to fail at time t_p . The relation found between t_γ and t_p in the example is only fictive. With use of the same statistical data $\in N(m, \sigma)$ and if the data is independent of each other and if the same safety index β is used, the two times should be the same.

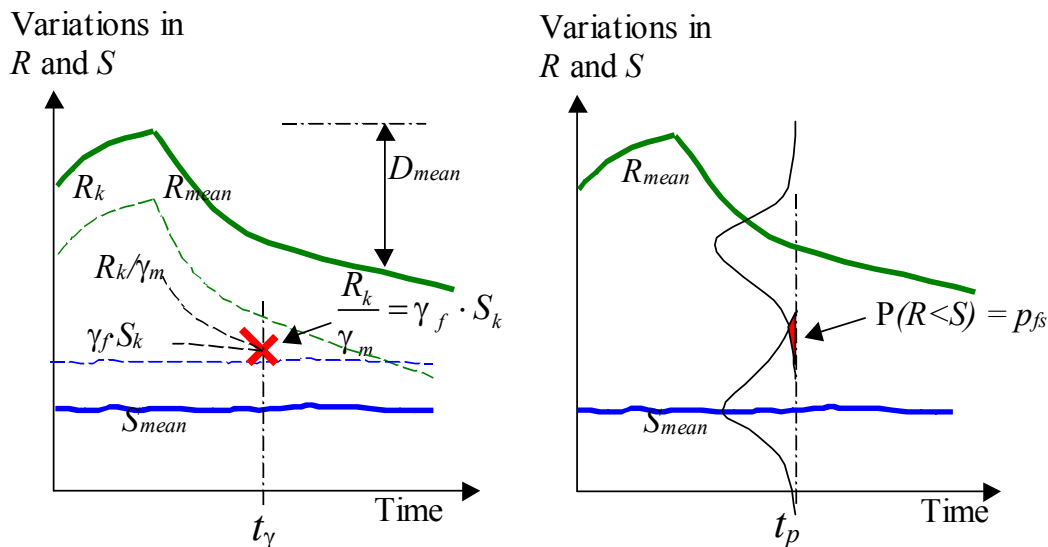


Figure 8.4 Principles involved in using a semi-probabilistic method such as the *partial coefficient method*, and a probabilistic method for estimating the residual life of a structure, where R = resistance; S = load effect; index k = characteristic value; γ = partial (uncertainty) factor; P = probability; and p_{fs} = specific probability.

Estimating if the condition $R > S$ is fulfilled requires that the distribution of the parameters involved be largely known, especially with use of the pure probabilistic method. For new structures built in a standardized way, the partial coefficients and the way they were calculated are often given in terms of a national or international code. For older structures, there may be no such help. The partial coefficient method is usually less suitable than probabilistic methods for analyzing time-dependent degradation problems in existing structures, since the determination of the partial factors is difficult.

Sarja and Vesikari (1996) described an approach of assessing older structures by introducing a time safety factor γ_t and by employing an assumed *mean* degradation D_{mean} value. If only the mean degradation is used, 50% of all structures are predicted to fail before the intended life t_m is terminated. By use of certain information regarding the variance of D_{mean} a time safety factor γ_t can be calculated. By use of this time safety factor, a design life t_d can be determined as $t_d = t_m / \gamma_t$ (Figure 8.5).

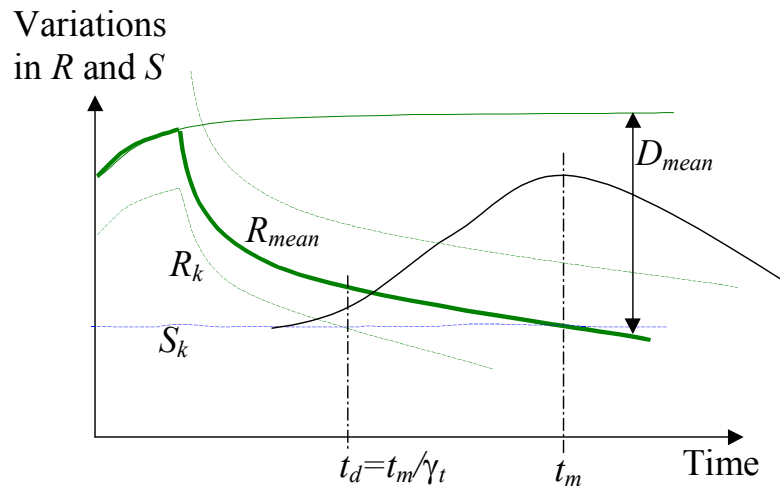


Figure 8.5 The principles involved in use of the *time safety factor* γ_t (b) (Sarja & Vesikari 1996) in calculating the safety of a structure.

Another useful method for assessing older structures is the Hasofer-Lind method (Schneider 1992). In this method a *safety index* β is used. This index is linked to the failure probability p_f by use of the standard normal distribution:

$$\beta = F^{-1}\{p_f\} \quad (8.1)$$

where the *failure probability* p_f is written as:

$$p_f = P[R - S \leq 0] \quad (8.2)$$

where β = safety index; R = strength; and S = load effect. A structure can be considered safe if the safety index β is above a certain level β_0 that is decided upon and which depends on the consequences of failure

$$\beta \geq \beta_0 \quad (8.3)$$

8.4 Example of the calculation of the durability of the front slab in a buttress dam

8.4.1 Introduction

The problem is to estimate when the bond strength will become lower than the bond stress, applied to the reinforcement bars at location (A) in a front slab in a buttress dam, see Figure 8.2 and Figure 8.6. The slab is assumed to serve as a cantilever-beam exposed to only hydraulic water pressure. The bending moment in the beam is taken up by tensile forces in the reinforcement and by a compression force in the concrete. It is important that the bars be bonded to the concrete so that the tensile force can be transferred from the bars to the concrete. Many different degradation mechanisms may affect the concrete in such a location either alone or together. In this example only leaching is considered.

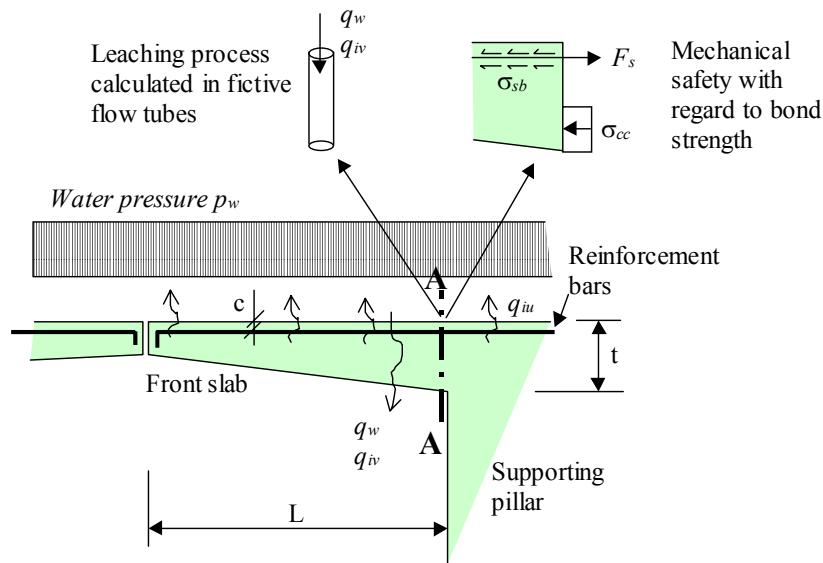


Figure 8.6 Calculations carried out on a fictive front slab in a buttress dam, where q_w = flow of water; q_{iu} = diffusion flow of dissolved ions; q_{iv} = convective flow of dissolved ions; F_s = force in reinforcement bars; σ_{cc} = concrete stress; and σ_{sb} = bond stress.

The bond stress between the reinforcement bars and the concrete is calculated as

$$\sigma_{sb} = \sigma_s \cdot \frac{\pi \cdot \phi^2}{4} / (\pi \cdot \phi \cdot L_b) = \sigma_s \cdot \frac{\phi}{4 \cdot L_b}; \quad \sigma_s = \frac{M}{z \cdot A_s}; \quad (8.4)$$

$$M = \frac{p_w \cdot L^2}{2}; \quad p_w = \rho_w \cdot g \cdot h; \quad z = 0.9 \cdot (t - c)$$

where σ_{sb} = bond stress between reinforcement and concrete (Pa); σ_s = stress in the reinforcement bars (Pa); ϕ = diameter of the reinforcement bars (m); L_b = the anchorage-length (m); M = bending moment of the concrete slab (N·m); z = internal lever between the reinforcement bars and the resultant of the compression force in the concrete (m); A_s = area of the reinforcement bars (m²); p_w = the hydraulic pressure applied (N/m²); L = length of the cantilever (m); ρ_w = density of water (1000 kg/m³); h = depth of water (m); t = thickness of the concrete slab at the abutment (m); c = thickness of the cover (m).

The bending moment is slowly increased since the pore pressure becomes gradually higher on the upstream part of the slab when this part is leached and the permeability in this part increases. This effect is, however, assumed to be insignificant. Therefore, it is omitted here.

The tensile force is carried by two types of reinforcement bars, one type (F_{s1}) that is as long as the cantilever plus an anchorage-length L_b and one other type (F_{s2}) that is only about half the length of the cantilever. The bond stresses and strength of reinforcement bars of type 2 is calculated in the present example, see Figure 8.7. The anchorage-length L_b is the part of the reinforcement bars that lies on the outside of the “displaced force-curve”. The displaced force-curve is the tensile force-curve in the reinforcement bars, adjusted for inclined shear cracks that can occur.

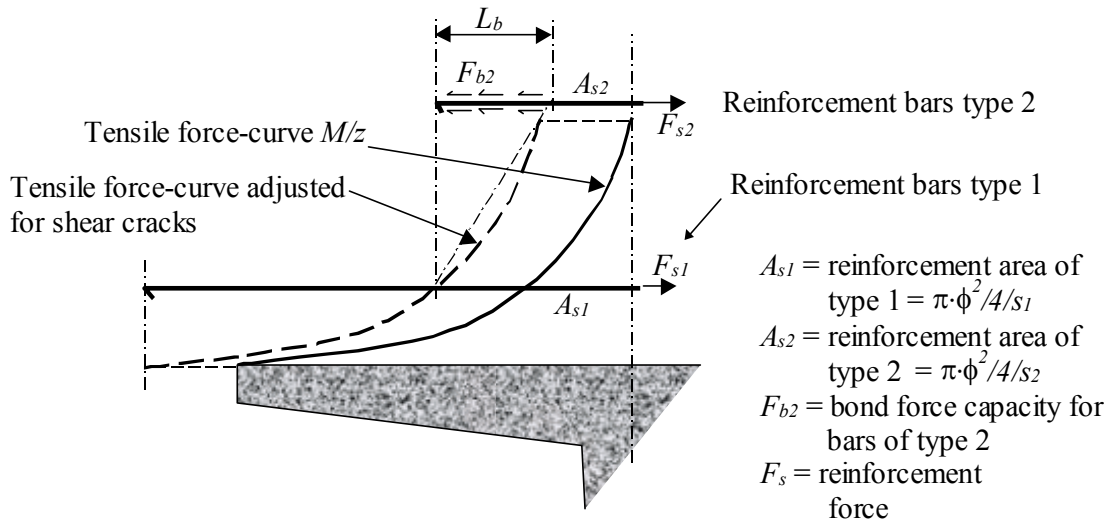


Figure 8.7 The tensile force-curve with and without adjustment for shear cracks. Reinforcement bars are of two lengths, adjusted to the adjusted tensile force curve. The bond stress and strength of reinforcement bars of type 2 are calculated in the present example.

The geometry of the cantilever and type of reinforcement are set according to Table 8.1.

Table 8.1 Input data for calculation of the bond stress. s_1, s_2 = space between each reinforcement bar of type 1 and 2, respectively (m).

| h | t | c | L | ϕ | s_1 | s_2 | A_{s1} | A_{s2} |
|-----|-----|-------|-----|--------|-------|-------|----------------------|----------------------|
| (m) | (m) | (m) | (m) | (m) | (m) | (m) | (mm ² /m) | (mm ² /m) |
| 10 | 1.0 | 0.050 | 2.8 | 0.020 | 0.750 | 0.250 | 419 | 1257 |

With input data from Table 8.1 and calculation according to equation (8.4), the steel stress (σ_s) and reinforcement forces (F_s) are calculated, see Table 8.2.

Table 8.2 Calculated force and stress in reinforcement bars.

| z | p_w | M | σ_s | F_{s1} | F_{s2} |
|-------|-------|---------|------------|----------|----------|
| (m) | (kPa) | (kNm/m) | (MPa) | (kN) | (kN) |
| 0.855 | 100 | 392 | 274 | 115 | 344 |

The bond force capacity F_b must be larger than the reinforcement force F_s

$$f_b \cdot \pi \cdot \phi \cdot L_b = F_b \geq F_s = \sigma_s \cdot \frac{\pi \cdot \phi^2}{4} \quad (8.5)$$

or rewritten to

$$f_b \geq \sigma_s \cdot \frac{\phi}{4 \cdot L_b} = \sigma_{sb} \quad (8.6)$$

where f_b = bond strength (Pa); F_b = bond force capacity (N); and F_{s2} = reinforcement force (N). It is assumed that the adjustment to shear cracks and the length of the

reinforcement bar of type 2 are such that the anchorage-length $L_b = 1.5$ m. The bond stress becomes

$$\sigma_{sb} = \sigma_s \cdot \frac{\phi}{4 \cdot L_b} = 274 \cdot \frac{0.020}{4 \cdot 1.5} = 0.9 \text{ MPa} \quad (8.7)$$

The bond strength is affected by leaching. The leaching of hydration products from the concrete is assumed to result in loss of bond strength to the reinforcement bars. Estimation of the material properties is carried out by use of a degradation model $D(t)$ and, for comparison, by fictive test values from investigations supposedly performed both at the time when the dam was new (t_0) and at the time of the current assessment (t_1). For comparison purposes, estimates of structural safety were made in two different ways: (i) by use a lifetime safety factor γ_t and (ii) by calculating the safety index β for different time periods.

8.4.2 Leaching process

The leaching of hydration products from the concrete involves the diffusion of ions from the concrete to the reservoir on the upstream side of the dam and it involves convective flow of ions by the water flow through the dam. The extent of the leaching is calculated by use of the following mathematical relations (the same balance equations and parameters as were used in calculations for the specimens in the present experimental work, Calc. 4 in Table 7.3, are used in the present example):

$$\text{Flow of water:} \quad \nabla \cdot (\mathbf{v}_w) = 0; \quad \mathbf{v}_w = -k_w \nabla P_w \quad (8.8)$$

$$\text{Flow of ions:} \quad \frac{\partial c_i}{\partial t} = \hat{c}_i - \nabla \cdot (\mathbf{F}_{iv} + \mathbf{F}_{iu}); \quad \mathbf{F}_{iv} = \mathbf{v}_w c_i; \quad \mathbf{F}_{iu} = -k_i \nabla c_i \quad (8.9)$$

$$\text{Leaching of solid compounds:} \quad \frac{\partial c_j}{\partial t} = -\hat{c}_i \quad (8.10)$$

$$\text{Change in total porosity:} \quad P_p = \frac{(V_p)_p + V_{leach}}{V_p} \quad (8.11)$$

The calculations were made by the same FEM-program as was used in section 7.8.

The conceptual model of the compressive strength of the concrete is based on the assumption that the latter corresponds approximately to the strength of the cement paste, which in its turn is strongly dependent upon the porosity. The solid phase $(V_0)_p$ of the paste, involving solid gel and unhydrated cement, is assumed to carry the entire load. The pores carry no load. The compressive strength is assumed to depend upon the porosity (see section 7.7)

$$f_{cc} = f_{pc} \cdot a \cdot (w/c)^b \quad (8.12)$$

$$f_{pc} = f_0 (1 - P_p)^{K_1} \quad (8.13)$$

where f_{cc} = a model describing the compressive strength of concrete (Pa); f_{pc} = the compressive strength of cement paste (Pa); a = a curve fitting parameter, $a = 1.2$ to fit f_{cc} in Ysberg (1979); b = a curve fitting parameter. $b = 0.5$ to fit f_{cc} in Ysberg (1979); f_0 =

the fictitious strength of the solid phase without pores (Pa); K_I = an empirical parameter, given as $2 \leq K_I \leq 3.5$ in the literature (-); P_p = the porosity of the cement paste (no air pores are included) (m^3/m^3); w/c = water to cement ratio (kg/kg); and α = degree of hydration (-). The fictitious strength in the strength-structure relations is proposed to $f_0 = 210$ MPa, (see section 7.7)

The tensile strength is assumed to be (Möller et al. 1989)

$$f_{ct} = A \cdot f_{cc}^B \quad (8.14)$$

where f_{ct} = model of the tensile strength of the concrete (Pa); and A , B = empirical parameters.

The bond strength is assumed to be (BBK 1994):

$$f_b = \eta \cdot f_{ct} = \eta_1 \cdot \left(\frac{1}{3} + \frac{2}{3} \cdot \frac{c}{\phi} \right) \cdot \eta_2 \cdot f_{ct} \leq \eta_1 \cdot 3 \cdot f_{ct}; \quad (8.15)$$

Where η_1 = parameter pertaining to the depth of the concrete under the reinforcement bars at casting, set here to 0.7 (-); $\eta_2 = 1.4$ for the profiled bars; ϕ = diameter of the reinforcement bars (m); and c = concrete cover (m).

The concentration of Ca in the pore solution and the content of Ca in the solid compounds are calculated over a period of 200 years and are shown in Figure 8.8 and Figure 8.9.

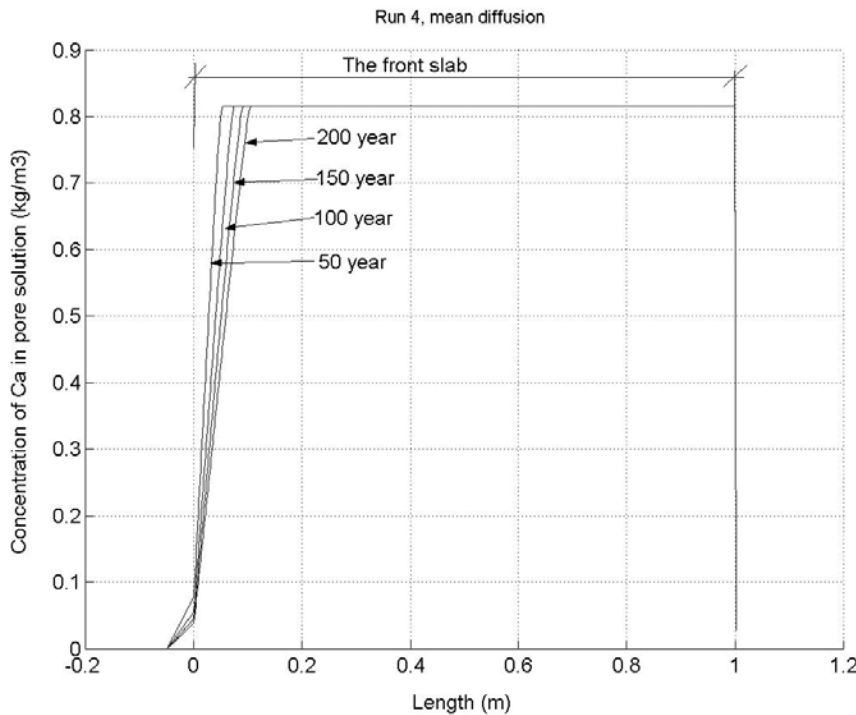


Figure 8.8 Calculated concentration of Ca in the pore solution in the concrete (mole/m^3) versus the depth (m) from the upstream surface at the 50, 100, 150 and 200 year time.

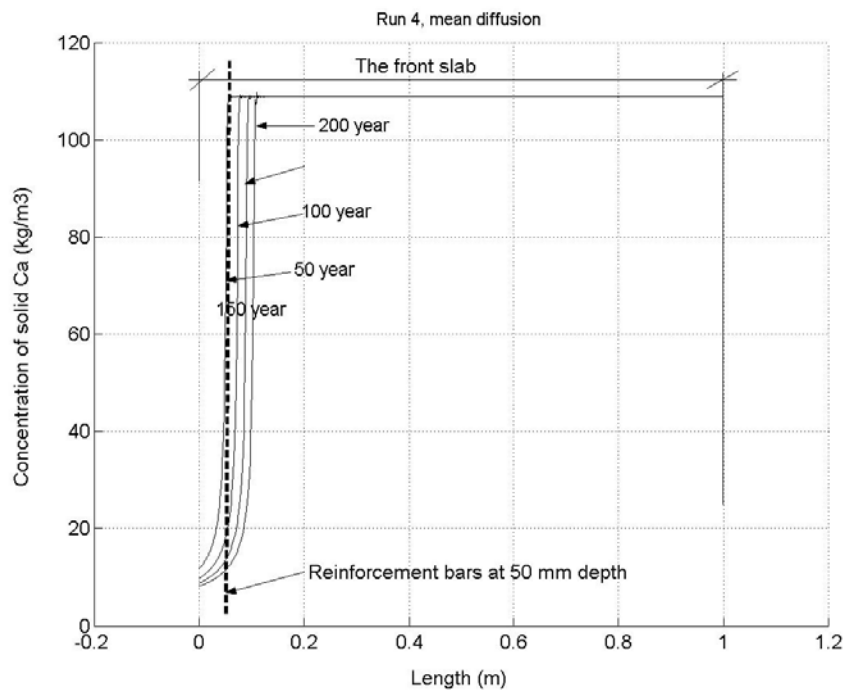


Figure 8.9 Calculated content of Ca in the solid compounds of the concrete (mole/m^3) versus the depth (m) from the upstream surface at the 50, 100, 150 and 200 year time.

The porosity is calculated by equation (8.11), using the FEM-calculation for leaching. Figure 8.10 shows the calculated total porosity at two different depths on the upstream surface of the concrete cantilever. At the level for the reinforcement bars, 50 mm, the porosity is increased first after about 55 year ($1.7 \cdot 10^9$ s), when the leaching front arrives.

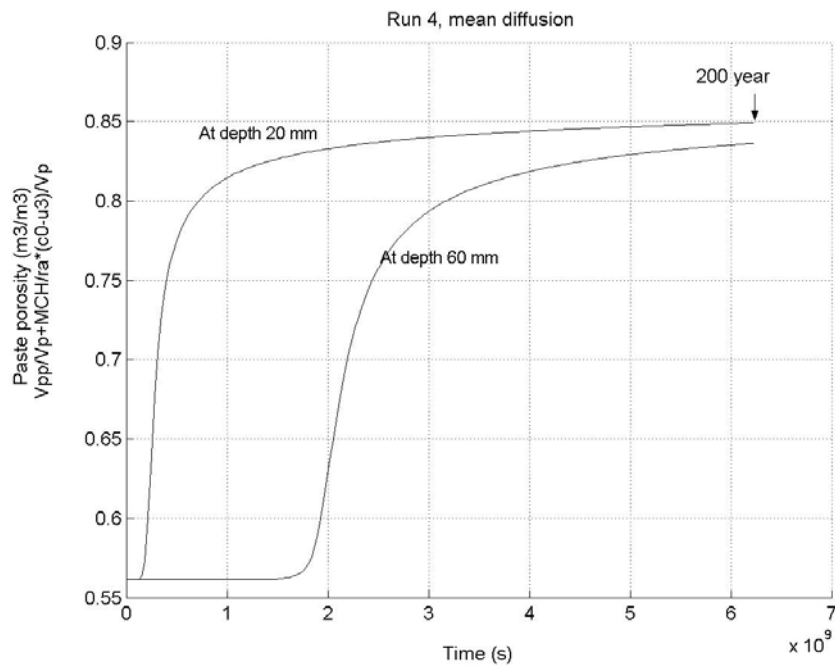


Figure 8.10 Calculated total porosity of the cement paste phase at two different depths on the upstream surface of the concrete.

8.4.3 Estimation of the "design service life" by a Lifetime safety factor

Sarja and Vesikari (1996) introduced a Lifetime safety factor γ_t utilizing the scatter contained in the variables used in the degradation model employed.

In structures of thin concrete or of concrete of high permeability, the major cause of destruction due to leaching is water flowing through the concrete, transporting dissolved lime out of the concrete. In thick concrete structures or structures composed of concrete of low permeability, the major cause of leaching damage is the diffusion of dissolved lime to water that is lower in ion strength, such as the water on the upstream face of a dam. In the present example, the major degradation of bond strength of the reinforcement bars at the upstream part of the concrete slab is assumed to be the diffusion of lime from the concrete to the reservoir. This leaching also causes an increase in porosity. The degradation rate D is assumed to be proportional to the square root of time $D \propto t^K$.

No report of statistical variation in the diffusion coefficient is found in the literature. For this example the mean value and standard deviation were assumed to be $\mu[k_s] = 10^{-13} \text{ m}^2/\text{s}$ and $s[k_s] = 0.5 \cdot 10^{-13} \text{ m}^2/\text{s}$, respectively.

Figure 8.11 shows the calculated load (bond stress) and the calculated strength (bond strength), for the model presented above, at a depth of 60 mm on the upstream part of the concrete slab. The reinforcement bars are at a depth of 50 mm. The bond strength is calculated using equations (8.12), (8.13), (8.14) and (8.15). When the bond strength becomes lower than the stress at this point, the safety is endangered. At the time 200 year after the structure is taken into use, the assumed mean bond strength, as based on a mean diffusion coefficient of $k_s = 10^{-13} \text{ m}^2/\text{s}$, is smaller than the mean bond stress. If the mean bond strength is also calculated using a higher diffusion coefficient,

with mean $\mu[k_s]=10^{-13}$ m²/s and standard deviation $s[k_s]=0.5\cdot 10^{-13}$ giving the characteristic diffusivity $k_{i0} = \mu[k_{i0}] + s[k_{i0}] = 10^{-13} + 0.5\cdot 10^{-13} = 1.5\cdot 10^{-13}$ m²/s, these new calculations indicate the technical service life to decrease to about 125 year.

The variance v of the degradation is calculated as the difference between the bond stress obtained in the two separate calculations in relation to the mean value. In Figure 8.11 it is approximated to 0.2. For $\beta_m=4.8, v= S/\mu= 0.2$ and $K= 0.5$, a lifetime safety factor of $\gamma_t= 3.83$ is obtained by use of the following calculating scheme (described by Sarja and Vesikari 1996):

Calculation scheme of the lifetime factor γ_t :

Step 1. Decide values of β_m , v and K and choose m

Step 2. Assume a value of γ_t

$$\text{Step 3.} \quad r_t = \frac{v_D \cdot m \cdot \beta_m}{(1-m) \cdot \gamma_t^K}; \quad \alpha_t = \frac{r_t}{\sqrt{1+r_t^2}};$$

$$\beta_t = \frac{(\gamma_t^K - 1)}{v_D}; \quad \beta_m = \beta_t \frac{\alpha_t}{1 - \sqrt{1 - \alpha_t^2}}$$

Step 4. If the calculated value of β_m = the decided value of β_m the last assumed γ_t is the right one. If the calculated $\beta_m \neq$ the decided β_m , go to step 2 again and choose a new value of γ_t and make new calculations again due to step 3.

where r_t = a variable for facilitate calculations (-); β_m = the total mechanical reliability index; β_t = the durability reliability index; v_D = the standard deviation of the degradation; m = the relative reduction of the load bearing capacity minus the load effect (R-S) during time; γ_t = the lifetime safety factor; α_t = the ratio of standard deviation due to degradation to the total standard deviation; and K = a rate coefficient.

With use of the Lifetime safety factor $\gamma_t = 3.83$ considered above, the “design service life” t_d is assumed to be approximately **52 year** ($t_d = t_m/\gamma_t = 200/3.83=52$), see Figure 8.11.

The selected safety index of $\beta = 4.8$ means a potential probability of 10^{-6} that a failure will occur ($R < S$).

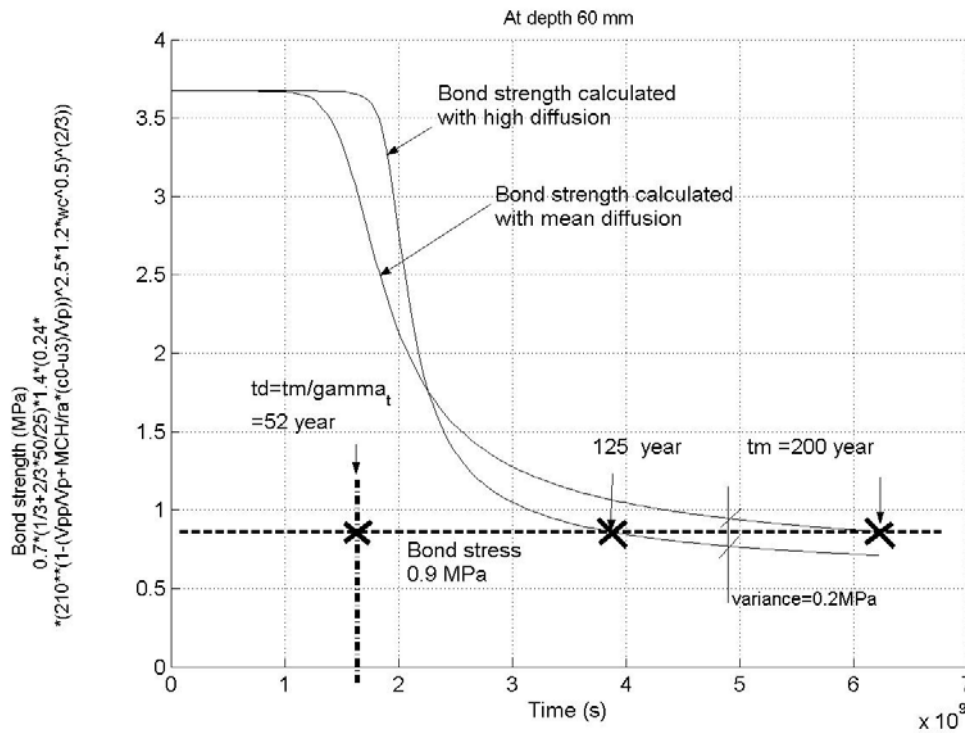


Figure 8.11 The principles involved in use of the *time safety factor* γ_t (b) (Sarja & Vesikari 1996) in calculating the safety of a structure, i.e. when the bond strength becomes lower than the bond stress for the reinforcement bars on the upstream part of the front slab. In this example, the “mean service life”, t_m , is calculated to be 200 years, but due to uncertainties in the degradation model the “real” service life t_d becomes approximately 52 year.

8.4.4 Estimation of the “design service life” by the Hasofer-Lind method

A safety index is calculated over time by the approximately probabilistic Hasofer-Lind method. The types of distribution and the mean and standard deviation values of the used parameters are only hypothetical in this example. It is only a parameter-study.

The failure equation, g , yields

$$g = \sigma_{sb} - f_b \leq 0 \quad (8.16)$$

where σ_{sb} = the bond stress (MPa); and f_b = the bond strength (MPa). The bond stress is calculated using equation (8.4) and data from Table 8.1:

$$\sigma_{sb} = \frac{\rho_w \cdot g \cdot h \cdot L^2 / 2}{A_s \cdot 0.9 \cdot (t - c)} \cdot \frac{\phi}{4 \cdot L_b} = \frac{10 \cdot h \cdot 2.8^2 / 2}{1676 \cdot 10^{-6} \cdot 0.9 \cdot (1 - c)} \cdot \frac{0.020}{4 \cdot 1.5} \quad (8.17)$$

The values of the water depth h and the cover thickness c are assumed to have a statistical variation according to Table 8.3.

The bond strength is calculated using equations (8.12), (8.13), (8.14) and (8.15):

$$\begin{aligned}
 f_b &= \eta \cdot f_{ct} = \eta_1 \cdot \left(\frac{1}{3} + \frac{2}{3} \cdot \frac{c}{\phi} \right) \cdot \eta_2 \cdot f_{ct} = \eta_1 \cdot \left(\frac{1}{3} + \frac{2}{3} \cdot \frac{c}{\phi} \right) \cdot \eta_2 \cdot f_{pc} = \\
 &= 0.7 \cdot \left(\frac{1}{3} + \frac{2}{3} \cdot \frac{c}{\phi} \right) \cdot 1.4 \cdot A \cdot \left(f_0 \cdot (1 - P_p)^{K_1} \cdot a \cdot 0.80^b \right)^B
 \end{aligned}
 \tag{8.18}$$

The values of the diameter ϕ of the reinforcement bars, the cover thickness c , the empirical parameters A , B and K_1 , the curve fitting parameters a and b , the fictitious strength f_0 are assumed to have a statistical variation according to Table 8.3. The values of the paste porosity P_p are coming from the FEM-calculation of the leaching as was performed above. The P_p is assumed to have a standard deviation of $0.01 \text{ m}^3/\text{m}^3$, see Table 8.3.

Table 8.3 Assumed values of the variables used for calculating the safety index β . G = gumbel, N = normal, LN = log-normal.

| Variable | Type of distribution | Mean | St. dev. |
|----------|----------------------|---------|----------|
| h | Gu | 10 m | 0.1m |
| c | N | 0.050 m | 0.005 |
| A | LN | 0.24 | 0.03 |
| B | LN | 0.67 | 0.05 |
| f_0 | LN | 210 MPa | 20 |
| P_p | LN | Varies | 0.04 |
| a | LN | 1.2 | 0.1 |
| b | LN | 0.5 | 0.1 |

The shortest distance perpendicular to the failure curve $g=0$ to the origo of the two standardised normal distributions of R' and S' in figure 8.12 (S' is termed E' in the figure) correspond to the safety index β and is calculated by use of the statistical program COMREL.

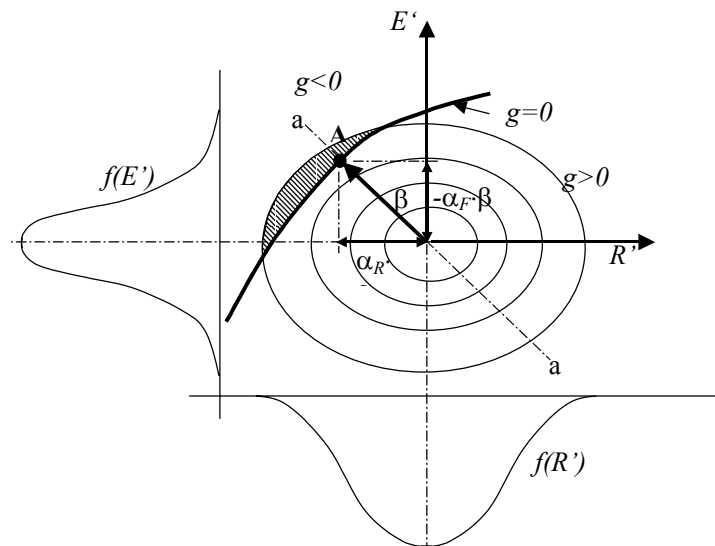


figure 8.12 Design point A on the failure curve $g=0$ and the safety index β for standardised, normally distributed independent variables (a modification of EN 1990 fig. C2).

The safety index β_{cal} as calculated at different times is shown in Figure 8.13. Calculations have been made by use of the computer program COMREL. When the calculated safety index decreases below the required level of $\beta_0 = 4.8$, after a period of approximately **57 years** the service life is assumed to be ended.

Calculations by use of COMREL also indicate the influence of each parameter on the solutions (α^2 in Figure 8.13). It can be seen that the porosity has a great influence on the calculation result. If an investigation indicate that the standard deviation of, for example, the porosity is considerably lower than the value estimated above, there will be a considerable increase in the safety index.

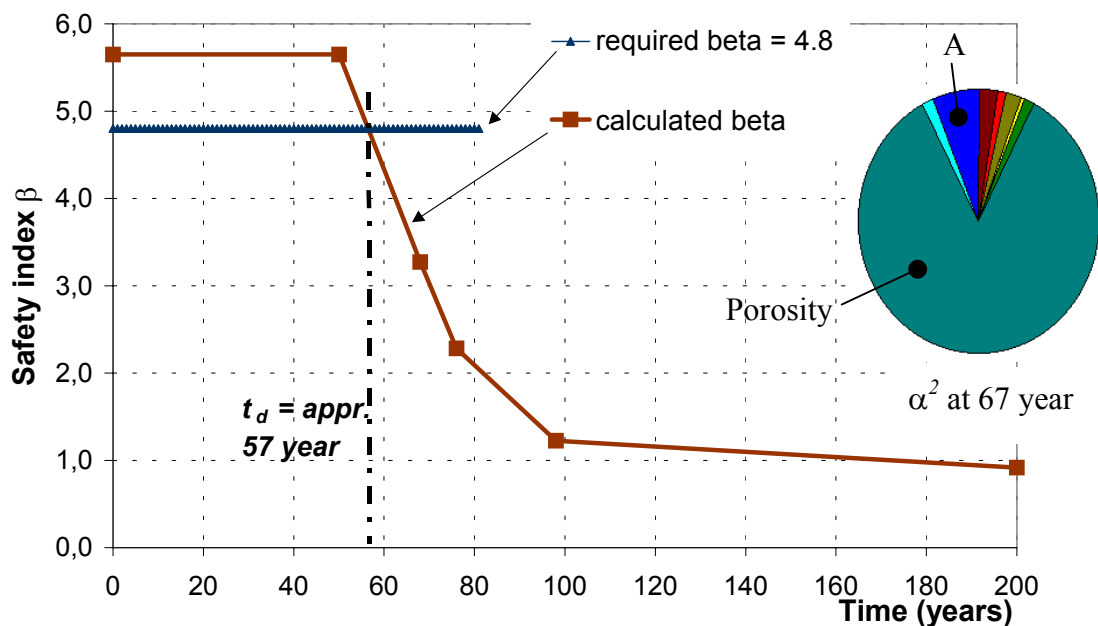


Figure 8.13 The principles involved in use of using safety index for estimate the technical target service life. In this example 57 year. Two of the variables (porosity and A defined by equation (8.14)) with the largest calculated α^2 are explicit shown.

8.5 Conclusions

It is important that relevant degradation models are developed and it is still more important that data from degradation tests always be presented so that account can be taken in degradation models of the statistical variance. It is also highly important that structural engineers become aware of that degradation of engineering materials occur over a period of time.

In the example given, the “design service life” was found to be 52 and 57 years respectively, as calculated by use of the Lifetime safety factor γ_t and the Safety index β methods. Although both methods are satisfactory, it is easier by use of the Hasofer-Lind method to take account of a large number of variables and the scatter in them. The

Hasofer-Lind method also yields the safety index, which can be used almost directly in connection with existing codes.

It is however essential that the degradation models assumed be calibrated not only to experimental data, but also, and still more importantly, to field data.

9 Conclusions

The work presented here consists of a survey of the literature, an experimental part and a modelling part. Only results from the experimental and modelling parts are commented below.

EXPERIMENTS:

- Three types of experiments were performed, involving
 - Homogenous steady-state percolation of water through defect-free concrete
 - Percolation through artificially-made holes in concrete
 - Surface leaching at free surfaces of concrete lying in stagnant water

All specimens were saturated with water prior to testing. Three w/c-ratios were used: 0.60, 0.80 and 1.29. Three types of pre-treatments of specimens were employed: (i) Virgin specimens stored in water two to three months prior to testing; (ii) Early-heated specimens heated at +55-60°C directly after unmoulding, followed by submersion in water for about two months; and (iii) Late-dried specimens dried at +55°C after a long period of leaching or after being submerged in water. The water that was pressed through the specimens was deionised.

Homogenous steady-state percolation of water through defect-free concrete:

- The laboratory test was *accelerated* in terms of: (i) the pressure gradient, which was approximately 50 times as high as in a real dam; (ii) the w/c ratio, which was mostly 0.80, whereas the normal values in new dam structures are about 0.55 to 0.60; and (iii) the use of aggressive deionised water used. On the other hand, the test was partly *retarded* in that no aggressive ions were present in the water (CO_2 , H^+ , SO_4^{2-} , etc.) and in that the temperature was held constant at 20°C.
- The test equipment developed worked very well. It consisted mainly of standard components.
- The experimental results showed that the percolation of pure water through concrete specimens is able to dissolve hydration products, mainly $\text{Ca}(\text{OH})_2$, and also to carry the dissolved ions out of the specimen by diffusion or convection.
- The measured permeability of the test specimens depended mainly on the way in which the specimens were pre-treated. Drying and heating led to permeability much higher (approximately 100 times as high) as in specimens in a virgin state.
- The permeability was often found to increase after approximately 10 liters of water had percolated through the specimens.
- The measured concentrations of Na and K in the percolated water decreased for all the specimens rather quickly after about 0.1 liters of water had percolated.
- The reduction in Na and K led to a corresponding decrease in pH, from about 13.3 to 12.5, $\text{Ca}(\text{OH})_2$ acting as a strong buffer.
- The concentration of Ca in the percolated water was uniform at approximately 0.6 g/l for all specimens except for the early-heated (EH) specimens, in which the concentration was uniform at approximately 1.1 g/l.
- The concentration of Ca in the percolated water decreased rapidly if the flow of water through the specimens increased rapidly, which happens, as said above, when about 10 litre of water has percolated. The leaching rate in terms of g/s remain

however constant, since the product of the increased water flow in l/s and the concentration (g/l) remain approximately the same ($l/s \cdot g/l = g/s$).

- From measurements of the ion concentrations in the inlet water it was obvious that ions diffused in large amounts from the upstream end of the specimens to the pure water at the inlet.
- In highly permeable concrete, water appeared to mainly flow in a rather small number of distinct passageways, or “flow channels”. In these channels, the flowing water dissolved solids from the channel walls, probably mainly Portlandite ($Ca(OH)_2$), the channels becoming wider, the water flow thus increasing, the channel walls becoming so depleted of soluble ions that the concentration of ions in the channels decreased sharply. Dissolution of the channel walls was a diffusion process from the interior of the solids towards the channel walls. The concrete around these channels became highly disintegrated, almost no continuous cementitious material being left to maintain strength and tightness.
- Between the flow channels, or in the less permeable portions of the concrete, leaching appeared to be largely driven by diffusion to the inlet water at the upstream end.
- Although there was often a very large reduction in strength, this was very much a local phenomenon, certain parts of the concrete (at the upstream surface and around the flow channels) becoming highly leached, with a considerable loss in strength, whereas other parts were leached to a much lesser degree. The measured compressive strength of the leached specimens showed a high degree of scatter. The measured split strength showed a lesser degree of scatter.
- Porosity analysis of the leached specimens showed a clear increase in porosity in the upstream part.
- Chemical analysis showed there to be a clear reduction in the elements present, calcium in particular, in the upstream part.
- Leaching was found to be very much governed by the permeability of the concrete (as are most other degrading mechanisms as well). For tight concrete subjected to deionised water under pressure, leaching was largely governed by the upstream diffusion of ions to the deionised water, whereas for very porous concrete leaching was largely governed by the convection of ions through the downstream flow of water through the concrete. If permeability is high but there are few flow channels, the concentration of ions in the percolating water decreases rapidly, the leaching rate decreasing too. If the permeability is high and there are many flow channels (highly porous concrete), the leaching rate remains high, the strength of the concrete decreasing rapidly.

Percolation through artificially-made holes in concrete:

- The matrix around the hole was leached of Portlandite at a distance of about 1.5 mm at the inlet to the hole and about 0.5 mm at the outlet of the hole. There were found to be two causes for the layer that was leached being thicker at the inlet: (i) the deionised water was more pure and therefore more aggressive at the inlet (ii) the diffusion of calcium from the matrix around the hole was not hindered at the inlet by a thick layer of tight calcite. Further downstream in the hole the concentration of calcium ions in the water was higher, making the water less aggressive, and the calcite layer also was thicker, see below.

- There was a very thin layer of calcite (approximately 1-3 μm thick) on the surface of the hole walls at the inlet to the holes, whereas the layer was somewhat thicker (20 μm) on the hole walls at the outlet. The thicker layer at the outlet was probably caused by the higher pH, leading to more calcite being precipitated. The higher pH can be ascribed to the amount of Portlandite dissolved being higher at the outlet.

MODELLING:

- Use of FEM calculations facilitates the application of the basic balance laws, allowing calculations to be performed for a wide variety of different leaching situations and widely varying geometries. The effective FEM software available today is well suited for parameter studies using the latest post-processing techniques. Such calculations provide highly informative pictures that contribute to an understanding of the processes involved. The FEM technique enables the same types of variables to be used for experiments as for real structures of large size.
- The calculations performed agree quite well with results of the experiments. The large database the work resulted in can serve as a basis for further calculations.
- The measured concentrations of ions in the inlet water to the specimens in the homogenous percolation experiment for example, could probably be analysed in a more detailed way using FEM-calculations.
- For the experiment involving percolation through holes, the observed leaching of Portlandite in the matrix around the hole, and the formation of a calcite layer on the surfaces of the hole, can probably best be calculated by the models employed here if account is taken of the balance and the reactions of CO_2 .
- The experiment on surface leaching was not carried out in such a way that diffusion coefficients could be obtained. However if the measured concentrations of ions in the exchanged water are used, certain information concerning the diffusion that occurred could probably be calculated using the models employed here. Such calculations are not made.

FUTURE RESEARCH:

The present work points to further research that is needed:

- The ions that diffused upstream were not measured with the same degree of exactness as the ions that were carried away downstream by the water. More exact measurements of upstream diffusion ought to be performed in future work.
- The experimental data and the models used in the present work should be calibrated more thoroughly to data from field investigations of real structures.

10 References

- Adenot F. (1992), "Concrete durability: characterisation and modelling of the chemo-physical processes inducing cement degradation, Ph.D. thesis (in french), Université d'Orléans, France.
- Andersson K. (1983), PhD Thesis, Chalmers University of Technology, Göteborg.
- Assarson G., Sundius N. (1929), "Dissolution of Portland cement in water" (in Swedish), From "Report of investigations regarding the causes of the destruction of concrete in hydraulic structures, The Royal Waterpower Board, Technical report, issue B no. 16, Trollhättan 1929.
- Atkins, P., Jones, L. (1997), "Chemistry Molecules, Matter, and Change", 3rd edition, W. H. Freeman and Company, New York.
- Atzeni C., Massidda L., Sanna U. (1987), "Effect of pore distribution on strength of hardened cement pastes", from "Pore Structure and Construction Materials Properties", vol. one, edited by J.C. Maso, Proc. 1st Int. Congr. RILEM, Versailles Sept. 7-11, 1987.
- Ayora, C. et al (1998), "Weathering of iron sulfides and concrete alteration: Thermodynamic model and observation in dams from central Pyrenees", Spain, Cem. & Concr. Res. Vol. 28, no. 9, pp 1223-1235.
- Bakker R.F.M. (1983), "Permeability of blended cement concretes", ACI Publication, SP-79, Vol. 1.
- Bal'shin (1949), "Relation of mechanical properties of powder metals and their porosity and the ultimate properties of porous metal-ceramic materials", Dokl. Akad. Nauk. SSSR, 67, 5.
- Bažant Z.P. (1975), "Pore pressure, uplift and failure analysis of concrete dams", Proc. of the Int. Symp. of "criteria and assumptions for numerical analysis of dams", 8-11 Sept., 1975, Swansea.
- BBK (1994), "Handbook for concrete structures" (in Swedish), Boverket, Sweden.
- Bear J. (1987), "Eight lectures on mathematical modelling of transport in porous media included in Modelling and applications of transport phenomena in porous media", Kluwer Academic publishers, Belgium.
- Bentz, D. P., Garboczi, E. J. (1991a) "A digitized simulation model for microstructural development", Advances in Cementitious Materials, Ceramic Transactions Vol. 16, pp. 211-226.
- Bentz, D. P., Garboczi, E.J. (1991b) "Percolation of phases in a three-dimensional cement paste microstructural model", Cement and Concrete Research, Vol. 21, pp. 325-344.

Bentz, D. P., Garboczi, E. J. (1992), "Modelling the leaching of calcium hydroxide from cement paste: effects on pore space percolation and diffusivity", *Materials and Structures*, Vol. 25, 523-533.

Bentz, D. P., Garboczi, E. J., Martys N.S. (1996), "Application of digital-image-based models to microstructure, transport properties, and degradation of cement-based materials", *The modelling of microstructure and its potential for studying transport properties and durability*, Kluwer Academic publishers, Netherlands.

Bentz, D. P. (1999), "Modelling cement microstructure: Pixels, particles, and property prediction", *Materials and Structures*, Vol. 32, 187-195.

Berner U. R. (1987), "Modelling porewater chemistry in hydrated portland cement", *Mat. Res. Soc. Symp. Proc.* Vol. 84.

Bourdette B., Ringot E., Ollivier J.P. (1995), "Modelling of the transition zone porosity", *Cement and Concrete Research*, Vol. 25, No. 4, pp. 741-751.

Bowen R. M. (1984), "Porous media model formulations by the theory of mixtures", from *Fundamentals of Transport Phenomena in Porous Media NATO ASI series No. 82*, Martinus Nijhoff Publishers.

Brakel J. Van (1975), "Pore space models for transport phenomena in porous media – Review and evaluation with special emphasis on capillary liquid transport", *Powder Technology*, 11 (1975) 205-236, Elsevier, Netherlands.

Breysse D., Gérard B. (1997), "Modelling of permeability in cement-based materials: Part 1-uncracked medium.

Brown P.W. (1987), "Thermodynamic aspects of concrete durability", from "Pore Structure and Construction Materials Properties", *Proc. 1st Int. Congr. Rilem, Versailles*, Sept. 7-11, 1987.

Cabrera J.G., Hassan K.E. (1997), "Controlling the quality of concrete by measuring its permeability", *13th Int. Baustofftagung, Weimar*.

Carde C., Francois R., Torrenti J-M. (1996), "Leaching of both calcium hydroxide and C-s-H from cement paste: Modelling the mechanical behaviour"; *Cem. and Concr. Res.*, Vol. 26, No. 8.

Carlson R.W. (1950), "Permeability, pore pressure, and uplift in gravity dams", Appendix to "*Permeability and Triaxial Tests of Lean Mass Concrete*", Corps of Engineer.

Cederwall K. (1979), "Hydraulics for civil engineers" (in Swedish), Liber läromedel, Malmö.

Chang J. C. (1984), "Handbook of Chemistry and Physics", 64th Ed., B-219, Boca Raton, CRC Press, Florida.

Chem. & Phys (1989), "Handbook of Chemistry and Physics", 70th edition, CRC Press.

Constantiner, D., Diamond, S. (1995), *Pore solution analysis: Are there pressure effects?*, Proceedings of the Materials Research Society's Symposium on Mechanisms of Chemical Degradation of Cement-based Systems, Boston, 27-30.

Contecvet (2001), "Contecvet – A validated Users Manual for assessing the residual service life of concrete structures. Manuals for assessing concrete structures affected by": Part I frost, Part II ASR and Part III corrosion, EC Innovation project IN309021, available from Lund Institute of Technology, Division of Building Materials.

Collins et al (1986)

Darcy H. (1856), "Les fontaines publiques de la ville de Dijon", Dalmont, Paris.

Derjaguin B., Zachavaeva N. (1965), "Physical properties of water and its mobility in fine pores", Inst. of Physical Chemistry of the Academy of Sciences, Moscow.

Deju R.A. (1970), "Physical and chemical models of fluid flow through porous media", from Flow – its measurement and control in science and industry, vol. one, ASME fluids engineering conference, Pittsburgh.

Dhir R.K., Hewlett P.C., Chan Y.N. (1989), "Near surface characteristics of concrete: Intrinsic permeability", Mag. Conc. Res., Vol. 41, No. 147.

Duchesne, J., Reardon, E. J. (1995), "Measurement and prediction of portlandite solubility in alkali solutions", Cement & Concrete Research, vol. 25, no. 5, pp 1043-1053.

Dullien F.A.L. (1991), "Porous media Fluid transport and pore structure", 2nd edition, Academic press, USA.

Edvardsen, C. (1996), "Water permeability and autogenous healing of cracks in concrete", (in German), Heft 455, Deutscher Ausschuss für Stahlbeton, Berlin.

Edvardsen, C. (1999), "Water permeability and autogenous healing of cracks in concrete", ACI Materials Journal, July-August 1999.

Ekström T. (1998), "Degradation of concrete dams due to lime leaching", Proc. Int. ICOLD Symp. on new trends and guidelines on dam safety, Barcelona 17-19 June, 1998.

Ekström T. (2000), "Leaching of concrete – Experiments and modelling", Licentiate report TVBM-3090, Div. of Building Materials, Lund Institute of Technology, Sweden.

Ekström T. (2001), "Durability check of existing concrete dams subjected to environmental degradation", Proc. ICOLD symposium, Geiranger, Norway, 2001.

Ekström T. (2003), "Leaching of concrete – experiments and modelling", submitted to ICOLD 21st Congress, Montreal, 2003.

Ekström T. (2003), "Estimation of current condition and remaining service life of a existing degrading concrete structure", submitted to ICOLD 21st Congress, Montreal, 2003.

Eriksson H. (2001), "Reparations for dams from different époques", KTH VASO – Dams and safety of dams, Royal Institute of Technology and Swedish Energy, Stockholm.

Fagerlund G. (1972), "Relationship between porosity and mechanical properties of materials", Report no 26, Div. of building technology (now materials), The Lund Institute of Technology, Lund.

Fagerlund, G. (1980a), "Structure", (in Swedish), The concrete Handbook Material, Svensk Byggtjänst, Stockholm.

Fagerlund, G. (1980b), "Moisture-mechanical properties", (in Swedish), The concrete Handbook Material, Svensk Byggtjänst, Stockholm.

Fagerlund, G. (1987), Relations between the strength and the degree of hydration or porosity of cement paste, cement mortar and concrete, Seminar on Hydration of Cement, Aalborg Portland, Aalborg.

Fagerlund, G. (1989), Concrete for hydraulic structures, (in Swedish), CEMENTA, Danderyd.

Fagerlund, G. (1991), Freeze testing of concrete from the Storfinnforsen dam, (in Swedish), Div. of Building Materials, Lund Institute of Technology.

Fagerlund, G. (1994), Structure and development of structure, (in Swedish), The concrete Handbook Material, Svensk Byggtjänst, Stockholm.

Fagerlund G. (1996), Service life prediction of concrete structures, (in Swedish), report TVBM-3070, Lund.

Fagerlund, G., "Calculations of residual life of concrete structures" (in Swedish), TVBM-3070, Lund 1996.

Fagerlund, G. (1997), Deterioration, service life and repair of concrete structures-knowledge and research needs, Div. of Building Materials, Lund Institute of Technology.

Fagerlund, G. (1997a), Composite models and composite formulas, (in Swedish), Compendium in Building Material Div. of Building Materials, Lund Institute of Technology.

Fagerlund, G. (1997b), The chemistry of cement based binder, (in Swedish), Compendium in Building Material Div. of Building Materials, Lund Institute of Technology.

Fagerlund, G. (1997c), Temperature development in concrete, (in Swedish), Compendium in Building Material Div. of Building Materials, Lund Institute of Technology.

Fagerlund, G. (2000), "Leaching of concrete", contribution to EU-project CONTECVET, Div. of Building Materials, Lund Institute of Technology.

Faucon, P., Bonville, P., Adenot, F., Genand-Riondet, N., Jacquionot, J., Virlet, J. (1997), ^{57}Fe Mössbauer study of cement water degradation, Advances in Cement Research, 9, No 35, pp. 99-104.

Faucon, P., Gerard, B., Jacquionot, J., Marchand, J. (1996), *Leaching of cement: study of the surface layer*, Cement and Concrete Research, vol. 26, no. 11, pp 1707-1715.

Faucon, P., Adenot, F., Jacquionot, J., Petit, J., Cabrillac, R., Jordan, M. (1998), "Long-term behaviour of cement pastes used for nuclear waste disposal: Review of physico-chemical mechanisms of water degradation", Cement & Concrete Research, vol. 28, No.6, pp. 847-857.

Feldman R.F., Sereda P.J. (1970), "A new model for hydrated Portland cement and its practical implications", Engineering Journal (Montreal), 1970(53):8-9.

FEMLAB, Computer program from COMSOL AB, Sweden.

Frost R.V., Virgin E.I. (1929), "Concrete and especially concrete pipes durability against water" (in Swedish), Betong 1929, p 100-160.

Garboczi, E. J., Bentz, D.P. (1992), Computer simulation of the diffusivity of cement-based materials, J. Mater. Sci. 27.

Garboczi, E. J., Bentz, D. P. (1996), Multi-Scale Picture of concrete and its transport properties: Introduction for non-cement researchers, NISTIR 5900, Gaithersburg, U.S.A.

Garboczi, E. J., Bentz, D.P. (1998), Modelling Analytical/Numerical theory of the diffusivity of concrete, Advances in Cement Based Materials 1998;8:77-88.

Gartner E.M, Jennings H.M. (1987), "Thermodynamics of calcium silicate hydrates and their solutions", J. Amer. Ceram. Soc., 70.

Gérard B., Torrenti J.M., Adenot F. (1998), "Nuclear Waste Management in France: A Review of the Strategies for Designing Durable Concrete Structures", 5th Int. Workshop on Material Properties and Design, Weimar, Oct. 1998, Aedificatioin Publishers.

Gjörv O.E., Löland K.E. (1978), "Effect of air on the hydraulic conductivity of concrete", Proc. of the First Int. Conf. of Durability of building materials and components, Ottawa, ASTM special tech. publ. 691, ed. Sereda & Litvan.

Glanville W.H. (1931), Building Research Techn. Paper no 3, revised ed. Dep. Of Scientific And Industrial Research, London.

Granholt H., Werner D., Giertz-Hedström S. (1934), "Investigation of the suitability of concrete pipes in roads", *Betong* 1934:1.

Grattan-Bellew, P. E. (1996), "Microstructural investigation of deteriorated Portland cement concrete", *Construction and Building Materials*, Vol. 10, No. 1, pp. 3-16.

Grube, H. and Rechenberg, W. (1989), "Durability of concrete structures in acidic water", *Cement and Concrete Research*, Vol. 19, pp. 783-792.

Gruner E. (1967), "The mechanism of dam failure", Q.34, R.12, ICOLD Conference in Istanbul 1967.

Hall C. (1994), "Barrier performance of concrete: A review of fluid transport theory", *Materials and Structures*, Vol. 27.

Hallström B. (1933), "Decay and repair of concrete and masonry dams", reprint from the *Structural engineer*, May 1933, p 1-19.

Halvorsen, U. (1966), "Corrosion of steel and leaching of lime near cracks in concrete structures" (in Swedish), Bulletin 1, Div. of Building Technology, Lund Institute of Technology.

The Handbook on Water Treatment (1990), published by Kemira AB, Water Treatment, Landskrona, Sweden.

Hansen T.C. (1986), "Physical structure of hardened cement paste. A classical approach",

Harris A.W., Manning M.C., Tearle W.M., Tweed C.J. (2002), "Testing of models of the dissolution of cements – leaching of synthetic CSH gels", *cement and concrete research* 32.

Hearn N. (1992), Saturated permeability of concrete as influenced by cracking and self-healing, Dissertation submitted to the University of Cambridge.

Hearn N. (1997), "Self-sealing property of concrete – Experimental evidence", *Mat. & Struct.*, Vol. 30.

Hearn N. (1998), "Self-sealing, autogenous healing and continued hydration: What is the difference?", *Materials and Structures*, Vol. 33, Oct. 1998.

Hearn N. (1994), "Water permeability and microstructure of three old concretes", *Cement and Concrete Research*, Vol. 24, No. 4.

Hedin, R. (1962), "Processes of Diffusion, Solution and Crystallisation in System $\text{Ca}(\text{OH})_2 - \text{H}_2\text{O}$ ", Swedish Cement and Concrete Research Institute, Stockholm.

Holly J., Hampton D., Thomas M.D.A. (1993), "Modelling relationships between permeability and cement paste pore microstructures", *Cement and Concrete Research*, Vol. 23.

Hooton R.D. (1989), "What is needed in a permeability test for evaluation of concrete quality", *Mat. Res. Soc. Symp. Proc.* Vol. 137.

Hughes D.C. (1985), "Pore structure and permeability of hardened cement paste", *Mag. Of Concrete Res.*, Vol. 37, No. 133.

ISO (1998) "General principles on reliability for structures", Int. Org. for Standardization.

ISO/FDIS 2394 (1998), "General principles on reliability for structures", Switzerland.

ISO/CD 13822 (1997), Bases for design of structures – Assessment of existing structures.

Johannesson, B. (1998), "Modelling of transport processes involved in service life prediction of concrete; important principles", Licentiate thesis report TVBM – 3083, Div. of Building Materials, Lund Institute of Technology.

Johannesson, B. (1999), "Diffusion of a mixture of cations and anions dissolved in water", *Cement and Concrete Research*, 29.

Johannesson, B. (2000), "Transport and sorption phenomena in concrete and other porous media", Doctoral thesis report TVBM – 1019, Div. of Building Materials, Lund Institute of Technology.

Kropp J. (1995), "Relations between transport characteristics and durability", from "Performance Criteria for Concrete Durability", edited by J. Kropp and H.K. Hilsdorf, E & FN Spon, London.

Kou S. (1996), "Transport phenomena and material processing", University of Wisconsin, John Wiley & Sons, U.S.A.

Lage J.L. (1998), "The fundamental theory of flow through permeable media from Darcy to turbulence", Presented in "Transport phenomena in porous media", edited by Ingham & Pop, Elsevier Science Ltd, U.K.

Larsen G. (1961), "Microscopic measuring, a quantitative petrographic method of determining the $\text{Ca}(\text{OH})_2$ content of the cement paste of concrete", *Magazine of Concrete Research* 1961:38.

Lea, F. M. (1983), "The chemistry of cement and concrete", third edition, Edward Arnold (Publishers) Ltd, London.

Linsley R.K., Franzini J.B., Freyberg D.L., Tchobanoglous G. (1992), "Water-Resource Engineering, Mcgraw-Hill, New York.

Maggion R., Bonnamy P., Levitz P., van Damme H. (1996), "A scaling model of the microstructural evolution in C₃S/S-S-H pastes", from the modelling of microstructure and its potential for studying transport properties and durability, Kluwer academic publishers, Netherlands.

Mainguy M., Tognazzi C., Torrenti J-M., Adenot F. (2000), "Modelling of leaching in pure cement paste and mortar", Cement and Concrete Research, Vol. 30.

Maréchal J. Le, Gérard B., Marchand J., Gagnon J.Ph., Didry O. (1997), "New accelerated leaching experiment: The LIFT procedure", Recent advances in concrete technology, pp. 951-980.

Markestad A. (1959), "Chemical problems in connection with concrete" (in Norwegian), Norger Tekniska Högskola, Publ. No. 58.

Markestad A. (1977), "An investigation of concrete in regard to permeability problems and factors influencing the results of permeability tests", Norwegian Institute of Technology, STF 65 A 77027.

Marr J., Glasser F.P. (1983), Proc. 6th Int. Conf. Alkali in Concrete, Copenhagen.

Mary, M. (1936), contribution to the discussion with Ruettgers, Proceedings of the ACI, vol. 32, pp. 125-129.

Mason P.J. (1990), "The effects of aggressive water on dam concrete", Water Power & Dam construction.

Mather B., Callan E.J. (1950), "Permeability and Triaxial Tests of Lean Mass Concrete", Corps of Engineer.

Mather K. (1950), "Leaching of lime from concrete", JACI, Discussion February 1950 with Terzaghi.

McMillan F.R., Lyse I. (1930), "Some permeability studies of concrete", Journal of the American Concrete Institute Nov. 1929 – June 1930.

Mehta P.K., Manmohan D. (1980), D., Proc. 7th Int. Congress of Chem. cement, V. II-1-5.

Mehta P.Kk. (1986), "Concrete – structure, properties and materials", Prentice-Hall, U.S.A.

Meyers S.L. (1935), "Discussion of a paper by Messrs. Ruettgers, Vidal and Wing" (see Ruettgers et al 1935), ACI Journal, Proceedings Nov. – Dec. 1935.

Mindess S., Young J.F. (1981), "Concrete", Prentice-Hall, U.S.A.

Mindess S. (2000), "The strength and fractures of concrete: The role of the calcium hydroxide", Proc. of the workshop on the role of calcium hydroxide in concrete, Florida.

Moragues A., Macias A., Andrade C., Losada J. (1988), Cem. Conc. Res.

Moskvin, V. (1980), "Concrete and reinforced concrete deterioration and protection", Mir Publishers, Moscow.

Möller, G., Petersons, N., Elfgren L. (1994), *Strength*, (in Swedish), The concrete Handbook Material, Svensk Byggtjänst, Stockholm.

Nyame B.K., Illston J.M. (1980), "Capillary pore structure and permeability of hardened cement paste", 7th Int. Symp. on the Chemistry of Cement paste", Paris, 1980, vol. III.

Nyame, B. K., Illston, J. M. (1981), "Relationships between permeability and pore structure of hardened cement paste", Magazine of Concrete Research, Vol. 33, No. 116.

Ottosen N., Petersson H. (1992), "Introduction to the Finite Element Method", Prentice Hall, Great Britain.

Peer L. B. B. (1990), Water flow into unsaturated concrete, Ph. D., U. Of Cambridge.

Pereira C.J., Rice R.W., Skalny J.P. (1988), "Pore structure and its relationship to properties of materials", Symp. of Pore structure and permeability of cementitious materials Nov. 28-30, Boston.

Poulsen E. et al (1985), "Sickness of concrete" (in Danish), Beton 4 – Statens byggeforskningsinstitut.

Powers T.C., Copeland L.E. (1954), Hayes J.C., Mann H.M., (1958), J. ACI, Proc., Vol. 5, pp. 285-98.

Powers T.C. (1958), J. Am. Ceram. Soc., Vol. 4, No. 1, pp. 1-5.

Powers T.C., Mann H.M., Copeland L.E. (1958), "Flow of water in hardened Portland cement paste", Highway Res. Branch, special report no 40.

Powers, T. C. (1962), "Physical properties of cement paste", From: Chemistry of cement. Proceedings of the 4th International Symposium, Washington, 1960. Washington D.C., 1962. National Bureau of Standards, Monograph 43, vol. II, pp. 577-613, 1962.

Powers T.C. (1969), "Physical properties of cement paste", Proc. 4th Int. Symp. on the Chemistry of Cement, Washington D.C.

Reardon E.J. (1989), "An ion interaction model for the determination of chemical equilibria in cement/water systems", Cement and Concrete Research, Vol. 20.

Reardon E.J. (1990), Cem. Conc. Res. 20, 175.

Reinius E. (1968), "Water construction part 3, Dams" (in Swedish), Royal Institute of Technology, Stockholm.

Rombèn L. (1978), "Aspects on testing methods for acid attack on concrete", CBI 1:78, Stockholm.

Rombèn L. (1979), "Aspects on testing methods for acid attack on concrete – further experiments", Swedish Cement and Concrete Research Institute, Stockholm.

Roy, D. M. and Jiang, W. (1995), "Concrete chemical degradation: Ancient analogues and modern evaluation", Proceedings of the Materials Research Society's Symposium on Mechanisms of Chemical Degradation of Cement-based Systems, Boston, USA, 27-30.

The Royal Waterpower Board (1929), "Investigations of the long-term water-tightness of concrete slabs", From "Report of investigations regarding the causes of the destruction of concrete in hydraulic structures", Technical report, issue B no. 16, Trollhättan 1929.

Ruetters, A., Vidal, E. N., Wing, S. P. (1935), "An investigation of the permeability of mass concrete with particular reference to Boulder Dam", ACI Journal, Proceedings 1935(31):4, pp. 382-416.

Scheidegger, A. E., (1960), "The physics of flow through porous media", 2nd ed., University of Toronto Press

Skalny J. P. (1989), "A generalised continuum theory for concrete", Cement and Concrete Research Vol. 19, pp. 929-938, USA.

Schneider J. (1992), "Some thoughts on the Reliability Assessment of Existing Structures", Structural Engineering International 1/92.

Stronach S.A., Glasser F.P. (1997), "Modelling the impact of abundant geochemical components on phase stability and solubility of the CaO-SiO₂-H₂O system at 25°C: Na⁺, K⁺, SO₄²⁻, Cl⁻ and CO₃²⁻", Ad. In Cem. Res., 9, NO. 36.

Sundius N. (1930), "About the question of carbonic acid influences on concrete" (in Swedish), The Swedish concrete association.

Sällström S. (1962), "Resistance of lime-leaching of porous mortar with LH-cement at different content of trass" (in Swedish), Statens vattenfallsverk, January 1962.

Sällström, S. (1964), Investigation of the durability of porous cement mortar exposed to continuing water percolation, (in Swedish), Statens Vattenfallsverk, Preliminary report, Stockholm.

Sällström S. (1968), "Watertightness of Dam concrete" (in Swedish), Nordisk Betong 1968:1, Stockholm.

Taylor H. F. W. (1990), "Cement chemistry", Academic Press, London.

Tremper, B. (1931), "The effect of acid waters on concrete", Proceedings of the ACI, vol. 28, pp. 1-32.

Wallin, M. (1988), "A fundamental analysis of the Rate of Limestone Dissolution from a Plane geometry", Licentiate thesis, Department of Chemical Engineer, University of Lund.

Westerberg G. (1933), "Methods for assessing the condition of concrete in hydraulic buildings" (in Swedish), Swedish association of waterpower, Publ. 256.

White F.M. (1979), "Fluid mechanics", McGraw-Hill.

De Wiest R.J.M. (1969), "Fundamental Principles of Ground-Water flow", from "Flow through porous media" edited by De Wiest, Academic Press, New York.

Winslow D. N., Diamond S. (1970), "A mercury porosimetry study of the evolution of porosity in Portland cement paste", Journal of Material, 1970(5):3, pp. 564-585.

Winslow D.N., Lovell (1981)

Winslow D.N., Cohen M.D., Bentz D.P., Snyder A., Garbozci E.J. (1994), "Percolation and pore structure in mortars and concrete", Cement and Concrete research, vol. 24.

Wisnicki B.P., Balbi R., Hula J., Matsuba D., Gutstein D., Lachnit F. (1969), "State of stress and permeability in concrete", University of British Columbia, Vancouver.

Wittman F.H. (1977), "Grundlagen eines Modells zur Beschreibung charakteristischer Eigenschaften des Betons", Deutscher Ausschuss für Stahlbeton, Heft 290.

Young J.F., Berger R.L., Bentur A. (1978), "Shrinkage of tricalcium silicate pastes: superposition of several mechanisms", Il Cemento, Vol. 75, No. 3.

Young J.F. (1988), "A review of the Pore Structure of Cement Paste and Concrete and its Influence on Permeability", Conference proc. Permeability of concrete, ACI.

Yokozeki K, Furusawa Y., Watanabe K., Koseki K. (2000), "Numerical modelling for predicting the degradation of cement-based materials due to calcium leaching", Proc. from Integrated life-cycle design of materials and structures ILCDES 2000, Helsinki.

Ysberg, G. (1979), "Connection between water cement ratio/water-air-cement ratio and compressive strength", report Ra 3:79, Swedish Cement and Concrete Research Institute, Stockholm.

Zienkiewicz, O. C., Taylor, R. L., (1989), "The Finite Element Method", 4th edition, Volume 2, McGraw-Hill, New York.

APPENDIX A STRUCTURE OF CONCRETE

A.1 Introduction

“Concrete has a highly heterogeneous and complex structure. Therefore, it is very difficult to constitute exact models of the concrete structure from which the behaviour of the material can be reliably predicted. However, knowledge of the structure and properties of the individual components of concrete and their relationship to each other is useful for exercising some control on the properties of the material. (...) The type, amount, size, shape, and distribution of phases present in a solid constitute its structure” (Metha 1986). Macrostructure is generally the whole structure visible by the naked eye and microstructure is the portion of the macrostructure that is visible with help of a microscope.

At the macroscopic level, concrete is made up of two main phases: aggregate and cement paste. The aggregate is fixed within the cement paste, which forms a thin “glue” between the particles of the aggregate. Concrete is usually composed of about 65-75% aggregate and 25-35% cement paste.

At the microscopic level it is obvious that the two phases, aggregate and paste, are neither homogeneously distributed with respect to each other, nor are themselves homogenous. For instance, each aggregate particle may contain several minerals, in addition to microcracks and voids. Similarly, hardened cement paste (hcp) generally contains different types and amounts of solid phases, pores, airvoids and microcracks distributed heterogeneously. At the casting of the concrete, air voids are entrapped due to treatment or compression work or are entrained when frost-entraining agents are added. Such air voids are much larger (0.3 – 1 mm) than the other pores in the paste, but are normally assigned to the paste phase (Fagerlund 1994). In the presence of aggregate, the structure of hcp in the vicinity of large aggregate particles is usually very different from the structure of the bulk paste. There is a third phase, the transition zone, which represents the interfacial region between the large aggregate particles and the hcp (Metha 1986). This zone is very thin and makes up a small fraction of the total volume in concrete, but has nevertheless large influence on such properties as strength, freezing resistance and permeability. A schematic picture of the composition of concrete is shown in A.1.

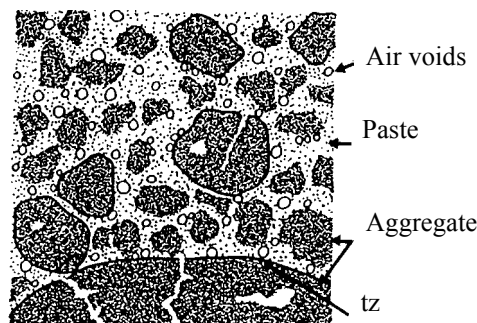


Figure A.1 Schematic picture of the composition of concrete (Fagerlund, 1994)

The properties of concrete are largely determined by the volume fractions of aggregate and cement paste and the individual properties of the aggregate and the paste. The

property of the aggregate are determined by the volume fractions and properties of the different minerals, as well as the amount of pores and cracks.

The properties of cement paste are largely determined by the porosity and the pore structure, which in turn depend on the w/c ratio, the degree of hydration, the air voids, the micro-cracks, possible leaching, etc.

If aggregate is added, this results in either *mortar* or *concrete*, depending upon whether the aggregate is fine or coarse. Aggregate “disturbs” the cement paste structure. The properties of the interfacial border between the cement paste and the aggregate differ from those of both the cement paste and the aggregate, the porosity there being greater, microcracks being common, water separation may have produced possible cavities under the aggregate, air voids having possibly been trapped and a larger number of calcium hydroxide crystals are present (Fagerlund 1980a). These properties make this zone weaker, more water-permeable and more sensitive to leaching.

The *chemical* and *physical* properties of concrete affect its engineering characteristics, such as its strength, elasticity, fracture toughness and permeability.

The chemical properties of concrete depend on the different compounds, how they are combined and how they interact with each other chemically.

The physical structure of concrete can be described by the shape and amount of the different phases it contains. Its physical properties are related to how the hydration products are formed and connected with each other, their geometrical size and connectivity, and the shape of the pores between them. Water permeability and leaching are strongly affected by the pore size distribution and connectivity. There are different types of pores in concrete: the gel pores in the cement gel, the capillary pores between the solids in the cement gel and finally, the pores in the interface between the cement gel and the aggregate. In addition, there can be air voids and cracks.

The chemical and physical structures interact with each other. For example, the physical properties of the pore system determine how easily water or substances dissolved in it, can penetrate the pores, whereas the chemical properties determine how easily this water and aggressive substances, can react with the solid material inside the pore system. Such important properties as permeability to water or to ions are determined by chemical interactions between molecules or ions.

The desirable engineering characteristics of hardened concrete – strength, dimensional stability, (permeability), and durability – are influenced not only by the proportion but also by the properties of the hcp, which, in turn, depend on the microstructural features, i.e. the type, amount, and distribution of solids and voids. (...) Strength and permeability of the hcp are two sides of the same coin in the sense that both are closely related to the capillary porosity or the solid/space ratio. (Metha 1986), see figure A.2.

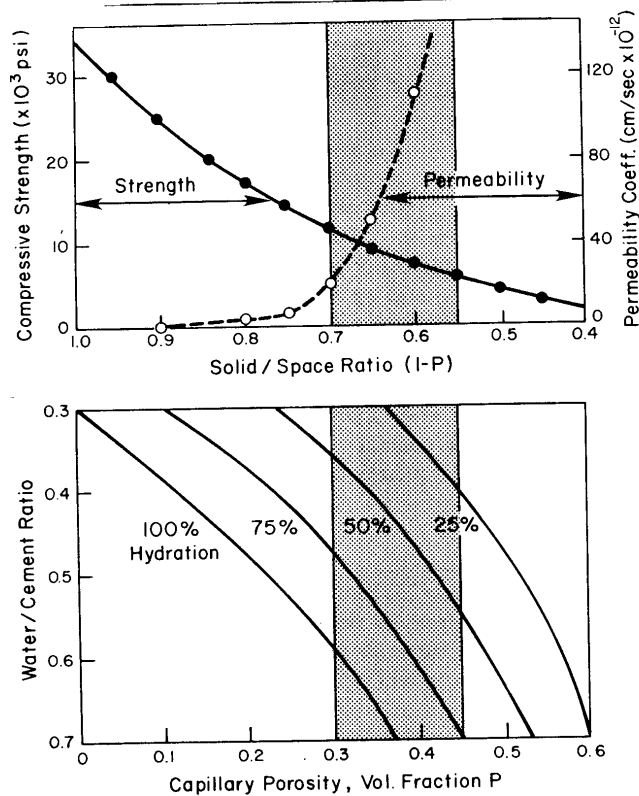


Figure A.2 Influence of the solid/space ratio and capillarity porosity on strength and permeability. From experimentally obtained values obtained by Powers, as presented in Metha (1986).

During recent decades, a number of models have been developed for describing concrete, cement paste and the interfacial zone between the paste and the aggregate. The aim of these models has varied. The early models (of Powers, Sereda, Wittman and others) aimed at an understanding of the physical behaviour, geometry and shape of the paste, from the nanoscale to the microscale. Later models (of Bentz, Garboczi and co-workers, van Breugel, Jennings and others) are frequently of numerical nature aiming at calculating the time development of specific properties such as the porosity and pore geometry, the heat of hydration, the strength, the transport properties, or aiming at developing numerical models regarding long-term properties, such as durability.

A.2 Cement

The cement in concrete can be of different types. Here, only Ordinary Portland cement (OPC) is considered. OPC consists mainly of raw materials obtained from limestone, sand and clay, The raw materials are mixed, heated and ground, the resulting product being *cement*. In OPC, the main clinker minerals are C_2S , C_3S , C_3A and C_4AF , see table A.1.

Table A.1 Notations for different compounds in Ordinary Portland cement

| Notations employed | Chemical formula | Mole weight (g) | Density ¹⁾ (kg/m ³) |
|-------------------------|---|-----------------|--|
| C | CaO | 56.08 | |
| S | SiO ₂ | 60.09 | |
| H | H ₂ O | 18 | 1000 |
| A | Al ₂ O ₃ | | |
| F | Fe ₂ O ₃ | | |
| M | MgO | | (3580) |
| \bar{S} | SO ₄ ²⁻ | 96.07 | |
| C ₃ S | 3CaO·SiO ₂ | 228.33 | 3210 (3500) |
| C ₂ S | 2CaO·SiO ₂ | 172.25 | 3280 |
| C ₃ A | 3CaO·Al ₂ O ₃ | | 3030 |
| C ₄ AF | 4CaO·Al ₂ O ₃ ·Fe ₂ O ₃ | | 3730 |
| $\bar{C}\bar{S}H_2$ | | | (2320) |
| $\bar{C}\bar{S}H_{1/2}$ | | | (2740) |
| Portland cement | | | (3150) |

¹⁾Bentz (1999), (Mindess & Young (1981) tab. 4.7)

A.3 The structure of cement paste

A.3.1 Chemistry of hydration

When cement is mixed with water, the most soluble compounds in the cement, particularly K⁺, Na⁺, Ca²⁺, SO₄⁻ and OH⁻, dissolve in the water with the release of heat. In this mixture, containing constituents that readily react with water molecules, and in which heat is available, many new compounds are formed, primarily of the cement constituents and water. Crystals of Ca(OH)₂ and ettringite precipitate. An increasing layer of hydration products, in which water diffuses and reacts with the cement, covers the residual cement grains. As the degree of hydration increases, less cement grains remain and more hydration products are formed. Amorphous or crystallite solids are formed in which water molecules, or water ions (H⁺ and OH⁻), are incorporated. These solid products, called *hydration products*, form the *cement paste*. The hydration products in hardened concrete have a very large internal surface in relation to their mass, their forming a porous complex. Some of the cement constituents (such as K⁺, Na⁺ and OH⁻) remain to a large extent dissolved in the pore solution between the hydration products. The dominant part of the hydration products in the OPC paste is made up of calcium silicate hydrates (C-S-H), calcium hydroxides (CH) and calcium aluminium iron hydrates. CH is formed as a by-product of the hydration of C₃S and C₂S.

Calcium silicates and calcium hydrates

The hydration reactions of the dicalcium silicate (belite) and the tricalcium silicate (alite) are stoichiometrically very similar, differing only in the amount of calcium hydroxide produced.



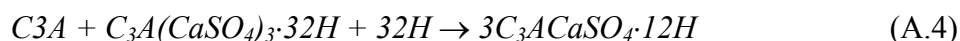
The composition of the C-S-H gel varies but can be written in approximate form as $1.7\text{CaO}\cdot\text{SiO}_2\cdot x\text{H}_2\text{O}$, where $x=1-4$ (Taylor 1990). $a\approx 1$ and $b\approx 3$.

Aluminium, ferrite and sulphate phases

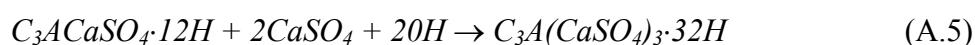
C_3A reacts with gypsum CaSO_4 to form ettringite



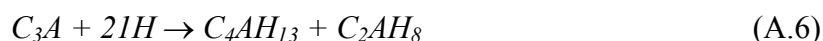
After awhile when more C_3A reacts, the ettringite is transformed into the monosulphate:



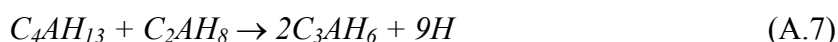
If the monosulphate in the hardened concrete is exposed to sulphate ions from the surroundings, ettringite can be formed once again causing what is called a sulphate attack. It can destroy the hardened concrete through expansion:



If no gypsum is added during casting, flash setting may occur due to the rapid formation of

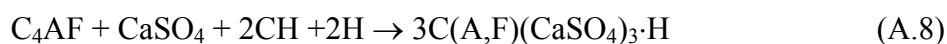


which is not stable and is later converted to hydrogarnet



This C_3AH_6 paste of is the same as formed in high alumina cement, but is formed so rapidly that it develops no strength.

If the clinker also contains ferrite, the reaction looks like the reaction with C_3A , but is slower. An example of the reaction is



The aluminium, ferrite and sulphate phases have the general composition $\text{C}_3(\text{A,F})\cdot x\text{CaX}\cdot y\text{H}$, where X can be different anions, e.g. SO_4^{2-} , OH^- or CO_3^- .

For the AFm phase there is one ($x=1$) CaSO_4 and for the AFt phase there are three ($x=3$) CaSO_4 .

Typical pore-water compositions of hydrated cement is shown in table A.2

Table A.2 Measured pore-water compositions of hydrated cement in mmoles/litre; from Andersson (1983) and Marr & Glasser (1983), as presented in Berner (1987) table IV.

| <i>Na</i> | <i>K</i> | <i>Ca</i> | <i>Mg</i> | <i>Al</i> | <i>Si</i> | <i>Fe</i> | <i>OH</i> | <i>Eh</i> (<i>mV</i>) | <i>pH</i> |
|-----------|----------|-----------|-----------|-----------|-----------|-----------|-------------------|----------------------------|-----------|
| 65.2 | 161.1 | 2.25 | <0.01 | <0.2 | <0.2 | <0.01 | 231 ¹⁾ | 139 | 13.4 |

¹⁾ OH^- is given as the sum $[\text{Na}^+] + [\text{K}^+] + 2\cdot[\text{Ca}^{2+}]$

Notations of the most common compounds in cement paste and theirs chemical formulas, mole weights and density are shown in table A.3.

Table A.3 Notations for different compounds contained in ordinary Portland cement paste.

| Notations employed | Chemical formula | Mole weight (g) | Density ¹⁾ (kg/m ³) |
|---|--|-----------------|--|
| 3CaO·2SiO ₂ ·3H ₂ O | C ₃ S ₂ H ₃ (C-S-H) | 342.42 | 2120 |
| CH | Ca(OH) ₂ | 74.08 | 2240 |
| 3CaO·Al ₂ O ₃ ·6H ₂ O | C ₃ AH ₆ | 378.2 | 2520 |
| 3CaO·Fe ₂ O ₃ ·6H ₂ O | C ₃ FH ₆ | 435.94 | |
| CaSO ₄ | Ca \bar{S} | 136.15 | |
| 3CaO·Al ₂ O ₃ ·3CaSO ₄ ·32H ₂ O | C ₃ A·3Ca \bar{S} ·32H (AFt) | 1254.65 | 1700 |
| 3CaO·Al ₂ O ₃ ·CaSO ₄ ·12H ₂ O | C ₃ A·Ca \bar{S} ·12H (AFm) | 622.35 | 1990 |
| <i>MH</i> | | | (2370) |
| <i>C₄AH₁₃</i> | | | (2020) |
| <i>C₂AH₈</i> | | | (1950) |

¹⁾Bentz (1999), (Mindess & Young (1981) tab. 4.7)

Example: An example is presented of the hydration products that are formed when OPC is hydrated. The example is rather realistic in terms of the type of cement used in the present work. The example is included so that correct estimates can be made, later on in the report, of the residual contents of leached concrete. For approximate weight parts of the different hydration products in the OPC reactions, see table A.4.

Table A.4 The main Portland cement reactions (weight parts) of pure clinker compounds in water.

| Reactants | | Products |
|---|---|--|
| 2 C ₃ S + 6H 1.00 + 0.24 | → | C-S-H + 3CH 0.75 + 0.49 |
| 2 C ₂ S + 4H 1.00 + 0.21 | → | C-S-H + CH 1.00 + 0.21 |
| C ₃ A + 6H 1.00 + 0.40 | → | C ₃ AH ₆ 1.40 |
| C ₄ AF + 2CH + 10H 1.00 + 0.31 + 0.37 | → | C ₃ AH ₆ + C ₃ FH ₆ 0.78 + 0.90 |
| C ₃ (A,F) + xCaX + yH X = e.g. SO ₄ ²⁻ , OH ⁻ , CO ₃ ⁻ | | C ₃ (A,F)·xCaX·yH (general) |
| C ₃ (A,F) + 3Ca \bar{S} + 32H (x=3, y=32) 1.0 + 1.51 + 2.13 | → | C ₃ (A,F)·3Ca \bar{S} ·32H ettringite (AFt) 4.64 |
| C ₃ (A,F) + Ca \bar{S} + 12H (x=1, y=12) 1.0 + 0.50 + 0.80 | → | C ₃ (A,F)·Ca \bar{S} ·12H monosulphate (AFm) 2.30 |

The hydration products formed in the cement used in the present work can be assumed to have the following clinker-composition:

$$a \cdot C_3S + b \cdot C_2S + c \cdot C_3A + d \cdot C_4AF + e \cdot \bar{S} \quad (\text{A.9})$$

where a, b, c, d, e = constants describing the weight fractions in cement clinker; and C₃S, C₂S, C₃A, C₄AF, \bar{S} , see above. The constants a, b, c, d and e are assumed to be 0.557, 0.228, 0.021, 0.131 and 0.0207 respectively. The figures are provided by the

supplier of the cement used in the concretes denoted 0.80a, 0.80b and 1.29 in the experimental study (see Table 4.3). For the concrete of types 0.60 and 0.80c, $a = 0.573$ and $b = 0.218$. Assume that half of the SO_4^{2-} in the cement becomes bonded as Aft and half as AFm. In the example, the following amount of hydration products were obtained (concrete types 0.80a, 0.80b and 1.29):

$$\alpha \cdot (0.557 \cdot C_3S + 0.228 \cdot C_2S + 0.021 \cdot C_3A + 0.131 \cdot C_4AF + 0.0207 \cdot \bar{S}) \cdot C \text{ (kg)} \quad (\text{A.10})$$

$$m_{CSH} = \alpha \cdot (0.557 \cdot 0.75 + 0.228 \cdot 1.00) \cdot C = \underline{\alpha \cdot 0.646 \cdot C} \text{ (kg CSH)} \quad (\text{A.11})$$

$$\begin{aligned} m_{CH} &= \alpha \cdot (0.557 \cdot 0.49 + 0.228 \cdot 0.21 + 0.131 \cdot (-0.31) + 0.0207 \cdot (-1.0 \cdot 74.08 / 40.08)) \cdot C = \\ &= \underline{\alpha \cdot 0.242 \cdot C} \text{ (kg CH)} \end{aligned} \quad (\text{A.12})$$

$$m_{C_3AH_6} = \alpha \cdot (0.021 \cdot 1.40 + 0.131 \cdot 0.78) \cdot C = \underline{\alpha \cdot 0.131 \cdot C} \text{ (kg } C_3AH_6) \quad (\text{A.13})$$

$$m_{C_3FH_6} = \alpha \cdot (0.131 \cdot 0.90) \cdot C = \underline{\alpha \cdot 0.118 \cdot C} \text{ (kg } C_3FH_6) \quad (\text{A.14})$$

$$m_{Aft} = \alpha \cdot 0.5 \cdot 0.0207 \cdot 4.64 \cdot C = \underline{\alpha \cdot 0.048 \cdot C} \text{ (kg Aft)} \quad (\text{A.15})$$

$$m_{AFm} = \alpha \cdot 0.5 \cdot 0.0207 \cdot 2.30 \cdot C = \underline{\alpha \cdot 0.023 \cdot C} \text{ (kg AFm)} \quad (\text{A.16})$$

Where α = degree of hydration (-); and C = content of cement (kg).

In table A.5, the part and total amount of calcium (Ca) in the different hydration products are shown for the present example. The total Ca, from the hydration products, in this example is $0.447 \cdot \alpha \cdot C$ (kg). If the degree of hydration is below 1.0, the remainder of the calcium in the cement is $(1-\alpha) \cdot 0.447 \cdot C$. In table A.6 is shown the same calculations but for cement used for the specimens 0.60 and 0.80c in the experimental study.

Table A.5 The amount of hydration products and of Ca contained in the hydration products at a degree of hydration of 1.0, as assumed for concrete of the types 0.80a, 0.80b and 1.29 used in the experimental study.

| unity | C-S-H | CH | C_3AH_6 | C_3FH_6 | Aft | AFm | Sum |
|--------------|---------------------|-------|-----------|-----------|-------|-------|-------|
| kg/kg cement | 0.646 | 0.242 | 0.131 | 0.118 | 0.048 | 0.023 | |
| (g/mole) | 342 | 74 | 378 | 436 | 1255 | 622 | |
| g Ca/mole | 3.40 | 40 | 3.40 | 3.40 | 6.40 | 4.40 | |
| Ca | 0.227 ¹⁾ | 0.131 | 0.042 | 0.032 | 0.009 | 0.006 | 0.447 |

¹⁾Example: $0.646 \cdot (3.40) / 342 = 0.227$ kg Ca/kg cement.

Table A.6 The amounts of hydration products and of Ca in the hydration products assumed for a degree of hydration of 1.0 of concrete of the types 0.60 and 0.80c used later in the study.

| unity | C-S-H | CH | C ₃ AH ₆ | C ₃ FH ₆ | Aft | AFm | Sum |
|--------------|---------------------|-------|--------------------------------|--------------------------------|-------|-------|-------|
| kg/kg cement | 0.648 | 0.248 | 0.131 | 0.118 | 0.048 | 0.023 | |
| (g/mole) | 342 | 74 | 378 | 436 | 1255 | 622 | |
| g Ca/mole | 3·40 | 40 | 3·40 | 3·40 | 6·40 | 4·40 | |
| Ca | 0.227 ¹⁾ | 0.134 | 0.042 | 0.032 | 0.009 | 0.006 | 0.450 |

¹⁾Example: $0.648 \cdot (3 \cdot 40) / 342 = 0.227$ kg Ca/kg cement.

A.3.2 The development of structure

When cement and water are mixed, the cement reacts with the water to form a porous conglomerated mass of fine crystal-like *gel* particles constituting the *cement gel*, see figure A.3. The main volume of the gel consists of calcium-silicate-hydrate products in which calcium hydroxide is incorporated. Besides it contain about 28% fine “gel-pores”. The gel volume grows as the hydration proceeds. Part of the original volume not occupied by gel consists of *capillary pores*, which are much coarser than gel pores. Young pastes have a inter-connected capillary-pore system, but as hydration proceeds the hydration products grow into the capillary pores, the capillary pore volume being reduced and at a certain hydration stage gel “blocks” the continuous capillary pore system gel.

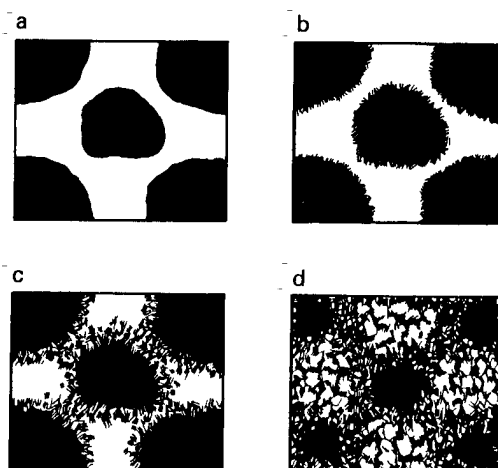


Figure A.3 Development of the structure of cement paste according to Powers (1962), (a) just after the mixing of cement and water, (b) after a few minutes, (c) when the hydration products become connected and (d) after a few months (presented in Fagerlund, 1994).

In table A.7, the approximate hydration age when all interconnected capillary pores are blocked by cement gel, is shown for cement pastes of differing w/c ratio.

Table A.7 Approximate hydration age when all interconnected capillary pores are blocked in cement paste of differing w/c ratios (Powers, Copeland & Mann, (1959) as presented in Fagerlund (1994).

| W/c ratio | 0.40 | 0.45 | 0.50 | 0.60 | 0.70 | >0.70 |
|-----------|--------|--------|---------|----------|--------|-------|
| Age | 3 days | 7 days | 14 days | 6 months | 1 year | never |

The development of the degree of hydration (α) is dependent upon the chemical properties of the cement and on the specific area involved, as well as on the w/c ratio, the temperature, the moisture conditions during curing, and any additives that used.

The C-S-H structure in the inner part of the hydrated layer of the cement grain is more massive and is almost amorphous (Taylor 1990). The outer part formed in the water-filled spaces forms columns of fibres radiating outwards. Only about 45% of a completely hydrated cement particle can occupy the original size of the particle. The remaining 55% of the gel formed is located outside the original cement particle (Fagerlund 1980a).

Photographs taken by an ESEM microscope of one of the specimen tested in the present work are shown in figure A.4. The physical structure of the cement paste can be discerned to some extent there. The “fluffy” balls consist of hydrated C-S-H gels that have grown into the capillary pores. The internal porosity of the cement paste is high, as can be seen. The CH grows inside the C-S-H, or between parts of it. It is limited in size by the space available.

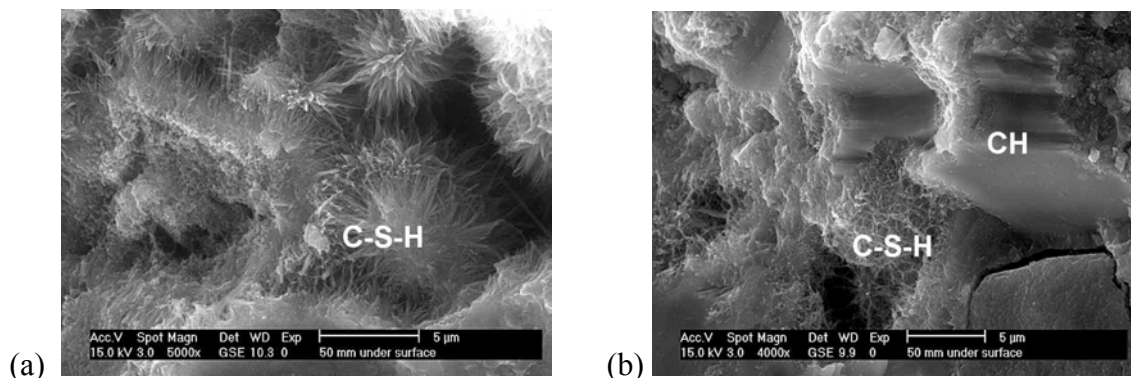


Figure A.4 ESEM photograph of one of the specimens tested in the study. (a) “Fluffy” Calcium-Silicate-Hydrate gel with capillary pores located in between. (b) Calcium-Silicate-Hydrate gel into which calcium hydroxide and capillary pores have become incorporated. Finger Institute, University of Weimar.

The older the cement paste becomes, the denser and more featureless the C-S-H gel appears. Tobermorite and Jennit are natural minerals that resemble C-S-H gel. This has an extraordinarily high internal surface area as measured by water adsorption, in the range of 250 – 450 m²/g (Mindess & Young 1981) or 100-700 m²/g (Metha 1986). Measurements by N₂-sorption gives considerably smaller surface area.

There are three major conceptual models of C-S-H gel presented in the literature, the *Powers-Brunauer* model (see e.g. Powers 1962), the *Feldman-Sereda* model (Feldman & Sereda 1970) and the *Munich* model.

According to Mindes and Young, the models have various features in common: *“recognition that water plays a very important role in the structure and behaviour of C-S-H. Also, the material is in a high-energy state because of the additional energy associated with the extensive free surface. (...) Water is held within C-S-H in a variety of ways, ranging from bulk water in capillary pores, through water physically adsorbed*

on surfaces or between surfaces (micropores) and water structurally associated with the solid (interlayer water), to hydroxyl water in the solid lattice. There appears to be no sharp distinction between the various forms but a gradual transition between them.”

According to Fagerlund (1994), the largest difference between the models of Feldman-Sereda and of Powers are that Feldman-Sereda regard water at low relative humidities (<11 %) as a part of the structure, whereas Powers regard this water as part of the pore solution.

A major advantage of the Powers model is that it can be used for quantitative calculations of porosity, permeability, strength, shrinkage, etc.

Bentz and Garbotczi (1991, 1992, 1996, 1997) have developed a 3-dimensional digital-image-based simulated microstructural model of cement hydration. They use a computer model in which cement particles of C_3S lie randomly within a 3-dimension space. Hydration is represented as a series of digital dissolution/diffusion/reaction steps. The particles are allowed to hydrate randomly and thereby grow by the following relation, $1.0C_3S \rightarrow 1.7(C-S-H) + 0.61CH$, where C-S-H is calcium silicate hydrate (cement gel) and CH is calcium hydroxide (volume ratios). Due to this, hydration, the porosity and the permeability decrease. The pixels used in the computer model can be solid phases or pore space. In the leaching process, the computer does the opposite, taking away hydration products (pixels) randomly, the porosity and the permeability increasing. At each degree of hydration or leaching ratio the computer tests how connected the pore-pixels are by investigating the percolation (or diffusion) ability. The approach Bentz and Garbotczi use is to utilise properties computed at one scale level of modelling as input in the computation procedures employed at a higher scale. The scales are: (i) a nano-scale (5nm) for the quasi-random growth of overlapping hydration products; (ii) a meso-scale (40 nm) involving spherical agglomerates, each composed of smaller nano-level particles; (iii) a micro-scale in 3 dimensions modelling microstructural development during hydration, using stoichiometric restrictions, and (iv) finally a macro-scale on which mortar and concrete are modelled as a continuum of cement paste containing rigid (non-overlapping) spherical and ellipsoidal aggregate particles. To utilise these solution technique, the properties of each phase in the microstructure must be known or assumed. The authors utilise properties computed at one scale level of modelling as input to the computation procedures employed at a higher scale (Garbotczi & Bentz 1996).

The 3D microstructural model is analysed in terms of material properties such as percolation characteristics, see for example figure A.5. When the solid fractions are connected $p = 0$, each of the sub-units is totally isolated from each of the other sub-units, whereas $p = 1$, all the sub-units are connected.

At a micro-scale level, percolation theory indicates the diffusion properties in particular, whereas at the macro-scale level percolation theory indicates the flow of viscous fluids. At the micro-scale, percolation occurs through channels in the paste, whereas at the macro-scale percolation occurs mainly through channels between aggregates in connected interfacial zones.

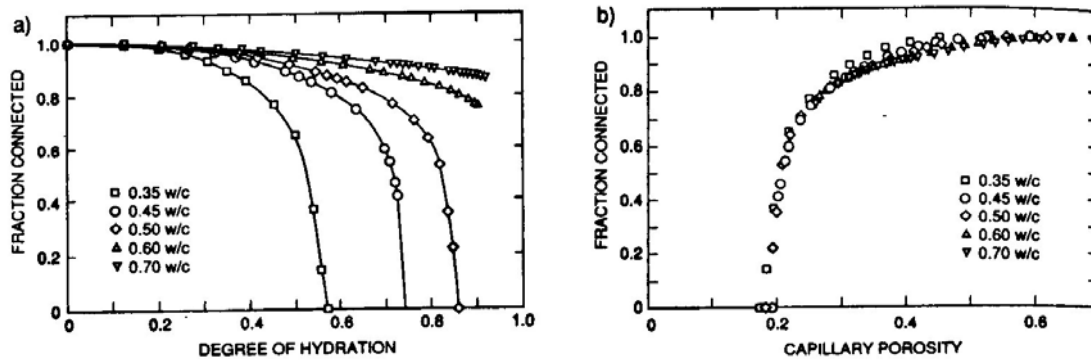


Figure A.5 Percolation plots of the calculated porosity in neat $C_s s$ pastes, showing (a) fractions connected by capillary porosity vs. degree of hydration and (b) fractions connected by capillary porosity vs. total capillary porosity (Bentz & Garboczi 1991).

Bentz and Garboczi have performed a large number of simulations on fictive cement pastes with use of this computer model. They have modelled such properties as porosity, fraction of pores connected, percolation in capillary pores and ionic diffusivity for both the hydration phase and any possible leached phase. The early hydration phase has also been simulated in terms of interfacial zone percolation, strength development, thermal development and self-desiccation, see Bentz and Garboczi (1991b), (1992), Garboczi and Bentz (1992), (1998), (1998) and Bentz (1999).

Eijk and Brouwers (1998), using the same modelling method as Bentz and Garboczi, provide other volume fractions for the hydration products by also taking account of chemical shrinkage using the reaction; $C_s S \rightarrow 1.52(C-S-H) + 0.61CH$.

Calcium hydroxide crystals constitute 20 to 25 % of the volume of the solids in the completely hydrated paste (Mindess & Young 1981, Metha 1986). Under ideal conditions of crystallisation, CH forms hexagonal plates with weak bonding forces between each of the plates (Taylor 1990). In contrast to the C-S-H, the calcium hydroxide, $Ca(OH)_2$ has definite stoichiometry. “*The morphology usually varies from nondescript to stacks of large plates, and is affected by the available space, temperature of hydration, and impurities present in the system*” (Metha 1986). Portlandite is a naturally occurring mineral that is similar to CH in cement paste. Crystals of CH grow where free space is available. If it is stopped in one direction it grows in another. If it encounters a hydrating cement grain it may well grow around it (Mindess & Young 1981). The morphology of CH, which depends on the hydration conditions, is described by (Mindess 2000) as follows:

- “*Separate or aggregate crystals and crystallites scattered in the cement paste;*
- *Layers covering the surfaces of aggregate particles, ranging in thickness from a few μm to more than 50 μm (figure A.14);*
- *In what were originally bleed water pockets on the undersides of coarse aggregate particles;*
- *In narrow spaces between aggregate particles;*
- *As CH shells of varying thickness precipitated around air-filled voids;*
- *And as large hexagonal crystals within air bubbles” (figure A.6b).*

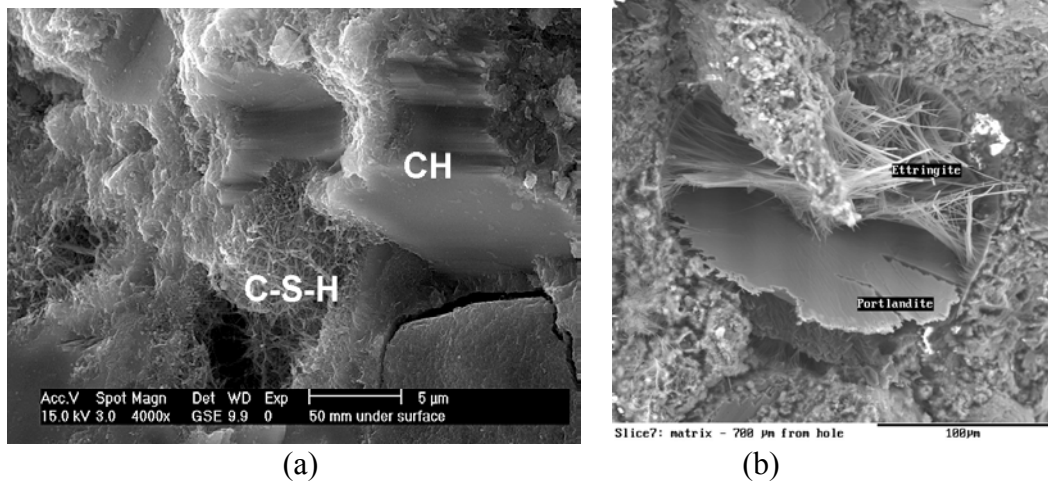


Figure A.6 ESEM photographs of one of the specimens tested in the study. (a) Portlandite (CH) incorporated into C-S-H-gel. Observe the crack between the aggregate and the paste. (b) Portlandite in an air void (b). Finger Institute, University of Weimar.

Aft phases form hexagonal prismatic crystals (Taylor 1990) with columns of $[\text{Ca}_3(\text{A},\text{F})(\text{OH})_6 \cdot 12\text{H}_2\text{O}]^{3+}$ running parallel to the prism, X-anions and H_2O are located between the columns. Figure A.7 shows Aft that has grown inside an air pore.

The AFm crystal looks similar to CH, but each third atom of Ca has been exchanged for an atom of Al or Fe. Between successive layers there are X-anions that level out the charge differences, as well as water molecules. The differences in size between the Ca-atoms and the atoms of Al and Fe make the layer which for CH was a perfect plane somewhat distorted.

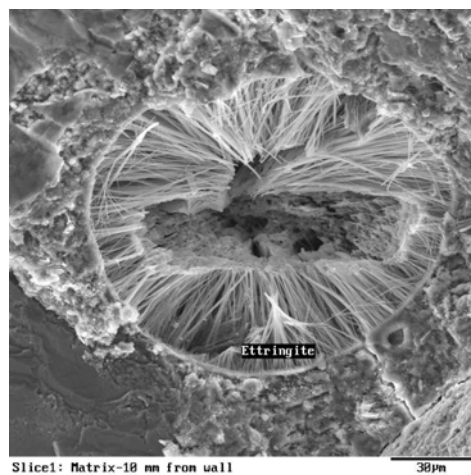


Figure A.7 Ettringite (Aft) within an air void. ESEM photograph of one of the specimens tested in the study. Finger Institute at the University of Weimar.

A.3.3 The porosity and density of cement paste

The pore structure influences almost all the properties of a porous material: the density, mechanical properties (strength, fracture energy, shrinkage, creep, elasticity) durability, thermal properties, permeability, electric properties, etc. (Fagerlund, 1972).

All hydration products are lower in specific gravity and higher in specific volume than the cement compound itself. Thus, every hydration reaction is accompanied by an increase in solid volume (Mindess & Young 1981). Yet since the hydration products C-S-H and CH grow into the spaces available between the cement particles (and the aggregate particles if any), the hydration of calcium silicates is not accompanied by any increase in the total volume. They only occupy space within the paste available to them.

“And, the generation of the much smaller hydration products subdivides the initial pore space between the anhydrous grain, resulting in increasingly smaller pore diameters”(Winslow & Lovell 1981). *“Thus cement hydration may be looked upon as a process during which the space originally occupied by cement and water is being replaced more and more by the space filled by hydration products. The space not taken up by the cement or the hydration products consists of capillary voids, the volume and size of the capillary voids being determined by the original distance between the anhydrous cement particles in the freshly mixed cement paste and the degree of cement hydration”* (Metha 1986). *“Quite the contrary occurs when ettringite is formed from C₃A or the ferrite phase. Ettringite crystals will make space for themselves when their crystal growth is impeded by solid material”* (Mindess & Young). This is not a problem in unhardened paste, where the ettringite can push aside obstructing cement grains, but in hardened paste large stresses can arise and lead to cracks in the paste.

From the ESEM-photographs presented above it can be seen that cement paste has a very complex system of pores, with large differences in pore sizes. There are considerable difficulties in describing such pore systems in quantitative terms. In attempts to measure them, most test methods includes drying of the cement paste, almost surely changing the pore structure. Besides, in analysing the results a simple particular geometrical shape must be assumed, even if the real pore structure is highly complex and can change very much. A classification of the porosity of cement paste is given in table A.8.

Table A.8 Classification of the pore sizes in hydrated cement paste (Mindess & Young 1981)

| Designation | Diameter | Description | Role of water | Paste properties affected |
|-----------------|--------------|--------------------------|---|--|
| Capillary pores | 50-10 000 nm | Large capillaries | Behaves as bulk water | Strength; permeability |
| | 10~50 nm | Medium-sized capillaries | Moderate surface tension forces generated | Strength; permeability; shrinkage at high humidities |
| Gel pores | 2.5-10 nm | Small (gel) capillaries | Strong surface tension forces generated | Shrinkage to 50% RH |
| | 0.5-2.5 nm | Micropores | Strongly adsorbed water; no menisci form | Shrinkage; creep |
| | <~0.5 nm | Micropores “interlayer” | Structural water involved in bonding | Shrinkage; creep |

Table A.8 shows there to be an enormous range of pore sizes, from 10 μm to less than 0.5 nm in diameter. “Thus, the water that occupies the pores plays many roles. It is useful to make a distinction between capillary pores and gel pores in a hydrated paste. The capillary pores are the remnants of water-filled space that exists between the partially hydrated cement grains; the gel porosity can be regarded as part of the C-S-H. The porosity seen in SEM micrographs is capillary porosity; the gel porosity cannot be resolved by the SEM and would be included in the volume occupied by C-S-H. In mature pastes the bulk of the porosity resides within the C-S-H. The size division between capillary and gel porosity is to a large extent arbitrary, as the spectrum of pore sizes is a continuous one. It should also be noted that gel pores include small capillary pores if we use the more accurate definition that a capillary pores one in which capillarity effects can occur (i.e., a meniscus can form). As can be seen (in table A.8), porosity over the whole size range of pores has an influence on paste properties. Yet it is difficult to get an exact assessment of pore-size distributions because no one measurement encompasses the whole size range and because it is difficult to interpret experimental data. Thus, comparisons of porosity should be made with care” (Mindess & Young 1981).

Figure A.8 shows both the solid phases and the voids in hcp (hardened cement paste).

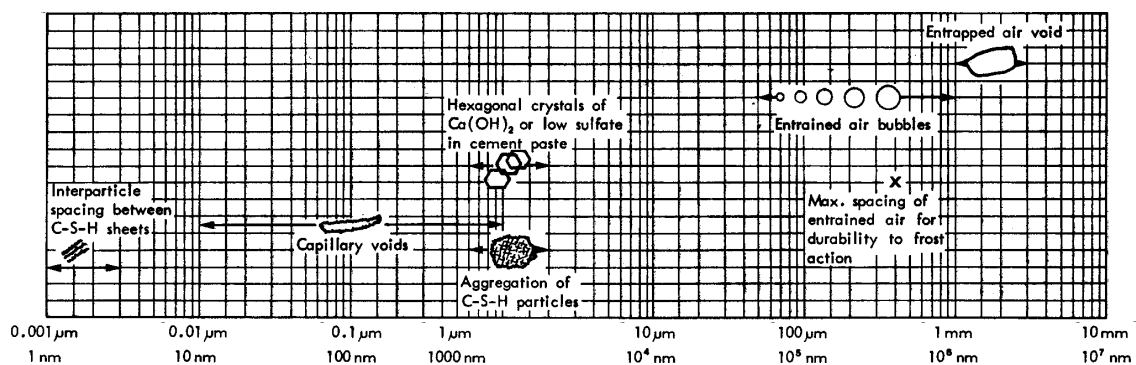


Figure A.8 Range in the dimensions of solids and pores in hydrated cement paste (Metha, 1986).

It is not the total porosity but the pore size distribution and the connectivity that control the strength, permeability, and volume changes in hcp. Pore size distributions are affected by the water/cement ratio, and age (degree of cement hydration). Large pores (larger than 50 nm) influence mainly the compressive strength and the permeability, whereas small pores (smaller than 50 nm) mainly influence the drying shrinkage and creep (Metha 1986).

“Whereas the capillary voids are irregular in shape, the air voids are generally spherical. (...). Air can be entrapped in the fresh cement paste during the mixing operation. Entrapped air voids may be as large as 3 mm; entrained air voids usually range from 50 to 200 μm . Therefore, both the entrapped and entrained air voids in the hcp are much bigger than the capillary voids, and are capable of adversely affecting its strength and impermeability” (Metha 1986).

Winslow and Lovell (1981) performed a mercury intrusion investigation of cement pastes. The pastes were mixed at two different w/c ratios: 0.4 and 0.6. Any entrapment of air appeared to have been avoided by the pastes being mixed in an evacuation chamber. Prior to the mercury intrusion, the specimens were dried at +105°C. The results show various general trends (figure A.9).

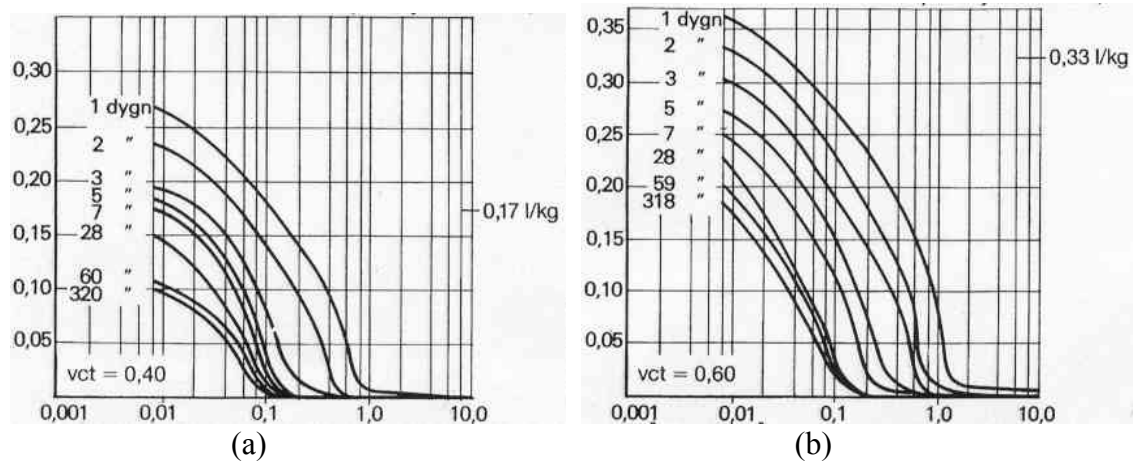


Figure A.9 Volume of mercury (l/kg) that penetrated in relation to the pore size distribution (μm) in hydrated cement pastes at w/c ratios of 0.4 (a) and 0.6 (b), from Fagerlund (1994) based on Winslow & Lovell (1970).

Typical pore size distribution plots of several hcp specimens tested by use of the mercury intrusion technique are also shown in figure A.10.

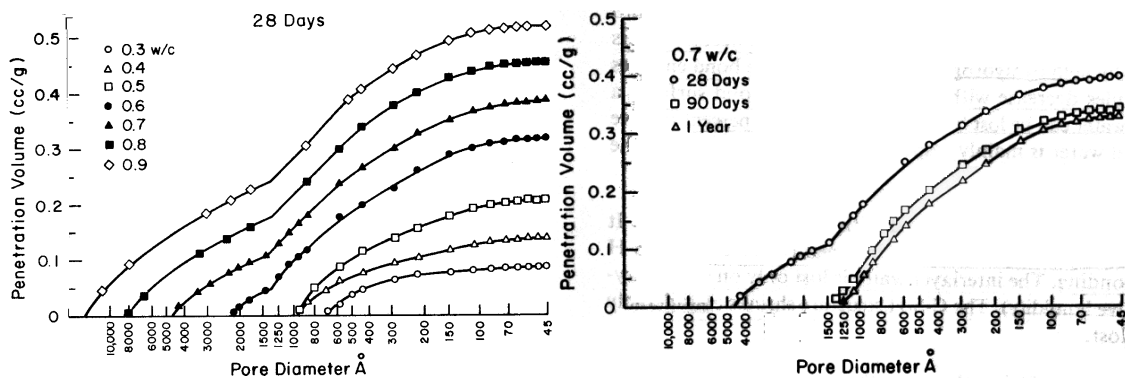


Figure A.10 The pore size distribution of hydrated cement pastes. From Metha & Manmohan, 1980, presented in Metha (1986).

The volume of mercury that intrudes is used to determine the pore volume, the pore size being calculated from the intrusion pressure. The following factors can limit the accuracy of mercury intrusion porosimetry (MIP), however, (Holly et al. 1993, Maggion et al. 1996):

- The method of drying can damage or change the microstructure of the pores.
- Intrusion in any pores that are only accessible by way of a narrow entrance will occur at a pressure corresponding to the pore size at the entrance.

- The high pressure that is necessary for intrusion into the smaller pores can damage and alter the microstructure of the pores.
- The simplifying pore-geometry assumptions necessary for analysing the results are not representative of the structure.

MIP therefore provides no true pore size distribution. It simply indicates the accessibility of the overall porosity as a function of pore size. If many large pores lie inside a narrow neck, MIP shows too large amount of pores with the size of that neck. This is especially pronounced for the pores and microcracks in the interfacial zone between the cement paste and the aggregate. Only if these pores or cracks provide a continuous passageway, are they recorded correctly by MIP in terms of volume and size (Winslow et al. 1994).

Basic volume relationships between cement, cement gel, gel pores, capillary pores and water in cement paste are shown in figure A.11.

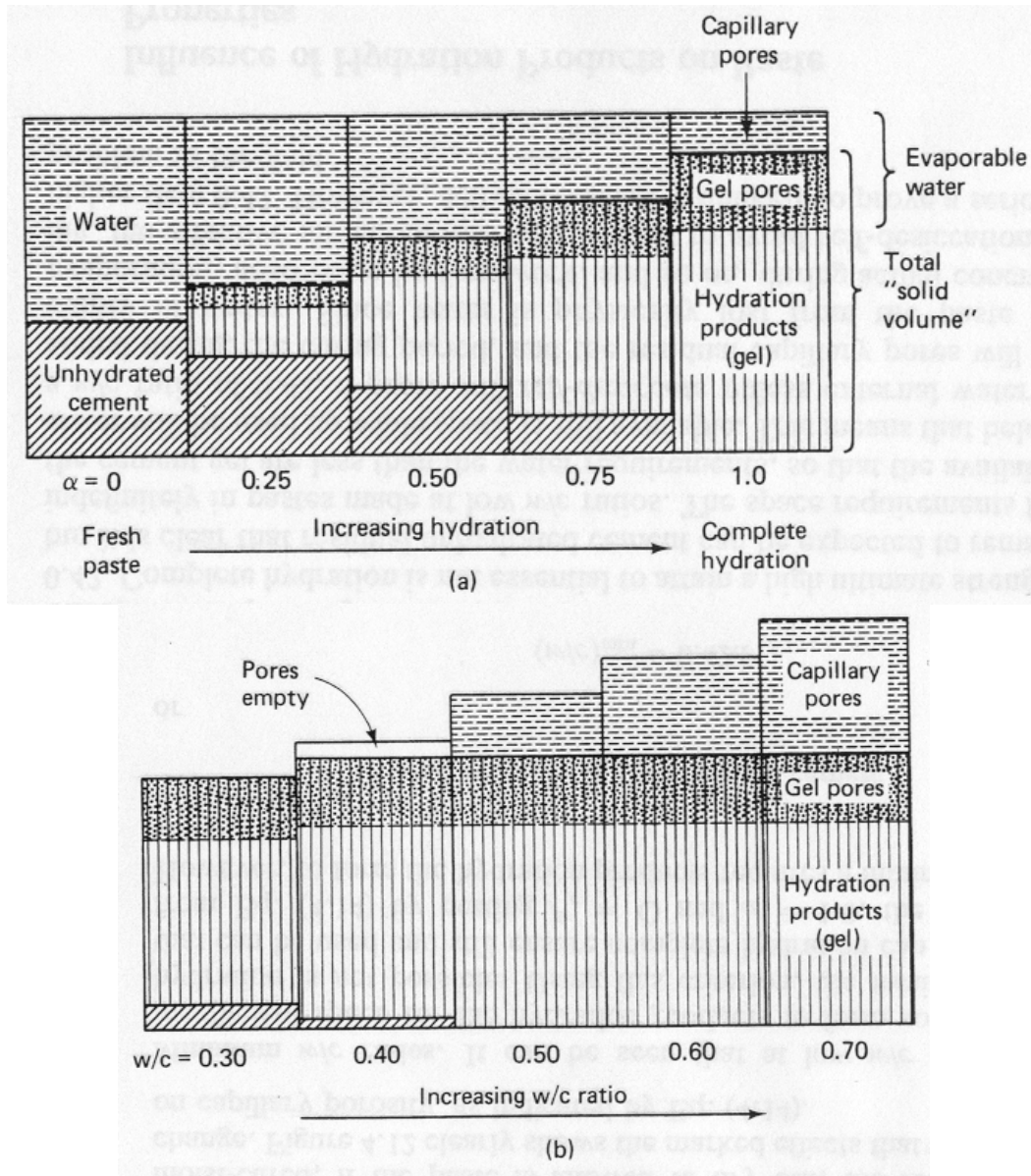


Figure A.11 Volume relationships between constituents of hydrated pastes: (a) a constant w/c ratio of 0.50 and changing degree of hydration α ; (b) changing w/c ratios and constant degree of hydration ($\alpha = 1.0$) (Mindess & Young 1981).

A.3.4 The water contained in hydrated cement paste

Capillary water is present in pores, in which capillary condensation can occur. This corresponds to a pore diameter of about 40 Å. The capillary condensed water has somewhat lower internal energy level than bulk water (free water). When this water dries, the material will contract (shrink). Water in pores with diameter larger than 1000 Å can be considered as free water. Its removal does not cause any change in volume.

Under the influence of attractive forces, water molecules are physically adsorbed onto the surface of solids in hcp. It has been suggested that up to six molecular layers of water (15 Å) can be physically held in the adsorbed layer. At relative humidity 45% at

which capillary condensation can occur the thickness correspond to about 2 molecules layers. The adsorbed layer is not completely lost until the cement paste is completely dry (RH=0). Loss of adsorbed layer leads to shrinkage.

Interlayer water is water associated with the C-S-H structure but not an integrated part of the solid gel particularly. Such interlayer water consist of a monomolecular water layer between the layers of C-S-H is strongly held by hydrogen bonding. The interlayer water is accordingly to Feldman and Sereda (1970) only lost if strong drying (below 11% RH) occurs. When the interlayer water is lost, the C-S-H structure shrinks considerably.

Chemically combined water is water that is an integral part of the C-S-H. It is assumed to be lost above +105°C.

A.3.5 The porosity of cement paste based on the Powers model

Only ordinary Portland cement (OPC) is dealt with here, the structure of the concrete that is assumed is one based on a structural model described in Fagerlund (1994), based on the work of Powers (1962). The model is described mathematically by a set of simple equations, for calculating the volume fraction of cement, hydration products (gel) and pores. Powers proposed certain empirically based equations, derived from experimental data. The equations do not distinguish between the various hydration states and different types of the hydration products, all are regarded as *cement gel*. Besides, a given increase in degree of hydration is assumed to create the same amount and structure of cement gel irrespectively of at what hydration state this additional hydration occurs.

Although this gives simple equations, the simplifications do not matter very much in reality, or as Hansen (1986) states “*structural differences among pastes are mainly due to differences in capillary porosity. Chemical composition is not very important because it turns out that physical characteristics of hcp gel influenced to only a minor extent by such differences in chemical composition as are found among different types of Portland cement*”.

In the model, the following is assumed:

- 1) The density of the cement grains is 3100 (kg/m³).
- 2) The water bound chemically in the hydration process is 0.25·α·C, where α = degree of hydration (-); and C = cement content (kg).
- 3) The chemically bound water “decreases” in volume to 0.75 of the volume it had prior to hydration.
- 4) The cement gel formed during hydration has a porosity of 28 %.
- 5) The air pores due to compaction or to air-entraining agents are omitted. Instead, they are added on the level of the concrete.

The total pore volume (V_p)_p of the cement paste is (figure A.12)

$$\begin{aligned} (V_p)_p &= \frac{W - 0.75 \cdot W_n}{\rho_w} = \frac{W - 0.75 \cdot 0.25 \cdot \alpha \cdot C}{\rho_w} = \frac{W - 0.19 \cdot \alpha \cdot C}{1000} = \\ &= \frac{C}{1000} (w/c - 0.19 \cdot \alpha) \end{aligned} \quad (\text{A.17})$$

where $(V_p)_p$ = total pore volume of the cement paste (m^3); W = content of water mixed (kg); W_n = chemically bound water (kg); ρ_w = density of water (kg/m^3); and w/c = water to cement ratio.

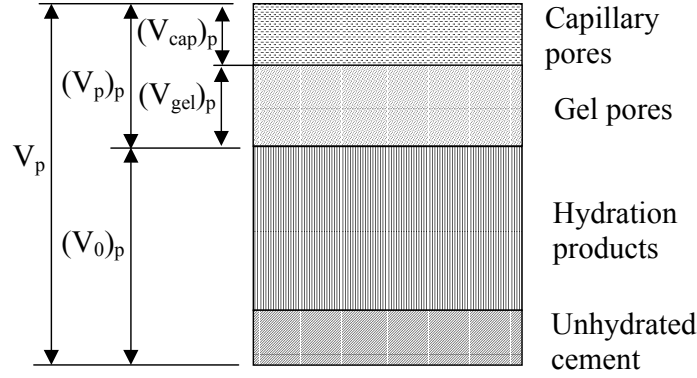


Figure A.12 Volume relationships among constituents of the hydrated pastes.

The compact volume, i.e. the solid volume without any pores, of the cement paste $(V_0)_p$ is

$$(V_0)_p = \frac{C}{\rho_c} + \frac{W_n}{\rho_w} = \frac{C}{3100} + \frac{0.19 \cdot \alpha \cdot C}{1000} = \frac{C}{1000} (0.32 + 0.19 \cdot \alpha) \quad (m^3) \quad (A.18)$$

where $(V_0)_p$ = compact volume of the cement paste (m^3); ρ_c = density of the cement (kg/m^3).

The total volume of the cement paste V_p is the sum of the pore volume and the compact volume

$$V_p = (V_p)_p + (V_0)_p = \frac{C}{1000} (0.32 + w/c) \quad (m^3) \quad (A.19)$$

The total porosity of the cement paste P_p is

$$P_p = \frac{(V_p)_p}{V_p} = \frac{(w/c - 0.19 \cdot \alpha)}{(0.32 + w/c)} \quad (m^3 / m^3) \quad (A.20)$$

The volume of the cement gel V_{gel} is

$$V_{gel} = \frac{C}{1000} \cdot 0.71 \cdot \alpha \quad (m^3) \quad (A.21)$$

The volume of the gel pores $(V_p)_{gel}$ is

$$(V_{gel})_p = 0.28 \cdot V_{gel} = \frac{C}{1000} \cdot 0.20 \cdot \alpha \quad (m^3) \quad (A.22)$$

The volume of the capillary pores $(V_p)_{cap}$ in the cement paste is

$$\begin{aligned}
 (V_{cap})_p &= (V_p)_p - (V_{gel})_p = \frac{C}{1000}(w/c - 0.19 \cdot \alpha) - \frac{C}{1000} \cdot 0.20 \cdot \alpha = \\
 &= \frac{C}{1000}(w/c - 0.39 \cdot \alpha) \quad (\text{m}^3)
 \end{aligned}
 \tag{A.23}$$

The capillary porosity $(P_{cap})_p$ of the paste is

$$(P_{cap})_p = \frac{w/c - 0.39\alpha}{0.32 + w/c} \quad (\text{m}^3/\text{m}^3)
 \tag{A.24}$$

A.4 The structure of the Aggregate

The structure of aggregate depends on the types of minerals in the aggregate and on its geological history, which differ markedly from one location to another. In Sweden, fractions of crushed granite and gneiss are normally used. Such aggregates are hard, tight and not easily dissolved. Although the porosity is low, only about 0-1 %, the pores in these types of aggregate are quite coarse and are often so interconnected that the permeability of for example, granite, is in parity with that of cement paste of a high w/c ratio (Fagerlund 1980a, Mehta 1986). See figures A.13 and A.14.

A.5 Interfacial zones between cement paste and aggregate

Between the cement paste and the aggregate there is a thin, rather porous inter-facial zone (sometimes called the transition zone, *tz*), see figure A.13. It becomes increasingly porous during hydration and normally has a larger content of CH-crystals than the bulk paste located farther from the aggregate does. This zone may also crack due to differences in modulus of elasticity and strength of aggregate and cement paste. Referring to the work of other researchers, Winslow et al. (1994) noted a region of approximately 50 nm thickness which, has quite different properties than the rest of the bulk paste.

Bourdette et al. (1995) estimated from the literature the transition zone (*tz*) to be 30 μm thick. Using their models of hydration around the *tz*, they obtained results for porosity three times as high in *tz* as in the bulk paste, although it decreased with hydration age, whereas the porosity of the bulk paste remained relatively constant.

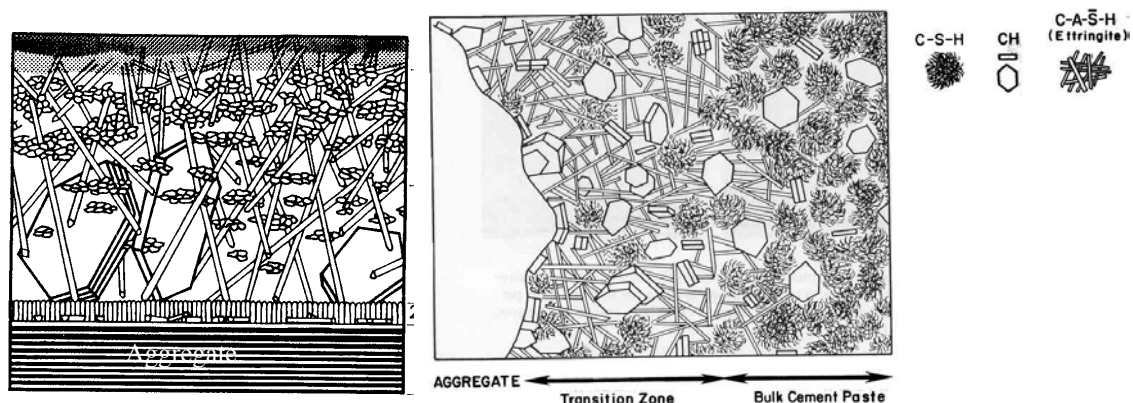


Figure A.13 Schematic representation of the transition zone (a) (Rehm et al., 1977) presented in Fagerlund (1994) and (b) Mehta (1986).

Figure A.14 shows Portlandite ($\text{Ca}(\text{OH})_2$) formed in the vicinity of the aggregate.

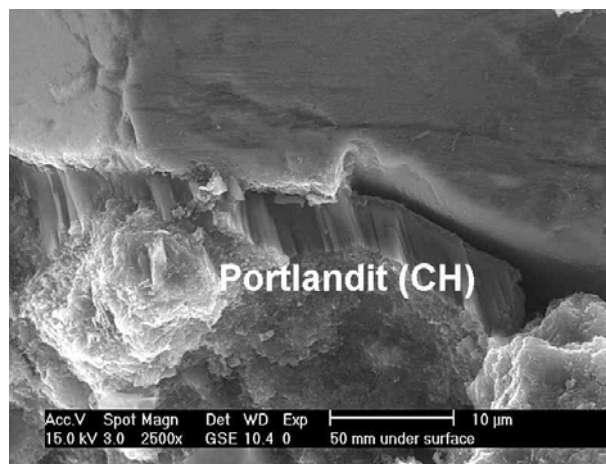


Figure A.14 An ESEM photograph of one of the specimens tested in the study. Calcium hydroxide formed close to the surface of an aggregate particle. Finger Institute, University of Weimar.

A reference to advanced modelling of the structure and properties of the transition layer is, for example, Garboczi and Bentz (1996).

A.6 The porosity and density of concrete

Winslow and Liu (1990) showed by means of mercury intrusion experiments that “*The paste in concrete is more porous, and the majority of the extra porosity has larger diameters than are found in plain paste*”, see A.15.

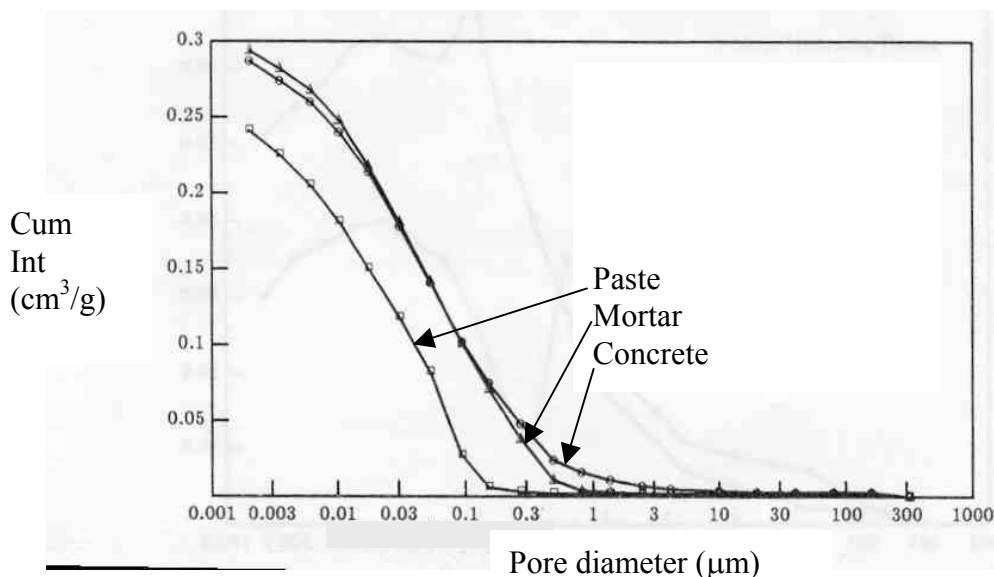


Figure A.15 Pore structure of well hydrated samples at $w/c = 0.55$ (Winslow & Liu, 1990).

“*For mortar and concrete, additional porosity occurs in pore sizes larger than the plain paste’s threshold diameter measured by mercury intrusion*” porosimetry (MIP)

(Winslow et al. 1994). In Winslow et al., mortars with a w/c of 0.4 were made with aggregate of different ratios. The samples were hydrated in lime-saturated water for 28 days and were then oven dried at 105°C. The pore size distributions of the pastes were obtained by MIP. An average thickness of the paste surrounding each aggregate particle was calculated by dividing the volume of paste in the mixture by the surface area of the sand in the mixture. A computer program for random particle placement, percolation assessment and phase fraction estimation was developed. By executing the program for different number of aggregate particles, the volume fraction of aggregate required for interfacial zone percolation for a given aggregate size distribution and interfacial zone thickness was determined and compared to experimental results (figure A.16). An interfacial zone thickness of 15-20 μm was found to be most consistent with results of the experiments.

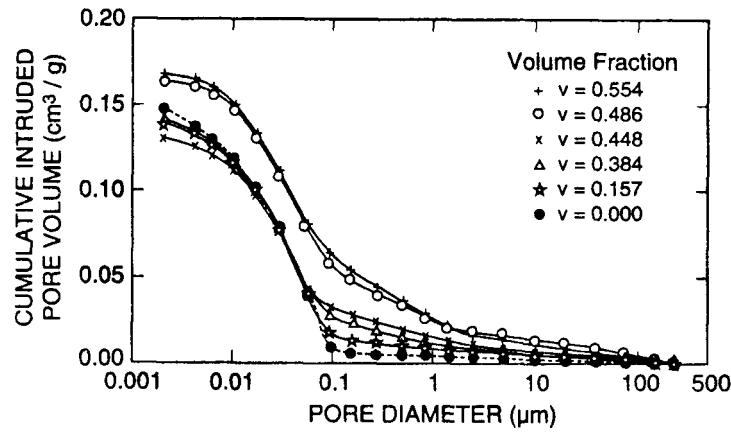


Figure A.16 Pore size distribution for different mortars (Winslow et al. 1994).

The volume of the aggregate is (see figure A.17):

$$V_a = (V_0)_a + (V_p)_a = A/\rho_a \quad (\text{A.25})$$

where V_c = volume of the concrete (m^3); V_a = volume of the aggregate (m^3); $(V_0)_a$ = volume of the compact volume of the aggregate (m^3); $(V_p)_a$ = volume of the pores of the aggregate (m^3); A = aggregate content (kg); and ρ_a = density of the aggregate (kg/m^3).

The total volume of concrete, the air pores included, is

$$V_c = V_a + V_p + V_{\text{air}} \quad (\text{A.26})$$

where V_{air} = air volume due to compaction or to air additives (m^3). Observe that in this model air is not included in the paste phase. Both during casting and afterwards during curing, additional air voids or cavities can appear in the concrete. The volume of these should be added to the air volume.

The porosity P_c (m^3/m^3) of the concrete is

$$P_c = [(V_p)_a + (V_p)_p + V_{\text{air}}] / V_c \quad (\text{A.27})$$

Usually the porosity of the aggregate is negligible, the porosity P_c of the concrete becoming

$$P_c = \frac{0 + w/c - 0.19 \cdot \alpha + V_{\text{air}}}{V_a + w/c + 0.32 + V_{\text{air}}} \quad (\text{A.28})$$

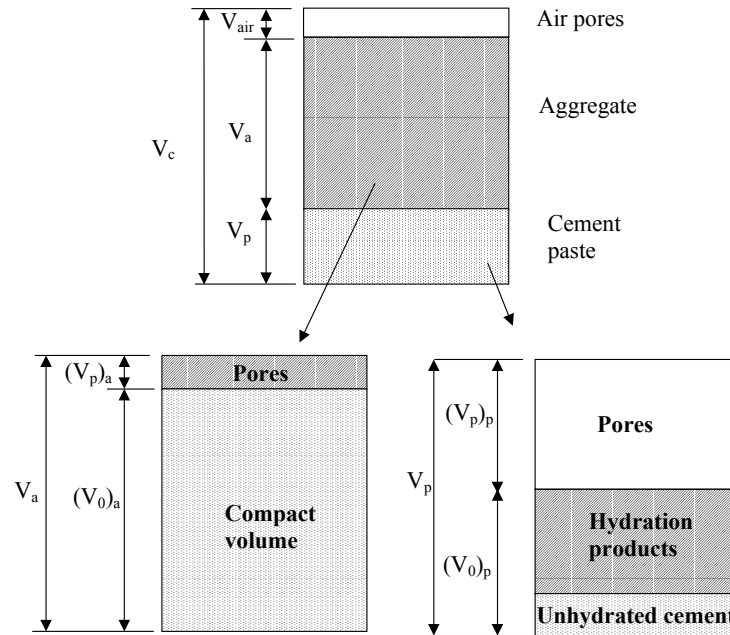


Figure A.17 Schematic volume fractions of pores and solid materials in concrete.

APPENDIX B EXPERIMENTAL RESULTS:

**Homogenous, steady-state percolation through defect-free
concrete - Flow of water and ions**

Figures B.1 to B.43 shows the flow of water, permeability and concentration of calcium, sodium, potassium and sulphate in the percolated water for all tested specimens of diameter $\phi 155$ mm. Two figures are shown for each specimen:

- One figure showing values of water flow, permeability and concentrations of Ca, Na, K and S
- One figure showing pH and the concentration of Ca, Na and K.

See chapter Table 4.1 and Figure 4.4 for description of type of concrete and testing history.

The flow of water is presented in two ways, as water flow q_w (m^3/s) and as water permeability k_w . By water permeability is meant the Darcy permeability k_w defined by the equation:

$$q_w = -k_w \cdot \nabla P_w \cdot A \quad (1.1)$$

The flow of ions presented in the figures is the measured concentration of calcium, $[Ca^{2+}]$, in the drainage water coming out from the downstream end of the specimens.

The arrows “Self sealing” denotes an observed reduction in water flow, probably caused of continued hydration. The arrows “Late-drying” denotes specimens that were dried in oven $+55^\circ\text{C}$ for a week. The arrows “leaching” denotes an observed increase in water flow, probably caused of a coarsening of the flow paths due to leaching.

Sometimes “6 to 3 bar” and “3 to 6 bar” are written in the figures. It means that the applied water pressure was changed from 6 to 3 and from 3 to 6 bar.

As can be seen in the figures, results are given first when the percolation (leaching) test was started. Up to that time, the specimens were cured, or stored.

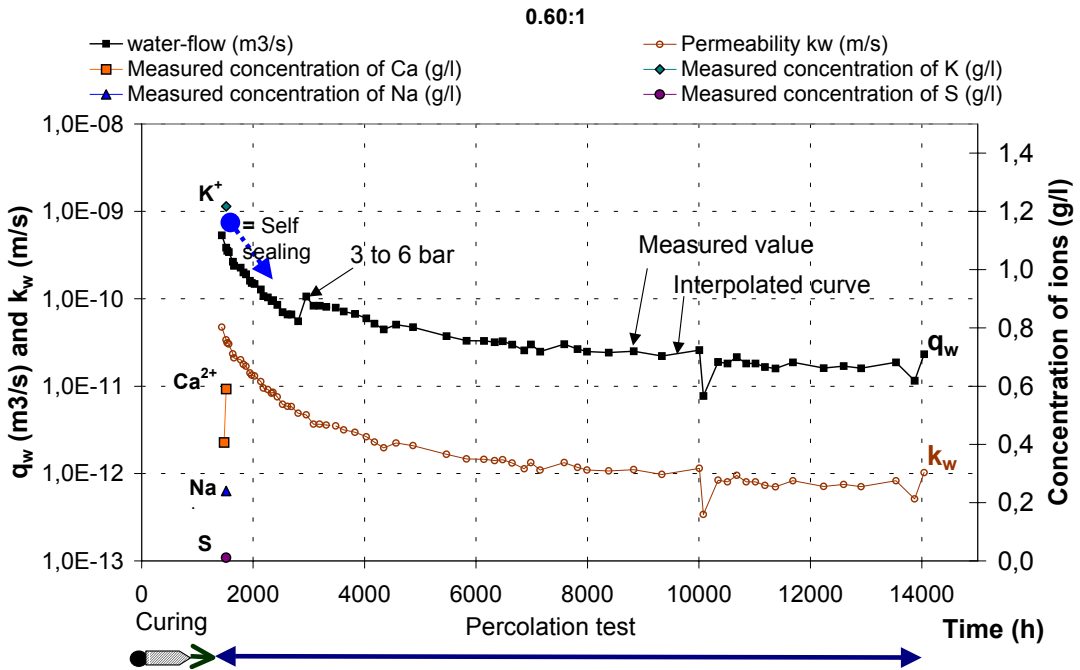


Figure B.1 Permeability and flow of water and ions for the leached specimen 0.60:1 (w/c 0.60, EH). q_w = water flow; k_w = permeability; Ca^{2+} , K^+ , Na^+ , S = ion concentration of calcium, potassium, sodium and sulphate respectively.

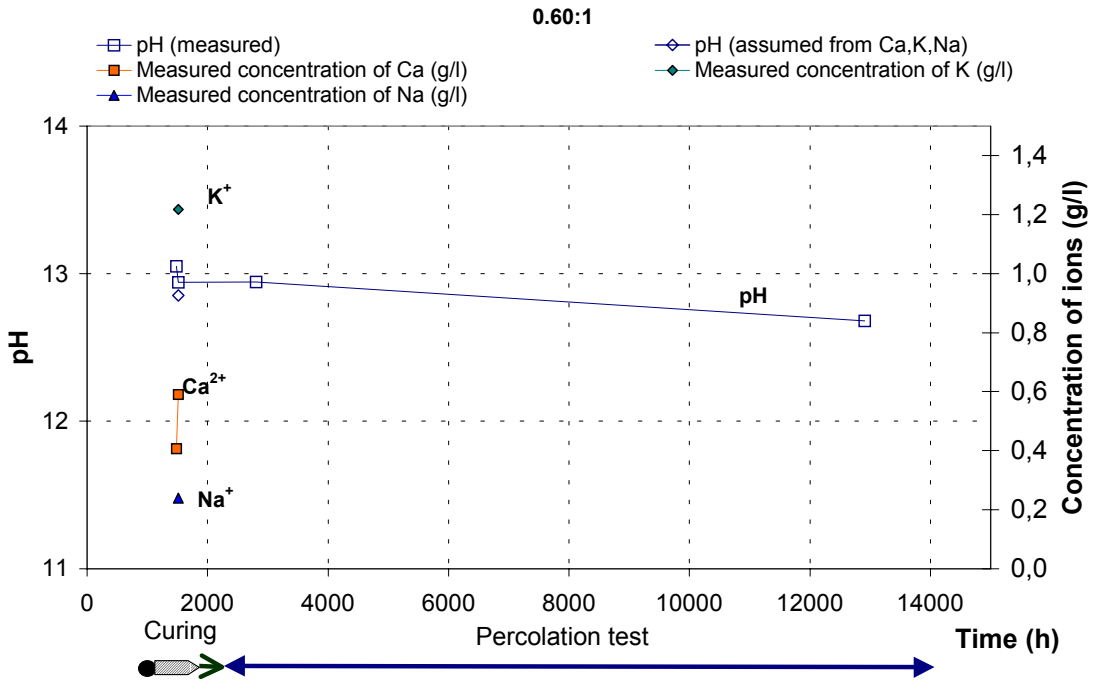


Figure B.2 Flow of ions and pH for the leached specimen 0.60:1 (w/c 0.60, EH).

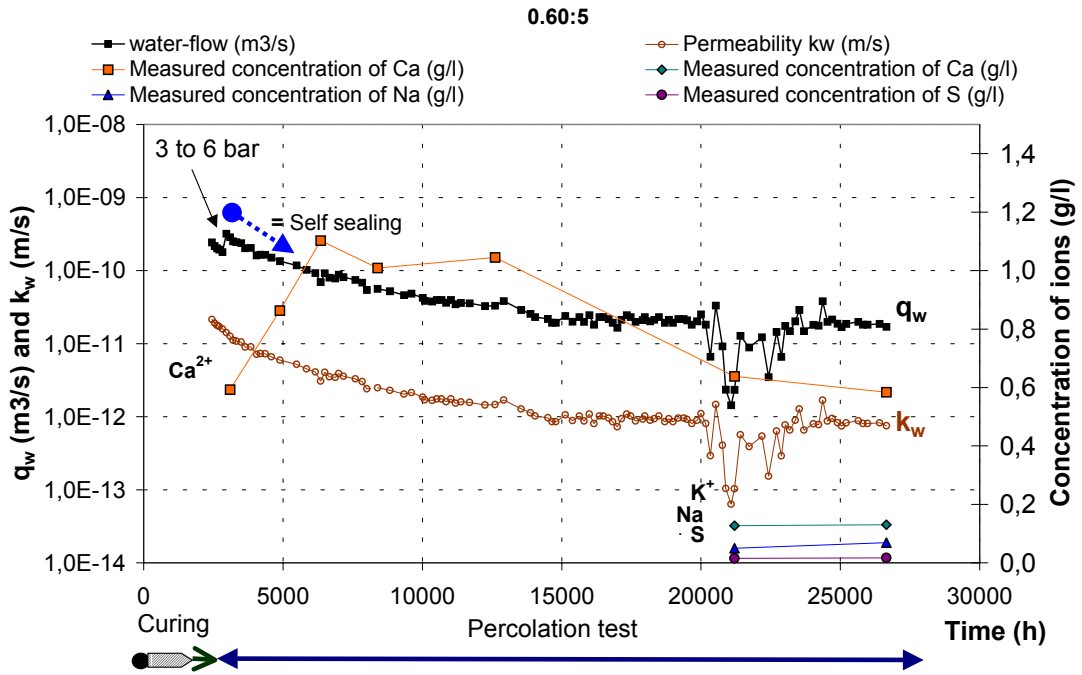


Figure B.3 Permeability and flow of water and ions for the leached specimen 0.60:5 (w/c 0.60, EH).

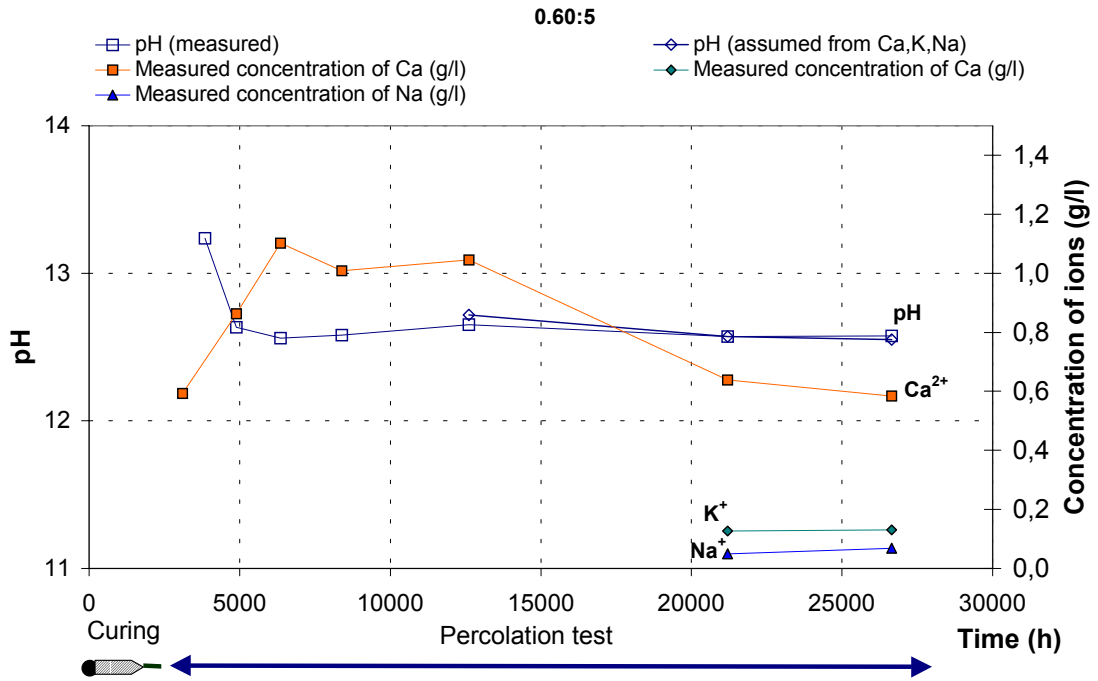


Figure B.4 Permeability and flow of water and ions for the leached specimen 0.60:5 (w/c 0.60, EH).

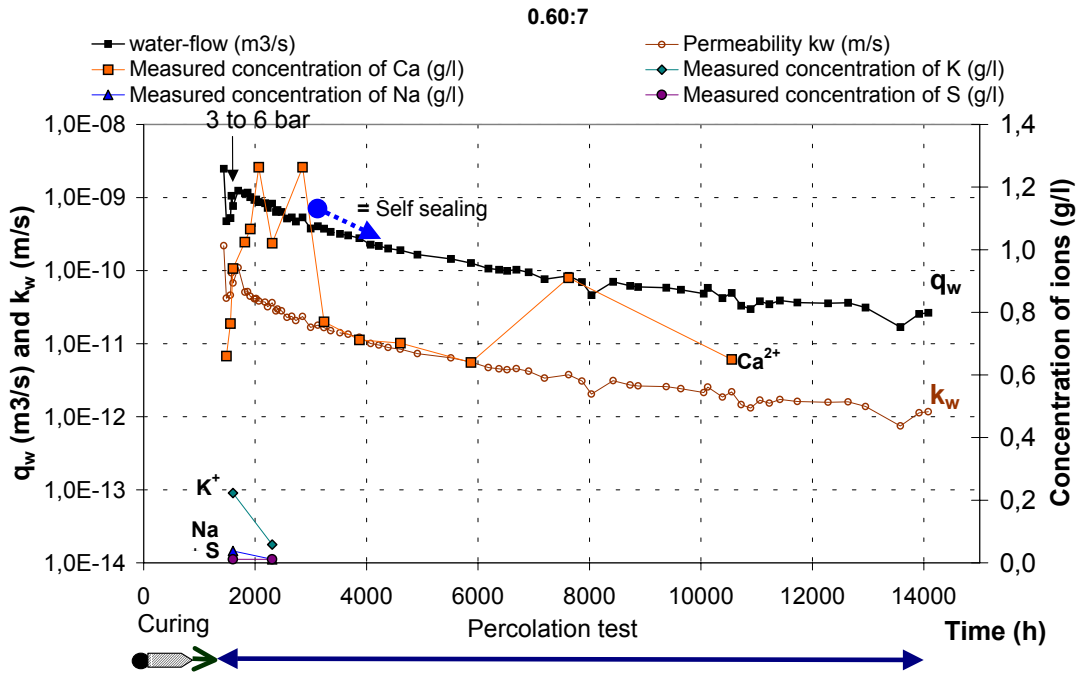


Figure B.5 Permeability and flow of water and ions for the leached specimen 0.60:6 (w/c 0.60, EH).

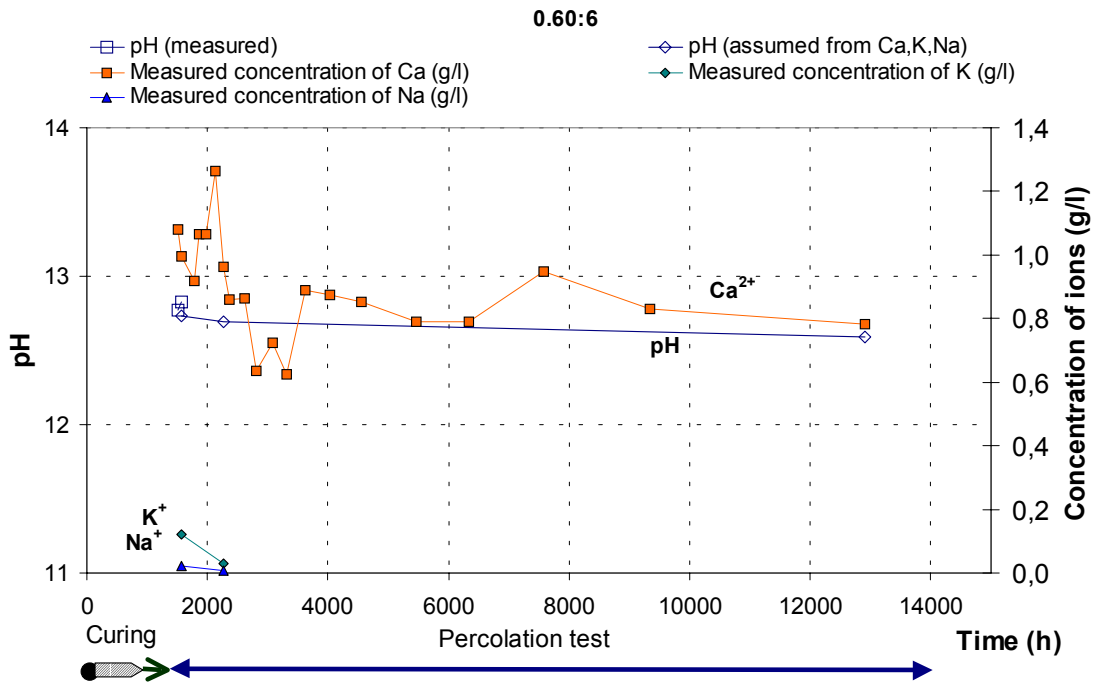


Figure B.6 Permeability and flow of water and ions for the leached specimen 0.60:6 (w/c 0.60, EH).

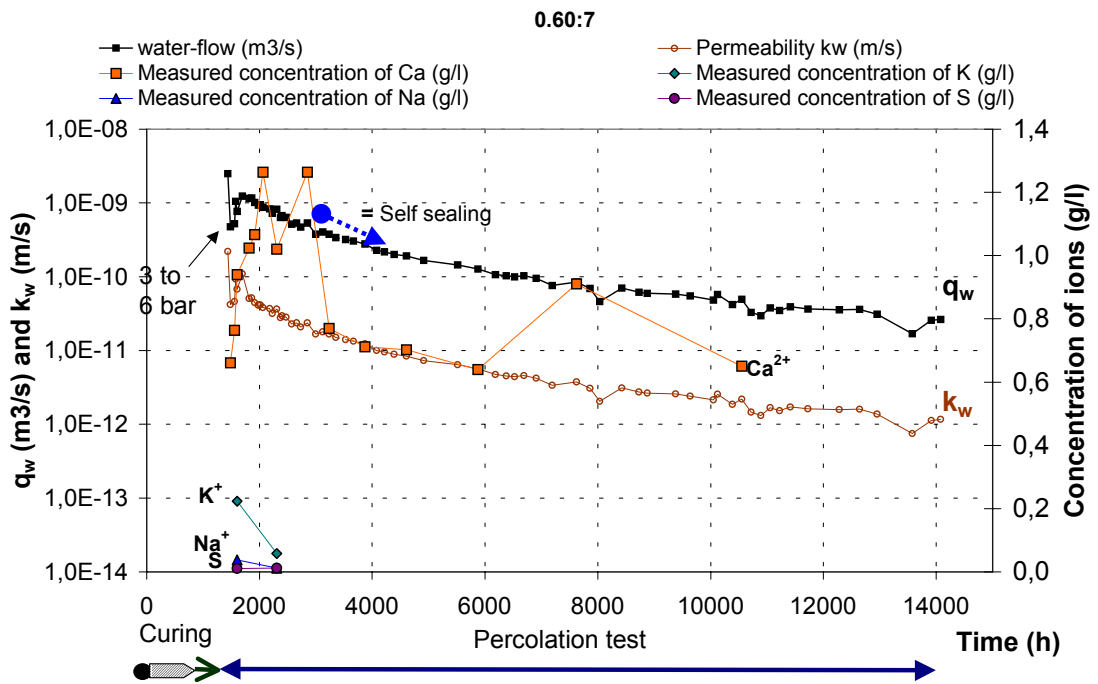


Figure B.7 Permeability and flow of water and ions for the leached specimen 0.60:7 (w/c 0.60, EH).

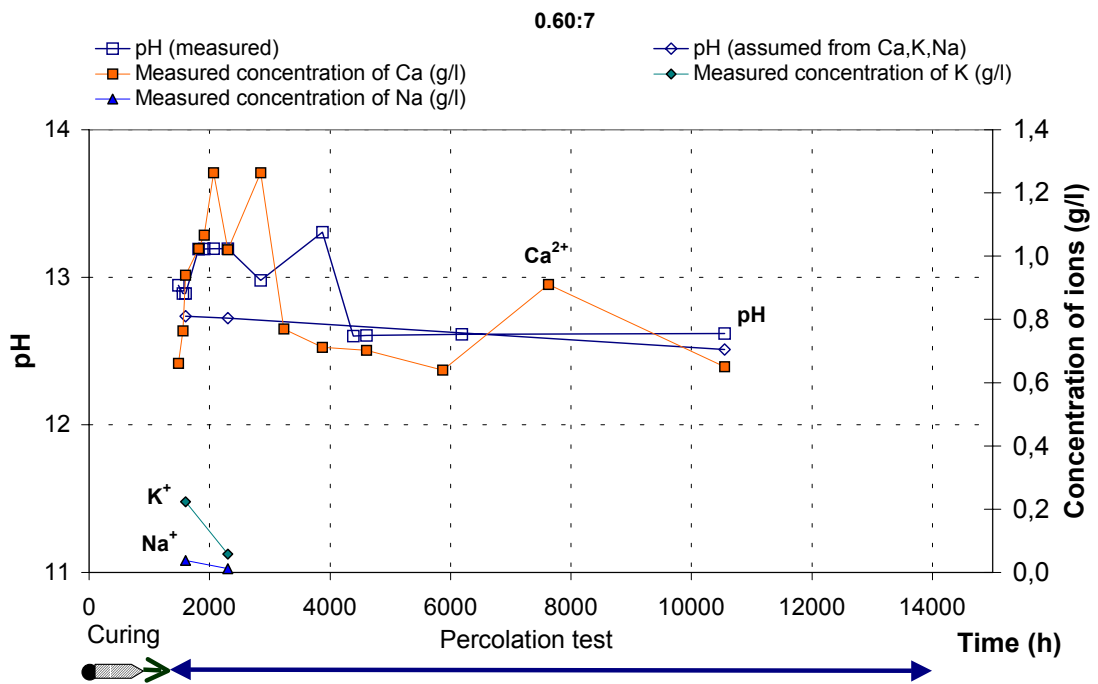


Figure B.8 Permeability and flow of water and ions for the leached specimen 0.60:7 (w/c 0.60, EH).

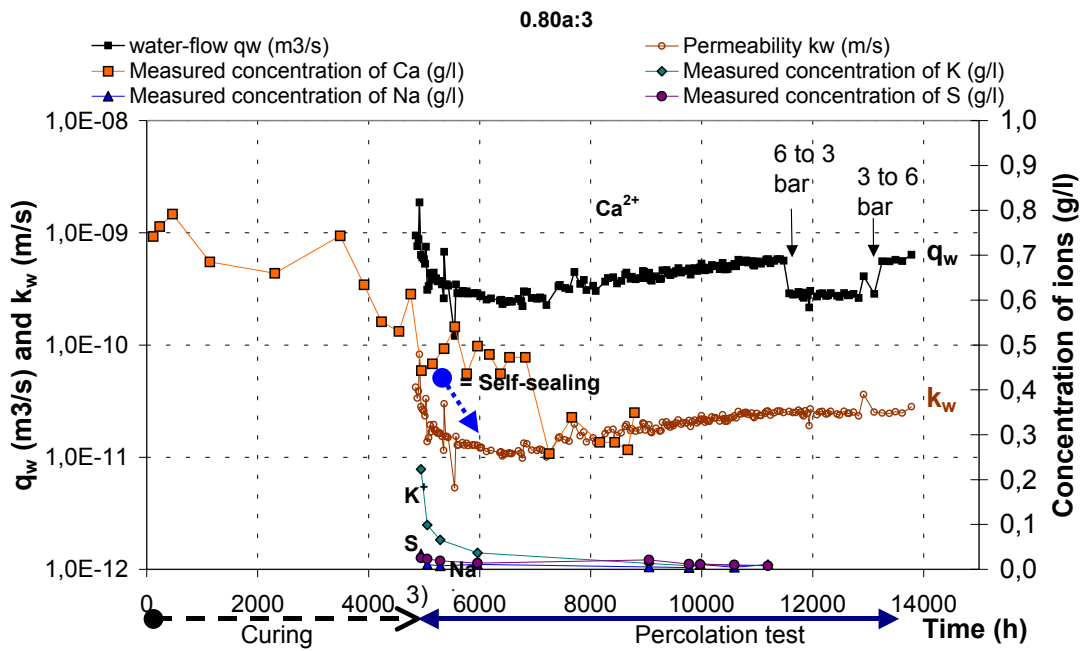


Figure B.9 Permeability and flow of water and ions for the leached specimen 0.80a:3 (w/c 0.80, LD).

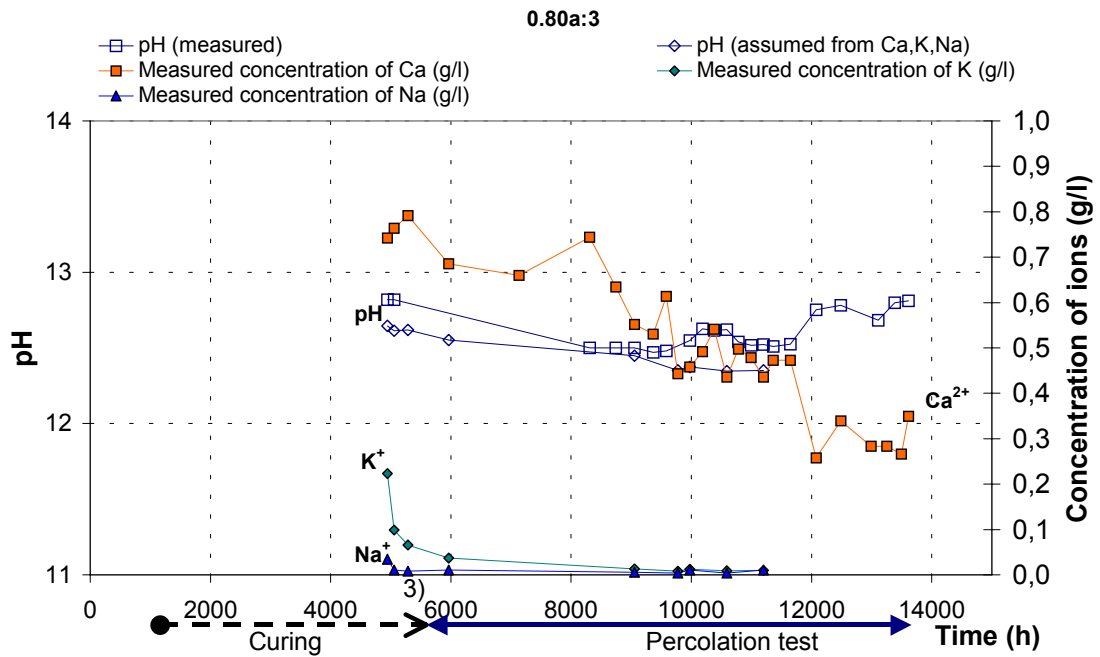


Figure B.10 Permeability and flow of water and ions for the leached specimen 0.80a:3 (w/c 0.80, LD).

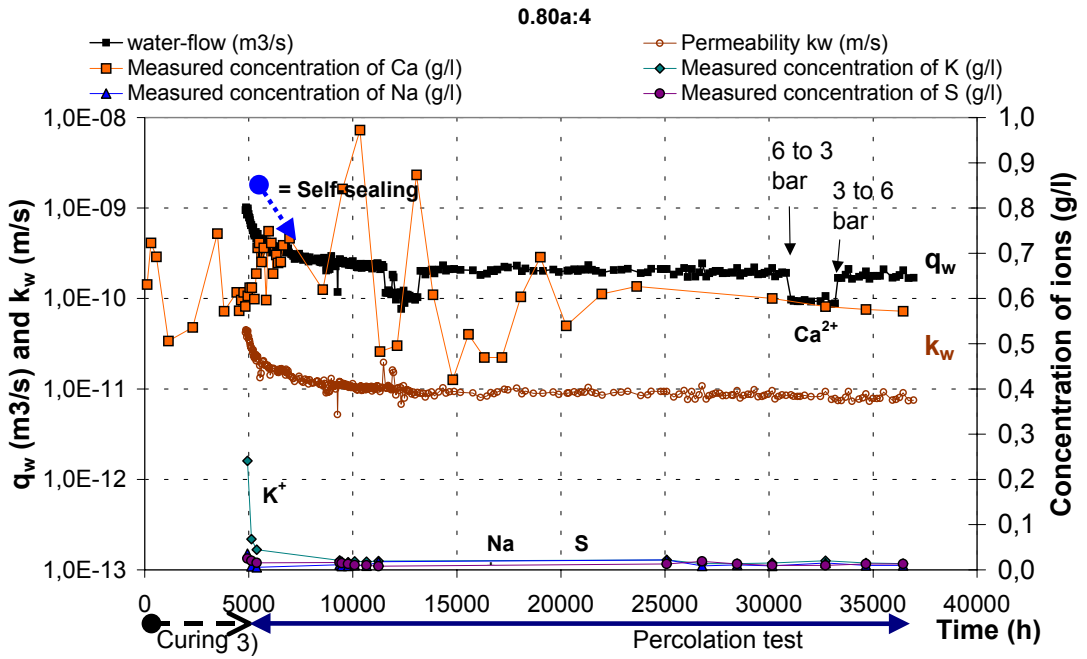


Figure B.11 Permeability and flow of water and ions for the leached specimen 0.80a:4 (w/c 0.80, LD).

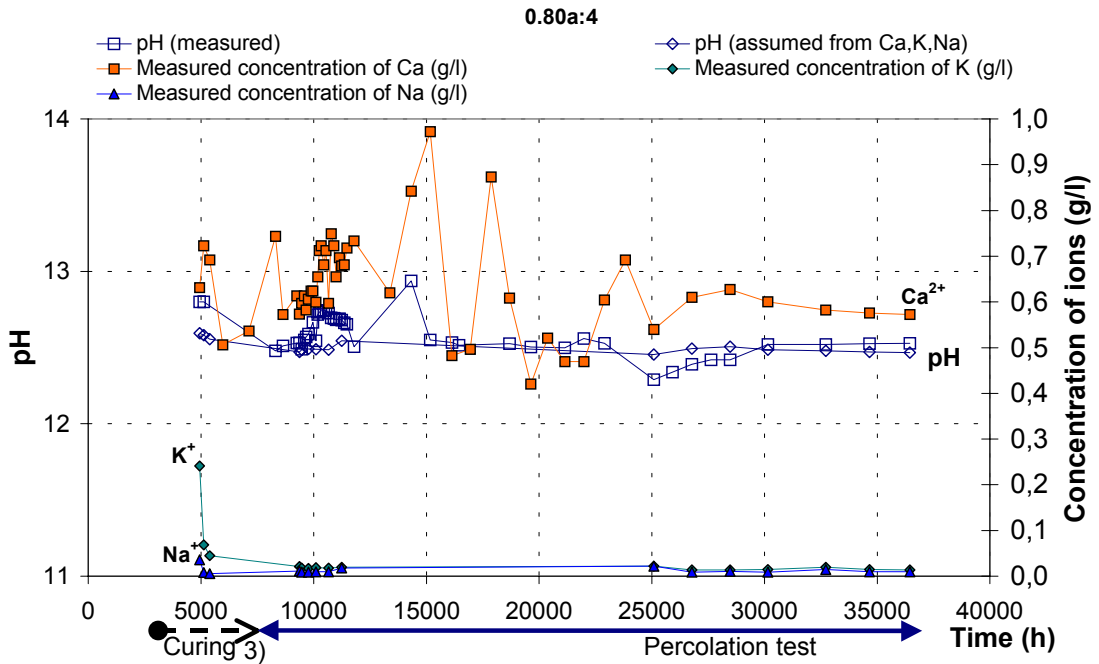


Figure B.12 Permeability and flow of water and ions for the leached specimen 0.80a:4 (w/c 0.80, LD).

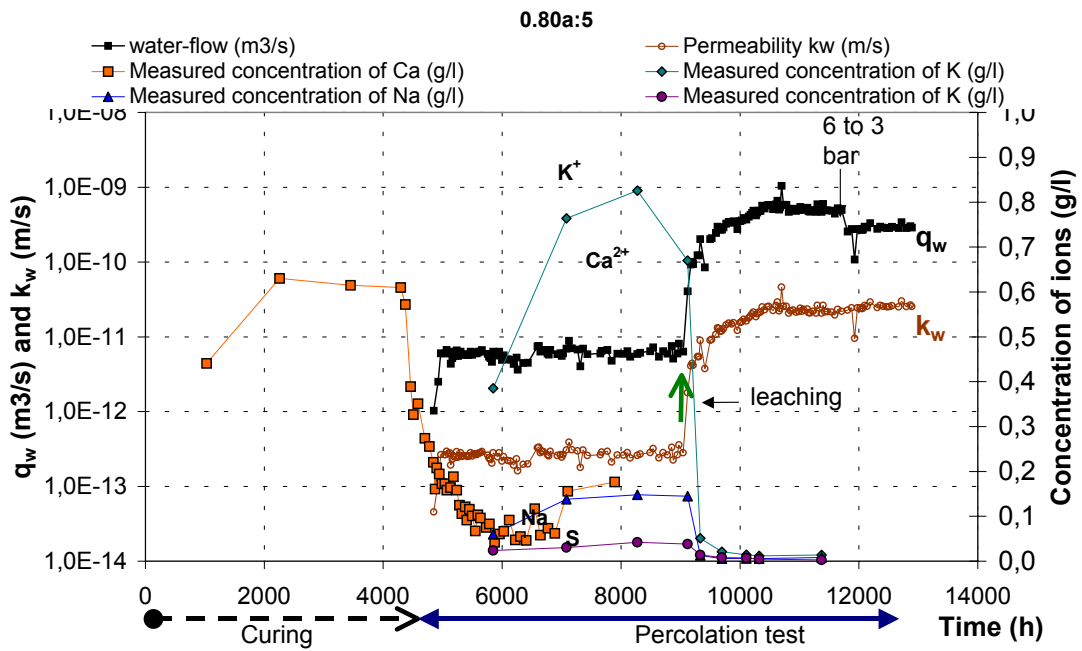


Figure B.13 Permeability and flow of water and ions for the leached specimen 0.80a:5 (w/c 0.80, V).

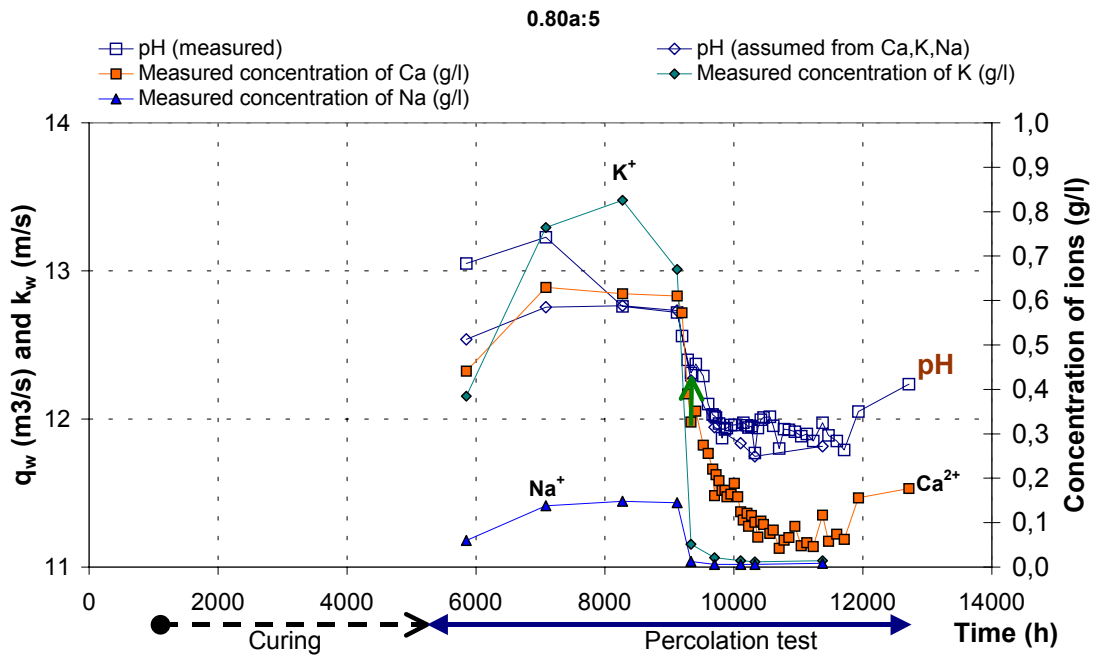


Figure B.14 Permeability and flow of water and ions for the leached specimen 0.80a:5 (w/c 0.80, V).

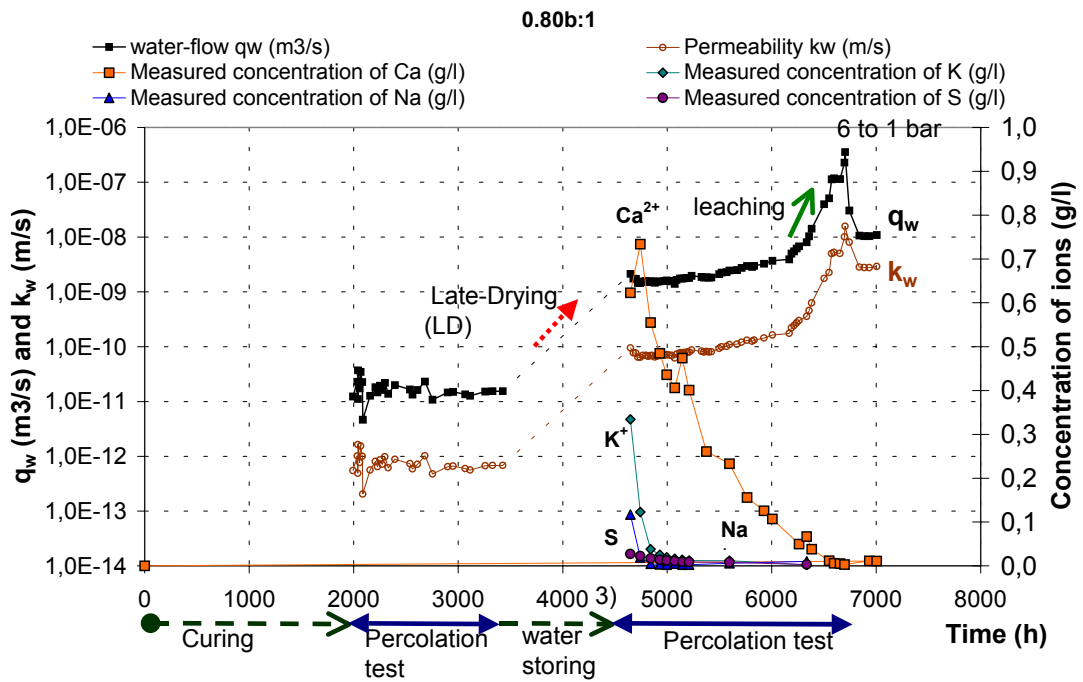


Figure B.15 Permeability and flow of water and ions for the leached specimen 0.80b:1 (w/c 0.80, V-LD).

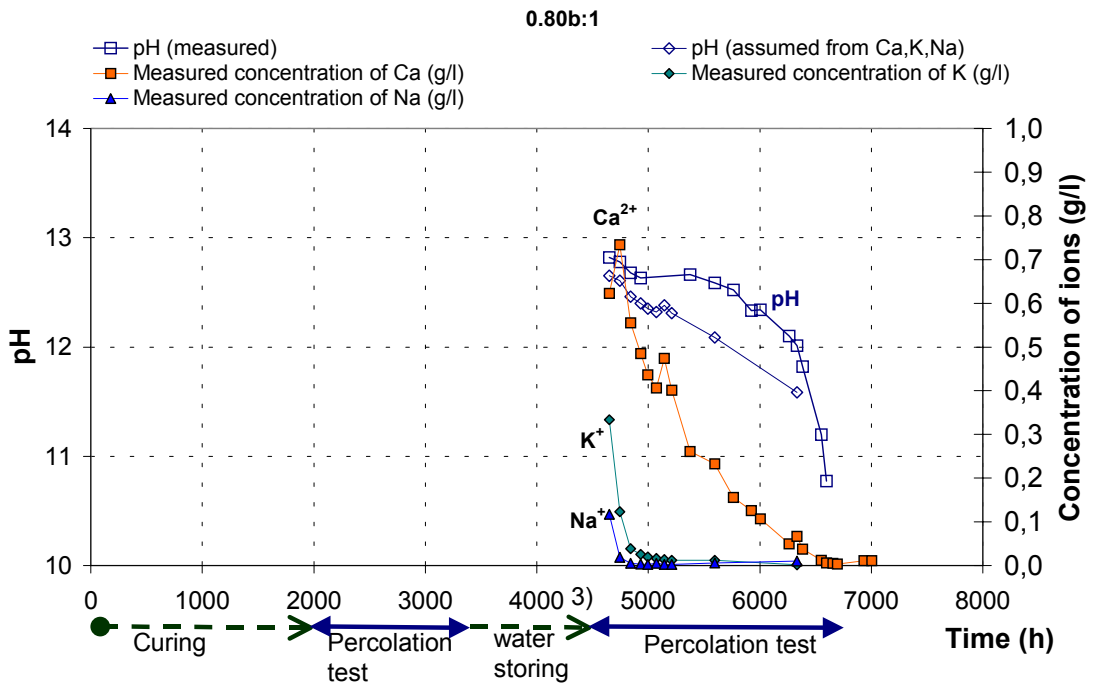


Figure B.16 Permeability and flow of water and ions for the leached specimen 0.80b:1 (w/c 0.80, V-LD).

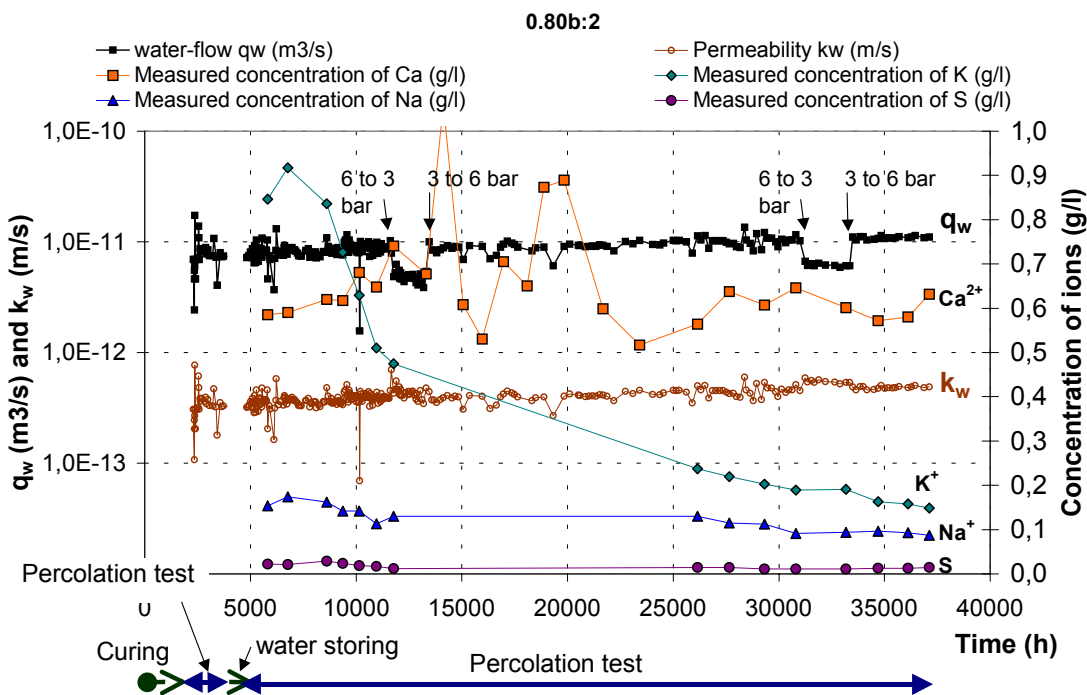


Figure B.17 Permeability and flow of water and ions for the leached specimen 0.80b:2 (w/c 0.80, V).

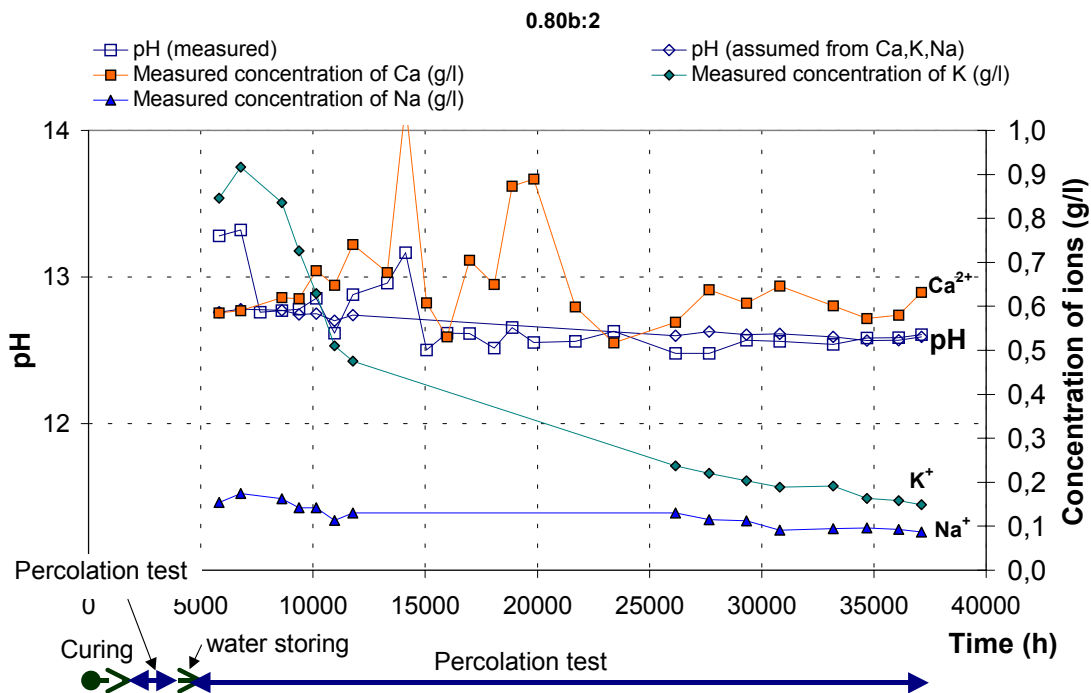


Figure B.18 Permeability and flow of water and ions for the leached specimen 0.80b:2 (w/c 0.80, V).

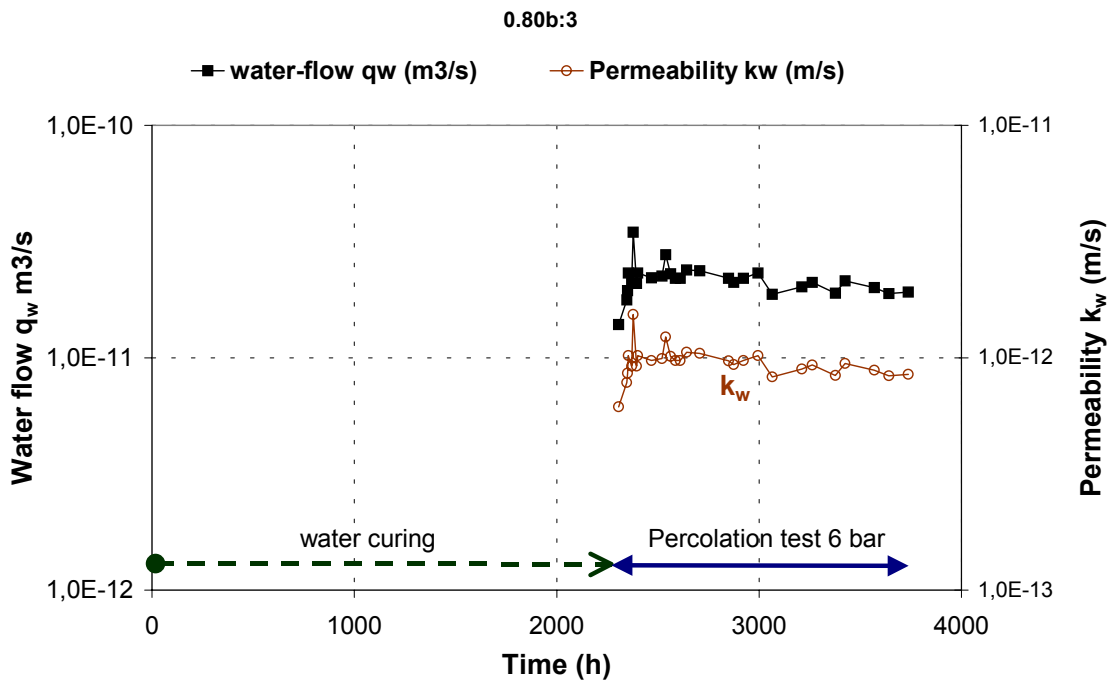


Figure B.19 Permeability and flow of water and ions for the leached specimen 0.80b:3 (w/c 0.80, V).

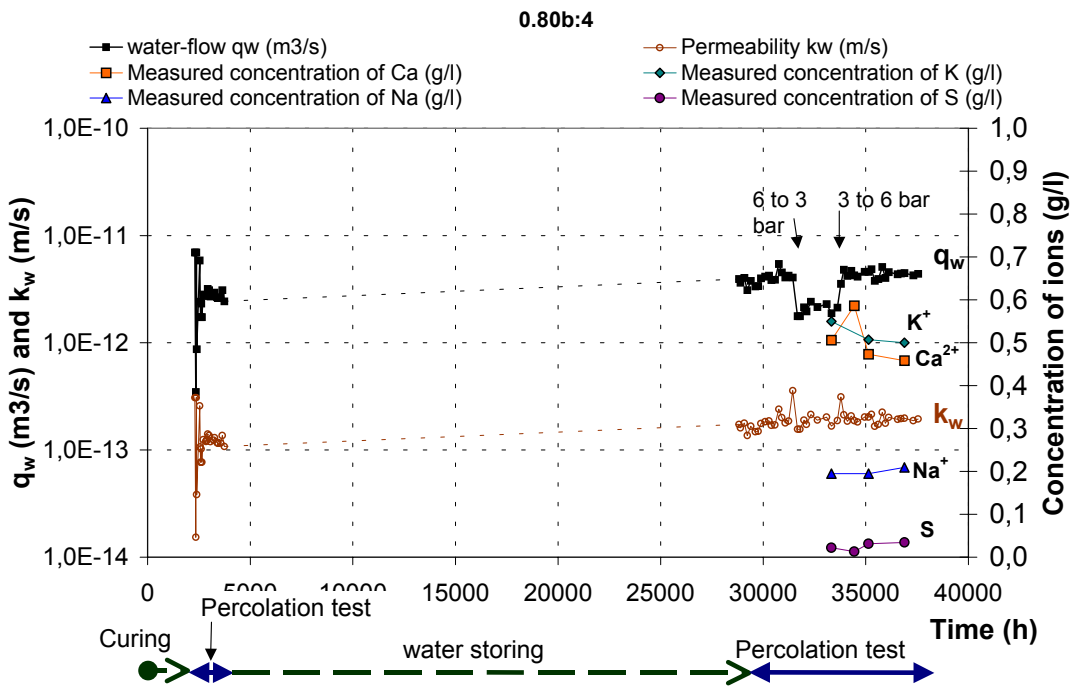


Figure B.20 Permeability and flow of water and ions for the leached specimen 0.80b:4 (w/c 0.80, V).

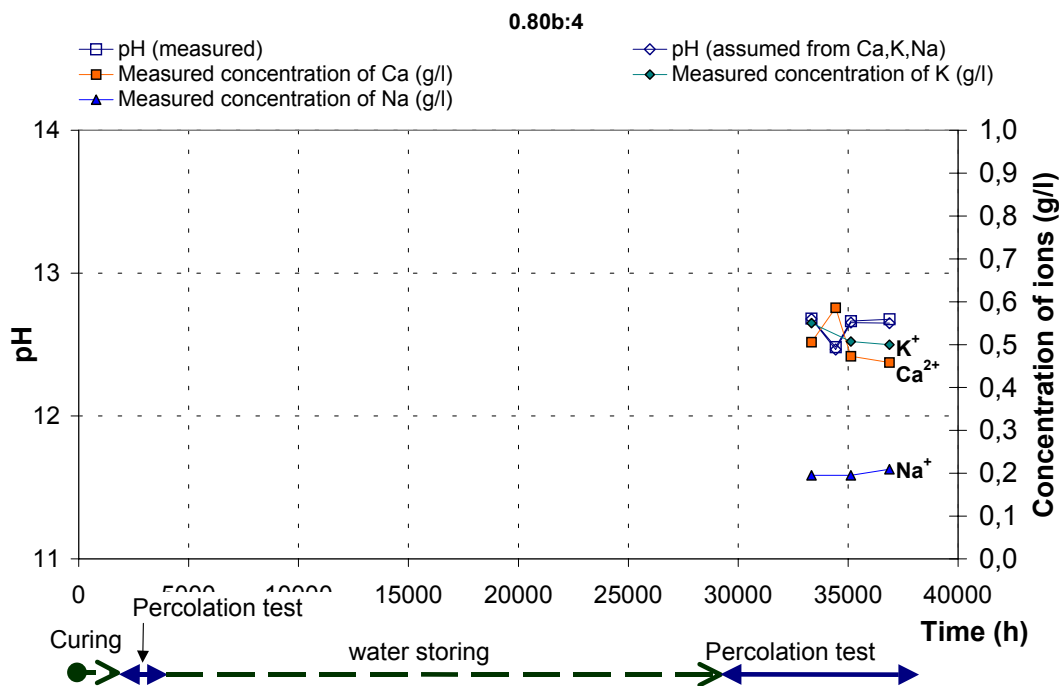


Figure B.21 Permeability and flow of water and ions for the leached specimen 0.80b:4 (w/c 0.80, V).

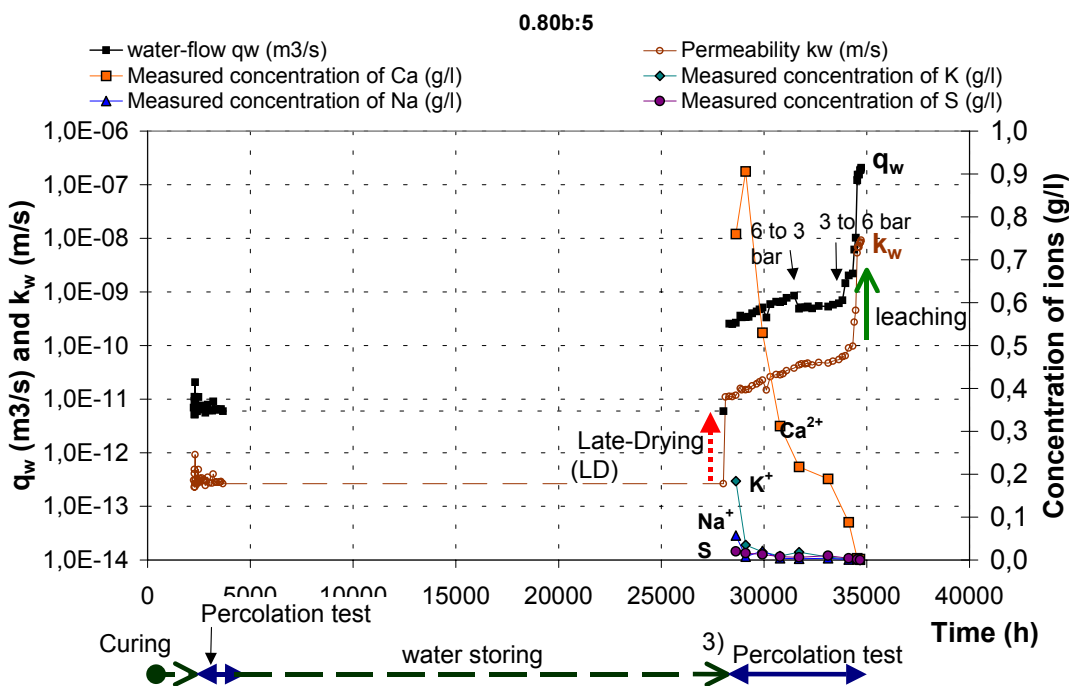


Figure B.22 Permeability and flow of water and ions for the leached specimen 0.80b:5 (w/c 0.80, V-LD).

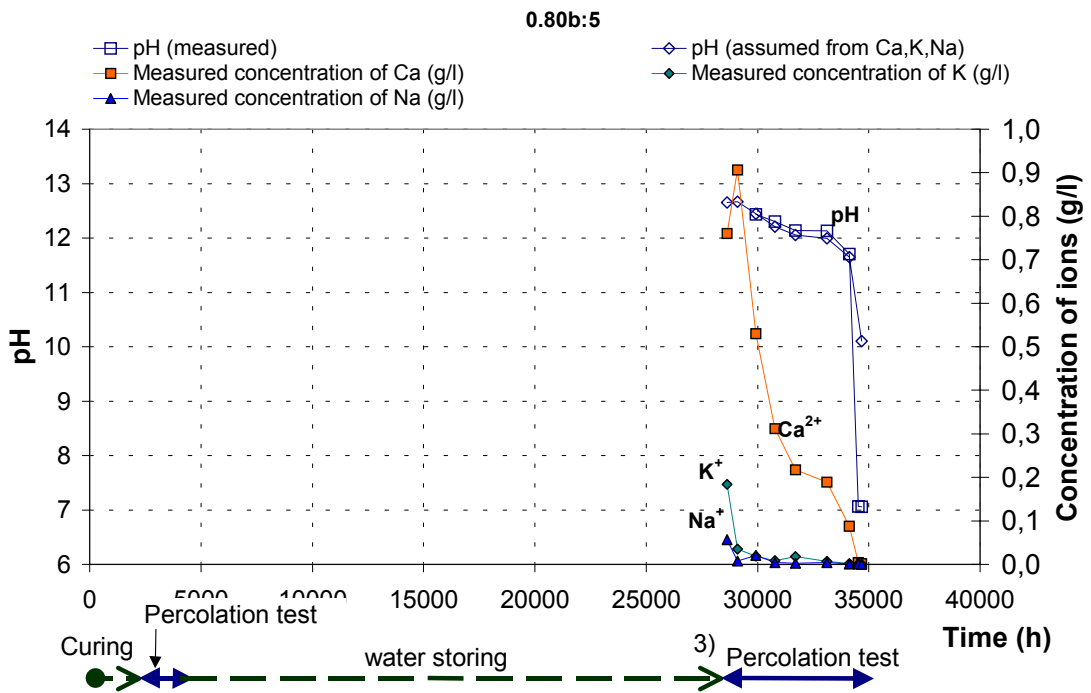


Figure B.23 Permeability and flow of water and ions for the leached specimen 0.80b:5 (w/c 0.80, V-LD).

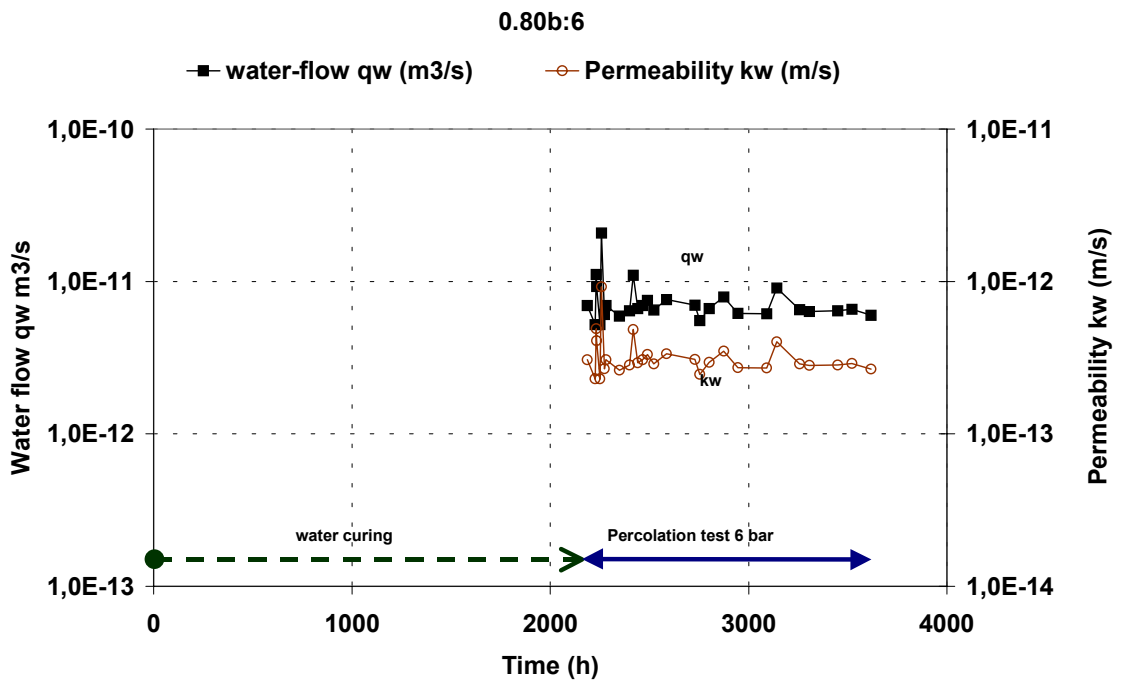


Figure B.24 Permeability and flow of water and ions for the leached specimen 0.80b:6 (w/c 0.80, V).

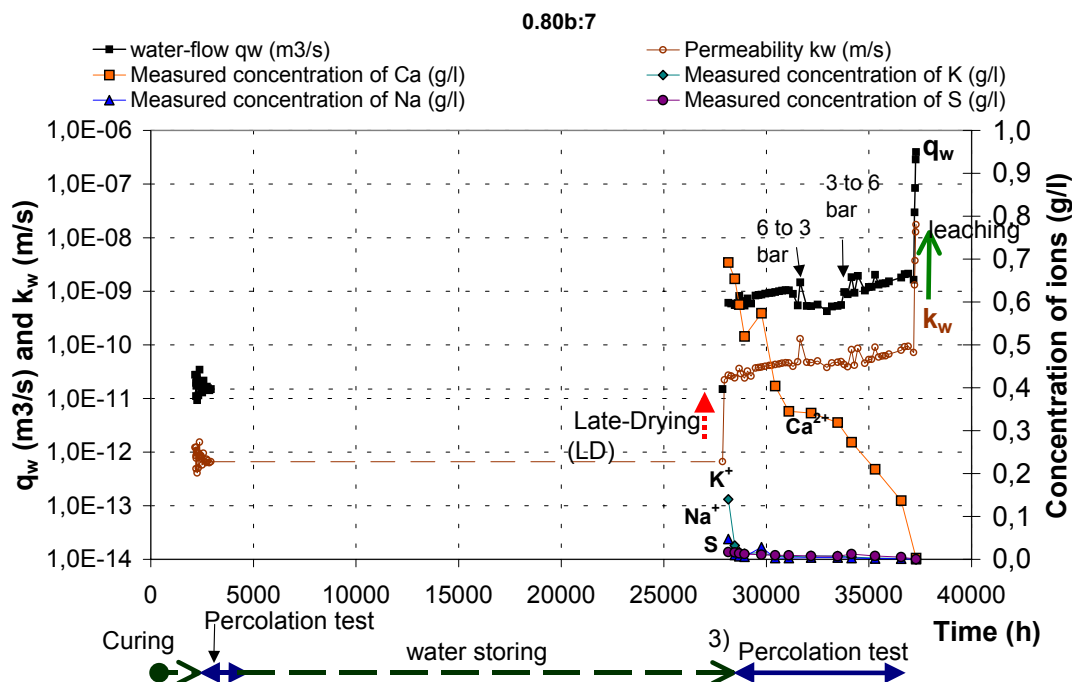


Figure B.25 Permeability and flow of water and ions for the leached specimen 0.80b:7 (w/c 0.80, V-LD).

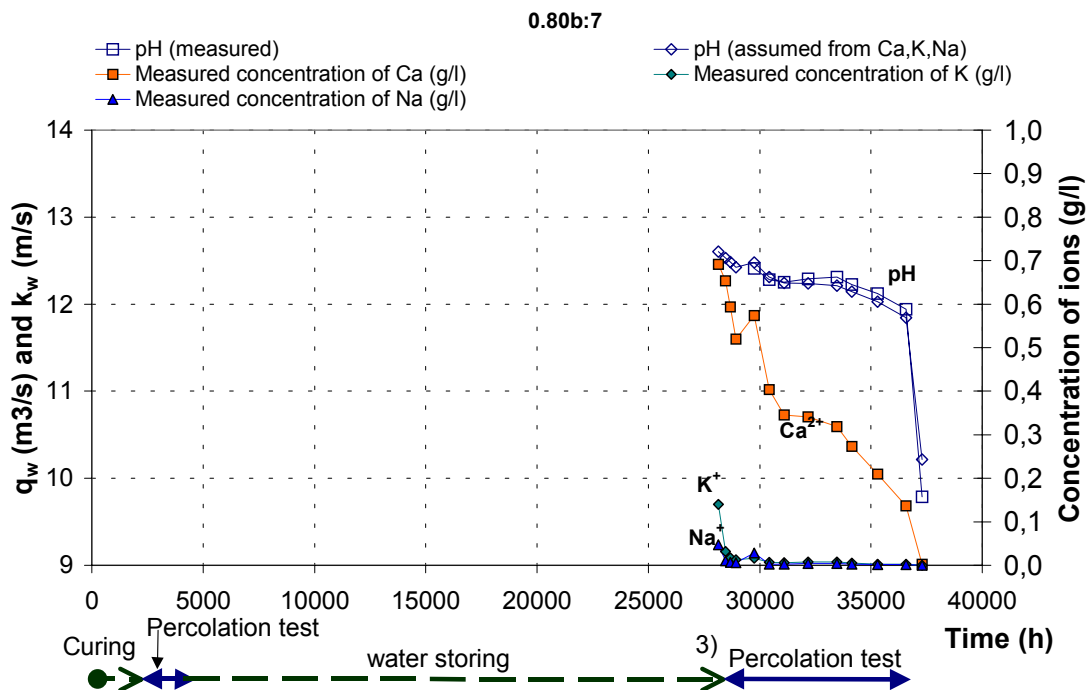


Figure B.26 Permeability and flow of water and ions for the leached specimen 0.80b:7 (w/c 0.80, V-LD).

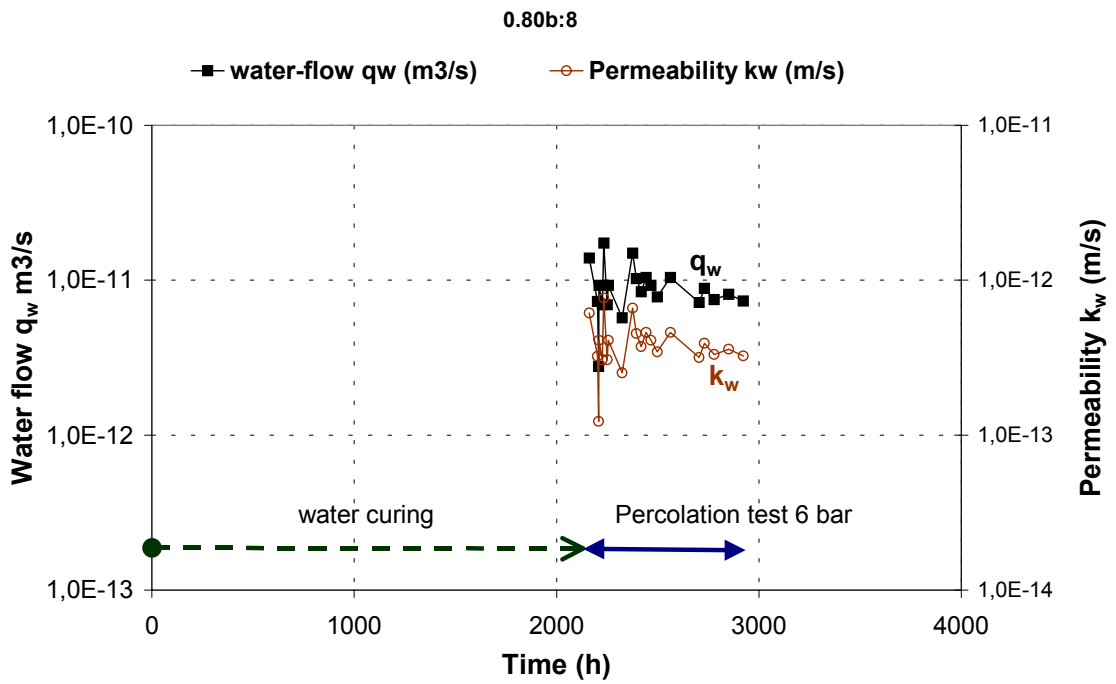


Figure B.27 Permeability and flow of water and ions for the leached specimen 0.80b:8 (w/c 0.80, V-LD).

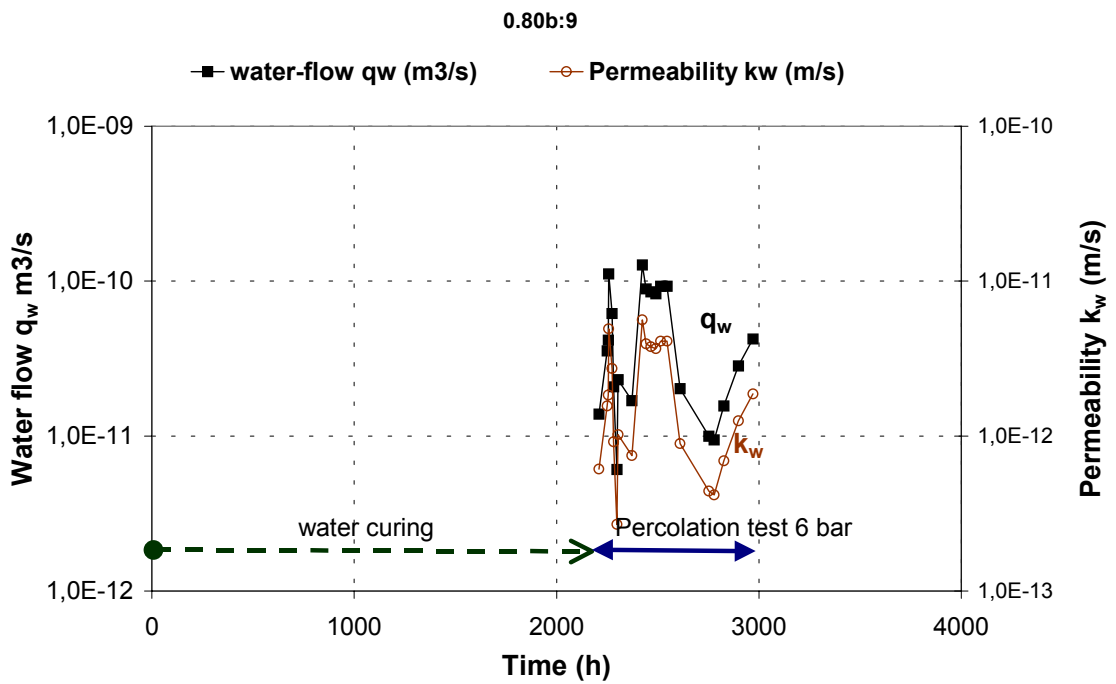


Figure B.28 Permeability and flow of water and ions for the leached specimen 0.80b:9 (w/c 0.80, V-LD).

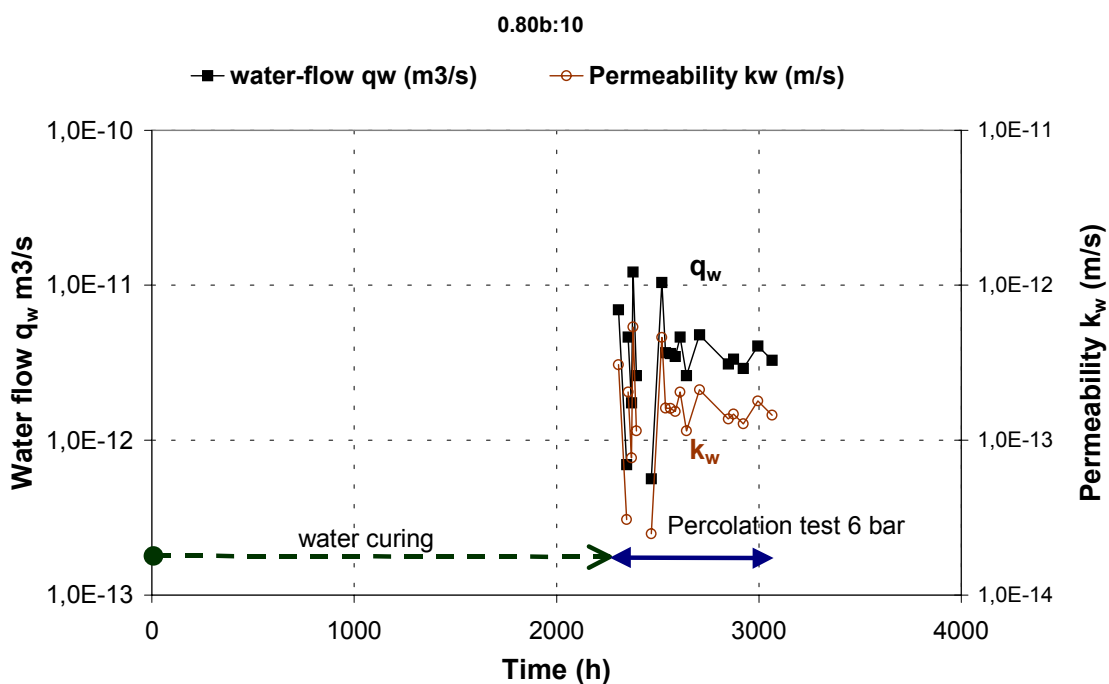


Figure B.29 Permeability and flow of water and ions for the leached specimen 0.80b:10 (w/c 0.80, V).

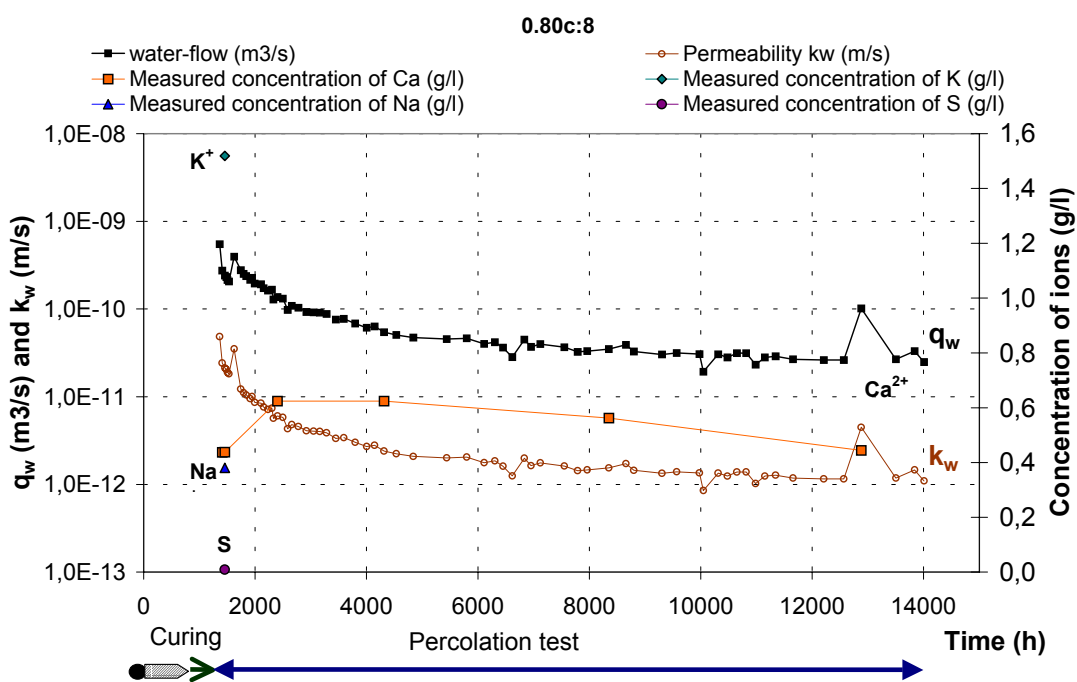


Figure B.30 Permeability and flow of water and ions for the leached specimen 0.80c:8 (w/c 0.80, EH).

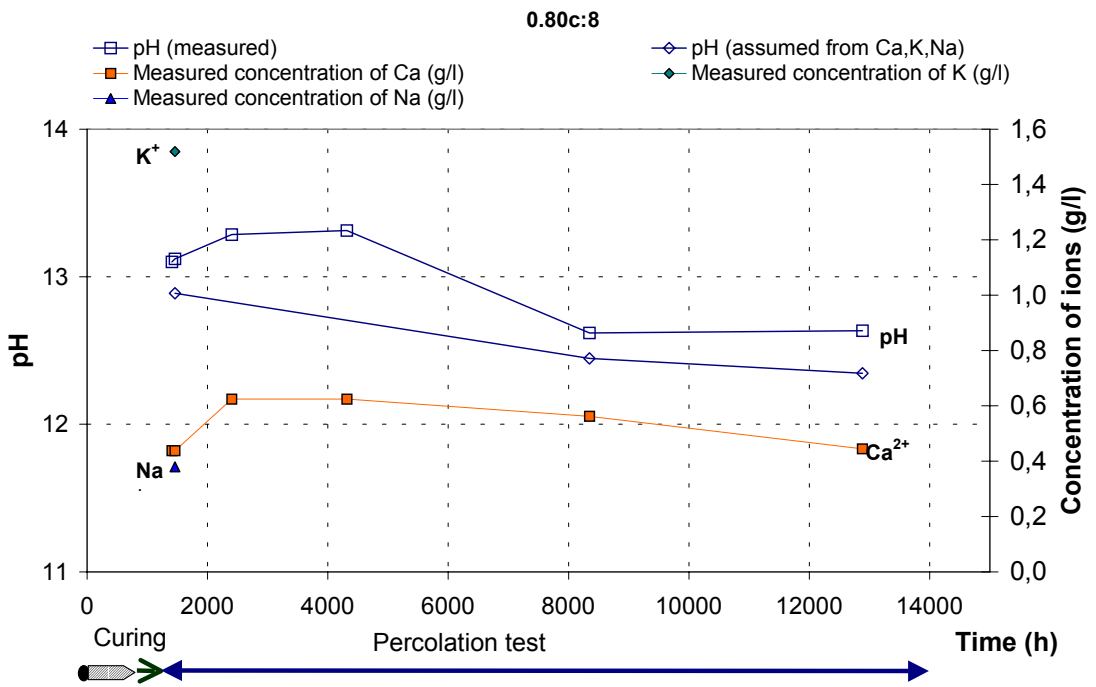


Figure B.31 Permeability and flow of water and ions for the leached specimen 0.80c:8 (w/c 0.80, EH).

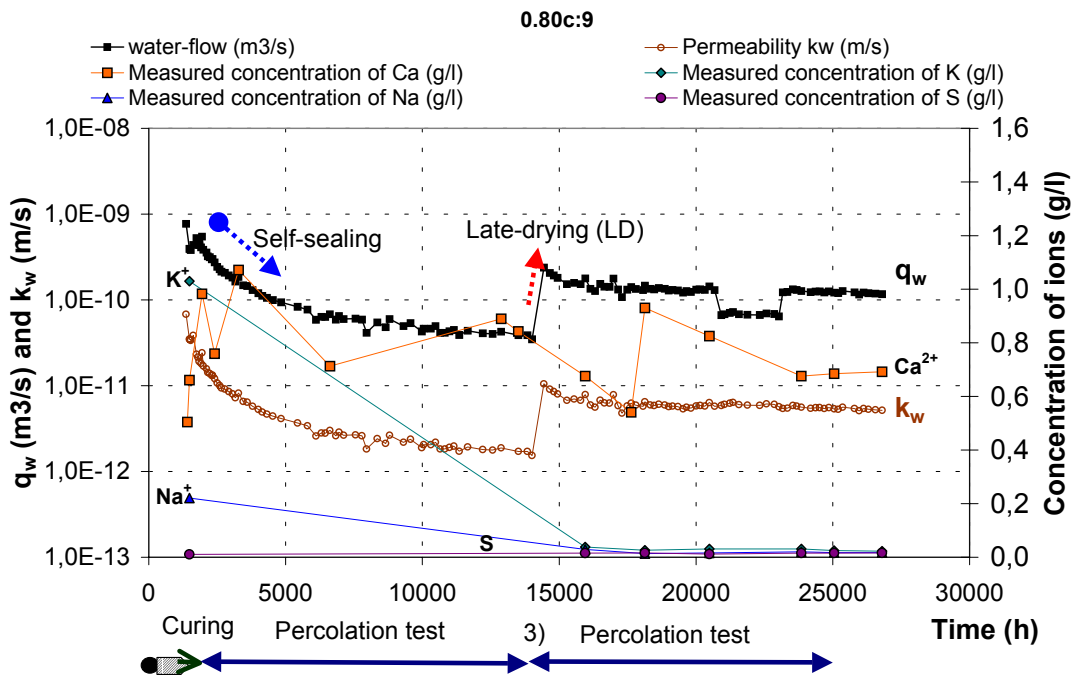


Figure B.32 Permeability and flow of water and ions for the leached specimen 0.80c:9 (w/c 0.80, EH-LD).

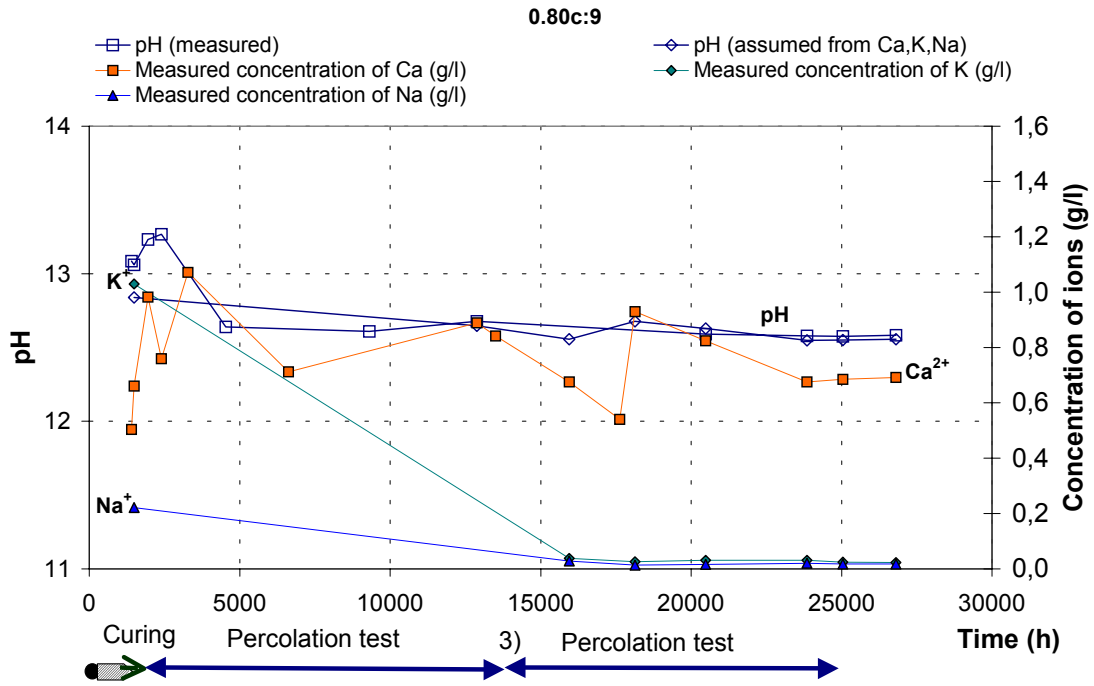


Figure B.33 Permeability and flow of water and ions for the leached specimen 0.80c:9 (w/c 0.80, EH-LD).

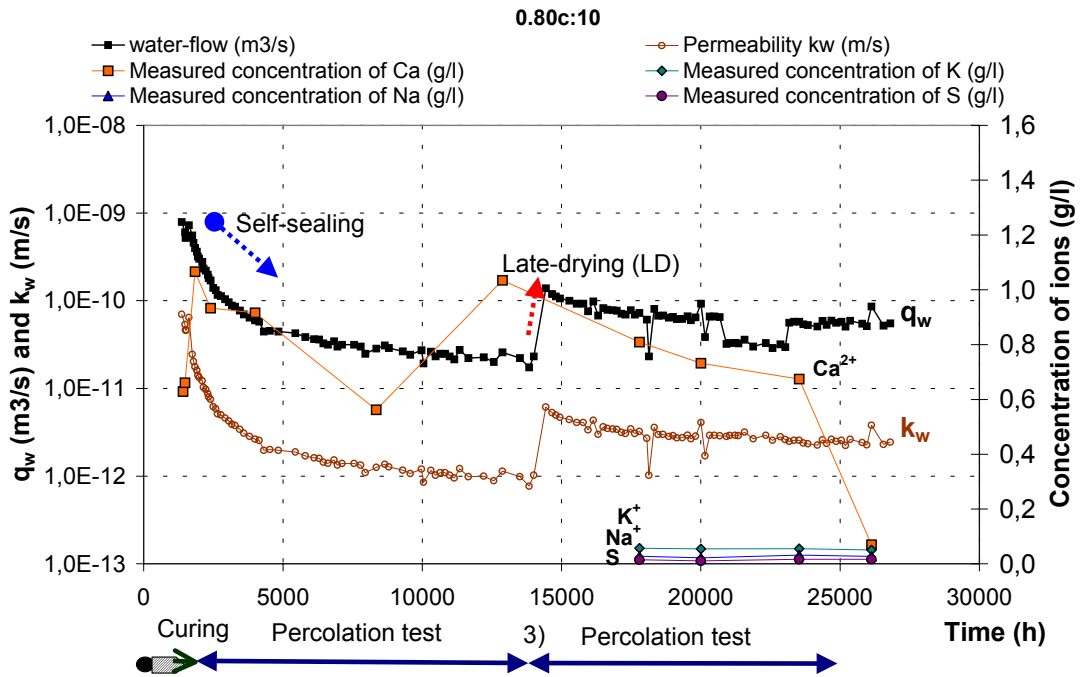


Figure B.34 Permeability and flow of water and ions for the leached specimen 0.80c:10 (w/c 0.80, EH-LD).

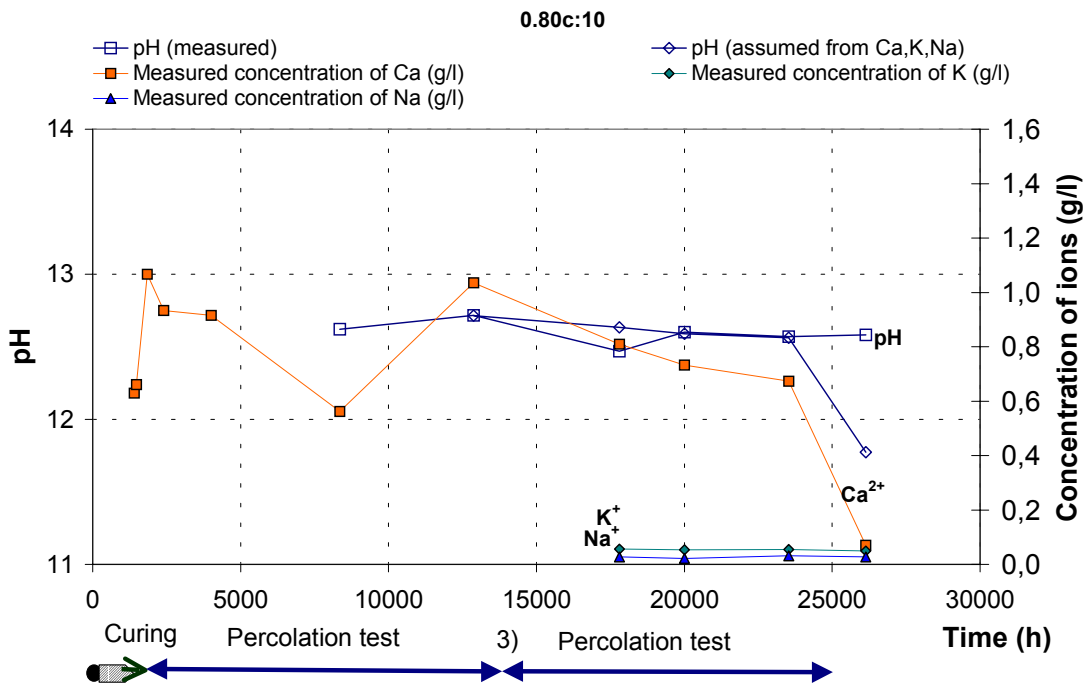


Figure B.35 Permeability and flow of water and ions for the leached specimen 0.80c:10 (w/c 0.80, EH-LD).

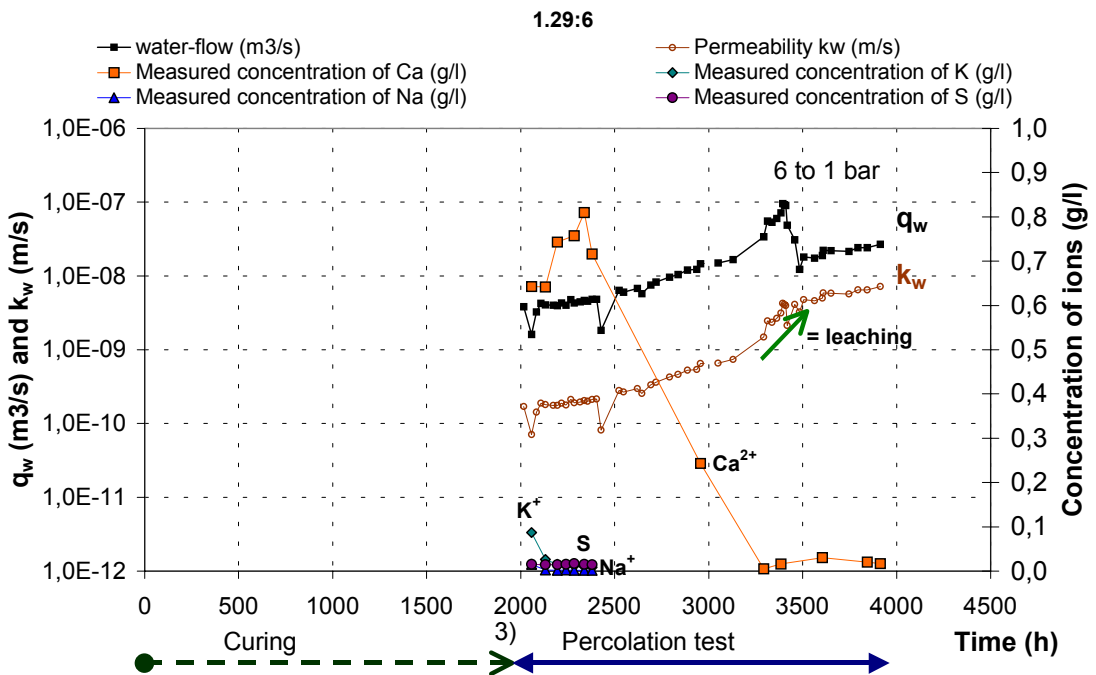


Figure B.36 Permeability and flow of water and ions for the leached specimen 1.29:6 (w/c 0.80, LD).

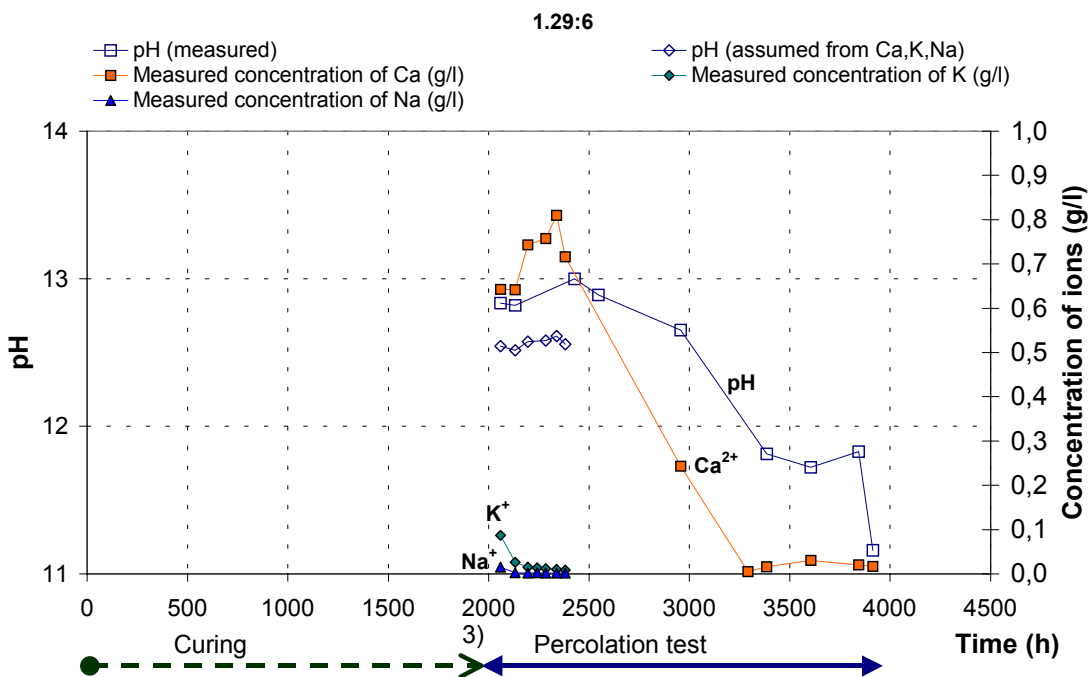


Figure B.37 Permeability and flow of water and ions for the leached specimen 1.29:6 (w/c 0.80, LD).

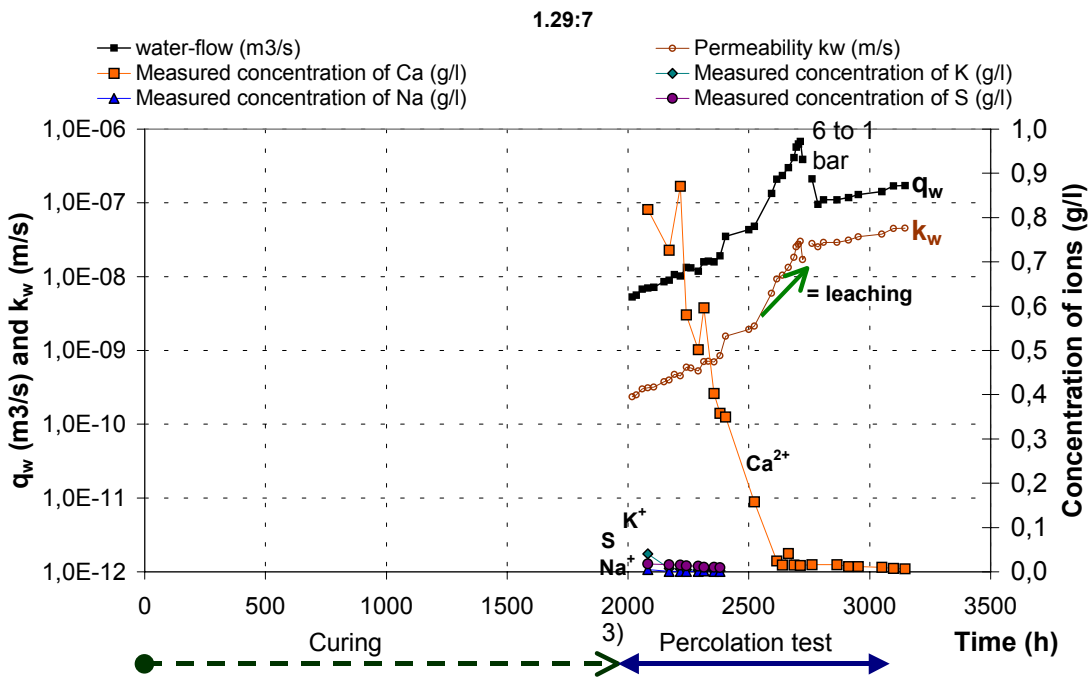


Figure B.38 Permeability and flow of water and ions for the leached specimen 1.29:7 (w/c 0.80, LD).

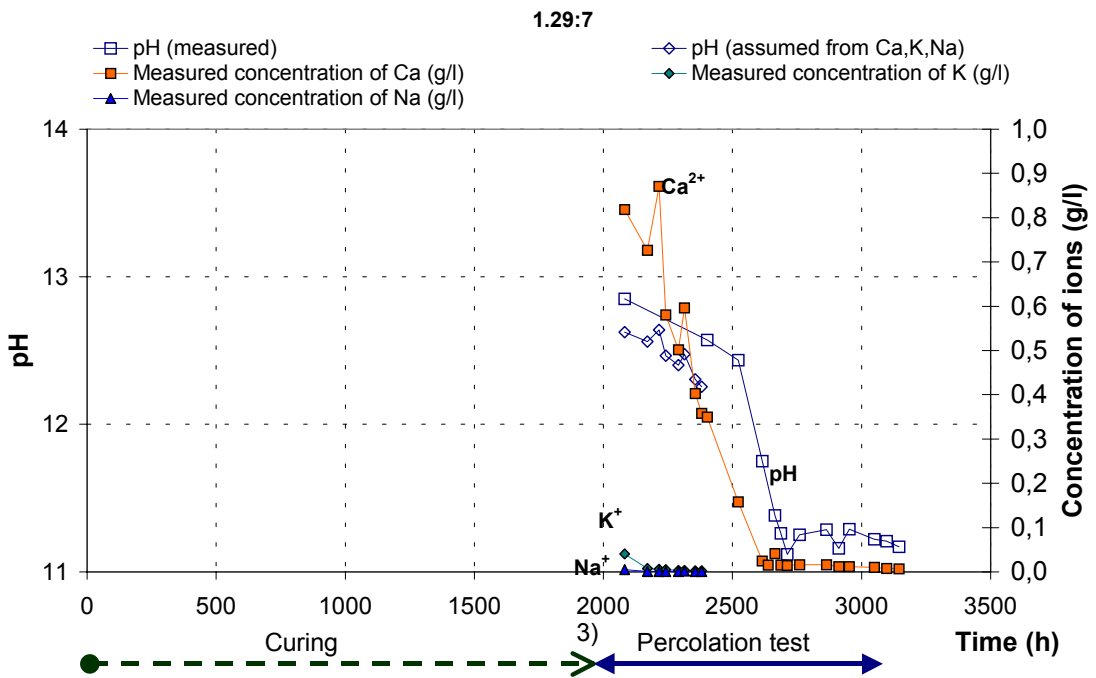


Figure B.39 Permeability and flow of water and ions for the leached specimen 1.29:7 (w/c 0.80, LD).

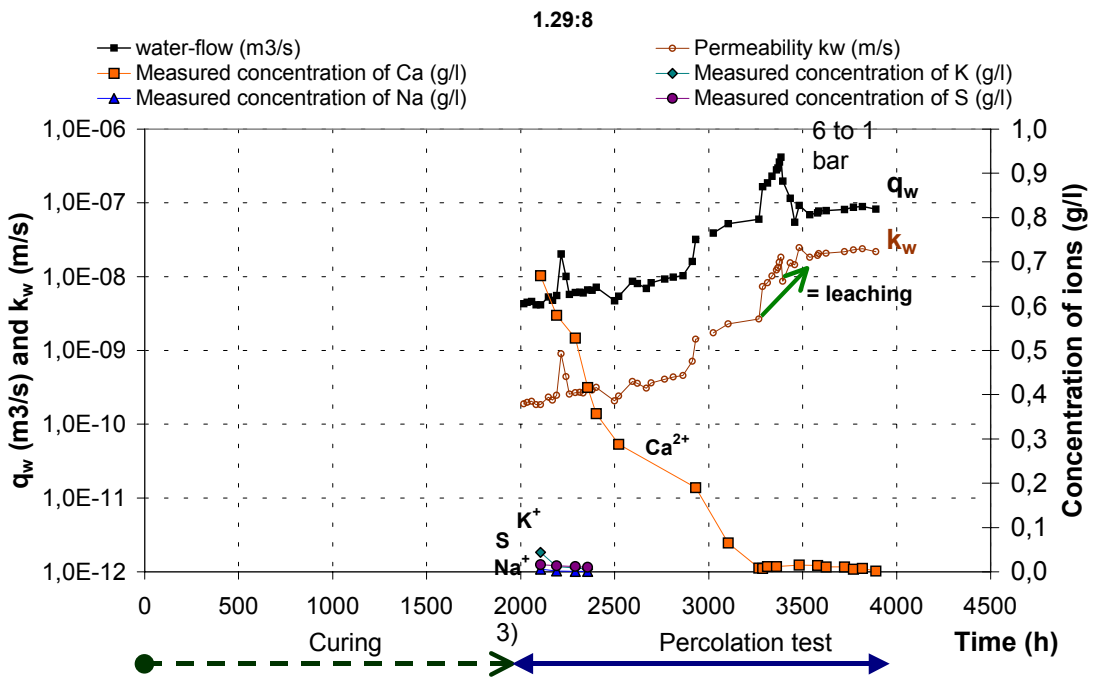


Figure B.40 Permeability and flow of water and ions for the leached specimen 1.29:8 (w/c 0.80, LD).

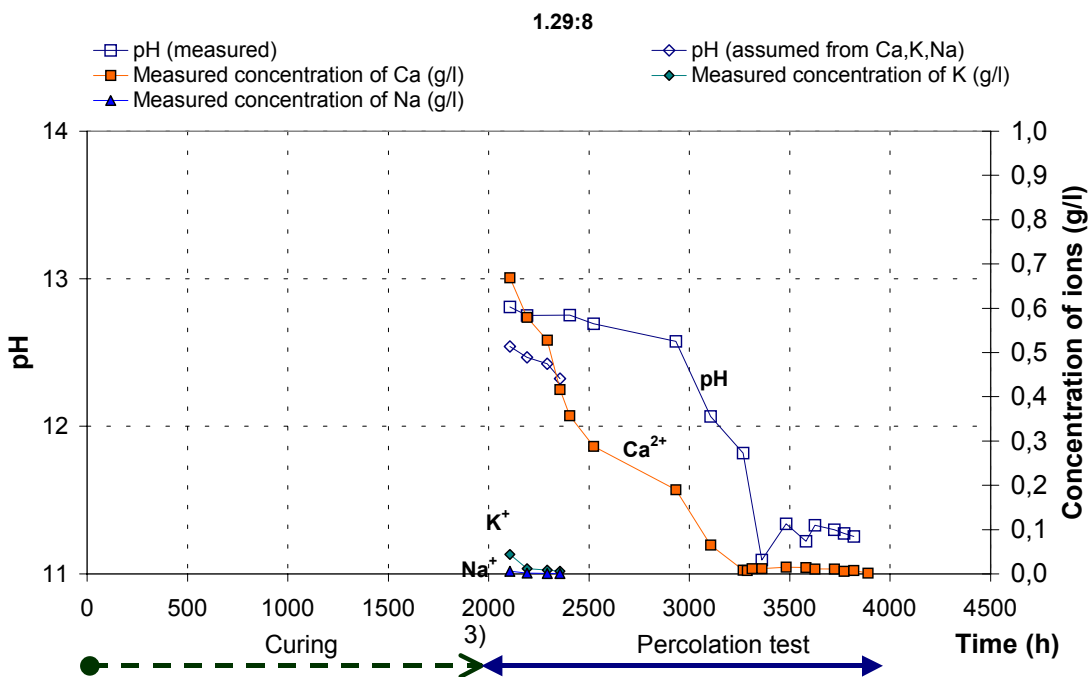


Figure B.41 Permeability and flow of water and ions for the leached specimen 1.29:8 (w/c 0.80, LD).

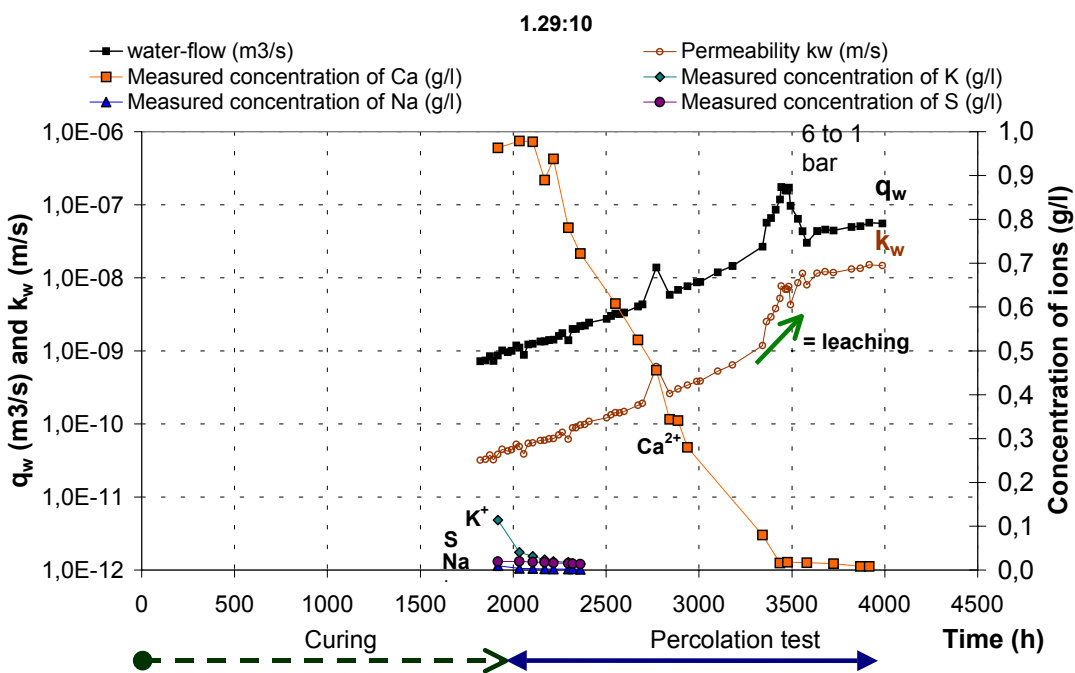


Figure B.42 Permeability and flow of water and ions for the leached specimen 1.29:10 (w/c 0.80, V).

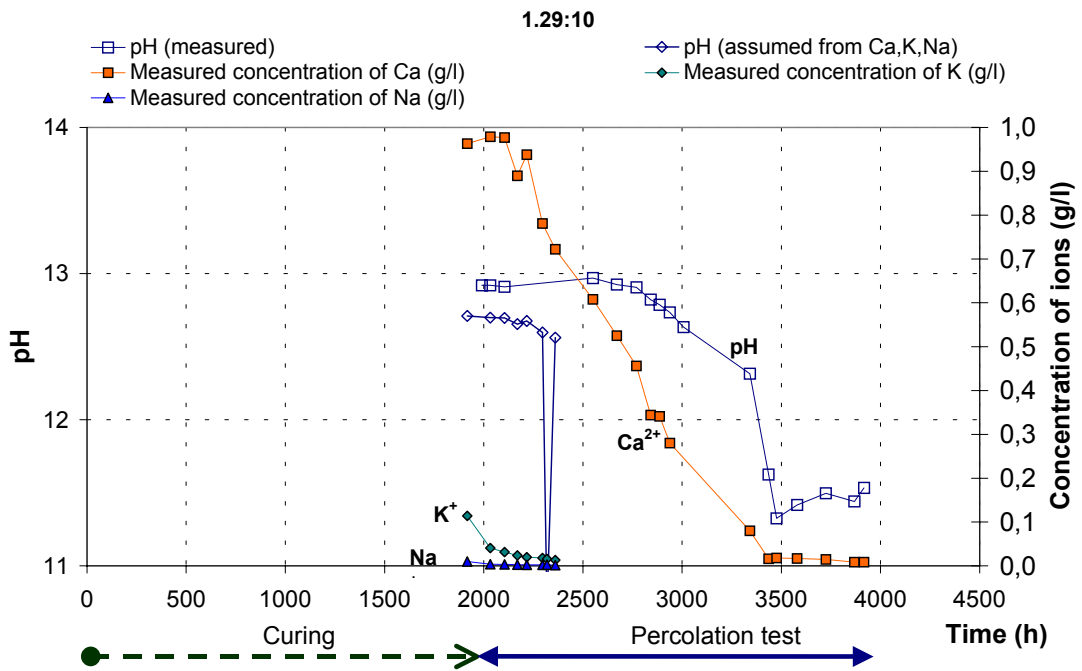


Figure B.43 Permeability and flow of water and ions for the leached specimen 1.29:10 (w/c 0.80, V).

APPENDIX C EXPERIMENTAL RESULTS:

**Homogenous, steady-state percolation of defect-free
concrete – effect of leaching on pore size distribution**

Figures C.1 to C.15 shows results from the pressure plate test, or suction test, described in section 4.10.2. A certain applied air pressure corresponds to a certain pore-radius. The relation between pressure and radius is given by Laplace's law. The total volume of water pressed out from the specimen when the pressure is increased from p_1 to p_2 is equal to the total pore volume in the pore size range r_1 to r_2 . Thus, by starting with a saturated concrete at atmospheric pressure and gradually increasing the pressure, and measuring the amount of water expelled, the size distribution can be determined. The minimum pore-size that can be observed is about $2 \cdot 10^{-8}$ m.

The different applied pressure values are assumed to correspond to certain pore radii's. The total volume of water that was pressed out of the samples at different pore radii (applied pressure levels) is assumed to correspond to certain values porosity. The figures show the accumulated porosity as a function of assumed pore radii.

See Table 4.1 and Figure 4.4 for description of type of concrete and testing history.

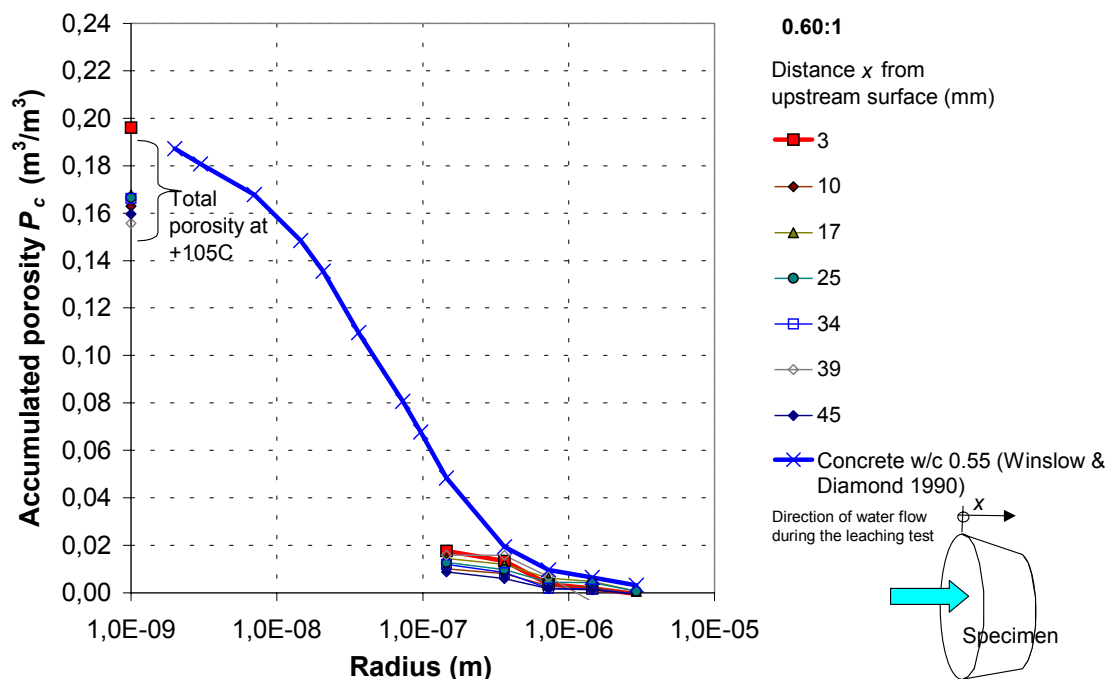


Figure C.1 Pore size distribution for the leached specimen 0.60:1 (w/c 0.60, EH). The values of “Total porosity at +105°C” are values achieved from measurements of weight after the samples have been in an oven (see section 4.10.3). A pore size distribution test of Winslow & Diamond (1990) is also given for comparison.

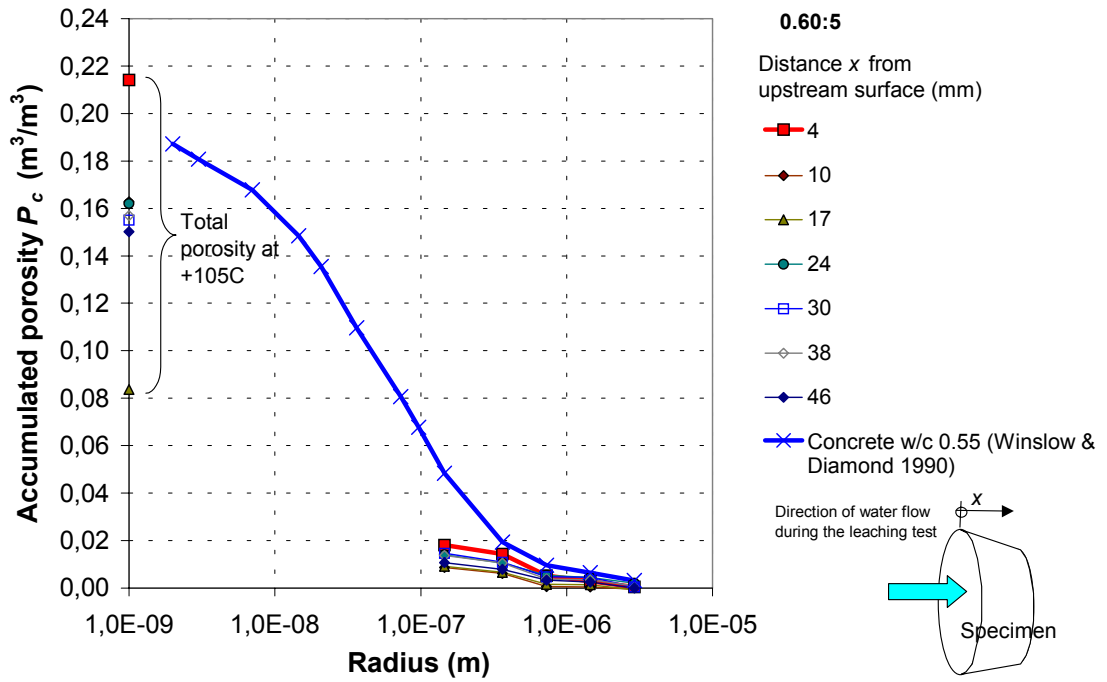


Figure C.2 Pore size distribution for the leached specimen 0.60:5 (w/c 0.60, EH).

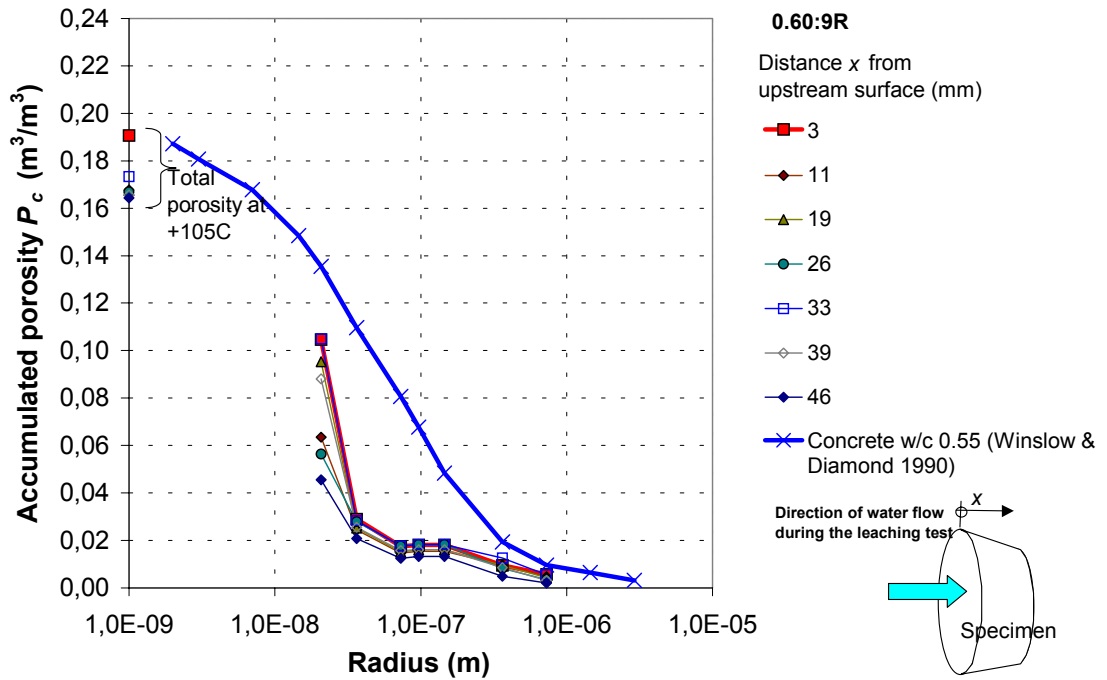


Figure C.3 Pore size distribution for the reference specimen 0.60:9R (w/c 0.60, EH, reference to 0.60:1).

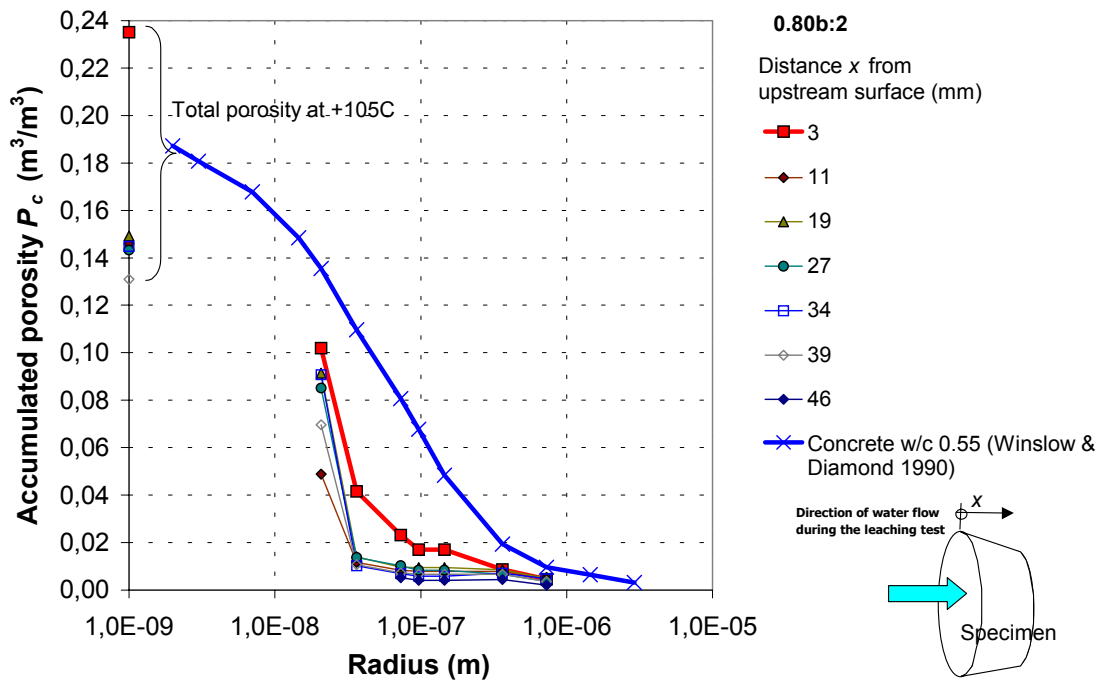


Figure C.4 Pore size distribution for the leached specimen 0.80b:2 (w/c 0.80, V).

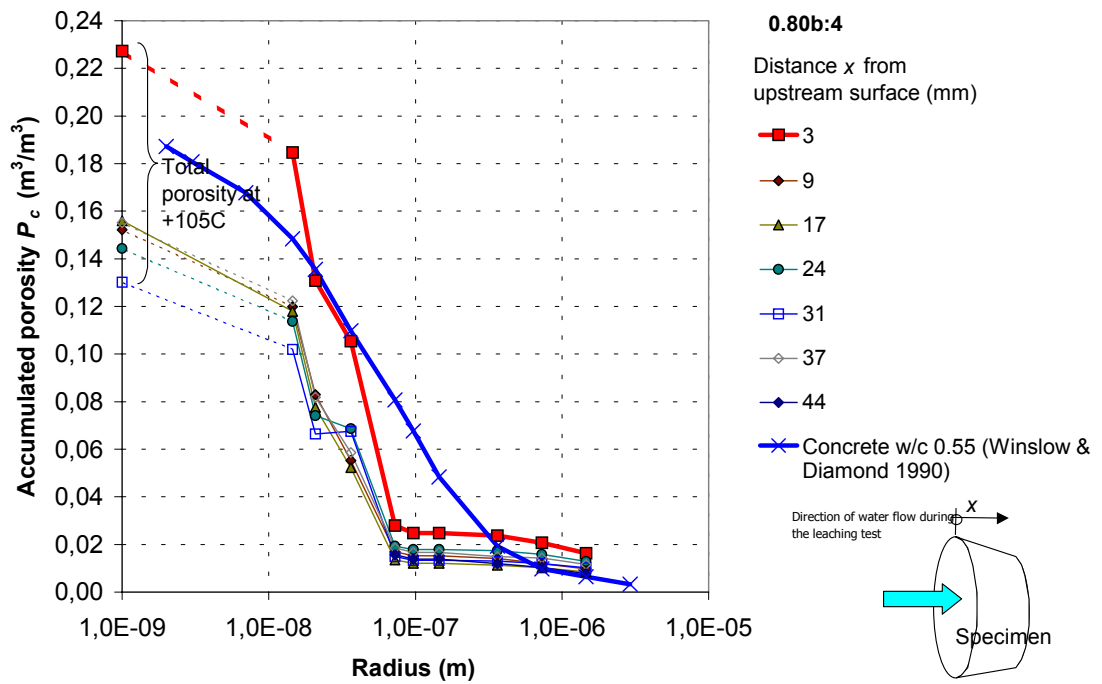


Figure C.5 Pore size distribution for the leached specimen 0.80b:4 (w/c 0.80, V).

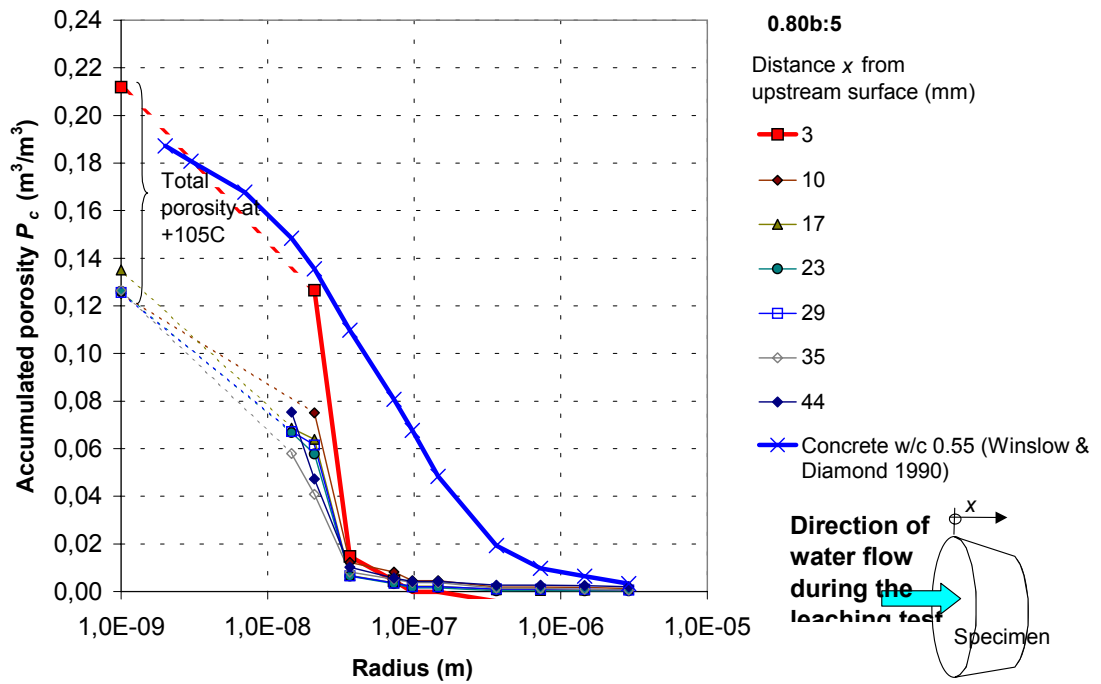


Figure C.6 Pore size distribution for the leached specimen 0.80b:5 (w/c 0.80, V-LD).

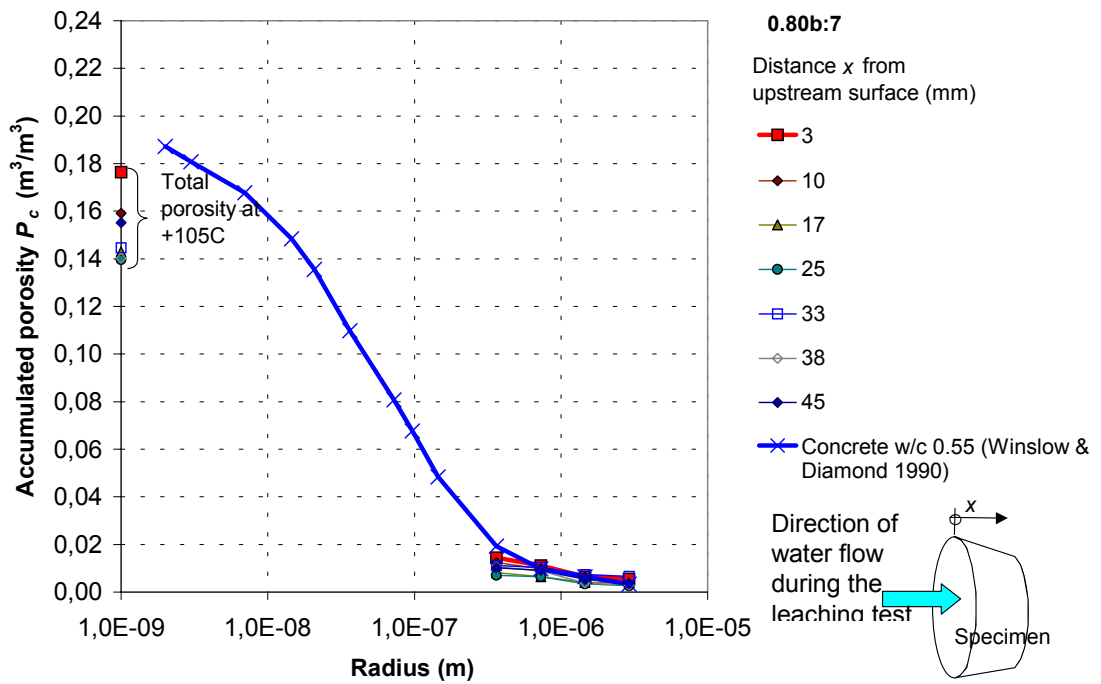


Figure C.7 Pore size distribution for the leached specimen 0.80b:7 (w/c 0.80, V-LD).

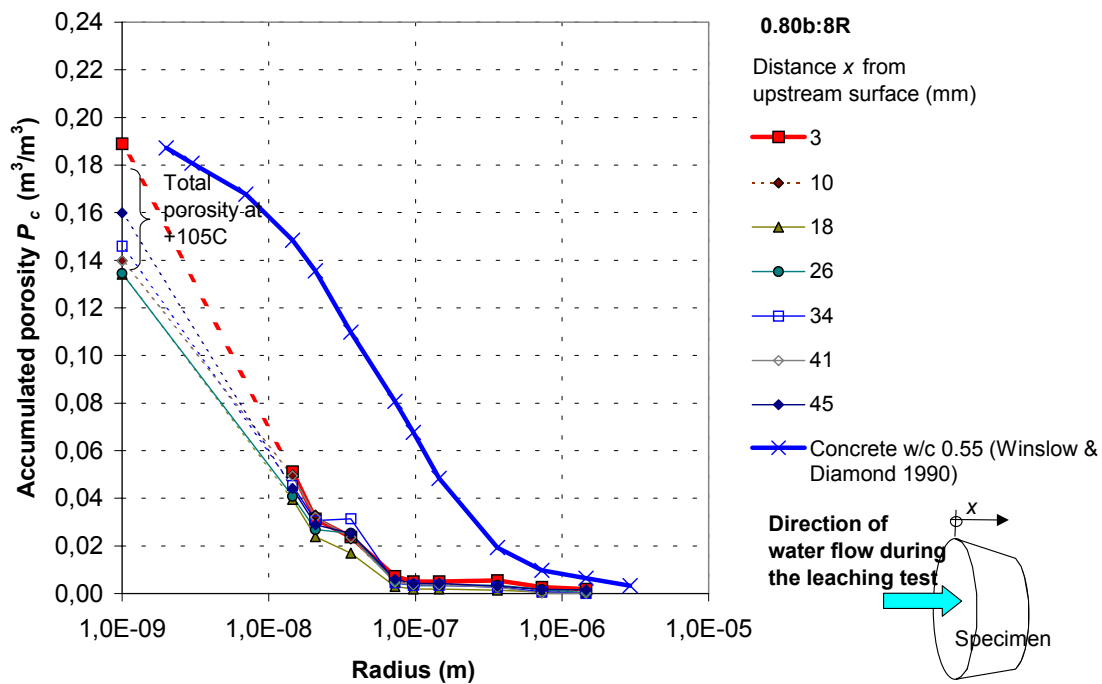


Figure C.8 Pore size distribution for the reference specimen 0.80b:8R (w/c 0.80, V-LD, reference to 0.80b:5&7).

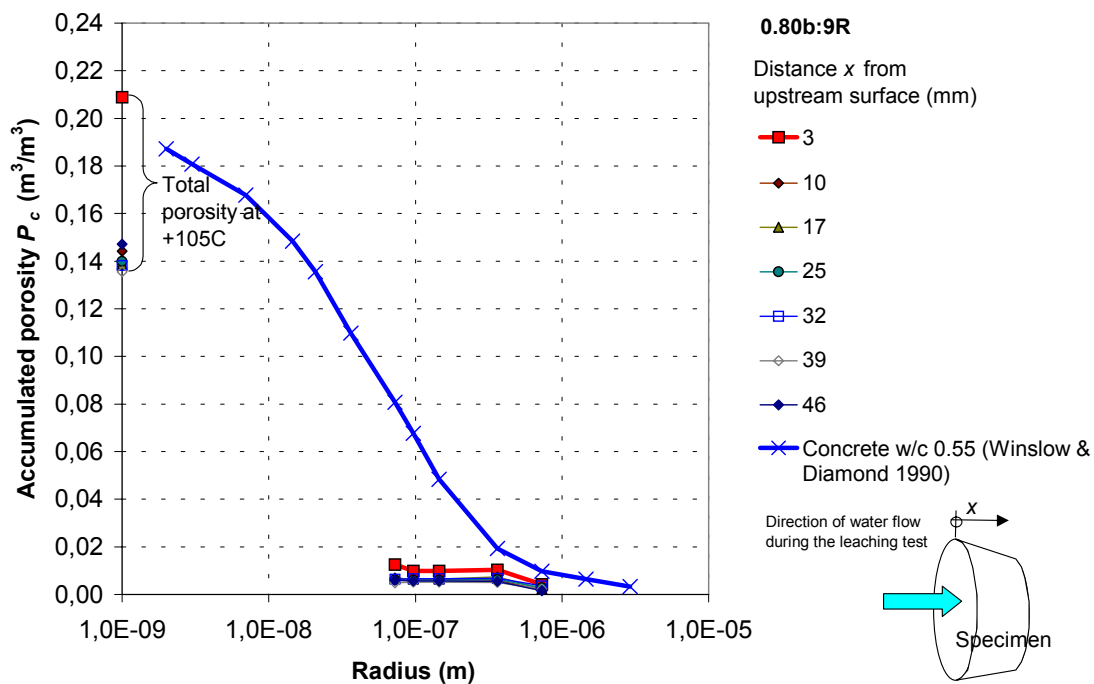


Figure C.9 Pore size distribution for the reference specimen 0.80b:9R (w/c 0.80, V-LD, reference to 0.80b:5&7).

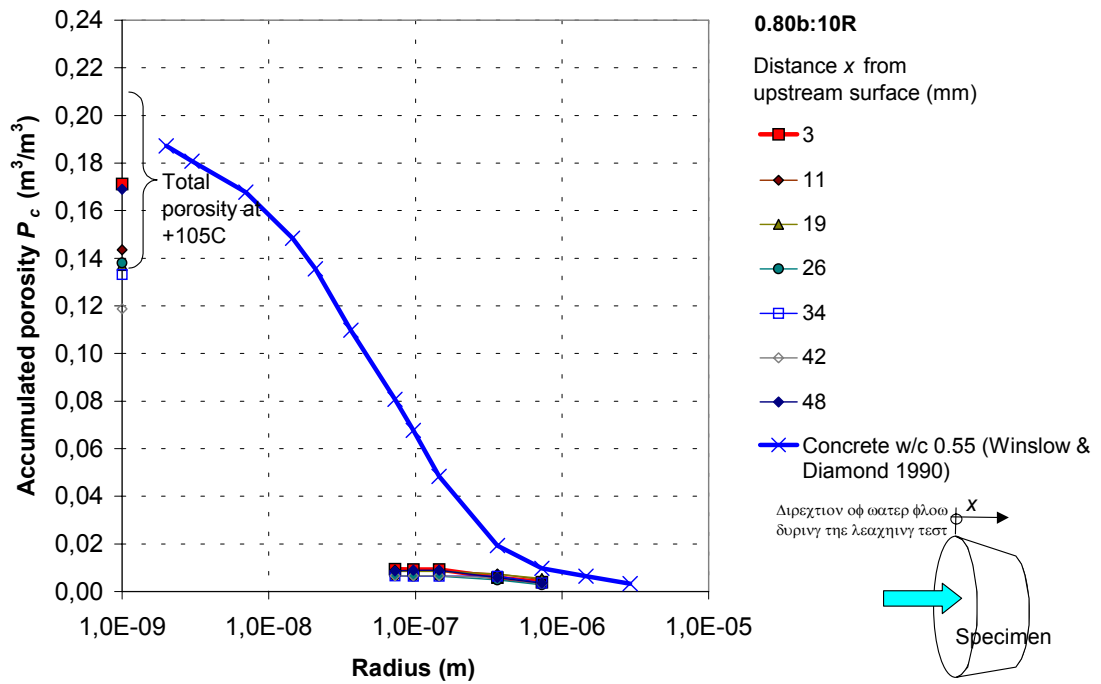


Figure C.10 Pore size distribution for the reference specimen 0.80b:10R (w/c 0.80, V, reference to 0.80b:2&4).

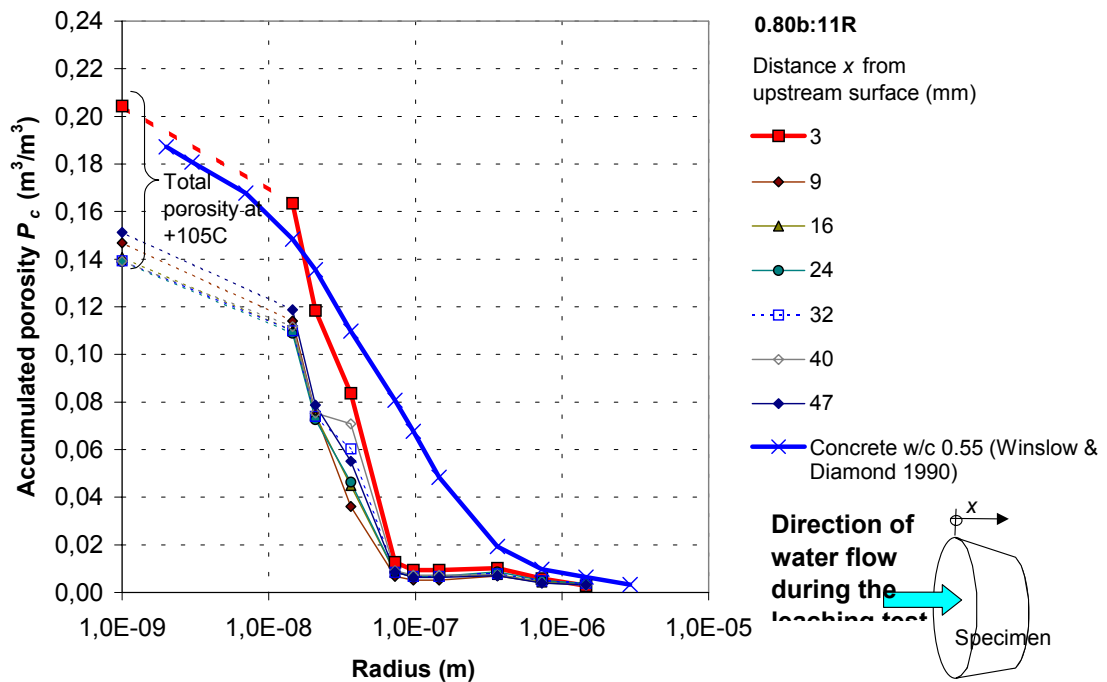


Figure C.11 Pore size distribution for the reference specimen 0.80b:11R (w/c 0.80, V, reference to 0.80b:2&4).

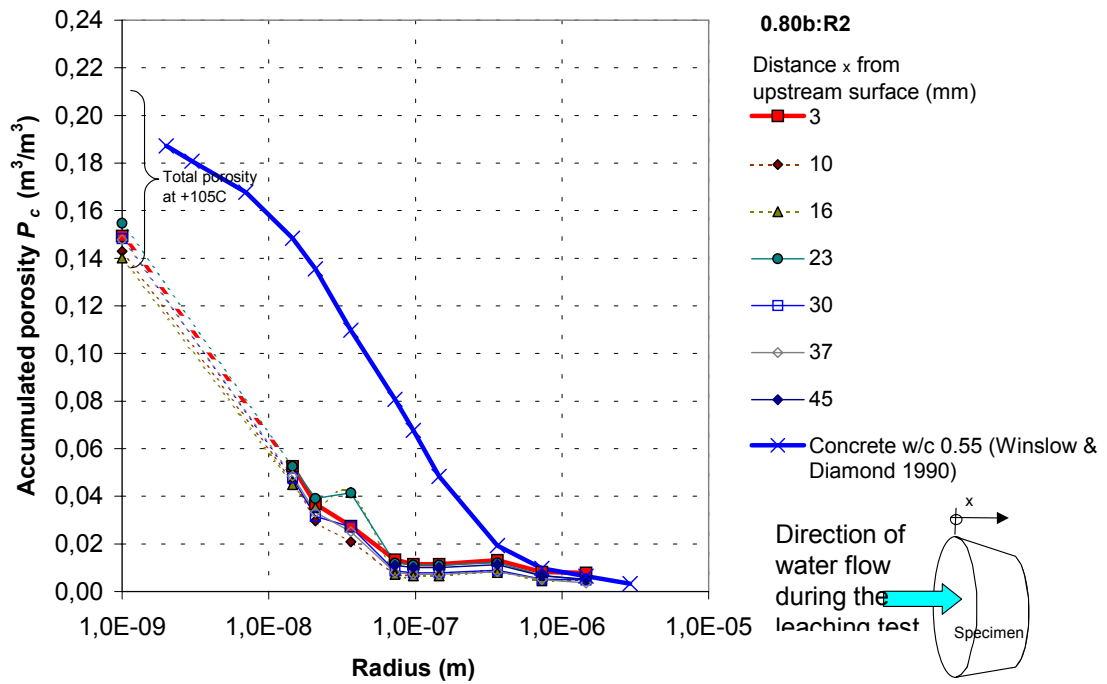


Figure C.12 Pore size distribution for the reference specimen 0.80b:R2 (w/c 0.80, V-LD, reference to 0.80b:5&7).

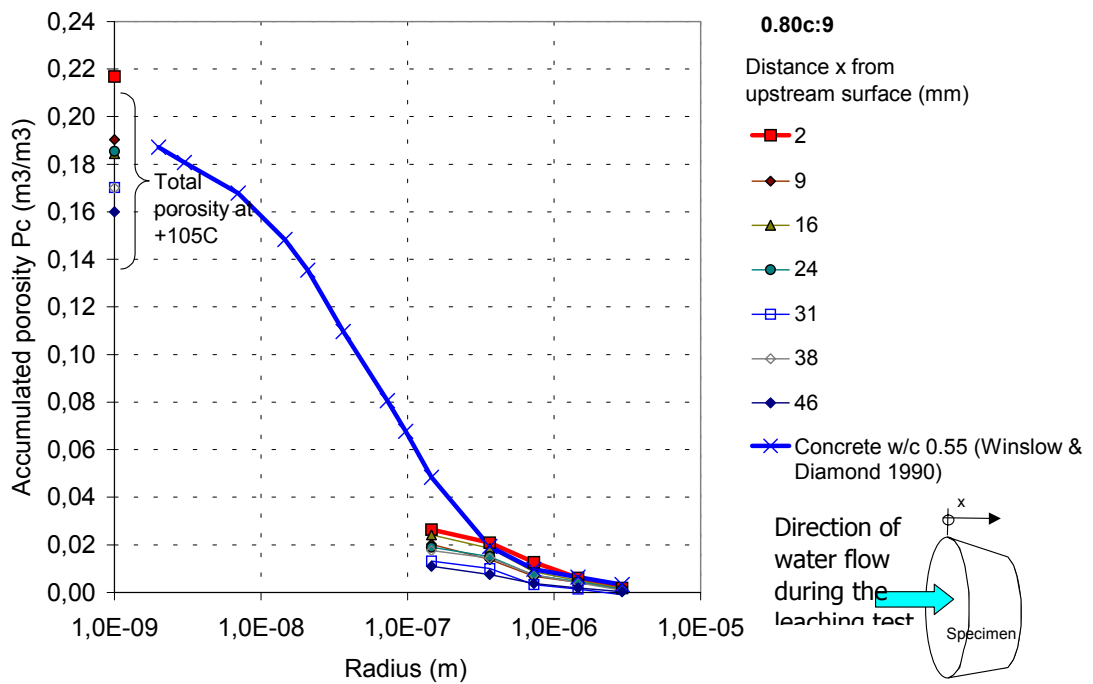


Figure C.13 Pore size distribution for the leached specimen 0.80c:9 (w/c 0.80, EH-LD).

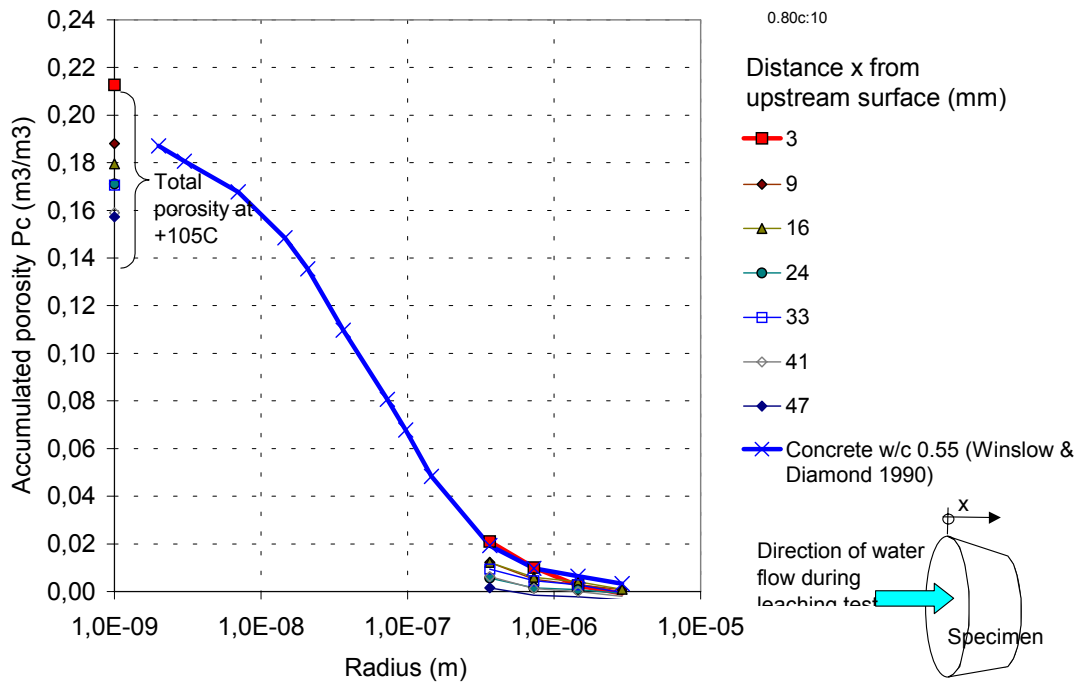


Figure C.14 Pore size distribution for the leached specimen 0.80c:10 (w/c 0.80, EH-LD).

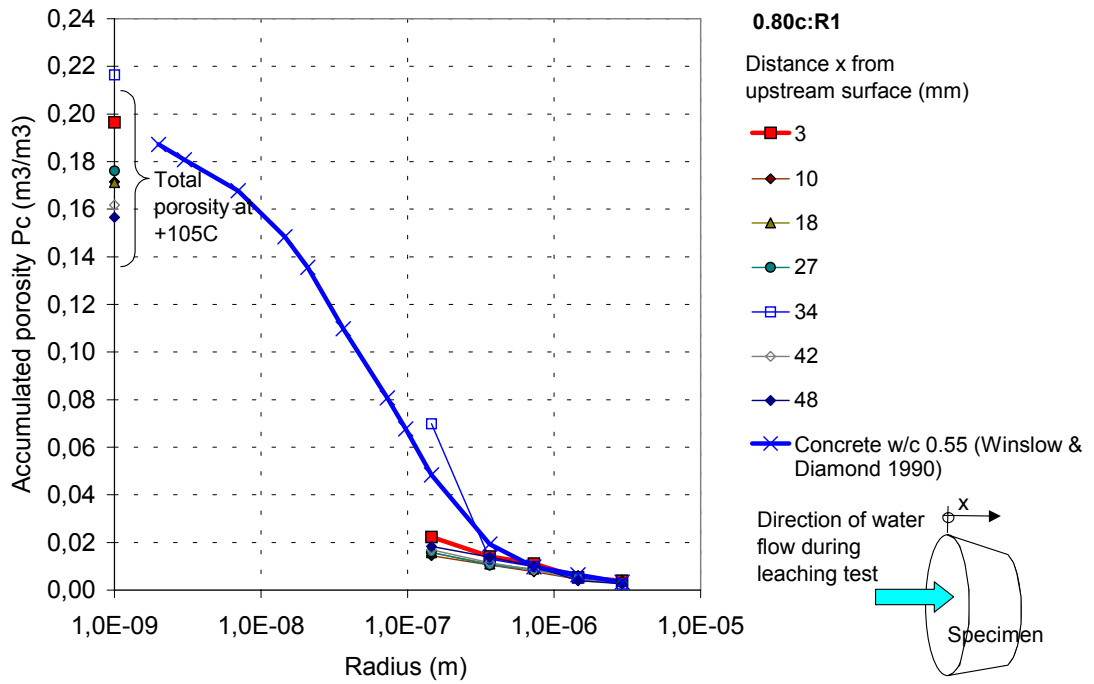


Figure C.15 Pore size distribution for the reference specimen 0.80c:R1 (w/c 0.80, EH-LD, reference to 0.80c:9&10).